SERDP

FINAL REPORT

Regenerable Resin Sorbent Technologies with Regenerant Solution Recycling for Sustainable Treatment of PFAS

Timothy Strathmann
Erin Sedlacko
Christopher Higgins
Colorado School of Mines

Treavor Boyer
Arizona State University

Charles Schaefer
CDM Smith

July 2023

SERDP Project ER18-1063

REPORT DOCUMENTATION PAGE

Form Approved
OMB No. 0704-0188

1. REPORT DATE *(DD-MM-YYYY)*	**2. REPORT TYPE**	**3. DATES COVERED** *(From - To)*
07-06-2023	SERDP Final Report	9/6/2018 - 9/5/2023

4. TITLE AND SUBTITLE

Regenerable Resin Sorbent Technologies with Regenerant Solution Recycling for Sustainable Treatment of PFAS

5a. CONTRACT NUMBER 18-C-0053

5b. GRANT NUMBER

5c. PROGRAM ELEMENT NUMBER

6. AUTHOR(S)
Timothy Strathmann, Erin Sedlacko, and Christopher Higgins: Colorado School of Mines
Treavor Boyer: Arizona State University
Charles Schaefer: CDM Smith

5d. PROJECT NUMBER ER18-1063

5e. TASK NUMBER

5f. WORK UNIT NUMBER

7. PERFORMING ORGANIZATION NAME(S) AND ADDRESS(ES)
Colorado School of Mines
1500 Illinois St.
Golden, CO 80401

8. PERFORMING ORGANIZATION REPORT NUMBER ER18-1063

9. SPONSORING / MONITORING AGENCY NAME(S) AND ADDRESS(ES)

Strategic Environmental Research and Development Program (SERDP), 4800 Mark Center Drive, Suite 16F16, Alexandria, VA 22350-3605

10. SPONSOR/MONITOR'S ACRONYM(S) SERDP

11. SPONSOR/MONITOR'S REPORT NUMBER(S) ER18-1063

12. DISTRIBUTION / AVAILABILITY STATEMENT
DISTRIBUTION STATEMENT A. Approved for public release: distribution unlimited.

13. SUPPLEMENTARY NOTES

14. ABSTRACT

The overall goal of this project was to evaluate the effectiveness and sustainability of resin-based treatment systems for treatment of groundwater contaminated by per- and polyfluoroalkyl substances (PFASs). This project undertook an in-depth analysis of the performance, regenerability, cost and sustainability of IX and other resins, work that will be critical to widespread adoption of these technologies at DoD sites impacted by aqueous film-forming foam (AFFF). Furthermore, work was undertaken to compare the efficacy of regenerable IX resins with emerging "PFAS-selective" resins, and to evaluate options for managing PFAS-contaminated concentrate streams.

15. SUBJECT TERMS
PFAS, aqueous film-forming foam, remediation, ion exchange, LCA

16. SECURITY CLASSIFICATION OF:			**17. LIMITATION OF ABSTRACT**	**18. NUMBER OF PAGES**	**19a. NAME OF RESPONSIBLE PERSON**
a. REPORT	**b. ABSTRACT**	**c. THIS PAGE**			Timothy Strathmann
UNCLASS	UNCLASS	UNCLASS	SAR	286	**19b. TELEPHONE NUMBER** 303-384-2226

TABLE OF CONTENTS

List of Tables

List of Figures

LIST OF ACRONYMS

6:2 FTS – 6:2 fluorotelomer sulfonate
6:2 FTSi – 6:2 fluorotelomer sulfinate
6:2 FTThA – 6:2 fluorotelomer thia acetic acid
6:2 FTTh-PrAd-DiMeEtS – 6:2 fluorotelomer thia propanoamido dimethyl ethyl sulfonate
8:2 FTS – 8:2 fluorotelomer sulfonate
8:2 FTSi – 8:2 fluorotelomer sulfinate
AEC – anion exchange capacity
AER – anion exchange resin
AFB – Air Force Base
AFCEC – Air Force Civil Engineering Center
AFFF – aqueous film-forming foam
ASU – Arizona State University
AmPr-FHxSA – N-dimethyl ammonio propyl perfluorohexane sulfonamide
BDD – boron doped diamond
bgs – below ground surface
BTEX – benzene, toluene, ethylbenzene, and xylenes
BV – bed volumes
CAS# - chemical abstract number
CE – collision energy
CEC – cation exchange capacity
CER – cation exchange resin
COD – chemical oxygen demand
CSM – Colorado School of Mines
CXP – collision cell exit potential
DFT – density functional theory
DGBE - diethylene glycol monobutyl ether
DI - deionized
DOC – dissolved organic carbon
DoD – Department of Defense
DOM – dissolved organic matter
DP – declustering potential
DPT – direct push technology
e_{aq}^- – hydrated electron
EBCT – empty bed contact time
ECT – electrochemical fluorination
EP – entrance potential
EPA – Environmental Protection Agency
ERSON – Environmental Restoration Statement of Need
ESI – electrospray ionization
ESTCP – Environmental Security Technology Certification Program
EtOH - ethanol
FASAs – fluoroalkyl sulfonamides
FTA – fire training area
FTSA – fluorotelomer sulfonate

FTOH – fluorotelomer alcohol
GAC – granular activated carbon
GC-ECD – gas chromatography with electron capture detection
GC-FID – gas chromatography with flame ionization detection
GC-MS/MS – gas chromatography with tandem mass spectrometry detection
GC-TCD – gas chromatography with thermal conductivity detector
gpm – gallons per minute
HAL – Health Advisory Level
HALT – hydrothermal alkaline treatment
HF – hydrofluoric acid
HIOCs – hydrophobic ionizable organic chemicals
HPLC – high pressure liquid chromatography
HPLC-DAD – high pressure liquid chromatography with diode array detection
HRMS – high resolution mass spectrometry
HTG – hydrothermal gasification
HTL – hydrothermal liquefaction
IC – ion chromatography
ICP-AES – inductively coupled plasma-atomic emissions spectrophotometry
I.D. – inner diameter
IPR – In-Progress Review
IPrOH – isopropyl alcohol
IS – internal standard
ISCO – in situ chemical oxidation
ISE – ion selective electrode
IX – ion exchange
JAX – Jacksonville Naval Air Station
k_{obs} – pseudo-first-order rate constants
LCA – life cycle assessment
LCC – life cycle costing
LCCA – life cycle cost analysis
LCI – life cycle impacts
LC-MS – liquid chromatography with mass spectrometry
LC-MS/MS – liquid chromatography tandem mass spectrometry
LC-QToF-MS – liquid chromatography with quantitative time-of-flight mass spectrometry detection
LCS – lab control sample
LOQ – limit of quantitation
MeOH – methanol
MMO – mixed metal oxide (electrode)
MURs – media usage rates
NAS – Naval Air Station
NF - nanofiltration
NIR – non-ionic resin
NMR – nuclear magnetic resonance
NOM – natural organic matter

O&M – operation and maintenance
PAER – PFAS-selective anion exchange resins
PAFB – Peterson Air Force Base
PCBs – polychlorinated biphenyls
PCE – tetrachloroethylene
PEs – person equivalents
PFAAs – perfluoroalkyl acids
PFASs – per- and polyfluoroalkyl substances
PFBA – perfluorobutanoic acid
PFBS – perfluorobutane sulfonate
PFCAs – perfluorocarboxylic acids
PFDoA – perfluorododecanoic acid
PFDS – perfluorodecane sulfonate
PFHpA – perfluoroheptanoic acid
PFHxA – perfluorohexanoic acid
PFHxS – perfluorohexane sulfonate
PFNA – perfluorononanoic acid
PFOA – perfluorooctanoic acid
PFOS – perfluorooctane sulfonate
PFOSA – perfluorooctane sulfonamide
PFPeA – perfluoropentanoic acid
PFSAs – perfluoroalkyl sulfonic acids
PFTeA – perfluorotetradecanoic acid
PFTrA – perfluorotridecanoic acid
PFUnA – perfluoroundecanoic acid
PSE – process systems engineering
QC – quality control
QToF – quantitative time-of-flight mass spectrometry
RPM – Remedial Project Manager
RT – retention time
SBA – strong base anion (exchange resin)
SDS – sodium dodecyl sulfate
SERDP - Strategic Environmental Research and Development Program
SON – statement of need
SPE – solid phase extraction
SRNOM – Suwanee River natural organic matter
TBA – tert butyl alcohol
TCE – trichloroethylene
TFA – trifluoroacetic acid
TOC – total organic carbon
TOP Assay – total oxidizable precursor assay
TRACI – Tool for Reduction and Assessment of Chemicals and Other Environmental Impacts
USEPA –United States Environmental Protection Agency
UV – ultraviolet light
UV-Vis – ultraviolet and visible light

VOC – volatile organic compound
WBS – work breakdown structure
WG – Willow Grove
XIC – extracted ion chromatogram

Abstract

Introduction and Objectives

The overall goal of this project was to evaluate the effectiveness and sustainability of resin-based treatment systems for treatment of groundwater contaminated by per- and polyfluoroalkyl substances (PFASs). Ion exchange (IX) resins have emerged as an economically viable alternative to granular activated carbon (GAC) adsorption treatment systems, so this project undertook an in-depth analysis of the performance, regenerability, cost and sustainability of IX and other resins, work that will be critical to widespread adoption of these technologies at DoD sites impacted by aqueous film-forming foam (AFFF). Furthermore, work was undertaken to compare the efficacy of regenerable IX resins with emerging "PFAS-selective" single-use resins, and to evaluate options for managing PFAS-contaminated concentrate streams produced upon IX resin regeneration.

Technical Approach

A series of experiments and modeling analyses were performed to meet the project objectives, including (1) Evaluating and comparing the effectiveness of commercially available ion exchange and non-ionic resins for removal of the full range of PFASs in AFFF-impacted water; (2) Comparing regenerable anion exchange resins (AERs) with emerging single-use "non-regenerable" AERs; (3) Identifying resin characteristics associated with increased adsorption of PFASs; (4) Assessing the effect of important non-target groundwater constituents on PFAS adsorption; (5) Evaluating the links between PFAS adsorption observed in batch experiments and continuous-flow adsorption studies; (6) characterizing the effectiveness of different salt brines, organic co-solvent, and other amendments for regenerating PFAS-loaded resins; (7) quantifying PFAS destruction in waste ion exchange regenerant solutions using electrochemical oxidation and hydrothermal alkaline treatment technologies; and (8) comparing the life cycle environmental impacts and treatment costs for different regenerable ion exchange treatment system design options, and identifying system variables that offer the greatest potential for improving system sustainability. Experiments were conducted using both batch and continuous-flow experimental systems in both laboratory and field site conditions.

Results

Results demonstrate that PFASs adsorb much more strongly to AERs than to nonionic and cationic resins as well as GAC, and the extent of adsorption to AERs varies extensively with both PFAS and resin structure. Longer-chain and sulfonic acid-based PFASs adsorb more strongly than shorter-chain and carboxylic acid-based structures due to a combination of electrostatic and van der Waals interactions. Adsorption is greatest with polystyrene-based PFAS-selective AERs possessing more hydrophobic functional groups. PFAS adsorption is relatively insensitive to most mobile counterions pre-loaded onto the resin (e.g., chloride versus sulfate). Regeneration of PFAS-loaded AERs, both strong- and weak-base forms, requires regenerant mixtures containing both salt brine and alcohol co-solvent; the shortest chain perfluorocarboxylic acids were the only PFASs appreciable desorbed from AERs using aqueous salt-only regenerants. Substitution of methanol with higher molecular weight alcohols can improve regeneration efficiencies at comparable co-solvent levels. Studies also found that "single-use" AERs could be regenerated, although typically this required higher co-solvent percentages. The regenerant wastes can be effectively treated using both electrochemical oxidation (ECO) and hydrothermal alkaline treatment (HALT) technologies. Rates of ECO were found to be superior in sulfate- and bicarbonate-based synthetic waste brines

compared to chloride-based brines. HALT was shown capable of destroying and defluorinating the full suite of PFASs detected in a waste IX still bottoms obtained from a DoD site, with destruction rates for individual PFASs in the mixture being consistent with results reported previously for other liquid solutions, including AFFF and AFFF-impacted groundwater. Comparative analysis under a baseline scenario indicates that AER systems employing single-use "PFAS-selective" resins have lower environmental impacts and costs than systems using regenerable resins or GAC adsorbents (either single-use or thermally reactivated processes) for nearly all impact categories. Use of GAC operated as a single-use adsorbent led to the highest impacts for most categories as well as the highest treatment costs, with thermally reactivated GAC proving to be less impactful than regenerable AER treatment. Generally, impacts of the adsorbent remediation systems were most sensitive to media usage rates or media regeneration frequency, which are highly dependent upon the PFAS breakthrough criteria used to determine when media replacement or regeneration was required. Environmental impacts of regenerable IX systems were found to be most dependent upon the mass of residuals disposed of or incinerated off-site, and practices that reduce the mass of these residuals such as maximizing the fraction of co-solvent and brine that can be recycled on-site.

Benefits

Results from this project support the continued deployment of IX treatment technologies for groundwater remediation at DoD sites contaminated AFFF. Results from both laboratory and field demonstration tests confirm successful removal of the broad suite of PFASs identified at AFFF-impacted sites from groundwater. Results show that both single-use and regenerable IX systems can be successfully applied, and critical factors to the sustainable and cost-effective deployment of these technologies have been identified. Results support future efforts aimed at demonstrating IX treatment of groundwater with diverse geochemical conditions and PFAS mixture composition.

Executive Summary

Introduction

Extensive use of per- and polyfluoroalkyl substances (PFASs) in aqueous film-forming foam (AFFF) has led to significant environmental releases at Department of Defense (DoD) facilities. As a result, soil and groundwater underlying these sites now represent major source zones for PFAS contamination of water supplies. Tests show that concentrations of PFASs in groundwater near DoD sites often exceed known adverse effect levels for human health. PFASs pose significant threats to human and environmental health due to their association with numerous health effects and potential for bioaccumulation. Recent studies have linked exposure to PFASs with various types of cancer, thyroid conditions, liver damage, and developmental issues, including adverse immune responses and infant low birth weights.

As a result of growing concerns listed above, the DoD and other Federal agencies have undertaken significant efforts to support the development, improvement, and deployment of technologies for treating AFFF-impacted groundwater. Removal of PFASs from water is most commonly accomplished using adsorption processes, where contaminated water is pumped through fixed beds of adsorbent media to induce separation of PFASs from water. Presently, granular activated carbon (GAC) adsorption is the most common adsorbent media used for PFAS treatment. Although GAC adsorbent beds can be effective in treating PFAS-contaminated water, long contact times are required and rapid breakthrough of PFASs from GAC adsorber beds is often observed, resulting in frequent media replacements that raise treatment costs and associated concerns about the environmental impacts from these practices.

More recently, use of anion exchange resins (AERs) have emerged as a cost-competitive alternative adsorption media. High affinity for PFAS adsorption to these polymeric resins is derived from a combination of electrostatic and hydrophobic molecular interactions between the resins and aqueous contaminants. Typically AER-based treatment systems for other water contaminants, most notably nitrate, involve the use of resins that are periodically regenerated through desorbing the contaminant with a concentrated salt brine solution that reverses the adsorption equilibrium. In addition to using resins that can be regenerated when resins have exhausted their capacity of PFAS adsorption, manufacturers have recently introduced PFAS-selective resins that are applied as single-use media that is disposed or incinerated after their adsorption capacity has been exhausted. These developments has led to growing interest in the potential of AERs, both regenerable and single-use media, as viable alternative for treatment of PFAS-contaminated water supplies. Navigating the trade-offs in terms of both treatment costs and long-term environmental sustainability of resin-based treatment systems in comparison to activated carbon adsorbents is a challenge faced by decision makers at a growing number of PFAS contamination sites. As such, this project was undertaken to examine the performance and potential of resin-based adsorption processes for treating AFFF-impacted water supplies. Experimental results were used to inform systems-level analyses of life cycle environmental impacts and treatment costs, aiming to identify resin properties and system design variables that have the greatest influence on performance, costs, and environmental sustainability.

Objectives

The overall goal of this project was to evaluate the effectiveness and sustainability of resin-based treatment systems for remediation and treatment of groundwater contaminated by per- and

polyfluoroalkyl substances (PFASs). Ion exchange (IX) resins have emerged as an economically viable alternative to granular activated carbon (GAC) adsorption processes, so this project undertook an in-depth analysis of the performance, regenerability, sustainability and costs for IX treatment systems for PFASs representative of contaminants detected at Department of Defense sites impacted by historical releases of aqueous film-forming foam (AFFF). Furthermore, work was undertaken to compare the efficacy of conventional regenerable IX resin treatment systems with emerging "PFAS-selective" single-use resin treatment systems, and to evaluate options for managing PFAS-contaminated concentrate streams produced as a byproduct of the resin regeneration process.

High resolution mass spectrometry techniques were applied, which enabled us to examine, for the first time, the effectiveness of resins for adsorbing a much wider range of PFASs detected in AFFF-impacted water matrices. Specific objectives of the project included:

(1) Evaluate and compare the effectiveness of commercially available ion exchange and non-ionic resins for removal of the full range of PFASs in AFFF-impacted water.

(2) Compare conventional regenerable resins with emerging single-use "non-regenerable" resins.

(3) Identify resin characteristics associated with increased adsorption of PFASs.

(4) Assess the effect of important non-target groundwater constituents (e.g., dissolved organic matter) on PFAS adsorption.

(5) Evaluate the links between PFAS adsorption observed in short-term batch experiments and longer-term continuous-flow adsorption experiments performed in both laboratory and field settings.

(6) Characterize regeneration of PFAS-contaminated resins with different salt brine, organic co-solvent, and other regenerant amendments.

(7) Quantify PFAS destruction in simulated and real waste ion exchange regenerant byproduct solutions using electrochemical oxidation and hydrothermal alkaline treatment technologies.

(8) Compare the life cycle environmental impacts and life cycle costs for regenerable and single-use resin treatment systems with GAC adsorption.

(9) Evaluate the life cycle environmental impacts of different resin regeneration options, and identify design variables that offer the greatest potential for improving sustainability.

Technical Approach

Overview: A series of experimental and modeling tasks (**Figure ES-1**) were performed to meet the project objectives and test associated hypotheses. Experimental methods are described below for (1) assessing both PFAS adsorption to resins, (2) comparing performance of resins under field conditions at a DoD site, (3) desorbing PFASs and regenerating resins, and (4) destruction of PFAS in simulated and real waste resin regenerant solutions. Experimental results were then used to inform a life cycle assessment and life cycle costing analysis (LCA/LCCA) of resin-based treatment systems is also described.

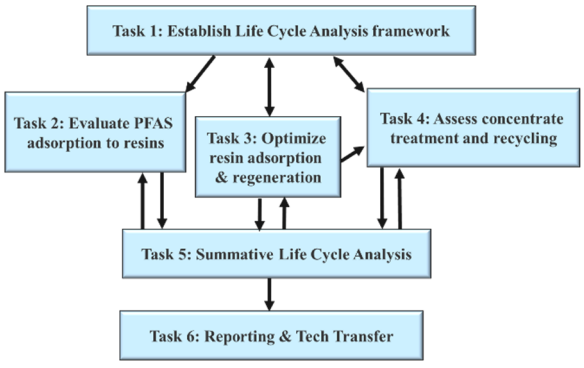

Figure ES-1. Schematic of major project tasks.

PFAS Adsorption to Resins: Both batch and continuous-flow experimental systems were used to quantify the adsorption of a wide range of PFASs, including widely detected perfluoroalkyl acids (PFAAs) and polyfluorinated structures that are precursors to formation of PFAAs at AFFF-impacted sites. Batch kinetics and equilibrium adsorption experiments were undertaken to quantify a PFAS adsorption to a wider range of commercially available anion exchange resins (AER), cation exchange resins (CER), and nonionic resins (NIR) with varying properties, including polymer matrix (polystyrene versus polyacrylic), porosity (macroporous versus gel-type), and ionic functional group identity. Experiments were conducted using AFFF diluted to a high enough degree that individual PFASs in the mixture adsorbed to the resins non-competitively. After mixing solutions with the target resin for the desired reaction time, supernatant was collected and analyzed by high resolution mass spectrometry to quantify the concentrations of each PFAS removed from the solution by adsorption to the resin. The resulting information was used to determine ion exchange adsorption equilibrium constants for each PFAS-resin combination. Separate batch experiments were also conducted to assess the impact of dissolved natural organic matter (NOM) and the identity of the adsorbed resin counterion (chloride versus sulfate versus bicarbonate) on PFAS and NOM adsorption to selected AERs. Finally, while most experiments focused on strong-base AERs where the resin functional group remains charged at all pH conditions, experiments also examined the adsorption of PFAAs to selected weak-base AERs to examine their performance under variable pH conditions.

Field Pilot Demonstration Comparing Different Resins: To extend results from the laboratory experiments, a 9-month field pilot study was conducted to compare performance of 5 anion exchange resins, including 2 regenerable resins (1 polystyrene, 1 polyacrylic) and 3 polystyrene-based single-use PFAS-selective resins treating AFFF-impacted groundwater at a DoD site located in Willow Grove, PA. Parallel packed columns of the 5 resins were treated with groundwater, and samples were collected for PFAS analysis following 30 seconds and 2 minutes of empty bed contact time (EBCT). For the regenerable resins, a third sample was collected following 3 minutes of total EBCT to better mimic manufacturer suggested contact times. Samples were collected weekly for 9 months, enabling treatment of >180,000 bed volumes of groundwater for the 2-minute EBCT sampling point and >750,000 bed volumes for the 30-second EBCT sampling point. The resulting effluent breakthrough data was analyzed using the Thomas Model. Following completion of the pilot study, a post-mortem analysis of the resins was performed to characterize the spatial distribution of individual PFASs adsorbed spatially along the packed beds of each resin.

Desorbing PFASs and Regenerating Resins: Batch and continuous-flow experiments were also conducted to measure desorption of PFASs from anion exchange resins in an effort to identify the effectiveness of different candidate regenerant solution components and constituents. Batch experiments were conducted with resins pre-loaded of either PFASs or surrogate hydrophobic ionizable chemicals that could be more easily measured using routine laboratory analysis methods. The pre-loaded resins were mixed in solutions containing a variety of potential components that may act to promote desorption of PFASs adsorbed on the resins, including many different salts, alcohol cosolvents, bases, surfactants, chelating agents, and organic anions. After mixing for the desired reaction time, supernatant was collected and analyzed to measure the extent to which individual PFASs or PFAS surrogate compound desorbed from the resin in question.

Several of the resins used in batch experiments described above, both in laboratory and field pilot settings, were also subjected to regenerant mixtures in continuous-flow conditions to better

reflect regeneration practices applied in practice. First, packed column laboratory adsorption-regeneration cycling experiments were conducted to evaluate PFAS adsorption and resin regenerability under continuous flow conditions that better mimic how resins are deployed in the field for groundwater treatment. Regenerable strong- and weak-base polystyrene and polyacrylic resins were loaded into 1-cm or 2.5-cm diameter glass columns and the mobile counterion was initially loaded as chloride, sulfate or bicarbonate anions. A mixture of perfluoroalkyl acids were then spiked into a real groundwater matrix to serve as the feed solutions. Breakthrough of the individual PFASs during treatment and regeneration phases were then measured by monitoring effluent from each of the packed columns. Separate column experiments were also performed using a recently introduced regenerable PFAS-selective resin where the feed solution was spiked with diluted AFFF. The regenerant mixtures, typically an aqueous salt brine combined with an alcohol cosolvent, were flushed through the PFAS-loaded resin beds, and effluent samples were collected to characterize the elution profile of individual PFASs that had adsorbed in the packed bed reactor during the adsorption phase. Experiments conducted using weak base anion exchange resins also examine the effects of raising pH of the regenerant solution to neutralize the resins' active sites for ion exchange. Finally, experiments were undertaken to evaluate the effect that co-adsorption of natural organic matter with PFASs has on the subsequent desorption of PFASs by regenerant salt brine/cosolvent mixtures.

Treatment of PFAS-Contaminated Regenerant Wastes: Experiments were conducted to assess the destruction of PFASs that accumulate in the waste regenerant byproduct solutions using two technologies: (1) electrochemical oxidation (ECO), and (2) hydrothermal alkaline treatment (HALT). ECO experiments using boron-doped diamond electrodes were conducted to evaluate treatment of PFASs in an AFFF mixture amended to a series of synthetic brine mixtures designed to mimic potential regenerant still bottoms waste streams. Batch experiments using a single-compartment micro flow cell were used and PFAS concentrations and inorganic fluoride ion were measured as a function of treatment time. ECO experiments were also performed for a still bottoms sample resulting from laboratory column regeneration following treatment of a groundwater matrix amended with AFFF. Batch HALT experiments were conducted with a still bottoms sample obtained from a field demonstration trial conducted at a DoD site. The still bottoms sample was extensively characterized before treatment, and individual PFASs and inorganic fluoride ion were monitored as a function of treatment time, and the resulting data was compared with findings from previous studies where HALT was applied to treat AFFF and AFFF-impacted groundwater.

Life Cycle Assessment and Life Cycle Cost Analysis of Resin-Based Treatment: Results of experiments were used to inform a life cycle assessment (LCA) and life cycle costing analysis (LCCA) of anion exchange treatment systems for PFAS-contaminated groundwater. Analysis focused on two major questions: (1) comparing anion exchange, both regenerable and single-use resin treatment systems, with GAC adsorption; and (2) comparing the environmental impacts of anion exchange treatment systems with different resin regeneration options. Analysis was conducted according to International Standards Organization (ISO) protocols. Life cycle inventories were prepared using detailed lists of materials, fuel, electricity, and processes were generated from consumables used during treatment and regeneration stages. Life cycle impact assessment was performed using the USEPA's TRACI methods, which transforms process inputs and emissions into tangible environmental impacts along the cause-and-effect chain of environmental degradation. The life cycle inventory for each remediation system was also used to estimate lifetime costs for treatment. Media usage rates were estimated based upon results of pilot

field studies, including the pilot study comparing anion exchange resins conducted in this project. Resin regeneration scenarios considered included full disposal of waste regenerant as well as partial and full recycling within the integrated treatment train. Analyses were first conducted for baseline treatment scenarios, and then separate sensitivity analyses were performed to identify system characteristics and design assumptions that have the greatest impact on estimated life cycle impacts.

Results & Discussion

Overview: The following is a summary of major findings from this multi-institution project that aimed to evaluate the performance and sustainability of resin-based adsorption technologies, both regenerable and single-use resin systems, for treatment of PFASs in AFFF-impacted groundwater. Major results are organized according to the following major areas of emphasis: (1) PFAS adsorption to resins; (2) field pilot demonstration study comparing different resins; (3) desorption of PFASs and regenerating resins; (4) treatment of PFAS-contaminated regenerant wastes; and (5) life cycle assessment and life cycle cost analysis of resin-based treatment systems for PFASs.

(1) PFAS Adsorption to Resins: Initially, the project team examined adsorption of a wide diversity of PFASs within AFFF to a series of commercially available resins. Batch experiments quantified the adsorption of 75 different PFASs, including 63 polyfluorinated substances, in a diluted AFFF mixture using 14 commercially available ion-exchange (IX)/non-ionic resins and granular activated carbon (GAC). Results of these experiments showed that anion exchange resins (AERs) exhibited significant adsorption of PFASs compared to cation exchange resins (CERs), non- ionic resins (NIRs), and GAC regardless of the PFAS's predicted charge. Isotherm data showed that macroporous AERs have a higher PFAS adsorption capacity compared to gel-type AERs. Equilibrium adsorption data was used to estimate PFAS/Cl^- selectivity coefficients (K_{ex}) for individual PFAS-AER combinations, yielding values that varied by >6 orders-of-magnitude. Cross-correlation of K_{ex} values for each PFAS-AER combination (**Figure ES-2**) showed that hydrophobicity of the AER functional group and polymer matrix played a dominant role in determining resin affinity for PFASs. The extent of PFAS adsorption was greatest for single-use PFAS-selective AERs (e.g., Purolite's PFA694E and Calgon's CalRes 2301). PFAS structural characteristics also significantly affected adsorption, with increasing chain length and a net negative charge increasing the extent of adsorption.

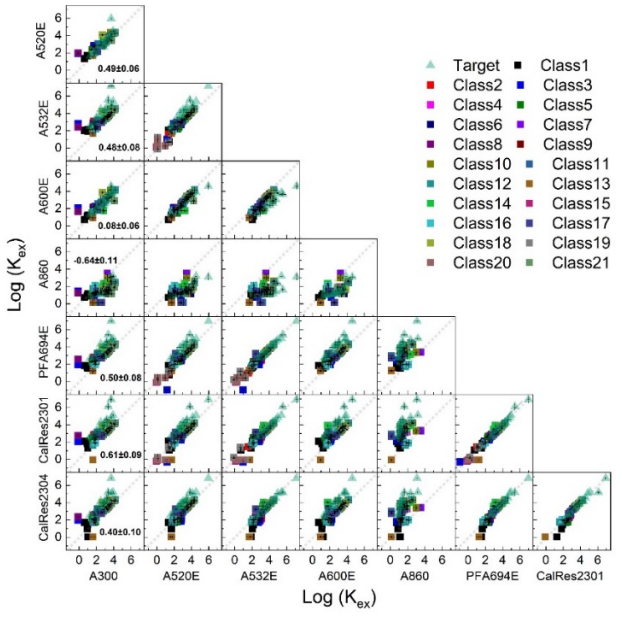

Figure ES-2. Cross-correlation comparison of PFAS/Cl^- selectivity coefficients (logK_{ex}) of seven AERs between the targeted PFAAs plus 63 additional PFASs identified in AFFF through suspect screening analysis. From Fang et al. (2021).

Batch studies also examined the combined removal of perfluoroalkyl acids (PFAAs) and natural organic matter (NOM) from real groundwater to polystyrene and polyacrylic regenerable AERs in both the chloride-loaded and sulfate-loaded forms. NOM is ubiquitous in natural waters and is often targeted for removal. PFAS occurrence in water resources is a human health concern. The polymer composition of the AER had a significant impact on contaminant removal with polystyrene resin (Purolite's A520E) being more effective for PFAA removal and polyacrylic resin (Purolite's A860) being more effective for SRNOM removal. The polystyrene resin showed greater removal of PFAAs with sulfonate than carboxylate head group and 8-carbon than 4-carbon chain length. Removal of NOM and PFAAs by both resin polymer compositions were greater when sulfate was the mobile counterion ion pre-loaded onto the resin than chloride. The results of this effort show that polymer composition and mobile counterion form of the resin can be selected to target specific contaminants and maximize contaminant removal.

A separate investigation was undertaken to examine PFAA adsorption at variable pH conditions by weak-base (WB) AERs that can be protonated or deprotonated depending on the solution pH. Two representative WB-AERs (polyacrylic IRA67 and polystyrene IRA96) and two representative strong-base (SB) AERs (polyacrylic IRA458 and polystyrene A520E), of differing polymer composition, were examined for the removal of six PFAAs. Under acidic (pH 4) and neutral (pH 7) conditions, the selectivity of AERs for each contaminant was predominantly influenced by polymer composition followed by the size of the resin functional group. This result reflected the WB-AERs being fully protonated and functioning identical to SB-AERs. Isotherm model parameters revealed WB-AER had higher capacity than SB-AER with analogous polymer composition and porosity regardless of resin selectivity for each contaminant. Under basic conditions (≥ pH 10), contaminant removal by WB-AERs declined due to deprotonation of the tertiary amine functional groups. Removal of PFAAs by the more hydrophobic polystyrene WB-AER (IRA96) remained approximately constant with changing pH, which was possibly due to electrostatic interactions with remaining protonated amine functional groups on the resin.

(2) Field Pilot Demonstration Comparing Different Resins: Building on laboratory adsorption studies, the project team conducted an 8-month pilot study comparing both regenerable and emerging single-use AERs at a source zone impacted by historical use of AFFF. Results demonstrate that single-use AERs (Purolite PFA694E, Calgon CalRes 2301, and Dowex PSR2+) significantly outperform regenerable resins (Purolite A860 and A520E), particularly for treatment of long-chain perfluoroalkyl carboxylic acids (PFCAs) and perfluoroalkyl sulfonic acids (PFSAs). **Figure ES-3** compares PFOA breakthrough data observed with each of the resins. from No detectable concentrations of ≥C7 PFCAs or PFSAs were observed within 150,000 bed volumes (BVs) after treatment with

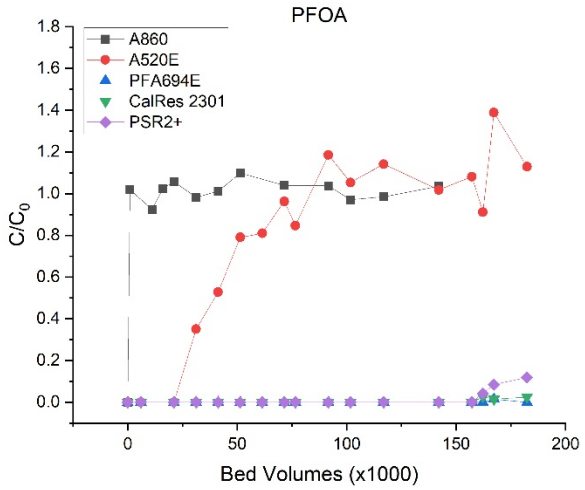

Figure ES-3. Breakthrough data for PFOA observed for different AERs using 2-min EBCT. From Ellis et al. (2022).

the single-use resins using a 2 minute empty bed contact time (EBCT). Analysis of effluent samples following 30 second of EBCT treatment shows that even the shortest-chain PFSAs do not reach 50% breakthrough within the first 350,000 BVs, though differences in removal of short-chain PFCAs was less dramatic. The regenerable polyacrylic A860 resin performed very poorly compared to all polystyrene resins, with >90% breakthrough of all PFASs occurring within 10,000 BVs. The greater affinity of polystyrene resins is attributed to increased hydrophobic interactions in addition to electrostatic ion exchange. Analysis of breakthrough profiles reveals empirical correlation with ion exchange affinity coefficients that were measured in batch experiments described above. Postmortem analysis of PFASs extracted from spent resins revealed chromatographic elution behavior and competition among PFASs for adsorption to the resins. PFSAs and long-chain PFCAs were preferentially adsorbed to earlier sections in the AER columns, whereas short-chain PFCAs were competitively displaced towards the later sections of the columns and into the effluent, consistent with effluent concentrations of the latter structures exceeding influent values.

(3) Desorbing PFASs and Regenerating Resins: Results of batch and continuous-flow experiments examining PFAs desorption and regeneration of AERs requires a regenerant solution containing both a concentrated salt brine (e.g., ≥1 wt% NaCl) and high alcohol cosolvent content (e.g., ≥70% methanol). This finding applies to both strong base and weak base AERs, to AERs that are classified as regenerable as well as those marketed as single-use PFAS-selective resins, and to polystyrene- and polyacrylic resins. For no AERs, did we observe significant desorption of the full suite of PFASs using salt-only or base-only regenerant mixtures, and attempts to regenerate resins with cosolvent only were also unsuccessful. Even weak base AERs could not be effectively regenerated using basic aqueous solutions that neutralize resin surface functional groups.

Increasing methanol cosolvent content (e.g., 90% vs. 70% cosolvent) and substituting more hydrophobic alcohol cosolvents (e.g., ethanol and n-propanol) for methanol led to enhanced contaminant desorption for equivalent cosolvent content . Similarly, increasing salt content (e.g., 0.05 to 5 wt% NaCl) improved contaminant desorption, but the effect was less dramatic than increasing cosolvent content. Substituting sulfate and carbonate salts for chloride led to less favorable desorption, and increasing temperature improved regeneration to only a small extent. Single-use PFAS selective resins required more bed volumes of regenerant or higher cosolvent contents to regenerate than conventional regenerable AER. Increasing pH of aqueous regenerant solutions

Generally, PFCAs were more readily desorbed from resins than PFSAs, and shorter-chain analogues were more easily desorbed than longer-chain structures, but this was not always the case. For example, co-adsorption of DOC with PFASs to Purolite's A592E resin (regenerable PFAS-selective resin) led to inhibited desorption of shorter chain PFCAs.

(4) Treatment of PFAS-Contaminated Regenerant Wastes: Experiments were conducted to evaluate the potential of electrochemical oxidation (ECO) and hydrothermal alkaline treatment (HALT) to degrade and defluorinate PFASs that accumulate in waste resin regenerant byproduct solutions. First, Bench-scale experiments were performed to evaluate the electrochemical oxidation, **via** direct anodic oxidation and indirect oxidation from salt-derived species, of diluted aqueous film forming foam (AFFF) in brine solutions to mimic anion exchange resin regenerant

solutions that are loaded with poly- and perfluoroalkyl substances (PFASs). Results showed that initial transformations of the polyfluorinated compounds, which accounted for approximately 45% of the organic fluorine, occurred primarily **via** an indirect oxidation pathway that targeted the non-fluorinated head groups. Depending on the brine solution, this indirect oxidation likely occurred **via** hydroxyl radical production or salt-derived oxidants (**e.g.**, $SO_4^{\cdot-}$ derived from anodic oxidation of sulfate). However, PFAA transformation and the overall rate of defluorination were controlled **via** a combination of direct and indirect electron transfer. Chloride levels (>0.2% by weight) and the presence of elevated concentrations of **tert**-butyl alcohol, a documented hydroxyl radical scavenger, substantially reduced rate constants for defluorination. Follow-up ECO experiments assessed treatment of a laboratory-generated still bottoms sample following distillation of the waste regenerant solution to recover the methanol cosolvent (e.g., **Figure ES-4**). Removal of both natural organic matter and PFAAs was observed during treatment over 24 hours, and, consistent with previous studies on the electrochemical oxidation of PFAAs, transient increases in the shorter-chained perfluorinated carboxylates (e.g., PFBA) were observed during the electrochemical treatment of the AFFF still bottom.

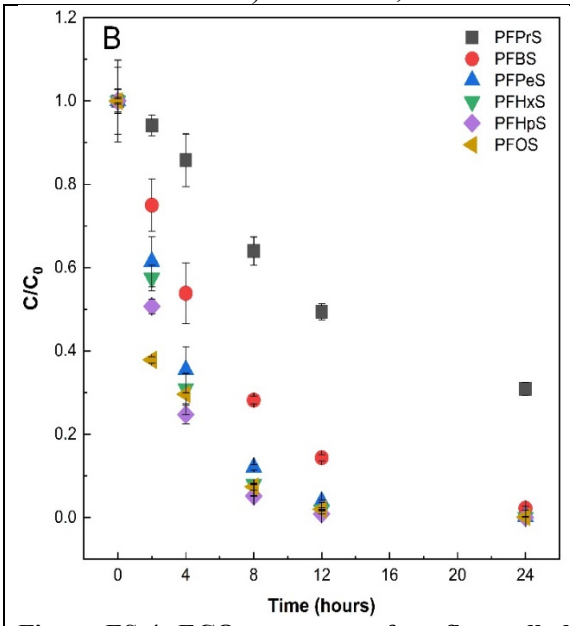

Figure ES-4. ECO treatment of perfluoroalkyl sulfonic acids in regenerant still bottoms

Treatment of a field-generated still bottoms with HALT showed rapid degradation of all PFASs detected in the concentrate stream. Reactivity trends among different PFASs was similar to results with other liquid matrices previously tested. Specifically, All of PFASs except sulfonic acid structures were removed >99% after only 15 minutes reaction, while sulfonic acids like PFOS are more recalcitrant to degrade. Still, analysis of fluoride ion generation demonstrated >85% defluorination of the PFAS mixture within 90 minutes of treatment. Tests also showed that >20% of the dissolved organic matter that accumulated in the still bottoms was mineralized during HALT treatment.

(5) Life Cycle Assessment and Life Cycle Cost Analysis of Resin-Based Treatment: Finally, results of experiments with ion exchange treatment processes informed life cycle assessment (LCA) and life cycle cost analysis (LCCA) of ion exchange treatment systems. First, we applied LCA to examine the relative environmental impacts of different options for management of waste regenerant solutions produced in regenerable ion exchange treatment processes, including disposing of waste regeneration solution via incineration, reusing the organic cosolvent and brine fractions of the waste regeneration solution, and altering the composition of the regeneration solution to avoid organic cosolvent or NaCl (**Figure ES-5**). The results show that disposing of waste regeneration solution via incineration, without recycling organic cosolvent or brine, had the greatest environmental impact, and that incineration accounted for the greatest impact among contributing processes. Recycling of the cosolvent (or cosolvent and brine) fraction of the waste regeneration solution resulted in lower environmental impacts due to reduced mass of waste

disposed of via incineration. Replacing NaCl in the brine with an alternative salt resulted in higher environmental impacts, with salts derived from chemical production, such as ammonium chloride and potassium carbonate, showing the largest increases in impacts. The results of this analysis highlight the importance of minimizing residual wastes that require off-site incineration to limit environmental impacts of regenerable ion exchange treatment systems used for PFAS treatment.

Next, we conducted a LCA and LCCA comparing regenerable and single-use ion exchange treatment systems with GAC adsorption, where we use results from field pilot studies to inform model inputs for media usage rates (MURs) and resin regeneration frequencies. Comparative analysis under a baseline scenario indicates that AER systems employing single-use "PFAS-selective" resins have lower environmental impacts and costs than systems using regenerable resins or GAC adsorbents (either single-use or thermally reactivated processes) for nearly all impact categories. Use of GAC operated as a single-use adsorbent led to the highest impacts for most categories as well as the highest treatment costs, with thermally-reactivated GAC proving to be less impactful than regenerable AER treatment. Sensitivity analysis highlighted the dominance of media usage rate (MUR) or regeneration frequency, factors that are highly dependent on the selected PFAS treatment goals to determine environmental impacts and treatment costs over a 30-year system life cycle. Selection of more stringent changeout criteria for media replacement/regeneration (e.g., detection of any PFASs in effluent) significantly reduces the advantages of single-use resins. For regenerable AER, environmental impacts were dominated by management/disposal of the PFAS-contaminated brine/co-solvent waste stream used to regenerate the adsorbent. Impacts were also sensitive to the cosolvent content of the regenerant mixture and the cosolvent recovery efficiency achieved by the on-site distillation system. High impacts estimated for GAC adsorption, the result of high MUR relative to ion exchange media, can be significantly reduced if spent adsorbents can be reused after thermal reactivation, but impacts are still greater than those predicted for single-use ion exchange systems. Pilot data from multiple studies indicates PFAS breakthrough is not highly sensitive to sourcewater PFAS concentrations, suggesting that many of the same conclusions may apply across a range of diverse sites, including higher-flow drinking water systems treating more dilute sources of PFAS contamination.

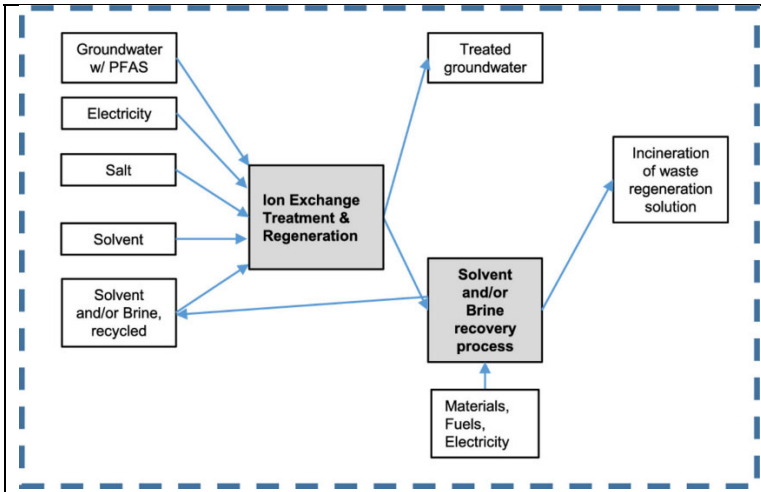

Figure ES-5. Material and energy inputs in the formulation of a LCA for regenerable ion exchange treatment of PFASs. From Boyer et al. (2021).

Implications and Benefits of Research

Findings from this project support the deployment of commercial anion exchange resins (AERs) and treatment technologies for groundwater impacted by historical AFFF use. In general, AERs are superior to GAC adsorbents in terms of the extent to which individual PFASs are

adsorbed and the effective adsorption bed volumes that can be treated before replacement or regeneration. Although costs of resins are greater than GAC adsorbents on a per-mass basis, overall treatment costs can be lower due to lower media usage rates. Differences between AER performance and GAC performance is greatest for sulfonic acids and longer-chain PFASs like PFOS, whereas performance for shorter-chain carboxylic acids like perfluorobutanoic acid (PFBA). Selection of optimal adsorbents will be heavily dependent upon the treatment criteria and contaminant group of interest. Life cycle analyses show that environmental impacts and costs are most heavily influenced by media usage rates or media regeneration frequencies, which again will be highly dependent upon the treatment criteria used at a particular site. Environmental impacts of regenerable AER treatment systems can be significantly reduced by minimizing the volume of waste residuals requiring offsite incineration or disposal. This can be accomplished by on-site destruction of PFASs in the waste regenerant solutions and recycling as much of the salt and cosolvent in the same waste streams.

Based on findings of this study, further deployment of ion exchange treatment technologies for PFASs would benefit from further research in the following areas:

- Widespread field pilot testing of AERs, both regenerable and single-use, at sites with variable groundwater chemistry
- Developing protocols for rapidly accessing the suitability of AER and GAC at sites, e.g., linking results from rapid small scale column testing to results of longer-term pilot testing at the same sites.
- Technologies for complete destruction of PFASs and recycling of waste regenerant solutions within regenerable AER systems.
- Development of resins with increased selectivity for shorter-chain perfluoroalkyl carboxylate structures that are poorly removed by existing resins and GAC adsorbent materials.

Publications and Technical Transfer

The project has resulted in ten peer-reviewed publications as of the date this report was submitted, with four additional publications currently under review or in preparation for publication. Technology transfer has also been supported by more than twenty-five conference presentations, lectures, and webinars to the broader community, as well as a fact sheet outlining recommended water quality parameters that site managers should evaluate when selecting adsorption-based treatment technologies for PFAS-contaminated water supplies.

1. Objectives

The overall goal of this SERDP project was to evaluate the effectiveness and sustainability of resin-based treatment systems for treatment of groundwater contaminated by per- and polyfluoroalkyl substances (PFASs). Batch and continuous-flow laboratory adsorption and resin regeneration studies were conducted to evaluate the effectiveness of commercially available regenerable and single-use resin sorbents (ion exchange + non-ionic). Ion exchange resins with variable properties were also compared under field conditions treating an aqueous film-forming foam (AFFF)-impacted groundwater, and PFAS destruction in simulated and real waste ion exchange regenerant brines was evaluated. Analysis of the treatment of complex PFAS mixtures was supported by high resolution LC-QToF-MS analysis, which enabled us to examine, for the first time, the effectiveness of adsorbents for a much wider range of PFASs detected in AFFF-impacted water matrices. Specific objectives of the project included:

(10) Evaluate and compare the effectiveness of commercially available ion exchange and non-ionic resins for removal of the full range of PFASs in AFFF-impacted water.

(11) Compare conventional regenerable resins with emerging single-use "non-regenerable" resins.

(12) Identify resin characteristics associated with increased adsorption of PFASs.

(13) Assess the effect of important non-target groundwater constituents (e.g., dissolved organic matter) on PFAS adsorption.

(14) Evaluate the links between PFAS adsorption observed in short-term batch experiments and longer-term continuous-flow adsorption experiments performed in both laboratory and field settings.

(15) Characterize regeneration of PFAS-contaminated resins with different salt brine, organic co-solvent, and other regenerant amendments.

(16) Quantify PFAS destruction in simulated and real waste ion exchange regenerant byproduct solutions using electrochemical oxidation and hydrothermal alkaline treatment technologies.

(17) Compare the life cycle environmental impacts and life cycle costs for regenerable and single-use resin treatment systems with GAC adsorption.

(18) Evaluate the life cycle environmental impacts of different resin regeneration options, and identify design variables that offer the greatest potential for improving sustainability.

2. Materials and Methods

2.1 Overview

A series of experimental and modeling tasks (**Figure 2.1.1**) were carried out to meet the project objectives and test associated hypotheses, with an ultimate goal of identifying the most effective and sustainable resin-based treatment technologies for treating PFAS-contaminated groundwater supplies. Experimental methods are described below for (1) assessing both PFAS adsorption to resins and resin regeneration in both batch and continuous-treatment systems, (2) comparing performance of regenerable and single-use AERs under field conditions at a DoD site, and (3) destruction of PFAS in simulated and real waste resin regenerant solutions. The framework and methodologies used for life cycle assessment and life cycle costing analysis (LCA/LCCA) of resin-based treatment systems is also described.

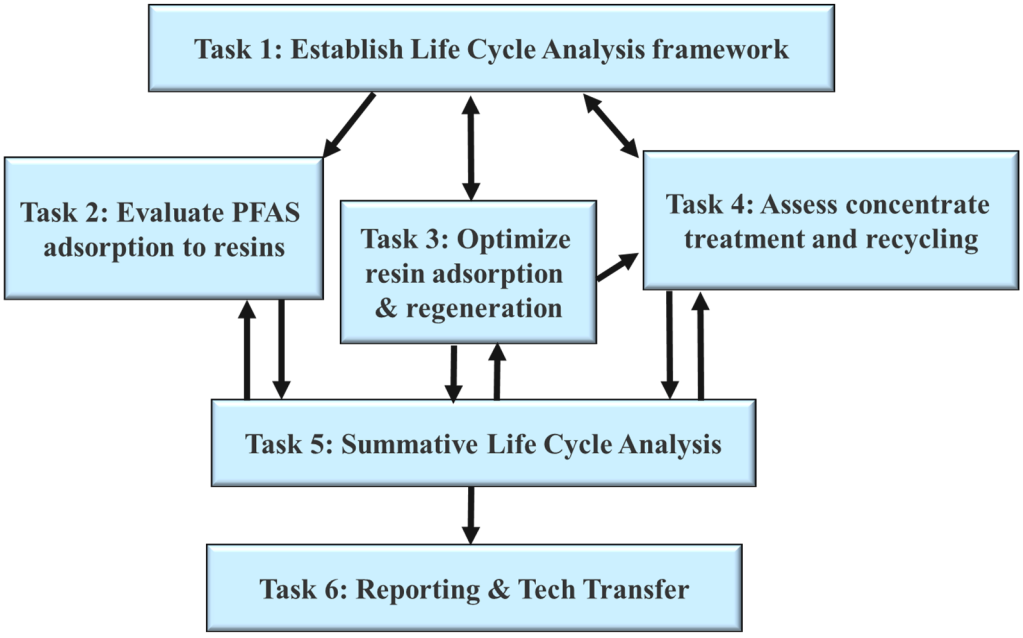

Figure 2.1 1 Schematic of major project tasks for ER18-1063.

2.2 Reagents and Materials

All chemical reagents are high purity and used without further purification once obtained from the vendor. Initial resin screening experiments are conducted using a wide range of commercially available resins (**Table 2.2.1**), including anionic exchange resins (AER), cation exchange resins (CER), and non-ionic resins (NIR). These include three PFAS-selective resins (PAER) that are typically operated in a non-regenerable fashion. These resins were pretreated with deionized water and methanol to remove impurities, and IX resins were pre-saturated with concentrated NaCl solutions to ensure saturation of adsorption sites with either Cl^- (AER) or Na^+ (CER). For comparison, batch adsorption experiments were also conducted using Calgon F400 as a representative granular activated carbon adsorbent material (**Table 2.2.2**).

Table 2.2.1. Ion exchange and non-ionic resins initially screened for PFAS adsorption. From Fang et al. (2021).

Resin	Vendor	Resin Type	Polymer	Particle size	Porosity	Functional Group	Capacity [a]
Regenerable Anion Exchange Resins (AER)[b]							
A300	Purolite	Type II, strong base	Polystyrene	avg. 750 µm	Gel	$R\text{-}N^+(CH_3)_2(C_2H_4OH)$	1.28
A520E	Purolite	Type I, strong base	Polystyrene	avg. 750 µm	Macroporous	$R\text{-}N^+(CH_2CH_3)_3$	0.84
A532E	Purolite	Strong base, other	Polystyrene	avg. 650 µm	Gel	Bifunctional quat amine	0.58
A600E	Purolite	Type I, strong base	Polystyrene	avg. 750 µm	Gel	$R\text{-}N^+(CH_3)_3$	1.40
A860	Purolite	Type I, strong base	Polyacrylic	avg. 750 µm	Macroporous	$R\text{-}N^+(CH_3)_3$	0.74
PFAS specific Anion Exchange Resins (PAER)							
PFA694E	Purolite	Strong base, other	Polystyrene	avg. 675 µm	Gel	N/A [c]	0.99 [d]
CalRes 2301	Calgon	Strong base, other	Polystyrene	avg. 785 µm	Macroporous	Tributylamine	1.20 [d]
CalRes 2304	Calgon	Strong base, other	Polystyrene	avg. 767 µm	Gel	Tributylamine	0.93 [d]
Cation Exchange Resins (CER)							
C100	Purolite	Strong acid	Polystyrene	avg. 750 µm	Gel	$R\text{-}SO_3^-$	1.55
C150	Purolite	Strong acid	Polystyrene	avg. 750 µm	Macroporous	$R\text{-}SO_3^-$	1.44
Non-Ionic Resins (NIR)							
XAD-4	Dow	Non-ionic, nonpolar	Polystyrene	avg. 590 µm	Macroporous	725 m^2g^{-1} [e]	N/A[f]
XAD-2	Dow	Non-ionic, nonpolar	Polystyrene	avg. 550 µm	Macroporous	300 m^2g^{-1} [e]	N/A
XAD-7HP	Dow	Non-ionic, Moderately polar	Polyacrylic	avg. 550 µm	Macroporous	450 m^2g^{-1} [e]	N/A

[a.] Unless otherwise indicated, capacity information provided by vendors. Unit: µmol (Cl^- or Na^+) / mg resin
[b.] Resins described by manufacturers as "regenerable" based upon non-PFAS treatment applications
[c.] Specific functional group information not provided by vendor
[d.] Measured by release of Cl^- when excess NO_3^- added to solution
[e.] Specific surface areas for NIRs obtained from vendors
[f.] Ion exchange capacities not applicable to NIRs

Table 2.2.2. Calgon F400 GAC properties. From Fang et al. (2021).	
Material	Coal
Specific surface area (m^2/g)	785
Total pore volume (cm^3/g)	0.27
Micropore volume (cm^3/g)	0.05
Mesopore volume (cm^3/g)	0.17
Macropore volume (cm^3/g)	0.05
Iodine number (mg/g)	1000
Effective size (mm)	0.55 – 0.75
Apparent density (g/ml)	0.54
Mass in column (kg)	10.2

2.3 Batch Adsorption Experiments Screening Different Resins

A series of batch reactors were prepared to assess the kinetic and equilibrium adsorption behavior of PFASs in the AFFF onto individual adsorbents. Individual reactors (1 L) were prepared with deionized water, 50 mg/L adsorbents, 5 mM electrolyte (NaCl), and 1 mM pH buffer (pH 8.3, $NaHCO_3$). After mixing the resin in electrolyte and buffer overnight, batch experiments were initiated by spiking an AFFF solution collected from a US Department of Defense facility to yield a diluted AFFF reactor solution (AFFF source diluted 1 to ~93,000). **Table 3.1.1** in the Results and Discussion summarizes the initial concentrations of quantifiable PFASs present in the AFFF

source. The total concentration of quantifiable and suspect screening PFASs after dilution ($\sum[PFAS]_0$) was estimated to be 0.5 μM, which is much lower than the total adsorption site capacity estimated for 50 mg/L resin suspensions (>50 μM Cl^- adsorption capacity for all AERs). The presence of excess ion-exchange sites ensures that individual PFASs in the AFFF mixture adsorb non-competitively to the resins. All reactions were conducted in duplicate and continuously mixed on stir plates at 75 ± 5 rpm at room temperature (21.6 ± 2.0 ºC) for 10 days. All adsorbent reactors were mixed at identical conditions with a uniform particle suspension observed in each reactor. Suspension aliquots were periodically collected and centrifuged to separate water from resins (21,000 g, 10 min), and stored at -20 ºC before PFAS analysis. Resin-free control reactions were also performed to account for any other potential losses of PFASs from the solution.

Separate batch reactions were conducted to further confirm the non-competitive nature of adsorption processes for individual PFASs in the 1-to-93,000 fold diluted AFFF containing a range of non-quantifiable PFASs (i.e., PFASs assumed to be present in the AFFF that cannot be measured with current LC-MS methods used in this study). plus even higher concentrations of uncharacterized organic constituents (e.g., co-solvents like butyl carbitol, hydrocarbon surfactants). The conditions of these reactions were the same as the AFFF adsorption experiments, except that a mixture of six PFAAs (PFOA, PFHxA, PFBA, PFOS, PFHxS, and PFBS) was spiked into each reactor with initial concentrations matching those measured for each in the diluted AFFF solutions ($\sum[PFAS]_0 = 0.27$ μM).

A series of batch reactors were also prepared for each of the selected AER and GAC to evaluate their maximum equilibrium adsorption capacity for PFOS in comparison to the manufacturer-reported capacities for Cl^- adsorption. Batch reactors were prepared with similar conditions described above, but varying PFOS concentration and 40 mg adsorbent. For each AER and GAC, reactors with 50-500 mg/L of PFOS were prepared and equilibrated overnight. The experiment was initiated after adding 40 mg of adsorbent to each reactor. After equilibrating 10 days, the residual aqueous concentration of PFOS was measured to quantify the extent of adsorption. The extent of PFOS adsorption was determined by comparing residual PFOS concentrations following equilibration with each AER or GAC with concentrations measured in a sorbent-free control reaction, to account for any other minor potential losses of PFOS from the solution (e.g., sorption to reactor walls, air/water interface).

2.4 Batch Experiments Assessing Impact of NOM and Resin Counterion

2.4.1. Materials

A520E and A860 (Purolite) AERs were used in this work. Both resins possess strong-base quaternary ammonium functional groups and macroporous structure. The resins differ in the nature of the quaternary ammonium groups and polymer composition. A520E has triethyl ammonium functional groups (total capacity, 0.9 eq/L) and polystyrene composition. A860 has trimethyl ammonium functional groups (total capacity, 0.8 eq/L) and polyacrylic composition. Although polymer composition was the focus of resin properties in this research, the differing functional groups between A520E and A860 does present a confounding factor. Nevertheless, the influence of polymer composition on the removal of ionizable organic compounds is well-documented in the literature [3-5], and previous research showed similar PFAA removal by A520E resin and a strong-base, polystyrene resin with trimethyl ammonium functional groups [6]. The resins were

received from the supplier in the chloride form (i.e., chloride present as mobile counterion). A portion of the resins were converted to the sulfate form by mixing resins in a highly concentrated solution of sodium sulfate (i.e., sulfate ion was present at 32× excess relative to AER on equivalent basis). The conversion of chloride-form resin to sulfate-form resin was assumed based on the knowledge from previous research [7, 8]. Mixing occurred in a jar test apparatus at 200 rpm for 24 h. Resins were separated from solution by filtration, rinsed with deionized (DI) water, and placed in a desiccator to dry. Resin density was calculated by measuring five, 1 mL wet resin samples in a graduated cylinder and then dried at room temperature in a desiccator for both types of resin in both the chloride and sulfate forms. Resins were measured and added to test waters as dry mass. Resin densities are reported in **Table A3.2.1** in the appendix. Resin doses are reported as volume of wet settled resin per volume of test water (i.e., mL/L) to allow for comparison with other published studies. Alternatively, resin dose can be expressed on equivalent concentration basis (e.g., meq/L) when there is significant difference in ion-exchange capacities between resins.

All test waters were composed of natural groundwater spiked with NOM and/or PFAA mixture. The groundwater was collected from a single groundwater well in Tempe, Arizona. The groundwater composition is reported in **Table A3.2.2**. Real groundwater was used as the test water for all experiments because of the prevalence of PFAS contamination in groundwater. There was no detectable PFAS in the groundwater, the DOC concentration was < 2 mg/L, and the concentration of inorganic ions was high as indicated by sodium, chloride, etc. (see **Table A3.2.2**).

The PFAA mixture used in this research included: perfluorooctanesulfonic acid (PFOS, CAS# 1763-23-1), potassium perfluorohexanesulfonate (K-PFHxS, CAS# 3871-99-6), potassium perfluorobutanesulfonate (K-PFBS, CAS# 29420-49-3), perfluorooctanoic acid (PFOA, CAS# 335-67-1), perfluorohexanoic acid (PFHxA, CAS# 307-24-4), perfluorobutanoic acid (PFBA, CAS# 375-22-4), purchased from Sigma Aldrich at ACS grade. Individual concentrated PFAA solutions were prepared in 10% by volume methanol in DI water to ensure complete dissolution of PFAAs. The individual PFAA stock solutions were combined and diluted in groundwater for each batch experiment. The residual methanol in the test water was < 0.1% by volume. Measured concentrations are listed in **Table 2.4.1**. The PFAA concentrations in this research are in-line with PFAA concentrations in groundwater near PFAS contamination souse zones [9, 10].

Suwannee River natural organic matter (SRNOM) isolate (2R101N, International Humic Substances Society) was used as the source of DOC in this work. SRNOM isolate was added to the groundwater at a dose of approximately 20 mg/L as NOM, with DOC concentrations given in **Table 2.4.1**. Because each batch of test water was made prepared separately, there is some variation in initial DOC concentration. The DOC concentration is representative of a high DOC groundwater [11, 12]. The test water was not filtered but AER-treated samples were filtered or centrifuged prior to analysis.

2.4.2. Experimental methods

Table 2.4.1 shows the experimental design including the measured concentrations of DOC and PFAAs in the untreated test waters. Batch tests were conducted with various doses of AER in 125 mL amber glass bottles containing 100 mL of test water. All samples were tested in triplicate. Sample bottles were placed on shaker tables (Thermo Scientific™ MaxQ™ 2000 and 3000 Benchtop Orbital Shakers) at 200 rpm for 24 h at room temperature (approx. 22 °C). The mixing

speed was selected to ensure that the AER was well mixed throughout the bottle. The mixing speed and equilibrium time were selected based on investigations in previous literature. Control samples of test water with no AER were included with each test condition. Afterwards, all samples without PFAAs were filtered through 0.45 µm filters and those containing PFAAs were centrifuged at 5000 rpm for 30 min. The entire sample (i.e., whole-bottle) was collected for analysis. The sample was diluted to fall within the PFAA calibration curve based on the expected PFAA concentration of the sample. Filtration through 0.45 µm filter is the standard definition for DOC (and standard approach for measurement of UV absorbance). However, previous research has shown that PFAS, such as PFOA, can adsorb to filters [13]. Therefore, it was decided to filter samples that did not contain PFAAs and centrifuge samples that did contain PFAAs. To support this approach, UV absorbance at 254 nm (UVA254) and DOC were measured in both filtered and centrifuged test water (i.e., groundwater plus SRNOM). The relative difference between filtered and centrifuged samples was 2.4% for UVA254 and 4.5% for DOC.

Table 2.4.1. Experimental design for removal of DOC and/or PFAAs by anion exchange resin. From del Moral et al. (2020).

Experiment	Test water	AER/counterion	DOC	PFBA	PFBS	PFHxA	PFHxS	PFOA	PFOS
1	GW	A520E/Cl, A860/Cl	1.3						
2	GW + SRNOM	A520E/Cl, A860/Cl	9.3						
3	GW + PFAAs	A520E/Cl, A860/Cl	1.6	321	333	587	417	289	375
4	GW + SRNOM + PFAAs	A520E/Cl, A860/Cl	8.2	337	309	652	395	298	404
5	GW	A520E/SO4, A860/SO4	1.6						
6	GW + SRNOM	A520E/SO4, A860/SO4	7.9						
7	GW + PFAAs	A520E/SO4, A860/SO4	1.5	317	487	585	308	215	167
8	GW + SRNOM + PFAAs	A520E/SO4, A860/SO4	8.5	460	548	479	289	250	167

Test water: Groundwater (GW), Suwannee River NOM (SRNOM), perfluoroalkyl acids (PFAAs)
DOC concentration in mg/L
PFBA, PFBS, PFHxA, PFHxS, PFOA, PFOS concentration in µg/L
PFOS concentration in Experiment 8 based on PFOS concentration in Experiment 7

2.4.3. Analytical methods

DOC was measured on a Shimadzu TOC-VCH Total Organic Carbon Analyzer following non-purgeable organic carbon method. DOC standards (RICCA Chemical Company) were analyzed every 15 samples with relative difference less than 15%. UVA254 was measured using a Hach DR6000 UV/visible spectrophotometer using a 1 cm quartz cuvette.

PFAAs were analyzed on an Agilent HPLC 1200 using gradient elution and a Phenomenex Gemini C18 column (110Å, 100×3 mm, 5 µm) equipped with a C18 guard column and Agilent Diol guard column (12.5×4.6 mm, 6 µm) coupled to a Sciex 3200 triple quadruple spectrometer in multiple reaction monitoring and negative electrospray ionization mode. The injection volume was

10 µL. To eliminate background PFAS contamination, Optima Grade LC/MS water and methanol (Fisher) were used for mobile phase and a delay column (Luna C18, 100Å, 30×3 mm, 5 µm) was placed between the pump and autosampler. The flow rate was 0.8 mL/min, and the gradient mobile phase consisted of 20 mM of ammonium acetate in water (A) and in methanol (B) starting at 5% B, increased to 60% B in 0.75 min, increased to 100% B for 4 min, and maintained for 3 min, decreased to 5% B in 1 min, and maintained at 5% B for 2 min. All PFAS standard compounds were purchased from Wellington Laboratory Inc. (Ontario, Canada). Acceptance criterion of analytical replicates prepared in triplicate was relative standard deviation ≤ 30%. This acceptance criterion encompasses sample preparation precision in the lab plus instrument analysis precision. **Table A3.2.3** lists analysis parameters and the limit of quantitation (LOQ) for the PFAAs analyzed in this research along with the isotope analytical standards.

2.4.4. Data analysis

Results for DOC are presented as the mean concentration of triplicate samples with error bars showing one standard deviation. Results for PFAAs are single measurements, and for calculations and plotting the LOQ was used for individual PFAA concentrations less than the LOQ. The precision for PFAA analysis is within 30% of true value. Two-factor ANOVA with replication was conducted for DOC removal by AER to investigate the significance of resin polymer composition and mobile counterion form of the resin. The null hypotheses were that DOC removal was the same for (i) A520E vs. A860 resin, (ii) chloride vs. sulfate counterion, and (iii) interaction between polymer composition and mobile counterion at significance level $\alpha = 0.05$. DOC removal was expressed as normalized concentration (i.e., C/C_0) to account for variability in initial concentration. Post-hoc analysis was conducted using paired t-tests following Bonferroni correction. The results are presented in **Tables A3.2.4 and A3.2.5** in the appendix.

2.5 Laboratory Continuous Resin Adsorption/Regeneration Experiments

2.5.1. Anion exchange resins and test waters

The AERs chosen for this study were Purolite A520E, a strong-base, polystyrene, macroporous resin, and Purolite A860, a strong-base, polyacrylic, macroporous resin. The resins were selected based on previous research that compared the impact of resin polymer composition [14, 15]. The resins were dosed volumetrically by measuring the volume of the wet settled resin in a graduated cylinder. Both AERs were received from the manufacturer with chloride (Cl^-) as the mobile counterion. A520E was converted to sulfate (SO_4^{2-}) as the mobile counterion using 10% sodium sulfate (Na_2SO_4) solution. A860 was converted to bicarbonate (HCO_3^-) as the mobile counterion using 8% sodium bicarbonate ($NaHCO_3$) solution. The solutions were pumped through the ion-exchange columns for 10 BVs and then rinsed with deionized (DI) water.

The chemical contaminants used in this work were perfluorooctanoic acid (PFOA, CAS# 335-67-1, Sigma Aldrich), perfluorooctane sulfonic acid (PFOS, CAS# 1763-23-1, Sigma Aldrich), perfluorohexanoic acid (PFHxA, CAS# 307-24-4, Sigma Aldrich), perfluorohexane sulfonic acid potassium salt (PFHxS, CAS# 3871-99-6, Sigma Aldrich), perfluorobutanoic acid (PFBA, CAS# 375-22-4, Sigma Aldrich), and perfluorobutane sulfonic acid potassium salt (PFBS, CAS# 29420-49-3, Sigma Aldrich). Stock solutions of 0.2 g/L were created for PFHxS, PFBS, PFBA, PFOS, and PFOA and a 0.3 g/L stock solution for PFHxA. Each stock solution was prepared in 30% methanol/nanopure water and the pH was adjusted to approximately 7 using sodium hydroxide.

For each ion-exchange column experiment, real Arizona groundwater was obtained in 55-gal plastic drums. The plastic drums were rinsed with DI water, then washed with 10% bleach solution, and rinsed three times again with DI water prior to collecting the groundwater. The raw groundwater water was spiked with a specified amount of each PFAS stock solution to achieve a desired overall concentration as listed in **Table 2.4.1**. The spiked groundwater was agitated to ensure mixing of the chemicals and then pumped in an up-flow configuration through the ion-exchange columns. The composition of the groundwater prior to spiking PFAS is given in **Table A3.3.1** in the appendix.

2.5.2. Ion-exchange column experiments

AER was loaded into 1 cm diameter, adjustable length glass columns (Diba Omnifit EZ Chromatogrphy columns). A previous study reported full PFAA recovery in the absence of AER after 10,000 BV of spiked groundwater [16]. Hence, losses of PFAS due to adsorption onto glass columns were assumed negligible in this study. All column tests were operated in one direction in up-flow mode for both the service cycle and regeneration cycle. The specific conditions for each experiment are listed in **Table 2.5.1**. Briefly, experiments 1–4 evaluated A520E resin converted to sulfate form and used test water with either low initial PFAS concentration (280 µg/L) or high initial PFAS concentration (11,200 µg/L) and different sulfate-based regeneration solutions. Experiment 5 evaluated A860 resin converted to bicarbonate form and used test water with high initial PFAS concentration (6,230 µg/L) and $NaHCO_3$ regeneration solution.

Table 2.5.1. Experimental design for column-mode anion exchange resin (AER) treatment for PFAS removal from water. From Dietz et al. (2021).

Experiment no.	AER-counterion	PFAS initial concentration, mg/L[a]	BV_{AER}, L[b]	SFR, mL/min	Regeneration solution
1	Purolite A520E-SO_4	0.02, 0.06, 0.1, 0.03, 0.04, and 0.03	0.003	0.6	0.5% $(NH_4)_2SO_4$ + 0.5% NH_4OH
2	Purolite A520E-SO_4	0.02, 0.06, 0.1, 0.03, 0.04, and 0.03	0.003	0.6	0.5% $(NH_4)_2SO_4$ + 50% methanol
3	Purolite A520E-SO_4	0.96, 2.5, 3.5, 0.81, 1.8, and 1.6	0.01	2.0	0.5% $(NH_4)_2SO_4$ + 0.5% NH_4OH
4	Purolite A520E-SO_4	0.96, 2.5, 3.5, 0.81, 1.8, and 1.6	0.01	2.0	0.5% $(NH_4)_2SO_4$ + 50% methanol
5	Purolite A860-HCO_3	0.52, 1.1, 2.1, 0.51, 0.9, and 1.1	0.004	0.8	8% $NaHCO_3$

Abbreviations: Bed volume of AER in column (BV_{AER}); Service flow rate (SFR).

[a] Initial, influent concentrations shown for PFBA, PFHxA, PFOA, PFBS, PFHxS, and PFOS. [b] Empty bed contact time (EBCT) was 5 min for all experiments.

During the treatment cycle, effluent samples were collected in polypropylene conical tubes at approximately 2,000 BV increments for experiments 1 and 2, while experiments 3–5 collected effluent samples at approximately 550 BV increments. All samples collected were centrifuged using an Eppendorf Centrifuge 5810R at 4,000 rpm for 25 min. A sample of 4 BV was collected for analysis. The sample was diluted to fall within the PFAA calibration curve based on the expected PFAA concentration of the sample.

Three regeneration solutions were evaluated in this study and made as follows: (i) 0.5% m/m ammonium sulfate ($(NH_4)_2SO_4$) (Fisher) and 0.5% v/v ammonium hydroxide (NH_4OH) (Fisher)

in nanopure water, (ii) 0.5% m/m ammonium sulfate ($(NH_4)_2SO_4$) and 50% v/v methanol (Sigma Aldrich) in nanopure water, and (iii) 8.0% m/m $NaHCO_3$ (Carolina Biological Supply Company) in nanopure water.

During each regeneration cycle, the resin was backwashed in down-flow mode at service flow rate for 1 BV with DI water to prevent physical clogging. After backwashing, the resin was treated with 10 BV of the regeneration solution followed by 4 BV of rinse with DI water. Both the 10 BV regeneration and 4 BV rinse were operated in the same direction as the service flow in up-flow mode. The flow rate during regeneration was reduced to half of the service flow rate and slowly increased to the service flow rate during the 4 BV of rinse. The entire 10 BV of regeneration solution was collected in polypropylene conical tubes and centrifuged at 4,000 rpm for 25 min.

2.5.3. PFAS analysis

PFAS analysis was performed on an Agilent high pressure liquid chromatograph (HPLC, 1100) system using gradient elution and a Phenomenex Gemini C18 column (110Å, 100×3 mm, 5 µm) equipped with a C18 guard column and Zorbax Diol guard column (12.5×4.6 mm, 6 µm) coupled to a Sciex 3200 triple quadruple mass spectrometer in multiple reaction monitoring (MRM) and negative electrospray ionization (ESI) mode. Injection volume was 20 µL and a delay column (Luna C18,100Å, 30×3 mm, 5 µm) was placed between the pump and autosampler. The addition of the delay column and the use of Optima Grade LC/MS water and methanol (Fisher) for the mobile phase were used to eliminate background PFAS contamination. The flow rate was 0.8 mL/min. The gradient mobile phase consisted of 20 mM of ammonium acetate in water (A) and in methanol (B) starting at 5% B, increased to 60% B in 0.75 min, increased to 100% B for 4 min, and maintained for 3 min, decreased to 5% B in 1 min, and maintained at 5% B for 2 min. PFAS standard compounds, [^{13}C] perfluorinated acid/sulfonate mix, was purchased from Wellington Laboratories (Ontario, Canada). **Table A3.3.2** lists analysis parameters for the PFAS analyzed in this research along with the isotope analytical standards.

2.5.4. Data analysis

Regeneration efficiency was calculated using the concentration data from the column experiments and PFAS analysis. The first step in calculating regeneration efficiency was to calculate the mass of PFAS in the influent solution:

$$M_{inf} = C_{inf} \times V_{tot} \quad (2.5.1)$$

where C_{inf} is the PFAS concentration (mg/L) in the influent solution, V_{tot} is the total influent volume (L), and M_{inf} is the mass of PFAS (mg) in the influent solution that the resin was exposed to. After verification of the influent PFAS concentrations and mass calculations, then the mass of PFAS adsorbed onto the resin was calculated using the concentration data from the experiment:

$$M_{Resin} = (C_{inf} - C_{eff}) \times (BV_N - BV_{N-1}) \times (AER\ BV) \quad (2.5.2)$$

where C_{eff} is the PFAS concentration (mg/L) of the effluent sample taken, BV_N is the BV of influent treated at the time of the corresponding sample was taken, BV_{N-1} is the BV of influent treated at the time of the previous sample taken, and M_{Resin} is the mass of PFAS (mg) that has

adsorbed onto the resin. Parameters of the experiments were also used in calculating the mass of PFAS adsorbed onto the resin such as the amount of resin per BV (liter of resin in column/BV).

The mass sorbed onto the resin was converted to milliequivalents (meq) of PFAS sorbed onto the resin:

$$meq_{Resin} = (M_{Resin} \times Valence_{PFAS})/MW_{PFAS} \quad (2.5.3)$$

where $Valence_{PFAS}$ is the valence of the specified PFAS, and MW_{PFAS} is the molecular weight of the specified PFAS (mg/mmol). After the meq of each sample was calculated, the meq of each sample during a regeneration cycle were added together to obtain the total meq sorbed onto the resin for the specified regeneration cycle. Using the PFAS concentrations obtained from analysis of the regenerant solution, the mass of PFAS desorbed from the resin into the regenerant solution is calculated using:

$$M_{Regen} = C_{Regen} \times V_{Regen} \quad (2.5.4)$$

where C_{Regen} is the PFAS concentration (mg/L) in the regenerant solution, V_{Regen} is the volume of regenerant solution (L) used for a specified cycle, and M_{Regen} is the mass of PFAS (mg) in the regenerant solution. The mass PFAS in the regenerant solution was then converted to milliequivalents (meq) of PFAS in solution:

$$mEq_{Regen} = (M_{Regen} \times Valence_{PFAS})/MW_{PFAS} \quad (2.5.5)$$

The total meq of PFAS that adsorbed onto the resin for a specified cycle and the meq that desorbed into the regenerant solution were used to calculate percent regeneration efficiency:

$$\% \text{ Regeneration Efficiency} = (meq_{Regen}/meq_{Resin}) \times 100 \quad (2.5.6)$$

Calculating percent regeneration efficiency using a mass balance is important as graphical analysis of treatment and regeneration cycles can be misrepresentative and lead to wrong conclusions.

2.5.5. Bench-scale flow through AER column adsorption and regeneration at CDM-Smith

The experimental design for the column testing was adopted from a previous study (Schaefer et al., 2019). Briefly, a series of glass columns (Econo0Column) with a diameter of 2.5 cm and a height of 10 cm was packed with the two selected AERs to assess their adsorption potential for PFAS. The columns were packed with 3.5 cm of glass beads (zirconia glass silica beads, 0.5 mm diameter) on the bottom, 3 cm of AER in the middle, and 3.5 cm of glass beads on top of the AER. The resulted AER empty bed volume (BV) is 14.7 cm3. Control columns were also prepared with only glass beads to confirm that PFAS are not adsorbing to other parts of the column assembly besides the AERs. The designed flow rate (i.e., 4.9 mL/min) for each column was based on a manufacturer-recommended empty bed contact time (EBCT) of 3 min. Before loading the AFFF spiked influent, all AER columns were pre-conditioned with 50 BVs of 5% (NH4)2SO4 solution to replace the Cl^- ions in the AERs with SO_4^{2-} (note: Cl^- ions are the default counter ion loaded onto each AER by the manufacturer). This step is to minimize the presence of Cl^- ion in the treatment system to reduce perchlorate production during ECO treatment. The AER columns were then pre-rinsed with 10 BVs of DI water to clean any impurities left within the column before the

adsorption experiment. A diluted AFFF (1:100,000) was used as the influent to initiate the column tests. A total of 2,000 BV of influent was treated through each AER column, and aqueous samples were collected periodically to monitor their water quality parameters (e.g., PFAS and TOC).

After loading the AER columns with AFFF-spiked groundwater, two regeneration recipes (i.e., two brine/co-solvent solutions (0.2% $(NH_4)_2SO_4$ + 80% MeOH and 0.2% NH_4Cl + 80% MeOH)) were developed to examine their ability to release PFAS from the spent AERs. A total of 10 BV of the three regenerants were flushed through the PFAS-loaded columns over three hours (i.e., 0.82 mL/min). The slower flow rate during the regeneration process provided increased contact time between the regenerants and impacted AERs for better regeneration efficiencies. A lower brine percentage was used in the two brine/solvent solutions due to sulfate's low solubility in organic solvents.

2.6 Pilot Field Comparison of Ion Exchange Resins

2.6.1. Pilot system design

Five resins were compared, down-selected from a larger group studied in batch systems (Fang et al., 2021). These AERs reflect the diversity of resin properties (**Tables 2.2.1-2.2.2**) that are commonly used in removing organic anions, as no AER used in this pilot shares the same porosity, functional group, polymer, and regenerability. While a major focus of the study was to compare regenerable and single-use AERs, other assessments of resin properties were considered, including polystyrene vs polyacrylic backbone and macroporous (20-100 nm pore size) vs gel-type resins (1-2 nm pore size). Maximum exchange capacities for chloride and maximum capacities for PFOS adsorption measured in batch isotherms are also listed in **Tables 2.2.1 and 2.2.2** 1. All AERs were obtained from manufacturers in the chloride form and were used as received. Although A860 was not found to be among the most effective resins in adsorbing PFASs in previous batch equilibrium adsorption studies (Fang et al., 2021), the polyacrylic resin was included in the study to compare with similar polystyrene resins. A520E, in particular, shares the same porosity, regenerability, uniformity, and particle size range as A860. This enabled assessment of the importance of polymer backbone in PFAS adsorption from groundwater under field conditions and comparison of relative resin performance trends in batch versus continuous-flow operation. Furthermore, while our earlier batch adsorption data suggested poor performance of A860, other recent reports have indicated that the resin is effective in adsorbing PFASs from groundwater (Dixit et al., 2020; Dixit et al., 2021a).

The pilot study was conducted at a U.S. Department of Defense site located in the Willow Grove, PA area where elevated groundwater PFAS concentrations have been documented due to historical releases of AFFF (Leeson et al., 2021). Total detected sourcewater PFAS concentrations ranged from 30-55 µg/L, more than 400 times greater than the EPA's lifetime health advisory level of 70 ng/L (PFOS+PFOA combined) (Goode and Senior, 2020). Resin quantities in each vessel were designed to allow prolonged PFAS loading while maintaining a vessel-to-particle diameter ratio >40 to prevent preferential flow paths due to walling effects (Tian et al., 2016). The pilot system was outfitted with 24 individual vessels packed with resin arranged in eight parallel columns (**Figures 2.6.1** and **2.6.2**), each containing three vessels in series with sample ports before and after each vessel. The system was constructed using vessels, fittings, and valves comprised of mostly Schedule 80 thick-walled PVC plastic. All infrastructure components were obtained from

McMaster-Carr Supply Company (Elmhurst, IL). Analog flow monitors were also obtained from McMaster-Carr, while digital flow monitors (Liquid Turbine Flow Meter Series 800) were obtained from JLC International, Inc. (New Britain, PA).

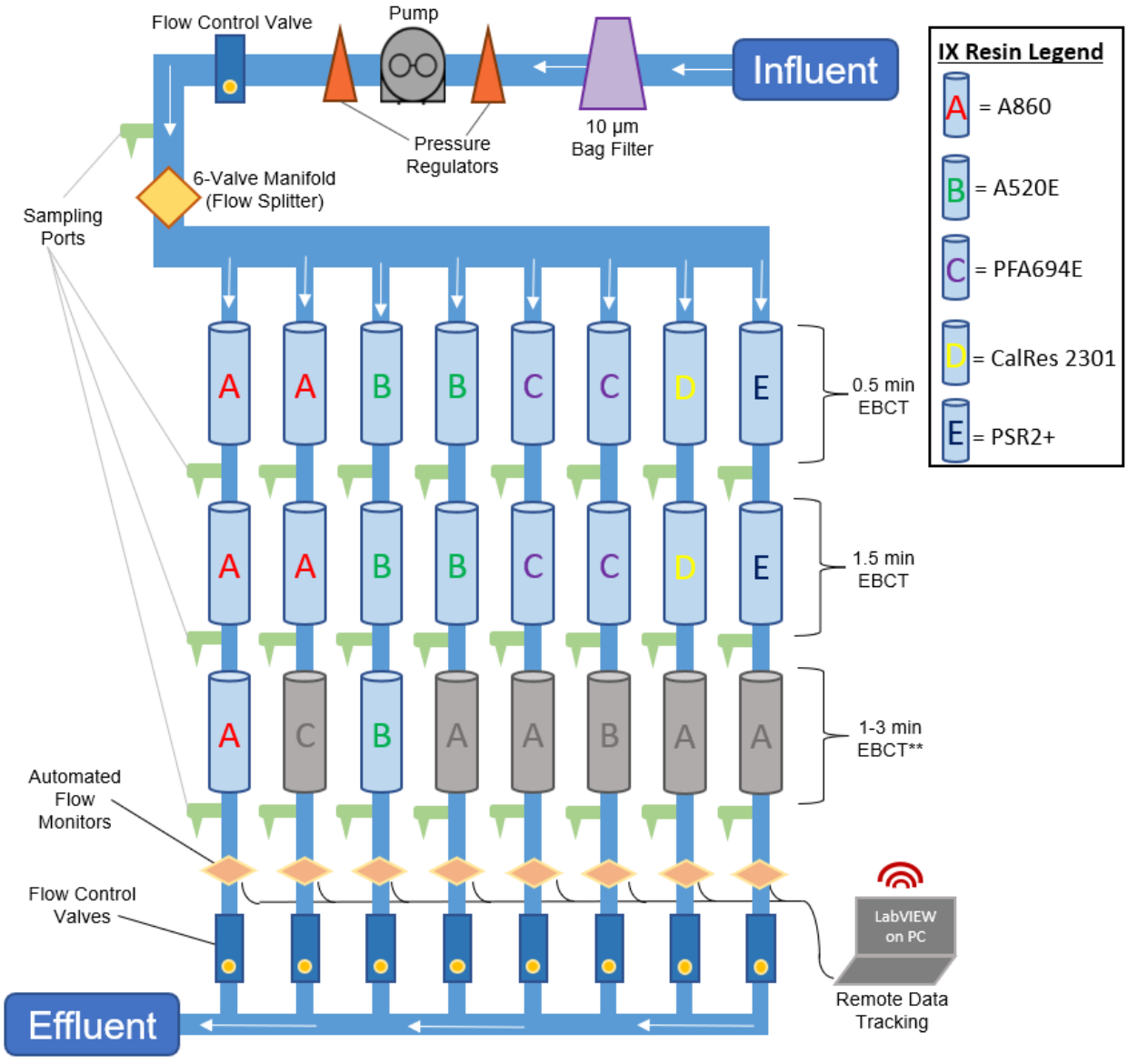

Figure 2.6.1. Schematic of the pilot-scale ion exchange system deployed at the treatment site in Willow Grove, PA (photograph provided in Figure 2.62). **Greyed vessels in the third row of each channel were excluded from analysis due to cost considerations. The third segment in channels #1 and #3 were assessed, each containing 1 min of additional EBCT to bring the total column EBCT to 3 min. From Ellis et al. (2022).

For each column, the first two vessels-in-series contained the same resin with the first vessel providing an EBCT of 30 sec and the second providing an additional 90 sec EBCT. Thus, influent waters pass through the given resin for a total of 2 min EBCT, consistent with manufacturer recommendations for single-use "PFAS-selective" resins (Boodoo et al., 2019). While recommendations for some resins, particularly regenerable AERs, are 3-5 min EBCT, the same

EBCTs were used for all resins to enable appropriate comparisons on a bed volume-equivalent basis. For three of the AERs (Purolite A860, A520E, and PFA694E), duplicate columns were included to assess variability in breakthrough data. Duplicate columns were not included for Calgon CalRes 2301 and Dowex PSR2+ due to system flow constraints. Although a third vessel of AER with 1-3 min of additional EBCT was included in the system design, breakthrough of nearly all these vessels was excluded from analysis due to cost considerations and poor performance of the resin used in the third vessel of most columns (Purolite A860). Analysis of effluent from the third vessel was conducted where a third segment of Purolite A520E and A860 was added to provide 1 min additional EBCT, providing a 3-min total EBCT, consistent with manufacturer recommendations for this regenerable AER. This also allowed us to compare breakthrough data for 0.5, 2, and 3 min EBCT for the same resin.

Figure 2.6.2 Field pilot system in operation. From Ellis et al. (2022).

Anion exchange resins (AERs) were measured by volume and added to the empty vessels prior to final vessel construction. Three of the AERs – A860, A520E, and PFA694E – were obtained from Purolite, CalRes 2301 was provided by Calgon Carbon Corporation, and the Dowex resin PSR2+ was obtained from Evoqua Water Technologies. Resin quantities were added to each vessel to achieve their design empty-bed contact times (EBCTs) through each of the eight parallel channels, with each channel receiving a flow of 450 mL/min (0.119 gpm). Sampling personnel ensured flows along each column were maintained at this value using flow control valves, and

flows were monitored remotely as well as in person by site personnel 5 days/week. Throughout the course of pilot system operation, pressures through the pumps were kept steady with no evidence of column plugging. A full description of the design parameters are provided in **Table 2.6.1**. Bed heights varied among the different AER vessels due to variations in density, uniformity, and particle size ranges of different resins. This field pilot was integrated into an existing larger onsite treatment system to ensure all effluent waters from the pilot were further treated prior to discharge.

Table 2.6.1. Parameters of AER vessels used in the field pilot system. From Ellis et al. (2022).

Total Flow Rate to Pilot System (mL/min)	3,600
Flow Rate for Individual Columns (mL/min)	450
Total Empty Bed Contact Time (min)	0.5 (Vessel 1), 2 (Vessels 1 + 2), 3 (Vessels 1 + 2 + 3)[c]
Column Inner Diameter (mm)	52.5
Vessel-to-Particle Diameter Ratio[a]	44-180
Bed Height (mm)[b]	100-110 (Vessel 1), 400-430 (Vessel 1 + 2), 1020-1070[d] (Vessels 1 + 2 + 3)
Hydraulic Loading Rate (gpm/ft^2)	5.101

[a.] Diameter ratios varied depending on the AER used (see Table 2.2.1).
[b.] Bed heights varied depending on AER density, uniformity, and particle size ranges (Table 2.2.1)
[c.] Third vessel-in-series for A520E and A860 provided a 1-min EBCT (total of 3 min of EBCT); effluent from third vessel-in series not analyzed for other columns.
[d.] Assumes a 3-minute EBCT for vessels in Row 3 (5-min total EBCT).

Operation of the pilot system was conducted over the course of 36 weeks (July 2020 – March 2021), with weekly samples collected from the influent and effluent of each resin vessel. Operation occurred continuously with minimal stoppages for maintenance (e.g., the changeout of 10 µm pretreatment bag filters located upstream of the field pilot intake). A total of 3600 mL/min (0.95 gpm) was drawn from a slipstream of a larger onsite treatment system and pumped through the resins, providing each parallel column with 450 mL/min (0.12 gpm) of groundwater. Treated water was routed back into the feedwater of the larger onsite treatment system to comply with discharge permits. Flow control valves along with both analog and digital flowmeters were included in every column to maintain desired flows that were monitored using a LabVIEW (National Instruments) remote interface.

2.6.2. Model fitting breakthrough data

Breakthrough data was fit using the Thomas Model presented in **Eq 2.6.1**,

$$\frac{C}{C_0} = \frac{1}{1+\exp\left[\left(\frac{k_{Th} q_e x}{Q}\right) - k_{Th} C_0 t\right]} \qquad (2.6.1)$$

In the above equation, all parameters in fitting are fixed with the exception of k_{Th}, the Thomas Model constant, and q_e, which reflects the resin capacity for sorbate uptake. Q represents the flow rate of the column, and x reflects the mass of adsorbent in the column. C and C_0 represent the effluent and influent contaminant concentrations, respectively, and t represents the time throughout treatment. This function was chosen from a larger list of nonlinear curve fits due to its documented utility and accuracy in fitting PFAS adsorption breakthrough curves and its simplicity as a two-parameter function that does not rely on extensive fitting factors (Grieco et al., 2021; Schaefer et al., 2019). Effluent C/C_0 values exceeding 1.0 were fixed at this value before least square fitting since the major goal was to identify BVs at which different thresholds for "breakthrough" (e.g., 10% of influent concentrations or 70 ng/L) were reached, rather than providing a prediction of the full breakthrough profile.

2.6.3. Characterization of spent ion exchange resins from field pilot

Upon completion of the pilot study, the vessels of used resin were transported from the site back to the Colorado School of Mines for postmortem analysis. The first two vessels from each column were frozen and cross-sectioned into five fractions before measuring the concentrations of adsorbed PFASs in each section. Resin from each column fraction was completely mixed to ensure homogeneity before extraction. Extraction of adsorbed PFASs from the resins was accomplished using a 90/9/1 (wt%) methanol/water/ammonium chloride mixture. Three rounds of extraction (100 mg resin in 25 mL extract solution; 24 h) were performed before pooling extracts for analysis. Validation of this extraction procedure was conducted by recovering >95% of a known quantity of PFOS, the major PFAS with the highest affinity for the resins (Fang et al., 2021), that was pre-loaded onto virgin resins.

2.7. Regeneration of PFAS-Contaminated Resins

2.7.1. Batch Regeneration Experiments

Anion Exchange Resins. The resins used in this experiment were PS SB-AERs, Purolite A502P, A520E, A532E, and A592E. These resins were chosen based ability to remove organic anions, including hydrophobic ionizable organic chemicals (HIOCs) and PFAAs, as well as possible reversibility [6, 17-21]. All resins were obtained in their chloride (Cl^-) mobile counterion form. **Table 2.7.1** provides the properties of the resins chosen. Resin A502P was chosen for its role as an organic scavenger and its high reversible adsorptive capacity as described by the manufacturer as well as a previous study showing its ability to remove DOC [22]. Past work on A520E has shown its ability to adsorb organic compounds in addition to its primary manufacturing purpose to adsorb nitrate [6, 23]. Resin A532E was chosen for its principal application of removing hydrophobic anions and high operating capacity, as well as being the only gel-type resin for comparison against macroporous resins [6]. Resin A592E was chosen for its ability to remove perfluoroalkyl substances (PFAS) with the hydrophobic ionizable organic compounds in the procedure serving as surrogates for different PFAS (Liu et al., 2021).

Hydrophobic Ionizable Organic Compounds. The two HIOCs probed for saturation onto resin and then regeneration were diclofenac sodium (CAS 15307-79-6, Spectrum Chemical) and sodium dodecylbenzene sulfonate (CAS 25155-30-0, Sigma Aldrich). A summary of their properties is included in **Table 2.7.2**. The molecular structures of diclofenac anion and dodecylbenzene

sulfonate can be found in **Figures A3.5.1** and **A3.5.2** in the appendix, respectively. The compounds were chosen for two primary reasons. Firstly, each compound represents a contaminant class present in wastewater and ground water; diclofenac sodium is a common pharmaceutical non-steroidal anti-inflammatory drug that has been detected in groundwater and drinking water .Sodium dodecylbenzene sulfonate is a long-chain surfactant used as a detergent and used generally in cleaning products and has been detected in groundwater and drinking water [24-26]. Secondly, each analyte serves as an ionizable organic compound surrogate to certain perfluoroalkyl acids (PFAAs). Diclofenac sodium contains a carboxylate group as do perfluorocarboxylic acids (PFCAs), and sodium dodecylbenzene sulfonate contains a sulfonate group as do perfluoroalkyl sulfonic acids (PFSAs).

Table 2.7.1. Strong base polystyrene anion exchange resin characteristics from manufacturer.

Resin	Functional Group	Structure	Moisture Retention	Total Capacity (wet, eq/L)	Specific Gravity (g/mL)
Purolite A502P	Quaternary Ammonium [a]	Macroporous	66 – 72%	0.85	1.04
Purolite A520E	Triethyl ammonium	Macroporous	50 – 56%	0.9	1.07
Purolite A532E	Bifunctional triethyl, trihexyl ammonium	Gel	40 – 48%	0.6	1.04
Purolite A592E	Tributyl ammonium	Macroporous	NA	0.9	NA

[a] Specific alkyl functional group(s) unknown

Table 2.7.2. HIOC solutes for adsorbance and regeneration with characteristics provided by manufacturer.

Solute Name	Chemical Formula	Molecular Weight (g/mol)	Functional Group	Class	pK_a [a]
Diclofenac Sodium	$C_{14}H_{10}Cl_2NNaO_2$	318.13	Carboxylate	Pharmaceutical NSAID	~ -6
Sodium Dodecyl-benzene Sulfonate	$CH_3(CH_2)_{11}C_6H_4SO_3Na$	348.48	Sulfonate	Surfactant	3.99

[a] Data sourced from suppliers and PubChem database

For the regeneration experiment of two resins saturated with PFAS, six different perfluoroalkyl substances were used, three carboxylate-group compounds and three sulfonate-group compounds: perfluorobutanoic acid (C4, PFBA, aqueous, CAS# 375-22-4), perflurohexanoic acid (C6, PFHxA, aqueous, CAS# 307-24-4), perfluorooctanoic acid (C8, PFOA, solid, CAS# 335-67-1), perfluorobutane sulfonate (C4, PFBS, sodium salt, CAS# 29420-49-3), perfluorohexane sulfonate (C6, PFHxS, sodium salt, CAS# 3871-99-6), and perfluorooctane sulfonate (C8, PFOS, aqueous, CAS# 1763-23-1). All six PFAS were purchased from Sigma-Aldrich at ACS grade. These PFCAs and PFSAs were chosen for their variability in aliphatic chain length and the two functional groups of carboxylate and sulfonate which correlate with diclofenac and dodecylbenzene sulfonate. The

six PFAS and their properties are listed in **Table 2.7.3**, and their deprotonated molecular structures can be seen in **Figure A3.5.3**.

Table 2.7.3. Perfluoroalkyl acids with sulfonate and carboxylate functional groups.

Perfluoroalkyl substance (PFAS)	Molecular Weight (g/mol)	Functional Group	Fluoroalkyl Chain Length	Dissociation Constant pK_a [a]	Log K_{ow} [a]
Perfluorobutanoic acid (PFBA)	214.04	Carboxylate	C_4	-0.20	2.82
Perfluorohexanoic acid (PFHxA)	314.05	Carboxylate	C_6	-0.13	4.06
Perfluorooctanoic acid (PFOA)	414.07	Carboxylate	C_8	-0.16	5.30
Perfluorobutane sulfonate (PFBS)	300.10	Sulfonate	C_4	-6.0	3.90
Perfluorohexane sulfonate (PFHxS)	400.11	Sulfonate	C_6	-6.0	5.17
Perfluorooctane sulfonate (PFOS)	450.12	Sulfonate	C_8	-6.0	6.43

Cosolvents for Regeneration. The cosolvents in solution with brine to test regeneration efficiency were methanol (CAS 67-56-1, Sigma-Aldrich), ethanol (CAS 64-17-5, Acros Organics), 1-propanol (CAS 71-23-8, Acros Organics), 1-butanol (CAS 71-36-3, Sigma-Aldrich), propylene glycol (CAS 57-55-6, MP Biomedicals), and glycerol (CAS 56-81-5, Sigma-Aldrich). The cosolvents were chosen for their variability in aliphatic chain length when compared to methanol or for their variability in hydroxyl group count when compared to 1-propanol. The effect of lengthening the alkyl chain length is greater hydrophobicity of the solvent as well as a higher boiling point which alludes to greater London dispersion forces in the monoalcohols as alkyl chain length increases [28]. A summary of characteristics of cosolvents is provided in **Table 2.7.4**. As salt content increased in the solution, the miscibility of salt water and cosolvent decreased, making certain mixtures fractionate and preventing them from being used in experiments. The miscibility profiles of the solutions were found empirically and can be found in the **Table A3.5.1**.

Resin Pretreatment. Resins were pretreated with excess Cl^- before use. 20 mL of each resin was determined by displacement in a 100 mL graduated cylinder initially filled with 50 mL water. The water was then decanted off, and the wet resins were desiccated for 24 h at 50°C. The 20 mL of each dried resin was submerged in 1L volumetric flasks containing NaCl solution at a concentration of ten times equivalency of the resins. A stir bar was submerged in each, and the resins were stirred at 250 rpm for 1 h to allow for complete saturation. The brine was decanted off, and the resins were washed continuously with DI water while the conductivity was measured. Once the conductivity dropped below 20 µS/cm, little to no aqueous Cl- remained. The resins were again desiccated at 50°C for 24 h, then weighed. The resin working density was then calculated as the dry mass of the resin divided by the wet volume to be used for all experiments.

Table 2.7.4. Cosolvent characteristics.

Cosolvent Name	Chemical Formula	Molecular Weight (g/mol)	Relative [a] Density at 20°C (g/mL)	$LogK_{ow}$[a]	Boiling Point (°C) [a]	Alkyl Chain Length	Hydroxyl Group Count
Methanol	CH_3OH	32.04	0.79	-0.77	64.7	1	1
Ethanol	C_2H_5OH	46.07	0.79	-0.31	78.2	2	1
1-Propanol	C_3H_7OH	60.10	0.81	0.25	97.2	3	1
1-Butanol	C_4H_9OH	74.12	0.81	0.88	117.7	4	1
Propylene Glycol	$CH_3CH(OH)CH_2OH$	76.09	1.04	-0.92	187.6	3	2
Glycerol	$CH_2(OH)CH(OH)CH_2OH$	92.09	1.26	-1.76	290.0	3	3

[a] Values sourced from PubChem

PFAS on Resin Regeneration. One combined solution of the six PFAS compounds (PFBA, PFHxA, PFOA, PFBS, PFHxS, PFOS) was prepared with each concentration at 120 µM in 2.1 L for a total of 720 µM PFAS solution. The mixture was sonicated to ensure complete dissolution of all PFAS. A 100 mL aliquot in a volumetric flask was taken for pre-saturation analysis. The remaining 2 L of master mix were dispensed into two 1 L volumetric flasks. In each flask, 240 µeq of A520E and A592E resin were added for a total of three-times equivalency, and a stir bar was added; each was stirred at 250 rpm for 48 hours. The resins were then isolated from the saturation solution and partially dried via vacuum filtration with a MilliporeSigma WP6211560 115V 60Hz pump. The total damp resins were vacuum dried and were weighed and transferred into 50 mL conical tubes for storage. The resins were then parceled into ten approximately equal masses and placed into 125 mL amber vials. A 100 mL aliquot of each post-saturation solution was recovered in a 100 mL volumetric flask from each filtrate. Resin regeneration was conducted for each parcel of resin saturated with PFAS. Regeneration solutions were synthesized in stock solutions in 1000 mL volumetric flasks. A 250 mL volumetric flask was used to measure the volume of solvent and volume of water needed for each regeneration solution. Solutions contained 0.5% NaCl on a m/m basis of the total regenerant solution. **Table 2.7.5** contains the cosolvent conditions used for regeneration.

Table 2.7.5. Regeneration cosolvent mixture conditions prepared in 1 L volumetric flasks for 6 PFAS.

Solvent	Volume % Solvent	Volume % Water	0.5% m/m NaCl (g)[a]
Methanol	25	75	4.7275
Ethanol	25	75	4.7250
1-Propanol	25	75	4.7388

[a] Mass per mass of total solution

The mass of sodium chloride on a total solution mass per mass basis was calculated based off the following equation:

$$Mass\ NaCl = (V_S\rho_S + V_W\rho_W) * (Mass\ Fraction\ Salt) \quad (2.7.1)$$

V_s is the volume of solvent (mL), ρ_s is the density of the solvent at 20°C (g/mL), V_w is the volume of water (mL), ρ_w is the density of water (g/mL).

To perform regeneration, 100 mL of each cosolvent, measured via graduated cylinder, was inserted into each amber bottle. The bottles were placed on a Thermo Scientific SHKE2000 MaxQ Shaker table and agitated at 250 rpm for 1 h which is consistent with past experiments (Dixit et al., 2020). After regeneration, each solution was passed through a 0.45 µm cellulose acetate syringe filter into a 50 mL conical tube. For the regenerant solutions and the saved pre-saturation and post-saturation solutions, 0.5 mL was pipetted into 9.5 mL of DI water for an initial twenty-times dilution. From the initial dilutions, 1 mL was pipetted into 50 mL volumetric flasks which were then filled to 50 mL for a second fifty-times dilution for a total of a thousand-times dilution. Before analysis, samples were diluted further by an additional factor of one hundred for a total of 100,000× dilution.

Diclofenac on Resin Regeneration. A total of four 9.0 mM solutions of diclofenac sodium, one for each of four resins (A502P, A520E, A532E, A592E), were prepared by dissolving 3.4538 g in 1.2 L which was distributed to a 1 L volumetric flask for the experiment and a 200 mL volumetric flask for pre-saturation analysis. A 0.5 mL aliquot was taken from the 200 mL volumetric flask and diluted with DI water into a 100 mL volumetric flask for analysis. Then, 3.0 meq of each resin was added to each 1 L volumetric flask for a three times equivalency of diclofenac sodium to resin. A stir bar was added to each flask, and the mixtures were stirred at 250 rpm for 24 h to allow full saturation of the diclofenac anion onto each resin. The resins were then isolated from the saturation solution and partially dried via vacuum filtration with the same pump used for diclofenac. The total damp resins were allowed to dry and were weighed and transferred into 50 mL conical tubes for storage. The resin was separated into 50 equivalent parcels in 20 mL scintillation vials. A 100 mL aliquot of each post-saturation solution was recovered in a 100 mL volumetric flask from each filtrate. These post-saturation solutions had 1 mL aliquot taken from each and diluted with DI water into 100 mL volumetric flasks for analysis.

Resin regeneration was conducted for each parcel of resin saturated with diclofenac anion. Regeneration solutions were synthesized in stock solutions in 250 mL volumetric flasks. A 200 mL graduated cylinder was used to measure the volume of solvent and volume of water needed for each regeneration solution. Solutions always contained 5% NaCl on a mass per mass basis of the cosolvent mixture. **Table 2.7.6** contains the conditions of the cosolvent solutions used to regenerate diclofenac-loaded resin.

To perform regeneration, 20 mL of cosolvent solution was pipetted into the 20 mL scintillation vials containing resin. The vials were placed on a Thermo Scientific SHKE2000 MaxQ Shaker table and agitated at 250 rpm for 1 hour, based off prior research [29]. A 1 mL aliquot was pipetted from the regeneration solution and diluted to 100 mL in a 100 mL volumetric flask. These dilutions were saved for analysis. The remaining resin and regeneration solution were disposed of in appropriate waste containers.

Dodecylbenzene Sulfonate on Resin Regeneration. Resin saturation for the dodecylbenzene sulfonate procedures was performed twice for the entire procedure. One batch of resin was used for all of the 5% NaCl m/m solution regenerations. A second resin batch was used for the 0.5 and 0.05% NaCl m/m solution regenerations. For the resins saturated with dodecylbenzene and

regenerated with 5% NaCl m/m cosolvent solutions, total of three 9.0 mM solutions of sodium dodecylbenzene sulfonate, one for each resin (A502P, A520E, A592E), were prepared by dissolving 3.4499 g in 1.1 L which was distributed to a 1L volumetric flask for the experiment and a 100 mL volumetric flask for pre-saturation analysis. A 1.0 mL aliquot was taken from the 200 mL volumetric flask and diluted with DI water into a 100 mL volumetric flask for analysis. Then, 3.0 meq of each resin was added to each 1L volumetric flask for three-times equivalency of sodium dodecylbenzene sulfonate to resin. A stir bar was added to each flask, and the mixtures were stirred at 250 rpm for 24 hours to allow full saturation of the dodecylbenzene sulfonate anion onto each resin. The resins were then isolated from the saturation solution and dried via vacuum filtration with a MilliporeSigma WP6211560 115V 60Hz pump. The total resins were weighed and transferred into 50 mL conical tubes for storage. The resin was separated into fifty roughly equivalent parcels in 20 mL scintillation vials. A 100 mL aliquot of each post-saturation solution was recovered in a 100 mL volumetric flask from each filtrate. These post-saturation solutions had 1 mL aliquot taken from each and diluted with DI water into 100 mL volumetric flasks for analysis. Loaded mass and saturation percent were calculated via the same method used for diclofenac and PFAS anions. The conditions for regenerant solutions are listed in **Table 2.7.7**.

Table 2.7.6. Regeneration cosolvent mixture conditions prepared in 250 mL volumetric flasks for diclofenac anion.

Cosolvent	Volume % Solvent	Volume % Water	5% m/m NaCl (g)[a]
None	0	100	12.463
Methanol	25	75	11.822
Methanol	50	50	11.181
Methanol	75	25	10.541
Ethanol	25	75	11.813
1-Propanol	25	75	11.856
Propylene Glycol	25	75	12.566
Propylene Glycol	50	50	12.669
Propylene Glycol	75	25	12.772

[a] Mass per mass basis of total regenerant solution

For the resins saturated with dodecylbenzene and regenerated with both 0.5% NaCl and 0.05% NaCl m/m cosolvent solutions, a similar method was followed with a few slight deviations. Firstly, although a three-times equivalency of dodecyl benzene sulfonate to resin was still maintained, the solution concentrations were lowered to 3.0 mM dodecylbenzene sulfonate, and the resin was 1.0 meq/L. The parcel sizes were smaller in mass, but this allowed for 10× dilutions rather than 100× dilutions for analysis.

For resin regenerations at 5% m/m NaCl was conducted for each parcel of resin saturated with dodecylbenzene sulfonate anion. Regeneration solutions were synthesized in stock solutions in 200 mL volumetric flasks. A 200 mL graduated cylinder was used to measure the volume of solvent and volume of water needed for each regeneration solution. Solutions always contained 5% NaCl on a mass per mass basis of the cosolvent mixture. The method for calculating the amount of NaCl needed for each regenerant solution followed the diclofenac procedure.

Regenerating with 0.5 and 0.05% NaCl followed the same procedure as above, but additional trials were performed so that each monoalcohol cosolvent solution would be analyzed for regeneration at 5, 25, 50, and 75% ABV excluding 1-butanol, and no further regeneration procedures were attempted for propylene glycol and glycerol. The regenerant cosolvent mixture parameters are listed below in **Table 2.7.8**. Regeneration was carried out via the same method used for diclofenac and PFAS anions. Regeneration efficiency was calculated via the same method as well.

Table 2.7.7. Regeneration cosolvent mixture conditions prepared in 200 mL volumetric flasks for dodecylbenzene sulfonate anion, 5% NaCl.

Solvent	Volume % Solvent	Volume % Water	0.5% m/m NaCl (g)[a]	0.05% m/m NaCl (mg)[a]
None	0	100	0.9970	99.7
Methanol	5	95	0.9867	98.7
Methanol	25	75	0.9455	94.6
Methanol	50	50	0.8940	89.4
Methanol	75	25	0.8425	84.3
Ethanol	5	95	0.9866	98.7
Ethanol	25	75	0.9450	94.5
Ethanol	50	50	0.8930	89.3
Ethanol	75	25	0.8410	84.1
1-Propanol	5	95	0.9872	98.7
1-Propanol	25	75	0.9478	94.8
1-Propanol	50	50	0.8985	89.9
1-Propanol	75	25	0.8493	84.9
1-Butanol	5	95	0.9877	98.8

[a] Mass per mass basis of total solution

Table 2.7.8. Regeneration cosolvent mixture conditions prepared in 200 mL volumetric flasks for dodecylbenzene sulfonate anion, 0.5 and 0.5% NaCl values.

Solvent	Volume % Solvent	Volume % Water	5% m/m NaCl (g)
None	0	100	9.970
Methanol	25	75	9.455
Methanol	50	50	8.940
Methanol	75	25	8.425
Ethanol	25	75	9.450
1-Propanol	25	75	9.478
1-Butanol	5	95	9.877
Propylene Glycol	25	75	10.053
Propylene Glycol	75	25	10.218
Glycerol	25	75	10.603
Glycerol	75	25	11.868

Analytical Methods. The pH and conductivity measurements were completed using an Orion Dual Star Multiparameter meter, Orion 9156BNWP Combination pH probe, and an Orion Star

A212 conductivity probe. Precision of regeneration of resin and reuptake of Cl^- was checked by running regenerations in triplicate, and triplicate results were averaged to determine values. The concentrations of both diclofenac anion and dodecylbenzene sulfonate anion were determined by UV absorbance using a UV-Visible Spectrophotometer (UV-Vis 2700, Shimadzu) operating in photometric mode at a single wavelength. Previous work has found diclofenac anion has a maximum peak absorbance around 275 nm [30, 31]. A 5-point calibration curve was created using serially diluted standard concentrations of 0.0 mmol/L, 0.01 mmol/L, 0.02 mmol/L, 0.05 mmol/L, and 0.075 mmol/L (R^2 = 0.99998). Measurements of experimental samples were checked by comparing standards with the calibration curve beforehand.

A previous study has found dodecylbenzene sulfonate has a maximum peak absorbance at 223 nm [25]. A 7-point calibration curve was created using serially diluted standard concentrations of 0.0 mmol/L, 0.001 mmol/L, 0.01 mmol/L, 0.02 mmol/L, 0.05 mmol/L, 0.08 mmol/L, and 0.095 mmol/L (R^2 = 0.99983). Each measurement of experimental samples was preceded by checking at least three standards with the calibration curve to maintain accuracy.

For the analysis of the six PFAS saturated onto resins then regenerated, an Agilent high pressure liquid chromatograph (HPLC, 1100) utilizing gradient elution and a Phenomenex Gemini C18 column (110 Å, 100×3 mm, 5µm) was used in accordance with past experiments [18]. The HPLC was outfitted with two additional guard columns, a C18 guard column and a Zorbax Diol guard column (12.5×4.6 mm, 6 µm). The total apparatus was paired with a Sciex 3200 triple quadruple mass spectrometer in multiple reaction monitoring and negative electrospray ionization mode. Between the pump and the autosampler was a Luna C18 delay column (100 Å, 30×3 mm, 5 µm), and injections were performed at 20 µL volume. The delay column and Optima Grade LC/MS water and methanol were used to eliminate possible background contamination of PFAS contamination. The flow rate was maintained at 0.8 mL/min, and the gradient mobile phase was comprised of 20 mM ammonium acetate in water and methanol, beginning with 5% methanol raised to 60% methanol in 45 seconds, further raised to 100% methanol over 4 minutes, and maintained for 3 additional minutes. The methanol concentration was then lowered to 5% over 1 minute and then maintained at 5% for an additional 2 minutes. PFAS standard compounds were attained from Wellington Laboratories.

Data Analysis. Regeneration efficiency was calculated on a mass basis. The amount of saturant on the resin was calculated by mass balance in the pre- and post-solutions. After the saturated resins were weighed, the mass of saturant on each parcel was determined by the mass fraction of the parcel to the total mass of saturated resin. All batch protocols were conducted in triplicate. Error was represented as standard deviation for regeneration experiments, and error bars on graphs represent one standard deviation from the mean in all cases. Comparing the concentrations of the initial pre-saturation solution and the post-saturation solution allows for the formulation of how much mass was loaded onto the resin, displacing Cl^- ion.

$$M_L = (C_i - C_f)V \tag{2.7.2}$$

M_L is the mass of saturant anion loaded onto the resin (mmol), C_i is the initial concentration of the saturant anion pre-saturation (mmol/L), C_f is the final concentration of the saturant anion post-saturation, V is the volume of solution used to saturate (L).

Resin saturation percent was also calculated based off the reported capacity of the resin compared to the capacity found experimentally.

$$Saturation\ \% = (M_L/M_P) * 100 \quad (2.7.3)$$

Saturation % is the ratio of the capacity of the resin determined experimentally to the capacities published by the manufacturer, M_L is the amount of saturant anion loaded onto the resin (mmol), M_P is mass of resin used based off its published equivalency (meq). Regeneration efficiency was calculated using the new concentration of diclofenac anion in the regeneration solution after the resin had been regenerated with Cl^-.

$$Regeneration\ \%\ Efficiency = \frac{C_R V_R}{(R_P/R_T) * M_L} * 100\% \quad (2.7.4)$$

C_R is the concentration of saturant anion in the regeneration solution (mmol/L), V_R is the volume of the regeneration solution (L), R_P is the resin parcel mass, R_T is the total mass of the saturated resin (mg). M_L is the mass of contaminant or saturant loaded onto the resin during saturation (mmol).

2.7.2. Regeneration of Spent Ion Exchange Resins from Field Pilot

Samples of 'spent' anion exchange resin (AER) were obtained from continuous-flow treatment columns used in a field pilot system treating groundwater impacted by aqueous film-forming foams (AFFF). These columns were operated for nearly eight months of continuous treatment, ultimately remediating >170,000 bed volumes (BVs) of water at a 2-minute empty-bed contact time (EBCT). All resins deployed at this field site experienced breakthrough of some PFAS analytes during operation, with full breakthrough data and elution profiles detailed in Ellis et al. (2022). For regeneration studies, two macroporous resins (regenerable A520E and single-use CalRes 2301) and two gel-type resins (PFA694E and PSR2+, both intended to be operated as single-use products) were selected for analysis. Samples from each cross-sectioned segment of the field columns were blended to create reference stocks of resin with known quantities of preloaded PFAS. **Table 2.7.9** details each of the resins used in this regeneration study with relevant parameters and expected PFAS loadings.

In the first phase of the regeneration study, batch experiments were conducted to screen each resin for their regenerability, as well as screen various regenerant solution mixtures for their efficacy in desorbing PFAS from the resins. Batch experiments were used to screen a wide range of regenerant solution constituents. Polyethylene reactors were filled halfway (25mL) with regenerant solution mixtures before adding 100 mg of PFA694E resin and mixing on a shaker table (160 rpm) for 24h at room temperature (20°C). Reactors were then centrifuged (10min, 1600 rpm) and supernatant was collected for PFAS analysis. The percent desorption of individual PFAS was determined by comparison with concentrations measured following application of the three-round extraction protocol previously validated (Ellis et al., 2022). Regenerable AERs (A520E) was excluded from analysis as its batch regenerability is described in literature (Conte et al., 2015) and to minimize analytical expenses.

Table 2.7.9. Resin parameters and PFAS loading from the field pilot

Resin Identity		A520E	PFA694E	CalRes 2301	PSR2+
Resin Details[a]	*Manufacturer*	Purolite	Purolite	Calgon	Dowex
	Operational Mode[c]	Regenerable	Single-Use	Single-Use	Single-Use
	Porosity	Macroporous	Gel	Macroporous	Gel
	Functional Group	Triethylamine	Complex amino	Tributylamine	Tributylamine
Sorbed PFAS Conc. (mg/g)[b]	*Total PFAS*	10.60±0.4	11.45±0.3	11.30±0.3	12.23±0.2
	PFCAs	0.14±0.00	1.28±0.05	1.13±0.01	1.33±0.01
	PFSAs[d]	2.29±0.1	3.12±0.1	2.89±0.1	3.03±0.2
	PFOS[d]	8.18±0.3	7.05±0.2	7.28±0.2	7.87±0.1

[a.] Resin properties obtained from manufacturer, with further details in Fang et al., 2021. All resins received in Cl- form for use in the field pilot study

[b.] PFAS loading of the virgin AERs occurred in the field pilot study described in Ellis et al., 2022, with breakthrough information described therein. PFAS loading values (sorbed PFAS concentrations) include all compounds regularly detected in PFAS sourcewater, including C4-C8 PFCAs and C3-C8 PFSAs. A full list of these analytes and their sourcewater concentrations are listed in Table 3.4.1.

[c.] A520E marketed as a regenerable resin, while the remaining three resins marketed as 'PFAS-selective' resins intended for single-use operation

[d.] PFSA values include PFOS, though PFOS is reported separately as it comprised >55% of total PFASs detected in field site groundwater

Continuous-flow regeneration experiments were conducted in packed-bed columns measuring 2.1 cm in diameter and 16.2cm in height, with metal screens inserted to ensure a 55 mL bed volume (**Figure 2.7.1)**. Regenerant solutions were pumped through columns using a peristaltic pump (Masterflex L/S; Cole-Parmer) at a design flow of 5.5 mL/min in upflow vertical configuration to achieve a 10-min EBCT. An experiment with 30-min EBCT was conducted using the same flowrate applied to larger columns (2.1 cm x 50 cm; 165 mL bed volume). Effluent samples were collected from a port at the top of the column after solution exited the resin bed, and the remaining waste regenerant was stored for subsequent analysis and use in distillation recovery experiments.

Evaluation of parameters and constituents used in regeneration began with batch screening of solution constituents, evaluating brine-only, cosolvent-only, and brine with cosolvent solutions, followed by screening of aqueous brines amended with different surfactants. A down-selected group of regenerants was then used for more extensive continuous-flow regeneration experiments.

The baseline regenerant mixture and condition used for continuous-flow regeneration was 70% methanol (v/v) and 1 wt% NaCl applied with a 10-min EBCT for 30 bed volumes (BVs; 1.65L of regenerant solution for a 55mL bed). While operation at longer EBCTs (e.g., 30-min) and fewer BVs (e.g., 10) may be more commonplace in practice (Dietz et al., 2021; Fang et al., 2023) to minimize solution requirements, use of 10-min EBCT has been documented in literature (Dixit et al., 2020) and effluent samples were collected throughout the 30-BV cycle to determine the optimal number of bed volumes required to reach target levels of PFAS desorption. **Table 2.7.10** summarizes the parameters evaluated in continuous-flow regeneration experiments, with each parameter varied independently to isolate its effects on overall AER regenerability.

Figure 2.7.1. Photograph of the continuous-flow regeneration apparatus.

Table 2.7.10. Amendments to regenerant solutions used in continuous-flow operation

Parameter	Baseline Condition	Alternate Conditions Examined[a]		
Resin Identity	PFA694E	A520E	CalRes 2301	PSR2+
Cosolvent Identity	Methanol	1-Propanol		
Cosolvent Fraction	70%	90%		
Salt Brine Conc.	1 wt% NaCl			
Empty-bed contact time (min)	10 min	30 min		
Number of BVs in regeneration	30 BVs	10 BVs		

[a.] Alternate conditions were explored by varying each parameter individually, keeping all other parameters from the baseline condition constant to isolate effects from each parameter on overall AER regeneration

2.8. Treatment of Waste Regenerant Solutions

2.8.1. Electrochemical oxidation

Bench-scale electrochemical experiments were performed using previously described methods (Schaefer et al., 2017, 2018). An AFFF solution collected from a US Department of Defense facility was used as the PFAS source in all electrochemical experiments. PFAS concentrations in the diluted AFFF are provided in **Table A3.6.1** in the Appendix. Brine solutions were prepared using salts (NaCl, Na_2SO_4, $NaHCO_3$, $(NH_4)_2SO_4$, $NaClO_4$) purchased from Sigma-Aldrich; NaOH was purchased from Integral Chemical; NH_4OH was purchased from Sigma-Aldrich. Tert-butyl alcohol (TBA) was purchased from Fisher Scientific. A single-compartment Micro Flow Cell (ElectroCell North America, Amherst, New York) with a stainless-steel cathode and a niobium-supported boron-doped diamond anode (Condias, Itzehoe, Germany) was used for the electrochemical experiments. The electrode spacing was 4 mm, and the active surface area of each electrode was 10 cm^2. Experiments were typically performed for 8 hours, at an applied current density of 40 mA/cm^2. Various brine solutions were evaluated, as shown in **Table A3.6.2**. These solutions were selected based on AER regeneration solutions previously considered for PFAS removal from AERs and in an effort to evaluate alternatives to chloride-based brines. A perchlorate brine was also included as an electrochemically inert brine to assess potential impacts of electrochemically generated sulfate- or bicarbonate-based radicals in the brine solutions on PFAS defluorination, as perchlorate is expected to remain inert during electrochemical treatment. TBA, which has been used as a hydroxyl radical scavenger, was used in several experiments at 100 mM (and, at 10 mM in one set of experiments to assess TBA dosage impacts on PFAS treatment) to evaluate the role of hydroxyl radicals and other potentially generated oxidants on treatment; the 100 mM TBA dosage represents approximately half the cosolvent organic carbon dosage previously observed in anion exchange regeneration fluid (Liang et al., 2018). TBA also served as a surrogate for evaluating the impacts of residual cosolvent on electrochemical treatment of AER regeneration fluids. While TBA was shown to behave similarly to methanol with respect to hydroxyl radical scavenging impacts on the electrochemical oxidation of an organic compound using BDD anodes, it is recognized that radical scavenging by TBA may not behave similarly to methanol. Brine solutions (550 mL) were amended with 1.1 mL of AFFF and placed in a 1 L Erlenmeyer flask. During the electrochemical experiments, 250 mL of this solution was recirculated through the electrochemical cell using a peristaltic pump at a rate of 0.1 L per minute. All experiments were performed in duplicate. Controls, performed identically but with no applied current, were also performed in duplicate. One long-term experiment was performed using the 0.2% sodium sulfate brine, in duplicate, for 30 hours to assess the fluorine mass balance. Most experiments used brines prepared from sodium salts, but one experiment was conducted using ammonium sulfate/ammonium hydroxide to assess the potential impacts of an alternate cation on PFAS treatment.

2.8.2. Hydrothermal alkaline treatment

A waste ion exchange still bottoms sample from a pilot regenerable IX treatment system run by ECT2 was obtained from the former Naval Air Station at Willow Grove. Still bottoms sample is a highly saline aqueous solution of concentrated PFAS waste generated from IX brine following resin regeneration and after distillation of the organic co-solvent (typically methanol). Because of its high salt and high concentration of PFASs, the treatment of still bottoms remains a problem.

Prior to use, the still bottoms sample was characterized for PFAS concentrations and other bulk water characteristics, including dissolved organic carbon (DOC, non-purgeable), major salt anions, and pH.

For this project, we evaluated the effectiveness of hydrothermal alkaline treatment (HALT) for destruction of PFASs in still bottoms. HALT is a destructive technology for PFASs that is being investigated in-depth through SERDP Project ER18-1501. Work in that project has demonstrated HALT to be effective for destruction of PFASs in aqueous film forming foam (AFFF) and AFFF-impacted wastes (groundwater and soil). Below is a brief summary of the results to date.

Hydrothermal treatment of still bottoms sample was conducted in stainless steel tube batch reactors (1.27 cm outer diameter × 10 cm length, 0.12 cm wall thickness; see **Figure 2.8.1a**). For each experiment, a 3 ml mixture of still bottoms samples (1.5 mL) and 2 M NaOH (1.5 mL) were added to the reactor. The reactor was then sealed and rapidly heated to 350 °C by immersing in a fluidized sand bath (Accurate Thermal Systems, FTBLL12; **Figure 2.8.1b**) for desired reaction time. After reaction, the reactor was quenched by immersion in cold tap water. Previous measurements showed that it took <3 min to heat/cool the reactor to the setpoint temperature. After cooling, the reactor was opened, and liquid contents were transferred to a 15 mL polypropylene centrifuge tube and stored at 4°C before analyses. All experiments were conducted at least in duplicate, with uncertainties representing the full range of values measured in the replicate experiments.

To evaluate the levels of target PFASs in still bottoms sample, the samples were diluted by large amounts and then analyzed by high-resolution liquid chromatography quadrupole time-of-flight mass spectrometry (LC-QToF-MS) with both ESI+ and ESI- analyses following the methods described in later sections. All still bottoms samples were measured at least in duplicate, with uncertainties representing the full range of values measured in the replicate experiments. The DOC of still bottoms sample was analyzed by a total organic carbon (TOC) analyzer (Shimadzu TOC-L). Analysis of common inorganic anions was performed on ion chromatography (IC) with conductivity detection (ICS-90, Dionex, Sunnyvale, CA).

(a) **(b)**

Figure 2.8.1 Reactors and heat source used for hydrothermal reactions. (a) Stainless steel tube reactors used for hydrothermal treatment reactions; (b) Fluidized sand bath used for heating reactors.

2.9. Analysis

2.9.1. PFAS analysis.

PFASs were measured using LC-QToF-MS and LC-MS/MS methods during the study. LC-QToF-MS analysis at the Colorado School of Mines was conducted using a Sciex x500r QTOF high-resolution mass spectrometer, while LC-MS/MS analysis was conducted using a Sciex 5500 QTRAP Triple Quad mass spectrometer. For both instruments, analysis was enabled using internal standard stocks prepared from analytical-grade reagents from 3M, Wellington Laboratories, Fluobon, and Synquest Laboratories. Aqueous eluents were prepared from Optima LC-MS grade water (Fisher Scientific) with 20 mM analytical-grade ammonium acetate while the organic eluent consisted of 100% Optima LC-MS grade methanol (Fisher Scientific). Total flows of eluent and sample through the instruments were set to 0.6 mL/min, with alternating stages of majority-aqueous and majority-organic phase elution. The stationary phase was a Phenomenex Gemini C18 LC column with 5 µm particle size and 110 Å pore size. All samples were prepared as a 1.5 mL mixture of sample, internal standards, Optima LC-MS grade water, Optima LC-MS grade isopropyl alcohol, Optima LC-MS grade methanol, and 99.8% trifluoroethanol from Acros Organics.

The Sciex X500R Quadrupole Time-of-Flight MS (QToF-MS) system using SWATH® Data-Independent Acquisition was operated in both positive and negative electrospray ionization (ESI+/-) mode for QToF-MS and MS/MS analysis. Sciex OS 1.5 was used to process collected QToF-MS data to quantify PFASs (i.e., targeted analytes) with available analytical standards and internal standards, and to identify additional PFASs (i.e., suspect analytes) using a custom extracted ion chromatogram (XIC) list. Detailed methods for target analyte quantification and suspect PFAS identification were adopted from previous studies (Hodgkins et al., 2019, Mejia-Avedano et al., 2017). Briefly, target analytes were identified when their retention times are within 30 seconds of their corresponding analytical standards, mass error < 10 ppm from the nominal isotopic m/z, and peak signal-to-noise ratio >10. The peak areas of each target analyte's internal standard were used to correct for matrix effects and instrumental variation. Target PFAS concentrations were only reported when their concentrations were at least three times higher than all instrument and method blanks. Identification of suspect analytes were based on the accuracy of mass measurement for the molecular ion, isotopic pattern matching scores, and the library purity score for compounds in the MS/MS library. Samples were screened by searching for the deprotonated molecular ion [M-H] for negative ionization and protonated molecular ion [M+H] for positive ionization using an XIC window of 0.008 Da, a signal: noise ratio of 3:1, and baseline subtraction over 3 min. Peaks collected from Sciex OS 1.5 were selected as suspect PFAS only when their mass error is <5 ppm and isotopic pattern error is <10% compared to the corresponding compound in the XIC list.

2.9.2. Other methods

During the electrochemical experiments, pH, temperature, voltage, fluoride, TBA (when added), and PFASs were monitored as a function of time. Anions were analyzed using ion chromatography. PFAS were analyzed at the Colorado School of Mines as described above. TBA was analyzed by APTIM (Lawrenceville, NJ) using gas chromatograph/mass spectrometry

(GC/MS) following EPA Method 8260C. Samples for PFAS analysis were preserved with 20 µL of 300 g/L sodium thiosulfate to limit potential oxidation of PFAA precursors due to the presence of any electrochemically generated residual oxidants. ^{19}F- nuclear magnetic resonance (NMR; ECA-500, JEOL) analysis, which has been shown to be an effective means for estimating the organic fluorine content in AFFF (Tenorio et al., 2020; Hao et al., 2021), was employed to determine the fluorine content of the AFFF using in this study.

2.10. Life Cycle Assessment and Life Cycle Costing Analysis

2.10.1. Comparison of ion exchange regenerant management options

Scope of study. The scope of the first LCA effort was to compare the environmental impacts of an AER remediation system with different regeneration options. Only the operating phase was considered given the regeneration options were based on hypothetical treatment scenarios seeking an attributional comparison [32]. The remediation system boundary included AER treatment and regeneration, methanol cosolvent recovery via onsite distillation, brine recovery via onsite GAC adsorption of PFASs, transport of chemicals to the site, transport of waste to off-site incinerator, and off-site hazardous waste incineration, and considered the input of materials and electricity to the processes and associated emissions (see **Figure 2.10.1**). The functional unit for the study was 1 m^3 of AER-treated groundwater with combined PFOA and PFOS concentration equal to 70 µg/L in untreated water and nondetectable concentration of PFOA and PFOS in treated water.

Each specific objective defined in section 1 was taken as an LCA scenario. In scenario 1a, the regeneration solution was composed of tap water, NaCl, and methanol (see **Figure 2.10.1a**). The waste regeneration solution, which contained water, NaCl, methanol, and desorbed PFOA and PFOS, was transported by truck and disposed of via off-site hazardous waste incineration.

In scenario 1b, the regeneration solution was composed of tap water, NaCl, and combination of new and recycled methanol (see **Figure 2.10.1b**). The methanol was recovered via onsite distillation process. Following distillation, the remaining PFAS-contaminated waste regeneration solution was transported by truck and disposed of via off-site hazardous waste incineration.

In scenario 1c, the regeneration solution was composed of tap water, NaCl, recycled brine, and combination of new and recycled methanol (see **Figure 2.10.1c**). The methanol recovery process was identical to scenario 1b. Following distillation, brine was recovered from the waste regeneration solution via onsite GAC adsorption of PFOA and PFOS. The GAC, which was loaded with PFOA and PFOS, was transported by truck and disposed of via off-site hazardous waste incineration. The regeneration facilities in scenarios 1a–c and 2a would require onsite fire suppression and other safety features due to solvent flammability, which was not considered here given the focus on the operating phase of the LCA.

The second set of scenarios focused on substitution of components in the regeneration solution make-up. Scenario 2a followed the same process flow as scenario 1b (see **Figure 2.10.1b**) with NaCl replaced with potassium chloride (KCl), ammonium chloride (NH_4Cl), sodium sulfate (Na_2SO_4), potassium sulfate (K_2SO_4), ammonium sulfate ($(NH_4)_2SO_4$), sodium carbonate (Na_2CO_3), potassium carbonate (K_2CO_3), or ammonium carbonate ($(NH_4)_2CO_3$). Methanol was used as the cosolvent in scenario 2a. Following methanol recovery (by onsite distillation), the

PFAS-contaminated waste regeneration solution was transported by truck and disposed of via off-site hazardous waste incineration.

Scenario 2b followed a similar process flow as scenario 1c (see **Figure 2.10.1d**), but methanol was replaced with sodium hydroxide (NaOH), potassium hydroxide (KOH), or ammonium hydroxide (NH_4OH) to produce an aqueous-only regeneration solution (i.e., caustic brine). Scenario 2b used brine based on chloride salt with the same co-ion as the base, e.g., NaCl paired with NaOH. Distillation was excluded since the regeneration solution did not contain organic cosolvent. The regeneration solution was recycled via onsite GAC adsorption of PFASs, which concentrated the PFOA and PFOS on GAC, and waste GAC was transported by truck and disposed of via off-site hazardous waste incineration. Scenario 2b is most applicable to weak-base AER that can be regenerated in brine/caustic solution [33-35], whereas brine/organic cosolvent solution used in scenarios 1a–c and 2a is most applicable to strong-base AER [17]. This is because weak-base AER exhibit pH-dependent charging behavior and nonionic character at alkaline pH [36].

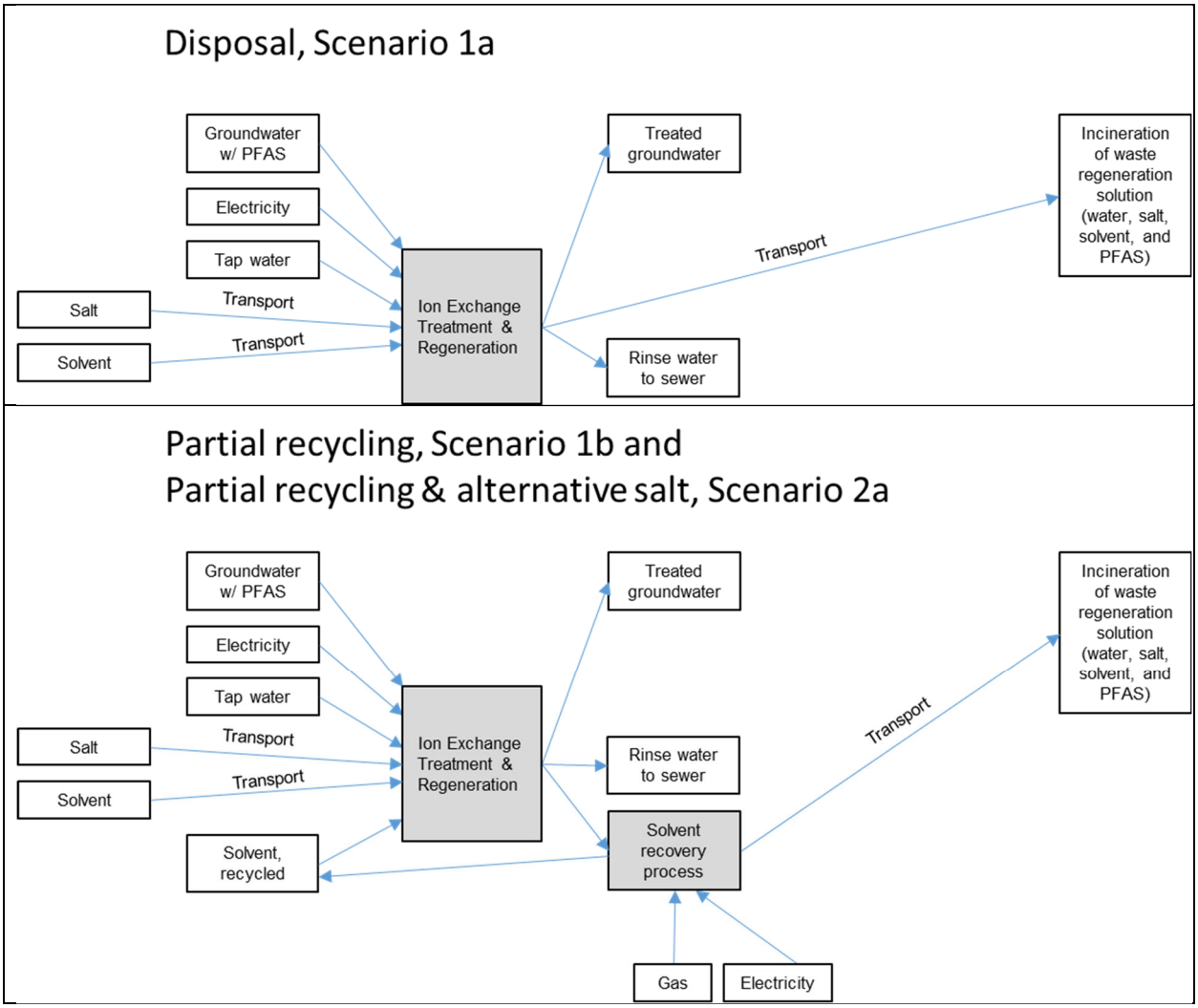

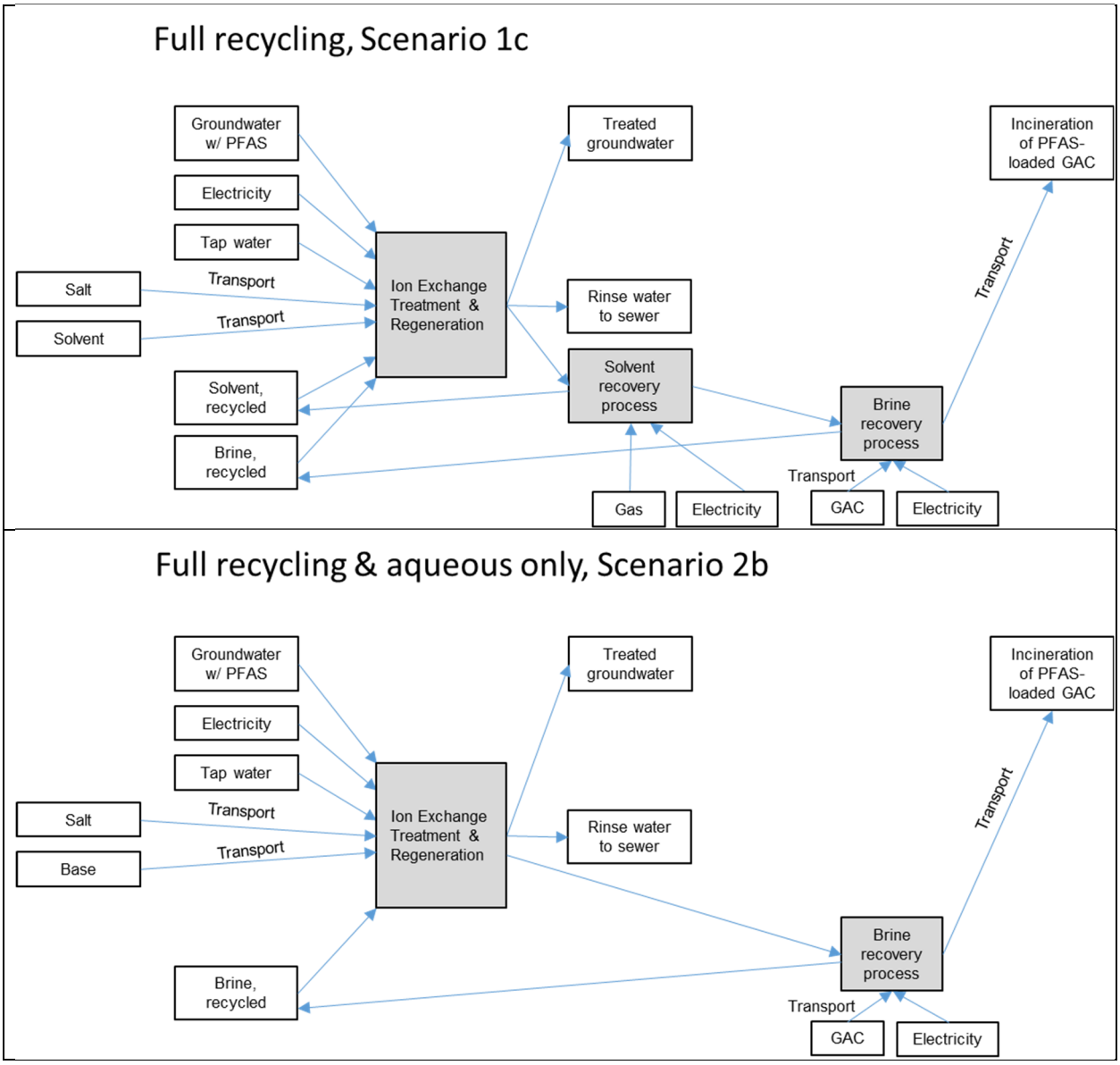

Figure 2.10.1. Inventory of materials, energy, transport, and emissions for AER remediation system with different regeneration options: (a) disposal of waste regeneration solution via incineration, scenario 1a, (b) recycle of organic solvent component of waste regeneration solution, scenarios 1b and 2a, (c) recycle of organic solvent and brine components of waste regeneration solution, scenario 1c, and (d) recycle of aqueous-only regeneration solution, scenario 2b. From Boyer et al. (2021).

Life cycle inventory. The inventory list of materials, fuel, electricity, and processes were generated from consumables used during AER treatment and regeneration (see **Table 2.10.1**). The inventory list was created based on a hypothetical AER remediation system treating groundwater with combined PFOA and PFOS concentration equal to 70 µg/L, and treated water with nondetectable (i.e., 0) concentration of PFOA and PFOS. The hypothetical AER remediation system including PFAS concentrations in groundwater was based on a previous LCA study by Emery et al (2019). Calculations, assumptions, and data sources in support of the hypothetical system are given in supplementary materials (Appendix A). The design calculations for the AER

system represent a hypothetical system where 100% adsorption capacity and regeneration efficiency are achieved. Regeneration of PFAS-loaded AER is an active area of research with studies showing >90% regeneration efficiency using brine and brine/organic cosolvent solutions [6, 33, 35]. The AER system operated at 5 min empty bed contact time (EBCT) and AER adsorption capacity for PFOA and PFOS of 1.66 g/kg based on pilot study of PFAS removal by AER [37]. The volume of AER (equivalent to 1 bed volume, BV) was calculated from the volumetric flow rate for the hypothetical AER system and EBCT. The BVs of water treated to resin saturation was calculated by mass balance from the AER adsorption capacity and influent concentration of 70 µg/L PFOA and PFOS assuming nondetectable (i.e., 0) concentration of PFOA and PFOS in the treated water. PFOA and PFOS concentrations of 70 µg/L represents a contaminated site source zone [9, 10], and was selected because a previous LCA study showed the AER remediation system to dominate environmental impacts at this concentration [38]. The AER system was regenerated once the resin was saturated with PFOA and PFOS. The volume of AER and the BVs of water treated to resin saturation were used to calculate the total volume of water treated per regeneration cycle, which was used to normalize all input parameters to the functional unit of 1 m^3 of AER-treated water.

Table 2.10.1. Inventory list for AER regeneration options for PFAS remediation of impacted water. From Boyer et al. (2021).

(a)

Input	SimaPro inventory item	Database	Unit[a]	Scenario 1a	Scenario 1b	Scenario 1c	Scenario 2a[b]	Scenario 2b[h]
Tap water	Tap water {RoW}| market for | Alloc Def, U	Ecoinvent 3	kg	0.23428	0.23428	0.07755	0.23428	0.1198
NaCl	Sodium chloride, at plant/RNA	USLCI	kg	0.01935	0.01935	0.001935	0.01159[c] 0.01935[d] 0.01935[e] 0.004063[f] 0.01935[g]	3.012e-4[i] 1.804e-4[j] 3.012e-4[k]
Methanol	Methanol, at plant/RNA	USLCI	kg	0.33398	0.0167	0.0167	0.0167	3.012e-4[i] 3.012e-4[j] 3.012e-4[k]
Methanol, recovered	Methanol, recovered	see part b	kg	NA	0.33398	0.33398	0.33398	NA
Brine, recovered	Brine, recovered	see part c	kg	NA	NA	0.1935	NA	0.6024
Truck transport	Transport, combination truck, diesel powered/US	USLCI	tkm	0.2814	0.1069	0.01896	0.1069	0.03015

Electricity	Electricity, at grid, US/US	USLCI	kWh	0.41	0.41	0.41	0.41	0.41
Incineration	Spent solvent mixture {RoW}| treatment of, hazardous waste incineration | Alloc Def, U	Ecoinvent 3	kg	0.52747	0.2102	0.03605	0.2102	0.06024

[a] Unit per m^3 water treated by anion exchange resin. [b] Salt type varied, other inventory items the same as scenario 1b. [c] Salt (SimaPro inventory item): KCl (Potassium chloride, as K2O {RoW}\| potassium chloride production \| Alloc Def, U). [d] Salt (SimaPro inventory item): NH_4Cl (Ammonium chloride {GLO}\| production \| Alloc Def, U). [e] Salt (SimaPro inventory item): Na_2SO_4 (Sodium sulfate, anhydrite {RoW}\| sodium sulfate production, from natural sources \| Alloc Def, U). [f] Salt (SimaPro inventory item): $(NH_4)_2SO_4$ (Ammonium sulfate, as N {RoW}\| ammonium sulfate production \| Alloc Def, U). [g] Salt (SimaPro inventory item): K_2CO_3 (Potassium carbonate {GLO}\| production, from potassium hydroxide \| Alloc Def, U). [h] Solvent replaced with base; same salt and base co-ion. [i] NaCl and NaOH (Sodium hydroxide, production mix, at plant/kg/RNA). [j] KCl and KOH (Potassium hydroxide {RoW}\| production \| Alloc Def, U). [k] NH_4Cl and NH_4OH (25% NH_3), see part d. Not applicable (NA).

(b)

Input	SimaPro inventory item	Database	Unit[a]	Amount
Natural gas	Natural gas, combusted in industrial boiler/US	USLCI	m^3	0.17
Electricity	Electricity, at grid, US/US	USLCI	kWh	8e-4

[a] Unit per kg "Methanol, recovered."

(c)

Input	SimaPro inventory item	Database	Unit[a]	Amount
Activated carbon	Activated carbon, at plant/RER Mass	Agri-footprint	kg	0.028
Electricity	Electricity, at grid, US/US	USLCI	kWh	0.0004
Truck transport	Transport, combination truck, diesel powered/US	USLCI	tkm	0.0154
Incineration	Hazardous waste, for incineration {RoW}| treatment of hazardous waste, hazardous waste incineration | Alloc Def, U	Ecoinvent 3	kg	0.028

[a] Unit per kg "Brine, recovered."

(d)

Input	SimaPro inventory item	Database	Unit[a]	Amount
Ammonia	Ammonia, steam reforming, liquid, at plant/RNA	USLCI	kg	0.25
Water	Water, deionized, from tap water, at user {RoW}| production | Alloc Def, U	Ecoinvent 3	kg	0.75

[a] Unit per kg "NH_4OH (25% NH_3)."

The regeneration procedure consisted of flushing 10 BVs of regeneration solution followed by 1 BV of rinse water through the AER bed based on pilot studies of PFAS removal by AER [6, 37]. For all scenarios, it was assumed that the regeneration process was 100% efficient in terms of desorbing PFOA and PFOS from the resin and restoring the initial AER adsorption capacity, which is supported by studies in the literature. Regeneration of PFAS-loaded AER is an active area of research with some solutions, e.g., methanol/NH_4Cl and NH_4Cl/NH_4OH, showing >90% regeneration efficiency as reviewed in [17]. Hence, 100% regeneration efficiency is conceivable and shows the lowest possible impacts that could be attained for a regenerable AER system. Regeneration efficiency < 100% would require more frequent regenerations and would increase the environmental impacts of the process. AER was not required as an input to the system since there was no resin loss during the operating phase. In a real system, AER would need to be periodically replaced due to attrition of resin beads and irreversible fouling, both of which reduce the ion-exchange capacity of the system.

For scenarios 1a–c, the regeneration solution was composed of 70% (v/v) methanol and 30% (v/v) brine based on previous studies comparing different regeneration solutions [6, 33]. The brine was composed of tap water containing 10% (m/m) NaCl. Upon mixing methanol and brine, the final regeneration solution contained 4% (m/m) NaCl. There is uncertainty in the literature on the impact of salt concentration on regeneration efficiency, with some studies suggesting increasing desorption with decreasing salt concentration [6, 33] and other studies showing the opposite trend [29]. In scenario 1a, the waste regeneration solution was transported 500 km to a hazardous waste incinerator. The transport distance was assumed; the impact of transport is explored in the sensitivity analysis described later. In scenarios 1b and 1c, distillation was used to recover 95% (m/m) methanol from the regeneration solution using natural gas and electricity as inputs based on similar assumptions in Emery et al. (2019). It was assumed that all water, NaCl, PFASs, and 5% (m/m) methanol were collected from the distillation process and either (i) transported 500 km to a hazardous waste incinerator in scenario 1b or (ii) used as input to brine recovery process in scenario 1c. In scenario 1c, GAC adsorption was used to remove PFASs from the waste regeneration solution and thereby enable the recovery of 90% (m/m) water and NaCl from the methanol-depleted regeneration solution. It was assumed that PFOA and PFOS were completely adsorbed by the GAC, thereby allowing the brine to be recycled and used for regeneration. The GAC adsorption process required GAC, electricity, and transport as inputs [38]. The PFAS-loaded GAC and a small amount of waste regeneration solution (10% (m/m) water and NaCl and 5% (m/m) methanol) were transported 500 km to a hazardous waste incinerator. The process of brine recovery via onsite GAC adsorption of PFASs is used hypothetically in this LCA based previous research investigating brine reuse [37, 38]. Future research is needed to confirm that GAC adsorption of PFASs in distillation bottoms can be used for recycling brine for regeneration. One reason the effectiveness of this process is not known is because of the variable level of dissolved organic carbon (DOC) possible in the distillation bottoms, which would inhibit GAC adsorption of PFASs similar to that observed in landfill leachate [39]. Scenario 2a followed the same composition of regeneration solution as scenario 1b with NaCl replaced by an alternative salt at the same mass fraction, which followed previous experimental and LCA study on alternative salt regeneration [40]. For scenario 2b, the regeneration solution was composed of aqueous solution of 0.5% (m/m) inorganic base and 0.5% (m/m) salt based on study comparing regeneration efficiency of brine, caustic brine, and brine/cosolvent [6]. In scenarios 2a and 2b, waste regeneration solution (and GAC,

if applicable) were transported 500 km to a hazardous waste incinerator. For all scenarios, waste rinse water was discharged without treatment (e.g., sewer); its disposal impact was not considered.

Regarding incineration, the Ecoinvent database contains inventory items for incineration of municipal waste (relevant options include municipal solid waste and spent AER) and hazardous waste (relevant options include hazardous waste and spent solvent mixture). In this LCA, the "spent solvent mixture" inventory item was used to represent incineration of liquid waste while the "hazardous waste" inventory item was used to represent incineration of spent GAC.

The electricity required to pump groundwater and operate the AER remediation system was assumed to be the same for all scenarios. The methanol recovery and brine recovery processes had separate electricity inputs. Hypothetical truck transport distances were assumed: 50 km for transport of regeneration chemicals to the AER remediation site and 500 km for transport of waste from the AER remediation site to an incinerator. It was assumed that the AER remediation site was connected to the electric grid, tap water, and sewer.

The scenarios were constructed using SimaPro 8.0.4.30 software. A procedure on the use of SimaPro for this research is given in supplementary materials. Inventory items were obtained from the following databases: Ecoinvent 3 (allocation, default - unit, version 3.1, compiled October 2014), U.S. Life Cycle Inventory (USLCI, updated October 2013), and Agri-footprint (mass allocation, version 1.0, May 2014). Inventory items were selected for United States (location code US) or North America (location code RNA), if available and consistent with input requirements for the study. Global inventory items (location codes RoW or GLO) were selected if United States or North America were not available or appropriate. Inventory items for material inputs and incineration were selected as transformation processes, which included inputs from production and associated emissions. Inventory items for electricity and tap water were selected as market processes, which included inputs from production and transportation and associated emissions.

Life cycle impact assessment. TRACI 2.1 (version 1.02) impact assessment method was used to evaluate the impacts of different regeneration options for the AER remediation system [41]. The impact assessment method transforms process inputs and emissions into tangible environmental impacts along the cause-and-effect chain of environmental degradation [42]. TRACI was developed by the U.S. EPA, so it has location-specific features for the United States and North America and uses midpoint impact categories that are associated with U.S. environmental regulations and guidelines [43]. TRACI uses ten midpoint impact categories: ozone depletion (kg CFC-11 eq), global warming (kg CO_2 eq), smog (kg O_3 eq), acidification (kg SO_2 eq), eutrophication (kg N eq), human toxicity cancer (CTUh), human toxicity non-cancer (CTUh), respiratory effects (kg PM2.5 eq), ecotoxicity (CTUe), and fossil fuel depletion (MJ surplus). The terms human toxicity cancer and human toxicity non-cancer are used interchangeably with carcinogens and non-carcinogens, respectively. Ozone depletion (air), global warming potential (air), smog (air), acidification (air and water), eutrophication (air and water), and ecotoxicity (air, water, and soil) represent categories of pollution with the affected environmental media listed in parentheses. Human toxicity cancer, human toxicity non-cancer, and respiratory effects represent categories of human health impacts. Fossil fuel depletion represents a category of resource depletion.

The environmental impact results are presented as scaled characterization values and normalized characterization values, as is typically done in LCA studies. Briefly, because the

impact categories have different units that cannot be compared, the characterization values were scaled such that the scenario or process with the highest characterization value in each impact category was set at 100%, with the other values scaled accordingly. To directly compare the magnitude of the different impact categories, the characterization values were normalized to the same unit, which is the average annual impact of a U.S. citizen in 2008 as the reference [44]. Because this LCA study was focused on groundwater remediation, impact categories of relevance included climate change impact as indicated by global warming, human health as indicated by human toxicity cancer and non-cancer, and environmental pollution as indicated by eutrophication and ecotoxicity.

Sensitivity analysis. A one-at-a-time sensitivity analysis was conducted for scenarios 1a–c and 2a by varying each input amount by ±50%. Based on the doubling of an input amount, an impact category was operationally defined as not sensitive (<10% increase), low sensitivity (10 to <25% increase), medium sensitivity (25 to <50% increase), or high sensitivity (>50% increase). The maximum possible increase from doubling an input amount is 100%. The relative change in the characterization value for each impact category was quantified to identify the most sensitive combinations of inputs and impact categories. The response of the LCA model to changing quantities of inventory items reveals the largest drivers of impact across the system.

The sensitivity of the impact assessment results to specific inventory items was also explored within the scenarios. For example, in scenarios 1a–c, different incineration inventory items were compared, and in scenario 2a different salt production inventory items were compared. The nature of the incineration process was examined by comparing the impacts of the available incineration inventory items in SimaPro—municipal solid waste, spent anion exchange resin, spent solvent mixture, and hazardous waste—at the same mass with other processes excluded. The nine salts considered in this research (Na^+, K^+, $NH_4^+ \times Cl^-$, SO_4^{2-}, CO_3^{2-}) can be divided into two categories: mined from natural deposits that require varying extents of purification (referred to as natural production, i.e., NaCl, Na_2SO_4, Na_2CO_3, and KCl) and produced from bulk chemicals and energy inputs (referred to as chemical production, i.e., K_2SO_4, K_2CO_3, NH_4Cl, $(NH_4)_2SO_4$, and $(NH_4)_2CO_3$). The salts were compared at the same mass with other processes within the AER system excluded.

2.10.2. Comparison of ion exchange and GAC adsorption technologies

Scope and boundaries of study. The scope of this second effort with LCA was to quantify the life cycle environmental impacts and costs for remediation of AFFF-impacted source zone groundwater using different ion exchange treatment system configurations (regenerable and non-regenerable) and compare these with each other and with treatment using GAC adsorption systems (**Figure 2.10.2**). The full remediation system lifecycle assumed treatment of 6,000 L/h (38,000 gal/d) of contaminated groundwater through two packed bed reactors arranged in a lead-lag configuration. Influent AFFF-impacted groundwater is assumed to contain a mixture of PFASs with concentrations up to 50 μg/L, consistent with the site where anion exchange pilot treatment data was collected (Ellis et al., 2022). Impacts from both the capital and operating phase for each technology were considered. The functional unit was remediation of 1 m^3 of contaminated groundwater.

The system boundary for each remediation system contained all sorbent media, contactors, pipes, fittings, pumps, regenerant solution, and associated infrastructure needed to construct the treatment apparatus. Where possible, specific components like material coatings (paint, corrosion inhibitors) crucial for system longevity are also included. Associated processes needed to operate the treatment system and deal with wastes (e.g., incineration, transportation, thermal energy inputs for reactivation) are also included within the 'system' even though these processes occur off-site due to their necessity in the overall treatment train. Certain elements assumed to be equivalent or identical for all three sorbent technologies were excluded from the analysis. Electricity required to pump groundwater to the surface is one such exclusion, as this electricity would be the same for all technologies as they all treat the same flow rate of water for each scenario. System containment buildings and groundwater pretreatment operations (e.g., bag filters or NOM-specific sorbent pretreatment) have been removed from this comparison as well, as these requirements would be expected to be equivalent among all four systems. The remediation systems were evaluated for a 20-year life cycle from cradle to grave, including the construction and operating phases as well as end-of-life waste disposal of the remediation system infrastructure.

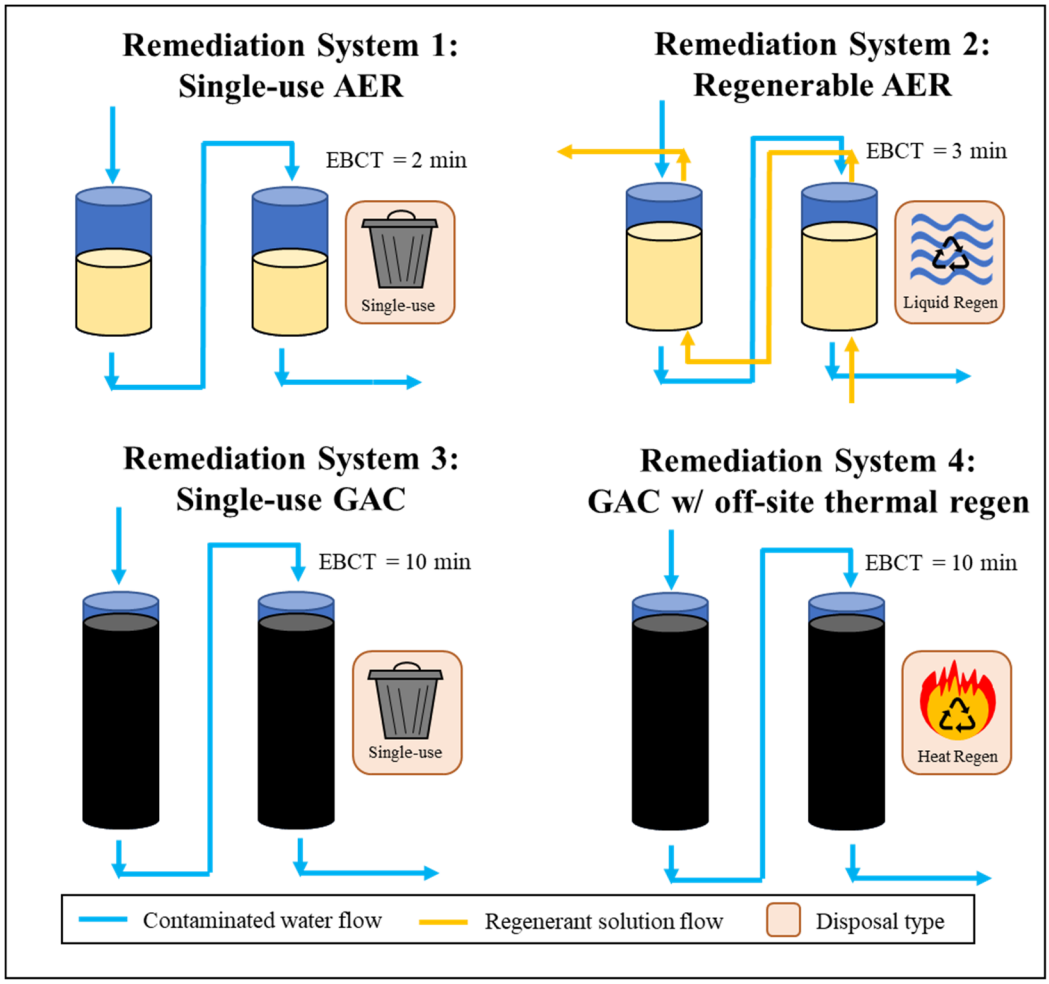

Figure 2.10.2. Schematic of each of the four PFAS remediation systems: (1) single-use anion exchange resins, (2) regenerable anion exchange resins, (3) GAC with off-site incineration, and (4) GAC with off-site thermal regeneration. From Ellis et al. (2023).

Table 2.10.2 summarized the assumed design and operating conditions of the four alternative remediation systems. The baseline scenario assumed changeout or regeneration of media upon detection of any perfluoroalkyl sulfonic acid (PFSA) in effluent from the lead adsorber bed, as estimated from pilot treatment data. *Remediation System 1* was a lead-lag series of adsorber vessels packed with single-use "PFAS selective" AER derived from a polystyrene polymer matrix. Individual adsorber vessels were sized to hold sufficient resin to provided 2-min of empty-bed contact time (EBCT), as recommended by resin suppliers. Upon PFAS breakthrough, PFAS-contaminated resin from the lead adsorber bed was replaced with virgin resin delivered by truck to the site. The contaminated resin was transported by truck and disposed of via off-site hazardous waste incineration.

Table 2.10.2. Assumed operating conditions for each of the four remediation systems under the baseline scenario.[a] From Ellis et al. (2023).

Operating Parameter[b]	Single-Use AER	Regenerable AER	GAC (Single-Use)	GAC (Thermal Regen)
Vessel Size (L)	200	300	1,000	1,000
Empty-Bed Contact Time (min)	2	3	10	10
Sorbent Mass (kg)	135	207	540	540
Sorbent Density (g/L)	675	690	540	540
BVs until Breakthrough[c]	162,200	31,200	13,000	13,000
Media Changeouts per Year[c]	1.62	5.62[d]	4.04	4.04
Sorbent Burn Rate (kg/mo)[c]	18.2	---	181.9	181.9
Management of Spent Media[e]	Incineration	Regeneration	Incineration	Reactivation

[a.] Utilizes field pilot data for specific brands enumerated in Section 1 of the Supplementary Materials (SM)

[b.] Assumes treatment of 6,000 L/hr of contaminated water through each system under the baseline scenario

[c.] Base case scenario assumed where changeout criteria is dictated by PFSA detection

[d.] Value for regenerable AER refers to the number of regeneration cycles per year as sorbent is reused after regeneration

[e.] AER and GAC operated as single-use are disposed of via hazardous waste incineration. Regenerable AER is subjected to brine + cosolvent to displace PFASs. GAC thermal regeneration is operated as hazardous at an offsite facility

Remediation System 2 was also a lead-lag series of adsorber vessels packed with regenerable AER-derived from polystyrene-based AER, but adsorber vessels were larger, sized to provide 3-min of EBCT, as recommended by suppliers. Upon breakthrough, PFAS-contaminated resin was regenerated using a salt brine/methanol co-solvent mixture (e.g., 70% methanol with 1 wt% NaCl), regenerated for 10 BVs at a 30-min EBCT to achieve complete regeneration. Recovery of the organic cosolvent was accomplished using a distillation module that is assumed to recover 80% of the solvent for reuse without enabling back-contamination of PFAS. Still bottoms containing the remaining cosolvent and aqueous brine were then transported offsite for hazardous waste incineration, and the freshly regenerated resin is flushed with 10 BVs of water to clear all regenerant solution out of the media.

The two anion exchange systems were compared to GAC adsorption systems, also designed and operated based upon recent field pilot treatment data. The general design of *Remediation System 3* was similar to *Remediation System 1* in that the adsorption media was considered to be single-use, with exhausted GAC being replaced with virgin GAC upon breakthrough, and being disposed of off-site by hazardous waste incineration. Spent GAC at some source zone remediation sites may be too heavily contaminated to be included in a recirculating pool of media undergoing off-site thermal regeneration, so must be disposed of after a single use. The GAC was assumed to be derived from bituminous coal and sourced from the manufacturer, and individual adsorber beds were sized to provide the recommended 10-min EBCT.

Remediation System 4 was comparable in design to Remediation System 3, except that the PFAS-contaminated GAC was transported off-site for thermal regeneration upon breakthrough. Thermal regeneration of GAC is much less energy intensive than incineration because the process is typically performed at lower temperatures of ~815°C compared to hazardous waste incineration temperatures of ~1200°C (Liu and Wagner, 1985; Long et al., 2021). 10% of the media is assumed to be lost to material volatilization in each reactivation cycle. Because this reactivation is modeled to be offsite, the GAC in this system is treated as fungible, meaning GAC sent to the site in each cycle may not be the exact same mix of GAC previously sent offsite for thermal reactivation.

Pilot system treatment data. Changeout or regeneration frequencies of individual media were estimated using field data collected in two recent pilot studies treating groundwater impacted by AFFF. **Table 2.10.3** summarizes the resulting bed volumes to breakthrough estimated for each media when using different PFAS breakthrough criteria. Single-use and regenerable AER breakthrough was estimated from pilot system treatment data collected at the Willow Grove, PA site (Ellis et al., 2022), where total PFAS concentrations in the untreated groundwater ranged from 30 – 55 μg/L. As all three single-use AERs exhibited similar performance, breakthrough data and Thomas-model fits of breakthrough data for CalRes 2301, a macroporous polystyrene resin functionalized with tributylamine, was chosen to represent the single-use AERs in *Remediation System 1*. Breakthrough data and model fits for Purolite A520E, a macroporous polystyrene resin with triethylamine functional groups, was selected to estimate regeneration frequencies for regenerable AER in *Remediation System 2*.

GAC adsorption was not included in the remediation pilot study conducted at the Willow Grove site, so media changeout frequency was estimated by comparing the relative performance of Calgon F400 with CalRes 2301 observed in another field pilot study (Liu et al., 2022). An earlier pilot study at the same site showed Calgon F400 to be the best-performing GAC media (Liu et al., 2019). While PFAS concentrations in sourcewater used in these pilots (150 – 250 ng/L), a drinking water utility's sourcewater, were much dilute than concentrations treated at the Willow Grove remediation site (30 – 50 μg/L), observed volumes of treated water before breakthrough were similar at both sites for CalRes 2301. Thus, by inference, we used breakthrough data and Thomas model fits of breakthrough data for Calgon F400 to estimate GAC media usage in *Remediation Systems 3* and *4*. A more detailed summary of the data aggregated from the field pilot systems and a detailed description of the process used to estimate media changeout/regeneration frequency is provided in Section S1 of the Supporting Information (SI).

Life cycle inventory. Each of the four treatment systems modeled in this study are constructed by aggregating every constituent product and process utilized across the entire lifespan of the system to create a life cycle inventory (LCI). These products and processes are added as inventory items, each intrinsically linked to all constituent processes needed to produce the item and all emission quantities associated with those processes. Because analyses were conducted from cradle to grave, all capital infrastructure was included with their quantities allocated over the 20-year operational lifetime of the system. Where possible, LCA quantities were chosen based on literature value ranges and from consulting industry experts, but informed assumptions were made where data was unavailable.

Table 2.10.3. Estimated BVs and MURs for each remediation system across a range of PFAS breakthrough criteria. From Ellis et al. (2023).

	Bed Volumes until Breakthrough			Media Usage Rate (g/m^3)		
Criteria	Single-Use AER	Regenerable AER	GAC[b]	Single-Use AER	Regenerable AER[c]	GAC[b]
Detection of any PFAS[d]	6,000	6,000	4,500	112.5	0.79	120.0
PFHxA Detection[d]	61,400	6,000	10,700	11.0	0.79	50.5
PFOS + PFOA Detection[d]	162,200	31,200	13,000	4.2	0.79	41.5
PFSA Detection[d]	182,400	51,400	10,700	3.7	0.79	50.5
PFOS Detection[d]	---[f]	91,700	28,100	---	0.79	19.2
10% UCMR3[e]	155,200	21,100	11,700	4.3	0.79	46.2
10% PFHxA[e]	86,800	31,200	12,100	7.8	0.79	44.6
10% PFOA[e]	197,200	31,200	19,800	3.4	0.79	27.3
10% PFHxS[e]	266,900	116,900	20,800	2.5	0.79	26.0
10% PFOS[e]	422,000	210,000	28,100	1.6	0.79	19.2
50% PFHxA[e]	102,000	31,200	20,800	6.6	0.79	26.0
50% PFOA[e]	362,000	41,300	43,200	1.9	0.79	12.5
50% PFHxS[e]	700,000	167,300	45,200	1.0	0.79	11.9
50% PFOS[e]	1,180,000	730,000	48,900	0.6	0.79	11.0

[a.] Estimated values assume treatment of 6,000 L/hr at design contact times. Values are derived from field pilot data.

[b.] Bed volume estimates for GAC determined from raw data and Thomas Model fit curves from Liu et al., 2022 and serve as conservative estimates for PFAS elution at a high-concentration source zone (as total sourcewater PFASs are far lower than those in Ellis et al., 2022.

[c.] Media usage rates for the regenerable AER system assume bed replacement every 5 years of operation, and do not correspond to the changing regeneration frequency that accompanies changes in breakthrough criteria

[d.] Detection criteria are obtained from raw breakthrough data as defined by the first detectable concentration over time

[e.] Criteria involving % breakthrough determined by the moment fitted Thomas Model elution curves exceed the criteria (Ellis et al., 2022)

[f.] PFOS remained at non-detect levels through the entirety of the field pilot (at a 2-min EBCT), thus calculation of MUR is precluded

Life cycle environmental impacts. The USEPA's TRACI 2.1 (Tool for Reduction and Assessment of Chemicals and Other Environmental Impacts) impact assessment model was used in conjunction with BEES 2.0 (Building for Environmental and Economic Sustainability) to convert life cycle inventory items into associated environmental impacts. Selection of all inventory items and the assessment of environmental impact using TRACI was conducted using SimaPro

v9.1 (PhD version, © PRé Sustainability) software. Grouping all impacts by their impact categories enables a straightforward assessment of the extent to which the environment is impacted by chemical releases. Impact categories specified by TRACI include ozone depletion (kg CFC-11 eq), global warming (kg CO_2 eq), smog formation (kg O_3 eq), acidification (kg SO_2 eq), eutrophication (kg N eq), human toxicity - carcinogens (CTUh), human toxicity – non-carcinogens (CTUh), respiratory effects (kg PM2.5 eq), ecotoxicity (CTUe), and fossil fuel depletion (MJ surplus). A complete description of all categories and their associated units is included in Section S3 of the SI.

Environmental impact data are presented in this study as scaled characterization values and normalized characterization values in line with existing LCA studies (Crenna et al., 2019; Boyer et al., 2021). Scaled values utilize the highest magnitude of impact among all systems in each impact category as a benchmark of '100%,' with values from the remaining systems scaled down between 0 and 100%. This scaling is performed for each category to normalize the y-axis, as every category has different units that cannot be directly compared. Conversely, data presented as normalized values are converted from various units of impact (e.g., kg CO_2) to units of 'person-years,' which reference the emissions of the average U.S. citizen in 2008 as the reference point for normalization (Ryberg et al., 2014).

Life cycle costing. The life cycle inventory for each remediation system was also used to estimate lifetime costs for treatment, both in terms of real dollars and on a per-unit-volume treated basis ($ per m^3 treated). Unit costs for consumables including sorbent media and solvents were obtained from industrial suppliers, while the costs for treatment infrastructure were estimated using the EPA-derived work breakdown structure (WBS) (U.S. EPA, 2022). AERs and GAC use different variations of this tool as iterations of the WBS exist for many different treatment technologies, but identical or equivalent items were chosen for all three technologies wherever possible. Additional expenses – particularly labor costs including O&M as well as service fees for transport and incineration – have been estimated from discussions with consulting firms and environmental service providers. While these service-related expenses are subject to greater uncertainties, and the estimated sum of unit costs may greatly exceed those when operators enter long-term service agreements where many unit operations are packaged together with fixed labor and analytical costs, we anticipate that the relative costs differences among the remediation systems would prove to be similar across a diverse range of treatment operations.

Assumptions and sensitivity analysis for ion exchange treatment. After evaluating the life cycle environmental impacts and costs for anion exchange and GAC adsorption systems under the baseline scenario, more detailed sensitivity analysis was conducted for each system to identify design and operational factors that have the greatest effects on estimated outcomes. A one-at-a-time sensitivity analysis was conducted by varying input quantities in the life cycle inventory (LCI) where assumptions were made in the model. These include variables like regenerant solution fractions (e.g., % organic cosolvent), bed volumes needed for regeneration, transport distance to the site from media suppliers. Where applicable, minimum and maximum reasonable values were chosen to constrain the range of input quantities (e.g., 50-95% organic cosolvent). For each input variation, the relative change in overall system environmental impact was quantified for each category to determine system sensitivity to each individual input.

Additionally, the sensitivity of each system to specific inventory item selection was examined by selecting different input items in the model where non-quantitative decision-making is necessary. Modeling of waste disposal is one such area, as numerous inventory items may be selected to model incineration, both in terms of disposal temperature (i.e., hazardous incineration or non-hazardous) and material-specific options (general incineration vs spent solvent mixture vs municipal incineration of resin). For *Remediation Systems 1* and *3*, emphasis was given to the temperature of incineration, while *System 2* focused on exploring material-specific options to best reflect disposal of a liquid waste stream. Other item-specific sensitivity options include the type of organic cosolvent, transportation options, and energy options for regenerant pumping and cosolvent distillation.

3. Results and Discussion

3.1 Screening of Resin Adsorbents for PFAS Adsorption

This section describes work aimed at characterizing the effectiveness of 13 commercially available resins (8 anion exchange resins, 2 cation exchange resins, and 3 non-ionic resins) in comparison to granular activated carbon (GAC) for adsorption of a wide range of PFASs present in an AFFF, including many structures identified through recent compound discovery efforts. Kinetic data were collected to establish the time required for resins to reach equilibrium with quantifiable PFAAs present in AFFF, then equilibrium adsorption was determined to assess resin adsorption capacities and the influences of resin properties and PFAS structure on adsorption affinity. Furthermore, resins were examined for adsorption of 63 additional PFASs, including polyfluorinated compounds, detected in the AFFF suspect screening analysis. Semi-quantitative methods recently developed were applied to estimate concentrations and adsorption affinity parameters for these structures, significantly expanding the data and providing improved insights into the structural factors controlling PFAS treatment with resin adsorbents.

PFAS composition in AFFF. A total of 12 target PFASs (all PFAAs) were identified in the diluted AFFF solution (from a target analyte list of 48 PFASs) (**Table 3.1.1**). Five compounds are perfluoroalkyl carboxylic acids (PFCAs), six are perfluoroalkyl sulfonic acids (PFSAs), and one is a chloro-perfluoroalkyl sulfonic acid (Cl-PFSA). Concentrations of these PFASs in the 1-to-93,000-fold diluted AFFF ranged from 0.74 µg/L (PFBA) to 97.7 µg/L (PFOS), with a sum total concentration of 137 µg/L. Collectively, these concentrations fall towards the high end of PFAS concentrations measured in groundwater near AFFF-impacted sites (Backe et al., 2013), but concentrations are high enough to enable quantification of most target compounds in solution following equilibration with the resin adsorbents.

Besides the targeted analytes, 63 additional PFASs were identified through LC-QToF-MS suspect screening analysis (**Table A3.1.3** in the appendix). The suspect PFASs are categorized into 21 different classes based on their perfluoroalkyl tails and nonfluorinated head groups; structural information for each suspect PFAS class was adopted from previous compound discovery work (Barzen-Hanson et al., 2017, D'Agostino et al., 2014, Rotander et al., 2015). This includes 22 analytes detected by both electrospray ionization negative (ESI-) and positive (ESI+) modes, 30 by ESI- only, and 11 by ESI+ only. The majority of the suspect analytes in this AFFF contain head groups derived from sulfonic acids, consistent with AFFF manufactured by electrochemical fluorination (ECF) (Buck et al., 2011). With respect to resin treatment, headgroup ionic charge is expected to be a critical parameter. SPARC (Archem LLC) was used to estimate the prevailing charges of the headgroups at pH conditions used in this study (pH 8.3). While most of the suspect analytes, are expected to be negatively charged, several structures were predicted to be zwitterions at pH 8.3, and four structures were predicted to be cationic.

Most of the suspect analytes have concentrations estimated by semi-quantification protocols (Nickerson et al., 2020) to be <1 µg/L in the diluted AFFF, but 21 have concentrations estimated to range from 1 to 13.4 µg/L. Collectively, the estimated concentration of all 63 suspect analytes was 91 µg/L, which is comparable to 137 µg/L for the 12 target analytes. Together, the target analytes and suspect structures are estimated to contribute 129 µg/L fluorine content to the diluted AFFF, accounting for 88% of the total fluorine content measured by ^{19}F-NMR.

Table 3.1.1 PFASs detected in 1-to-93,000 fold diluted AFFF by targeted LC-QToF-MS analysis and PFOS capacity for each AER. From Fang et al. (2021).

Compound class and structure	*n*	*Compound Acronym*	C_0 *(μg/L)*	*Log* (K_{ex})								
				A300	A520E	A532E	A600E	A860	PFA694E	CalRes 2301	CalRes 2304
Perfluoroalkyl carboxylic acids (PFCAs)	3	**PFBA**	0.74±0.01	1.26±0.01	1.61±0.02	2.55±0.01	1.33±0.02	0.88±0.02	2.69±0.01	2.58±0.00	2.56±0.01
	4	**PFPeA**	1.20±0.02	1.75±0.01	1.96±0.02	2.95±0.03	1.62±0.02	0.97±0.00	2.77±0.02	2.86±0.04	2.71±0.03
	5	**PFHxA**	3.23±0.05	2.00±0.00	2.32±0.04	3.51±0.02	1.96±0.04	1.03±0.01	3.30±0.04	3.31±0.02	3.25±0.04
	6	**PFHpA**	0.91±0	2.31±0.01	2.86±0.04	3.74±0.00	2.41±0.04	1.17±0.01	3.53±0.00	3.55±0.00	3.52±0.00
	7	**PFOA**	3.38±0.01	2.51±0.00	3.33±0.05	4.47±0.00	3.04±0.04	1.48±0.01	4.36±0.00	4.29±0.00	4.17±0.00
Perfluoroalkyl sulfonic acids (PFSAs)	3	**PFPrS**	1.86±0.03	2.87±0.06	2.68±0.01	4.10±0.01	2.36±0.02	1.06±0.01	3.94±0.02	3.90±0.04	3.84±0.03
	4	**PFBS**	3.46±0.02	3.01±0.07	3.02±0.04	4.41±0.02	2.65±0.06	1.18±0.01	4.25±0.03	4.32±0.07	4.15±0.01
	5	**PFPeS**	3.23±0.04	3.21±0.05	3.47±0.05	4.76±0.00	3.07±0.03	1.40±0.01	4.60±0.06	4.59±0.05	4.51±0.04
	6	**PFHxS**	16.5±0.10	3.36±0.01	3.80±0.03	5.56±0.06	3.65±0.04	1.62±0.01	5.41±0.00	6.09±0.04	5.19±0.04
	7	**PFHpS**	1.86±0.01	3.75±0.06	4.12±0.03	4.97±0.02	3.78±0.02	2.35±0.09	4.81±0.00	4.84±0.00	5.07±0.00
	8	**PFOS**	97.7±0.73	3.71±0.04	5.96±0.00	7.16±0.00	4.60±0.05	3.09±0.03	6.98±0.00	6.92±0.04	6.83±0.00
Chloro-perfluoroalkyl sulfonic acids (Cl-PFSA)[a]	8	**Cl-PFOS**	2.04±0.03	3.93±0.02	4.53±0.00	5.41±0.00	3.86±0.00	3.19±0.04	4.96±0.00	5.11±0.00	5.21±0.00
				A300	A520E	A532E	A600E	A860	PFA694E	CalRes 2301	CalRes 2304
PFOS capacity (μmol/mg)				0.27±0.01[b]	1.36±0.06[b]	0.07±0.04[c]	0.26±0.01[b]	0.88±0.04[b]	0.08±0.01[c]	0.66±0.03[b]	0.04±0.02[c]
$PFOS_{capacity}/Cl^-_{capacity}$ (%)				17.06	114.03[d]	6.08	12.81	83.14	6.17	56.98	3.45

[a] Class structure is presented in the Appendix
[b] Calculated based on the Langmuir isotherm model
[c] Calculated based on the averaged capacity points near the plateau of each resin.
[d] The larger PFOS capacity is likely a result of the uncertainly existed in the manufacturer's Cl^- capacity data

Establishing adsorption equilibria for PFAAs in AFFF. Because a major objective of the study was to characterize equilibrium adsorption of AFFF-derived PFASs to resins, it was important to assess adsorption kinetics in batch reactors to identify an appropriate minimum time for equilibration. Timecourse data for adsorption of the 12 target PFAAs in AFFF was monitored for a period of 10 days in suspensions of the AERs and GAC (**Figure 3.1.1**). These results indicate that most adsorbents showed higher adsorption percentage for PFSAs (10-90%) after 1 day compared to PFCAs (5-65%), but equilibrium for both classes of PFAAs is generally reached within 5 days. Such results agree with the equilibration time observed by other resin/PFAS studies (Zaggia et al., 2016, Deng et al., 2010). However, because the residual PFAS aqueous concentrations can continue to drop for a longer period of time even when >95% adsorption has occurred (Park et al., 2020), a 10-day equilibration time was used for subsequent experiments to ensure PFAS equilibrium with the resins. Furthermore, initial concentrations remained unchanged in resin-free control reactors, consistent with the reported recalcitrance of PFAAs to degradation (Prevedouros et al., 2006, Houde et al., 2006, Remde et al., 1996, Nancy et al., 2016).

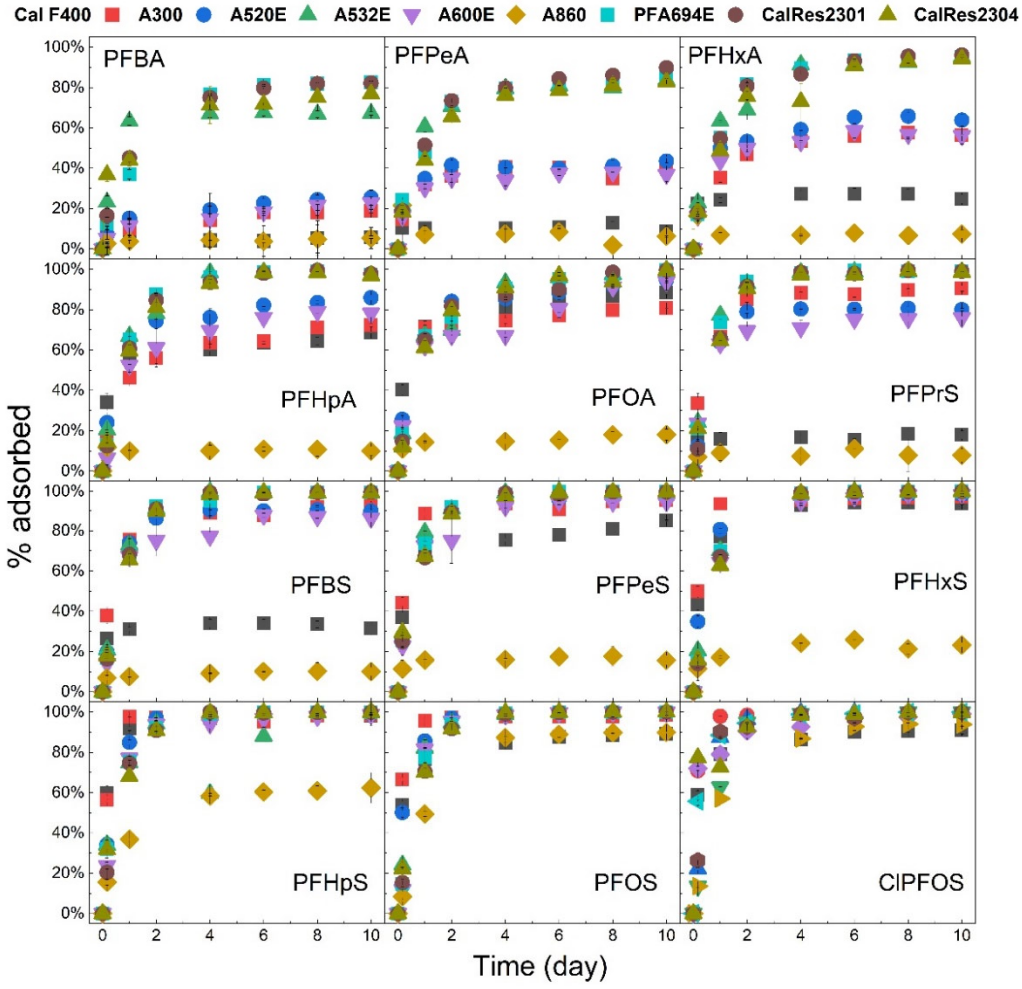

Figure 3.1.1. Time courses for the adsorption of 12 PFAAs in the presence of nine adsorbents. Reaction conditions: Individual PFAA's initial concentration is provided in Table 3.1.1, 50 mg/L adsorbent, pH 8.3 (1 mM $NaHCO_3$ + 5 mM NaCl), room temperature. Error bars represent min/max values of duplicate experiments. From Fang et al. (2021).

Further, since our intention was to quantify adsorption equilibrium for individual PFASs present in the AFFF mixture containing many other constituents, including co-solvents, hydrocarbon surfactants, and PFASs not measured by the QToF-MS method, it was important to verify that the presence of these other constituents did not significantly affect the adsorption behavior of individual PFASs (i.e., that adsorption to resin sites is non-competitive). To confirm this, we measured the adsorption of six PFAAs (PFBA, PFHxA, PFOA, PFBS, PFHxS, and PFOS) after spiking from purified reagents into suspensions of selected AER at the same initial concentrations measured in the diluted AFFF. The extent of adsorption for all six PFAAs measured after 4 h, 1 d, and 10 d was comparable to values measured in experiments where diluted AFFF was equilibrated with the same resins (**Figure 3.1.2**). This provides validation for the measurements of individual PFASs conducted in the diluted AFFF mixtures. The non-competitive nature of the adsorption process is also consistent with the fact that the total concentration of ion exchange sites in the resin suspensions (≥50 µM for 50 mg resin per liter) was much greater than the total PFAS concentration in diluted AFFF estimated from targeted and suspect screening analysis (0.5 µM).

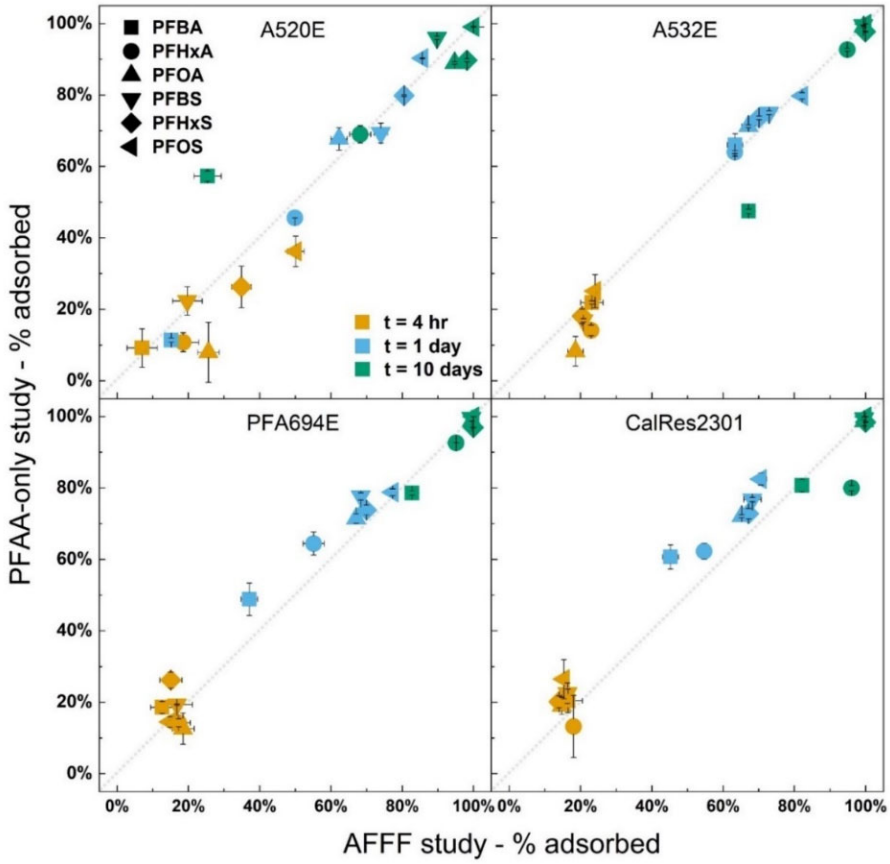

Figure 3.1.2. Close agreement between PFAA adsorption data measured in PFAA-only experiments and diluted AFFF experiments with 4 AERs. Supernatant samples collected for analysis after 4 h, 1 d, and 10 d of reaction. Reaction conditions: Initial PFAA concentrations provided in Table 3.1.1, 50 mg/L resin, pH 8.3 (1 mM $NaHCO_3$ + 5 mM NaCl), room temperature. Dashed line shows 1:1 correlation of results for the two experiments. Error bars represent min/max values of duplicate experiments. Symbol shapes correspond to individual PFAAs, and symbol colors correspond to different reaction times. From Fang et al. (2021).

Equilibrium adsorption of target PFAAs. **Figures 3.1.3** and **Table A3.1.2** in the appendix show the extent of adsorption of the target PFAAs measured after equilibration for 10 d with all the resins listed in **Table 2.2.1** (50 mg/L resin). Whereas significant adsorption of the PFAAs was observed for all the AERs examined (**Figure 3.1.3a-b**), minimal adsorption was observed to the CERs and NIRs (**Figure 3.1.3c**; <20% adsorbed in most cases). These trends are consistent with the anionic nature of the PFAAs. As reported previously, the extent of PFCA and PFSA adsorption to the AERs increased with increasing perfluoroalkyl chain length, and PFSAs adsorbed more strongly than PFCAs of comparable perfluoroalkyl chain length (Zaggia et al., 2016, Higgins et al., 2006, Laura del Moral et al., 2020). Adsorption to the PFAS-specific AERs (PAERs) was generally greater than to the regenerable AERs, especially for the shorter-chain analogues. Among the AERs, PFAA adsorption to A860 was significantly weaker than the other resins, which was notable in that this was the only resin examined with a polyacrylic base polymer (all others were polystyrene). This outcome agrees with the result of a recent study where the adsorption percentage of PFAAs were much lower for polyacrylic AERs compared to polystyrene AERs (Laura del Moral et al., 2020). Since activated carbon surfaces are generally non-polar, GAC was found to be more effective in adsorbing the longer-chain PFASs that are more hydrophobic than the shorter-chain analogues (Xiao et al., 2017, Du et al., 2014). With the exception of the A860 resin, greater adsorption of the PFAAs was generally observed for the same mass loadings of AER than for GAC.

The maximum capacity for PFOS adsorption was evaluated for each resin and compared to reported capacities for Cl^- adsorption (**Table 3.1.2** and **Figure 3.1.4**). The measured PFOS capacities at different initial concentration for gel-type resins (e.g., A520E and PFA694E) showed similar values when measured after 10 days (0.37 and 0.072 µmol/mg for A520E and PFA694E, respectively) and 150 days (0.38 and 0.078 µmol/mg for A520E and PFA694E, respectively) of equilibration, indicating adsorption equilibrium is reached within 10 days (see **Table 3.1.1**). Results from these experiments showed much higher PFOS capacities for the macroporous AERs (0.66-1.36 µmol/mg) compared to the gel-type AERs (0.04-0.27 µmol/mg). Whereas the PFOS capacities for macroporous resins were within a factor of 2 of the reported Cl^- capacities (57–114%), PFOS capacities for the gel-type resins were a much smaller percentage of the Cl^- capacities (3-17%), consistent with exclusion from internal exchange sites.

Anion exchange equilibria can be modelled as a surface exchange reaction between the aqueous target anion (e.g., individual PFAS anion) and the mobile counterion pre-adsorbed on the resin (e.g., adsorbed Cl^-),

$$PFAS_{aq} + Cl^-_{ads} \rightleftharpoons PFAS_{ads} + Cl^-_{aq} \qquad (3.1.1)$$

where $PFAS_{aq}$ and Cl^-_{aq} are the aqueous concentration of PFAS and Cl^- (µg/L) and $PFAS_{ads}$ and Cl^-_{ads} are the amount of PFAS and Cl^- adsorbed onto a resin (µg/mg) after 10 days. The selectivity coefficient (K_{ex}) then relates the ratios of adsorbed and aqueous anions at equilibrium:

$$K_{ex} = \frac{[PFAS]_{ads}[Cl^-]_{aq}}{[Cl^-]_{ads}[PFAS]_{aq}} \qquad (3.1.2)$$

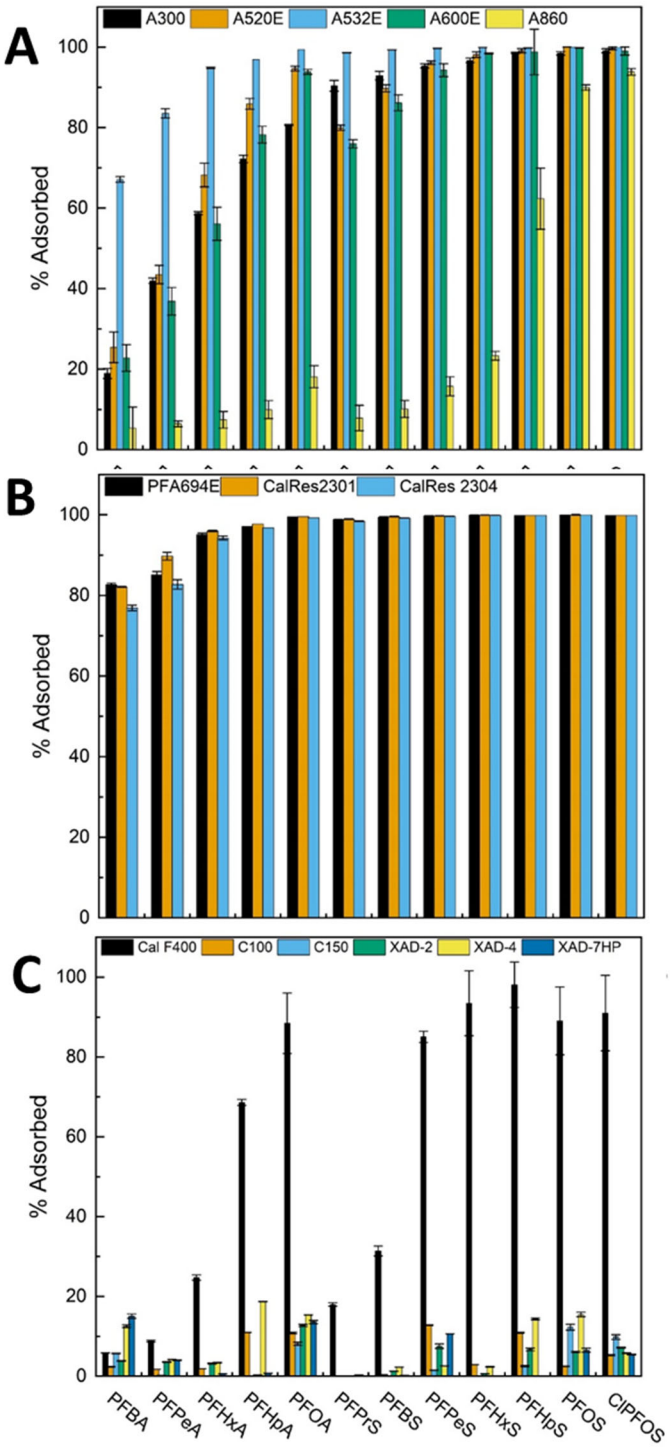

Figure 3.1.3. Extent of equilibrium adsorption of target PFAAs in 1-to-93,000 fold diluted AFFF to (a) regenerable AERs, (b) PFAS-selective AERs, (c) GAC (Cal F400), two CERs (C100, C150), and three NIRs (XAD-2, XAD-4, XAD-7HP). Initial PFAA concentrations provided in Table 3.1.1, 50 mg/L resin, pH 8.3 (1 mM $NaHCO_3$ + 5 mM NaCl), room temperature, t = 10 d. Error bars represent min/max values from duplicate experiments. From Fang et al. (2021).

The ratio of aqueous to adsorbed Cl^- ions was fixed by maintaining a large excess of chloride in the solution phase (5 mM NaCl as background electrolyte) and providing a large excess of resin sites relative to the PFASs present in the diluted AFFF solutions (50 mg/L AER initially possess 55-90 µM exchange sites occupied by Cl^- versus ~0.5 µM total PFASs in the diluted AFFF solution). It follows then that the PFAA adsorption data can be used to determine K_{ex} values for each of the PFAA-AER combinations (**Table 3.1.1**). It is worth noting that the K_{ex} values of a resin towards PFASs is independent of its maximum available PFAS capacity because isotherm derived PFAS capacities only represent a resin's maximum number of sites that can be occupied by PFAS molecules rather than the selectivity of that PFAS towards the resin. Examination of the resulting selectivity coefficients shows more than 6 orders-of-magnitude variations among the PFAA-resin combinations, ranging from $10^{0.7}$ (PFBA adsorbing on A860) to $10^{6.9}$ (PFOS adsorbing on PFA694E and CalRes2301). The K_{ex} values at the higher end of this range reflect the high selectivity of AER for adsorbing PFASs over inorganic anions like Cl^-.

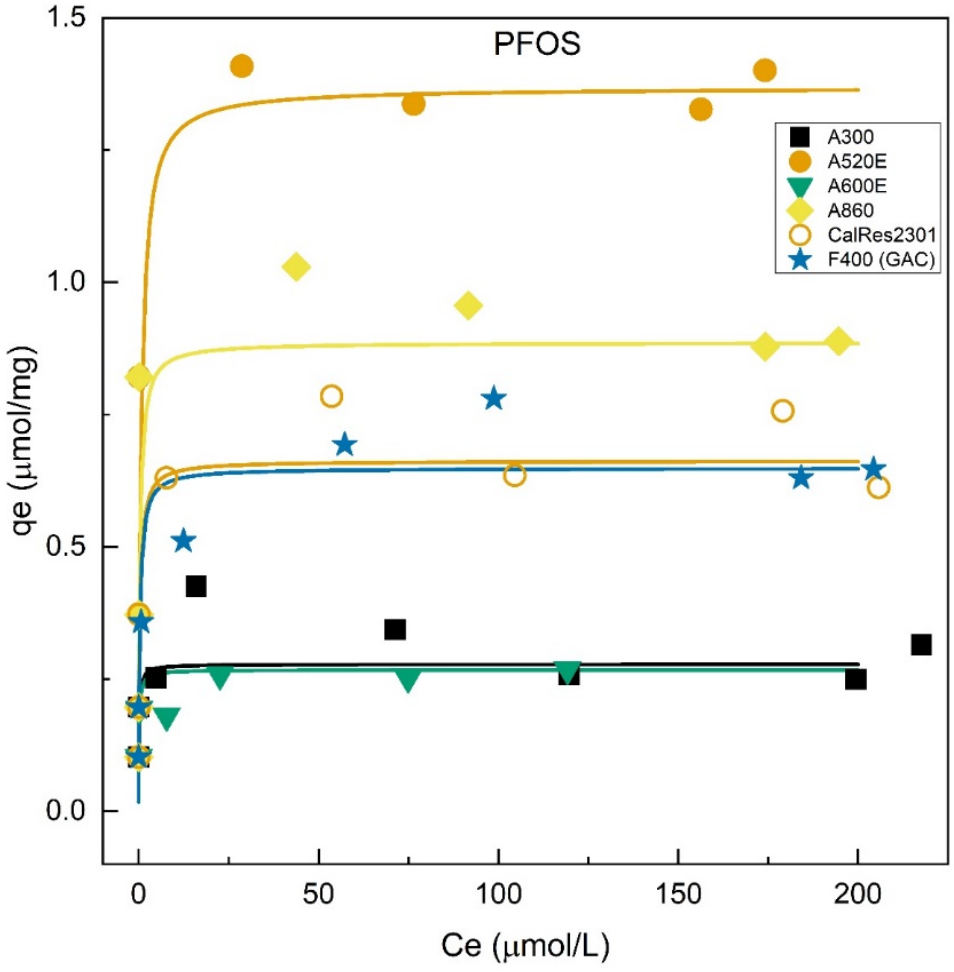

Figure 3.1.4. Adsorption profile of 9 adsorbents in reactors with varying PFOS concentration. Reaction conditions: 40 mg/L adsorbent, pH 8.3 (1 mM $NaHCO_3$ + 5 mM NaCl), room temperature. Solid lines represent model fit of eq S2 (r^2 > 95±3%). Isotherm fits were not performed for A532E, PFA694E, and CalRes2301 due to their low PFOS capacity and limited data points. From Fang et al. (2021).

Table 3.1.2. Fit-derived Langmuir isotherm parameters and PFOS capacity for AERs and GAC. From Fang et al. (2021).

	A300	A520E	A600E	A860	CalRes2301	F400 (GAC)
Q_0 (μmol/mg)	0.27±0.01	1.36±0.06	0.26±0.01	0.88±0.04	0.66±0.03	0.64±0.03
b (L/μmol)	7.49±0.37	1.42±0.07	7.01±0.35	2.80±0.14	3.01±0.15	2.90±0.14
PFOS capacity [a] (μmol/mg)	0.30±0.06	1.36±0.04	0.23±0.04	0.91±0.08	0.68±0.08	0.65±0.09

[a]Estimated from the plateau points of each AER and GAC. The averaged capacity was found identical or similar to the values calculated using the Langmuir model

Examination of the K_{ex} values reveals a number of notable trends. First, consistent with the adsorption data presented in **Figure 3.1.3** and previous reports (McCleaf et al., 2017, Zaggia et al., 2015, Higgins et al., 2006, Laura del Moral, 2020), we generally find that perfluoroalkyl sulfonic acids have larger K_{ex} values for a given resin than the corresponding carboxylic acid. The average logK_{ex} increase from a PFSA to a PFCA with equal chain length ranged from 0.82 to 2.02. This outcome agrees with a past study where the selectivity coefficients for adsorption of benzenesulfonate ($C_6H_5SO_3^-$) were found to be greater than for benzoate ($C_6H_5COO^-$) when examining adsorption to strong base AERs with Type I and Type II quaternary ammonium functional groups. It follows that the higher selectivity of sulfonates towards AERs is likely the result of the stronger negative inductive effect compared to carboxylates due to its resonance structure with one more oxygen atom. Through DFT calculations, Park et al. (2020) discovered that sulfonic PFASs can induce greater negative atomic charges per unit oxygen than carboxylic PFASs due to resonance stabilization. This increased negative atomic charge per oxygen and the additional oxygen atom in the sulfonate head group significantly increases the total negative charge of the headgroup interacting with the cationic amine surface functional groups on the resin (Park et al., 2020). Within each PFAA class, the K_{ex} values also increase with increasing perfluoroalkyl acid chain length (**Figure 3.1.5**). The average logK_{ex} change per CF_2 group is found ranged between 0.14 -0.65 for the studied AERs. This trend is consistent with favorable polymer interactions with longer-chain PFAAs and polar head groups that contribute to increased hydrophobicity (Higgins et al., 2006).

The importance of non-electrostatic contributions to PFAA adsorption is further highlighted by the much wider range in K_{ex} values observed across the 8 AERs for individual PFAAs that exhibit greater hydrophobicity (**Figure 3.1.5**). For example, while little variation among the AER is observed for K_{ex} values obtained for PFBA ($0.73 \leq \log K_{ex} \leq 2.30$), nearly 4 orders-of-magnitude variation is observed for PFOS ($2.93 \leq \log K_{ex} \leq 6.91$). This is consistent with the reported observation that short-chain PFAAs tend to still break through rapidly for PFAS-selective AERs in the field even though breakthrough volumes for longer-chain PFASs can be extended significantly in comparison to non-selective AER.

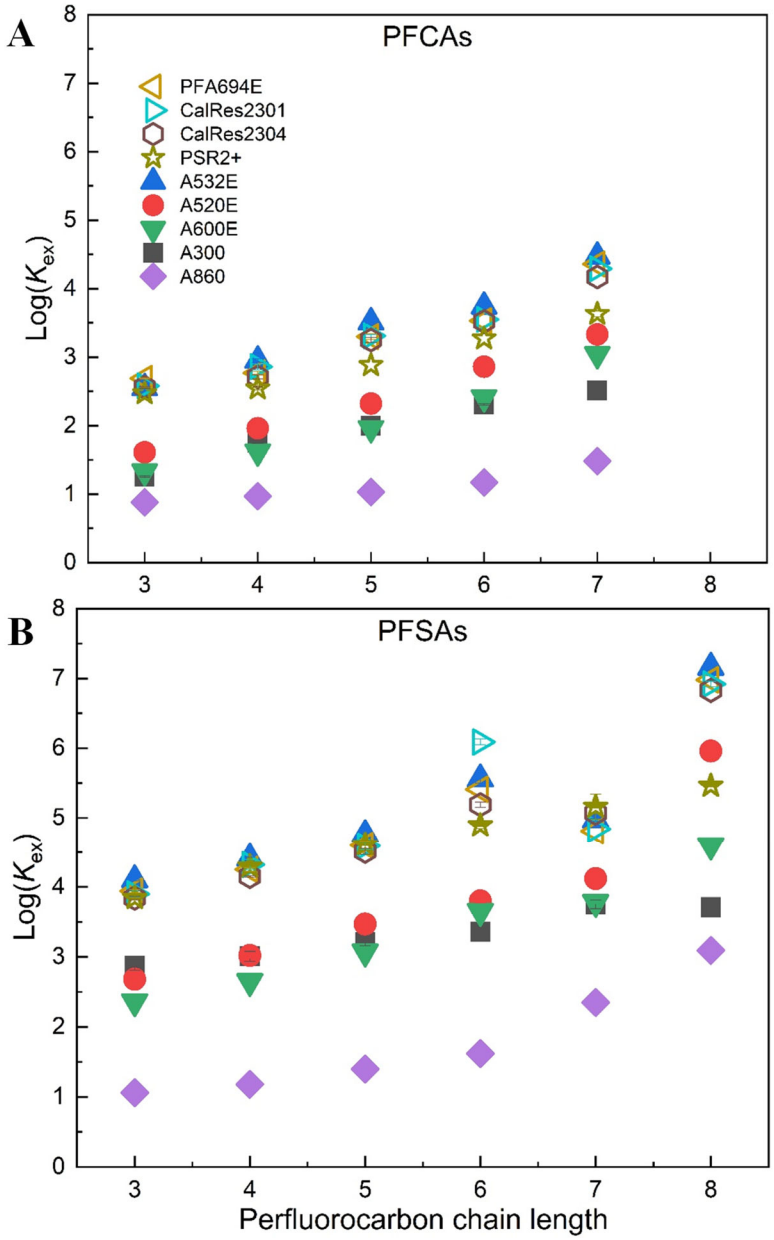

Figure 3.1.5. Effect of perfluoroalkyl carbon chain length and polar head group identity on the PFAS/Cl^- selectivity coefficients (eq 3.1.2) of 8 AERs for (a) PFCAs and (b) PFSAs. Open symbols represent PAERs, filled symbols represent regenerable AERs. Error bars representing min/max values from duplicate experiments are smaller than the size of the symbols shown. From Fang et al. (2021).

A number of notable trends are also revealed by collectively comparing K_{ex} values for the full range of target PFAAs among AERs. A cross-correlation analysis among resins (**Figure 3.1.6A**) can be useful for visualizing these differences and help to identify AER properties that influence K_{ex} values. This comparison reveals the superior performance of selected resins, in particular the PFAS-selective AERs over the non-selective AERs. Beyond this, comparison among resins reveals the importance of other resin properties to PFAA adsorption. For example, the cross-correlation

reveals that A860 exhibited the lowest affinity for the target PFAAs among the eight AERs, with average logK_{ex} values that negatively deviated most from the other resins. The AERs examined differ in three major aspects: polymer matrix, porosity, and functional group. Among the AERs, A860 is the only resin with a polyacrylic matrix. The other AERs all contain a more hydrophobic polystyrene matrix. Comparison of A860 with A520E is most revealing since they share similar characteristics besides the polymer matrix, but the latter resin yields much larger K_{ex} and $\Delta\log K_{ex}$ values per CF_2 group for the target PFAAs (**Figure 3.1.5**). Thus, while both resins provide a similar electrostatic attraction for the PFAAs, hydrophobic interactions are muted for the more polar polyacrylic resins where their open-chain aliphatic structure containing less hydrophobic carbonyl groups (Du et al, 2015, Yu et al., 2009, Li et al, 1996). Although similar trend is observed for other organic chemicals, such as pentachlorophenol, with polyacrylic resins (Li et al, 1996), findings from this work contradict with the result of a previous study where polyacrylic AERs exhibited higher selectivity for PFOS compared to polystyrene AERs (Deng et al., 2010). This discrepancy is likely caused by differences in initial PFAS concentrations used in the studies, where the total initial PFAA concentration in the present study is ~1300 times lower than the PFOS concentration applied in the previous report (Deng et al., 2010). It follows that when PFOS is present at a higher initial concentration (i.e., mg/L level), it may not only adsorb to the resin through electrostatic interactions with charged surface functional groups and hydrophobic interactions involving the fluoroalkyl tail, but also may accumulate within the resin pores via formation of micellar aggregates; this may be more important for acrylate-based AERs due to their higher polarity in comparison to styrene-based AERs (Schuricht et al., 2017). That said, such phenomena is not expected to be an important mechanism for PFAS uptake at more environmentally relevant concentrations (i.e., ng/L to µg/L levels). In general, hydrophobic polystyrene resins have a much greater affinity for adsorption of PFASs than do polyacrylic reins (Laura del Moral et al., 2020, Li et al., 1998), and this is supported by the fact that all of the merging PFAS-selective resins being introduced by manufacturers contain a polystyrene, rather than polyacrylic, matrix.

The importance of AER functional group was assessed by comparing three AERs that possess the same porosity and polymer matrix but different functional groups (A300, A532E, and A600E). Comparison between the three resins shows that, while A300 and A600E yield similar logK_{ex} values for the PFAAs, A532E yields much larger values, with average logK_{ex} values being 1.45 units higher than those measured for the other two resins. This higher selectivity of A532E is also reflected in its $\Delta\log K_{ex}$ values per CF_2 group compared to the other two resins (**Figure 3.1.5**). The greater affinity of A532E might be attributable to its non-traditional bifunctional structure containing two types of quaternary amine groups, one with long alkyl chains (4-6 carbons) and another with short alkyl chains (2-3 carbons) (Zaggia et al., 2016). In comparison, A600E and A300 are functionalized only with less hydrophobic amine groups. A600E contains trimethylammonium groups, whereas A300 has one of the methyl groups substituted with an ethanol group, further reducing resin hydrophobicity (SenGupta, 2017). Thus, while all three resins provide similar electrostatic interactions with PFAAs, the functional groups in A532E provide additional hydrophobicity that enhances adsorption of PFAAs, especially the longer-chain analogues. Although there is limited information available for the functional groups of PFA964E, its similarity in logK_{ex} values with A532E suggests it share similar physical characteristics where more hydrophobic moieties are utilized.

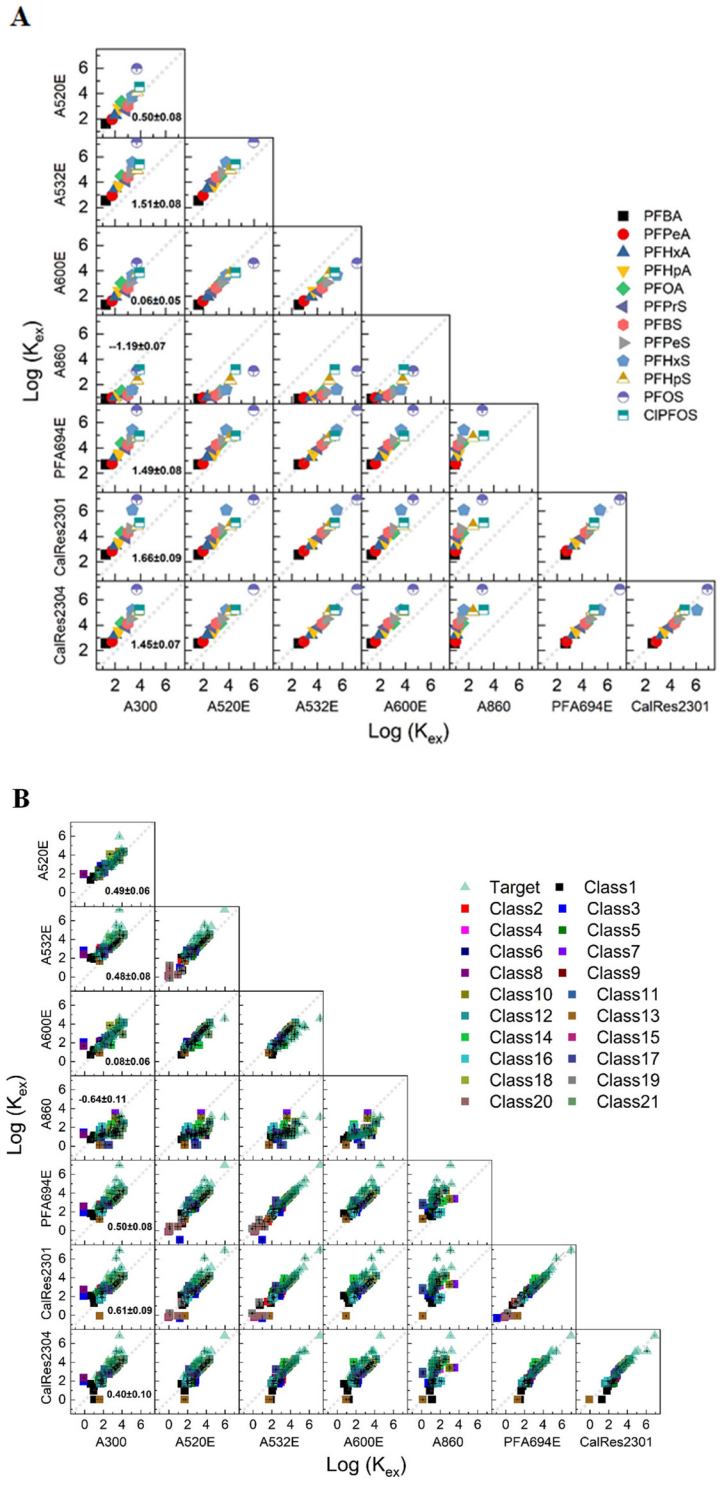

Figure 3.1.6. Cross-correlation comparison of PFAS/Cl⁻ selectivity coefficients (eq 3.1.1) of seven AERs between (a) 12 PFAAs analyzed by targeted analysis, and (b) the targeted PFAAs plus 63 additional PFASs identified through suspect screening analysis (Classes described in the appendix). Dashed line represents 1:1 correlation between logK_{ex} values for the two resins being compared. x and y axis. Error bars representing min/max values from duplicate experiments are smaller than the size of the symbols shown. From Fang et al. (2021).

Both gel-type and macroporous AERs were examined, and the selectivity coefficients obtained for two AERs that only differ in porosity (i.e. macroporous CalRes2301 vs. gel-type CalRes2304) were found closely related to each other (i.e., their logK_{ex} values are closely aligned with the 1:1 ratio line in **Figure 3.1.6A**), with only a slight preference for the macroporous CalRes2304. Past study has shown macroporous AERs are much more selective for PFASs in systems with elevated PFAS concentration (e.g., >100 mg/L) (Zaggia et al., 2016). This suggests the role of pore size is more significant in environments where PFASs are saturating the adsorption sites of individual resin. Such result resonates with the data from earlier sections (**Table 3.1.1**) where the capacity of PFOS for macroporous AERs was found significantly higher than the gel-type AERs.

Adsorption of other PFASs to resins. In addition to anionic PFASs, zwitterionic or cationic PFASs are also important contaminants that are frequently detected in AFFF-impacted source area waters where direct PFAS treatment is required before discharging to the environment. Therefore, it is crucial to evaluate the adsorption behavior of these chemicals along with anionic PFASs in order to achieve total PFAS removal goal. By applying semi-quantitative analysis, we were able to quantify the adsorption of 63 additional PFASs identified in the AFFF (**Table A3.1.1**), including 44 structures predicted to be anionic, 4 predicted to be cationic, and 15 predicted to be zwitterionic at experimental pH conditions. To our knowledge, this is the first study that evaluated the adsorption of a diverse group of zwitterionic or cationic PFASs onto commercially available resins. **Table A3.1.3** summarizes the extent to which each of the suspect compounds was adsorbed to each of the resins and GAC. In general, regardless of predicted charge, a larger number of the suspect PFASs tended to adsorb more strongly to AERs than to CERs, NIRs or GAC.

Like the targeted PFAAs, very little adsorption of the suspect PFASs was observed for both CERs examined, including the four structures predicted to be cationic. This indicates that the selected sulfonate-functionalized CERs, unlike amine-functionalized AERs, do not exhibit inherent selectivity for PFASs relative to the bulk counterion (Na^+) present in the solutions at much higher concentrations (6 mM) than the PFASs in diluted AFFF (< 1 μM). This is despite having a similar polystyrene polymer matrix that provides for favorable non-electrostatic interactions with the PFASs.

Selected PFASs adsorb to the NIRs, in particular some of the PFASs that contain long perfluoroalkyl tails and/or are cationic and zwitterionic (e.g., AmPr-FASA, MeEtCMeAmPr-FAAD, TAmPr-FASA, and TAmPr-FASAPrA). Since NIRs are resins without actively charged functional groups, the high adsorption percentages yielded from the long chain and non-anionic PFASs are likely a result of their strong hydrophobic interaction with NIRs' nonpolar structure. This conclusion is supported by the fact that a greater extent of PFAS adsorption was observed for NIRs with more nonpolar character (e.g., XAD-2 and XAD-4) compared to the NIR with moderately polar character (e.g. XAD-7 HP).

Consistent with results already discussed for PFAAs, the majority of the suspect PFASs adsorbed to the polystyrene based AERs to a greater extent than to GAC, whereas less adsorption was observed for the polyacrylic A860 resin (**Table A3.1.3**). Selectivity coefficients for the 63 suspect PFASs were estimated by applying eq 3.1.2 to the semi-quantitative estimates of aqueous and adsorbed concentrations of each suspect PFAS (**Table A3.1.4)**, and **Figure 3.1.6B** shows the resin cross-correlation plots expanded to include both the targeted PFAAs and the suspect PFASs.

In general, the trends already noted in terms of PFAS-selective vs. non-selective AER, polymer matrix, functional group, and resin porosity hold when the suspect PFASs are added to the targeted PFAAs.

Unlike the PFAAs, increasing perfluoroalkyl chain length within individual PFAS classes only led to larger K_{ex} values for the more hydrophobic AERs (e.g., AmPr-FASA, AmPr-FASA-PrA, and CEtAmPr-FASA-PrA in the presence of A532E, PFA964E and CalRes2301). Because the diverse perfluoroalkyl tails and the nonfluorinated head groups of the suspect PFASs can affect their overall structural hydrophobicity, the observed trend for the more hydrophobic PFASs is likely caused by strong hydrophobic interactions with the AERs. The diverse nonfluorinated head groups identified from the suspect PFAS classes also influenced adsorption behavior. For example, replacing the carboxylate head group in PFPeA with a complex amide functionality (e.g., MeEtCMeAmPr-FPeAd) markedly decreases the logK_{ex} value for AERs. Similar changes are also observed when the sulfonate group in PFHxS is replaced with a sulfonamide (e.g., FHxSA, a PFAS frequently detected in AFFF impacted groundwater) (Xiao et al., 2017) or sulfonamidoacetic acid (e.g., MeFASAA) (**Figure 3.1.7**). In general, we find that PFAS structures with head groups that are bulkier (i.e., higher steric hindrance) and/or predicted to be zwitterionic at pH 8.3 adsorb to a lesser degree than anionic PFAAs with similar perfluoroalkyl chain lengths, and the noticeable adsorption for these compounds are largely due to their non-electrostatic interaction with AERs. Nonetheless, the observed adsorption of Class 13 and Class 8 onto AERs may suggest that the prevailing charge for these compounds is not consistent with the predicted pK_a values. Follow up work with individual analytes are recommended to evaluate the pK_a values and adsorption trends for these structures.

Reduced adsorption to AERs was generally observed for PFASs containing zwitterionic or cationic headgroups. Adsorption of the zwitterionic PFASs ranged between 1 – 60% among all the investigated AERs, with <30% adsorption being observed for most PFAS-resin combinations (**Table A3.1.3**). PFASs possessing cationic head group (e.g., TAmPr-FASA) showed even less adsorption compared to the zwitterionic PFASs, with adsorption to the AERs ranging from 1 – 22%. Moreover, the logK_{ex} values of zwitterionic and cationic PFAS classes (e.g., AmPr-FASA, MeEtCMeAmPr-FAAd, TAmPr-FASA, and TAmPr-FASAPrA) were also the lowest among the 21 classes of suspect PFASs. The low adsorption of PFASs with zwitterionic and cationic headgroups are consistent with unfavorable interactions between resins and the localized cationic charges in the headgroup.

While low adsorption affinity may be expected for zwitterionic and cationic PFASs, more surprising was the low extent of adsorption observed for three suspect PFASs that are poly-ionic with one cationic and two anionic moieties (e.g., CEtAmPr-FEtSA-PrA, OAmPr-FPeSA, and OAmPr-FHxSA). As shown in **Table A3.1.4**, the highest logK_{ex} value among all AERs for these compounds is 1.45, corresponding to only 26% adsorption (to 50 mg/L resin). The low adsorption affinity of these PFASs indicates that cationic functional groups can negatively impact a PFAS's adsorption to AERs even if the net charge on the PFAS is negative. One reason for the lower adsorption of zwitterionic PFASs (especially if the negative charge falls in the middle of the molecule as opposed to the headgroup) may be steric hindrance to access the anion exchange site.

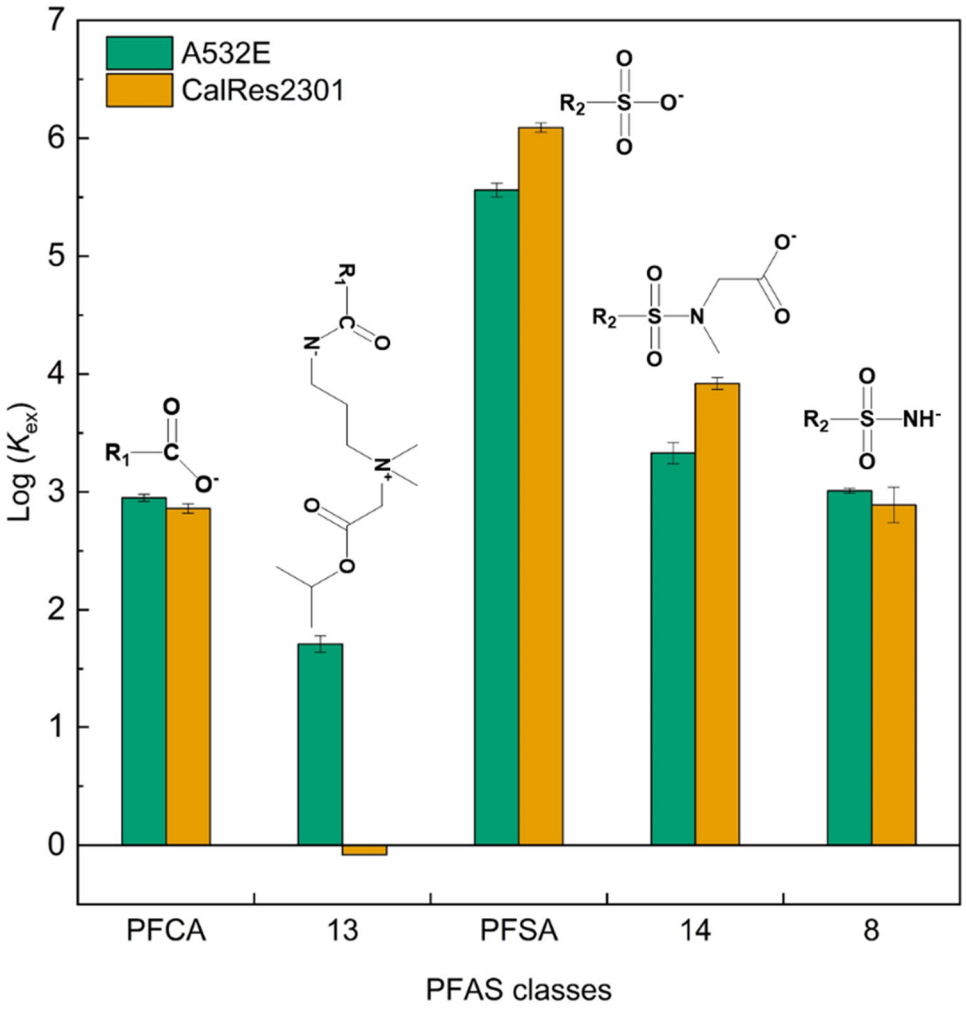

Figure 3.1.7. Effect of non-fluorinated head group on the selectivity of suspect PFAS classes of equal chain length in the presence of Purolite A532E and CalRes 2301. R_1 = $F(CF_2)_5$, R_2 = $F(CF_2)_6$. Class 13 = MeTeCMeAmPr-FAAd, Class 14 = MeFASAA, Class 8 = FASA. Error bars represent min/max values of duplicate experiments. From Fang et al. (2021).

Lastly, AmPr-FEtSA, AmPr-FPrSA, AmPr-FEtSA-PrA, CEtAmPr-FEtSA-PrA, and PFASs with 3-5 CF_2 moieties from TAmPr-FASA and TAmPr-FASAPrA did not adsorb significantly (<50%) to any of the studied resins. As all of these compounds contains localized cationic functional groups and limited CH_2 moieties, it is likely their hydrophobic interaction with all resins are inhibited by the shorter perfluoroalkyl tails while the positively charged moieties in their headgroups further diminished the electrostatic interaction with AERs.

3.2 Effect of NOM and Resin Counterion on PFAS Adsorption

3.2.1. Removal of DOC by anion exchange

Figure 3.2.1 shows the reductions in DOC by anion exchange highlighting differences in resin polymer composition and mobile counterion form of the resin. DOC was measured on a Shimadzu

TOC-VCH Total Organic Carbon Analyzer following non-purgeable organic carbon method. **Figure A3.2.1** in the appendix shows the corresponding results for UVA254 as well as UVA254 and DOC results normalized by initial concentration. The DOC and UVA254 measurements represent the combination of NOM from both the natural groundwater and the Suwannee River NOM isolate. Polystyrene A520E and polyacrylic A860 resins are compared within each subplot. The impact of changing the mobile counterion form of the resin (i.e., chloride vs. sulfate) is compared between the subplots. **Table A3.2.4** presents the ANOVA results corresponding to **Figure 3.2.1**. The major results encompassing **Figure 3.2.1**, **Figure A3.2.1**, and **Table A3.2.4** are as follows. UVA254 was reduced to a greater extent than DOC for all AER conditions except sulfate-form A520E resin at 0.25 and 0.5 mL/L. Because UVA254 is correlated with aromatic-rich and higher molecular weight sub-fraction of DOC [45], it explains why previous studies, and this study, show that UVA254 is reduced to a greater extent than overall DOC by AER [46].

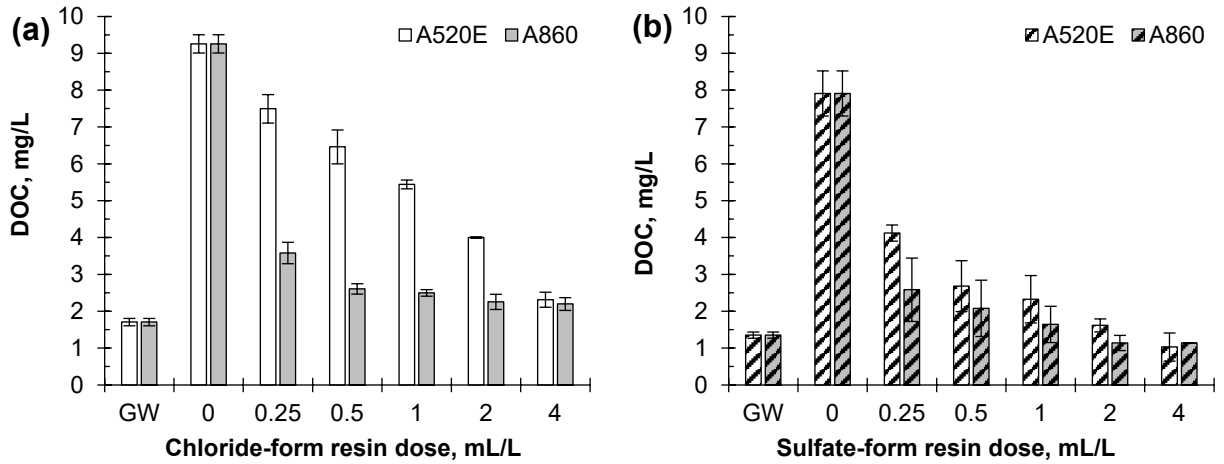

Figure 3.2.1. Impact of resin polymer composition (polystyrene A520E resin vs. polyacrylic A860 resin) and mobile counterion (chloride vs. sulfate) on DOC removal by AER. GW is groundwater. Test water (resin dose 0–4 mL/L) is combination of groundwater DOC and Suwannee River NOM. Bar is mean of triplicate samples with error bars showing one standard deviation. DOC concentration for sulfate-form, A860 resin, 4 mL/L is single sample. DOC was measured on a Shimadzu TOC-VCH Total Organic Carbon Analyzer following non-purgeable organic carbon method. From del Moral et al. (2020).

Polyacrylic A860 resin, in both the chloride- and sulfate-forms, showed greater reductions in DOC and UVA254 than polystyrene A520E resin in both mobile counterion forms. The greater reductions in DOC by A860 resin than A520E resin were statistically significant with p-value = 2.2×10^{-7} (**Table A3.2.4**), which suggests that resin polymer composition affects DOC removal and polyacrylic resin is preferred over polystyrene resin for DOC removal. Previous comparisons of resin polymer composition have reported greater DOC removal by polyacrylic resin than polystyrene resin, which was attributed to the hydrophilic nature of polyacrylic resins and higher water content of the resin that facilitates intraparticle pore diffusion of the DOC and more favorable conformation of DOC within the resin [47-50].

A860 and A520E resins, in both the chloride- and sulfate-forms, showed similar reductions in DOC and UVA254 at the highest resin dose of 4 mL/L. Furthermore, for both resins in both mobile counterion forms, the DOC concentration in the 4 mL/L sample was approximately equal to the DOC concentration in the natural groundwater before Suwannee River NOM was added, meaning

the SRNOM was highly favorable for removal by AER. Anion exchange experiments using natural groundwater without SRNOM showed low DOC removal, approx. 20%, regardless of resin dose or resin conditions (see **Figure A3.2.2**). Hence, the DOC present in the natural groundwater was not amenable to removal by AER. Previous studies have documented that portions of DOC can be non-removable by AER [51]. However, only 20% removal of DOC by AER is very low and likely attributable to competition by inorganic anions such as sulfate (see **Table A3.2.2**). Due to low removal of groundwater DOC by AER, no further results or discussion are presented for the groundwater only.

The most important result in **Figure 3.2.1** is the greater reduction in DOC by AER when the resin was in the sulfate form compared with the chloride form. The difference in DOC removal by chloride-form and sulfate-form resins was statistically significant regardless of resin polymer composition (p-value = 1.0×10^{-5}, **Table A3.2.4**), which indicates that the mobile counterion form of the resin influences DOC removal and specifically sulfate can increase DOC removal. Previous research on altering the mobile counterion form of AER has overlooked the potential benefits of sulfate-form resin. For example, most research has focused on bicarbonate-form resin as an alternative to chloride-form resin [7, 8, 52] with the main benefit being easier disposal of waste regeneration solution for bicarbonate than chloride. The results of these studies showed similar levels of DOC removal by chloride- and bicarbonate-form resin with polyacrylic composition. It is important to emphasize that this benefit pertains to DOC removal by AER in the absence of PFAS. The other benefit of bicarbonate-form resin relative to chloride-form resin is less corrosive water following AER treatment due to lower chloride concentration in the treated water [53, 54]. In the few studies that have evaluated sulfate-form AER, the results did not suggest the benefits of sulfate-form resin observed in this study. For example, Rokicki and Boyer (2011) compared AER in the chloride, bicarbonate, nitrate, and sulfate forms, and did not show increased contaminant removal by sulfate-form resin. Possible reasons for the increased DOC removal by sulfate-form resin than chloride-form resin are discussed after considering additional results.

Figure 3.2.2 shows the reductions in DOC by anion exchange in an identical format as **Figure 3.2.1** with the key difference being the addition of PFAAs to the natural groundwater spiked with SRNOM. **Figure A3.2.3** shows the corresponding results for UVA254 as well as UVA254 and DOC results normalized by initial concentration. **Table A3.2.5** presents the ANOVA results corresponding to **Figure 3.2.2**. Most of the trends described in **Figure 3.2.1** hold for **Figure 3.2.2**. For example, DOC reduction was statistically greater for A860 resin than A520E resin (p-value = 0.022, **Table A3.2.5**), again suggesting that resin polymer composition affects DOC removal with greater DOC removal for polyacrylic resin than polystyrene resin. The most important result from Figure 1, of the greater reduction in DOC by anion exchange when the resin was in the sulfate form compared with the chloride form, was also statistically significant in **Figure 3.2.2** regardless of resin polymer composition (p-value = 7.1×10^{-5}, **Table A3.2.5**). This further supports that changing the mobile counterion of the resin from chloride to sulfate can increase DOC removal. For the experiments shown in **Figures 3.2.1** and **3.2.2**, the test waters only varied due to the absence or presence of PFAAs; both test waters were based on Tempe groundwater matrix with addition of SRNOM.

Looking collectively at the results in **Figures 3.2.1** and **3.2.2** and **Tables A3.2.4** and **A3.2.5**, it appears that changing the mobile counterion form of a resin from chloride to sulfate had a greater

impact on A520E resin than A860 resin. Considering the mean difference in DOC removal between resin conditions, the difference between A520E and A860 resins decreases in going from chloride form resins to sulfate form resins, and the difference between chloride and sulfate forms of A520E resin is greater than the corresponding difference for A860 resin. Although A520E and A860 resins differ in polymer composition, they also differ in the identity of the quaternary ammonium functional group being triethyl ammonium vs. trimethyl ammonium, respectively. A520E resin is designed to be selective for nitrate over sulfate by increasing the size and spacing of the quaternary ammonium functional groups to favor monovalent anions over divalent anions [8, 55]. Therefore, it is possible that converting A520E resin from the chloride form to the sulfate form results in unfavorable conditions for the mobile counterion in the resin. In turn, this results in a greater driving force for exchanging the counterion in the resin with the counterion in solution, in this case DOC. The different functional groups could also impact uptake kinetics, but it was not studied here.

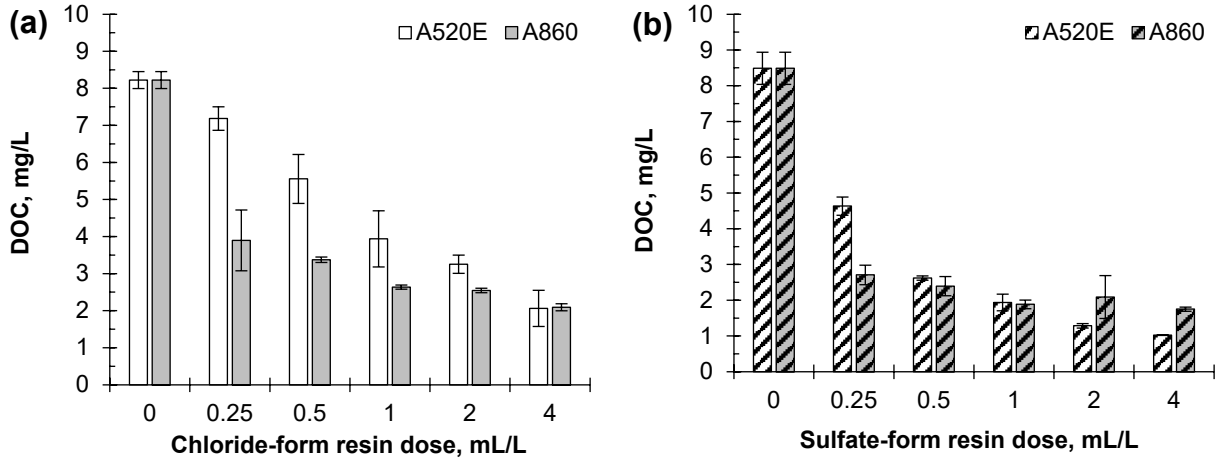

Figure 3.2.2. Impact of resin polymer composition (polystyrene A520E resin vs. polyacrylic A860 resin) and mobile counterion (chloride vs. sulfate) on DOC removal by AER in presence of perfluoroalkyl acids (PFAAs). Test water (resin dose 0–4 mL/L) is combination of groundwater DOC, Suwannee River NOM, and six PFAAs. Bar is mean of triplicate samples with error bars showing one standard deviation. From del Moral et al. (2020).

Comparing DOC removal by AER between **Figures 3.2.1** and **3.2.2**, the noteworthy change is the presence of six PFAAs in the test water in **Figure 3.2.2**. Because a different separation method was applied prior to DOC analysis, a statistical comparison was not conducted on the results in **Figures 3.2.1** and **3.2.2**. That said, the results in **Figures 3.2.1** and **3.2.2** follow the same trends, which suggests that the presence of PFAAs did not impact DOC removal by anion exchange for the resin conditions mentioned. For example, in both **Figures 3.2.1** and **3.2.2**, A860 resin removed more DOC than A520E resin regardless of mobile counterion, and sulfate-form resin removed more DOC than chloride-form resin regardless of polymer composition (see **Tables A3.2.4** and **A3.2.5**). There is limited previous research on the impact of PFAAs on DOC removal by AER. Kothawala et al. (2017) studied a single polystyrene AER and showed minimal impact of DOC on PFAA removal by AER. Dixit et al. (2019) studied a single polyacrylic AER and evaluated the impact of different types of NOM on removal of PFOS and PFOA by anion exchange. Neither study evaluated the impact of PFAAs (i.e., absence vs. presence) on DOC removal by AER. In general, trace organic contaminants, such as pharmaceuticals and pesticides, are present at orders of magnitude lower concentrations than DOC and are not expected to interfere with DOC removal

[56, 57]. The main competitor of DOC removal by AER is typically inorganic anions such as sulfate [8]. In the context of this research with average PFAA-to-DOC mass ratio of 0.056 and average PFAA-to-DOC equivalent ratio of 0.086, the results suggest that the presence of PFAAs did not interfere with DOC removal by AER.

3.2.2. Removal of PFAAs by anion exchange

Figure 3.2.3 shows the reductions in PFAAs by polystyrene A520E resin and evaluates the impact of DOC (absence vs. presence of SRNOM) and mobile counterion form of the resin (chloride vs. sulfate). Because the PFAAs were present at different initial concentrations (see **Table 3.2.1**), the results in **Figure 3.2.3** show normalized concentrations to facilitate comparisons. The general trend for PFAA removal by AER was sulfonates removed to a greater extent than carboxylates and C6 and C8 PFAAs removed to greater extent than C4 PFAAs. Previous studies show similar trends, with removal of PFAAs by AER increasing with increasing carbon chain length and greater removal of sulfonate functional groups than carboxylate functional groups [6, 58]. The clearest consensus among previous studies is the greatest removal of PFOS and lowest removal of PFBA by AER. This is hypothesized to be due to the combination of electrostatic and van der Waals forces of attraction contributing to PFOS removal versus electrostatic attraction only for PFBA removal. To elaborate, Li and Sengupta (1998) showed that it is favorable to transfer hydrophobic organic ionizable compound from water to non-polar phase such as AER, regardless of polymer composition. However, there are additional favorable interactions (i.e., van der Waals) between the hydrophobic organic ionizable compound and polystyrene resin matrix that are not present with the polyacrylic resin matrix [3]. The results of Rahmani and Mohseni (2017) support the first assertion whereby adsorption to polyacrylic resin increases for more hydrophobic organic compounds. The results of Landry and Boyer (2013) support the second assertion whereby the anionic pharmaceutical diclofenac exhibited greater adsorption to polystyrene resin than polyacrylic resin. Regarding PFAA removal by AER, PFAAs become more hydrophobic (less favorable interactions with water) as carbon chain length increases, which translates to greater AER adsorption of C8 PFAA than C4 PFAA regardless of polymer composition. In addition, adsorption is expected be greater to polystyrene resin than polyacrylic resin because of stronger van der Waals forces of attraction that increase with increasing carbon chain length (i.e., increasing polarizability).

A statistical analysis was not conducted on the results in **Figure 3.2.3** because only one sample out of the triplicate samples for each resin dose was analyzed for PFAAs. Comparing the results in **Figure 3.2.3**, on average subplot b shows lower C/C_0 bars than subplot a and subplot d shows lower C/C_0 bars than subplot c. This trend is most noticeable at AER doses on 0.25 and 0.5 mL/L and for PFBA at all resin doses. This was a similar result as DOC removal, which supports the conjecture of enhanced contaminant removal using a divalent counterion with a monovalent-ion-selective resin (e.g., A520E). To confirm this conjecture, additional comparisons of divalent vs. monovalent counterions would be needed. The results did not show an obvious impact of the presence of SRNOM on PFAA removal by AER, meaning that the presence of SRNOM did not interfere with PFAA removal. Although limited data are available, previous studies also show minimal impact of NOM on PFAA removal by AER [59, 60]. This indicates that AER (A520E in this case) is highly selective for PFAAs because the average DOC-to-PFAA equivalent ratio was 11.6 meaning there was >10× more NOM than PFAAs competing for ion-exchange sites.

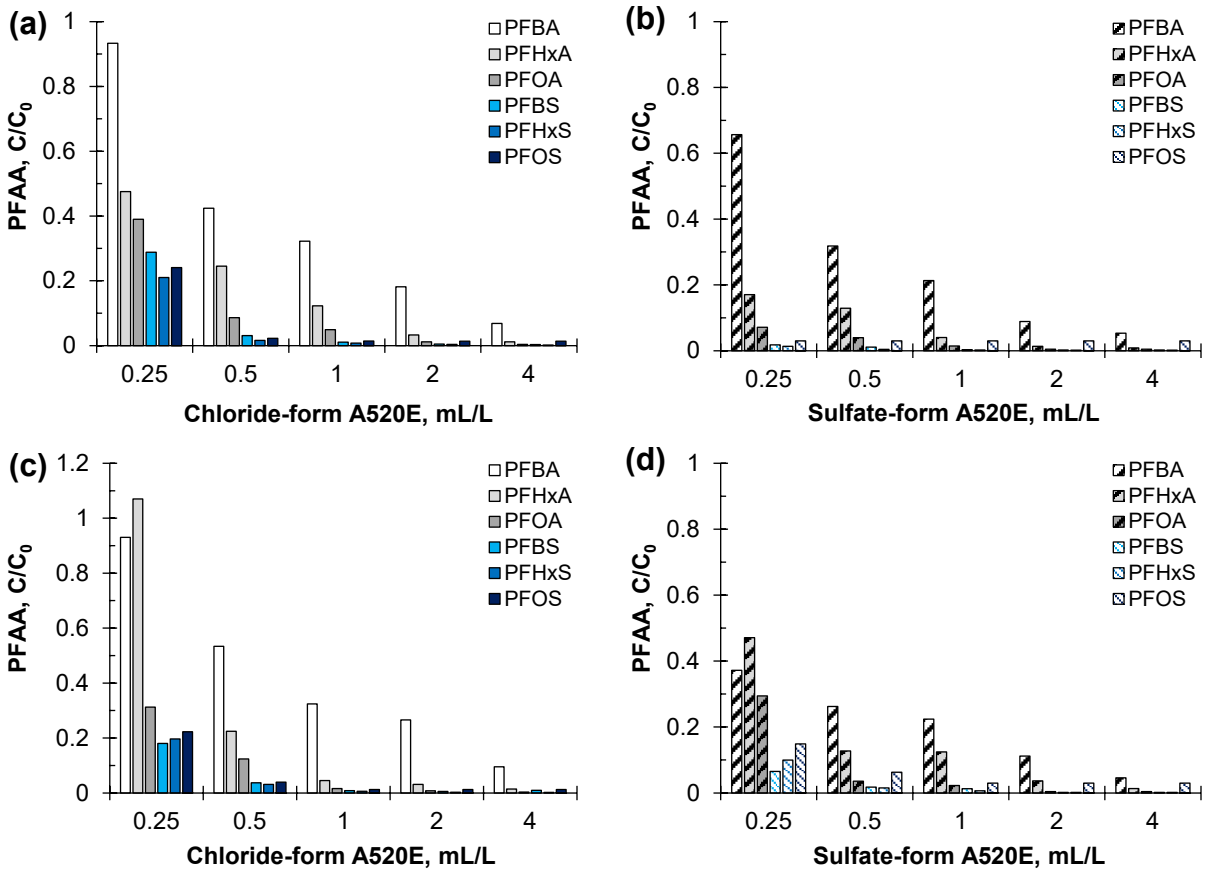

Figure 3.2.3. Removal of perfluoroalkyl acids (PFAAs) by polystyrene A520E resin in the absence of Suwannee River NOM (parts a and b) and presence of Suwannee River NOM (parts c and d) considering the impact of mobile counterion (chloride vs. sulfate). Normalized PFAA concentrations are single sample per resin dose. Initial concentrations given in Table 3.2.1: Experiment 3 (part a), Experiment 7 (part b), Experiment 4 (part c), Experiment 8 (part d). See note in Table 3.2.1 on initial PFOS in Experiment 8. From del Moral et al. (2020).

Figure 3.2.4 shows the reductions in PFAAs by polyacrylic A860 resin and evaluates the impact of DOC (absence vs. presence of SRNOM) and mobile counterion form of the resin (chloride vs. sulfate) in the identical format as **Figure 3.2.3**. The main result in **Figure 3.2.4** is the higher normalized PFAA concentrations by polyacrylic A860 resin than polystyrene A520E resin for all resin and solution conditions meaning that polyacrylic A860 resin was less effective for PFAA removal. Only PFOS was consistently removed greater than 50% by polyacrylic A860 resin. PFBA showed the least removal. Due to the low removals of PFAAs by polyacrylic A860 resin, there was not a major impact of changing the mobile counterion form of the resin or evaluating the absence or presence of SRNOM. The lower removal of PFAAs by polyacrylic A860 resin than polystyrene A520E resin is hypothesized to be due to weaker van der Waals forces of attraction between PFAAs and polyacrylic resin than PFAAs and polystyrene resin, as described above. For example, the same trend has been observed for removal of pharmaceuticals by AER with higher removal by polystyrene resin than polyacrylic resin [61], and more selective removal of hydrophobic pharmaceuticals than hydrophilic pharmaceuticals by polystyrene resin [62]. A860 polyacrylic resin was shown by Dixit et al. (2019) to effectively remove PFOS and PFOA in the presence of SRNOM. However, their results did not include a comparison with polystyrene resin or consider

short-chain PFAAs such as PFBA and PFBS. The impact of NOM in **Figures 3.2.3** and **3.2.4** is limited to SRNOM where it is known that NOM hydrophobicity and molecular weight can influence the ion-exchange process [63]. The results in **Figures 3.2.3** and **3.2.4** illustrate the importance of evaluating PFAA removal by AER considering short- and long-chain carboxylates and sulfonates to obtain a more complete understanding of removal performance. For example, both polystyrene A520E and polyacrylic A860 resins showed high removal of PFOS; however, only A520E resin achieved > 50% removal of shorter-chain PFAAs.

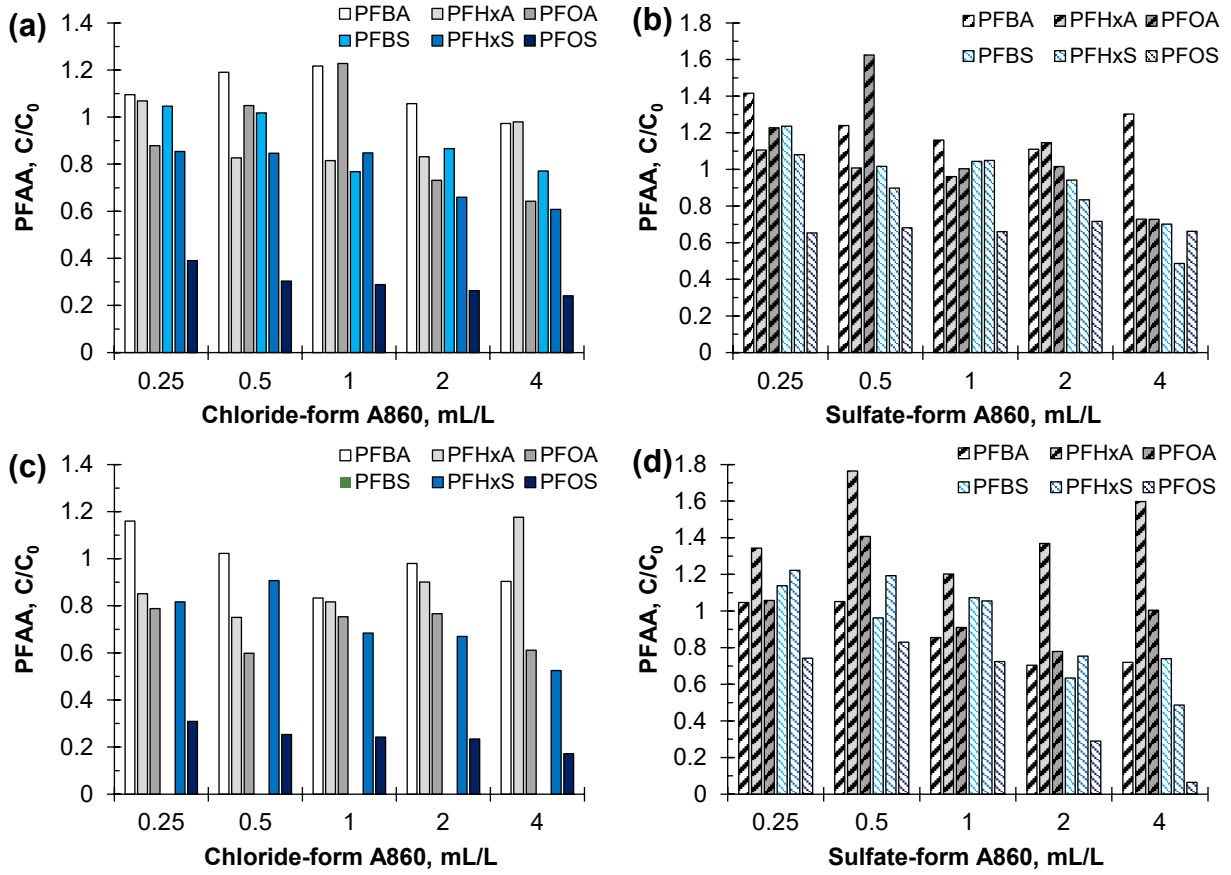

Figure 3.2.4. Removal of perfluoroalkyl acids (PFAAs) by polyacrylic A860 resin in the absence of Suwannee River NOM (parts a and b) and presence of Suwannee River NOM (parts c and d) considering impact of mobile counterion (chloride vs. sulfate). Normalized PFAA concentrations are single sample per resin dose. Initial concentrations given in Table 3.2.1: Experiment 3 (part a), Experiment 7 (part b), Experiment 4 (part c), Experiment 8 (part d). No PFBF data for part c. See note in Table 3.2.1 on initial PFOS in Experiment 8 (part d). From del Moral et al. (2020).

Table 3.2.1. Experimental design for removal of DOC and/or PFAAs by anion exchange resin. From del Moral et al. (2020).

Experiment	Test water	AER/counterion	DOC	PFBA	PFBS	PFHxA	PFHxS	PFOA	PFOS
1	GW	A520E/Cl, A860/Cl	1.3						
2	GW + SRNOM	A520E/Cl, A860/Cl	9.3						
3	GW + PFAAs	A520E/Cl, A860/Cl	1.6	321	333	587	417	289	375
4	GW + SRNOM + PFAAs	A520E/Cl, A860/Cl	8.2	337	309	652	395	298	404
5	GW	A520E/SO4, A860/SO4	1.6						
6	GW + SRNOM	A520E/SO4, A860/SO4	7.9						
7	GW + PFAAs	A520E/SO4, A860/SO4	1.5	317	487	585	308	215	167
8	GW + SRNOM + PFAAs	A520E/SO4, A860/SO4	8.5	460	548	479	289	250	167

Test water: Groundwater (GW), Suwannee River NOM (SRNOM), perfluoroalkyl acids (PFAAs)
DOC concentration in mg/L
PFBA, PFBS, PFHxA, PFHxS, PFOA, PFOS concentration in µg/L
PFOS concentration in Experiment 8 based on PFOS concentration in Experiment 7

3.2.3. Implications for AER treatment

The results of this research have several limitations that should be considered when interpreting the results. Regarding the AER experiments, there was some variability in initial DOC and PFAAs concentrations that make exact comparison difficult. However, all test waters were based on the same groundwater matrix. Although comparison of resin polymer composition was an important aspect of this research, it could be not conclusively separated from the different functional group chemistry and ion-exchange capacity. However, previous research comparing polystyrene resins with different functional groups [6, 64] shows smaller differences in resin selectivity than comparing polystyrene and polyacrylic resins [3, 5, 61].

The results of this research show that changing the mobile counterion form of the resin from chloride to sulfate can increase contaminant removal, especially for A520E resin, which is designed to be selective for monovalent anions over divalent anions. The benefits of sulfate-form AER go beyond contaminant removal to include less corrosive treated water (i.e., higher sulfate

concentration in treated water decreases the chloride-to-sulfate mass ratio), more disposal options for sulfate-based waste regeneration solution when hazardous contaminants are not present, and expanded options for treatment of hazardous contaminants in waste regeneration solution, e.g., sulfate-based regeneration solution is expected to eliminate the potential for perchlorate formation during electrochemical treatment. Studies on the destruction of PFAAs in sulfate-based regeneration solutions the use strongly oxidizing sulfate radical or persulfate are the next logical step in this research.

3.3 Laboratory Continuous-Flow Adsorption/Regeneration of Resins

PFAS breakthrough profiles. The specific conditions for each experiment are listed in **Table 3.3.1**. **Figure 3.3.1** shows the breakthrough of PFCAs and PFSAs as a function of BVs treated over three regeneration cycles for A520E polystyrene resin treating test water with low initial PFAS concentration (280 µg/L). PFBA showed breakthrough first, reaching 10% breakthrough between 4,000 and 6,000 BVs within the first regeneration cycle. PFBA remained above 10% breakthrough during the second and third regeneration cycles. PFCAs reached 10% breakthrough before PFSAs. PFBS and PFHxS treated the most BVs to 10% breakthrough occurring at approx. 21,000 BVs during the third regeneration cycle. The highest effluent concentration observed was for PFOS reaching $C/C_0 > 0.6$ at 33,000 BVs after the third regeneration cycle was performed. Regeneration using aqueous-only $(NH_4)_2SO_4$ + NH_4OH solution did not have a noticeable effect on the breakthrough results.

Table 3.3.1. Experimental design for column-mode anion exchange resin (AER) treatment for PFAS removal from water. From Dietz et al. (2021).

Experiment no.	AER-counterion	PFAS initial concentration, mg/L[a]	BV_{AER}, L[b]	SFR, mL/min	Regeneration solution
1	Purolite A520E-SO_4	0.02, 0.06, 0.1, 0.03, 0.04, and 0.03	0.003	0.6	0.5% $(NH_4)_2SO_4$ + 0.5% NH_4OH
2	Purolite A520E-SO_4	0.02, 0.06, 0.1, 0.03, 0.04, and 0.03	0.003	0.6	0.5% $(NH_4)_2SO_4$ + 50% methanol
3	Purolite A520E-SO_4	0.96, 2.5, 3.5, 0.81, 1.8, and 1.6	0.01	2.0	0.5% $(NH_4)_2SO_4$ + 0.5% NH_4OH
4	Purolite A520E-SO_4	0.96, 2.5, 3.5, 0.81, 1.8, and 1.6	0.01	2.0	0.5% $(NH_4)_2SO_4$ + 50% methanol
5	Purolite A860-HCO_3	0.52, 1.1, 2.1, 0.51, 0.9, and 1.1	0.004	0.8	8% $NaHCO_3$

Abbreviations: Bed volume of AER in column (BV_{AER}); Service flow rate (SFR).

[a] Initial, influent concentrations shown for PFBA, PFHxA, PFOA, PFBS, PFHxS, and PFOS. [b] Empty bed contact time (EBCT) was 5 min for all experiments.

Experiment 2 operated under the same conditions as experiment 1 (A520E polystyrene resin, test water with low initial PFAS concentration) with the difference being the regeneration solution included organic cosolvent (i.e., methanol). **Figure 3.3.2** shows the breakthrough data for PFCAs and PFSAs corresponding to experiment 2. Ten percent breakthrough was reached first by PFBA at approx. 4,000 BVs before the first regeneration occurred. PFBA continued to see 10–20% breakthrough throughout the remainder of the experiment. PFHxA and PFOA tracked PFBA with slightly lower effluent concentrations. PFBS and PFHxS displayed very similar breakthrough, and much greater BVs treated than PFCAs. Ten percent breakthrough for both PFBS and PFHxS occurred at approx. 20,000 BVs and then again at 30,000 BVs. Similar to experiment 1, PFOS achieved the highest effluent concentration of $C/C_0 = 0.6$ at approx. 31,000 BVs after the third

regeneration cycle was performed. Regeneration using $(NH_4)_2SO_4$ + methanol solution appeared to result in small recovery in AER adsorption capacity based on effluent samples immediately after regeneration.

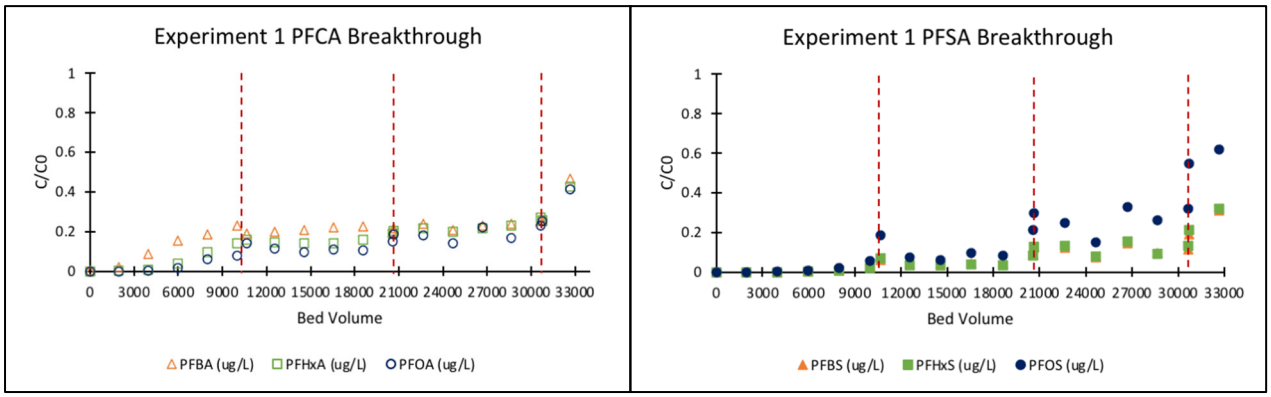

Figure 3.3.1. Experiment 1 breakthrough curves for polystyrene A520E resin using 0.5% $(NH_4)_2SO_4$ + 0.5% NH_4OH regeneration solution. Dashed vertical red lines represent regeneration. Each point represents an effluent sample. Total initial PFAS concentration equal to 280 µg/L; individual initial concentrations listed in Table 3.3.1. From Dietz et al. (2021).

Experiments 1 and 2 used the same composition test water (total initial PFAS concentration of 280 µg/L) and A520E polystyrene resin in the sulfate form. Therefore, the results for the first treatment cycle should be the same for the two experiments. The order of increasing BVs to 10% breakthrough was PFBA < PFHxA ≈ PFOA < PFBS ≈ PFHxS ≈ PFOS, which was the same order for removal of PFAAs observed for sulfate-form A520E resin in batch experiments [14] thereby confirming the usefulness of batch adsorption experiments to predict column adsorption behavior.

Experiments 3 and 4 had approximately 40 times higher total initial PFAS concentration (11,200 µg/L) than experiments 1 and 2. Breakthrough of PFCAs and PFSAs over 5 regeneration cycles is shown in **Figure 3.3.3** for A520E polystyrene resin using aqueous-only 0.5% $(NH_4)_2SO_4$ + 0.5% NH_4OH regeneration solution (experiment 3). PFBA breakthrough occurred first reaching >10% at 1,100 BVs before the first regeneration occurred. PFCAs had higher effluent concentrations than PFSAs, and short-chain PFCAs had higher effluent concentrations than long-chain PFCAs (i.e., PFOA), whereas PFSAs showed similar breakthrough behavior regardless of chain length. Regeneration resulted in slight reductions in effluent concentration in the samples collected immediately after regeneration.

Breakthrough of PFCAs and PFSAs over 5 regeneration cycles is shown in **Figure 3.3.4** for A520E polystyrene resin using 0.5% $(NH_4)_2SO_4$ + 50% methanol regeneration solution (experiment 4). The six PFAAs reached breakthrough of 10% or higher at 545 BVs and then decreased to less than 10% breakthrough (except for PFBA). PFBA consistently showed the highest effluent concentration and PFOS showed the lowest effluent concentration throughout the experiment. PFCAs had higher effluent concentrations in comparison with PFSAs, and short-chain PFAAs had higher and faster breakthrough than the long-chain PFAAs. Under the higher initial PFAS concentration in experiments 3 and 4 (100–1000 µg/L range for individual species), the PFSAs all had very similar removal while under the lower initial PFAS concentration in experiments 1 and 2 (10–100 µg/L range for individual species), PFBS and PFHxS removal were

similar and greater than PFOS removal. Regeneration did not have an obvious impact on the effluent samples collected immediately after regeneration.

Experiment 5 used polyacrylic A860 resin instead of polystyrene A520E resin, bicarbonate mobile counterion instead of sulfate mobile counterion, and $NaHCO_3$ regeneration solution instead of Na_2SO_4 for regeneration solution (see **Figure 3.3.5**). A520E and A860 resins were previously compared in both the chloride- and sulfate-form [14], with A520E resin exhibiting significantly greater removal of PFAS than A860 resin. Excluding PFOS, PFAAs reached >10% breakthrough with the first sample at 500 BV and PFAAs showed higher effluent concentrations for A860 polyacrylic resin than A520E polystyrene resin. PFOS reached its highest breakthrough of 17% at 8,500 BV after the fourth regeneration cycle, and showed similar or greater removal by A860 resin than A520E resin. Following the trends of the other experiments, the PFCAs had faster and higher breakthrough than PFSAs, and short-chain PFAAs exhibited faster and higher breakthroughs than long-chain PFAAs. Regeneration resulted in a decrease in effluent concentration for the samples collected immediately after regeneration.

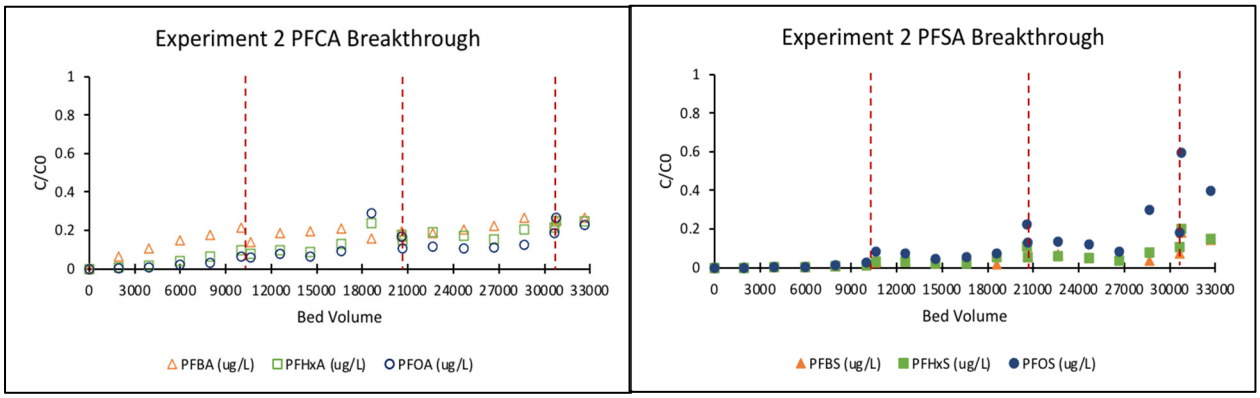

Figure 3.3.2. Experiment 2 breakthrough curves for polystyrene A520E resin using 0.5% $(NH_4)_2SO_4$ + 50% methanol regeneration solution. Dashed vertical red lines represent regeneration. Each point represents an effluent sample. Total initial PFAS concentration equal to 280 µg/L; individual initial concentrations listed in Table 3.3.1. From Dietz et al. (2021).

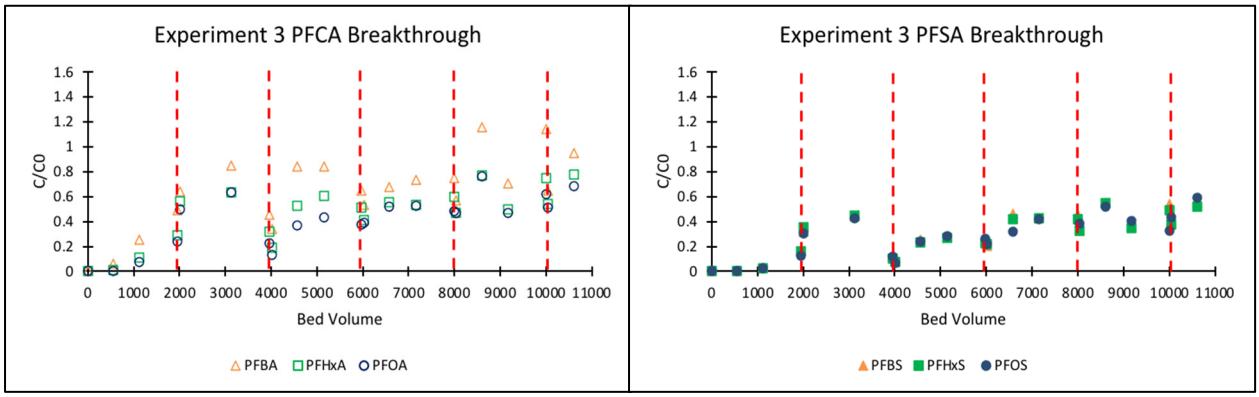

Figure 3.3.3. Experiment 3 breakthrough curves for polystyrene A520E resin using 0.5% $(NH_4)_2SO_4$ + 0.5% NH_4OH regeneration solution. Dashed vertical red lines represent regeneration. Each point represents an effluent sample. Total initial PFAS concentration equal to 11,200 µg/L; individual initial concentrations listed in Table 3.3.1. From Dietz et al. (2021).

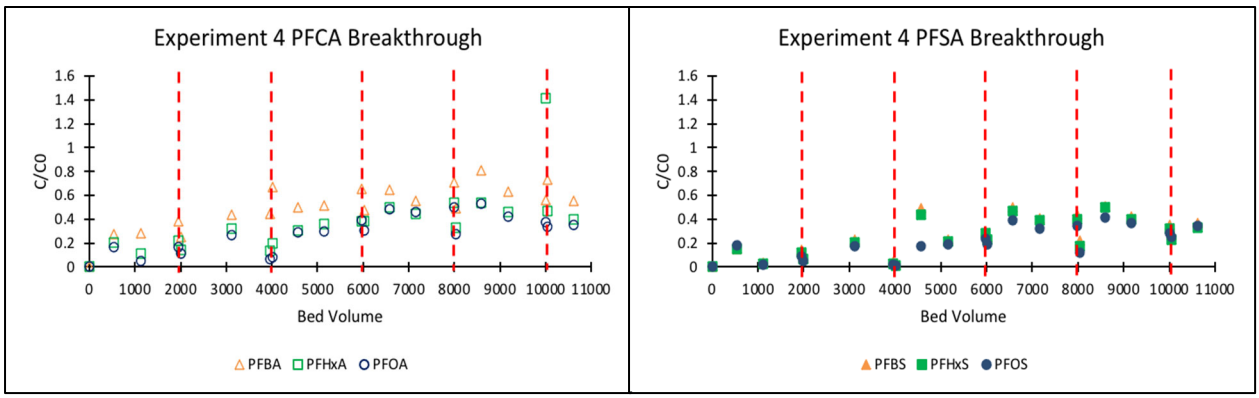

Figure 3.3.4. Experiment 4 breakthrough curves for polystyrene A520E resin using 0.5% $(NH_4)_2SO_4$ + 50% methanol regeneration solution. Dashed vertical red lines represent regeneration. Each point represents an effluent sample. Total initial PFAS concentration equal to 11,200 µg/L; individual initial concentrations listed in Table 3.3.1. From Dietz et al. (2021).

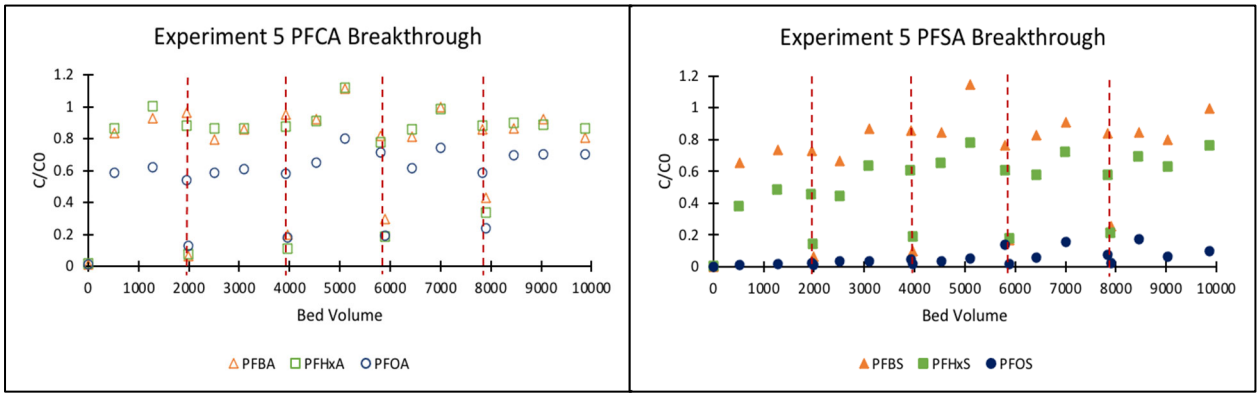

Figure 3.3.5. Experiment 5 breakthrough curves for polyacrylic A860 resin using 8% $NaHCO_3$ regeneration solution. Dashed vertical red lines represent regeneration. Each point represents an effluent sample. Total initial PFAS concentration equal to 6,230 µg/L; individual initial concentrations listed in Table 3.3.1. From Dietz et al. (2021).

PFAS regeneration efficiency. **Table 3.3.2** shows the regeneration efficiency of each PFAS tested in experiments 1–5 over the multiple treatment and regeneration cycles. From the breakthrough curves for experiment 1 (see **Figure 3.3.1**), it appears that the concentration of PFBA was the only chemical that decreased slightly after the first regeneration cycle occurred. During all other regeneration cycles, the concentrations of each PFAS increased suggesting that 0.5% $(NH_4)_2SO_4$ + 0.5% NH_4OH solution was ineffective at desorbing PFAS from polystyrene resin. This was supported by mass balance calculations that showed essentially 0% regeneration efficiency under lower PFAS concentrations in the influent. Because the PFAS concentration in the influent was 10–100 µg/L range, the resin had ion-exchange sites available allowing for >80% PFAS removal to occur even after ineffective regeneration cycles.

Table 3.3.2. Regeneration efficiency of ion-exchange column experiments over multiple treatment and regeneration cycles. Regeneration efficiency data are given as percentage. From Dietz et al. (2021).

		Experiment 1[a,d]	Experiment 2[b,d]	Experiment 3[a,e]	Experiment 4[b,e]	Experiment 5[c,f]
Regeneration cycle 1	PFBA	0	0.21	1.1	12	0.014
	PFHxA	0	0.30	0.25	11	0.010
	PFOA	0.41	0.30	0.082	13	0.015
	PFBS	0	0	0.010	1.5	0.018
	PFHxS	0	0.070	0.010	2.0	0.015
	PFOS	0	0.23	0	2.9	0
Regeneration cycle 2	PFBA	0	0	6.1	9.6	1.85
	PFHxA	0	0.40	1.2	9.3	1.41
	PFOA	0	0.58	0.34	9.0	0.40
	PFBS	0	0	0.13	0.84	0.70
	PFHxS	0	0.17	0.058	1.1	0.30
	PFOS	0	0.82	0.037	1.7	0.010
Regeneration cycle 3	PFBA	0	0.020	4.9	20	1.82
	PFHxA	0	0.080	1.0	21	1.94
	PFOA	0	0.11	0.25	18	0.54
	PFBS	0	0	0.11	2.8	1.64
	PFHxS	0	0.067	0.050	3.4	0.52
	PFOS	0	0.27	0.031	5.1	0.010
Regeneration cycle 4	PFBA	-	-	5.6	18	1.14
	PFHxA	-	-	1.4	21	1.64
	PFOA	-	-	0.37	21	0.52
	PFBS	-	-	0.19	3.6	1.85
	PFHxS	-	-	0.072	4.5	0.56
	PFOS	-	-	0	6.8	0.011
Regeneration cycle 5	PFBA	-	-	0	18	0.85
	PFHxA	-	-	1.51	-	1.14
	PFOA	-	-	0.42	19	0.53
	PFBS	-	-	0.19	4.0	1.32
	PFHxS	-	-	0.040	4.9	0.47
	PFOS	-	-	0.074	6.9	0.010

Dash (-) used to indicate that no sample was collected; experiments 1 and 2 show no values for regeneration cycles 4 and 5 because only three regeneration cycles were tested. Zero percent is used to signify that sample analysis was below quantification. [a] Regeneration solution used 0.5% $(NH_4)_2SO_4$ + 0.5% NH_4OH. [b] Regeneration solution used 0.5% $(NH_4)_2SO_4$ + 50% methanol. [c] Regeneration solution used 8% $NaHCO_3$. [d] Total initial PFAS concentration was 0.28 mg/L. [e] Total initial PFAS concentration was 11.2 mg/L. [f] Total initial PFAs concentration was 6.23 mg/L.

Breakthrough curves for experiment 2 (see **Figure 3.3.2**), under the same initial conditions as experiment 1, show somewhat better results with a slight decrease in PFCA concentrations after the first and second regeneration cycles, and a decrease in PFSA concentrations after the second regeneration cycle. Because the decreases in concentration seen in the breakthrough curves were small, a mass balance was conducted to examine the regeneration efficiency. The mass balance calculations showed that 0.5% $(NH_4)_2SO_4$ + 50% methanol did not desorb PFAS. Like experiment 1 and because of the lower PFAS concentrations in the influent, the resin had ion-exchange sites available that could adsorb PFAS over multiple treatment and regeneration cycles even with ineffective regeneration.

Using the 0.5% $(NH_4)_2SO_4$ + 0.5% NH_4OH regeneration solution, experiment 3 operated at higher initial PFAS concentrations to allow for the resin to become saturated with PFAS to better

evaluate the regeneration solution efficiency. In general, PFCA and PFSA concentrations decreased after each regeneration cycle (see **Figure 3.3.3**). Subjecting the resin to a higher PFAS loading appeared to give better regeneration results. However, mass balance calculations showed <1% regeneration efficiency for most PFAS using 0.5% $(NH_4)_2SO_4$ + 0.5% NH_4OH solution. PFBA showed the highest regeneration efficiency (up to 6.1%) followed by PFHxA (up to 1.5%), while the regeneration efficiencies of PFOA, PFBS, PFHxS, and PFOS were consistently below 1%.

Experiment 4 evaluated 0.5% $(NH_4)_2SO_4$ + 50% methanol regeneration solution at high PFAS concentrations in the influent water. The general trend shows that both PFCAs and PFSAs decreased in concentration after each regeneration cycle occurred, suggesting that the regeneration solution desorbed PFAS from the polystyrene resin. This was confirmed by mass balance calculations that showed regeneration efficiencies as high as 24% for PFBA and 9–21% for PFOA (see **Table 3.3.2**). PFCAs were desorbed more effectively than PFSAs from the polystyrene resin over multiple regeneration cycles. For instance, regeneration efficiencies were approximately 10–20% for PFCAs while 1–6% for PFSAs.

Experiment 5, which operated at high initial PFAS concentrations similar to experiments 3 and 4, evaluated 8% $NaHCO_3$ solution for regeneration of PFAS-loaded A860 polyacrylic resin. The breakthrough curves show high effluent concentrations of PFAS (e.g., C/C_0 = 0.8–1 for PFBA and PFHxA), and immediately after regeneration a decrease in effluent concentration (C/C_0 = 0.1–0.2). However, high effluent concentration was measured in the next sample. The trends in the breakthrough curves suggest that $NaHCO_3$ has some potential to desorb PFAAs from polyacrylic resin. However, mass balance calculations showed <2% regeneration efficiency (see **Table 3.3.2**) indicating that $NaHCO_3$ was not an effective regeneration solution for polyacrylic resin. PFBA, PFHxA, and PFBS achieved the highest regeneration efficiencies using 8% $NaHCO_3$.

Discussion of initial PFAS concentration. Regarding the PFAS concentrations used in this research, the low concentration condition (Experiments 1 and 2 in **Table 3.3.1**) had total PFAS concentration of 280 µg/L, which is not relevant to drinking water supplies but is possible in source zone contamination and groundwater remediation [9, 37]. The high concentration condition (Experiments 3–5 in **Table 3.3.1**) had total PFAS concentration of 6,230 and 11,200 µg/L (>1 mg/L), which is above concentrations detected in the environment and used as pragmatic approach for loading PFAS on the resin. The effect of initial PFAS concentration on breakthrough behavior can be compared in **Figures 3.3.1** and **3.3.3** (both used aqueous-only 0.5% $(NH_4)_2SO_4$ + 0.5% NH_4OH regeneration solution) and **Figures 3.3.2** and **3.3.4** (both used 0.5% $(NH_4)_2SO_4$ + 50% methanol regeneration solution). Increasing the initial PFAS concentration from 280 µg/L to 11,200 µg/L reduced the BVs treated to breakthrough and increased the effluent concentrations. For example, BVs treated to 10% breakthrough for PFBA, PFHxA, and PFOA were reduced by approx. a factor of 10 when total PFAS concentration was increased 40 times. The effect of higher initial PFAS concentration on BVs treated and effluent concentration was compounded over multiple regeneration cycles when the regeneration process did not effectively desorb PFAS from the resin.

Total initial PFAS concentration also impacted regeneration efficiency trends in **Table 3.3.2**. Foremost, higher initial PFAS concentration resulted in higher regeneration efficiency when all other conditions were constant. For example, regeneration efficiency for PFBA increased from 0%

to 1–6% for experiments 1 and 3 using aqueous-only 0.5% $(NH_4)_2SO_4$ + 0.5% NH_4OH regeneration solution, and regeneration efficiency for PFBA increased from <1% to 10–20% for experiments 2 and 4 using 0.5% $(NH_4)_2SO_4$ + 50% methanol regeneration solution. In addition to total initial PFAS concentration, the composition of the regeneration solution played a key role influencing regeneration efficiency with the presence of organic cosolvent increasing the desorption of PFAS from polystyrene resin.

Discussion of AER polymer composition. Experiments 1–4 evaluated the polystyrene resin, A520E, and experiment 5 evaluated the polyacrylic resin, A860. A520E resin exhibited greater removal of PFSAs than PFCAs, and within the PFCAs subgroup increasing removal with increasing length of perfluoroalkyl tail (the impact of tail length was less pronounced for PFSAs). A520E and A860 resins were not directly compared in this study; however, A520E and A860 resins were directly compared in both chloride- and sulfate-forms in a previous study [14], and A520E resin showed significantly greater removal of PFAS than A860 resin. The results for A520E resin are believed to reflect both electrostatic and non-electrostatic interactions between PFAS and resin. This is based on previous research that shows polystyrene AERs have higher selectivity for monosulfonic acids than monocarboxylic acids, and higher selectivity for aromatic carboxylic acids than aliphatic carboxylic acids [5]. The oxygen atoms in sulfonic acid have greater negative charge than the oxygen atoms in carboxylic acid, resulting in stronger electrostatic interactions between sulfonic acid and strong-base functional groups of resin. In addition, the aromatic portion of aromatic carboxylic acids has favorable van der Waals interactions with polystyrene resin [3]. Density functional theory (DFT) calculations support the stronger electrostatic interactions between sulfonate group of PFSAs and quaternary ammonium functional group of resin than between carboxylate group of PFCAs and functional group of resin [65]. Interestingly, DFT calculations suggested that increasing length of perfluoroalkyl tail resulted in greater net negative charge on PFAAs resulting in stronger electrostatic interactions with resin, and did not use van der Waals interactions to explain the results [65].

A860 resin exhibited low removal of PFAS except for PFOS. Removal of PFOS by A860 resin was greater than removal by A520E resin. While testing conditions for both AERs were slightly dissimilar (i.e., service flow rate, BV of AER in column, initial PFAS concentration and mobile counterion), previous research has consistently shown AER polymer composition to be the dominant variable in PFAS removal (Boyer et al., 2021; del Moral et al., 2020; Dixit et al., 2021). Therefore, one of the key differences between the two testing conditions was the more hydrophilic nature of polyacrylic resin (A860) than polystyrene resin (A520E) [3, 50], and therefore weaker van der Waals interactions. In addition, polyacrylic resin typically have higher water content than polystyrene resin, which facilitates mass transfer especially for larger chemicals like PFOS. Although removal trends for A520E resin support the importance of electrostatic interactions between PFAAs and polystyrene resin, the lack of van der Waals interactions between PFAAs and polyacrylic resin suggest that electrostatic interactions alone are not sufficient for PFAS removal by AER. A similar result was observed for the removal of the hydrophobic ionizable organic compound diclofenac by AER [61]. The high removal of PFOS by polyacrylic resin was influenced in part by favorable interactions between PFOS and polyacrylic resin due to high water content. However, the differences between PFOS and other PFAAs in terms of physicochemical properties (e.g., molecular weight, octanol-water partition coefficient Log K_{ow} and the distribution coefficient Log D) suggests that unfavorable hydrophobic interactions between PFOS and water are driving

the adsorption process (Zeng et al., 2020). Another PFAS adsorption study showed the Langmuir model to accurately fit PFAS adsorption to AER with the exception of PFOS [66]. This supports the idea of solute-solute interactions (i.e., bilayer adsorption) such as micelle and hemi-micelle formation within the resin pore water at high concentration range (i.e., mg/L) [67].

The effect of co-existing inorganic anions such as sulfate and chloride in groundwater was not evaluated in this study. However, results in the literature have shown that competing inorganic anions minimally impact the removal of long-chain PFSAs (i.e., PFHxS and PFOS) regardless of polymer composition. For instance, PFHxS uptake by polystyrene resin was reduced by 10% when the molar concentration of common inorganic anions was 100 times greater than that of PFHxS (Maimaiti et al., 2018). A similar trend was shown for the removal of PFOS by polyacrylic resin at the presence of 1 mmol/L sulfate (Deng et al., 2010). The higher affinity of PFOS and PFHxS to AER over inorganic anions is explained by the combination of electrostatic, van der Waals, and hydrophobic interactions, with the non-electrostatic interactions not relevant for inorganic anions. It is therefore expected that competition from background inorganic anions on PFCAs and short-chain PFAAs be more noticeable (Boyer et al. 2021). This is consistent with the faster and higher breakthrough of PFBA observed in this research.

The PFAS removal results in **Figures 3.3.1–3.3.5** were further explored by calculating the molar speciation of PFAAs in the influent and PFAAs adsorbed onto the resin as presented in **Table A3.3.3**. **Figures A3.3.1** and **A3.3.2**, corresponding to experiments 1 and 2, show that the speciation of adsorbed PFAAs remains the same as what is found in the influent. The results corresponding to experiments 3 and 4 (see **Figure A3.3.3** and **Figure 3.3.6**), show the same trends as experiment 1 and 2 despite having the higher initial PFAS concentrations, i.e., speciation on resin matches speciation in influent. **Figure 3.3.7**, corresponding to experiment 5, shows that the speciation of PFAS adsorbed to the resin is different than the speciation of influent. **Figure 3.3.7** shows that although PFOS represented 13% of the total PFAAs in the influent, PFOS adsorbed the most (33–42%) onto the resin in comparison with the other PFAS. The greater removal of PFOS than other PFAS supports the notion that physicochemical properties of PFOS lead to hydrophobic interactions with the polyacrylic resin.

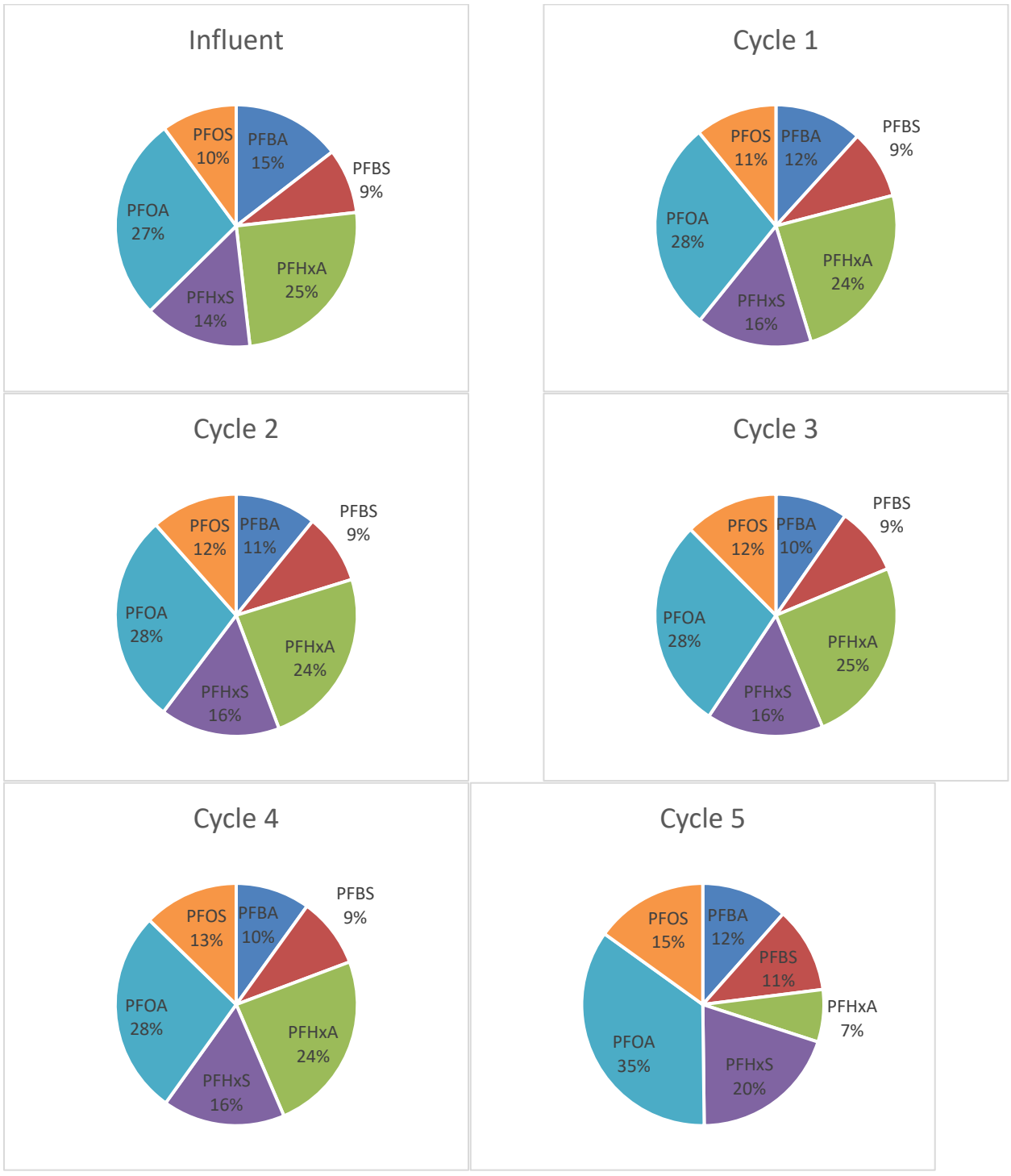

Figure 3.3.6. Experiment 4 molar speciation of the six PFAS chemicals in the influent (top left), and the molar speciation of PFAS chemicals that adsorbed onto A520E resin during the first (top right), second (middle left), third (middle right), fourth (bottom left), and fifth regeneration cycle (bottom right). Total initial PFAS concentration equal to 11,200 µg/L; individual initial concentrations listed in Table 3.3.1. From Dietz et al. (2021).

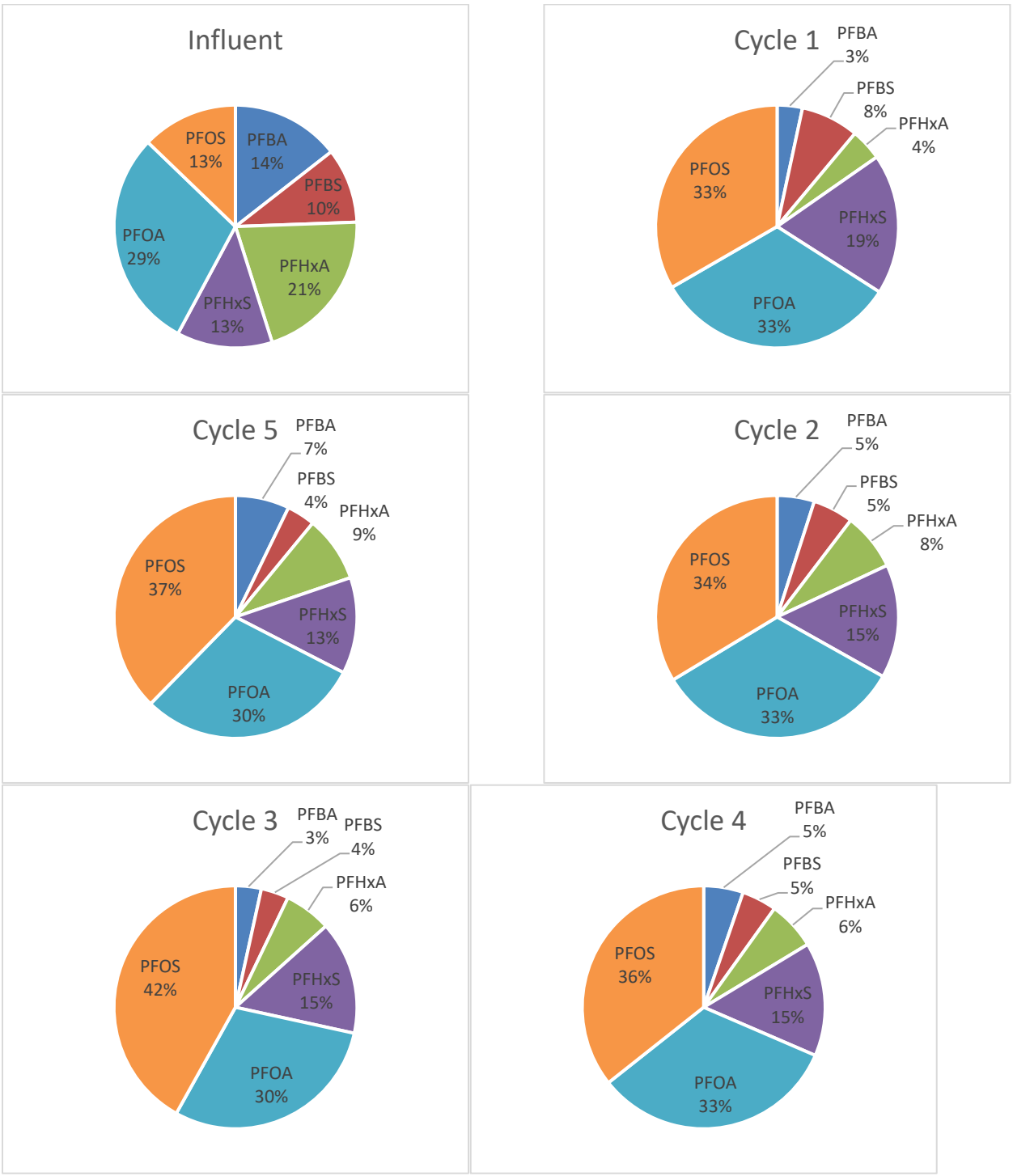

Figure 3.3.7. Experiment 5 molar speciation of the six PFAS chemicals in the influent (top left), and the molar speciation of PFAS chemicals that adsorbed onto A860 resin during the first (top right), second (middle left), third (middle right), fourth (bottom left), and fifth regeneration cycle (bottom right). Total initial PFAS concentration equal to 6,230 µg/L; individual initial concentrations listed in Table 3.3.1. From Dietz et al. (2021).

Discussion of Regeneration solution composition. The results for regeneration efficiency (see **Table 3.3.2**) support the discussion above on the influence of AER polymer composition on PFAS adsorption. For A520E polystyrene resin, $(NH_4)_2SO_4$ + methanol regeneration solution resulted in greater desorption of PFAS than aqueous-only $(NH_4)_2SO_4$ + NH_4OH regeneration solution underscoring the importance of both electrostatic and non-electrostatic interactions. That is, PFAS desorption from resin occurred by sulfate ion disrupting electrostatic interactions and water/methanol cosolvent weakening non-electrostatic interactions. For aqueous-only $(NH_4)_2SO_4$ + NH_4OH regeneration solution, PFBA and to a lesser extent PFHxA were the only PFAAs to desorb. These PFAS have weaker electrostatic interactions with the resin due to carboxylic acid head group and weaker non-electrostatic interactions with resin because of shorter perfluoroalkyl tail. For $(NH_4)_2SO_4$ + methanol regeneration solution, the three PFCAs showed similar regeneration efficiency and greater regeneration efficiency than for PFSAs. This is consistent with sulfonic acid head group having stronger electrostatic interactions. Considering future research on PFAS desorption from strong-base AER, it is possible that increasing the salt concentration would increase regeneration efficiency by further disrupting electrostatic interactions [29]; however, others have shown the opposite effect [33]. It is also possible that greater BVs or contact time of the regeneration solution are needed to improve PFAS recovery (Dixit et al., 2020). Or that a higher fraction of organic cosolvent is needed to further weaken non-electrostatic interactions [33], which presents concerns due to the flammability of methanol. The 0.5% m/m ammonium sulfate salt was used in this study considering the low solubility of PFOS in high ionic strength water matrices (Deng et al., 2010). Ammonium was used as the co-ion in the regeneration solution because ammonium is known to form stronger ion-pairs with PFAAs than sodium or potassium [6]. The potential for ion-pair formation to benefit regeneration efficiency was not able to be confirmed in this research.

PFAS adsorption-desorption from "regenerable" PFAS-selective resins. The results of the adsorption experiment showed a minimal difference between the two sets of AER columns, with the high DOC groundwater flushed columns displaying only ~10% breakthrough for shorter chain PFCAs (e.g., PFBA, PFPeA, and PFHx), and no breakthrough was observed for the non-DOC groundwater flushed columns. Such high removal of PFAS from both sets of columns is expected because the initial PFAS concentration in both influents is relatively low (e.g., 1:100,000 diluted AFFF), and the adsorption capacity of the AER columns is not expected to reach full with the quantity of water being treated (e.g., 2,000 BVs) through each column. Nonetheless, the small percentage of breakthroughs of the short-chain PFCAs in the DOC-impacted AER column indicates that NOM in groundwater can reduce the adsorption capacity of AERs for PFAS. On the other hand, the regeneration profiles of both sets of flow-through columns showed a significant difference, likely due to the different DOC concentrations in their influent. As shown in **Figure 3.3.8**, the amount of PFAS desorbed from each regeneration cycle was much more prominent in the non-DOC-impacted columns (**Figure 3.3.8B**) compared to the DOC-impacted columns (**Figure 3.3.8A**). For example, PFBA on the non-DOC-impacted columns was 100% desorbed after the second regeneration event, while only 45% of its mass was desorbed from the DOC-impacted columns after three regeneration events. This result suggests that high DOC presented in the groundwater hindered the regeneration of PFAS, potentially by blocking AER's pores that allow PFAS transport within the resin and/or lowering the regenerants affinity towards PFAS.

Other observations found in both data sets are PFCAs desorbed first before PFSAs with the same chain length and long-chain PFAS with the same head group generally desorb first compared to

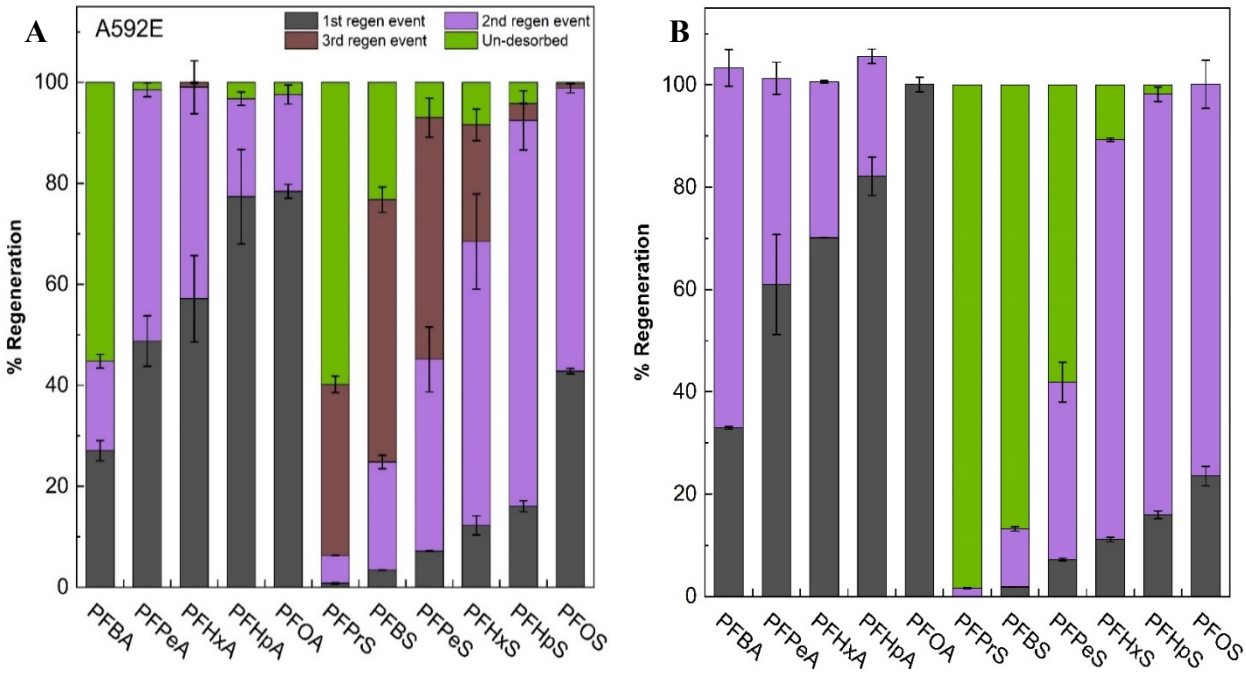

Figure 3.3.8. Regeneration profiles of A592E columns for PFAAs with the influent being: A) a groundwater with 7 mg/L DOC and B) a non-DOC groundwater. Regeneration schemes: 1st = 0.2% $(NH_4)_2SO_4$ + 80% MeOH, 10 BVs; 2nd = 0.2% $(NH_4)_2SO_4$ + 80% MeOH, 30 BVs; 3rd = 0.2% NH_4Cl + 80% MeOH, 30 BVs

their short-chain analogs.

3.4 Field Continuous-Flow Pilot Study Comparing Ion Exchange Resins

This section describes the results of a field pilot study and subsequent sorbent analyses aimed at improving understanding of PFAS removal by AERs under continuous-flow conditions. Five commercial AERs (both polystyrene and polyacrylic) were compared for PFAS treatment at an AFFF-impacted source zone, including two regenerable resins and three single-use resins with a range of functional groups and porosities. This system treated >180,000 bed volumes (BVs) with a combined EBCT of two minutes for the first two media vessels in each column while >750,000 BVs were treated through the lead vessel (30-sec EBCT) in each column. The goals of this field pilot were to evaluate (1) regenerable vs single-use resin performance, (2) the sorbent properties most important for PFAS removal, (3) the effects of EBCT on PFAS elution, (4) identify structure-reactivity patterns among PFASs and relate individual PFAS breakthrough behavior with batch-derived adsorption parameters, and (5) how to best optimize ion exchange system configuration. The Thomas Model was fit to breakthrough data to provide objective quantification of breakthrough parameters for individual PFASs on each resin. Postmortem analysis of the spent resins was performed to characterize adsorption zones for individual PFASs along each sorbent column to obtain a deeper understanding of how competitive adsorption among target PFASs influences sorbent capacity and analyte breakthrough. Breakthrough data and postmortem

adsorbate profiles were used to identify important factors, including site-specific treatment criteria, that will determine media usage rates (MURs) across a range of diverse sites.

Site and sourcewater characterization. Twelve PFASs including the C4-C8 perfluorocarboxylic acids (PFCAs), C3-C8 perfluoroalkyl sulfonic acids (PFSAs), and the fluorotelomer acid 6:2 FTS were consistently detected in the sourcewater above quantifiable limits (**Table 3.4.1**). Collectively, these analytes had a total PFAS concentration ranging from 30,000-55,000 ng/L. PFOS (22,500 ng/L) accounted for approximately 57% of the total PFAS, where 'total PFAS' is defined as the mean summation of all individual analytes present in the sourcewater with concentrations exceeding the detection limits of LC-QToF-MS analysis in replicate samples taken throughout system operation As a subclass, PFSAs also dominated, comprising >78% of total PFAS mass, whereas PFCAs constituted ~15% and 6:2 FTS the remainder. The predominance of PFSAs is consistent with other AFFF-impacted sites (Hu et al, 2016). A small number of additional nontarget PFASs, mostly perfluoroalkyl sulfonamide precursors, were detected using a suspect screening protocol (McDonough et al., 2020a). Semi-quantitative estimates of concentration for suspect analytes that were consistently detected ranged from 0.1 – 0.5 µg/L, representing less than 3% of the total detected PFASs. **Table 3.4.1** also includes water quality parameters and concentrations of important groundwater co-constituents detected at the site, including dissolved organic carbon (DOC). Concentrations of non-target anions were well below the levels expected to compete with PFASs for available exchange sites, and the DOC range of 0.7-1.3 mg/L is consistent with global median groundwater concentrations (Fang et al., 2021; McDonough et al, 2020b).

Table 3.4.1. Concentrations of PFASs and other sourcewater parameters.[a] From Ellis et al. (2022).

Sourcewater PFASs			Groundwater Co-Constituents	
Compound	**Acronym**	**Concentration (ng/L)**	**Constituent**	**Concentration (mg/L)**
Perfluorobutanoic acid	PFBA	564±105	TOC[b]	1.15±0.43
Perfluoropentanoic acid	PFPeA	819±322	DOC[b]	1.02±0.30
Perfluorohexanoic acid	PFHxA	1,720±380	TDS[b,c]	357±75
Perfluoroheptanoic acid	PFHpA	361±131	Alkalinity[d]	104±17
Perfluorooctanoic acid	PFOA	2,530±710	Dissolved O_2[b,c]	7.70±2.63
Perfluoropropane sulfonate	PFPrS	409±101	Cl^-	36.9±3.0
Perfluorobutane sulfonate	PFBS	894±283	NO_3^-	2.36±0.99
Perfluoropentane sulfonate	PFPeS	842±182	SO_4^{2-}	14.3±0.8
Perfluorohexane sulfonate	PFHxS	5,390±1,040	Na	19.5±0.4
Perfluoroheptane sulfonate	PFHpS	715±259	Ca	49.7±1.8
Perfluorooctane sulfonate	PFOS	22,500±5,200	Fe[c]	0.085±0.03
6:2 fluorotelomer sulfonate	6:2 FTS	2,520±800	Mg	14.5±0.6
Total PFAS	ΣPFAS	39,300±9,500	pH	6.85±0.64

[a.] Concentrations obtained at Colorado School of Mines unless otherwise noted

[b.] TOC = total organic carbon, DOC = dissolved organic carbon, TDS = total dissolved solids

[c.] Concentrations obtained from a consulting firm report provided by treatment site managers

[d.] Alkalinity units in mg/L as $CaCO_3$

Anionic resin selection for use in the field pilot system was informed by results from the resin screening detailed in Section 3.1, with a particular emphasis on selecting resins with a diverse variety of AER properties that may be available on the market (e.g., varied polymer, pore structure, etc.). Of the fourteen initial sorbents in the screening, both regenerable and PFAS-selective anionic resin groups outperformed all cationic resins, non-ionic resins, and GAC (Figure 3.1.3), thus those six adsorbents were removed from consideration. Because all PFAS-selective AERs were comprised of polystyrene, a direct comparison of AER polymer required one polystyrene regenerable AER (A520E) and the lone polyacrylic AER (A860), as these two resins share similar properties with the same porosity and size range. Because the PFAS-selective resins were found to have the strongest affinity for PFASs as a class, three of these products were chosen for inclusion. PFA694E and CalRes 2301 were selected as they have different porosities (gel and macroporous, respectively), but their different functional group types prevented direct isolation of each parameter. To assess the roles of AER porosity and functional group type, PSR2+ (a PFAS-selective resin more recently introduced to market) was included as its gel porosity and tributylamine functional group enabled comparison with PFA694E (gel, complex amino group) and CalRes 2301 (macroporous, tributylamine). Overall, these five resins allowed for direct comparison of AER regenerability, porosity, functional groups, and polymeric composition to evaluate which parameters most significantly influence PFAS removal.

PFAS treatment with regenerable AERs. The pilot test included two regenerable AERs: a polyacrylic resin (A860) and a polystyrene resin (A520E). The polyacrylic A860 performed very poorly at a 2-min EBCT, with all PFASs being detected in effluent samples after just 960 BVs – or 32 h of system operation, and all PFAAs reached >90% of influent concentrations within 10,000 BVs (**Figure A3.4.1**). Thus, further discussion of this resin's performance is limited. **Figure 3.4.1a** shows breakthrough curves for individual PFAAs from effluent of the second vessel in each column (2-min total EBCT) for the regenerable polystyrene resin (A520E) and the three single-use resins in **Figures 3.4.1b-d** (PFA694E, CalRes 2301, and PSR2+, to be discussed in next section). For A520E (**Figure 3.4.1a**), both short- and long-chain PFCAs, as well as 6:2 FTS (shown separately in **Figure A3.4.2**), eluted through the column fully in <75,000 BVs, whereas most PFSAs did not fully elute even after treating 180,000 BVs. Short-chain PFSAs were first detected at ~50,000 BVs, with only PFPrS and PFBS reaching complete breakthrough within 180,000 BVs. By the end of the pilot test, intermediate length PFSAs (PFPeS and PFHxS) reached ~50% breakthrough, but PFOS – the dominant PFAS detected in the sourcewater – reached only 4% breakthrough. For PFASs that fully broke through, many samples showed effluent concentrations that exceeded influent concentrations, sometimes reaching >170% of the influent values, consistent with competitive displacement of lower-affinity PFASs by higher-affinity structures like PFOS as observed in prior studies (McCleaf et al., 2017).

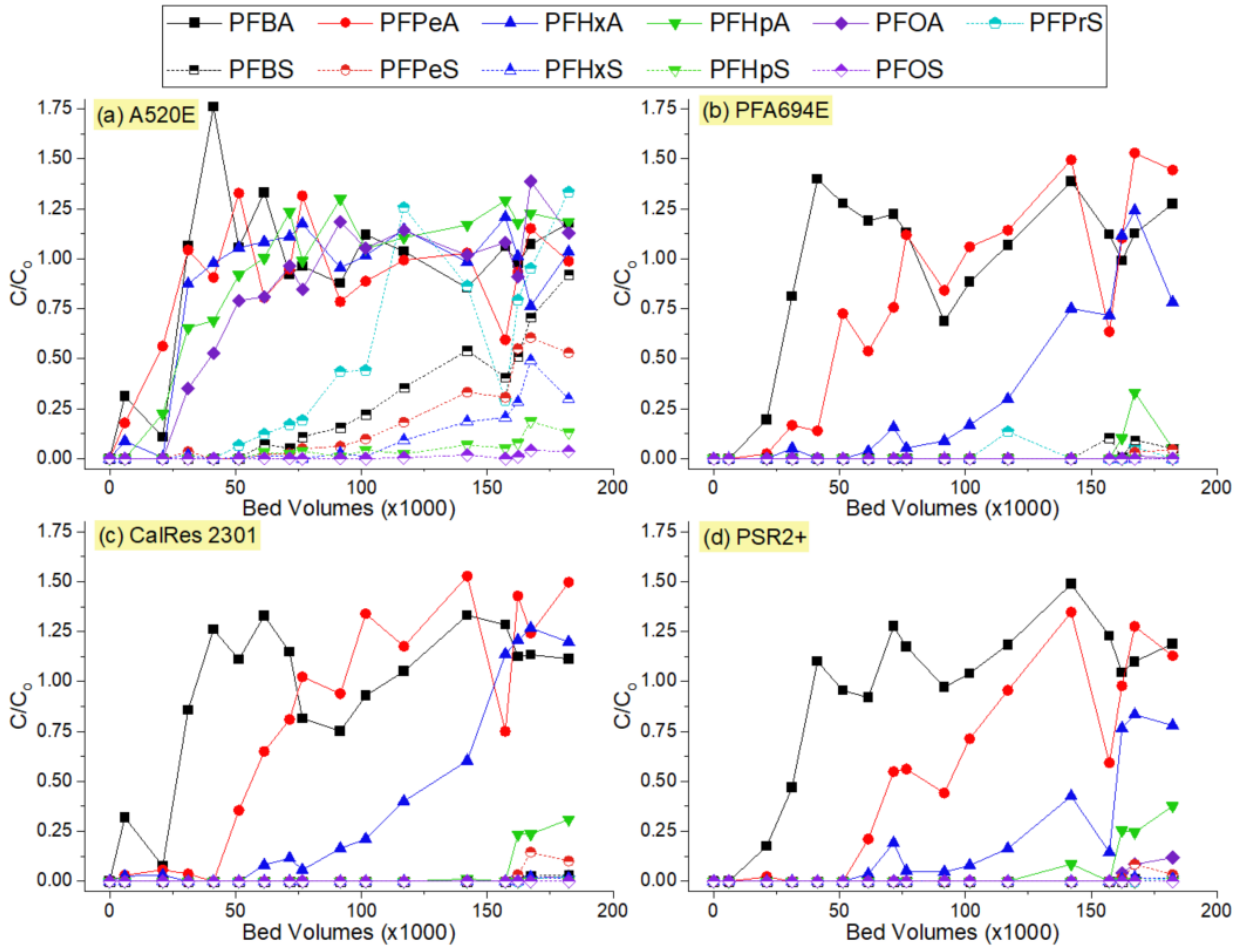

Figure 3.4.1. Breakthrough data for PFAAs after treatment with AERs at a 2-min EBCT. Data shown for resins including (a) A520E, (b) PFA694E, (c) CalRes 2301, and (d) PSR2+. From Ellis et al. (2022).

While complete breakthrough of many PFASs was not be observed for 2-min EBCT (**Figure 3.4.1a**), more complete breakthrough was observed in effluent collected following 30-sec of EBCT (**Figure 3.4.2a**), where >700,000 BVs were treated during the pilot study. Results for A520E are generally consistent with observations for 2-min EBCT, with rapid elution of PFCAs within the first 50,000 BVs. However, all PFSAs were also detectable within 25,000 BVs. PFPrS, the shortest-chain PFSA, first reaches 50% breakthrough by 114,000 BVs, whereas PFOS does not exceed 50% breakthrough until >650,000 BVs. Comparison of breakthrough data for individual analytes on a bed volume-equivalent basis (**Figures A3.4.14-A3.4.25**) shows breakthrough of most PFASs at lower BVs when monitoring effluent after 30-sec EBCT than 2-min EBCT, particularly for PFSAs. This can be attributed to kinetic limitations and greater opportunities for preferential flow path development in the shorter bed depths (Murray et al., 2021). Still, breakthrough data collected after the shorter EBCT is valuable for revealing PFSA breakthrough that would not otherwise be observed within the pilot study timescale. Effluent data collected from a third segment of A520E (**Figures A3.4.26-A3.4.37**) that provided an additional 1-min EBCT (total of 3-min EBCT) was similar to results for 2-min EBCT, reinforcing the notion that data collected

with 2-min EBCT likely reflects results that would be observed when using the longer recommended EBCTs for regenerable resins (e.g., 3-5 min).

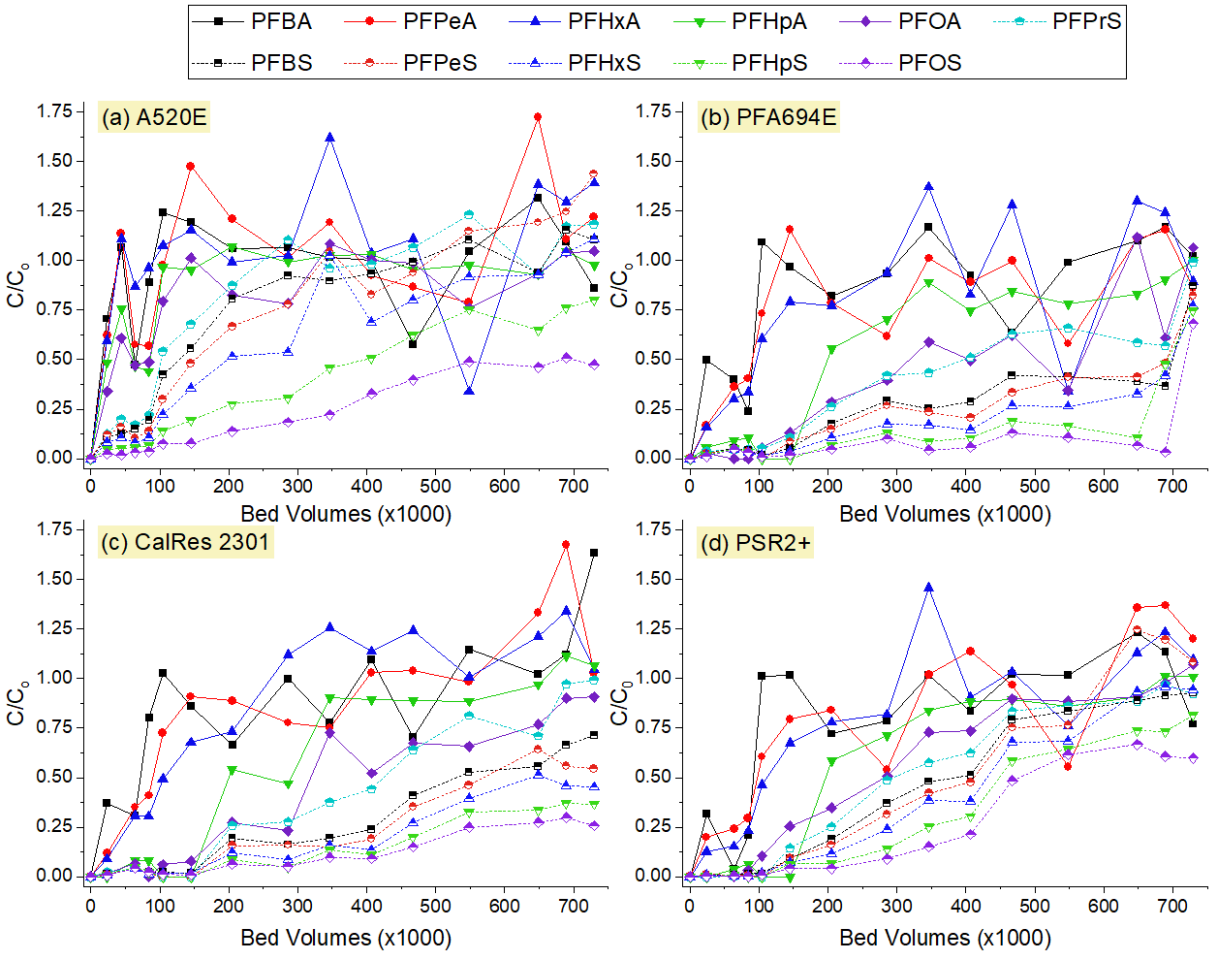

Figure 3.4.2. Breakthrough data for PFAAs after treatment with AERs at a 30-sec EBCT. Data shown for resins including (a) A520E, (b) PFA694E, (c) CalRes 2301, and (d) PSR2+. A860 data was not assessed at a 30-sec EBCT due to the immediate breakthrough observed in 2-min EBCT samples. From Ellis et al. (2022).

PFAS treatment with single-use AERs. Compared to the regenerable AERs, much longer BVs to breakthrough were observed for most PFASs using the three single-use resins (**Figures 3.4.1b-d, 3.4.2b-d**; PFA694E, CalRes2301, and PSR2+). With a 2-min EBCT, >50% breakthrough within 180,000 BVs was only observed for ≤C6 PFCAs. PFHpA is initially observed in the effluent, at ~25% of influent levels, between 150,000 and 180,000 for all three resins, and PFOA is initially observed in the effluent for PSR2+ after 160,000 BVs. Nearly all PFSAs remained undetected with the single-use resins throughout the pilot study, though some short-chain PFSAs were detected at trace levels after 160,000 BVs at a 2-min EBCT. Though there is considerable scatter in the sourcewater concentrations of 6:2 FTS and the resulting breakthrough data (**Figure A3.4.2**), similar trends hold where single-use resins show far more BVs to breakthrough than regenerable resins. Direct comparison of breakthrough data for individual PFASs on different resins is provided in **Figures A3.4.2-A3.4.13**.

The lack of substantial breakthrough for most PFAAs within 100,000 BVs using a 2-min EBCT indicates that these single-use AERs are promising options for PFAS treatment. However, the lack of actual breakthrough data precludes exact quantification of the extent to which these sorbents outperform regenerable AERs. Instead, data collected with 30-sec EBCT (**Figure 3.4.2**) can provide some measure of comparison between resins. While >50% breakthrough of short-chain PFCAs occurs within 100,000 BVs on all three single-use resins, >200,000 BVs is required for long-chain PFCAs. In contrast to the 2-min EBCT data, both long- and short-chain PFSAs are detected in the first 25,000 BVs for the single-use resins at a 30-sec EBCT, though no compounds reach 10% of their influent concentrations until >150,000 BVs. Long-chain compounds of regulatory concern like PFOA are better treated by all single-use AERs compared to the regenerable AERs, as PFOA does not reach 50% breakthrough on any single-use resin until 300,000 BVs compared to <65,000 BVs with regenerable resins. As seen in the case of regenerable resins, PFSA breakthrough curves after single-use AER treatment exhibit gradual breakthrough with long-chain PFSAs never reaching complete breakthrough by 700,000 BVs on any of the resins. However, AER removal of all PFASs is superior for all three single-use resins compared to A520E. Comparing single-use breakthrough data between the 30-sec and 2-min EBCTs for A520E (**Figures A3.4.38-A3.4.49**) reveals that the 30-sec EBCT reasonably predicts 2-min breakthrough for PFCAs, but PFSAs experience more rapid breakthrough at a 30-sec EBCT, indicating this contact time is inadequate for use in the field.

Treatment of nontarget PFASs. Screening of suspect compounds in the sourcewater revealed four additional structures with semi-quantitative estimates of concentration exceeding 100 ng/L. Three of these four compounds were short-chain fluoroalkane sulfonamides (FASAs) with $\leqslant$5 carbon atoms, which are uncharged at environmentally-relevant pH (Nguyen et al., 2020). Quantitative analysis of suspect breakthrough was precluded by the lack of native standards for these PFASs, though semi-quantitative analysis showed that these structures fully broke through all AER beds within the first five weeks, earlier than any of the PFAAs. The fourth suspect compound, H-PFDA, is a C10 polyfluoroalkyl carboxylic acid where one fluorine on the fluoroalkyl chain has been replaced by hydrogen. H-PFDA showed strong affinity for AERs and was not detected in effluent samples from four AERs analyzed throughout pilot system operation.

Postmortem analysis of resins. After conclusion of the field pilot, columns of used resin were cross-sectioned and PFASs were extracted from each segment to characterize the spatial distribution of adsorbed PFASs along each column. The first two of the five sections were derived from the initial 30-sec EBCT vessel, while the remaining three sections came from the second vessel in each channel that provided an additional 90 sec of EBCT. The resulting profiles are shown in **Figure 3.4.3**, with each bar representing the spatial distribution of an individual PFAS' mass along the length of the AER column, with flow proceeding from top to bottom. The numbers at the top of each bar represent the percentage of total influent analyte mass that was retained by the resin over the course of the pilot (i.e., the percentage of total sourcewater mass that did not break through). Consistent with the breakthrough data, the adsorbed data show that the single-use resins retained a much larger percentage of the sourcewater PFASs than the regenerable A520E resin. The retained masses of PFASs were similar for all three single-use resins.

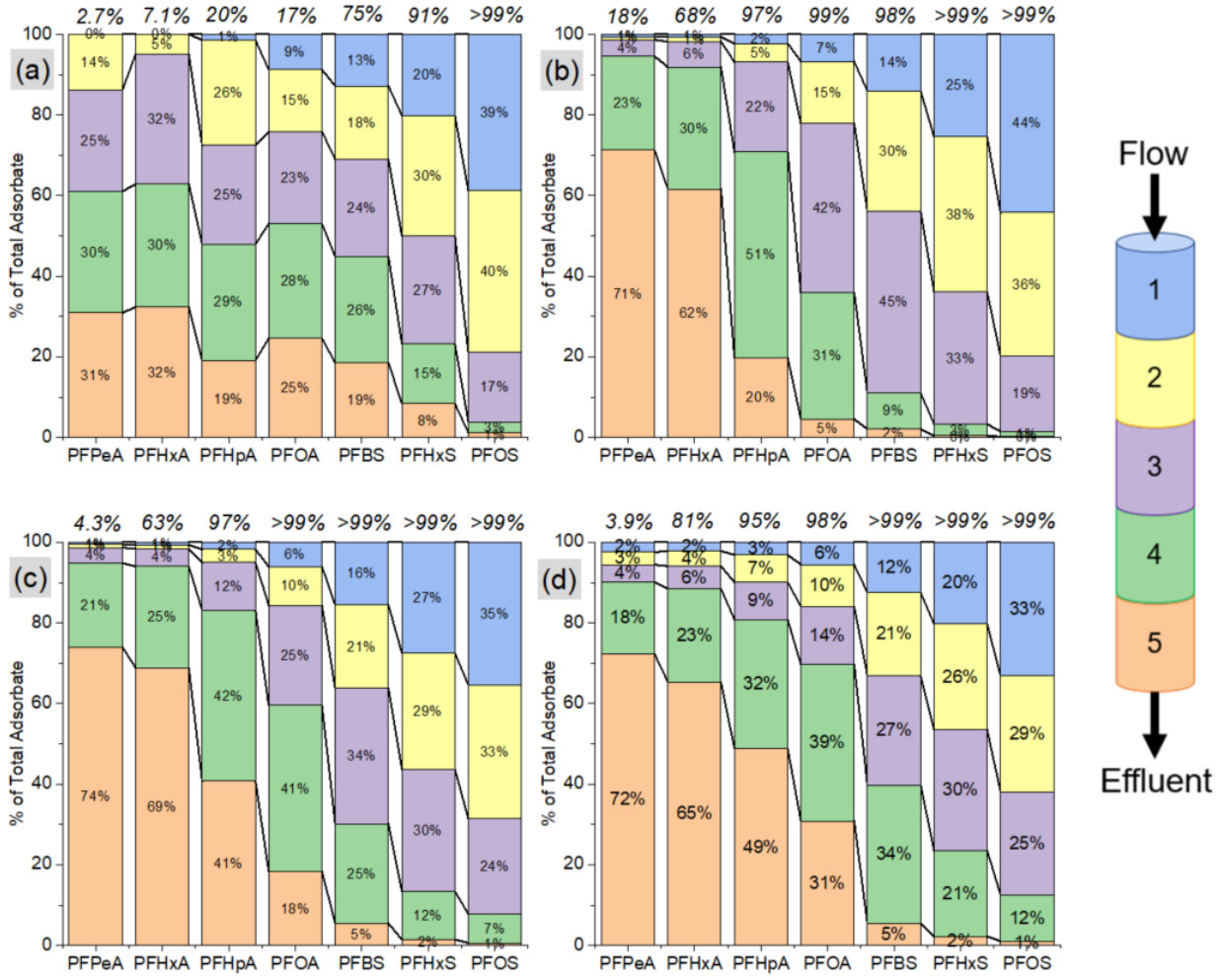

Figure 3.4.3. Used ion exchange column profiles obtained after extracting adsorbed PFAS. Data shown for resins including (a) A520E, (b) PFA694E, (c) CalRes 2301, and (d) PSR2+. Percentages at the top of each bar represent the percent of total influent PFAS mass that remained adsorbed to the column over the duration of the 36-week pilot study. Colors and numbers in legend refer to the sequence of cross-sections in the packed resin bed, where sections 1 and 2 each represent 15 sec of EBCT and sections 3-5 each represent 30 sec of EBCT. From Ellis et al. (2022).

For all resins, a clear trend is apparent where PFASs with higher affinity for a resin (i.e., PFSAs and long-chain PFCAs) were more heavily concentrated in the early segments of each column, whereas lower-affinity compounds were primarily found in the latter segments. Conceptually, this follows the chromatographic trends observed in the breakthrough data where the active adsorption zone of short-chain PFCAs has progressed further along the column by the conclusion of the study while higher-affinity compounds remain concentrated in the earlier sections. Because nearly all the PFOS mass is located in the early segments of each column, whereas PFPeA mainly exists in the latter segments, it can be inferred that – in the final days of pilot operation – the majority of PFOS uptake was occurring in the 30-sec EBCT vessel while PFPeA was primarily adsorbing in the latter segments of the second vessel. Additionally, the absolute mass of lower-affinity structures like PFPeA is much higher in the latter sections (e.g., 0.66 mg/g of resin in Section 5 vs

0.19 mg/g in Section 1 for CalRes 2301), consistent with an analyte that is being displaced from upstream sections by competitive adsorption of higher-affinity compounds like PFOS.

Analysis of PFAS breakthrough behavior. Breakthrough of individual PFAS analytes follows a chromatographic trend wherein short-chain structures break through earlier than long-chain homologues. This phenomenon is due to the hydrophobic and van der Waals forces that attract the hydrophobic, nonpolar fluorocarbon tail of the PFAS molecule to the hydrophobic components of the polymeric resin. Because overall molecular hydrophobicity increases with increasing length of the fluorocarbon tail, PFAS affinity for AERs increases with increasing tail length, leading to longer times before elution through the sorbent column (Boyer et al., 2021; Wang et al., 2019). Among structures with the same fluorocarbon chain length, PFCAs break through far earlier than PFSAs, indicating stronger attraction between the sulfonate head group of the PFSA and the cationic quaternary amine resin functional groups when compared to the carboxylate group of PFCAs. These functional groups located on the resin exchange sites attract PFAS head groups via electrostatic exchange, resulting in a combination of both electrostatic and hydrophobic forces in AER adsorption of PFASs. In fact, the shortest-chain PFSAs (PFPrS and PFBS) are generally retained longer than the longest-chain PFCA (PFOA). Surprisingly, breakthrough of 6:2 FTS, a polyfluoroalkyl sulfonate, was more similar to that observed for PFCAs than even short-chain PFSAs, demonstrating a critical effect of substitution at the α-carbon position on resin affinity. As expected, nonionic FASA structures identified through suspect screening analysis were not effectively adsorbed by AERs. These trends of chain length-dependent breakthrough, chromatographic elution, and the role of head groups are supported by existing literature (McCleaf et al., 2017, Maimati et al., 2018; Wang et al., 2019), with greater in-depth explanation of PFAS structure-reactivity relationships and AER characteristic-reactivity patterns available in our prior work (Fang et al., 2021).

From an operational perspective, the most important distinction between these sorbents is the resins' regenerability. All three single-use AERs treat both PFCAs and PFSAs for many more BVs before breakthrough than either regenerable resin. PFOA, the PFCA of primary interest to regulators, is treated to non-detect levels (<0.1 ng/L) through >150,000 BVs with all single-use resins (2-min EBCT), compared with only 31,000 BVs for the regenerable A520E (and <1,000 BVs for A860). This disparity holds true for the PFSA class as well, as every PFSA present in the sourcewater other than PFOS is detected in A520E effluent samples within 61,000 BVs, whereas long-chain PFSAs remain at non-detect levels for ≥150,000 BVs with all three single-use resins. Among the three single-use resins, PFAS treatment performance is similar for all analytes after 2 min of EBCT.

Although some recent reports have indicated successful use of polyacrylic AERs (Deng et al., 2010; Dixit et al., 2021a), findings from this study and recent laboratory investigations (del Moral et al., 2020; Dietz et al., 2021) demonstrate the superiority of polystyrene AERs. The four polystyrene-based resins removed PFSAs through ≥40,000 BVs with complete PFOS removal through ≥75,000 BVs, whereas near-immediate breakthrough was observed with the polyacrylic resin. The success of A860 in prior studies might result from longer contact times (e.g., >10 min) and lengthy batch reactions that do not reflect treatment site conditions in the present study, as well as the presence of elevated NOM levels in the earlier bench-scale studies. Because A860 has been found to remove NOM better than polystyrene PFAS-selective resins (Dixit et al., 2020; Dixit

et al., 2021a), the presence of higher NOM levels may improve PFAS adsorption by cooperative adsorption mechanisms. The superiority of polystyrene-based resins for PFAS adsorption observed in the present study can be attributed to their greater hydrophobicity in comparison to polyacrylic-based resins.

It is interesting to note the similar performance of three single-use resins despite large differences in maximum PFOS adsorption capacity measured in batch equilibrium experiments (**Tables 2.2.1-2.2.2**). Although the macroporous CalRes 2301 yielded a maximum batch adsorption capacity >4 times greater than either of the other two gel-type single-use resins, breakthrough data for PFOS was similar for all three resins. Thus, other factors beyond maximum adsorption capacity control uptake and competition among PFASs on these resins. Influent PFAS concentrations is likely one such factor, as other pilot-scale treatment systems at lower-concentration sites experienced complete PFAS breakthrough after adsorption of significantly lower total PFAS masses (Liu et al, Under Review; Dixit et al., 2021b). Other factors specific to individual AERs including polymer, exchange site density, and functional group type have been known to play a major role in the adsorption and desorption of various PFASs to AERs (Fang et al., 2021; Deng et al., 2010).

Breakthrough curve fitting using the Thomas Model. Measured PFAS breakthrough data, where sufficient breakthrough was observed before the pilot study ended, was fit with the Thomas Model as shown for CalRes 2301 in **Figure 3.4.4**. Similar fits for other resins are provided in **Figures A3.4.51-A3.4.57** in the appendix; data for A860 was excluded since >50% breakthrough of all PFASs was observed within one week of pilot operation. The resulting fit-derived parameters, k_{Th} (Thomas Model constant) and q_e (resin capacity for individual sorbate uptake) are listed in **Table A3.4.2**. Statistical variances of these fits are reasonable ($r^2 > 0.9$ for most analytes) and sigmoid inflection points (**Table 3.4.2**, representing 50% breakthrough) were obtained from these fits to serve as an objective reference point to compare various analytes' breakthrough profiles. Fitting efforts focused on data from 30-sec EBCT vessels because breakthrough was more complete within the 725,000 BVs of data collected, enabling broader comparison among all PFASs and resins. While breakthrough was not observed for many PFAAs using a 2-min EBCT, Thomas model fits are provided for the few analytes that did breakthrough sufficiently during the pilot study.

Although breakthrough data and model fits for 30-sec EBCT are not expected to perfectly represent breakthrough when using a longer 2-min EBCT, it is worth noting that the model predictions of 50% breakthrough with 30-sec and 2-min EBCT generally agreed for the few analytes that did experience sufficient breakthrough at a 2-min EBCT to perform a model fit. **Figure A3.4.58** compares the BVs at which 50% analyte breakthrough is predicted at both EBCTs, with the majority of analytes falling very near the 1:1 correlation line. Still, the lack of PFSA breakthrough for single-use AERs at 2-min EBCT during the pilot study prevents conclusions from being drawn for PFSAs. Overall, the general agreement between the two EBCTs supports the use of the 30-sec data for Thomas Model fitting and breakthrough predictions.

The trends in 50% breakthrough values observed for individual PFAA-resin combinations are generally consistent with trends in equilibrium ion exchange affinity constants measured in batch experiments (Fang et al., 2021). **Figure 3.4.5** shows the relationship between the BVs at which breakthrough reaches 50% for different analytes (**Table 3.4.2**) and the PFAS-Cl^- exchange

coefficients (logK_{ex}) measured for the same analyte-AER combinations in batch adsorption experiments; corresponding linear correlation fits for individual resins provided in **Figures A3.4.59-62**. These empirical correlations – particularly strong for the single-use AERs – suggest that field performance of new resins under development may be roughly estimated from batch adsorption experiments for the new resin in tandem with pilot breakthrough data already collected for existing resins where these correlations have been observed. While such predictions need further validation, this suggests an approach that could be used to rapidly screen and downselect new adsorbents before investing in more costly and lengthy pilot studies at a contaminated site.

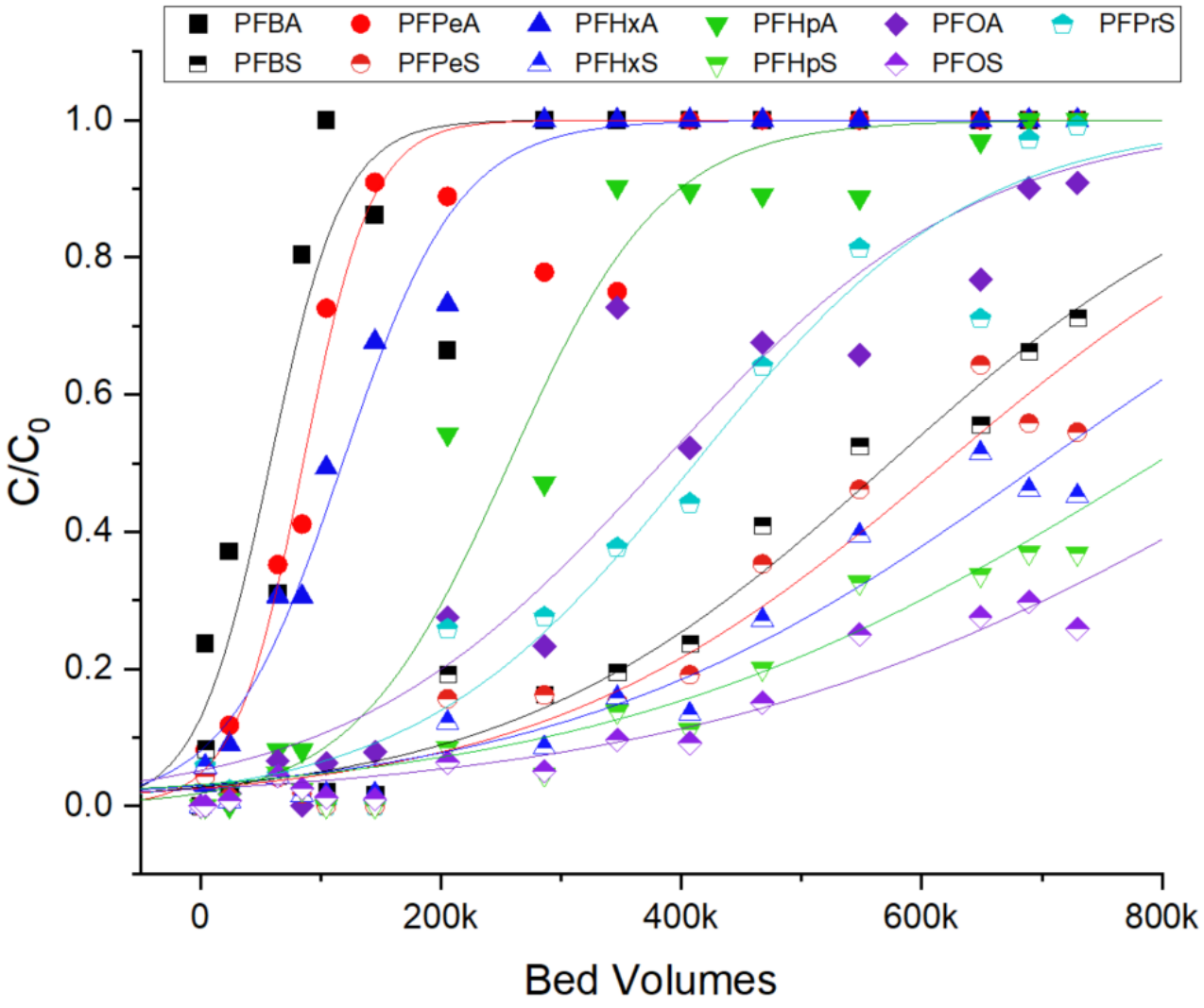

Figure 3.4.4. Sigmoid curve fits to breakthrough data for all PFAS structures after treatment using CalRes 2301 at a 30-sec EBCT. From Ellis et al. (2022).

Table 3.4.2. Bed volumes treated until breakthrough observed for a number of treatment criteria. From Ellis et al. (2022).

Resin	A860	A520E	PFA694E	CalRes 2301	PSR2+
	50% Breakthrough BVs as Obtained from Fitted Curves[a,b]				
PFBA	<1,000 ± 75	17,000 ± 1,300	67,000 ± 13,000	151,000 ± 82,000	70,300 ± 17,000
PFPeA	<1,000 ± 100	19,000 ± 1,200	84,000 ± 7,200	83,000 ± 10,000	101,000 ± 21,000
PFHxA	<1,000 ± 100	20,000 ± 1,700	97,000 ± 17,000	102,000 ± 18,000	108,000 ± 16,000
PFHpA	<1,000 ± 100	25,000 ± 7,200	186,000 ± 32,000	197,000 ± 32,000	182,000 ± 29,000
PFOA	<1,000 ± 100	80,000 ± 15,000	315,000 ± 64,000	362,000 ± 116,000	278,000 ± 25,000
PFPrS	3,000 ± 2,000	117,000 ± 6,000	411,000 ± 82,000	385,000 ± 32,000	292,000 ± 12,000
PFBS	3,700 ± 1,900	134,000 ± 5,900	639,000 ± 162,000	542,000 ± 31,000	350,000 ± 19,000
PFPeS	1,300 ± 1,500	166,000 ± 12,000	732,000 ± 243,000	581,000 ± 47,000	371,000 ± 35,000
PFHxS	2,900 ± 1,900	219,000 ± 30,000	681,000 ± 51,000	700,000 ± 55,000	390,000 ± 29,000
PFHpS	3,000 ± 2,000	396,000 ± 29,000	696,000 ± 12,000	907,000 ± 73,000	432,000 ± 23,000
PFOS	3,000 ± 1,600	730,000 ± 58,000	715,000 ± 10,000	1,180,000 ± 236,000	503,000 ± 40,000
	BVs Treated before Breakthrough Observed for Specific Criteria				
10% of Influent PFOS[b,c]	<4,000 BVs	160,000 BVs	440,000 BVs	422,000 BVs	346,000 BVs
70 ng/L PFOS + PFOA[c]	<1,000 BVs	<24,000 BVs	105,000 BVs	64,000 BVs	84,000 BVs
Detection of UCMR3 Listed Structures[d,e]	<1,000 BVs	21,000 BVs	157,000 BVs	142,000 BVs	142,000 BVs
Detection of any PFAS[e]	<1,000 BVs	<6,000 BVs	21,000 BVs	<6,000 BVs	21,000 BVs

[a.] BVs determined by the point at which the analyte reaches 50% of its influent conc. on the fitted breakthrough curves

[b.] BVs determined by the point at which PFOS reaches 10% of its influent conc. on the fitted breakthrough curves

[c.] Estimates provided here using 30-second EBCT data for all AERs

[d.] UCMR3 defined by the EPA in 2012 to include PFHpA, PFOA, PFNA, PFBS, PFHxS, and PFOS

[e.] BVs as provided here obtained from the raw 2-minute EBCT data for all AERs

To enable direct comparison of different AERs, **Figure 3.4.6** shows pairwise scatterplots comparing the fit-derived 50% breakthrough BVs (30-sec EBCT) for individual analytes on each of the four polystyrene-based resins. The plots reinforce the superiority of all three single-use AERs compared to the regenerable A520E. Further, we see that all PFSAs reach their 50% breakthrough point earlier for PSR2+ than either PFA694E or CalRes 2301. While these trends are consistent for all PFSA structures, the 30-sec EBCT does not reflect treatment conditions in full-scale systems where 2-3 min EBCT is recommended, thereby precluding a definitive determination of a singular "optimal" resin. While PSR2+ appears to be the least effective single-use AER in treating PFSAs at a 30-sec EBCT, this resin actually shows superior treatment of short-chain PFCAs (PFBA, PFPeA, and PFHxA) when using a 2-min EBCT (**Figure 3.4.1 and A3.4.2-A3.4.4**). Thus, while selection of an optimal single-use resin will depend on the breakthrough criteria that dictates resin changeout, the collective data supports a conclusion that all three single-use resins will be highly effective in PFAS treatment.

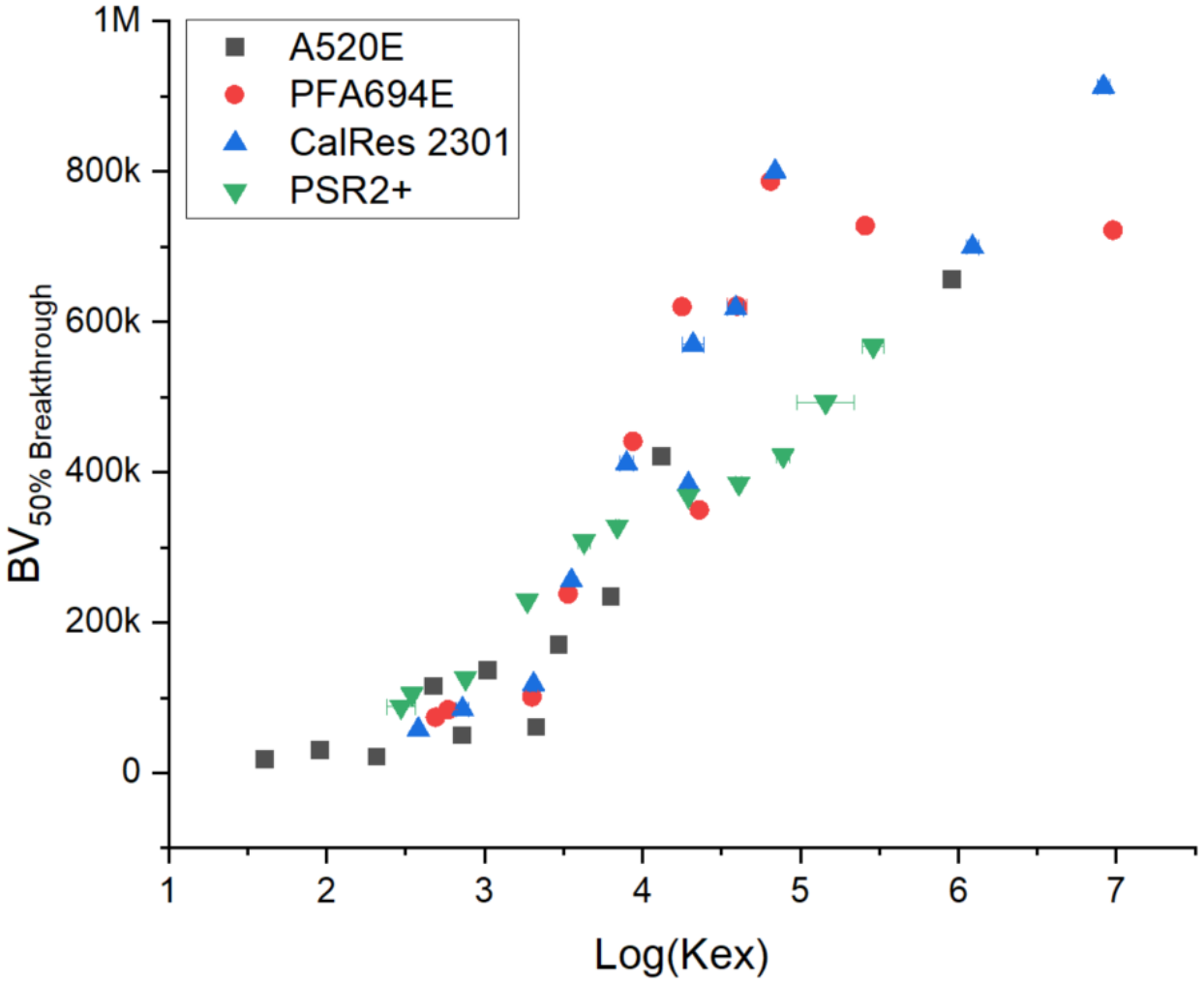

Figure 3.4.5. Relationship between pilot system breakthrough data and batch-derived PFAS-chloride ion exchange coefficients for polystyrene resins. From Ellis et al. (2022).

Media usage rates. Breakthrough data and the Thomas Model fit-derived parameters can be used to predict BVs at which different thresholds for media changeout/regeneration are met (e.g., when 10% PFOS breakthrough occurs). The bottom portion of **Table 3.4.2** summarizes BVs where different thresholds are reached, including BVs treated by each resin before "detection of" criteria are met including "detection of any PFASs" and "detection of UCMR3 structures" since these are common treatment criteria at some sites. In these situations, the values were derived from the raw breakthrough data observed with 2-min EBCT. Predicting the BVs at which media replacement will be required can be directly used to calculate expected media usage rates (MURs). For the single-use AERs, using a changeout criteria of detection of any PFASs in effluent at a site similar in concentration to this study would likely necessitate frequent vessel changeout ≤20,000 BVs since PFBA is detectable within 21,000 BVs for all resins. However, sites only concerned with compounds listed under the EPA's UCMR3 could treat PFAS-impacted waters for well over 100,000 BVs prior to detection using any of the single-use resins. This disparity is even more pronounced in cases where only PFSAs or long-chain structures are of concern. For all three single-use resins, none of the PFSAs reach 50% breakthrough before 325,000 BVs. Thus, media replacement/regeneration criteria will have a significant effect on MURs.

Although single-use AERs treat most PFASs much longer than regenerable AERs when using 50% breakthrough as the changeout/regeneration criteria, differences are not so large when changeout/regeneration criteria is the detection of any PFASs. The superiority of single-use AERs is most pronounced for long-chain PFCAs and short-chain PFSAs. Using detection of UCMR3 structures as the changeout criteria is one scenario where single-use resins substantially outperform regenerable AERs, with estimates that >7 times more water can be treated using single-use resins than either of the regenerable resins. This trend indicates that emphasizing more highly selected-for PFASs (e.g., PFSAs, long-chains) leads to larger disparities between single-use and regenerable AERs. Finally, it is worth noting that PFAS concentrations, mixture composition, and groundwater geochemistry at given site can significantly influence breakthrough and MURs. This pilot test was performed at a source zone with elevated PFAS concentrations (i.e., >10 μg/L), and media replacement at such a site can be expected to be quite different from sites where PFAS concentrations are much lower.

Adsorption zone identification. Postmortem analysis of the spatial distribution of adsorbed PFASs on the resins provided a snapshot of the active adsorption zone for each analyte at the time the pilot study was completed. These data reinforce the trends seen in the breakthrough data, indicating long-chain structures and PFSAs have higher affinity for all AERs than short-chain structures and PFCAs, respectively. This suggests that not only does the increased hydrophobic character of PFASs with longer fluorocarbon tails lead to greater resin affinity, but also that PFASs with shorter tails are more easily displaced from resins due to the lower hydrophobic attraction between the target analytes and the hydrophobic resin polymer. While chromatographic elution of PFAS analytes is well-established, these adsorbate distribution profiles underscore the importance that competitive displacement mechanisms play in the breakthrough behavior of individual PFASs when treating PFAS mixtures in AFFF-impacted water sources.

Comparison of the total PFAS mass found on each section shows that the total adsorbed mass decreases substantially along the length of the column. On a molar basis, the total PFAS mass adsorbed in the first section of each single-use resin is >15-fold higher than that adsorbed in last

section. In fact, the masses extracted from section 1 exceed isotherm-derived PFOS capacities for CalRes 2301 and PFA694E. Possible explanations for this include size exclusion, where lower molecular weight PFASs may access more internal exchange sites than PFOS, or potential bilayer/micellar formation on the surface of the AER beads that enables hydrophobic uptake beyond the electrostatic exchange capacity. Potential for bilayer and micellar formation has been documented for PFASs adsorbing onto charged surfaces including AERs (Dixit et al., 2021b; Xiao et al., 2019; Zaggia et al., 2016), as well as for hemi-micelle aggregation on NOM macromolecules (Gagliano et al., 2020).

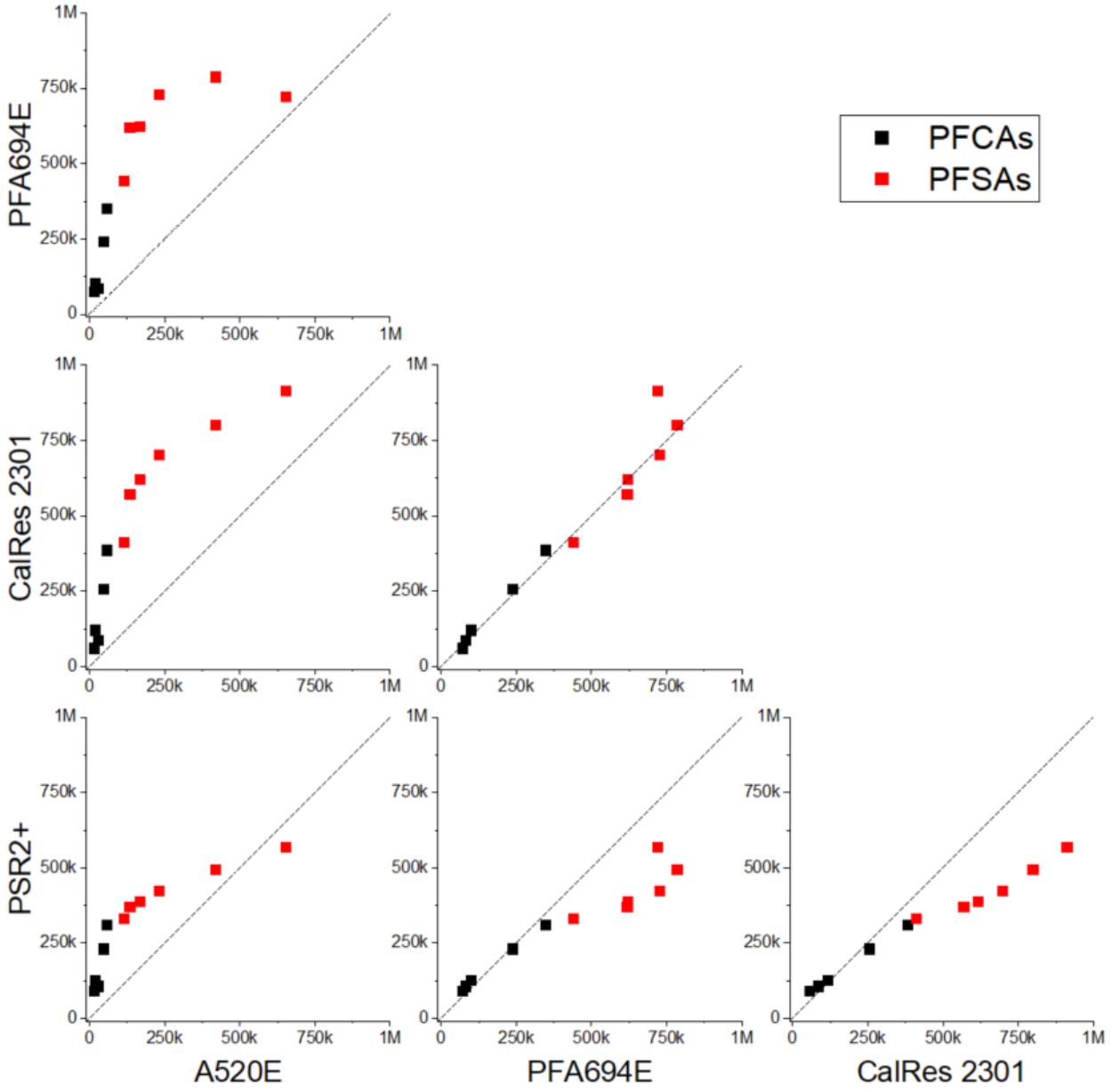

Figure 3.4.6. Pairwise scatter of the estimated bed volumes treated until PFAA breakthrough reaches 50% for various combinations of resin. Axes represent bed volumes treated in thousands (k) or millions (M). Individual points represent a single analyte's estimated breakthrough for a given pairing of resins. From Ellis et al. (2022).

Implications for full-scale treatment operations. The enhanced mass uptake in earlier sections of the column identified in the postmortem resin analyses is that sites with stringent treatment objectives may potentially reduce MURs by arranging multiple sorbent vessels in series (e.g., lead → lag 1 → lag 2) and operating the lead vessel to greater degrees of breakthrough before media changeout. Such a configuration would enable operators to replace resin with high PFAS loading in the lead vessel while continuing to facilitate adsorption in the lag vessels containing resin that would otherwise be replaced during changeout of a single vessel. Given that the extract profiles of the spent AERs imply that the earliest sections of the column have higher sorbed PFAS masses than the later sections, it would be expected that lengthier operation of a lead vessel would result in a greater overall PFAS uptake per mass of resin and ultimately lower MURs. Total system EBCT is recommended to be ≥2 minutes, as shorter EBCTs (e.g., 30-sec) experienced more rapid detection of numerous PFAS analytes. This may be accomplished by multiple vessels with shorter individual EBCTs, thereby enabling a lead-lag configuration that can achieve a total of 2-3 minutes of contact.

Results from this field pilot study also inform operators as to how to best select resins for treatment of PFAS mixtures. Polystyrene resins are strongly recommended due to their increased hydrophobic character while single-use resins provide even greater uptake of PFASs due to the specialized functional groups containing quaternary amines with long hydrocarbon chains, furthering the strong hydrophobic attraction to the adsorbent. However, selection of an optimal resin for remediation will ultimately depend on criteria used to determine the compounds of regulatory concern and their relative concentrations in the PFAS mixture. Sites predominated by long-chain PFASs would benefit from use of high-capacity single-use AERs while sites concerned with short-chain PFASs may opt for regenerable resins that experience breakthrough of PFBA and PFPeA at similar times to single-use AERs. Pilot-scale testing of AERs using site sourcewater is recommended, which may be paired with the correlations identified in this study to approximate expected breakthrough times for more slowly eluting compounds like PFOS.

3.5 Resin Regeneration

3.5.1. Batch resin regeneration experiments

Two polystyrene macroporous anion exchange resins (A520E, A592E) were saturated with six PFAS anions, three carboxylates and three sulfonates, and then regenerated with three different alcohols (methanol, ethanol, 1-propanol) all at 25% ABV with 75% water and 0.5% NaCl m/m of total solution. The results of this experiment can be found below in **Figure 3.5.1**. The results show that desorption of PFBA, PFHxA, and PFOA increased as the carbon skeleton of the alcohol increased from methanol to ethanol to propanol. PFSAs showed lowed desorption of PFCAs for all conditions. The greatest desorption of PFSAs occurred using the propanol-based regeneration solution. Follow-on experiments were conducted using anion exchange resin saturated with either diclofenac or dodecylbenzene sulfonate to evaluate a wide range of regeneration solution conditions. Diclofenac and dodecylbenzene sulfonate were studied as proxies for PFAS since the chemicals display similar interactions with anion exchange resin as PFAS and anion exchange resin, i.e., combination of electrostatic and non-electrostatic interactions. In addition, diclofenac possesses carboxylic acid functional group like PFCAs and dodecylbenzene sulfonate possesses sulfonic acid functional group like PFSAs.

Evaluation of diclofenac saturant regeneration. Four polystyrene anion exchange resins were probed for regeneration after being saturated with diclofenac which features a carboxylate head group. Three of the resins were macroporous (A502P, A520E, A592E), and one resin was gel-type (A532E). Past work has shown that resin uptake of diclofenac anion is characterized by electrostatic interaction between the deprotonated carboxylate head group on diclofenac and the quaternary ammonium complex on the resin as well as by Van der Waals forces and the π–- π interactions between the resin divinyl benzene group and the aromatic rings on diclofenac. [19, 30, 68]. This suggests that regenerating the resin requires a cosolvent solution that promotes these same or similar interactions but between the cosolvent and the HIOC. **Figure 3.5.2** shows the results of the regeneration experiment comparing mono-alcohols and diol at different ABV.

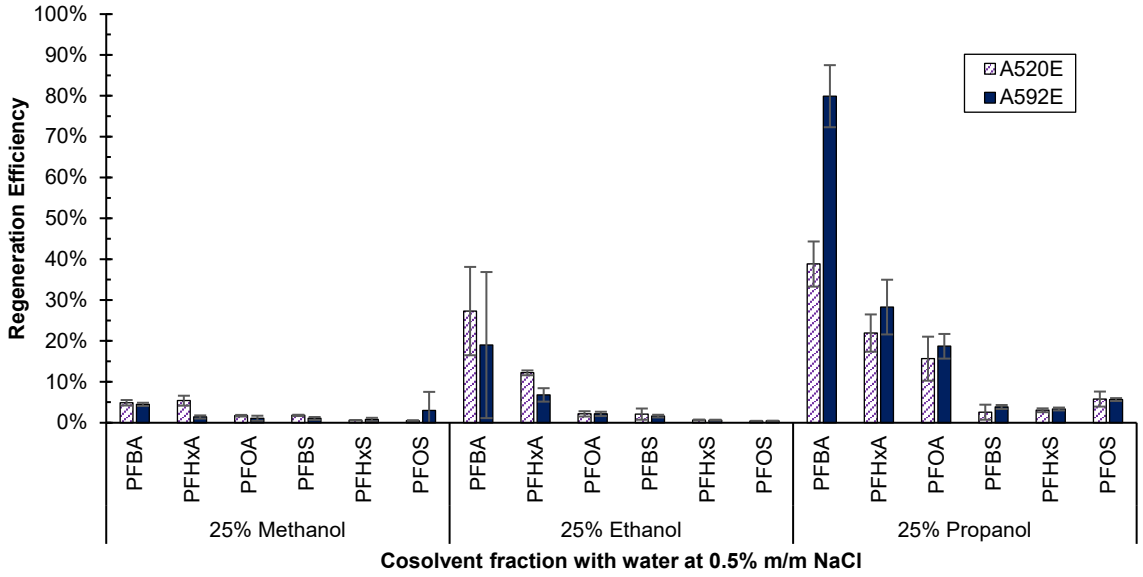

Figure 3.5.1. Regeneration efficiency of two Purolite strong-base polystyrene anion exchange resins saturated with three perfluoroalkyl carboxylates: perfluorobutanoate (PFBA), perfluorohexanoate (PFHxA), and perfluorooctanoate (PFOA), as well as three perfluoroalkyl sulfonates: perfluorobutane sulfonate (PFBS), perfluorohexane sulfonate (PFHxS), and perfluorooctane sulfonate (PFOS) and regenerated with 0.5% NaCl on a mass per mass basis for each given cosolvent parameter. Legend: Purolite Resin A520E (diagonal striped purple), Purolite Resin A592E (solid navy). All data are measured values. All measured data are mean values of duplicate samples with error bars showing one standard deviation.

As can be seen in **Figure 3.5.2**, increasing the volume fraction of methanol led to greater regeneration for all four resins. At 75% methanol by volume, all three macroporous resins achieved 90+ % regeneration. This result was to be expected as this is the common volume ratio of methanol that is conventionally used for optimal regeneration of organic-loaded resin. When comparing volume ratios that were the same, i.e. 25% methanol versus ethanol versus 1-propanol, all resins achieved greater regeneration with 1-propanol than with ethanol than with methanol. This shows that for equivalent alcohol concentrations, the HIOCs will more readily desorb when the alkyl chain of the cosolvent alcohol is longer. This is in part due to the non-electrostatic Van der Waals intermolecular interactions between the nonpolar tail of the alcohol and the nonpolar body of the HIOC, promoted by the decreased dielectric constant of the overall solution [28, 69]. Because salt concentrations were held equal, and regeneration at 25% ABV varied across alcohols, electrostatic forces between the resin quaternary ammonium and the carboxylate in competition with chloride

counterion were not the determination of regeneration efficiency. Propylene glycol was probed as a polyol alternative due to its nontoxicity, ready availability, nonflammability, and similar structure to 1-propanol. However, propylene glycol did not achieve even 50% with any of the resins or at 25% or 75% volume fraction. The single gel-type resin A532E showed the lowest regeneration across all experiments which matched prior literature on the difficulty of regenerating gel type PS SB-AERs [6]. Although resin A532E has been shown to be effective for removal of HIOCs, regeneration of the resin is higher with macroporous PS SB-AERs.

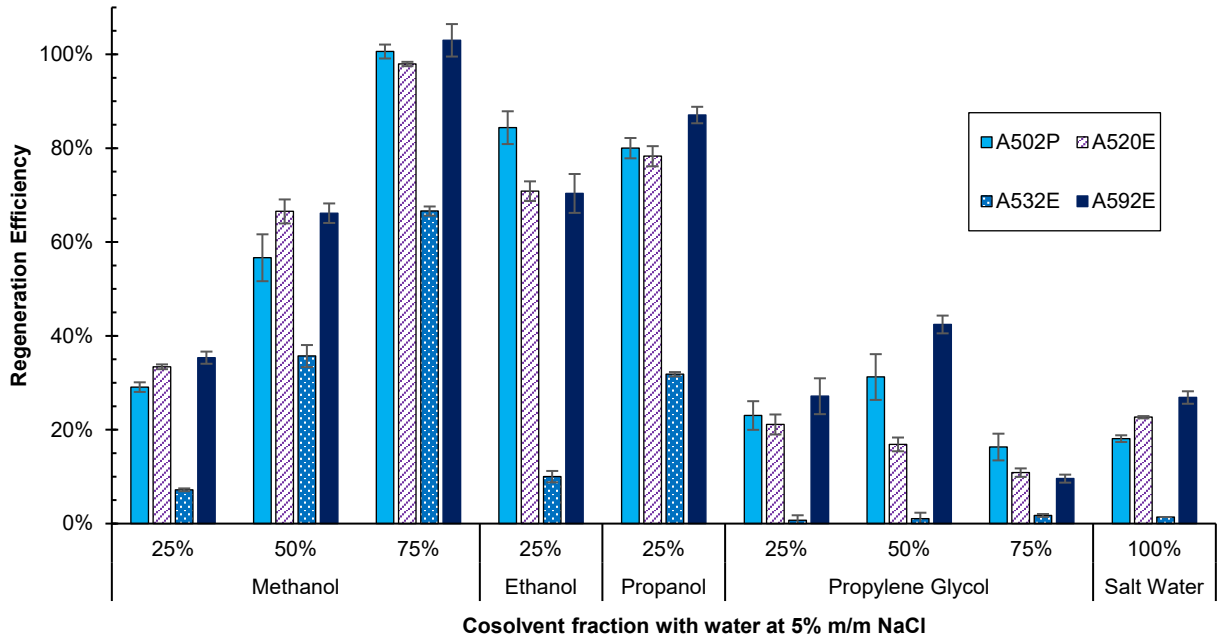

Figure 3.5.2. Regeneration efficiency of four Purolite strong-base polystyrene anion exchange resins saturated with diclofenac anion and regenerated with 5% NaCl on a mass per mass basis for each given cosolvent parameter. Legend: Purolite Resin A502P (solid sky blue), Purolite Resin A520E (diagonal striped purple), Purolite Resin A532E (dotted blue), Purolite Resin A592E (solid navy). All data are measured values. All measured data are mean values of duplicate samples with error bars showing one standard deviation.

Dodecylbenzene sulfonate. Three PS SB-AERs were saturated with surfactant dodecylbenzene sulfonate ion then regenerated under different cosolvent conditions. Whereas diclofenac contains a carboxylate functional group, dodecylbenzene sulfonate contains a sulfonate functional group. The regenerant solutions were made of different alcohols and polyols at varying ABV with brine at different NaCl concentrations. For the 5% NaCl m/m regeneration experiments, high salt concentration prevented miscibility with high ABV ethanol and methanol. The diol propylene glycol and triol glycerol were examined in addition with the monoalcohols. The results of this experiment are seen in **Figure 3.5.3**.

Similar to the results seen with the diclofenac procedure at 5% m/m NaCl, increasing the volume fraction of methanol led to greater regeneration and desorption of dodecylbenzene sulfonate across all resins. When comparing 25% ABV across alcohols, i.e. methanol versus ethanol versus 1-propanol, all resins achieved greater regeneration with 1-propanol than with ethanol than with methanol. In addition, even though the 1-butanol regenerant solution was only

5% ABV, it achieved 63.2 ± 5.4%. Again, these results highlight the effect that the decrease in polarity of the regenerant solution has on the ability of the HIOC to desorb from the resin and dissolve in solution. Similar to the diclofenac procedure, propylene glycol was not an effective regenerant, and glycerol proved to be worse, achieving approximately the same regeneration as the brine solution without cosolvent.

For the 0.5 and 0.05% m/m NaCl regenerant solutions, the decreased salt concentration allowed greater miscibility for high ABV solutions with methanol, ethanol, and 1-propanol. Propylene glycol and glycerol, given their poor results with 5% m/m NaCl regenerant solutions were not continued. The results of these procedures are found in **Figure 3.5.4**, below.

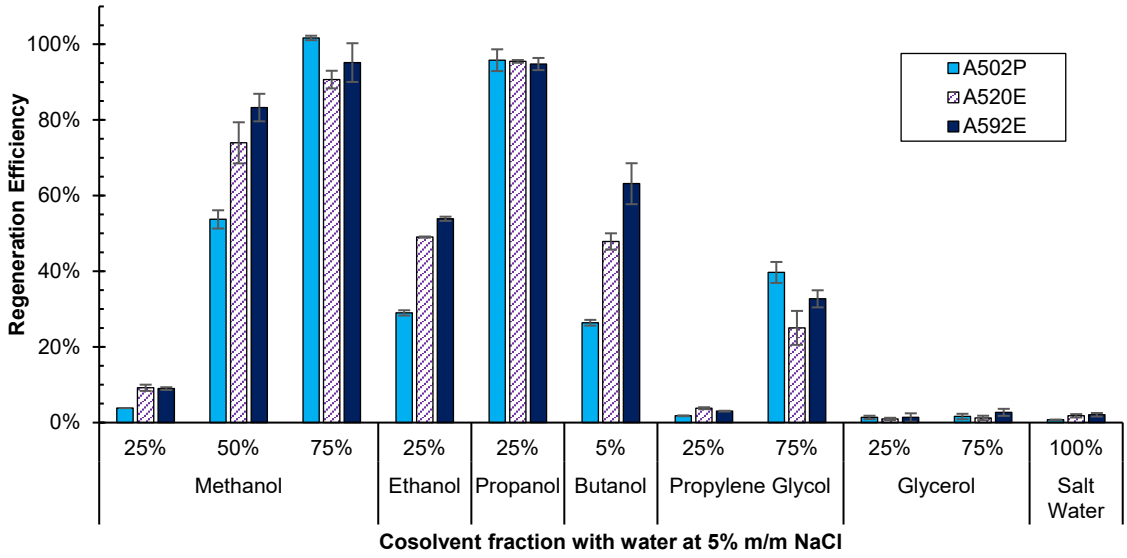

Figure 3.5.3. Regeneration efficiency of three Purolite strong-base polystyrene anion exchange resins saturated with dodecylbenzene sulfonate anion and regenerated with 5% NaCl on a mass per mass basis for each given cosolvent parameter. Legend: Purolite Resin A502P (solid sky blue), Purolite Resin A520E (diagonal striped purple), Purolite Resin A592E (solid navy). All data are measured values. All measured data are mean values of duplicate samples with error bars showing one standard deviation.

The key takeaways from interpreting the results of the 0.5% and 0.05% NaCl regenerations are again the cosolvent solution parameters. For 0.5% NaCl regenerative cosolvent solutions, 75% ethanol and 75% 1-propanol achieved greater than 90% regeneration for all resins, and 75% methanol did not. In addition, 50% 1-propanol achieved greater than 90% regeneration while 50% ethanol did not. These results show the favorability of the HIOCs to desorb off the resin back into a more nonpolar solution where nonpolar interactions dominate. That said, electrostatic effects still play a large role as regeneration decreased for all cosolvent solutions when the salt concentration dropped from 0.5% to 0.05%. Because no cosolvent matrix with 0.05% NaCl achieved at least 90% regeneration, this salt concentration was determined to be too low for adequate regeneration. The correlative relationship between salt concentration and regeneration is further evidenced by comparing the regeneration experiments at 5% m/m NaCl for equivalent ABV. For 25% ABV ethanol and 25% 1-propanol, decreasing the salt concentration from 5% to 0.5% saw a loss in regeneration efficiency which further decreased when the salt concentration dropped to 0.05%.

This demonstrates that regeneration of the resin and desorption of the HIOC is both dependent on the polarity of the cosolvent as well as the concentration of the counterion.

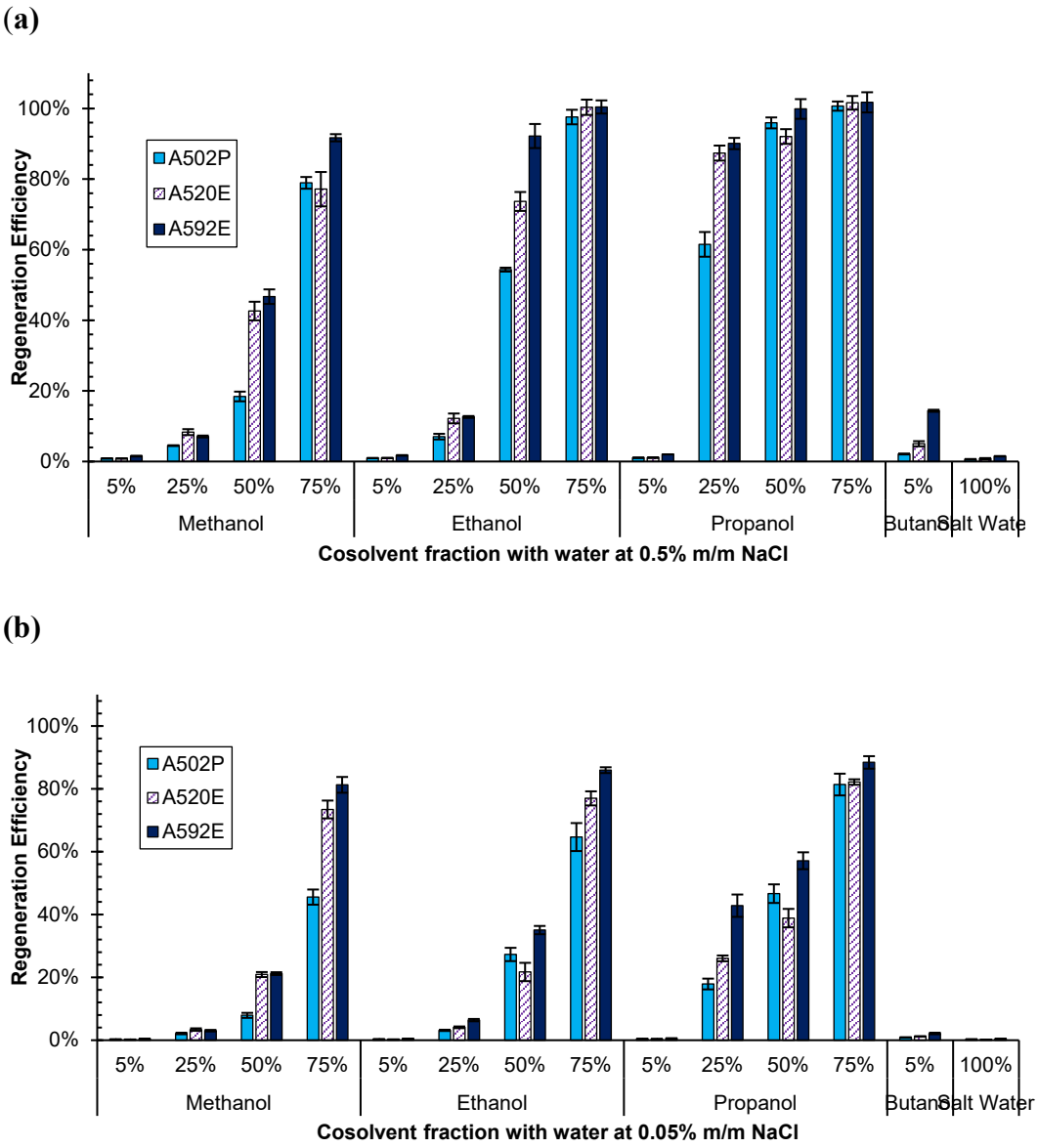

Figure 3.5.4. Regeneration efficiency of three Purolite strong-base polystyrene anion exchange resins saturated with dodecylbenzene sulfonate anion and regenerated with 0.5% NaCl (a) and 0.05% NaCl (b) on a mass per mass basis for each given cosolvent parameter. Legend: Purolite Resin A502P (solid sky blue), Purolite Resin A520E (diagonal striped purple), Purolite Resin A592E (solid navy). All data are measured values. All measured data are mean values of duplicate samples with error bars showing one standard deviation.

During desorption, the strong electrostatic bond between the HIOC sulfonate group and the quaternary ammonium is disrupted by the introduction of an alcohol cosolvent. The oxygen in the hydroxyl group on the alcohol draws electrons towards itself and away from the hydrogen due to

its electronegativity, and the hydrogen atom maintains a slight positive charge for ionic hydrogen bonding with the sulfonate group [70]. This electrostatic force is weaker than the cation/anion electrostatic force exhibited by the quaternary ammonium and sulfonate, so additional forces are needed to desorb dodecylbenzene sulfonate from the resin. Increasing cosolvent ABV and salt concentration decreases the dielectric constant which allows for greater solubility of dodecylbenzene sulfonate. Finally, longer chain alcohols, and the London dispersion forces between the HIOC alkyl tail and the alcohol alkyl tail assist in desorption from the resin. These interactions are only possible for the longer chain alcohols and do not occur with methanol. A qualitative figure displaying this phenomenon is found below in **Figure 3.5.5**.

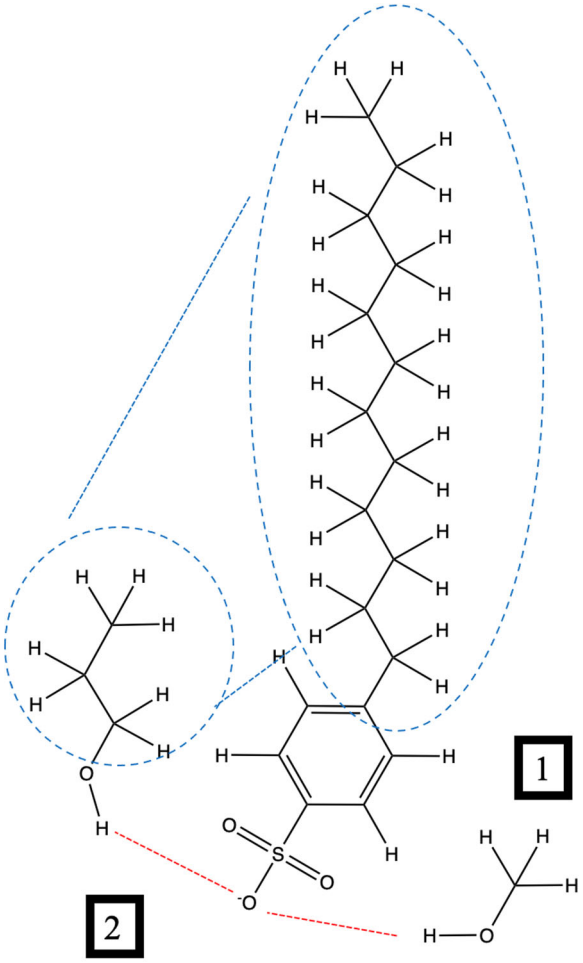

Figure 3.5.5. Intermolecular relationships between dodecylbenzene sulfonate ion and (1) methanol, showing only ionic hydrogen bonding (red), and (2) 1-propanol, showing both ionic hydrogen bonding (red) and London dispersion forces (blue). Note that explicit hydrogen atoms are shown.

Modeling the regenerative capabilities of three polystyrene macroporous anion exchange resins saturated with dodecylbenzene sulfonate was performed as a multivariate linear analysis with ten initial parameters in backwards step-wise function. The regeneration of resin A502P was found to be a function of four statistically significant parameters: cosolvent volume fraction,

cosolvent molar mass, ionic strength, and K_{OW}. Regeneration of resin A520E was found to be a function of three statistically significant parameters: cosolvent volume fraction, cosolvent molar mass, and ionic strength. Regeneration of resin A592E was also found to be a function of three statistically significant parameters: cosolvent volume fraction, ionic strength, and K_{ow}. The empirically determined equations are found below in **Figure 3.5.6**.

(a)

$$A502P\ Regeneration\ Efficiency\ =\ -0.809 + \begin{pmatrix} Cosolvent \\ volume \\ fraction \end{pmatrix} * 1.16 + \begin{pmatrix} Cosolvent \\ molar \\ mass \end{pmatrix} * 0.0158 + \begin{pmatrix} Ionic \\ Strength \end{pmatrix} * 0.391 + (K_{OW}) * 0.0570$$

(b)

$$A520E\ Regeneration\ Efficiency = -0.524 + \begin{pmatrix} Cosolvent \\ volume \\ fraction \end{pmatrix} * 1.26 + \begin{pmatrix} Cosolvent \\ molar \\ mass \end{pmatrix} * 0.00861 + \begin{pmatrix} Ionic \\ Strength \end{pmatrix} * 0.411©)$$

$$A592E\ Regeneration\ Efficiency = -0.140 + \begin{pmatrix} Cosolvent \\ volume \\ fraction \end{pmatrix} * 1.32 + \begin{pmatrix} Ionic \\ Strength \end{pmatrix} * 0.373 + (K_{OW}) * 0.0435$$

Figure 3.5.6. Three multivariate linear functions of regeneration efficiency for resins A502P (a), A520E (b), and A592E (c). Statistical significance was defined at 95% confidence interval $p < 0.05$ for each parameter.

They primarily serve to illuminate the key parameters relevant to regeneration and how those parameters will either increase or decrease regeneration of the resin. Firstly, cosolvent volume fraction was one of two parameters that was statistically significant for all three resins used in the experiment. For all three resins, the coefficient was positive, indicating that increasing the amount of cosolvent volume fraction increased regeneration. The other parameter that was common across all three models was ionic strength. The ionic strength coefficient was also always positive, indicating that as salt concentration in the solution increased, the regeneration efficiency increased. The tradeoff here is that as more salt is dissolved in solution, the more nonpolar alcohols will no longer be miscible with the brine solution. Surprisingly, dielectric constant was not determined to be a significant variable which does not match expectations from previous literature that cites dielectric constant of the regenerant solution as one of the most important factors for regeneration [71, 72]. This highlights some of the limitations of the model used. As alcohol volume fraction and salt concentration increase, the dielectric constant of the overall solution will decrease. While there are both empirical datasets and various models for dielectric constant determinations of binary alcohol and water solutions as well as single solute with water solutions and single solute in alcohol solutions, there is limited data on solutions that contain water, alcohol, and salt [73, 74]. Therefore, the pure solvent dielectric constant did not significantly correlate with resin regeneration per the models.

One safety consideration when handling alcohol cosolvent is the flammability of the mixture. As the volume percent of alcohol increases, the flashpoint temperature decreases. For the purposes of this study, a flashpoint above room temperature (20 °C) was operationally defined as the "safe" limit. Regeneration solutions that achieved ≥ 90% regeneration for at least one resin and had a flashpoint above 20 °C were considered to be both effective and safe for regeneration when considering flammability. A scatterplot of regeneration efficiency versus solution flashpoint is below in **Figure 3.5.7**.

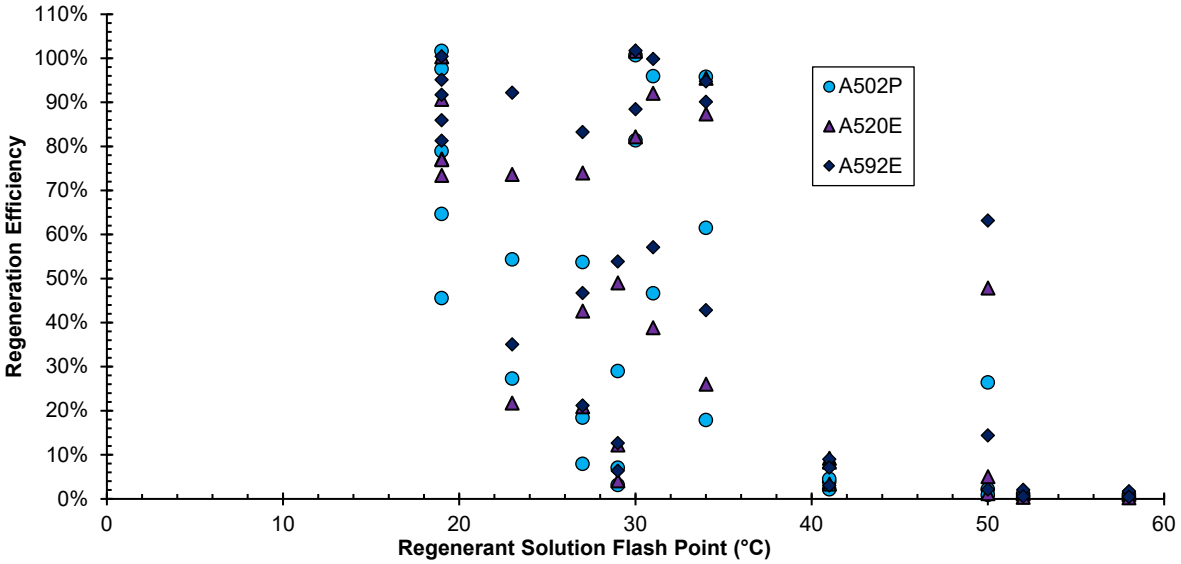

Figure 3.5.7. Regeneration efficiencies for various cosolvent compositions across three resins compared to regenerant solution flashpoint for three resins

The solutions that achieved both objectives for regeneration and flashpoint for at least one resin were 25% 1-propanol with 5% NaCl; 50% and 25% ethanol with 0.5% NaCl; and 25, 50, and 75% 1-propanol with 0.5% NaCl. Most regenerant solutions fell outside the optimal range, and a general trend was observed that as flashpoint temperature increased, regeneration decreased. This is not surprising based off the data and models that showed that increasing cosolvent volume fraction increased regeneration, and increasing cosolvent fraction of an alcohol decreased flashpoint.

Cost of regenerant solution is another practical consideration for engineering. Each regenerant solution was normalized to the cost of 1 L from the average of two large chemical suppliers. The results of this analysis are shown below in **Figure 3.5.8**.

The results of this analysis show a wide discrepancy to the point where a logarithmic scale was needed to display the results together. The most cost-effective regenerant solution for any resin loaded with dodecylbenzene sulfonate ion was found to be A592E with 5% ABV 1-butanol at 5% NaCl. The cost per regeneration percent was $0.16/Regen%. However, this solution only achieved 63.2 ± 5.4%. If the results are truncated to only include regeneration efficiencies of 90+ %, the best performing regenerant solution for the three resins is 25% ABV 1-propanol with 5% NaCl at an average of $0.27/Regen%. Similar to the flashpoint determination, the 25% ABV 1-propanol with 5% NaCl solution is the optimal solution.

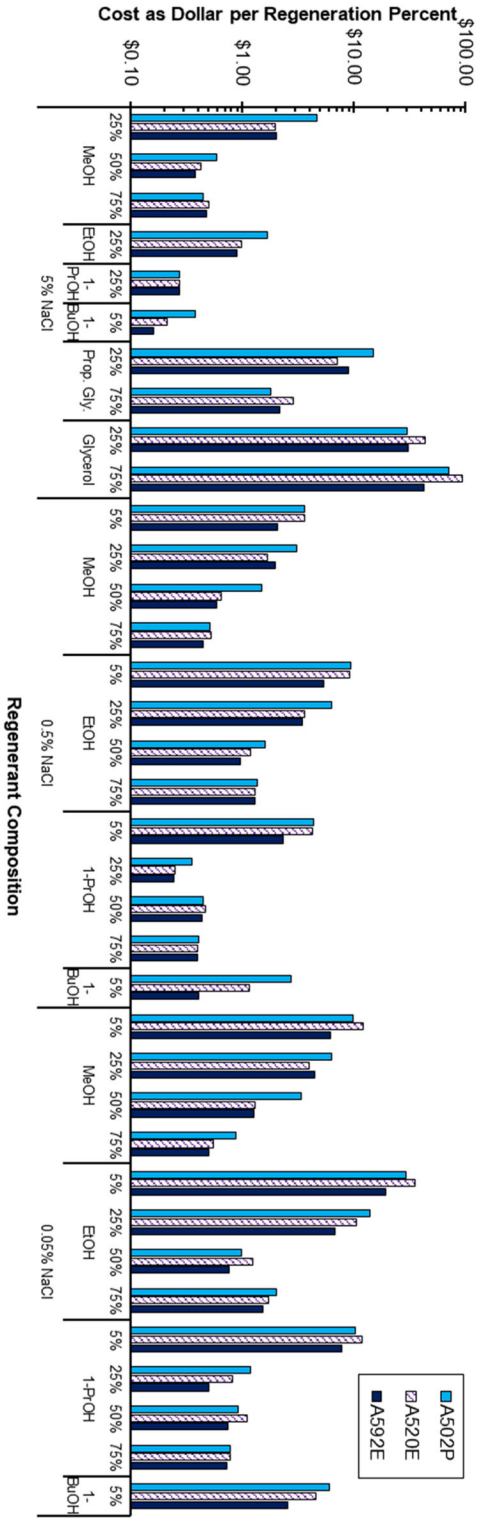

Figure 3.5.8. Cost effectiveness of regenerant solutions for dodecylbenzene sulfonate determined by normalized cost of 1L regenerant solution divided by regeneration for the given experiment. Note the Y-axis is logarithmic. Legend: Purolite Resin A502P (sky blue circle), Purolite Resin A520E (purple triangle), Purolite Resin A592E (navy diamond). MeOH = methanol; EthOH = ethanol; PrOH = propanol; BuOH = butanol; Prop. Gly. = propylene glycol

Sustainability considerations were determined by the CO_2 emission potential of 1 L of normalized solvent. The results of this analysis are shown below in **Figure 3.5.9**.

An overall trend positive is seen for regeneration efficiency vs. carbon dioxide emission potential. The regeneration experiments established that increasing the CO_2 emission potential generally increased with regeneration efficiency. If an arbitrary designation is made to consider only regeneration that achieved 90+ % and had a CO_2 emission potential of 500 g CO_2/Lsol., only 25% ABV 1-propanol accomplishes that goal at 445 g CO_2/Lsol. Based off the above assessments for safety, cost-effectiveness, and sustainability, 25% ABV 1-propanol with 5% NaCl is determined to be the optimal regenerant, being the only one to meet all three criteria.

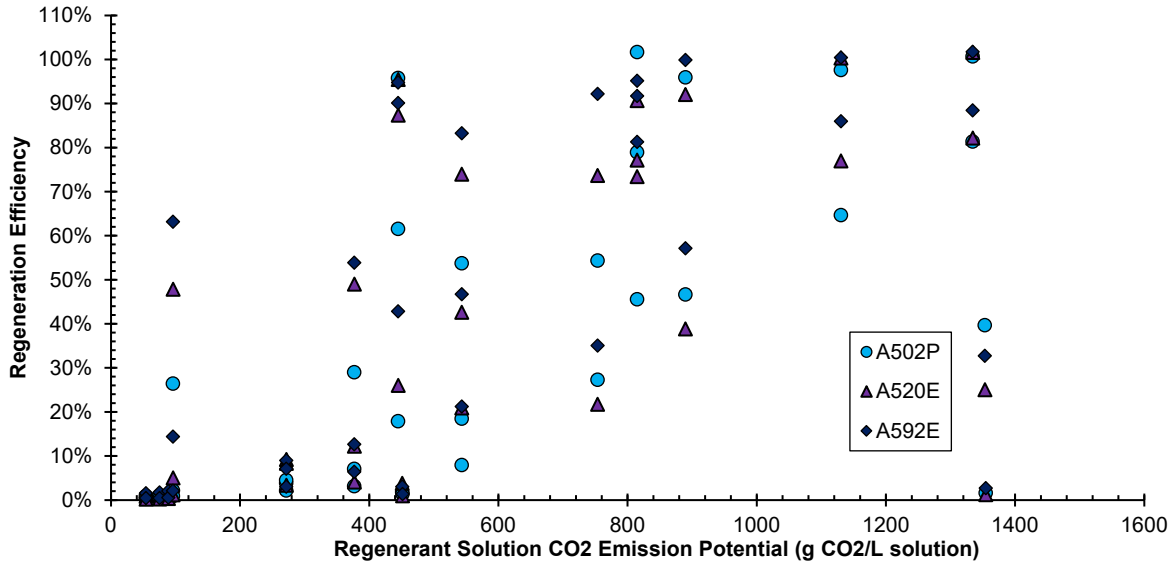

Figure 3.5.9. Regeneration efficiencies for various cosolvent compositions across resins compared to g CO_2 emission potential per L regenerant solution. Legend: Purolite Resin A502P (sky blue circle), Purolite Resin A520E (purple triangle), Purolite Resin A592E (navy diamond).

Considering future sustainability practices when using regenerative cosolvents for spent anion exchange resin, particularly when regenerating resins saturated with organic compounds, distillation byproducts from ethanol fermentation could play a role in resin regeneration. Distilleries make three cuts during the distillation process to separate the desired consumable product from which are the head, heart, and tail for spirit production [75, 76]. The cuts are designed to separate the ethanolic spirit from unpleasantly flavored and even toxic compounds like methanol, propanol, butanol, and fusel oils which are also included in the initial mash [77]. If longer chain alcohols are successful in regenerating saturated resins, then these distillation byproducts could be considered for recycled use as regenerant solutions for AERs. Efforts have been made to decrease the concentration of methanol in the heart which would allow for greater concentrations of methanol as byproduct to be recycled for use in anion exchange resin [78]. Furthermore, carbon dioxide is generated during fermentation, and the process is a significant contributor to the global

carbon budget, so recycling the distillation byproducts would reduce the overall carbon budget on two fronts [79]. The limitation to implementation of distillation byproducts as novel regenerant hinges on a few factors. An analysis of the heads, hearts, and tails cuts of distillate from fermented *Arbutus unedo* found that the concentration of ethanol in the heads cut was 64.77% v/v with far lower concentrations of other alcohols at 3.87 g/L methanol, 0.10 g/L 1-propanol, and 0.45 g/L isobutanol [76]. If combined with salt, this solution could act as a regenerant, provided the other organic anions in the head cut distillate do not exchange onto the resin. This could be mitigated with acid addition to protonate any organic anions.

3.5.2 Regeneration of Resins Loaded During Field Pilot Demonstration Study

Screening of Regenerant Solution Constituents. Assessment and optimization of AER regeneration began with a comprehensive screening of constituents and solution amendments that may be used in practice to desorb PFASs and replenish exchange capacity of the resin. This screening began with a component-level examination of salts and cosolvents in the presence of nanopure water. **Figure 3.5.10** depicts the regeneration efficiencies (represented by desorption of C6 and C8 PFCAs and PFSAs) of the screening for the single-use resin PFA694E, with **Figure 3.5.10A** specifically addressing brine-only and cosolvent-only aqueous solutions. As seen in this figure, neither brine-only (1 wt% salts) nor cosolvent-only solutions (90% MeOH and 1-PrOH) led to even 10% desorption of PFASs, both for short- and long-chain PFCAs and PFSAs. Shorter-chain structures saw greater desorption than long-chain structures when using brine-only solutions while long-chain structures experienced greater desorption when using cosolvent-only solutions than their shorter-chain analogues. This phenomenon is likely due to the comparatively larger role of electrostatic attraction in short-chain PFAS adsorption, as longer fluoroalkyl chains induce greater hydrophobic attraction to the resin. Because anions from the salt brine disrupt electrostatic forces while organic cosolvent disrupts hydrophobic attraction (Li et al., 2020, brine-only solutions disproportionately desorb short-chain PFASs while solvent-only solutions disproportionately affect long-chain PFASs. While none of these solutions would ever be used in practice, this finding may be useful in optimization of regenerant solutions to displace the full suite of PFASs from spent anionic resins. The addition of hydrocarbon surfactants was also found to be ineffective in regenerating resins as indicated in **Figure 3.5.10B**. Dodecylbenzene sulfonate (DBS), sodium dodecylsulfate (SDS), and methylimidazolium ethyl sulfate (EtSO4) surfactants as well as the chelating agent nitrilotriacetic acid (NTA) were all examined as these ionizable compounds share similar amphiphilic behavior of PFASs, however none of these structures proved competitive with PFASs for exchange sites, even despite their elevated amendment concentrations (1-100 mM).

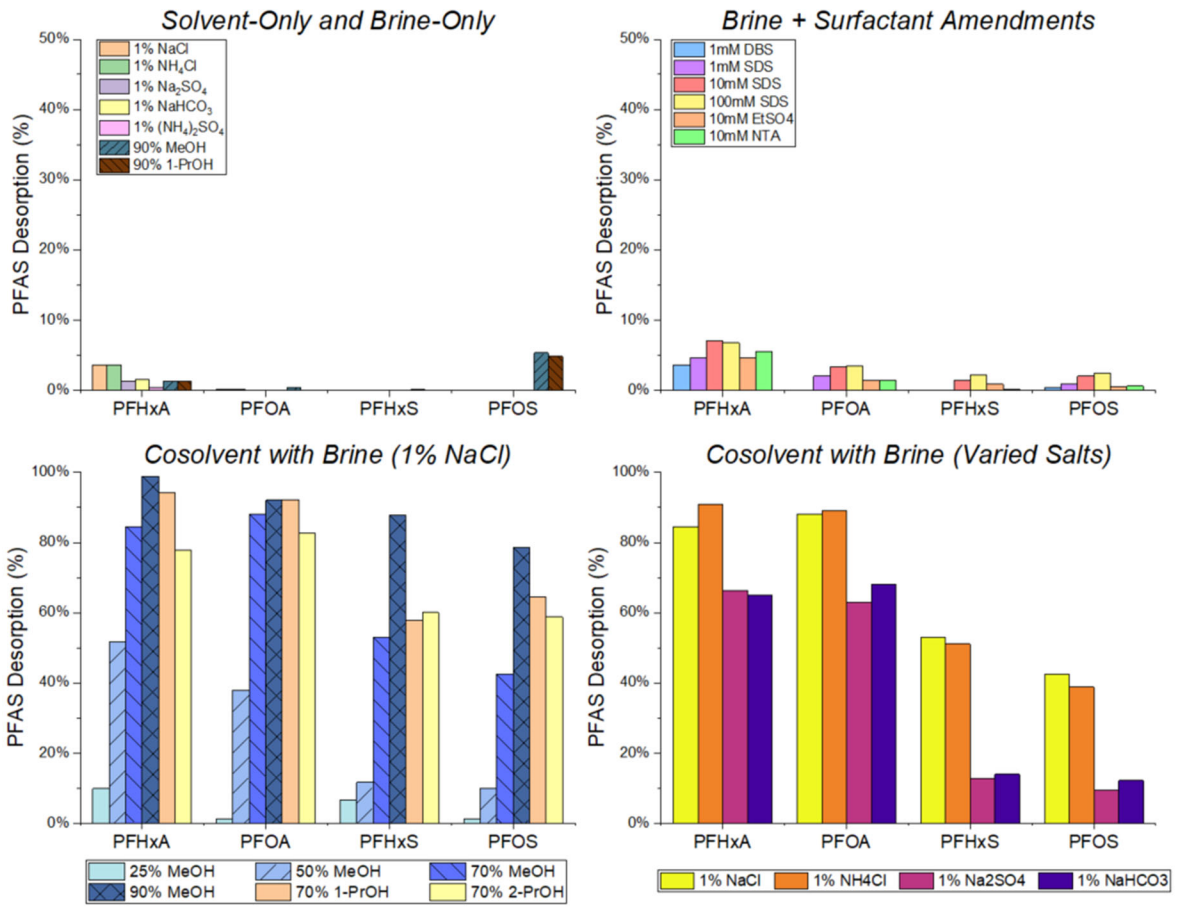

Figure 3.5.10. PFAS desorption from field pilot-loaded resin (PFA694E) conducted in 24-hour batch experiments. Data shown for (A) solvent-only and brine-only solutions, (B) brines with surfactant amendments, (C) cosolvent + brine solutions (all using 1% NaCl) and (D) cosolvent + brine solutions (all using 70% MeOH).

While neither brine-only, cosolvent-only, nor brine with surfactant solutions demonstrated efficacy in AER regeneration, combinations of brine and organic cosolvent displayed significantly greater success in desorbing PFASs from spent resins. **Figures 3.5.10C-D** highlight PFAS desorption from PFA694E using varied cosolvent fractions in the presence of NaCl brine (**Figure 3.5.10C**) and varied salts used in the presence of 70% methanol (**Figure 3.5.10D**). Of all the solution combinations displayed in these two panels, the use of 90% methanol with 1 wt% NaCl demonstrated the greatest PFAS desorption, with even PFOS being displaced despite a chloride exchange coefficient of 10^7 (Fang et al., 2021). Among cosolvents, 1-propanol and 2-propanol were found to desorb PFSAs to a greater extent than methanol at a 70% solvent fraction, with all three solvents exhibiting similar regeneration efficiencies for PFCAs. However, the increase in cosolvent fraction to 90% methanol led to more efficient regeneration than use of alternate solvents at 70% fractions. Additionally, the lower solubility of salts like NaCl in propanol solutions prohibits formation of a 1 wt% NaCl solution in 90% 1- or 2-propanol solution at room temperature (De Santis et al., 1976). Thus, 90% methanol with 1 wt% salt was found to be an optimal mixture. Among different salts, NaCl and NH_4Cl demonstrated promise in desorbing PFASs when in a 70% methanol mixture compared to Na_2SO_4 and $NaHCO_3$. This follows a known trend of chloride having a higher resin selectivity than bicarbonate and sulfate, as bicarbonate has poor selectivity

(Hu et al., 2016) and the divalency of sulfate prohibits ideal exchange with PFAS for quaternary amine sites (Gu et al., 2004). Among chloride salts, the marginal difference between the two forms was within the analytical uncertainty range for all PFASs. Because NaCl is a much cheaper, more abundant, and more commonly used salt in traditional regeneration than NH_4Cl, this compound was used as the salt for all regenerant mixtures used in subsequent continuous-flow regeneration studies.

Continuous-Flow Regeneration of AER Columns. Continuous-flow regeneration of PFAS-laden AERs began with a baseline aqueous solution comprised of 70% methanol and 1 wt% NaCl brine. This solution was first applied to columns of A520E (regenerable) and PFA694E (PFAS-selective) resin at a 10-min EBCT, with effluent regenerant solution sampled throughout 30 BVs. Regeneration efficiencies are shown in **Figure 3.5.11**, with panels A and B reporting absolute regeneration (mg/BV desorbed) while panel C reports cumulative regeneration of total PFASs over time (% regenerated). Temporal results indicate that desorption kinetics occur much more rapidly for the regenerable A520E (**Figure 3.5.11B**) than the single-use PFA694E (**Figure 3.5.11A**), as PFASs experience >60% regeneration by the tenth bed volume for A520E compared to <20% for PFA694E. This lack of rapid desorption for PFA694E is attributable to sulfonate PFASs, as all sulfonate analytes experienced a plateau-like desorption behavior wherein PFSA elution holds constant between the 8th and 30th bed volume (**Figure 3.5.11A**), resulting in a near-linear cumulative profile (**Figure 3.5.11C**). A520E, conversely, experiences ~90% PFSA regeneration by the 15th bed volume when using 70% methanol in solution. While this trend may be expected given the significantly higher selectivity coefficients reported for single-use AERs (Fang et al., 2021), these results indicate that PFASs can be appreciably desorbed from PFAS-selective resins.

While A520E does experience rapid and near-complete PFAS desorption under the baseline condition, the single-use PFA694E did not achieve full restoration of exchange capacity. To assess whether this is a facet of perceived 'regenerability' or pore structure, further resins and regenerant solution conditions were tested. **Figure 3.5.12** depicts the regeneration results for three 'PFAS-selective' resin brands used in the original field pilot study (Ellis et al., 2022) using 70% and 90% methanol regenerant solutions with 1 wt% NaCl. Results indicate that for both macroporous and gel-type single-use resins, regeneration with elevated cosolvent fractions (90% MeOH) can achieve >95% PFAS desorption while all three resins were incompletely regenerated using lower fractions (70% MeOH) as none of them achieved >45% regenerations. This trend holds true across different AER porosities, as the macroporous CalRes 2301 experienced similar desorption profiles to the gel-type resins. A deeper dive into the analyte-specific data reveals that incomplete regeneration is driven by sulfonate PFASs, as PFCAs are fully desorbed at 70% solvent fractions while PFSAs experience a plateau-like regeneration profile for all three resins. Thus, it can be reasonably concluded that attempts to regenerate AERs marketed as single-use adsorbents necessitates use of >70% solvent, with 90% being a potential optimal solution mixture.

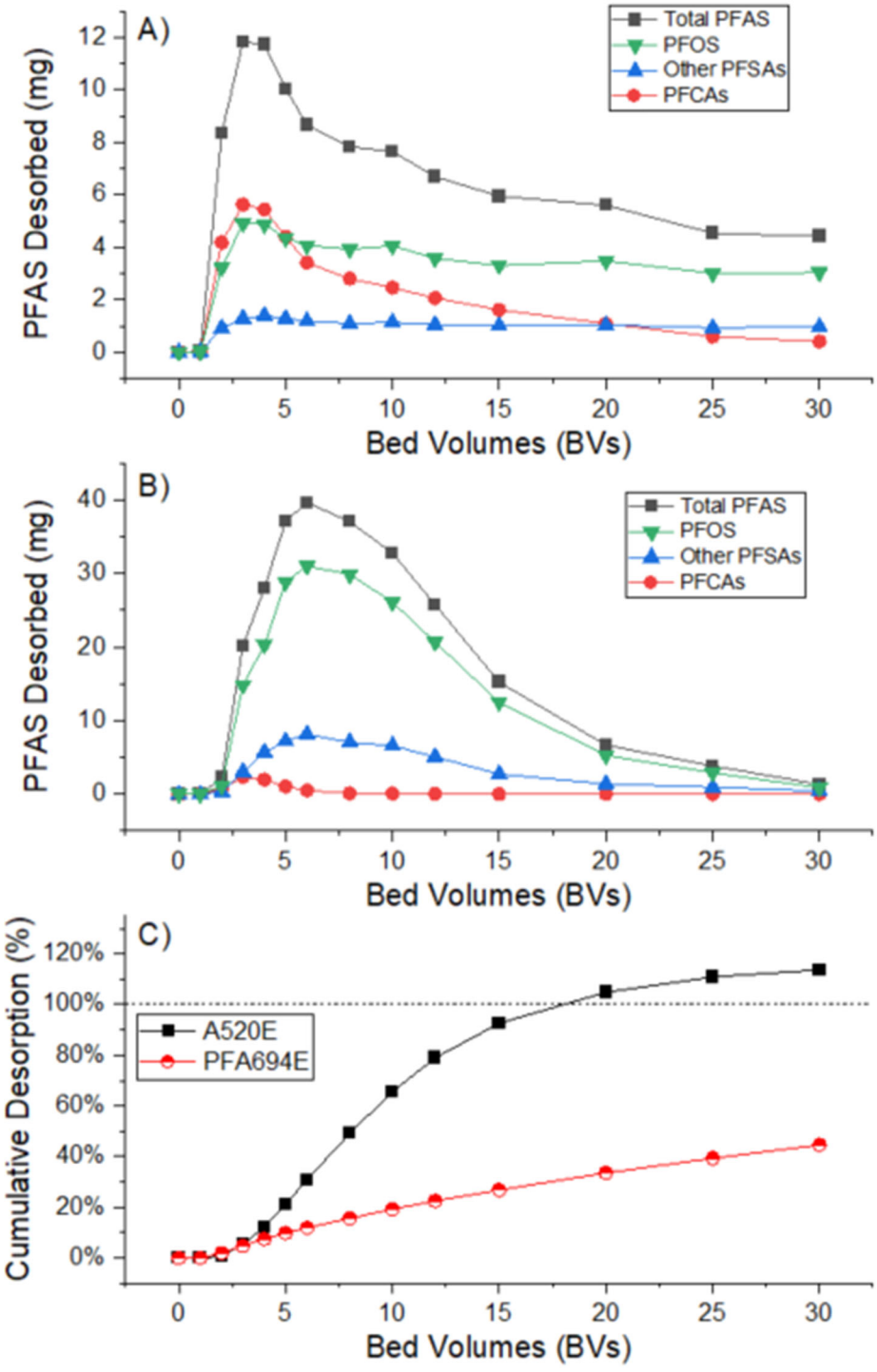

Figure 3.5.11. Temporal PFAS desorption from (A) PFA694E and (B) A520E using a 70% MeOH, 1 wt% NaCl. (C) Cumulative desorption also shown for both resins over 30 BVs based on expected adsorbate concentrations.

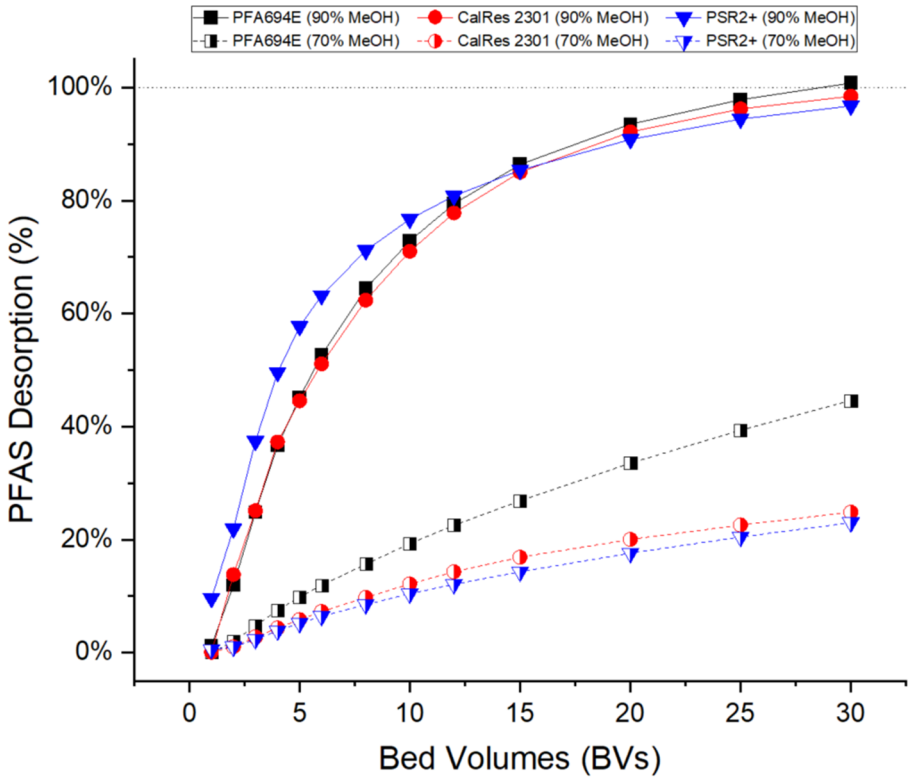

Figure 3.5.12. Cumulative PFAS desorption from PFAS-selective 'single-use' resins (PFA694E, CalRes 2301, and PSR2+) compared to their expected concentrations using 70% and 90% methanol solutions, all in the presence of 1 wt% NaCl.

Beyond the effects of increased cosolvent fraction, alternate methods to optimize resin regeneration were explored. Cosolvent identity and empty-bed contact time are two potential pathways to improve regenerability, as longer-chained solvents are known to be more hydrophobic than shorter-chained solvents (Li et al., 2023) and EBCT has been found to enable greater diffusion of PFAS anions through resin pores (Schaefer et al., 2019; Ellis et al., 2022). Two columns of spent PFA694E were subjected to regeneration using 70% 1-propanol (10-min EBCT) and 70% methanol (30-min EBCT), respectively, to ascertain the effects of varying solvent identity and EBCT with all other parameters set to the baseline condition. **Figure 3.5.13** displays the regeneration efficacy of these two conditions against the baseline (70% MeOH) and the 90% methanol solution for PFA694E (both using 10-min EBCT). Use of 70% 1-propanol in regenerant solution was found to markedly improve regeneration compared to 70% methanol, with an overall increase of 73% in PFAS desorption. PFOS – the dominant fluoroalkyl compound on the AER – experienced a 125% increase in desorption when using 1-propanol. Generation of a 90% 1-propanol solution was attempted to compare against 90% methanol, though salt precipitation prevented achievement of a 1 wt% solution. Given the high efficacy of 90% methanol solutions in regeneration, further column testing of 1-propanol solutions was omitted.

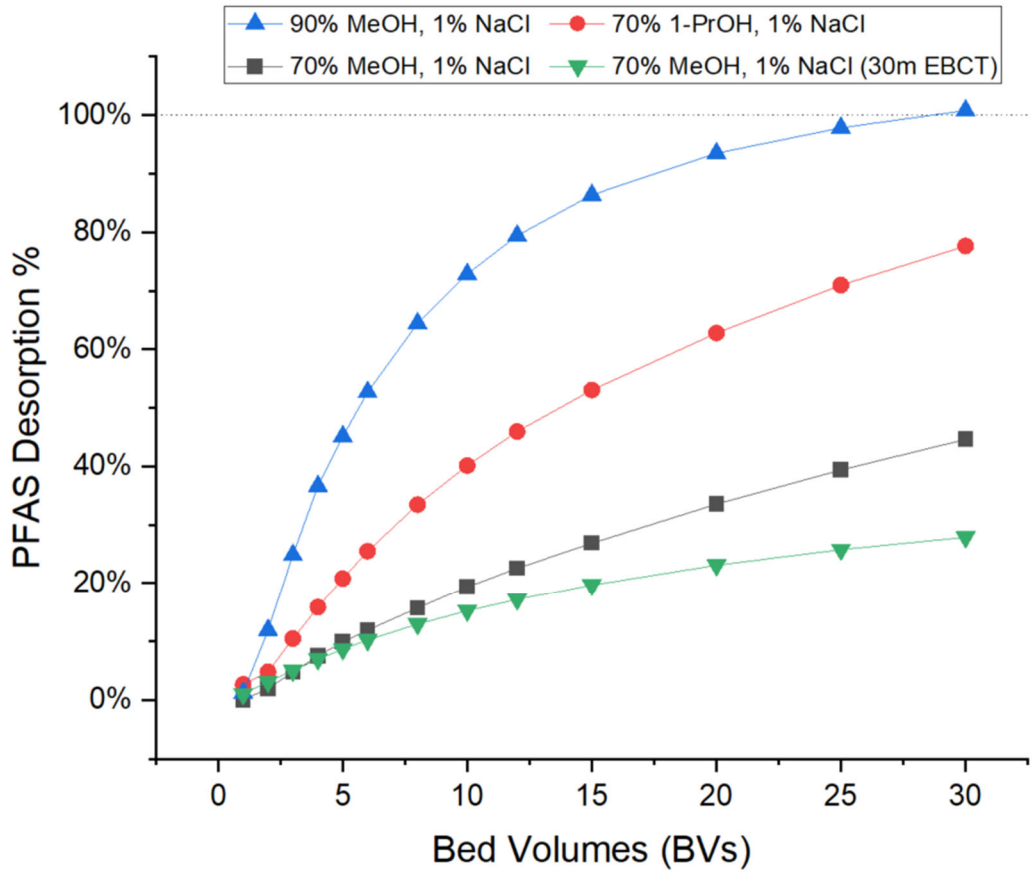

Figure 3.5.13. Regeneration efficiency of PFA694E using various regenerant solution conditions and operational considerations. All regeneration occurred for 30 BVs using a 10-min EBCT unless otherwise stated.

Perhaps even more striking, the increase in EBCT from 10 to 30 minutes did not lead to an increase in PFAS desorption for PFA694E. While this AER column was three times the size of the column used in 10-min regeneration, it exhibited similar regeneration percentages throughout the 30-BV cycle to the 10-min PFA694E column. This finding does not by itself disprove the prevailing theory that increased EBCT leads to more effective regeneration, though it may indicate that prioritizing regenerant solution optimization and recovery of high cosolvent fractions over operational considerations such as regenerant solution flow rate and EBCT. Because prior sustainability studies found remediation costs and environmental impacts to be reduced when using high cosolvent fractions with efficient distillation recoveries, use of a large number of bed volumes at a lower EBCT (e.g., 30 BVs at a 10-min EBCT) may not be cost-prohibitive and will likely lead to better resin regeneration than 10 BVs at a 30-min EBCT, despite both regeneration processes requiring the same amount of time.

Regenerability of 'Single-Use' and 'Regenerable' AERs. Anion exchange resins are often viewed as a monolithic category of treatment technologies, though the disparate contaminant affinities, adsorption kinetics, and operational configurations lead to significant performance differences between individual resin brands and classes, particularly for PFASs (Zaggia et al., 2016). While resins used in practice to remediate PFASs are often distinguished by their supposed

regenerability, this marketing moniker often signifies differences in exchange affinities rather than indicating irreversible adsorption caused by hysteresis behavior, as evidenced in a screening of many different resin brands for their selectivity coefficients. Resins marketed as 'PFAS-selective' or 'single-use' have been found to have high affinities for PFASs both in equilibrium batch isotherms (Fang et al., 2021) and continuous-flow treatment of real AFFF-impacted groundwater (Ellis et al., 2022; Liu et al., 2022) compared to their 'regenerable' counterparts. However, results from this study support the potential regenerability of 'PFAS-selective' resins, even in the presence of nontarget adsorbed constituents like NOM and precipitates. These AERs offer enhanced adsorption kinetics and PFAS capacities in addition to their high selectivities for PFASs, which extend their bed lives such that disposal upon PFAS breakthrough is economically feasible, unlike GAC and regenerable AERs (as discussed in Chapter 3). Findings from this study indicate that these cost and sustainability benefits may be even further expanded when considering regeneration of PFAS-selective resins using optimized regenerant solutions.

Although many of the regenerant solution mixtures tested lead to poor PFAS desorption, particularly for PFAS-selective resins, optimized solutions with high cosolvent fractions were found to be highly effective in regenerating resins within 30 BVs. Class-specific breakdowns of regeneration efficacy are presented in **Table 3.5.1**, which indicates that over 95% of adsorbed PFASs can be desorbed regardless of chain length or head group type. Use of 90% methanol yielded higher desorption efficiencies for all three PFAS-selective resins than using lower solvent fractions, alternate cosolvents, or longer empty-bed contact times. While certain analytes yielded incomplete desorption (e.g. 72-90%), this is believed to be an artifact of analytical uncertainty and low temporal resolution, as analytical costs constrained the quantity of samples able to be analyzed for each experiment. It is worth noting, however, that PFOS is well-characterized as the structure with the highest resin affinity of those studied (Fang et al., 2021) and achieved >90% desorption from all PFAS-selective resins when using 90% cosolvent. Furthermore, PFOS comprises the majority of the total adsorbate concentration on the single-use resins (60-65%), indicating that shorter-chained PFSAs with far lower adsorbate concentrations would at minimum achieve the desorption efficacy observed for PFOS. This lack of complete regeneration was validated by analyzing replicate samples from the pooled 'waste' regenerant solution, which collected the entire spent regenerant solution (other than those samples each BV) in a single container. Results from these analyses indicate that total desorbed PFCAs and C3-C7 PFSAs are within 15% of their expected concentrations for all analytes and replicates, which is within the 20% range of analytical uncertainty. Thus, operators can confidently expect these adsorbents to be fully regenerated under the optimized solution conditions (90% methanol, 30 BVs).

Unlike PFAS-selective AERs, resins marketed as being regenerable have extensive academic validation of their regenerability when using combinations of salt and organic cosolvent (Dixit et al., 2021). In particular, A520E was found to be regenerable for both short-and long-chain PFCAs and PFSAs loaded from a drinking water source at an 80% cosolvent fraction (Gagliano et al., 2020). While this finding relied on batch regeneration experiments, results from this study support the feasibility of regenerating packed beds of AER in continuous-flow regeneration at a lower (70%) cosolvent fraction. Despite much of the literature on AER adsorption utilizes long EBCTs to enable PFAS diffusion from the resin into the regenerant solution (e.g., 30-min EBCT: Dixit et al., 2020), the present study found EBCT to have minimal effect on both PFAS-selective and regenerable resins.

Table 3.5.1. Regeneration efficacy of various regenerant solution conditions

Regeneration Experiment[a]	Desorption of PFAS Analytes from Resin[b]				% of PFASs Remaining on Resin[c]		
	ΣPFAS	**PFCA**	**PFOS**	**Other PFSA**	**10 BVs**	**20 BVs**	**30 BVs**
PFA694E, 70% Methanol	45%	>95%	39%	26%	80.7%	66.4%	55.4%
PFA694E, 90% Methanol	>95%	87%	>95%	80%	27.1%	6.5%	---
PFA694E, 70% 1-Propanol	78%	>95%	88%	38%	59.9%	37.2%	22.4%
PFA694E (70%), 30m EBCT	28%	>95%	17%	19%	84.8%	76.9%	82.1%
A520E, 70% Methanol	>95%	>95%	>95%	>95%	32.8%	---	---
A520E (70%), 30m EBCT	>95%	>95%	>95%	>95%	34.4%	---	---
CalRes 2301, 70% Methanol	25%	>95%	13%	25%	87.8%	80.0%	75.1%
CalRes 2301, 90% Methanol	>95%	>95%	91%	>95%	29.0%	7.8%	---
PSR2+, 70% Methanol	23%	66%	18%	17%	89.6%	82.4%	77.0%
PSR2+, 90% Methanol	>95%	>95%	>95%	77%	23.3%	9.2%	3.2%

[a.] Regeneration occurred at a 10-min EBCT unless otherwise noted

[b.] Desorption efficiencies compared against replicates of spent resins subjected to a 3-round extraction protocol described in Ellis et al., 2022

[c.] % of PFASs remaining on the resins calculated from expected sorbate concentrations and regeneration profiles

Role of Organic Cosolvent in PFAS Desorption. Perhaps the most significant finding from this study is the dominant role of organic cosolvent fraction in enabling PFAS desorption from anionic resins. As evidenced in **Figure 3.5.11** and **Figure 3.5.13**, cosolvent fraction is the most

significant determinant of PFAS desorption compared to all other parameters screened in this study. Cosolvent type was also found to be a major factor in regenerant solution efficacy, as 70% 1-propanol regeneration exceeded the efficacy of 70% methanol in both batch and column regeneration efforts. Comparing all parameters evaluated in the study, the relative importance of each regeneration parameter follows in decreasing order: cosolvent fraction > number of BVs > cosolvent type > salt brine type > EBCT. While temporal regeneration profiles presented in **Figure 3.5.11** clearly demonstrate the necessity of ≥10 bed volumes to regenerate AERs, **Table 3.5.1** illustrates how greater PFAS desorption is achieved through only 10 BVs using a 90% methanol solution than through 30 BVs using 70% methanol for all three PFAS-selective AERs. Use of an alternate cosolvent (1-propanol) did lead to improved AER regeneration, though improvements fell below those found when using 90% methanol fractions. While salt type was found to have an effect on PFAS desorption from resins in batch reactions, the superiority of chloride salts combined with the ubiquity, affordability, and solubility of NaCl prevented further testing with emphasis given to cosolvents in continuous-flow experiments.

The crucial importance of organic cosolvent type and fraction stem from the hydrophobic character they provide to the overall regenerant solution. Because the hydrophobic fluoroalkyl tail of the PFAS molecule comprises the majority of its mass and size, use of aqueous-only regenerant solutions do little to disrupt the Van der Waals forces attracting the PFAS to the hydrophobic polymer (Liu and Sun, 2021). It then follows that solutions with greater hydrophobic character (e.g., lower polarity) lead to better PFAS desorption, as evidenced in **Figure 3.5.11C**. While this trend underpins the rationale behind selection of regenerant solutions with higher cosolvent fractions, it also provides support for certain solvents leading to better regeneration outcomes than others at the same solvent fraction. 1-propanol, for example, has a lower relative polarity than methanol (Reichardt and Welton, 2010), leading to a less polar overall solution when mixed with water at a 70/30 volume ratio. Because relative polarity decreases with increasing alcohol chain length (Atamna et al., 1990), it can be surmised that use of longer-chained alcohols leads to better PFAS desorption. However, the lower salt solubility of long-chained alcohol solvents compared to shorter-chained analogues places methanol in a unique position to effectively desorb PFASs without incurring undue risk to humans and the environment (Ferrari et al., 2023). While cosolvent parameters play a determining role in selection of regeneration parameters, use of cosolvent in regenerant solutions can be optimized from a cost and sustainability perspective through recovery processes like distillation.

3.6 Treatment of PFAS-Contaminated Regenerant Brines

3.6.1. Electrochemical oxidation of synthetic waste brines

Electrochemical oxidation experiments were first conducted to evaluate treatment of a wide range of PFASs derived from diluted AFFF (**Table A3.6.1**) in various synthetic brine solutions (**Table A3.6.2**) being considered for AER regeneration schemes, thereby providing insights in developing hybrid AER/electrochemical treatment strategies. Hitherto a systematic study on the impacts of these brine matrices on PFAS treatment has not been performed. In this work, the impacts of hydroxyl radical scavenging on PFAS treatment were assessed (particularly with respect to oxidation of the polyfluorinated compounds, and the relative importance of direct versus indirect oxidation mechanisms), as well as the impacts of various brine anionic and cationic species on overall treatment effectiveness. Comparison of non-chloride containing brines (to prevent the

formation of perchlorate) to chloride-containing brines traditionally used for AER regeneration also was a focus of this study, as was potential beneficial impacts of the elevated sulfate and bicarbonate brine concentrations on overall PFAS treatment. Herein, we focused on assessing the extent to which electrochemically generated oxidants derived from various brine solutions impact overall treatment effectiveness. Treatment assessment was based on fluorine mass balances, and insights into the oxidation pathways of the polyfluorinated compounds was attained.

PFAS Defluorination in Different Salt Brines. Fluoride generation in the 5 brine solutions is shown in **Figure 3.6.1 (A-C)**. First-order rate constants and R^2 values regressed to the fluoride data, shown in **Table A3.6.3**, suggest an overall pseudo first-order electrochemical defluorination process. With the exception of the NaCl brines, the pseudo first-order rate constants for fluoride generation in each of the brines (without TBA) was statistically identical. For the $NaHCO_3$ and Na_2SO_4 brines, where differing brine concentrations were tested, the fluoride generation also was independent of the brine concentration for the corresponding range of applied voltages examined. The perchlorate brine, which is expected to be inert during electrochemical treatment (the perchlorate ion is not further oxidized), yielded statistically identical pseudo first-order fluoride generation rate constants as the sulfate and bicarbonate-based brines. Together, these results suggest that the sulfate and bicarbonate salts which have potential to scavenge hydroxyl radicals (Chaplin et al., 2010) or produce secondary radicals, did not influence the PFAS defluorination rate constant during the electrochemical treatment. This also confirms that these electrolytes do not inhibit reactions by competing for reactive sites on the BDD anode. Furthermore, experiments performed with ammonium salts (**Figure 3.6.1A**) resulted in fluoride generation rate constants similar to the corresponding sodium salt brines, indicating that replacement of the sodium cations with ammonium had a negligible impact on PFAS defluorination under the conditions tested.

A small layer of foam was observed in all experiments. This foam did not notably dissipate during the duration of the 8 hour electrochemical experiments, and no visual differences in foam generation were observed among the various brine types or concentrations. It is likely that the elevated levels of PFAS and/or hydrocarbon surfactants known to be present in AFFF, coupled with electrochemically generated hydrogen and oxygen gases, facilitated this foam formation. The foam phase served as a potential sink for some PFASs during treatment, as will be discussed with respect to fluoride generation and observed PFAS transformation.

The fluoride generated in the brines (with the exception of the NaCl brines) represents approximately half of the 27 mg/L of total fluorine estimated by ^{19}F-NMR analysis to be present in the 500-fold diluted AFFF solution. A long-term 30 hour experiment using a 0.2% sodium sulfate solution (**Figure A3.6.1**) yielded a maximum fluoride concentration of 22 mg/L, representing ~81% defluorination of the PFASs initially present, as determined by ^{19}F-NMR. It is noted that fluoride levels were still slowly increasing at the end of this experiment, so additional treatment time likely would have resulted in a slightly greater fluoride recovery. Foam was no longer present after 24 hours reaction, thereby eliminating the potential for any undissolved fluorine sinks by 24 hours.

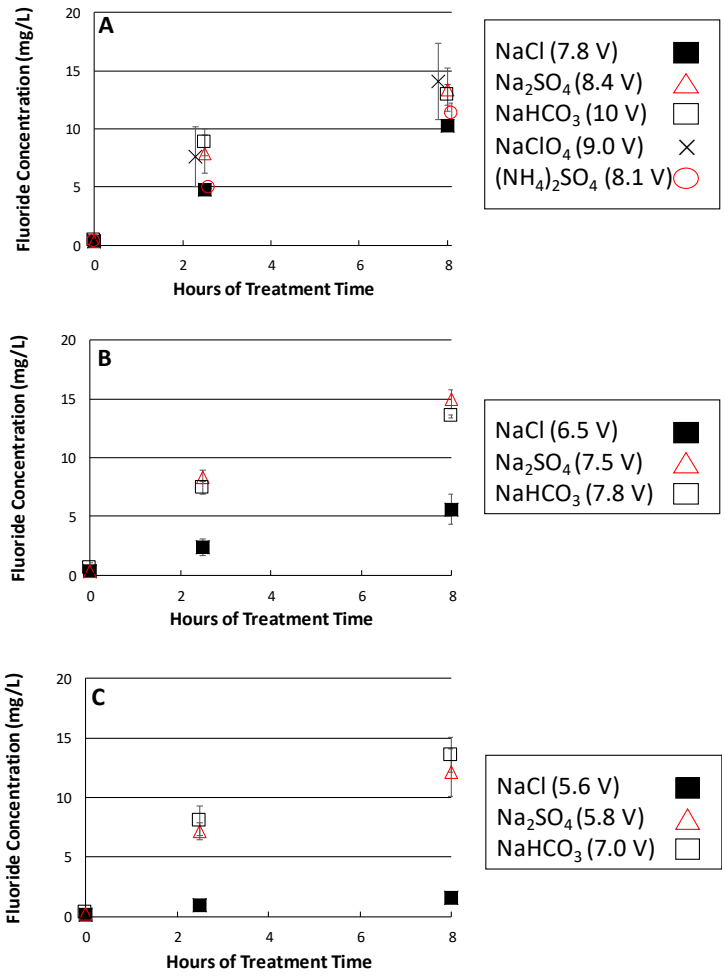

Figure 3.6.1. Fluoride generation during electrochemical treatment in brine solutions at 0.2% (A), 1% (B), and 5% (C) concentrations. The $NaHCO_3$ brine concentration in panel C was limited to 2.5% due to solubility constraints. All experiments were performed at a current density of 40 mA/cm^2, and with an applied voltage (V) shown in the parentheses in the legends. The pH values were approximately 12.6, 12.4, 10.3 and 12.2 for the chloride, sulfate, carbonate, and perchlorate experiments, respectively. Average of duplicate results with 95% confidence intervals are shown. The $NaClO_4$ and $(NH_4)SO_4$ data in panel A are offset for clarity. From Schaefer et al. (2020).

For the NaCl brines, the fluoride generation was less than in the sulfate, bicarbonate, or perchlorate brines, and the fluoride generation in the NaCl solutions decreased with increasing NaCl concentration (**Figure 3.6.1 A-C**). The pseudo first-order fluoride generation rate constant decreased from 0.065 h^{-1} to 0.0079 h^{-1} as the NaCl brine concentration increased from 0.2 to 5%. While NaCl at concentrations less than 0.02% have been shown to not impact PFAA defluorination (Schaefer et al., 2017), the elevated NaCl concentrations used herein (0.2% to 5%) had a measurable adverse impact on defluorination. The decreased fluoride generation in the NaCl brine solutions was likely due to chloride oxidation on the anode surface (and ultimately the formation of perchlorate) (Polcaro et al., 2009), which was observed as the primary transformation product of chloride oxidation in previous experiments using the same type of BDD anodes (Schaefer et al.,

2018). Decreases in chloride concentrations were observed during electrochemical treatment, consistent with this chloride oxidation process (**Figure A3.6.2**); **Figure A3.6.2** also shows that perchlorate was the primary chloride transformation product. This direct chloride anodic oxidation likely competed with the direct electrode oxidation defluorination step that has been shown to be the rate limiting step in the defluorination of PFAAs, and potentially other PFASs (Schaefer et al., 2018, Le et al., 2019).

To further examine the decreased defluorination in the NaCl brines, residual PFAA concentrations for the highest concentration NaCl, $NaHCO_3$ and Na_2SO_4 brines were evaluated. These results (**Figures A3.6.3** and **A3.6.4**) show that removal of the long-chained PFAAs (e.g., perfluorooctane sulfonate (PFOS), perfluorooctanoic acid (PFOA), perfluoroheptane sulfonate (PFHpS) was nearly identical among all three brines, with >90% removal of PFOS and PFHpS by the 2.5 hour sampling point, and >80% removal of PFOA by the 2.5 hour sampling point. The organic fluorine present in these three long-chained PFAAs accounted for >90% of the organic fluorine present as PFAAs in the initial AFFF solution. While shorter-chained PFAAs (e.g., PFHxA, PFPeS) exhibited less transformation in the 5% NaCl brine compared to the other brines, removal of PFOS, PFHpS, and PFOA did not decrease in the presence of the elevated 5% NaCl brine, despite the fact that fluoride generation at the elevated NaCl concentration was substantially reduced (**Figure 3.6.1C**) relative to the other brines. This observation likely was due to the fact that PFOS, PFOA, and PFHpS removal was due to their accumulation in the foam. Longer-chained PFAAs are more surface active than shorter-chained PFAAs (Schaefer et al., 2019, Brusseau and Van Glubt, 2019), and therefore are more likely to migrate into the foam. To verify this, a separate set of experiments was performed where the foam generated over 8 hours was collected, and either dissolved in methanol for PFAS analysis, or re-dissolved in sulfate brine where it was subsequently electrochemically treated and fluoride generation was measured. Results showed that at least 80% of the PFOS-associated fluorine had partitioned into the foam, while the mass of polyfluorinated compounds in the foam relative to the aqueous phase was negligible (<1%).

No decreases in PFAA concentrations were observed in the no-current controls (which did not produce any foam due to the absence of gas generation at the electrodes).

Consistent with previous studies on electrochemical oxidation of PFAAs (Schaefer et al., 2018, Gomez-Ruiz et al., 2017), transient increases in the shorter-chained perfluorinated carboxylates were observed during electrochemical treatment of the diluted AFFF solutions shown in **Figures A3.6.3** and **A3.6.4**. Increases in PFPrS also were observed. These transient increases are likely due to the sequential head group oxidation reactions of the longer-chained perfluorinated carboxylates and sulfonates, but may also be due to the oxidation of PFAA precursor compounds to perfluorinated carboxylates (Schaefer et al., 2018). These shorter-chained PFAAs are less surface active than the longer-chained PFAAs (Schaefer et al., 2019, Brusseau and Van Glubt, 2019), thus are less likely to be removed from the bulk aqueous phase during foam formation. For the NaCl brine, transformation of the shorter-chained perfluorinated carboxylates and sulfonates occurs more slowly compared to the other brines, suggesting that the elevated NaCl levels inhibit defluorination of these shorter-chained compounds due to competition for active sites on the anode surface [23]. Similar to observations for fluoride generation, NaCl had a measurable adverse impact on short-chained PFAA transformation. Partitioning into the foam likely masked these chloride inhibition effects for the longer-chained PFAAs. It is noted that the fluorine mass associated with

any observed increases in short-chained PFAAs was negligible when considering the overall F mass balance and fluoride generation.

While evaluation of the PFAAs provides useful insight, the PFAAs initially present in the diluted AFFF account for only 14.8 mg/L of F, suggesting that the remaining 12.2 mg/L (based on ^{19}F-NMR analysis) of fluoride was initially present as polyfluorinated compounds or at least compounds that were not part of the targeted PFAA analysis. The 22 mg/L fluoride generated in the 30-hour experiment (**Figure A3.6.1**) is consistent with this mass balance. More importantly, due to the partitioning of PFOS, PFHpS, and PFOA into the foam, at least 65% of the fluoride generated over the 8-hour electrochemical experiments (**Figure 3.6.1 A-C**) originated from the polyfluorinated compounds.

The polyfluorinated species showing the most abundant area counts (>10^5) in the diluted AFFF were the N-dimethyl ammonio propyl perfluoro sulfonamides (AmPr-FASAs) and the N-dimethyl ammonio propyl perfluoroalkane sulfonamido propanoic acids (AmPr-FASA-PrA), with perfluorinated chain lengths of 3 to 6. Transient increases observed during electrochemical treatment were observed for N-oxidedimethylammoniopropyl-perfluoro sulfonamides (OAmPr-FASAs), N-methylperfluoroalkane sulfonamido acetic acids (MeFASAAs), and perfluorosulfonamides (FASAs), with perfluorinated chain lengths of 3 to 6. Representative structures of these compounds are provided in **Figure A3.6.5**. Together, these polyfluorinated compounds account for approximately 84% of the organic fluorine present in the identified polyfluorinated compounds (estimated based on the fluorine number and area counts).

Relatively rapid transformation of these polyfluorinated compounds was observed during electrochemical treatment for all the brines tested (**Figure 3.6.2**), likely due to transformations associated with the non-fluorinated head groups. For the NaCl, Na_2SO_4, and $NaHCO_3$ brines, at least 80% transformation was observed by the 2.5 hour sampling point; no transformation was observed in the no-current controls. Based on the negligible (<1% of what was in the bulk aqueous phase) accumulation of polyfluorinated compounds in the foam, the observed removal of the polyfluorinated compounds was due to electrochemical oxidation. Formation of transient oxidation products during electrochemical treatment is shown in **Figure A3.6.6**; these transients were observed in the NaCl, Na_2SO_4, $NaHCO_3$ and $NaClO_4$ brines. OAmPr-FASAs were likely formed from the oxidation of the AmPr-FASA-PrA, and with the FASAs forming from the subsequent oxidation of the OAmPr-FASAs. A similar AmPr-FASA-PrA oxidative pathway has been observed in previous electrochemical oxidation experiments using AFFF (Schaefer et al., 2018), where PFAAs were the final products formed before defluorination occurred.

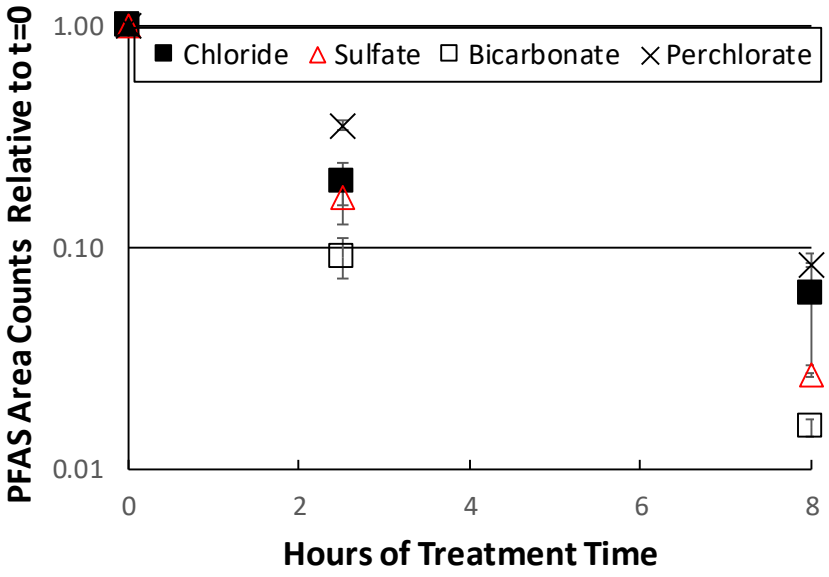

Figure 3.6.2. Relative (to t=0 hours) transformation of N-dimethyl ammonio propyl perfluoro sulfonamides (AmPr-FASAs and N-dimethyl ammonio propyl perfluorohexane sulfonamido propanoic acid (AmPr-FHxSA-PrA) during electrochemical treatment in the 0.2% sodium salt brines. Average of duplicate results are shown. Error bars represent 95% confidence intervals.91%, 83%, and 80% PFAS removal in the bicarbonate, sulfate, and chloride brines (respectively) were observed by 2.5 hours, while only 64% of the PFAS was removed by 2.5 hours in the perchlorate brine. From Schaefer et al. (2020).

Comparison of the 5% Na_2SO_4 and NaCl brines in **Figures A3.6.4** and **A3.6.7** shows that removal of PFOS, PFHpS, PFHxS and polyfluorinated compounds were nearly identical (the slower removal of the other PFAAs shown in **Figures A3.6.3** and **A3.6.4** was insignificant with respect to the overall fluorine mass balance). However, the fluoride generation (**Figure 3.6.1C**) for the 5% Na_2SO_4 and NaCl brines differed by approximately 11 mg/L fluoride (or, approximately 41% of the total fluorine present in the diluted AFFF). Thus, at 8 hours of treatment, the 5% NaCl brine had 41% less identified fluorine than the corresponding sulfate brine (since identified PFAA and polyfluorinated levels were the same in the 5% Na_2SO_4 and NaCl brines). This discrepancy in fluorine mass balance is likely attributable to unidentified polyfluorinated compounds – either in the raw diluted AFFF solution, and/or as intermediate oxidation products. To ensure that the observed discrepancy in fluoride generation and fluorine mass balance was not due to any re-dissolution of PFAS from the foam, but rather the presence of unidentified polyfluorinated compounds in the bulk aqueous phase, an additional experiment was performed using the Na_2SO_4 brine where the foam was continuously removed (via pipetting) during the 8-hour electrochemical treatment. The fluoride generated in the bulk aqueous phase during this experiment (**Figure A3.6.8**). was identical to that measured in experiments where the foam was not removed, indicating that (over an 8 hour period) PFAS transferred to the foam did not measurably re-dissolve into the bulk aqueous phase to facilitate subsequent electrochemical defluorination.

Previous studies have shown that the electrochemical oxidation of AmPr-FASAs yielded intermediate oxidation products that were not identified (Schaefer et al., 2018), thus the fluorine

mass balance results reported herein are consistent with previous observations. This is a notable result for electrochemical treatment, as transformation of PFAAs and suspect analytes identified in current mass spectral libraries may not be sufficient for confirming the success of electrochemical treatment with respect to defluorination, as unidentified fluorine containing species may persist.

The decreased precursor transformation in the presence of the perchlorate brine, and further exploration of PFAS transformation during electrochemical oxidation, are discussed in the following section.

Impacts of Radical Formation and Scavenging. As previously discussed, and shown in **Figure 3.6.1A**, fluoride generation in the $NaClO_4$ brine was identical to that in the $NaHCO_3$ and Na_2SO_4 brines, but defluorination was inhibited in the presence of NaCl. PFAA oxidation in inert perchlorate electrolyte was the same as observed in the $NaHCO_3$ and Na_2SO_4 brines (**Figure A3.6.9**). Together, these results suggest that any radical formation or scavenging by bicarbonate or sulfate species did not measurably impact the PFAA transformation that occurs via direct anodic oxidation, as results in inert $NaClO_4$ brine were identical. In contrast, transformation of the polyfluorinated compounds in the presence of chloride, bicarbonate, and sulfate was enhanced relative to that of the inert perchlorate brine, as clearly observed at the 2.5 hour timepoint in **Figure 3.6.2**. This difference for the perchlorate brine is not explained by any difference in applied voltage or pH, as the voltage and pH were within the ranges observed for the other brines (**Figure 3.6.1A**). One plausible explanation for the lower polyfluorinated compound transformation observed in the perchlorate brine is the absence of any carbonate radicals that likely were generated in the bicarbonate brine (Velazquez-Pena et al., 2013), sulfate radicals generated in the sulfate brine (Davis et al., 2014) and/or reactive chlorine species generated in the NaCl brine (e.g., chlorate radicals or hypochlorite) (Azizi et al., 2011). Reactive chlorine species, which are generated during electrochemical oxidation when chloride is present (Schmalz et al., 2009), have been shown to oxidize the non-fluorinated head groups of PFAA precursors (Xiao et al., 2018). Interestingly, Pica et al. (2019) also observed that sulfate-based electrochemically generated radicals using BDD anodes enhanced the transformation of PFASs, but did not enhance fluoride generation, which is consistent with results observed herein. Thus, it appears that oxidants that are likely generated in the NaCl, Na_2SO_4, $NaHCO_3$ brines contribute to at least the initial transformation of the polyfluorinated compounds (e.g., AmPr-FASAs and AmPr-FHxSA-PrA) via indirect oxidation mechanisms, but rate-limiting defluorination steps are still controlled by direct reactions on the anode surface. These results also suggest that chloride and bicarbonate, in addition to sulfate, have an overall effect that enhances the transformation of polyfluorinated compounds (relative to the inert perchlorate solution), rather than having a net inhibitory effect due to potential oxidant scavenging.

To further explore the potential role of electrochemically generated oxidants, additional electrochemical experiments were performed with the radical scavenger TBA added to both the 0.2% $NaClO_4$ and 0.2% Na_2SO_4 solutions. TBA concentrations, initially at 100 mM, decreased by approximately 50% during the duration of the electrochemical experiments. TBA addition resulted in an approximately 6-fold decrease in the first-order fluoride generation rate constant (**Figure 3.6.3** and **Table A3.6.3**); decreasing the initial TBA concentration to 10 mM decreased the fluoride generation pseudo first order rate constant by approximately 50% (**Table A3.6.3**) compared to

experiments without TBA. TBA also inhibited transformation of the perfluorinated sulfonates (**Figure A3.6.10**), although TBA impacts on the longer-chained PFAAs could not be fully assessed due to (as previously discussed) their partitioning into the foam phase. In addition, TBA (100 mM) inhibited the transformation of the polyfluorinated compounds initially present in the diluted AFFF, decreasing the first-order rate constant associated with their transformation in the sulfate and perchlorate brines by approximately a factor of 2 (**Figure A3.6.11** and **Table A3.6.4**). These results suggest the importance of electrochemically generated radicals on the initial oxidation steps of the polyfluorinated compounds, and on PFAS defluorination.

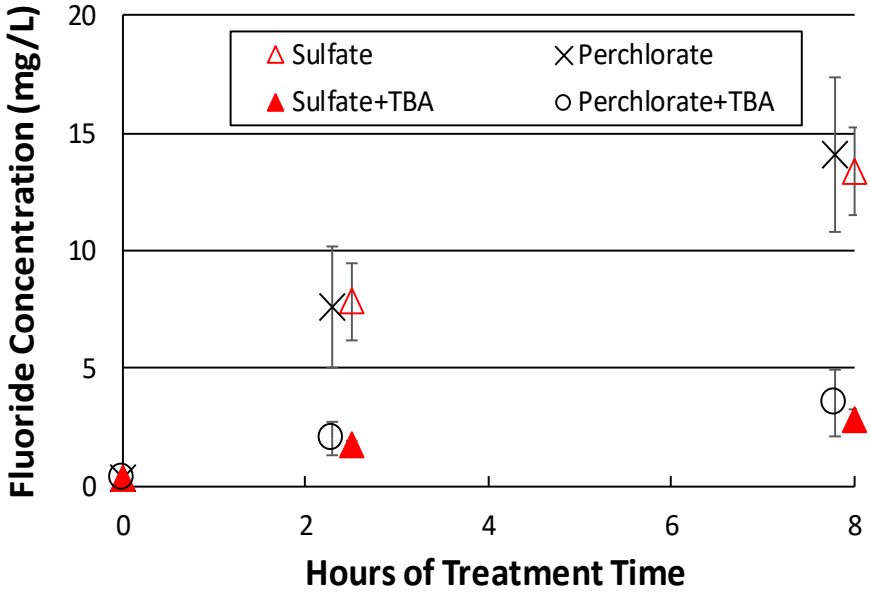

Figure 3.6.3. Fluoride generation during electrochemical treatment in 0.2% Na_2SO_4 and $NaClO_4$, with and without TBA. All experiments were performed at a current density of 40 mA/cm^2. Average of duplicate results with 95% confidence intervals are shown (in some cases, error bars are smaller than the data markers). Perchlorate data are offset 0.2 hours for clarity. From Schaefer et al. (2020).

Together, the results described in the previous two paragraphs explain the slow PFAS defluorination in the presence of a radical scavenger such as TBA. The conceptual model is presented in **Figure 3.6.4**, which in general shows indirect oxidation transforming non-fluorinated head groups, while direct anodic oxidation is responsible for defluorination. Previous work (Schaefer et al., 2018) showed that AmPr-FHxSA-PrA yields identifiable oxidation intermediates (OAmPr-FASAs, MeFASAAs, and FASAs), leading to PFAA formation and ultimately defluorination. This pathway was observed herein, but since AmPr-FHxSA-PrA consisted of less than 20% of the organic fluorine present as polyfluorinated compounds in the AFFF (estimated based on its relative area counts compared to the other polyfluorinated compounds), this pathway played a minor role in terms of fluorine mass balance. Previous work (Schaefer et al., 2018) also has shown the electrochemical oxidation of AmPr-FASAs results in the formation of unidentified intermediates (which is the suspected cause of the fluorine mass balance discrepancy previously discussed), thus two oxidation pathways are shown in **Figure 3.6.4**.

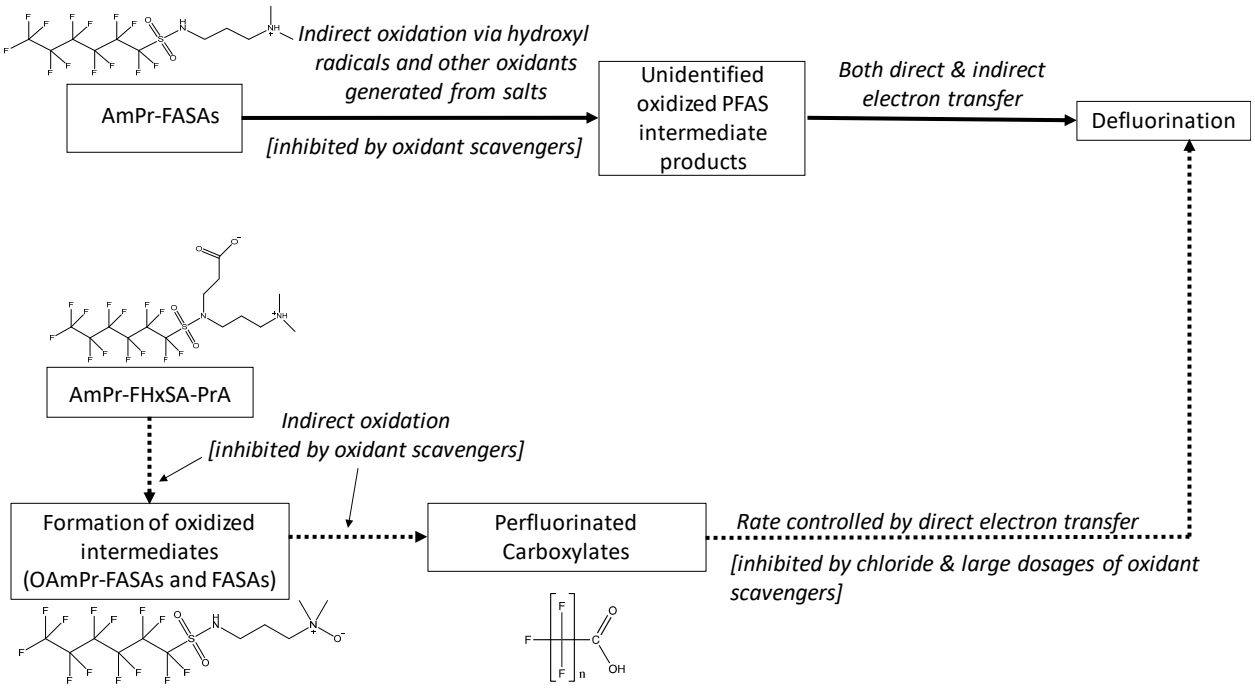

Figure 3.6.4. Proposed electrochemical oxidation pathway for the most abundant polyfluorinated compounds observed in the diluted AFFF. The differing pathways for the AmPr-FASAs and AmPr-FHxSA-PrA are consistent with previous electrochemical studies with BDD anodes. From Schaefer et al. (2020).

The inhibited transformation of both the AmPr-FASAs and AmPr-FHxSA-PrA (which together contain approximately 40% of the organic fluorine in the AFFF, and account for the majority of the polyfluorinated compounds shown in **Figure A3.6.11**) in the presence of TBA indicates that transformation of these compounds is largely controlled by indirect oxidation (e.g., via generation of hydroxyl or other salt-based oxidants). Increased AmPr-FASA and AmPr-FHxSA-PrA transformation in the presence of sulfate, bicarbonate, or chloride compared to perchlorate (**Figure 3.6.2**) further suggests electrochemically generated oxidants contribute to the indirect oxidation of these polyfluorinated compounds. In the AmPr-FASA oxidation pathway, initial transformation of AmPr-FASA results in the generation of unidentified polyfluorinated compounds, consistent with the previously discussed discrepancy in fluorine mass balance.

Inhibited transformation of the perfluorinated sulfonates in the presence of 100 mM TBA was observed (**Figure A3.6.10**); the only exception is PFOS, which (as previously discussed) was controlled by partitioning into the foam. Previous work showed that a TBA dosage of approximately 1.3 mM showed no inhibition of fluoride generation from PFAAs (Schaefer et al., 2017). At a swamping dosage of hydroxyl radical scavenger (such as the 100 mM TBA used herein), which may be representative of cosolvent dosages used in brine regeneration (Zaggia et al., 2016), secondary perfluorinated sulfonate oxidation steps that require hydroxyl radicals (Chaplin, 2018) likely become rate limiting, resulting in a decrease in perfluorinated sulfonate oxidation. This interpretation is consistent with the results of Lin et al. (2018), who noticed a substantial decrease in PFAA transformation in the presence of elevated NaCl and methanol cosolvent.

Current Efficiency and Energy. To quantify the overall efficiency of the applied current to oxidative PFAS defluorination, the dimensionless coulombic efficiency (CE) is defined as follows (Bagastyo et al., 2012) :

$$CE = FVe\frac{C_F}{At} \quad (3.6.1)$$

where F is Faraday's Constant (94,486 C mol^{-1}), V is the volume of the batch system (0.25 L), *e* is the moles of electrons needed per mole fluoride (assume 1 electron per C-F bond cleavage), C_F is the measured fluoride generation (mol L^{-1}), A is the applied current (0.40 A), and t is the time at the end of the electrochemical experiments. Applying this to the 30-hour sodium sulfate solution (no TBA), **Figure A3.6.12** shows that the CE varies from 2 x 10^{-3} near the beginning of the experiment to 0.6 x 10^{-3} at the end of the experiment. These low values are due, in part, to the transformation and mineralization of other organic carbon present in the diluted AFFF, including polyfluorinated compounds. These CE values are, however, nearly 10-times greater than the CE values measured previously in diluted AFFF and AFFF-impacted groundwater using BDD anodes (Schaefer et al., 2018). The reason for this large difference is likely due to the approximately 10-fold greater PFAS concentration (based on fluorine content) used herein compared to the previous study, highlighting the fact that electrochemical oxidation of PFASs becomes more efficient at high concentrations.

Using data in **Figure A3.6.1**, 90% PFAS defluorination requires approximately 430 W-h L^{-1} for the 0.2% sulfate brine solution; this energy demand decreases to 280 W-h L^{-1} if the 5% sulfate brine were used (due to the lower voltage, as shown in **Figure 3.6.1C**). While these energy demands are high, two considerations are noteworthy. First, treatment of regeneration solutions is expected to be less than 0.1% of the volume that is treated by the anion exchange resin (Zaggia et al., 2016). Thus, the energy demand per volume of total water treated is at least 1,000-times less than calculated based on the data in **Figure A3.6.1** (i.e., less than 0.3 W-h L^{-1} using 5% sulfate brine). Second, due in large part to the very high PFAS concentrations used herein, electrochemical treatment in this study was inhibited by foam formation, as PFAS partitioned into the foam. Given that nearly half of the PFAS-associated fluorine partitioned into the foam within the first few hours of treatment, the treatment time and calculated energy demand in the absence of foam generation (i.e., at lower PFAS concentrations than those used herein) likely would have been nearly half that measured in this study.

3.6.2. Electrochemical oxidation of IX still bottoms

Results of the post-distillation solution (still bottoms) showed that negligible PFAS losses occurred during the distillation process, and the methanol mass decreased by more than 5 orders of magnitude compared to the non-distilled solution. The properties of the reconstituted (with DI water) still bottoms for the high TOC groundwater impacted columns before and after the ECO treatment are provided in **Table 3.6.1**. An ECO cell voltage of 7.9 V was applied throughout the experiment to produce a constant 40 mA/cm2 current density. The TOC removal in the still bottom was more than 99% and no significant change in temperature occurred during the treatment (e.g., 23 – 24 ^{0}C). Removal of the selected PFAAs is shown in **Figure 3.6.5**. Consistent with previous studies on the electrochemical oxidation of PFAAs, transient increases in the shorter-chained perfluorinated carboxylates (e.g., PFBA) were observed during the electrochemical treatment of

the AFFF still bottom. Such transient increases are likely due to the sequential head group oxidation reactions of the longer-chained perfluorinated carboxylates, but may also be due to the oxidation of PFAA precursor compounds to perfluorinated carboxylates.

Table 3.6.1. Anions and other relevant parameters of the still bottom 1 before and after ECO treatment

	Baseline	After 24 hr treatment
Fluoride (mg/L)	*<0.18*	*8.02±0.88*
Chloride (mg/L)	*543.5±6.6*	*<0.15*
Nitrite (mg/L)	*<0.5*	*<0.5*
Nitrate (mg/L)	*<8.6*	*376.1±36.6*
Sulfate (mg/L)	*2904.1±92.8*	*2868.6±470.6*
pH	*4.4±0.1*	*7.0±0.1*
TOC (mg/L)	*215*	*<2*
Applied Voltage (V)	*0*	*7.9±0.04*

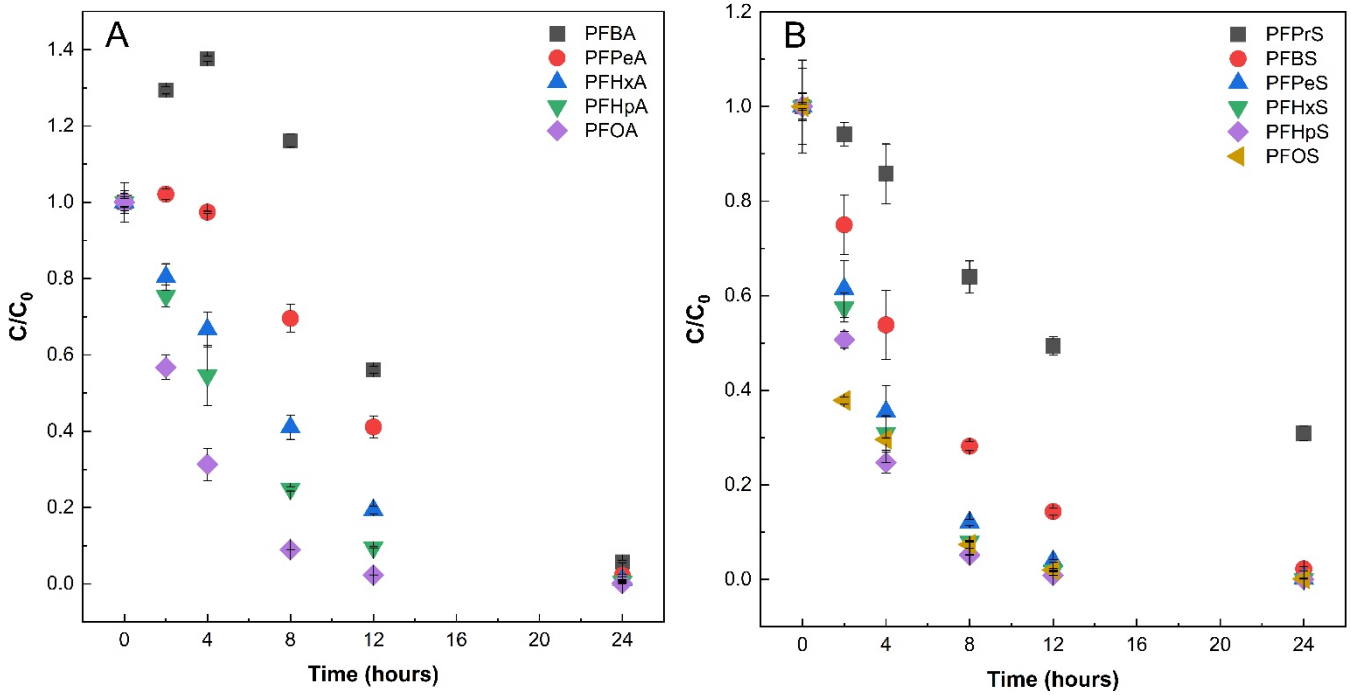

Figure 3.6.5. Time course for the degradation of selected A) PFCAs and B) PFSAs in the still bottom. Error bars represent the min/max of duplicate samples.

3.6.3 Hydrothermal treatment of field-generated IX still bottoms

The received still bottoms sample is an aqueous solution with dark color (**Figure 3.6.6**). The water quality results were shown in **Table 3.6.2**. As expected, still bottoms sample has high TOC (13.9 g/L, non-purgable) and high salts (chloride up to 82.7 g/L and nitrate up to 5 g/L). The still bottoms sample is slightly basic with pH of 9.64. **Table 3.6.3** summarizes PFAS concentrations measured via targeted analysis with reference standards and suspect screening analysis with semi-quantitative analysis. As shown, high concentrations of PFASs were detected in this still bottoms sample. The total PFASs including targeted and suspected analytes is ~872 mg/L. A series of perfluoroalkyl acids (PFAAs) including perfluorocarboxylic acids (PFCAs) and perfluoroalkyl sulfonic acids (PFSAs) with different perfluorinated carbon chain lengths were present. Among them, PFOS (64.7 mg/L) and PFOA (603 mg/L) were measured at the highest concentrations. The concentration of PFOA is around 10-fold higher than PFOS, indicating the site is somewhat atypical of AFFF-impacted sites. In addition to PFAAs, some fluorotelomer acids, including X:2 fluorotelomer sulfonate (X:2 FTS) and perfluoroalkane sulfonamide (FASA) were detected at not very high levels (total <20 mg/L). The semi-quantitative analysis showed that 14:2 FTS has the highest concentration (10.6 mg/L). The residue methanol in still bottoms sample was measured at 5.5 g/L from vendor's information. This amount is likely in addition to the measured dissolved organic carbon which used a non-purgeable DOC methodology. Overall, still bottoms sample in this study has high concentration of PFASs, high TOC, high salt, and some cosolvent which challenges most of PFAS treatment technologies.

Figure 3.6.6. Photo of waste IX still bottoms sample.

Table 3.6.2 Water quality of waste IX still bottoms sample obtained from Willow Grove pilot treatment system.

Water quality	Unit	Conc.	Uncertainty
pH		9.64	
TDS	g/L	177	
TOC(purge)	g/L	12.8	
TOC(non purge	g/L	13.9	
Fluoride	mg/L	3.7	± 0.03
Chloride	mg/L	82700	± 300
Bromide	mg/L	38	± 1.0
Nitrate(NO3-)	mg/L	5000	± 50
Sulfate	mg/L	2940	± 7

Figure 3.6.7 shows individual PFAS degradation during HALT of still bottoms sample. All of PFASs except PFSAs were removed >99% after only 15 min reaction while PFSAs are more recalcitrant to degrade. This is consistent with our previous studies on HALT of AFFF and AFFF-impacted groundwater. **Figure 3.6.7c** shows the defluorination increased to >85% after 90 min reaction demonstrating the effectiveness of HALT for this complex matrix. The suspect screening analysis did not show any suspected PFAS present in the post-treatment sample. We also estimated the k_{obs} of individual PFSAs and compared them with previous measurements conducted in different matrices (AFFF and AFFF-impacted groundwater). No big difference was found among different matrices, despite still bottoms have very high salt and DOC. This further demonstrated the high tolerance of matrices for HALT to treat PFAS waste.

We also tracked changes in DOC during HALT reaction (**Figure 3.6.8**). The DOC was removed by >20% after 15 min of reaction, but then remain at almost constant with longer reaction times. This is consistent with what we observed in another project which applied HALT to foam fractionation-derived concentrate sample. The first DOC drop was likely due to the PFAS mineralization and other easily degradable organic components that makeup the DOC. The remainder of DOC was more recalcitrant, even more than PFASs, during HALT. The presence of these recalcitrant compounds needed to be characterized when considering the disposal of final waste stream after HALT. Project ER18-1501 is examining the fate of groundwater-derived natural organic matter during HALT in greater depth as well as testing methods for further mineralizing these components during the treatment process.

The degradation of PFASs in still bottoms sample was not affected by the residue methanol which we thought it may promote or inhibit degradation as methanol has some co-solvent effect on chemistry reaction. This might be due to the low percentage of methanol (mass percentage <1%) in still bottoms sample. However, we did find the presence of methanol affected the sealing of stainless steel tube reactor. In future efforts, as part of ER18-1501, we intend to systematically evaluate the co-solvent effect on HALT of PFASs. If cosolvent was demonstrated to not inhibit or even promote PFAS degradation, the distillation of methanol can be eliminated, and the post-treatment solution can be reused to regenerate ion exchange resin.

Table 3.6.3. Targeted and semiquantitative analysis of PFAS in still bottoms samples.

Analysis	PFAS	Conc. (mg/L)	Uncertainty
Targeted PFAS	PFBA	1.21	0.03
	PFPeA	9.4	0.44
	PFHxA	25.1	0.6
	PFHpA	17.4	0.3
	PFOA	603	36
	PFNA	1.47	0.06
	PFDA	1.16	0.01
	PFPrS	4.58	0.27
	PFBS	15.8	0.6
	PFPeS	19.2	0.3
	PFHxS	59.1	0.7
	PFHpS	2.34	0.02
	PFOS	64.7	1.4
	PFNS	0.29	0.01
	PFEtCHxS	2.23	0.01
	FBSA	2.86	0.08
	FOSA	0.32	0.02
	FHxSA	11.9	0.3
	6:2 FTS	4.07	0.02
	8:2 FTS	2.24	0.08
	Cl-PFOS	0.13	0.01
	Total	848	36
Suspected PFAS	14:2 FTS	10.66	-0.37
	FPeSA	3.50	-0.07
	UPFOS	1.46	-0.03
	O-U-PFNA	2.64	0.04
	SPr-FHxSA	1.53	-0.11
	FPrSA	0.91	-0.03
	PFHxSi	0.57	0.01
	PFMeCHxC/	1.38	-0.04
	K-PFOS	0.18	-0.01
	K-PFHxS	0.24	0.00
	FHxSAA	0.26	0.00
	UPFHxS	0.21	0.00
	SPr-FPeSA	0.24	-0.03
	UPFHpS	0.10	0.00
	K-PFPeS	0.10	0.00
	MeFPrAA	1.22	-0.09
	Total	23.99	0.40

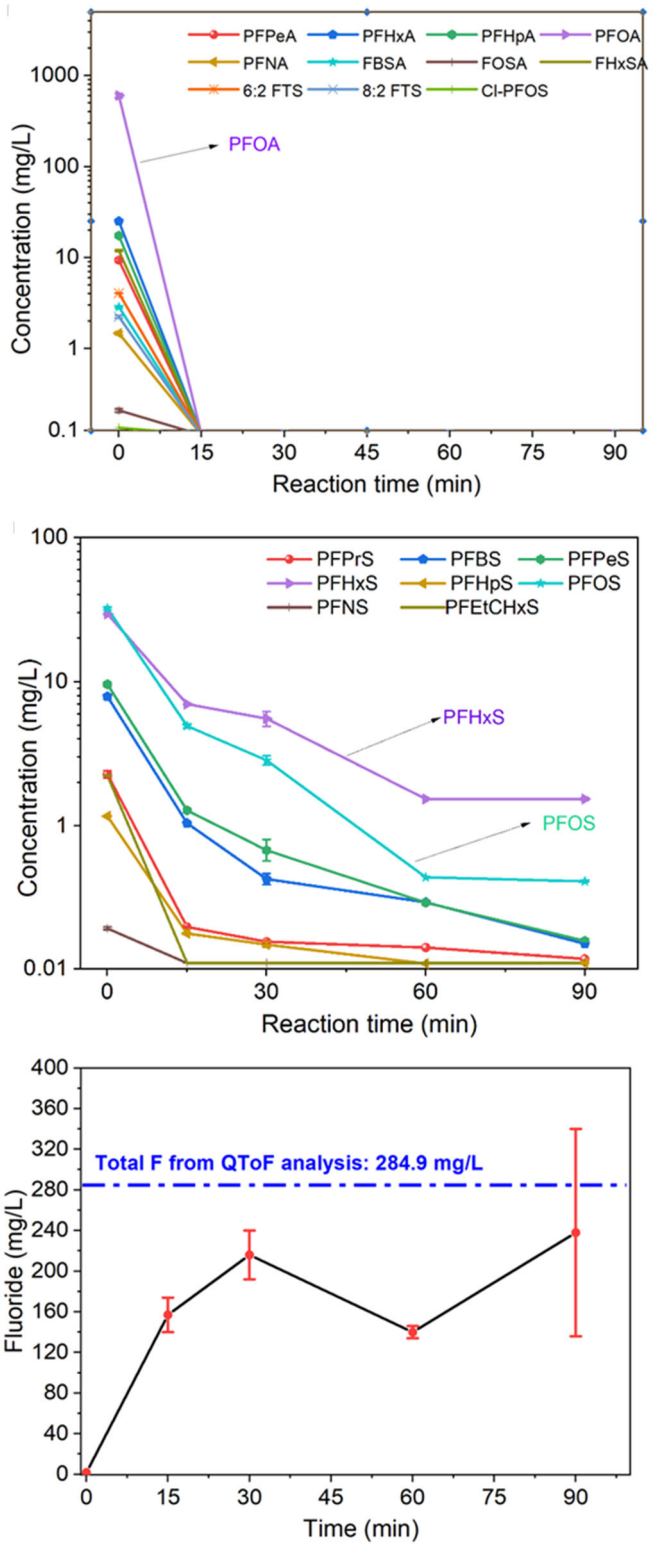

Figure 3.6.7. Individual non-PFSA (a) and PFSA degradation (b) and fluoride release (c) during HALT of still bottoms sample.

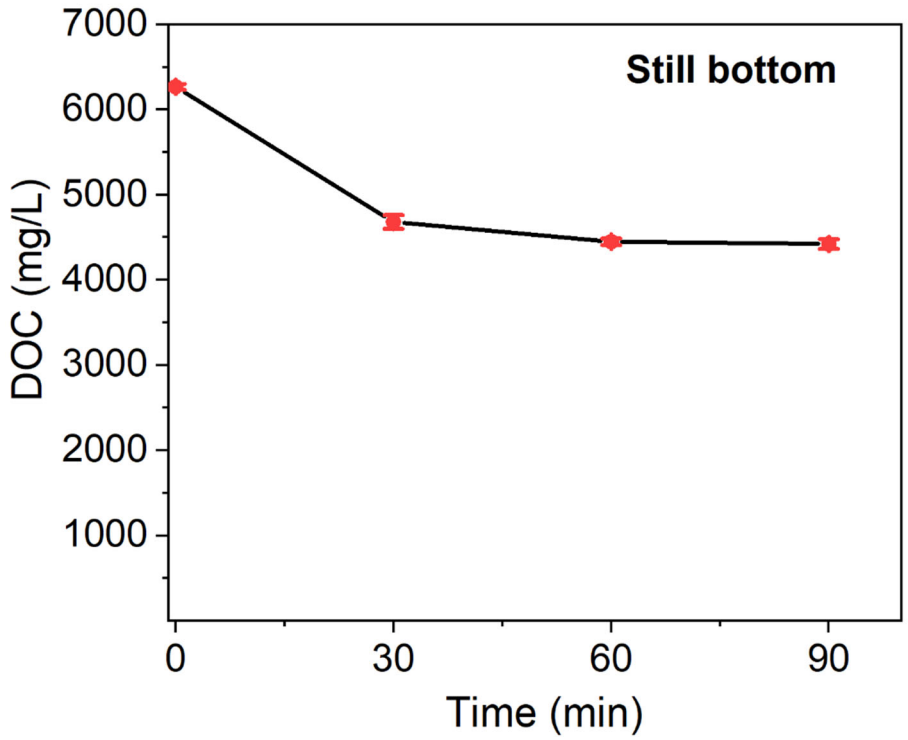

Figure 3.6.8 DOC degradation during HALT of still bottoms sample.

3.7 Life Cycle Assessment of Regenerable Ion Exchange Treatment Design Options

3.7.1. Impact of disposal vs. recycling of waste regeneration solution

The environmental impacts of the different options for management of waste regeneration solution, i.e., disposal (scenario 1a), partial recycling (scenario 1b), and full recycling (scenario 1c), are explored in this section (see **Figure 3.7.1**). The regeneration conditions were selected as hypothetical scenarios that could be used to motivate future laboratory research and pilot studies. The results are considered first with respect to the overall impact between scenarios (**Figure 3.7.2**, scaled characterization values) followed by the impacts of contributing processes within the scenarios (**Figure 3.7.3a–c**, normalized characterization values). **Figure 3.7.2** shows that for all impact categories, the order of decreasing environmental impact was disposal (scenario 1a) > partial recycling (scenario 1b) > full recycling (scenario 1c). The main changes occurring in the scenarios from disposal to full recycling included decreasing mass of chemical inputs and decreasing mass of waste being transported for off-site incineration (see **Table 3.7.1**). Among the impact categories, fossil fuel depletion and ecotoxicity showed the greatest decrease in relative impact going from disposal to partial recycling (scenario 1a to 1b), and eutrophication showed the greatest decrease in relative impact going from disposal to full recycling (scenario 1a to 1c) and partial recycling to full recycling (scenario 1b to 1c). The reduction in fossil fuel depletion was due to a significant decrease in methanol consumption in transitioning from disposal to partial recycling (i.e., methanol recovery was assumed to be 95% efficient). The reductions in ecotoxicity and eutrophication were due to significant decreases in the amount of waste incinerated in

transitioning from disposal and partial recycling to full recycling (i.e., replacing liquid waste stream by solid adsorbent). Smog showed the smallest decrease in relative impact when going from disposal to partial recycling and disposal to full recycling. This was because electricity dominates smog formation, and overall electricity use increased as more of the regeneration solution was recycled via methanol recovery and brine recovery processes. Fossil fuel depletion, acidification, and respiratory effects showed the smallest decreases in relative impact going from partial recycling to full recycling, as both scenarios recovered and recycled methanol.

Figures 3.7.3a–c show the normalized characterization results for disposal, partial recycling, and full recycling scenarios, respectively, illustrating the processes that contribute to the scenarios. Note that the scale of the y-axis in **Figure 3.7.3** decreases going from disposal to full recycling. (**Figure A3.7.1** compares the normalized characterization results for the three scenarios in the same plot.) Among the impact categories, human toxicity cancer (i.e., carcinogens) had the highest impact in the three scenarios. Ecotoxicity, acidification, and fossil fuel depletion had the next highest impacts and varied by scenario. Both the human toxicity-cancer and ecotoxicity impact categories reflect the release of chemicals to the environment (air, water, and land) and the pathways of exposure to humans and biota, whereas acidification reflects environmental pollution and fossil fuel depletion reflects resource consumption. In this LCA, PFAS emissions are not considered in human toxicity (cancer or non-cancer) or ecotoxicity; however, research is underway to include PFAS emissions in impact categories [80]. The climate change impact of AER regeneration was lower than human toxicity and environmental pollution impacts. For the disposal scenario, global warming potential was similar to non-carcinogens and less than carcinogens, ecotoxicity, acidification, and eutrophication.

Ozone depletion, which results from the release of halogen-containing chemicals to the atmosphere, showed the smallest impact, at least two orders of magnitude lower than the other impact categories, and is not considered in subsequent results and discussion. It should be noted, however, that production of AER requires halogen-containing chemicals, and as such, ozone depletion is an important impact category when AER is an input to the system such as using non-regenerable AER or when regenerable AER is compared with another technology [81].

For disposal of waste regeneration solution, the greatest environmental impacts and corresponding contributing process were to carcinogens by incineration, fossil fuel depletion by methanol consumption, eutrophication by incineration, and ecotoxicity by incineration and methanol consumption (see **Figure 3.7.3a**). Incineration accounted for the greatest contribution to global warming potential, but its impact was less than carcinogens, ecotoxicity, and eutrophication by incineration. Considering all impact categories, the overall environmental impact of each contributing process in the disposal scenario was as follows: 47.5% incineration, 37.8% methanol consumption, 11.7% electricity use, 2.7% transportation, 0.18% NaCl consumption, and 0.15% tap water use. The results for the disposal scenario illustrate the high environmental impacts associated with methanol consumption for preparing the regeneration solution and incineration of the waste regeneration solution. The results indicate that decreasing the methanol content of the regeneration solution and/or decreasing the mass of waste regeneration solution disposed of via incineration would decrease the environmental impacts of the AER system.

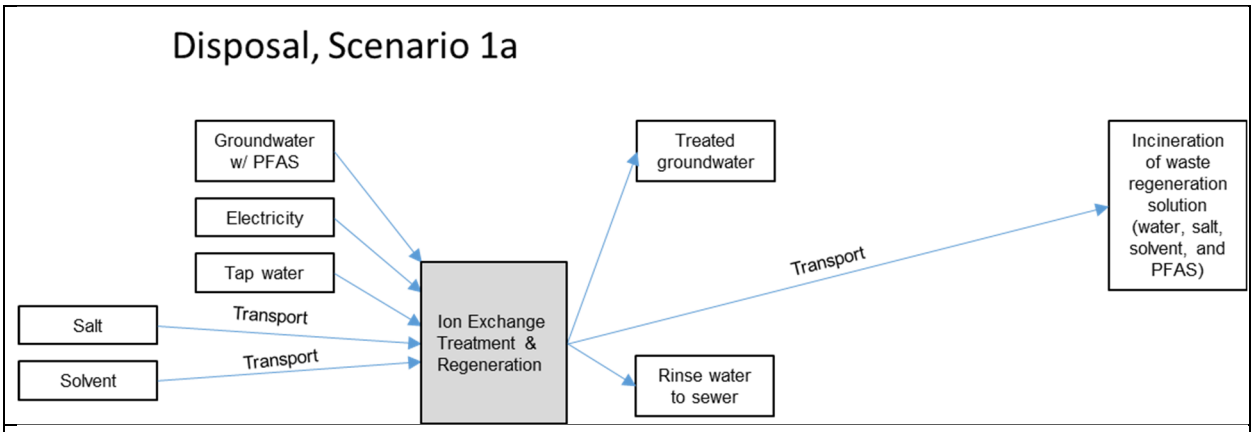
Disposal, Scenario 1a
Groundwater w/ PFAS
Electricity
Tap water
Salt
Solvent
Transport
Transport
Ion Exchange Treatment & Regeneration
Treated groundwater
Rinse water to sewer
Transport
Incineration of waste regeneration solution (water, salt, solvent, and PFAS)

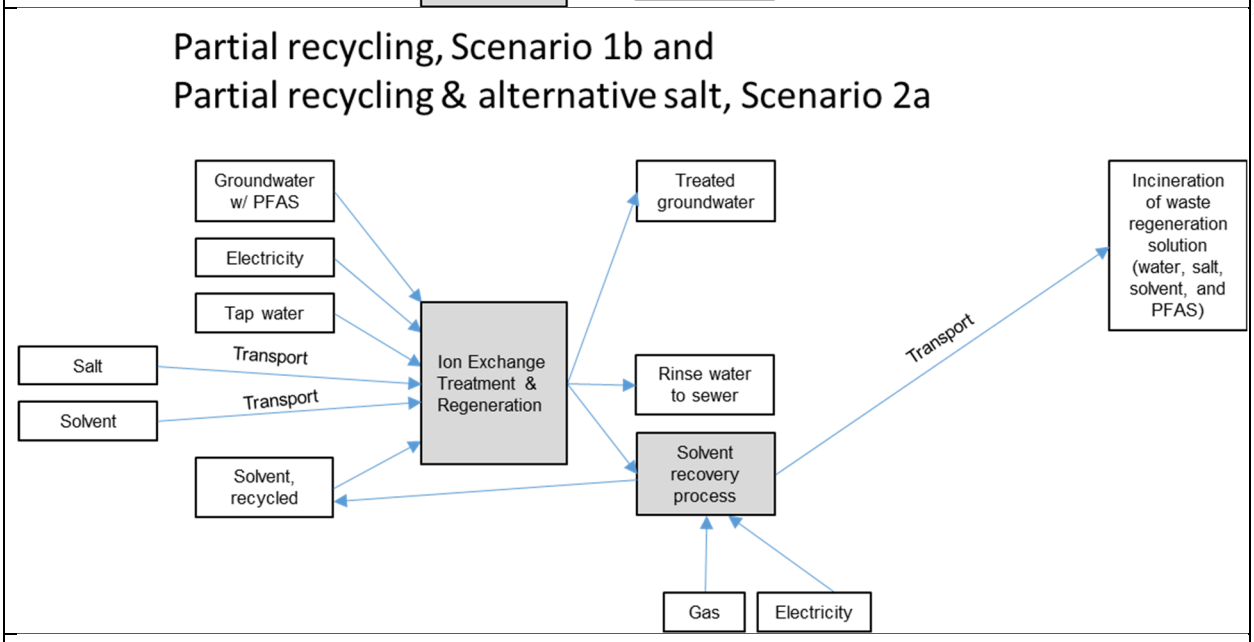
Partial recycling, Scenario 1b and
Partial recycling & alternative salt, Scenario 2a
Groundwater w/ PFAS
Electricity
Tap water
Salt
Solvent
Transport
Transport
Solvent, recycled
Ion Exchange Treatment & Regeneration
Treated groundwater
Rinse water to sewer
Solvent recovery process
Transport
Incineration of waste regeneration solution (water, salt, solvent, and PFAS)
Gas
Electricity

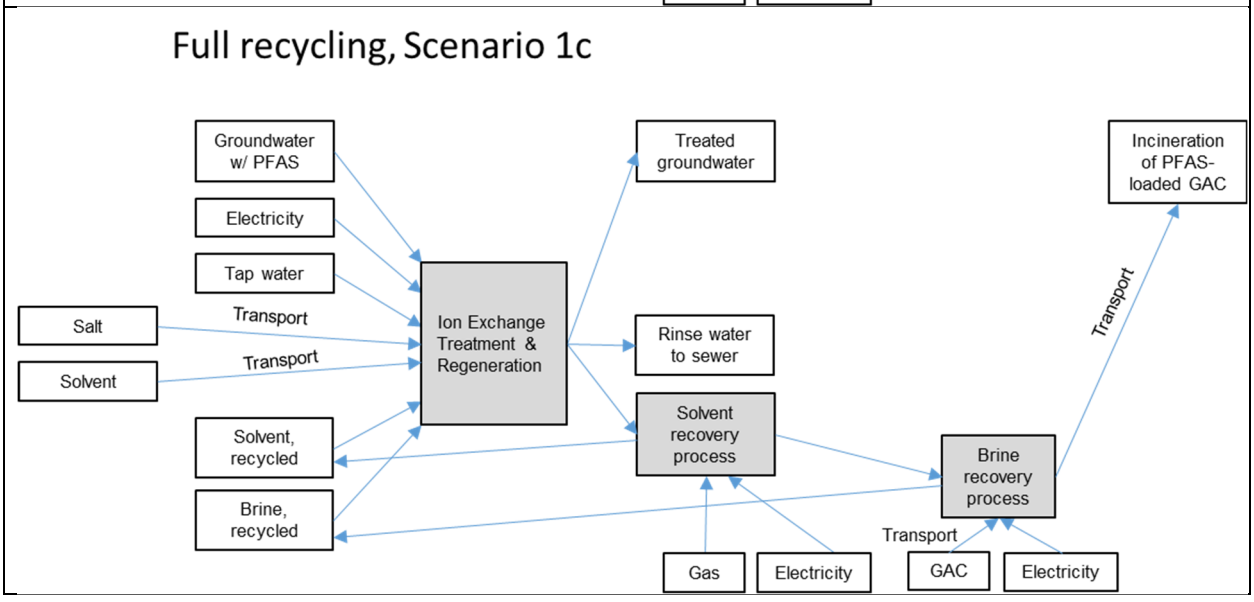
Full recycling, Scenario 1c
Groundwater w/ PFAS
Electricity
Tap water
Salt
Solvent
Transport
Transport
Solvent, recycled
Brine, recycled
Ion Exchange Treatment & Regeneration
Treated groundwater
Rinse water to sewer
Solvent recovery process
Brine recovery process
Transport
Incineration of PFAS-loaded GAC
Transport
Gas
Electricity
GAC
Electricity

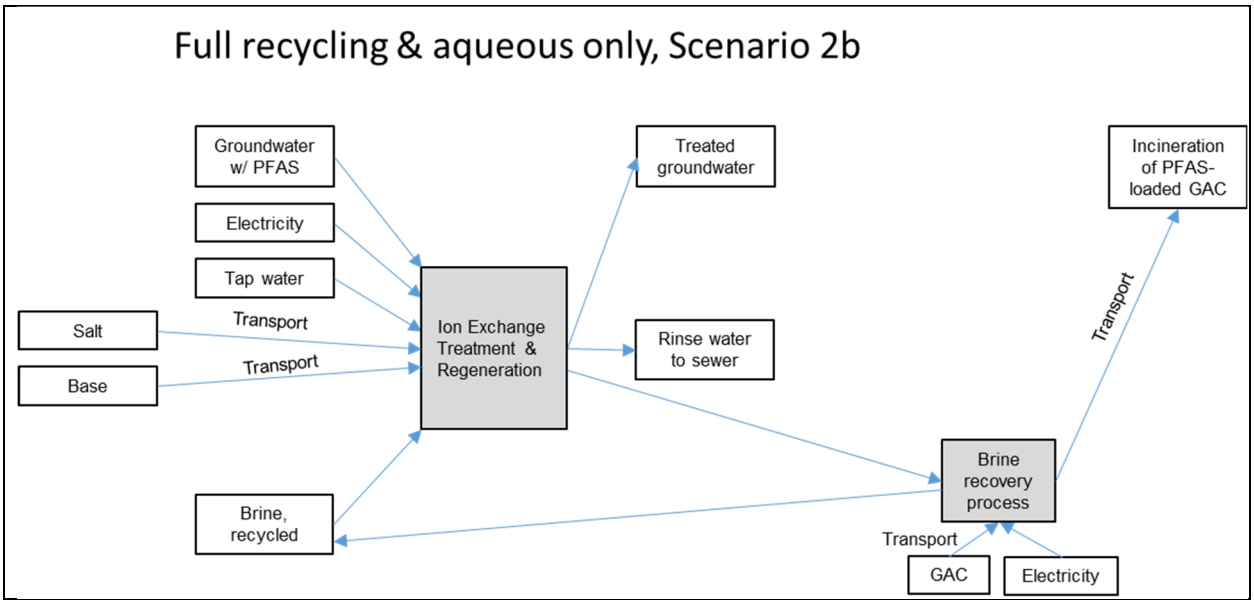

Figure 3.7.1. Inventory of materials, energy, transport, and emissions for AER remediation system with different regeneration options: (a) disposal of waste regeneration solution via incineration, scenario 1a, (b) recycle of organic solvent component of waste regeneration solution, scenarios 1b and 2a, (c) recycle of organic solvent and brine components of waste regeneration solution, scenario 1c, and (d) recycle of aqueous-only regeneration solution, scenario 2b. From Boyer et al. (2021).

For partial recycling of waste regeneration solution, the greatest environmental impacts and corresponding contributing process were carcinogens, eutrophication, ecotoxicity by incineration, and acidification by electricity use (see **Figure 3.7.3b**). Incineration and electricity use contributed similarly to global warming potential, and their impact was less than several other categories, especially those related to human health and environmental pollution. Considering all impact categories, the overall environmental impact of each contributing process in the partial recycling scenario was as follows: 44.8% incineration, 27.6% electricity use, 19.9% methanol recovery process (which included natural gas and electricity inputs), 4.5% methanol consumption, 2.4% transportation, 0.43% NaCl consumption, and 0.36% tap water use. The results for the partial recycling scenario show that incineration had the greatest environmental impacts, although the magnitude of the impacts was reduced relative to disposal (see Figure S1 comparing disposal and partial recycling scenarios). Recycling methanol decreased the impacts associated with methanol consumption and shifted the impacts to electricity use both directly and as part of the methanol recovery process. Because the methanol recovery process required fossil fuel and electricity as inputs, it contributed to many of the same environmental impact categories as methanol consumption.

For full recycling of waste regeneration solution, the greatest environmental impacts were to carcinogens by brine recovery process, acidification by electricity use, and fossil fuel depletion by methanol recovery process (see **Figure 3.7.3c**). In a shift from the previous scenarios, electricity use accounted for the greatest contribution to global warming potential. However, global warming potential and its impact from electricity use was smaller than several other environmental impacts and contributing processes. Considering all impact categories, the overall environmental impact

of each contributing process shown in the full recycling scenario was as follows: 36.8% electricity use, 26.5% methanol recovery process, 19.8% brine recovery process (which included activated carbon consumption, electricity use, transportation, and incineration), 10.2% incineration, 6.0% methanol consumption, 0.57% transportation, 0.16% tap water, and 0.06% NaCl consumption. The results for the full recycling scenario show that electricity use was associated with the greatest environmental impacts, which is consistent with previous research that shows electricity use is often the dominant contributor to environmental impacts for water and wastewater treatment [32, 82]. The brine recovery process decreased the mass of waste regeneration solution sent to incineration (see **Table 3.7.1**), which resulted in smaller impacts by incineration to several environmental impact categories, and lower environmental impacts overall relative to the other scenarios (see **Figure A3.7.1**). However, the brine recovery process was the dominant contributor to carcinogens, so there was some shifting of environmental impacts.

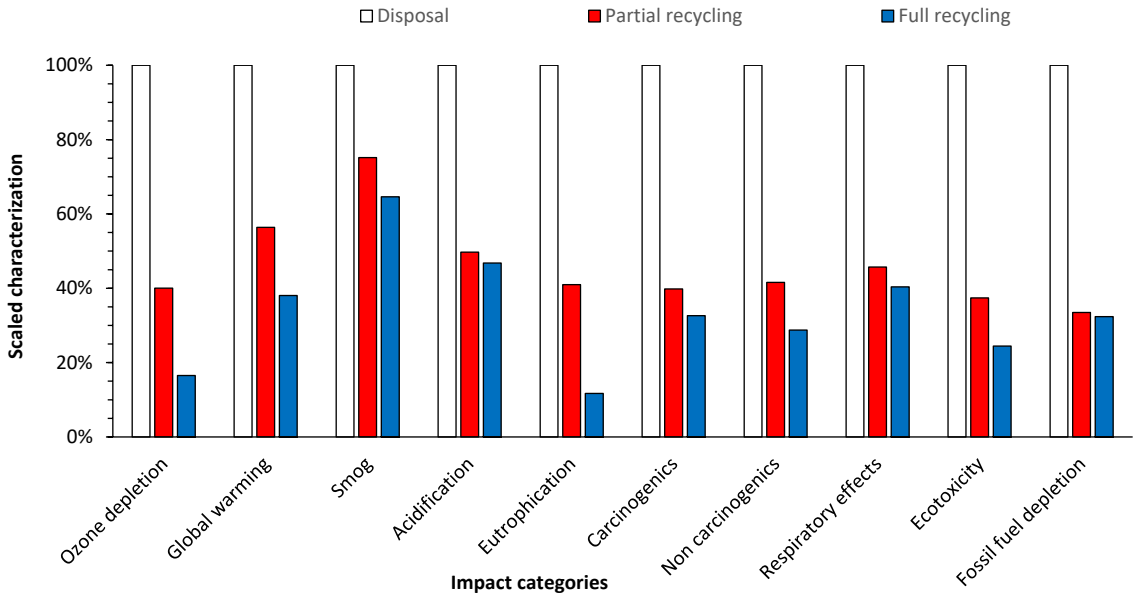

Figure 3.7.2. Overall environmental impact of AER regeneration options as calculated by TRACI 2.1. Results expressed such that the scenario with the greatest impact for a given impact category is 100% (Disposal scenario for all impact categories), and the other scenarios are a percentage of that scenario. From Boyer et al. (2021).

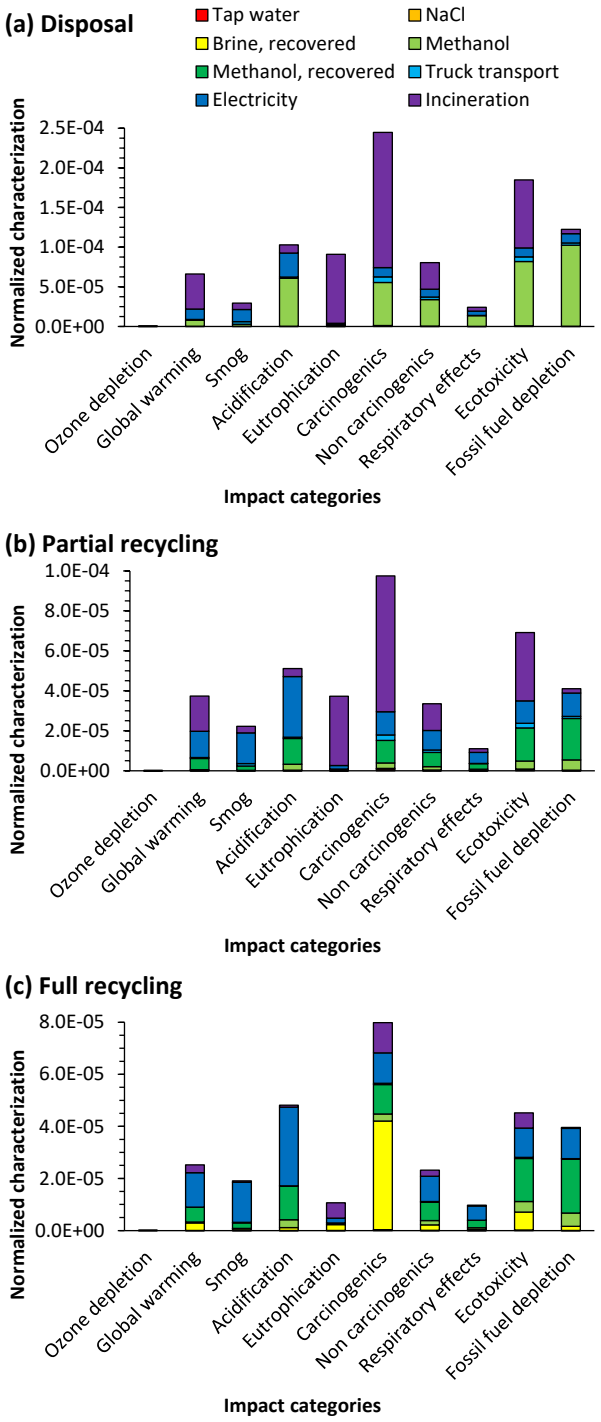

Figure 3.7.3. Impact assessment results for AER regeneration options (a) Disposal, scenario 1a, (b) Partial recycling, scenario 1b, and (c) Full recycling, scenario 1c calculated by TRACI 2.1 normalized to the average annual impact of a U.S. citizen in 2008. Color coding for each inventory item is consistent across subplots. From Boyer et al. (2021).

Table 3.7.1. Inventory list for anion exchange resin regeneration options for PFAS remediation of impacted water. From Boyer et al. (2021).

(a)

Input	SimaPro inventory item	Database	Unit[a]	Scenario 1a	Scenario 1b	Scenario 1c	Scenario 2a[b]	Scenario 2b[h]
Tap water	Tap water {RoW}| market for | Alloc Def, U	Ecoinvent 3	kg	0.23428	0.23428	0.07755	0.23428	0.1198
NaCl	Sodium chloride, at plant/RNA	USLCI	kg	0.01935	0.01935	0.001935	0.01159[c]	3.012e-4[i]
							0.01935[d]	1.804e-4[j]
							0.01935[e]	3.012e-4[k]
							0.004063[f]	
							0.01935[g]	
Methanol	Methanol, at plant/RNA	USLCI	kg	0.33398	0.0167	0.0167	0.0167	3.012e-4[i]
								3.012e-4[j]
								3.012e-4[k]
Methanol, recovered	Methanol, Recovered	see part b	kg	NA	0.33398	0.33398	0.33398	NA
Brine, recovered	Brine, recovered	see part c	kg	NA	NA	0.1935	NA	0.6024
Truck transport	Transport, combination truck, diesel powered/US	USLCI	tkm	0.2814	0.1069	0.01896	0.1069	0.03015
Electricity	Electricity, at grid, US/US	USLCI	kWh	0.41	0.41	0.41	0.41	0.41
Incineration	Spent solvent mixture {RoW}| treatment of, hazardous waste incineration | Alloc Def, U	Ecoinvent 3	kg	0.52747	0.2102	0.03605	0.2102	0.06024

[a] Unit per m^3 water treated by anion exchange resin. [b] Salt type varied, other inventory items the same as scenario 1b. [c] Salt (SimaPro inventory item): KCl (Potassium chloride, as K2O {RoW}\| potassium chloride production \| Alloc Def, U). [d] Salt (SimaPro inventory item): NH_4Cl (Ammonium chloride {GLO}\| production \| Alloc Def, U). [e] Salt (SimaPro inventory item): Na_2SO_4 (Sodium sulfate, anhydrite {RoW}\| sodium sulfate production, from natural sources \| Alloc Def, U). [f] Salt (SimaPro inventory item): $(NH_4)_2SO_4$ (Ammonium sulfate, as N {RoW}\| ammonium sulfate production \| Alloc Def, U). [g] Salt (SimaPro inventory item): K_2CO_3 (Potassium carbonate {GLO}\| production, from potassium hydroxide \| Alloc Def, U). [h] Solvent replaced with base; same salt and base co-ion. [i] NaCl and NaOH (Sodium hydroxide, production mix, at plant/kg/RNA). [j] KCl and KOH (Potassium hydroxide {RoW}\| production \| Alloc Def, U). [k] NH_4Cl and NH_4OH (25% NH_3), see part d. Not applicable (NA).

(b)

Input	SimaPro inventory item	Database	Unit[a]	Amount
Natural gas	Natural gas, combusted in industrial boiler/US	USLCI	m^3	0.17
Electricity	Electricity, at grid, US/US	USLCI	kWh	8e-4

[a] Unit per kg "Methanol, recovered."

(c)

Input	SimaPro inventory item	Database	Unit[a]	Amount
Activated carbon	Activated carbon, at plant/RER Mass	Agri-footprint	kg	0.028
Electricity	Electricity, at grid, US/US	USLCI	kWh	0.0004
Truck transport	Transport, combination truck, diesel powered/US	USLCI	tkm	0.0154
Incineration	Hazardous waste, for incineration {RoW}| treatment of hazardous waste, hazardous waste incineration | Alloc Def, U	Ecoinvent 3	kg	0.028

[a] Unit per kg "Brine, recovered."

(d)

Input	SimaPro inventory item	Database	Unit[a]	Amount
Ammonia	Ammonia, steam reforming, liquid, at plant/RNA	USLCI	kg	0.25
Water	Water, deionized, from tap water, at user {RoW}| production | Alloc Def, U	Ecoinvent 3	kg	0.75

[a] Unit per kg "NH_4OH (25% NH_3)."

3.7.2. Sensitivity analysis of disposal vs. recycling of waste regeneration solution

Table 3.7.2 shows the results of the one-at-a-time sensitivity analysis on the input amounts to the AER regeneration scenarios of disposal, partial recycling, and full recycling. The scenarios were most sensitive to the amount of waste sent to incineration and electricity use across several impact categories, with eutrophication being the most sensitive impact. For the disposal and partial recycling scenarios, when the incineration amount was doubled, the impact to eutrophication almost doubled, which is the maximum sensitivity possible. Global warming potential, human toxicity cancer and non-cancer, and ecotoxicity showed medium to high sensitivity to the incineration amount for the disposal and partial recycling scenarios. The full recycling scenario showed lower sensitivity to incineration amount than the other scenarios because the amount of waste regeneration solution sent to incineration was reduced by implementing both methanol and brine recovery. Human toxicity cancer was highly sensitive to the brine recovery amount in the full recycling scenario. The scenarios became more sensitive to electricity use as the scenarios transitioned from disposal to partial and full recycling of waste regeneration solution because the cosolvent and brine recovery processes required additional electricity inputs and the amount of waste sent to incineration decreased.

Several impact categories for the disposal scenario (i.e., acidification, respiratory effects, and fossil fuel depletion) were sensitive to methanol consumption, whereas the same impact categories for the partial and full recycling scenarios were not sensitive to methanol consumption and instead were sensitive to the amount of methanol recovered. The impact categories were not sensitive to the amount of NaCl consumption, transportation, or tap water use. The fact that the AER regeneration scenarios were not sensitive to the amount of NaCl consumed is a surprising and important result given previous LCA studies showing the high environmental impacts of AER regeneration [83, 84]. The lack of sensitivity to NaCl consumed reflects the unique composition of the regeneration solution (i.e., only 30% v/v brine) and the need to incinerate the waste produced.

For 8 out of 10 impact categories, the general order of decreasing environmental impact was hazardous waste incineration > spent solvent mixture incineration > spent AER incineration > municipal solid waste incineration, whereas for non-carcinogens and ecotoxicity, the order of decreasing environmental impact was municipal solid waste incineration > hazardous waste incineration > spent solvent mixture incineration ≈ spent AER incineration (see **Figure A3.7.2a**). For the normalized characterization results, the highest impacts were attributed to carcinogens and ecotoxicity (see **Figure A3.7.2b**).

In the context of the AER regeneration scenarios, replacing incineration of spent solvent mixtures (default inventory item) with incineration of spent AER would decrease environmental impacts, whereas replacing incineration of spent solvent mixtures with incineration of hazardous waste would increase environmental impacts. Replacing incineration of spent solvent mixtures with incineration of municipal solid waste would decrease environmental impacts for most categories; however, it would increase the impacts of carcinogens, non-carcinogens, and ecotoxicity. Recalling that carcinogens and ecotoxicity had some of the highest normalized characterization values across the scenarios (see **Figure A3.7.1**), these impacts would increase if incineration of municipal waste or hazardous waste was used in place of incineration of spent solvent mixtures to represent incineration of waste regeneration solution. Hence, the environmental impacts of the AER regeneration scenarios are highly sensitive to the amount of waste regeneration solution sent to incineration and the nature of the incineration process. Finally, the LCA impact categories do not consider PFAS emissions [80], and in the case of incineration, PFAS destruction is an active area of research [85, 86].

Table 3.7.2. One-at-a-time sensitivity analysis on inputs to anion exchange resin regeneration options of disposal (scenario 1a), partial recycling (scenario 1b), and full recycling (scenario 1c). Each input amount was varied by 0.5× and 2× from the baseline value in Table 3.7.1, and the percent decrease and percent increase, respectively, is listed.[a] From Boyer et al. (2021).

Impact category	Scenario	Electricity		Tap water, total		NaCl		Methanol		Transport, total		Incineration		Methanol recovered		Brine recovered	
Ozone depletion	1a	0%	0%	0%	0%	0%	0%	0%	0%	0%	0%	-50%	100%				
Ozone depletion	1b	0%	0%	0%	0%	0%	0%	0%	0%	0%	0%	-50%	99%	0%	0%		
Ozone depletion	1c	0%	0%	0%	0%	0%	0%	0%	0%	0%	0%	-21%	41%	0%	0%	-29%	58%
Global warming	1a	-10%	17%	0%	0%	0%	0%	-6%	12%	-1%	2%	-33%	67%				
Global warming	1b	-18%	35%	0%	0%	0%	0%	-1%	1%	-1%	1%	-24%	47%	-8%	15%		
Global warming	1c	-26%	52%	0%	0%	0%	0%	-1%	2%	0%	0%	-6%	12%	-11%	22%	-6%	11%
Smog	1a	-26%	34%	0%	0%	0%	0%	-5%	9%	-5%	10%	-14%	28%				
Smog	1b	-35%	69%	0%	0%	0%	0%	0%	1%	-3%	5%	-7%	15%	-5%	10%		
Smog	1c	-40%	81%	0%	0%	0%	0%	0%	1%	-1%	1%	-1%	3%	-6%	11%	-2%	3%
Acidification	1a	-15%	23%	0%	0%	0%	0%	-29%	59%	-1%	2%	-5%	10%				
Acidification	1b	-30%	59%	0%	0%	0%	0%	-3%	6%	-1%	1%	-4%	8%	-13%	25%		
Acidification	1c	-31%	63%	0%	0%	0%	0%	-3%	6%	0%	0%	-1%	1%	-13%	27%	-1%	2%
Eutrophication	1a	-1%	2%	0%	0%	0%	0%	-1%	2%	0%	0%	-48%	96%				
Eutrophication	1b	-2%	5%	0%	0%	0%	0%	0%	0%	0%	0%	-46%	93%	-1%	1%		
Eutrophication	1c	-8%	17%	0%	0%	0%	0%	0%	1%	0%	0%	-28%	56%	-2%	5%	-11%	21%
Carcinogenics	1a	-2%	5%	0%	0%	0%	0%	-11%	22%	-1%	3%	-35%	70%				

Carcinogenics	1b	-6%	12%	0%	1%	0%	0%	-1%	3%	-1%	3%	-35%	70%	-6%	12%		
Carcinogenics	1c	-7%	15%	0%	0%	0%	0%	-2%	3%	0%	1%	-7%	15%	-7%	14%	-26%	52%
Non carcinogenics	1a	-6%	11%	0%	0%	0%	0%	-21%	42%	-2%	4%	-21%	42%				
Non carcinogenics	1b	-15%	29%	0%	0%	0%	1%	-3%	5%	-2%	4%	-20%	40%	-11%	21%		
Non carcinogenics	1c	-21%	42%	0%	0%	0%	0%	-4%	7%	0%	1%	-5%	10%	-15%	31%	-5%	9%
Respiratory effects	1a	-11%	19%	0%	0%	0%	0%	-28%	57%	0%	0%	-10%	20%				
Respiratory effects	1b	-25%	50%	0%	0%	0%	0%	-3%	6%	0%	0%	-9%	17%	-13%	26%		
Respiratory effects	1c	-28%	56%	0%	0%	0%	0%	-4%	7%	0%	0%	-2%	3%	-15%	29%	-2%	4%
Ecotoxicity	1a	-3%	6%	0%	0%	0%	0%	-22%	44%	-2%	3%	-23%	46%				
Ecotoxicity	1b	-8%	16%	0%	1%	0%	0%	-3%	6%	-2%	3%	-25%	49%	-12%	24%		
Ecotoxicity	1c	-12%	25%	0%	0%	0%	0%	-4%	9%	0%	1%	-6%	13%	-18%	37%	-8%	15%
Fossil fuel depletion	1a	-5%	9%	0%	0%	0%	0%	-42%	83%	-1%	2%	-2%	4%				
Fossil fuel depletion	1b	-14%	28%	0%	0%	0%	1%	-6%	12%	-1%	3%	-3%	5%	-25%	51%		
Fossil fuel depletion	1c	-15%	29%	0%	0%	0%	0%	-6%	13%	0%	0%	0%	1%	-26%	52%	-2%	4%

[a] For input varied by 0.5× from baseline, the results were considered: Not sensitive, <5% decrease; low sensitivity, 5 to <12.5% decrease; medium sensitivity, 12.5 to <25% decrease; high sensitivity, >25% decrease. For input varied by 2× from baseline, the results were considered: Not sensitive, <10% increase; low sensitivity, 10 to <25% increase; medium sensitivity, 25 to <50% increase; high sensitivity, >50% increase.

3.7.3. Impact of altering the salt used for regeneration solution

Table A3.7.1 compares the environmental impacts of altering the type of salt used in the regeneration solution. Considering all impact categories, the overall trend of decreasing environmental impact was $NH_4Cl \approx K_2CO_3 > (NH_4)_2CO_3 \approx NH_4Cl$ (modified Solvay process) > $K_2SO_4 > Na_2CO_3$ (modified Solvay process) > $KCl \approx (NH_4)_2SO_4 > Na_2CO_3 >$ NaCl (powder) > NaCl (brine solution) $\approx Na_2SO_4 \approx$ NaCl (see **Table A3.7.1a**). NaCl, which was used as the default salt inventory item in scenarios 1a–c, had the lowest impact in all categories. Based on the

normalized characterization values, the categories with highest impact were human toxicity-cancer and ecotoxicity, followed by human toxicity non-cancer and eutrophication. Global warming potential was one of the lowest impact categories. Hence, both human health and ecosystems would receive adverse impacts from mining and production of alternative salts to NaCl.

The results showed higher environmental impacts for salts obtained by chemical production and lower environmental impacts for salts obtained by natural production (see **Table A3.7.1**). For example, NH_4Cl and K_2CO_3 had the highest scaled characterization values across impact categories, whereby NH_4Cl production requires ammonia and hydrochloric acid and K_2CO_3 production requires potassium hydroxide, which are products from other chemical and energy demanding processes. In contrast, NaCl, Na_2SO_4, and Na_2CO_3, which had the lowest scaled characterization values across impact categories, are mined from natural deposits that require lower chemical and energy inputs. In some cases, the mined salt requires more chemical and energy inputs to purify, which results in a higher environmental impact, e.g., KCl [40]. In other cases, the manufactured salt is a co-product or byproduct of another chemical process so its environmental impacts are lower, such as $(NH_4)_2SO_4$ as byproduct of nylon production in the Ecoinvent database.

Figure 3.7.4 shows the scaled and normalized characterization values for partial recycling (scenarios 1b using NaCl and 2a using KCl, NH_4Cl, Na_2SO_4, $(NH_4)_2SO_4$, and K_2CO_3), and Figure S3 shows the normalized characterization values for each alternative salt in partial recycling (scenario 2a) in terms of the contributing processes. The order of decreasing environmental impact, based on scaled characterization values, was $NH_4Cl \approx K_2CO_3 >$ KCl $\approx Na_2SO_4 \approx (NH_4)_2SO_4 \approx$ NaCl (see Figure 4a). The highest impact categories for all salts were human toxicity-cancer and ecotoxicity based on normalized characterization values. The impact categories of human toxicity cancer and non-cancer, ecotoxicity, and eutrophication showed the greatest difference in environmental impact between salts obtained by natural production (NaCl, KCl, Na_2SO_4) vs. chemical production (NH_4Cl, K_2CO_3) with $(NH_4)_2SO_4$ exhibiting similar impacts as natural production but produced by chemical production. **Figure A3.7.3** shows that the higher impact of scenario 2a for NH_4Cl and K_2CO_3 in categories like human toxicity cancer and ecotoxicity was due to salt consumption, which reflects chemical production of the salts.

The results in **Figure 3.7.4** indicate that replacing NaCl with another salt obtained by natural production had a minimal change in environmental impact, whereas replacing NaCl with another salt obtained by chemical production resulted in higher environmental impacts, especially for human toxicity cancer and non-cancer, ecotoxicity, and eutrophication. **Table A3.7.2** further explores the impact of salt selection and shows the contributions of the processes in scenarios 1b and 2a. For example, NaCl consumption accounted for 0.4% of total environmental impacts in scenario 1b with incineration and electricity use accounting for 45% and 28%, respectively. In contrast, in scenario 2a, NH_4Cl and K_2CO_3 consumption accounted for nearly 25% of total environmental impacts with incineration and electricity use accounting for 34% and 21%, respectively. Replacing NaCl with KCl, Na_2SO_4, or $(NH_4)_2SO_4$ resulted in impacts due to salt consumption increasing from 0.4% to 3.5–6.7% of total environmental impacts. Hence, consumption of non-NaCl salts obtained by natural production can result in total environmental impacts greater than methanol consumption or transport in scenario 1b, and non-NaCl salts

obtained by chemical production can result in total environmental impacts greater than methanol recovery and similar to electricity use in scenario 1b.

A one-at-a-time sensitivity analysis for the results in **Figure 3.7.4** showed that human toxicity cancer and non-cancer, ecotoxicity, and eutrophication were moderately sensitive to the amount of NH_4Cl and K_2CO_3 consumed. Comparing the sensitivity results in **Tables 3.7.2** and **A3.7.3**, human toxicity cancer and non-cancer, ecotoxicity, and eutrophication were most sensitive to incineration amount followed by NH_4Cl and K_2CO_3 consumed and then electricity use. Human toxicity cancer and ecotoxicity showed low sensitivity to the amount of KCl and $(NH_4)_2SO_4$ consumed. Environmental impacts were not sensitive to the amount of Na_2SO_4 consumed, which was the same result shown in **Table 3.7.2** for NaCl. The conclusion from section 3.2 that the regenerable AER system was not sensitive to the amount of NaCl consumed remains valid; however, with the important caveat that the system is sensitive to the type and amount of non-NaCl salt consumed, especially for salts obtained from chemical production. Two additional factors for salt selection are cost and PFAS destruction, as NaCl is typically the cheapest salt [40] but NaCl interferes with electrochemical oxidation of PFASs [87].

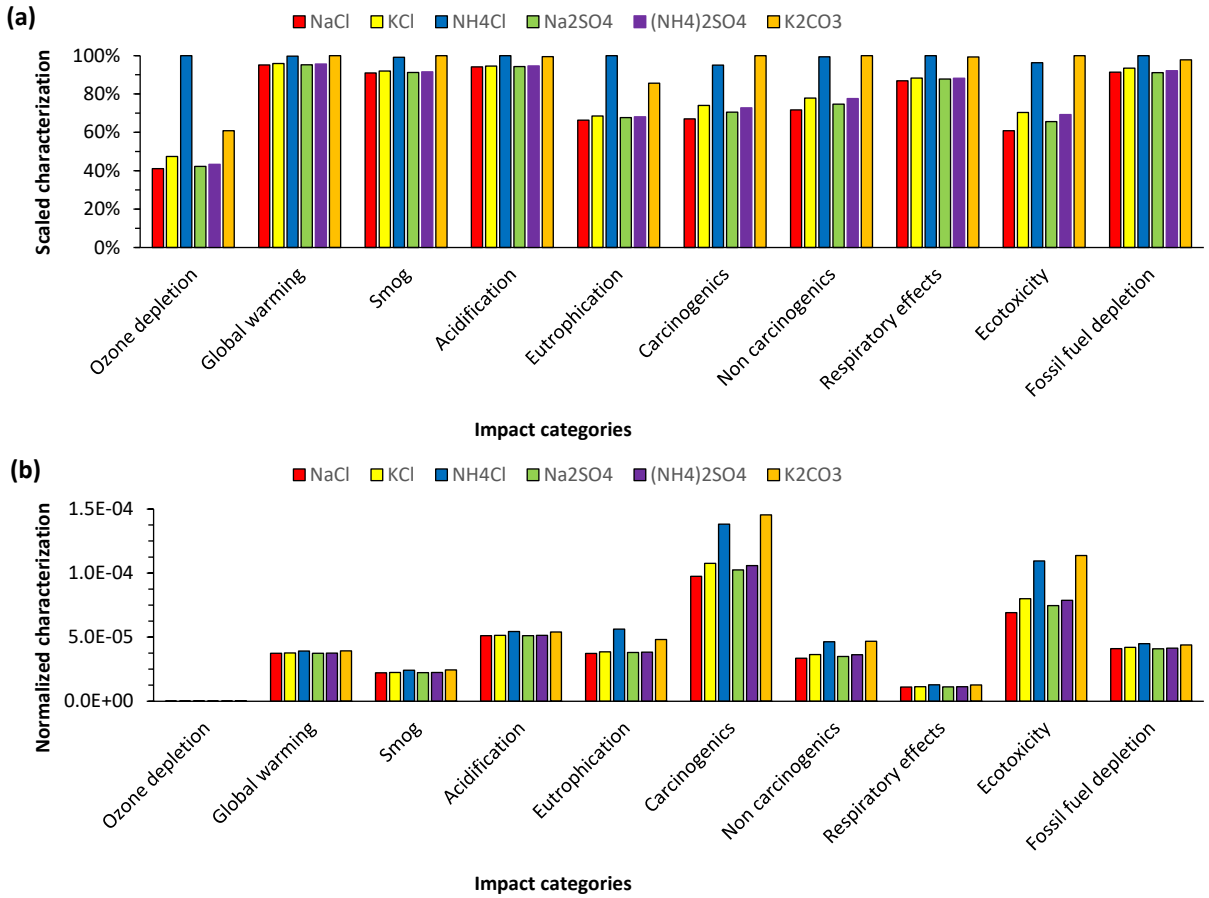

Figure 3.7.4. Overall environmental impact of AER regeneration option of partial recycling for the salts NaCl (scenario 1b) and KCl, NH_4Cl, Na_2SO_4, $(NH_4)_2SO_4$, K_2CO_3 (scenario 2a) calculated by TRACI 2.1 (a) results expressed such that the salt with the greatest impact for a given impact category is 100% and the other salts are a percentage of that salt, and (b) normalized to the average annual impact of a U.S. citizen in 2008. From Boyer et al. (2021).

3.7.4. Impact of eliminating organic cosolvent from regeneration solution

Figure 3.7.5 compares the impact of full recycling of brine/methanol (scenario 1c) with full recycling of brine/caustic (scenario 2b using NaCl/NaOH, KCl/KOH, and NH_4Cl/NH_4OH). Brine/caustic had greater relative impact than brine/methanol for ozone depletion, eutrophication potential, and human toxicity cancer, whereas brine/methanol had greater relative impact than brine/caustic for acidification, human toxicity non-cancer, respiratory effects, and fossil fuel depletion (see **Figure 3.7.5a**). Global warming potential, smog, and ecotoxicity were similar for brine/methanol and brine/caustic scenarios. In terms of magnitude of impacts, impacts to human toxicity cancer were the highest, with brine/caustic having a higher impact than brine/methanol. The brine recovery process was the greatest contributor to the human toxicity cancer impact category and the single greatest contributor overall. This follows from **Table 3.7.2**, where human toxicity cancer was highly sensitive to the amount of brine recovered. Due to the assumptions of the hypothetical AER system, the full recycling of brine/caustic had approximately twice the mass of brine recovered than the full recycling of brine/methanol (see **Table 3.7.1**), which manifested itself as higher impacts in the human toxicity cancer category. This was because the brine recovery process was applied to the entire volume of brine/caustic solution, whereas the brine recovery process was only applied to the aqueous fraction (i.e., 30%) of the brine/methanol solution. If researchers can confirm that brine/caustic can effectively desorb PFASs from weak-base AER [17], then the next step is to reduce the volume of waste regeneration solution prior to brine recovery, possibly through membrane separation [37, 58] or even evaporation. For the results in **Figure 3.7.5**, the different formulations of brine/caustic showed similar impact within an impact category, suggesting that formulations of brine/caustic should be selected based on regeneration efficiency and the possibility of coupling to PFAS destruction technologies [87, 88].

3.8. LCA and LCCA comparison of Ion Exchange and GAC Adsorption Technologies for Treatment of PFAS-Contaminated Groundwater

3.8.1. Technology comparison for baseline scenario

Life cycle environmental impacts. **Figure 3.8.1** compares the life cycle environmental impacts for each of the four remediation systems treating AFFF-impacted groundwater under the baseline scenario described in **Table 2.10.2**. All life cycle models constructed in this comparison relied on system assumptions made in **Table 2.10.2** (e.g., assumed EBCT, flow rates, bed lifetimes). Assumptions for EBCT are determined from manufacturer recommendations in product specification sheets, assumptions of bed lifetimes and changeout frequencies are sourced from breakthrough data obtained in the field pilot system (**Table 3.4.2**), though some assumptions (vessel size, total flow rate) were chosen to best reflect a small-to-moderately-sized remediation site operation. A full list of assumptions made for this comparison is available in **Table A3.8.1**. Results for each environmental impact category are scaled characterization values based on the system with greatest impacts (100%). Because all ten impact categories are associated with different units of impact (e.g., kg CO_2 for global warming vs CTUh for ecotoxicity), this enables all systems to be compared on an equivalent basis for each segment of environmental impact.

Perhaps the most striking finding within this comparison is that the single-use GAC process (*Remediation System 3*) is associated with the highest environmental impacts for most categories, often by a wide margin. This results principally from the high MUR for GAC (41.5 g/m^3 water

treated) due to rapid PFAS breakthrough (changeout after 13,000 bed volumes), large bed size, and the fact that the spent media is transported offsite for hazardous waste incineration in this process. With the exception of ozone depletion, all impacts from single-use AER and thermally-reactivated GAC treatment are ≤30% of those estimated for the single-use GAC system. GAC systems utilizing off-site thermal reactivation and reuse of the spent GAC significantly reduces impacts in all categories simply from the net reduction in new adsorbent material required for treatment and the much lower temperature of thermal reactivation processes (e.g., 815°C) compared to hazardous waste incinerators (e.g., 1200°C).

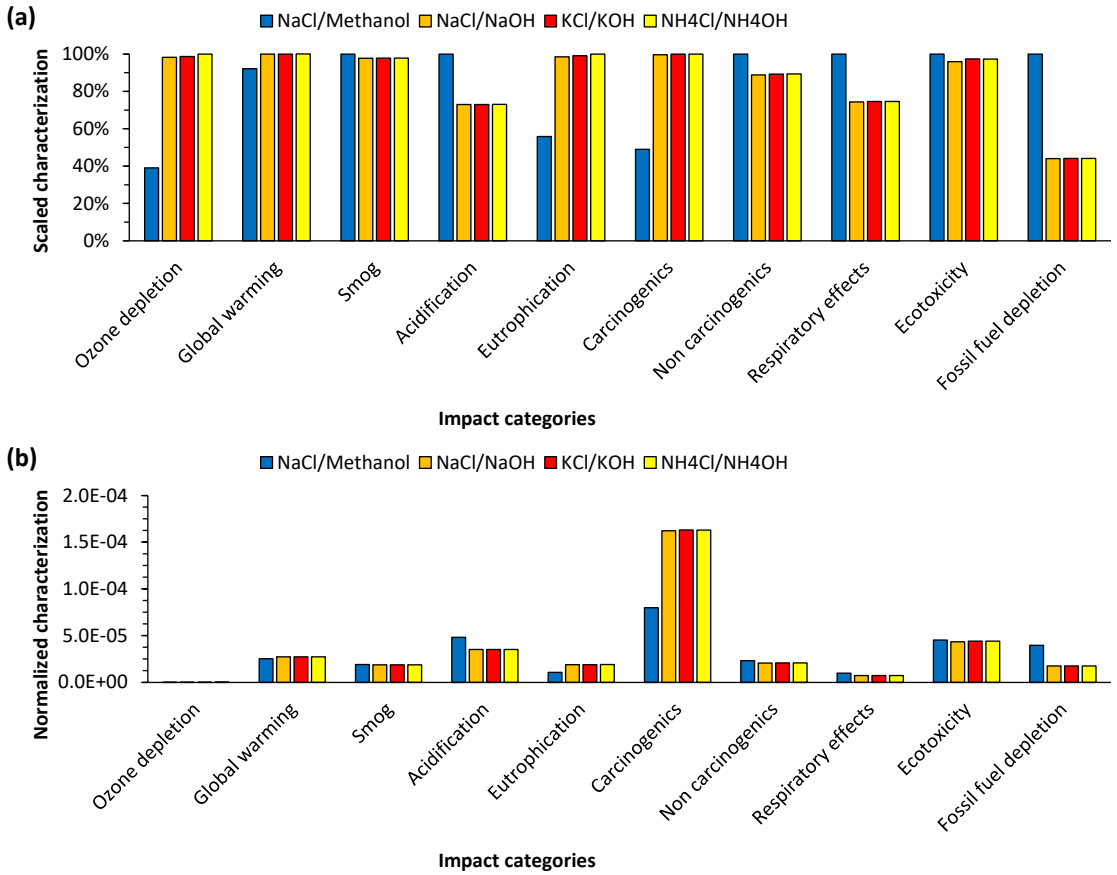

Figure 3.7.5. Overall environmental impact of AER regeneration option of full recycling for NaCl/methanol (scenario 1c) and aqueous-only NaCl/NaOH, KCl/KOH, and NH_4Cl/NH_4OH (scenario 2b) calculated by TRACI 2.1 (a) results expressed such that the solution with the greatest impact for a given impact category is 100% and the other solutions are a percentage of that solution, and (b) normalized to the average annual impact of a U.S. citizen in 2008. From Boyer et al. (2021).

Besides ozone depletion, treatment using single-use AERs is associated with reduced environmental impacts in comparison to all other systems, even outperforming the two systems with media recycling. This is mostly due to the much lower MURs (e.g., 4.2 g/m^3 for single-use resin, nearly an order of magnitude lower than GAC) resulting from the much longer bed volumes to PFAS breakthrough compared to GAC (**Table 2.10.3**). Comparing the two AER systems, it is apparent that single-use AERs provide significantly lower impacts in all categories beyond ozone depletion. Despite its reusable nature, the regenerable AER proves to be the second most impactful

remediation system after single-use GAC. This is because regenerable AERs include added infrastructure and chemical-intensive processes to regenerate resins and recycle the regenerant solution cosolvent. Although the process uses much less resin over the 30-year treatment system life cycle, this is more than offset by other inputs (e.g., salt, cosolvent) and wastes (PFAS-contaminated waste still bottoms). Regenerable AER is anticipated to have greater environmental impacts than the thermally regenerated GAC system across most categories due to its large quantity of still bottom (larger volume than the adsorber bed) requiring incineration as well as impacts from cosolvent used during frequent resin regeneration.

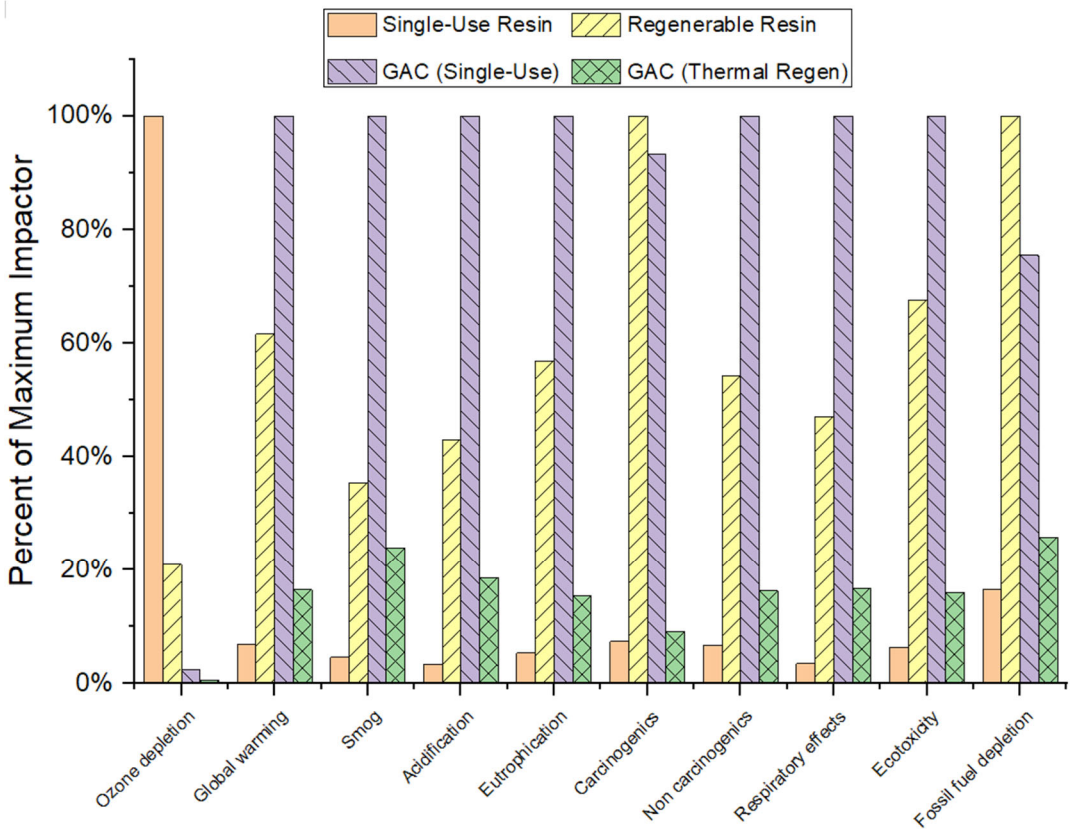

Figure 3.8.1. Life cycle environmental impact comparison for each of the four PFAS remediation systems under the baseline scenario described in Table 2.8.2. Impacts are normalized to values estimated for the most impactful remediation system in each impact category. From Ellis et al. (2023).

For most categories of environmental impacts, the relative environmental impacts follow single-use AER < thermally-reactivated GAC < regenerable AER < single-use GAC. The major exception to this trend was noted for the ozone depletion impact category, where impacts for single-use AER are much greater than the three other remediation systems. This stems from emissions of ozone-depleting chemicals during polymer synthesis and amination processes, which dwarfs the impacts from any other segment of adsorbent treatment. While regenerable AER also uses polymer-based AER, net use of new polymer-based media is much lower since the media is regenerated upon PFAS breakthrough rather than being replaced with virgin media (baseline scenario assumes replacement of regenerable AER every 5 years).

Contributions to impacts. **Figure 3.8.2** shows the breakdown of major factors contributing to each of the predicted impact categories for each of the four remediation systems. For single-use AER (**Figure 3.8.2A**) and single-use GAC (**Figure 3.8.2C**), nearly all impacts result from media production and incineration. Single-use AER treatment experiences a greater fraction of impacts from incineration than GAC as the mining of bituminous coal and energy needed to activate carbon have greater impacts per unit mass than resin production. Impacts associated with the capital infrastructure were minimal, but these are non-negligible for single-use AER as its very low MUR decreases impacts associated with the operational phase to a point where the relative contribution of capital phase impacts are nontrivial. Capital also plays a larger role for reactivated GAC, as the lack of high-temperature incineration allows for more relative contributions from other segments of treatment including infrastructure.

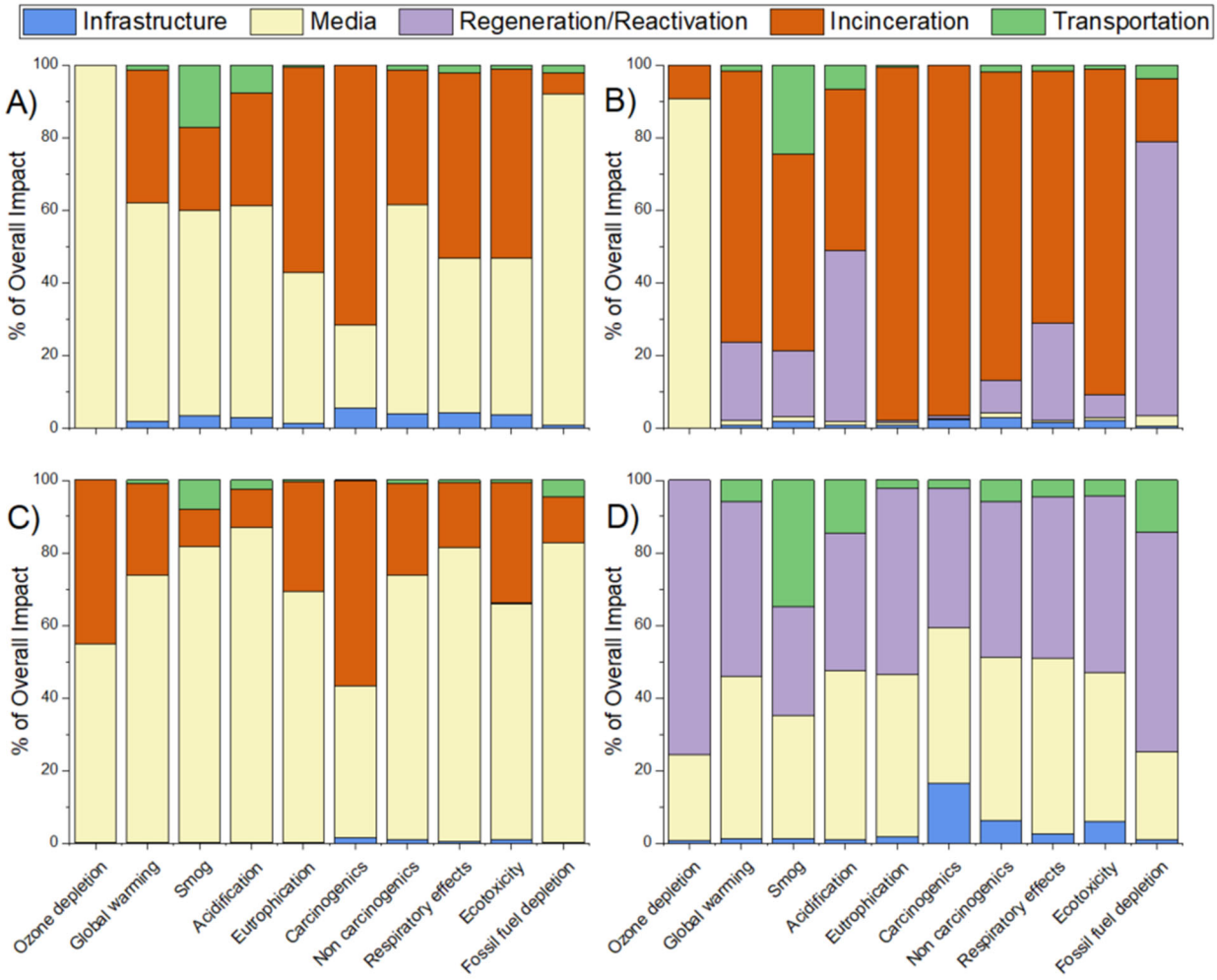

Figure 3.8.2. Impact breakdown for each of the four PFAS remediation systems under the baseline scenario described in Table 2.10.2. Impacts shown are for PFAS remediation systems using (A) single-use AER, (B) regenerable AER, (C) single-use GAC, and (D) GAC with thermal reactivation. From Ellis et al. (2023).

For GAC with off-site thermal reactivation (**Figure 3.8.2D**), reactivation process used to recycle spent GAC is the dominant contributor to environmental impact, closely followed by virgin GAC production. The near-equivalent contributions of these processes is striking given that 90% of each bed is reactivated GAC while only 10% is virgin GAC, but the minimization of coal mining reduces impacts from GAC treatment significantly. Transportation of spent/virgin media plays the largest role in the case of thermally reactivated GAC as the lack of hazardous incineration allows for greater contributions from other segments as seen for capital infrastructure.

Environmental impacts from the regenerable AER system (**Figure 3.8.2B**) are more multifaceted as this system is more complex in design. Unsurprisingly, ozone depletion is almost entirely attributable to AER production since this category is highly sensitive to polymer synthesis. In contrast, the large quantity of waste still bottoms (10 BVs of 30% water; more than thrice the volume of the adsorber bed) requiring incineration leads to overwhelmingly dominant impacts from incineration across the board. In the case of eutrophication, carcinogens, and ecotoxicity, >90% of impacts stem from incineration. Because incineration is modeled on a mass-basis, the higher density of the still bottom (1 kg/L) than any adsorbent media (540-700 kg/L) further adds to the high incineration requirements. In the case of acidification and fossil fuel depletion, the production of regenerant solution comprises the majority of impact, even when assuming that most of the cosolvent (90%) is recovered for reuse by distillation. This primarily stems from methanol production, which is more impactful than NaCl production on a mass basis for all categories. Unlike the other three remediation systems, the regenerable AER system has the added complexity of the on-site regeneration system that is included in construction, though these impacts are largely dwarfed by those stemming from incineration and regeneration.

Impact normalization. Although comparison among the treatment processes may be enabled by each category's raw impact value, a methodology for unit normalization is possible to directly compare the magnitude of each impact category against one another. Such standardization utilizes 'impact per person per year' data aggregated for the average American citizen in a given year (2008), which is then used to divide the raw impact quantity in each category thereby yielding units presented in "person-years" (Ryberg et al., 2014). While the relative importance of each category is context- and site-specific (e.g., coastal regions may be more concerned with acidifications while urban areas may emphasize smog), this methodology enables comparison across all categories. **Figure 3.8.3** presents the impact data of all four remediation systems for all impact categories normalized in terms of these person-year units on a log scale. Presenting the data in this way reveals several notable findings. First, the normalized impacts of single-use GAC and regenerable AER dominate every category with the exception of ozone depletion. Additionally, the impacts stemming from carcinogens and ecotoxicity are, in that order, the two most impactful categories relative to average US emissions for each of the four remediation systems. Thus, these two categories can be used as indicator categories warranting additional exploration to observe how changing parameters influence these emissions. While ozone depletion is disproportionately caused by AER-based remediation systems, the impacts in this category actually have the lowest maximum impact of any category. Therefore, while care must be given to the high quantities of CFC-11 equivalents from resin-based systems, the relative impact of PFAS treatment on the ozone layer compared to other compartments of the environment may be of lesser concern.

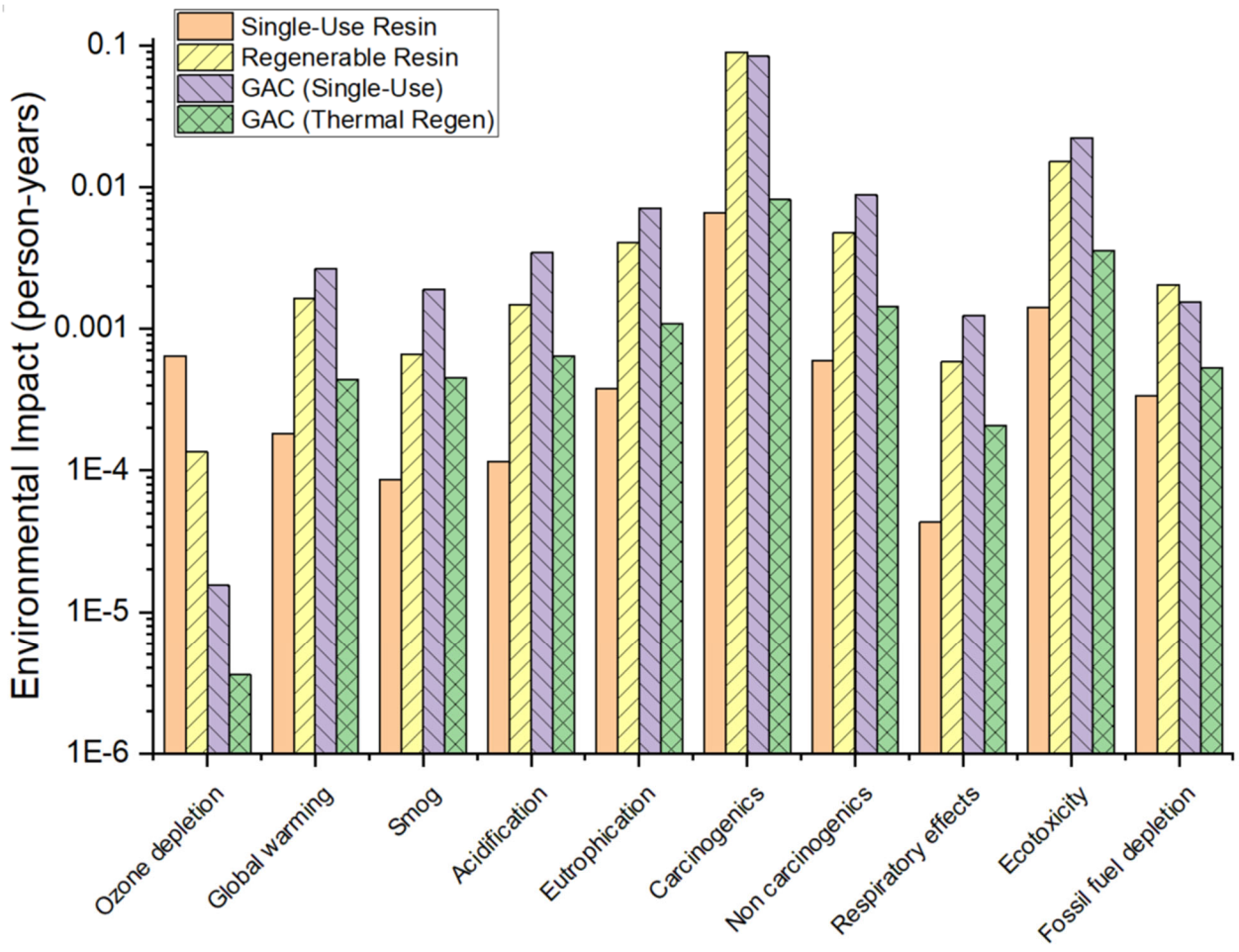

Figure 3.8.3. Normalized environmental impacts for of treatment of PFAS-contaminated water with the four remediation systems, where impacts are normalized using the Ryberg (2008) annual impact data to standardize all units in terms of person-years. Y-axis shown in log(base 10) scale. From Ellis et al. (2023).

Life cycle treatment costs. Life cycle costing data was obtained using the EPA's work breakdown structure (WBS) in conjunction with sorbent pricing provided by manufacturers. A breakdown of costs for each of the four remediation systems is provided in **Table 3.8.1**. Sized to treat 6,000 L/h, capital costs for the single-use AER system are far lower than those of the regenerable AER system due to the slightly larger contactor as well as the additional pumps, piping, and storage and mixing vessels required to enable AER regeneration. While neither GAC system requires these additional components as all disposal/regeneration is performed off-site, the capital costs for GAC are remarkably similar to those of the regenerable AER system. These differences are largely due to the significantly larger contactors needed to provide an EBCT of 10-min relative to the 2-3 min required for the AER systems.

While capital costs may influence decision-making of site managers, capital costs for all four systems are well below the recurring costs during the operational phase of treatment. In the operational phase, the single-use AER system proves to be the most economical option due to its low MUR, as this system can operate through >160,000 BVs prior to PFOS or PFOA

breakthrough. The expected operational cost of $11,246 for single-use AERs (and annual capital cost of $3,526) comes in below the operational and capital costs of any other remediation system. Given uncertainties in cost estimates and changing bulk chemical prices of regeneration constituents, operational costs for single-use and regenerable AERs can be considered comparable. However, estimated costs may not perfectly encapsulate potential added labor costs associated with operating the more complex regenerable AER system.

Table 3.8.1. Life cycle costing estimates for each of the four remediation schemes for PFAS. From Ellis et al. (2023).

Remediation System	Cost of Capital Infrastructure[a]	Financed Capital Cost[b]	Cost of Annual Operation	Cost per m^3 Treated Water[c]
Single-Use Resin	$44,164	$3,526	$11,246	$0.28
Regenerable Resin	$77,571	$6,193	$14,746	$0.40
Single-Use GAC	$78,445	$6,263	$19,879	$0.50
GAC with Thermal Regen	$78,445	$6,263	$16,634	$0.44

[a] Does not include potential site needs (e.g., concrete pad) and assumes groundwater well is already drilled

[b] Assumes capital and first-year costs financed up-front at a 7% APR

[c] Cost per m^3 determined by combining annual capital and operational costs divided by the volume of water treated in a year

While the cost of GAC media is lower than either type of resin on a mass-normalized basis ($2.90/kg for GAC compared to $15.70/kg for single-use resin), the much higher MURs associated with GAC more than offset the price savings. This is partly due to GAC adsorber vessels needing changeout every 2.5 months whereas AER beds only require changeout every 5.1 months, but the much larger vessel size of GAC (5x that of single-use AER) multiplies the cost difference even more. Therefore, despite the lower unit cost of GAC, the total cost for treatment with single-use GAC is $0.45/$m^3$, nearly double that of the single-use AER system ($0.28/$m^3$). The thermally-reactivated GAC system is estimated to be slightly cheaper than single-use GAC as costs mainly stem from reactivation, though significant uncertainty exists in the estimated reactivation costs due to the need for hazardous reactivation and potential inclusion of reactivation in contract pricing. While the low cost of carbon may be attractive to operators, the high MURs and large bed sizes make GAC less economically beneficial than AER treatment of PFAS.

Sensitivity analysis. The LCA and LCCA discussed above compared the four different remediation systems under a baseline scenario representing site remediation of AFFF-impacted groundwater that was informed by performance of adsorptive media documented in recent pilot field studies (Woodard et al., 2017; Liu et al., 2019; Ellis et al., 2022; Liu et al., 2022). However, this baseline scenario included a number of assumptions of major process variables that influence relative impacts and costs of each remediation system. To ascertain the effects of each variable, a deeper sensitivity analysis was undertaken to identify design and operational factors for which environmental impacts and costs are most sensitive.

Sensitivity of single-use AER treatment systems. Due to the simple design and operation of single-use AER systems, only a small number of consumables and system design parameters are

expected to influence life cycle impacts, including MUR, changeout criteria, transportation distances (from resin supplier and to the site of resin disposal), resin identity, and disposal method (e.g., incineration type). A one-at-a-time sensitivity analysis was first conducted to identify the factors that most strongly influence environmental impacts and treatment costs. Because impacts stemming from transportation are minimal for this system, variations in transportation type and distance have a minimal effect (<2%) on environmental impact for nearly all categories. Additionally, because single-use AER performance among all resin identities was near-identical (Ellis et al., 2022), resultant changes in environmental impact are also insignificant. Because impacts from adsorbent media and incineration comprise >90% of the impacts in nearly all categories and scale linearly with AER usage, life cycle environmental impacts and costs were determined to be most sensitive to MUR.

The dominance of MUR in determining environmental impacts and costs is critical because MUR will be largely determined by site-specific PFAS breakthrough behavior and the selected breakthrough criteria used for media changeout. The baseline scenario was informed by breakthrough behavior of PFAS from a relatively concentrated source area (ΣPFAS = 30 – 50 µg/L (Ellis et al., 2022)) and a changeout criteria of "detection of PFOS or PFOA". This criterion was selected as PFOA is the lowest-affinity compound set to be regulated by the EPA (Fang et al., 2021; EPA 2023), meaning changeout upon PFOA detection is adequate to prevent elution of any regulated PFAS analyte. Further, these two compounds have the most documentation regarding their behavior and toxicity (Fenton et al., 2020; Zareitalabad et al., 2013). Site-specific criteria will undoubtedly influence MURs, which can be observed in **Figure 3.8.4** for numerous potential breakthrough criteria. As indicated in **Table 2.10.3**, the bed volumes for media changeout depend massively on the breakthrough criteria selected, varying from as little as 6,000 BVs (when using 'detection of any PFASs' including low-affinity short-chain PFCAs) to 1,180,000 BVs (when using 50% breakthrough of strongly-adsorbing PFOS). This translates to nearly a 200-fold difference in MUR for remediation of the same site, indicating large sensitivities in projected environmental impacts. Furthermore, site-specific differences in PFAS concentrations and matrices as well as groundwater geochemistry that may alter breakthrough behavior will indirectly influence treatment costs and environmental impacts by their effect on MURs; these impacts require evaluation through pilot testing.

Environmental impacts and costs will also be affected by the choice of disposal option. The baseline scenario assumed hazardous waste incineration of wastes because it seems increasingly likely that this more stringent level of incineration will be required in the future, and that municipal solid waste (MSW) incineration will not be permitted for PFAS-containing wastes. However, the choice of hazardous waste incineration leads to much higher environmental impacts compared to choosing generic MSW incineration, MSW incineration of AERs, or hazardous waste incineration of waste solvent when calculating environmental impacts. Landfilling, while not examined in depth, proved to be less impactful than incineration for all categories (20-30% impact reductions), though databases are lacking in entries for hazardous-specific landfills, thus extensive analysis was precluded.

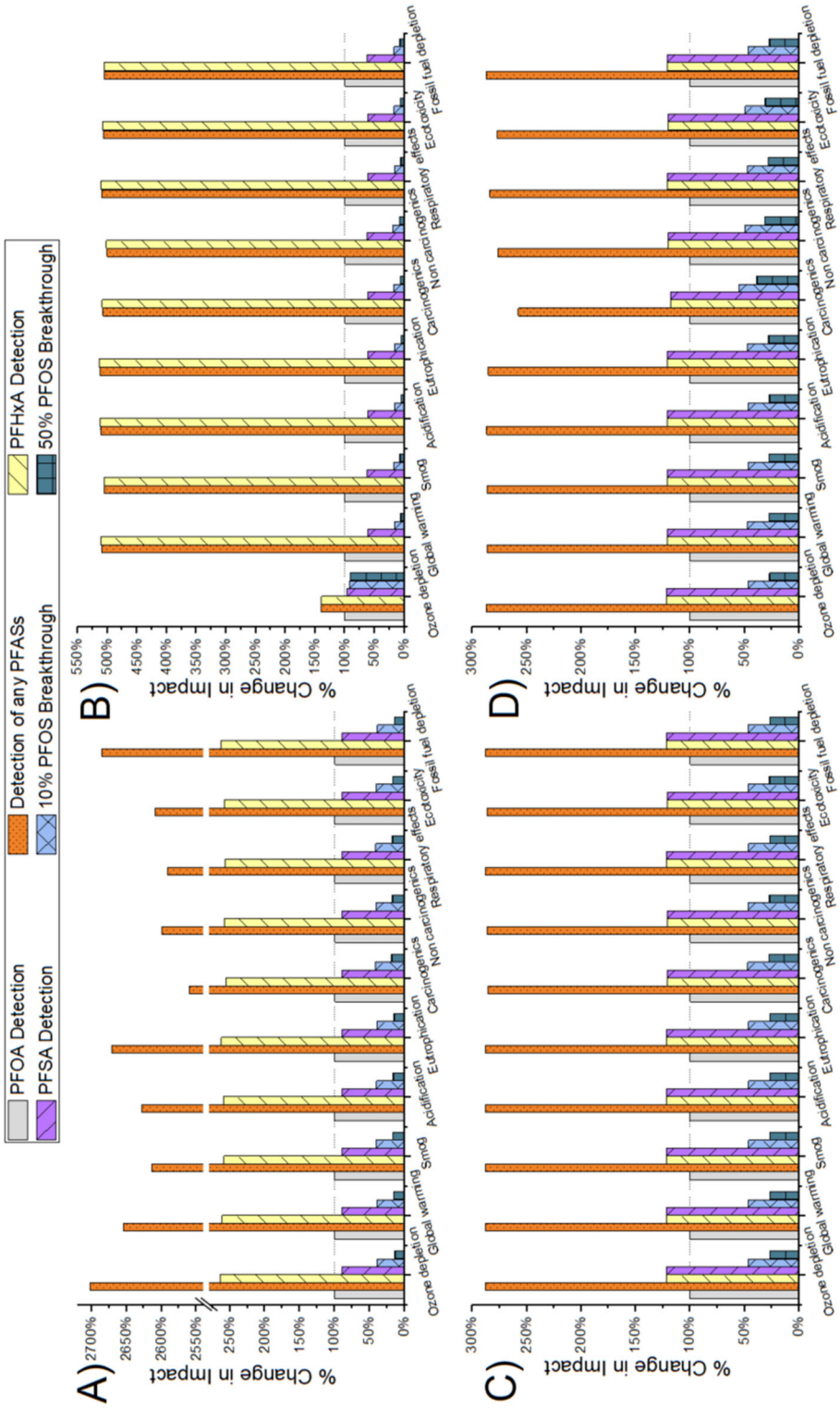

Figure 3.8.4. Percent change in environmental impacts across various criteria used to dictate vessel changeout or regeneration (relative to impacts of the baseline criteria of PFSA detection). Figures shown for (A) single-use AER, (B) regenerable AER, (C) single-use GAC and (D) GAC with thermal reactivation. Note the y-axis break between 250%-2550% in panel A. From Ellis et al. (2023).

Sensitivity of GAC treatment systems. Like single-use AER treatment systems, GAC adsorption systems are simple in design. Moreover, environmental impacts and costs are dominated by MURs to an even larger degree than single-use AER because of the comparatively high impacts of GAC production relative to AER production. However, the criteria for media changeout for GAC is less dependent on PFAS treatment goals than single-use AER, varying from 4,500 BVs to 48,900 BVs (~10-fold variation compared to nearly 200-fold variation for AER). The difference in MUR between single-use GAC and single-use AER varies considerably depending on the changeout criteria used. Whereas this resulted in a nearly 10-fold difference in MURs under the baseline scenario, differences in MURs may be much smaller when selecting alternative media changeout criteria. To highlight this point, **Figure 3.8.5** shows selected impacts and costs for single-use GAC relative to those for single-use AER when selecting different elution criteria to define PFAS breakthrough. Relative life cycle costs (**Figure 3.8.5A**) can favor single-use GAC when selecting stringent breakthrough changeout criteria whereas single-use AER is about half the cost when using less stringent criteria. Reactivated GAC systems were found to be highly sensitive to the temperature of incineration, as low-temperature incineration can reduce carcinogens by 38% while higher-temperature incineration similar to those used in hazardous waste lead to >500% increases in carcinogens. Environmental impacts stemming from thermally reactivated GAC (**Figure 3.8.4D**) mirror closely the impacts from single-use GAC (**Figure 3.8.4C**) as both systems share the same assumed MUR and have impacts that scale linearly with media usage.

Sensitivity of regenerable AER systems. Regenerable AER systems are more sensitive to a diverse set of factors given the greater system complexity compared to single-use AERs. The baseline scenario showed that system impacts were dominated by operations associated with incineration and resin regeneration (**Figure 3.8.2B**). Boyer et al. (2021b) previously showed that minimization of waste quantity and chemical inputs is paramount to reducing impacts stemming from regeneration, which is readily accomplished using alternate salts in regenerant solution brine. Overall impacts for this system are driven by three variables: cosolvent fraction, the percentage of cosolvent recovered from the solution after regeneration, and the number of bed volumes required for complete regeneration. The number of bed volumes used was found to have the strongest effect on system sustainability, as this correlates directly with the quantity sent for incineration and has a near-linear effect on emissions. Impacts were not found to be sensitive to the type of salt or cosolvent used for regeneration.

Figure 3.8.6 depicts the change in environmental impacts for the overall regenerable AER system expected from changes to the methanol percentage in the regenerant feed solution and the percentage of methanol recovered from the waste regenerant through distillation. As seen here, certain categories like ozone depletion and acidification are not at all sensitive to these variations as their impacts are not primarily from cosolvent management. However, other categories (e.g., eutrophication, carcinogens, and ecotoxicity) are highly sensitive to these parameters. Overall system impacts in these three categories can be reduced by >50% when using high methanol fractions and distillation efficiencies, as this greatly reduces the quantity of waste sent for incineration. Fossil fuel depletion is also highly sensitive to methanol use, as any cosolvent recovery efficiencies below 70% lead to massive increases in fossil fuel depletion associated with increased waste masses sent for hazardous waste incineration. Clearly, improving efficiency of

cosolvent use is key to reducing impacts of the regenerable AER system; however, the percent cosolvent used in practice must maintain complete regeneration of the resin.

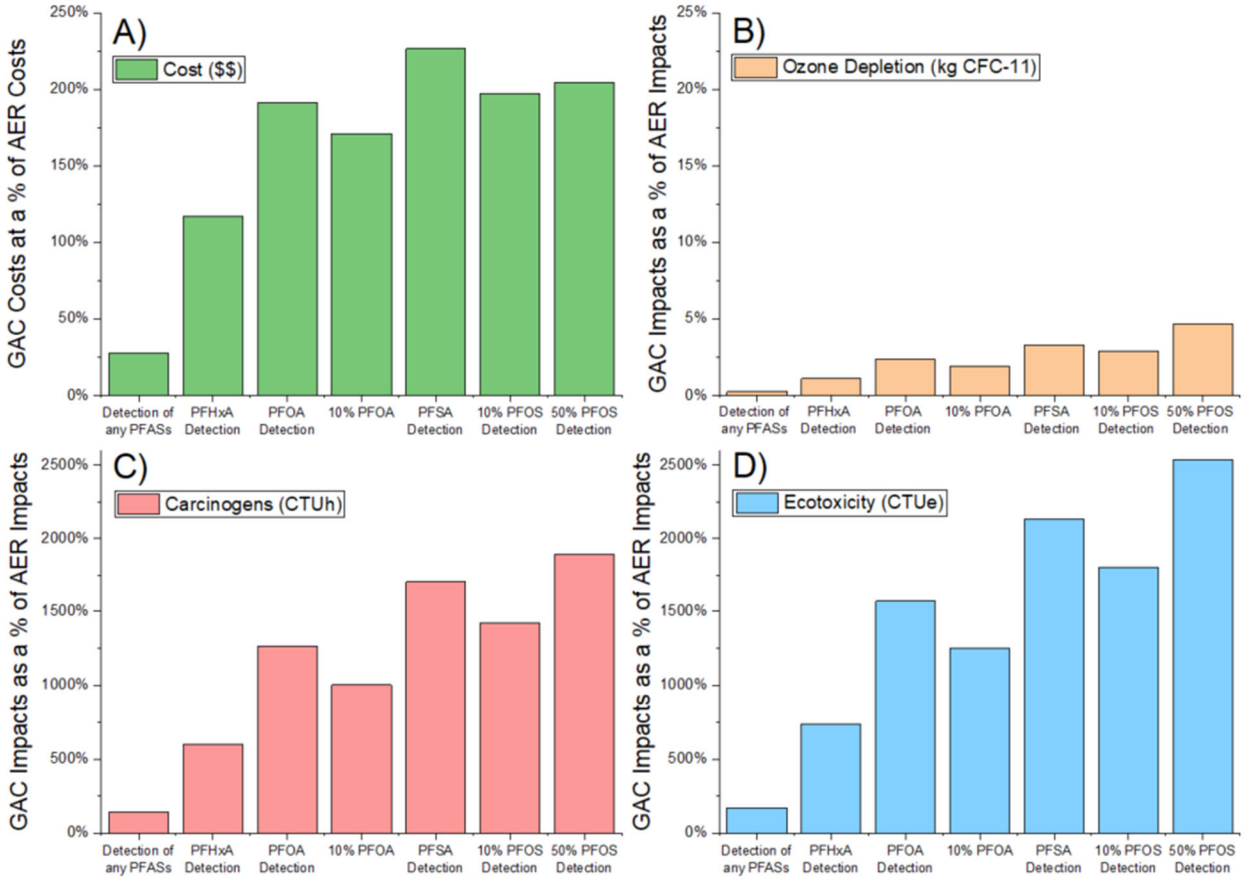

Figure 3.8.5. Percentages of single-use AER treatment costs and impacts stemming from use of single-use GAC. Values shown for (A) cost, (B) ozone depletion, (C) carcinogens, and (D) ecotoxicity. Note the differing y-axes for figures A, B, and C/D. From Ellis et al. (2023).

Importance of media changeout/regeneration criteria. While each remediation system is comprised of many inputs, the key parameter in determining the frequency of media usage or regeneration is the criteria used to determine when 'PFAS breakthrough' is reached. Because contaminated sites are typically associated with many different PFASs, particularly in the case of AFFF-impacted groundwater (Hu et al., 2016), the BVs treatable before media replacement/regeneration is needed varies widely depending on how breakthrough is defined (**Table 2.10.3**). While research has established the superiority of AERs in collectively adsorbing PFASs compared to GAC (Fang et al., 2021; Liu et al., 2022), the specific criteria chosen for a site has a direct effect on the extent to which these resins outperform GAC, as these sorbents' effective lifetimes are highly sensitive to breakthrough criteria. **Figure 3.8.4** depicts how breakthrough criteria can lead to massive disparities in impact and costs for all four remediation systems. While certain systems are more sensitive to media usage than others (e.g., single-use AER disparities of 200-fold versus 10-fold for GAC), these changing criteria can also influence selection of an 'optimal' system as illustrated in **Figure 3.8.5**. While differences in MUR are much narrower in

cases where more stringent breakthrough criteria are used, the single-use AER system results in lower impacts than single-use GAC for all but the single most stringent criteria. Because many key sources of impact (e.g., incineration) scale linearly with MUR for single-use systems, these technologies are more sensitive to breakthrough criteria than any other parameter. While the balance between complete PFAS removal to safeguard human and environmental health must be weighed against other environmental impacts indirectly related to implementation of a treatment system, effluent PFAS limits are often set by regulators. Therefore, an examination of other system sensitivities must be conducted to identify areas of improvement to optimize PFAS treatment systems.

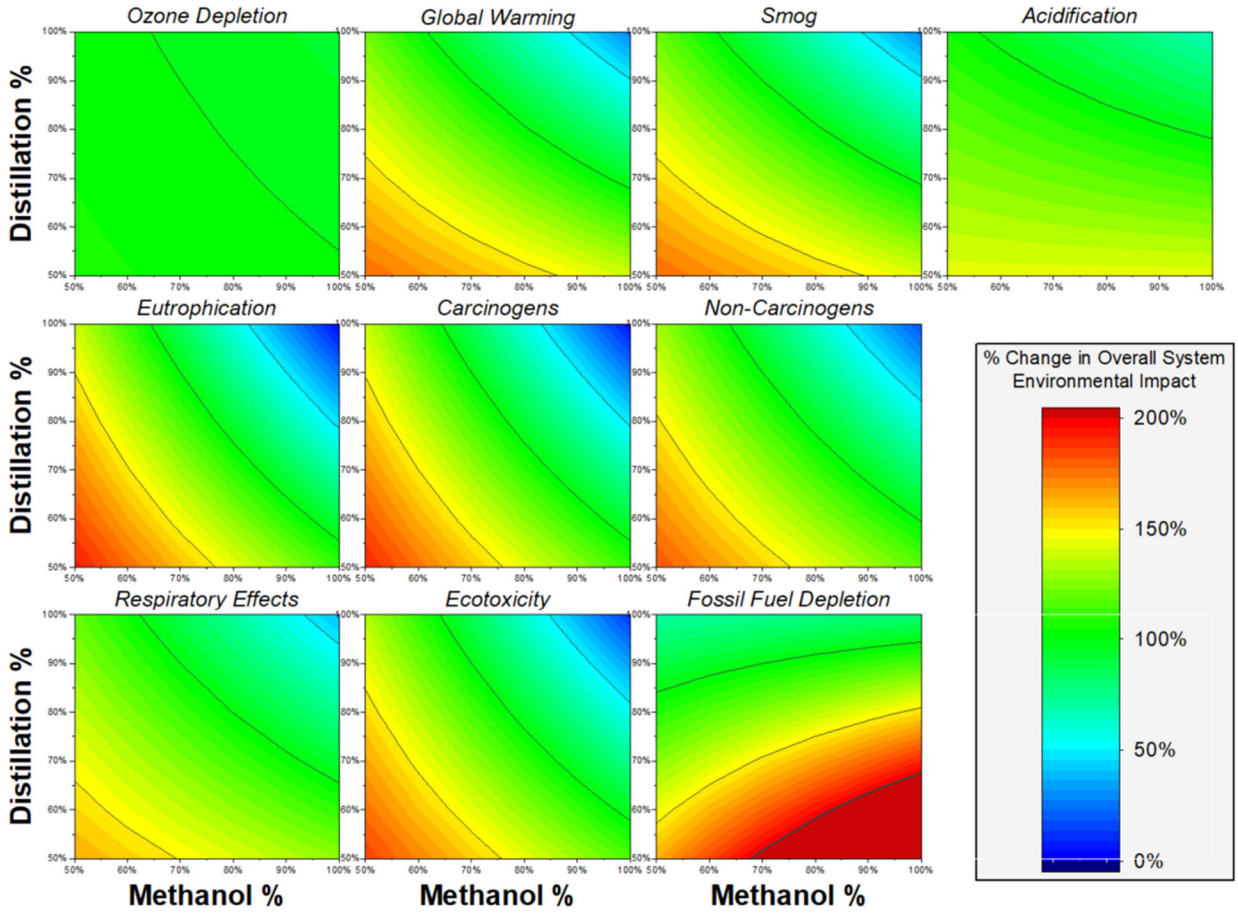

Figure 3.8.6. Heatmap showing influence of methanol percentage in the regenerant mixture and the methanol recovery by distillation percentage on environmental impacts of the overall regenerable AER system. Legend bar indicates the extent to which the estimated impact changes relative to the baseline scenario (70% methanol, 90% recovery). From Ellis et al. (2023).

Other key drivers of system sensitivity. While the foremost factors in driving overall system sensitivity is MUR and breakthrough criteria, systems are also sensitive to many other operational considerations. Beyond MUR, the primary driver of environmental impact common to all four systems is the management of wastes generated by each system. In this study's LCA models, solid waste (single-use systems) and still bottoms were disposed of using 'hazardous waste incineration'

and treatment of thermally reactivated GAC was modeled as 'treatment of spent activated carbon, reactivation' both from the Ecoinvent 3 database. While research on incineration of PFAS waste streams is still ongoing, the impacts from waste disposal are inextricably tied to the quantity of generated wastes, indicating that minimization of waste is key to reduce remediation system environmental impact.

While the quantity of AER and GAC sorbents cannot be significantly reduced, waste still bottom volume produced in regenerable AER systems can be reduced by increasing recovery of organic cosolvent, increasing cosolvent fraction (**Figure 3.8.6**), and reducing the number of bed volumes required for brine/cosolvent regeneration each cycle. High cosolvent fractions and high recoveries can lead to very low volumes of waste still bottoms (e.g., <20% of the total regenerant volume is produced as a waste still bottom when regenerant makeup includes >90% cosolvent that is recovered with 90% efficiency). While increasing the cosolvent fraction does increase impacts stemming from its production, it also decreases the volume of the still bottoms requiring incineration. Moreover, increasing cosolvent fraction may result in fewer required bed volumes for resin regeneration due to increased hydrophobicity, thereby offsetting any of the preceding benefits. The parameter most strongly linked to environmental impact was found to be the number of BVs required to regenerate the resin each cycle. While the baseline scenario assumes 10 BVs are needed to regenerate the bed, halving or doubling this volume leads to impacts that are ~50% and ~200% of those estimated for the baseline scenario for most categories. However, any amendments to regenerant solution or the number of BVs must maintain complete AER regeneration. In summary, the regenerable resin system impacts are most sensitive to the number of BVs needed for regeneration > cosolvent distillation efficiency > cosolvent fraction >> salt or cosolvent identity.

All four systems exhibited minimal sensitivity to transportation distance compared to sorbent media replacement/regeneration and disposal options, though transportation type was found to be a more significant factor than transportation distance for many categories. System environmental impacts were also found to be minimally sensitive to system size (e.g., flow rate and vessel size) as nearly all facets of treatment including MUR and incineration scale linearly with the quantity of water treated. Furthermore, some variables like EBCT are static and do not influence system impacts when varied; because additional contact time beyond recommended contact time was not found to increase treated BVs until breakthrough (Boodoo et al., 2019; Ellis et al., 2022), remediation systems are not sensitive to EBCT provided manufacturer recommendations are followed.

Implications for site operators and design engineers. Findings from this study may benefit operators by helping improve remediation system efficiency while minimizing environmental impact and superfluous costs. For any site manager tasked with selecting between sorbents or optimizing an existing system, it is recommended that decision-makers begin by determining site-specific PFAS analytes of concern and treatment goals that dictate breakthrough criteria. The stark difference in sorbent MURs detailed in **Table 2.10.3** for different criteria supports the use of the least stringent criteria allowable to maximize PFAS uptake in the lead bed and reduce treatment-derived environmental impacts. Once a criterion is determined, the MURs for each sorbent media and associated cost constraints can be used to select an optimal treatment technology based on tradeoffs in costs and environmental impacts. Once a remediation system has been selected and

installed, operators can further reduce environmental impacts and costs by optimizing the treatment system in tangible ways to most efficiently remove PFASs from groundwater. Close monitoring of effluent from reactor beds can refine and possibly extend times between media changeouts/regenerations. For regenerable AER systems, another tangible method for system optimization is to increase cosolvent distillation to the maximum extent possible without risking back-contamination of PFAS in methanol. While distillation requires increasingly greater energy inputs to marginally improve recovery percentage above 80% (Kong et al., 2022), the natural gas needed for distillation is both cheaper and more sustainable than additional methanol production, which has high associated costs and impacts.

Sensitivity results regarding breakthrough criteria and associated MURs support the notion that a trade-off exists between complete remediation of all PFAS analytes and treating impacted water efficiently at a reasonable cost and minimal environmental harm. The dominant role of breakthrough criteria significantly influences these trade-offs, as remediation focused on longer-chain compounds and PFSAs can remove over 90% of the total PFAS at many sites including high-concentration sites like Willow Grove, PA. However, changing criteria to the detection of any PFAS increases the MUR by >2500% in the case of single-use resin, and the costs associated with these more stringent criteria can increase by over 20-fold when using single-use AERs (>2-fold for the GAC systems). While maximum uptake per unit mass could be achieved using very relaxed criteria (e.g., 50% PFOS), this would lead to elution of other long-chain and sulfonate PFASs from the lag bed, therein risking the safety of human health and environmental systems. Thus, a balance is required in operator decision-making between unfeasibly rapid bed changeout and elution of some PFASs to attain optimal, efficient PFAS removal.

Utilizing results to guide future research. Results from this analysis can also inform priority research areas to reduce environmental impacts and costs associated with adsorbent technologies for PFAS treatment, including (1) improvements to sorbent affinity for PFASs, particularly short-chain structures, (2) coupling adsorbents and other separation technologies with destruction technologies that eliminate the need for PFAS waste disposal, and (3) quantitative evaluation of the threat posed by lower-toxicity short-chain PFCAs compared to increased environmental threats posed by emissions associated with remediation. Over the past decade, the emergence of target-selective sorbents including single-use "PFAS-selective" resins has led to increased mass loading of PFASs onto sorbent media compared to GAC and more traditional resins (Liu et al., 2022; Ellis et al., 2022). While these single-use AERs exhibit significantly improved affinities for long-chain and sulfonate PFASs, improvements in retention of short-chain PFCAs would greatly extend sorbent lifetimes and decrease MURs, leading to overall reductions in environmental impact and costs. While this may be achieved through specialized functional groups targeting short-chain compounds, another option could be coupling high-affinity single-use AERs with a lag bed of lower-affinity regenerable AERs to maximize mass loading of PFAS onto the lead vessel while enabling concentration of PFASs in the regenerant solution from the lag bed. Although this would lead to both solid and liquid waste streams, the lower affinity for short-chain PFCAs may enable brine-only regeneration or use of solutions containing low fractions of brine and cosolvent. Future sorbent development and pilot study efforts would also benefit from thorough examination of the role played by nontarget co-constituents (e.g., TOC and anions like nitrate), as even the most ideal adsorbents may be fouled by these constituents. While removal of PFASs should be prioritized,

novel adsorbents should also be resilient to these constituents across a range of groundwater matrices.

Perhaps more ideally, separation technologies like those compared in this study could be coupled with emerging technologies that demonstrate promise for destroying PFAS on site, potentially enabling low- or no-waste treatment system, including liquid phase thermal technologies like supercritical water oxidation (SCWO; Krause et al., 2022) and hydrothermal alkaline treatment (HALT; Hao et al., 2021), plasma treatment (Singh et al., 2019), electrochemical oxidation (ECO; Schaefer et al., 2020), and photochemical and photocatalytic technologies (Tenorio et al., 2020; Amador et al., 2023). Since these destructive technologies are energy intensive, their most efficient application is for treatment of concentrate streams like those produced from regenerable AER. Concentrate streams can be further optimized via waste minimization through solvent recovery, highlighting the need for additional research into low-brine AER regeneration as well as solvent regeneration of GAC (Siriwardena et al., 2021). Future research is suggested to evaluate and compare life cycle impacts of treatment trains coupling sorbent media with different destruction technologies.

These findings highlight the major role breakthrough criteria plays in the environmental impacts and costs associated with remediating groundwater contaminated with PFAS mixtures. To that end, future research is recommended to evaluate trade-offs between operating remediation systems to achieve complete removal of all PFASs versus allowing for variable release of different PFASs (e.g., allowing higher effluent limits for PFASs determined to pose much lower health and ecological risks). Treating sites to the most stringent PFAS limits may be optimal from an PFAS exposure viewpoint, but risk much larger overall environmental impacts due to embedded impacts of the required treatment systems.

Alternative strategies for management of exhausted adsorbents. Sorbent regeneration/reactivation options as presented in this study may offer further benefits to system sustainability and life cycle costs by enabling coupling of these separation technologies with destruction modules to eliminate PFASs from waste streams. In the case of AER treatment, aqueous still bottom wastes require high-emission and costly disposal options including hazardous waste incineration or hazardous waste landfilling. However, overall system emissions and costs are expected to be reduced by treating this liquid waste byproduct with technologies like hydrothermal alkaline treatment (HALT) or supercritical water oxidation (SCWO), which require concentrated aqueous streams laden with PFASs. Because technologies like HALT have been found to fully defluorinate even the most recalcitrant long-chain PFAS structures (e.g., PFOS; Hao et al., 2021), HALT treatment of regenerant still bottoms would prevent the need for environmentally-damaging hazardous waste disposal methods. While technologies like HALT and SCWO are energy-intensive and require additional inputs of electricity to pump liquid wastes and operate destruction modules, the emissions and costs associated with this energy increase may be far below those for hazardous waste disposal. Moreover, operation of still bottoms treatment systems on-site may reduce impacts and costs associated with off-site transport to centralized sites for hazardous waste management.

These destructive techniques would likely also reduce the impacts from GAC systems, though processes like solvent washing would require an aqueous component with solvent distillation to concentrate PFASs in water, as solvents may interfere with destruction due to subcritical expansion

of methanol in HALT and interference with oxidants in SCWO. Additionally, because GAC reactivation processes are assumed to fully remove PFAS from GAC at a lower temperature than hazardous waste incineration, coupling sorbent systems with destruction technologies is expected to have greater relative benefit for AER systems than GAC systems. These improvements to sustainability and affordability also depend on regeneration configuration, as lower-cosolvent regenerant solutions (e.g., 70% MeOH) lead to larger volumes of less-concentrated still bottoms compared to high-cosolvent solutions (e.g., 90% MeOH) when both have efficient solvent recovery processes. While a brief analysis found environmental impacts to be reduced by >70% for key categories (including carcinogens and ecotoxicity) when solvent is distilled for reuse and treated aqueous wastes with minimal PFAS concentrations are blended back into the feed stream, the cost benefits are less clear. Coupling destruction techniques with sorbent separation may depend on the relative infrastructure costs and complexity of operating HALT or SCWO modules, as capital infrastructure and labor plays a much more significant role in estimated costs compared to estimated environmental impacts. Further field demonstration of this technology pairing is recommended, as field results could inform future analyses of the LCA/LCCA implications of adding destruction modules to a sorbent-based treatment train.

4. Conclusions and Implications

As described in the preceding report, this project has had a number of significant findings that both address the project's stated objectives and advance the science and engineering of ion exchange treatment processes for AFFF-impacted water sources. Below is a summary of significant findings and major conclusions from the project, organized by topic.

PFAS Adsorption

- Equilibrium adsorption data and ion exchange selectivity coefficients were measured for 75 unique PFAS structures identified in an AFFF mixture (categorized into 21 different PFAS classes) adsorbing to 13 different commercial resin adsorbents (5 regenerable AER, 3 PFAS-selective AER, 2 regenerable CER, and 3 NIR) and to a reference GAC material. Kinetic data was also collected for a subset of PFASs and AERs that will be useful in model predictions. To our knowledge, this represents the largest and broadest data set to date on equilibrium and kinetics of adsorption of PFASs. A manuscript is currently in preparation that will report these results and discuss PFAS- and resin- structure-specific reactivity trends.
- Results showed that anion-exchange resins (AERs) exhibited significant adsorption of PFASs compared to cation-exchange resins (CERs), nonionic resins (NIRs), and GAC regardless of the PFAS's predicted charge.
- Structure-reactivity trends are consistent with PFAS selectivity for resins being driven by a combination of electrostatic and van der Waals interactions between the PFASs and the resin functional groups and supporting polymeric matrix. Perfluoroalkyl sulfonic acids (PFSAs) adsorb to AERs much more than the corresponding perfluoroalkyl carboxylic acids (PFCAs) Both PFAS sorbate and resin characteristics that increase hydrophobicity increase selectivity for AERs.
- PFASs adsorb much more strongly to polystyrene-based than polyacrylic-based AERs.
- Both equilibrium batch adsorption data and continuous-flow adsorption studies confirm the greater affinity of most PFAS classes for PFAS-selective AERs (PAERs), and support the industry trend of adopting these materials for treatment of dilute PFAS-contaminated water sources.
- Results demonstrate that single-use AERs significantly outperform regenerable resins, particularly for treatment of long-chain perfluoroalkyl carboxylic acids (PFCAs) and perfluoroalkyl sulfonic acids (PFSAs). No detectable concentrations of ≥C7 PFCAs or PFSAs were observed within 150,000 bed volumes (BVs) after treatment with the single-use resins (2-min EBCT). Analysis of effluent samples following 30-sec EBCT treatment shows that even the shortest-chain PFSAs do not reach 50% breakthrough within the first 350,000 BVs, though differences in removal of short-chain PFCAs was less dramatic.
- Although PAERs are highly effective for adsorbing longer-chain PFAAs and other higher molecular weight PFASs, their effectiveness for adsorption and treatment of short-chain PFAAs remains limited like the regenerable AERs. This suggests the need for resin manufacturers to prioritize development of resins that will be selective for these structures to achieve removal of the broadest possible suite of PFASs in contaminated water sources.

- Analysis of breakthrough profiles for different PFASs during a 9-month pilot study reveals empirical correlation of breakthrough behavior with ion exchange affinity coefficients (logK_{ex}) measured in batch experiments.
- While batch adsorption isotherm data indicate much greater total PFAS adsorption capacity of macroporous resins than gel-type resins, results from long-term field pilot experiments shows similar capacities for both types of resins.
- Postmortem analysis of PFASs extracted from spent resins from the field pilot study revealed chromatographic elution behavior and competition among PFASs for adsorption to the resins. PFSAs and long-chain PFCAs were preferentially adsorbed to earlier sections in the AER columns, whereas short-chain PFCAs were competitively displaced towards the later sections of the columns and into the effluent, consistent with effluent concentrations of the latter structures exceeding influent values.
- Experiments with regenerable AER demonstrate that adsorption of PFAAs are relatively insensitive to the mobile counterion loaded onto the resin (chloride versus sulfate). This is significant because it supports the use of non-chloride salts for resin regeneration, which is desirable for electrochemical treatment of PFASs in the waste regenerant solutions so that formation of toxic oxyanions (e.g., perchlorate) can be avoided.
- Changing the mobile counterion form of the resin from chloride to an alternative anion can have multiple benefits. For sulfate-form resin, the benefits include higher contaminant removal especially for resin with triethyl ammonium functional groups, less corrosive treated water, and expanded options for brine disposal and treatment of contaminants in the waste regeneration solution. The higher contaminant removal for sulfate-form resin is believed to be more pronounced for resins with functional groups that are selective for monovalent anions over divalent ions, e.g., triethyl ammonium.

Resin Regeneration

- Confirming earlier reports, results of this research project support the conclusion that effective regeneration of PFAS-contaminated AERs requires regenerant mixtures containing both salt brine and alcohol co-solvent.
- Both components are required in significant levels, but there are tradeoffs in regeneration efficacy with higher co-solvent allowing for effective regeneration with lower salt levels.
- In laboratory loading/regeneration studies, $(NH_4)_2SO_4$ + methanol solution achieved the highest regeneration efficiency in terms of desorbing PFAAs from the resin. Although the highest regeneration efficiencies were achieved using $(NH_4)_2SO_4$ + methanol solution, the 50% v/v methanol was only moderately effective in desorbing PFAAs from polystyrene AER indicating that higher methanol content is needed. PFBA was the only PFAA studied that desorbed appreciably using aqueous-only $(NH_4)_2SO_4$ + NH_4OH regeneration solution. PFBA, PFHxA, and PFOA exhibited similar desorption and greater desorption than PFBS, PFHxS, and PFOS using $(NH_4)_2SO_4$ + methanol regeneration solution. The results suggest additional research is needed to assess the possibility of developing treatment schemes where short-chain PFAS can be desorbed through periodic aqueous-only regeneration thereby extending treatment run times.

- Results here show that AERs marketed as "single use" can also be regenerated using salt/co-solvent mixtures. Optimal regeneration of single use Purolite PFA694A gel-type resin requires 90% methanol with 1 wt% NaCl. Only perfluoroalkyl carboxylates were effectively desorbed using 70% cosolvent fractions. Counterintuitively, increased empty bed contact time (30 min vs 10 min) does not improve regeneration.
- Both macroporous and gel-type resins loaded with real groundwater constituents (e.g., PFASs, NOM, precipitates) were effectively regenerated using 90% methanol, supporting the use of any PFAS-selective resin brand with high-cosolvent regeneration infrastructure.
- Weak base AERs still require co-solvent for regeneration, even when pH is raised to neutralize the resin functional group.
- Substitution of methanol with higher molecular weight alcohols, particularly n-propanol, can yield improved regeneration for the same percent co-solvent composition.
- Attempts to regenerate using other solution amendments, including hydrocarbon-based anionic surfactants, chelating agents, and organic acids, were unsuccessful in aqueous-only regenerant mixtures. Similarly, raising temperature of aqueous regenerants had limited effect on regeneration.
- Regarding weak-base AER (WB-AER), at neutral pH, contaminant removal was not influenced by the basicity of the resin functional groups. This indicated the potential for WB-AER to be used in place of SB-AER in water and wastewater treatment applications.
- WB- and SB-AER of polystyrene composition were proven most effective for PFAA removal with a greater selectivity for PFSAs than PFCAs and for PFOS than remaining PFAAs. To minimize the impact of competing sulfate and carbonate anions on PFAA adsorption, AERs with large alkylamine functional groups and polystyrene composition are suggested. These conclusions are limited to synthetic solutions containing the six PFAAs tested in this work. Future research should evaluate real test waters rich in competing organic matter and explore WB-AER with functional groups that are more selective for monovalent anions to extend its use in PFAA-impacted water.
- For regeneration, as the alkyl chain length of the alcohol cosolvent increased from methanol to ethanol to 1-propanol to 1-butanol, regeneration efficiency of resin increased for perfluoroalkyl acids and other organic anions when other variables were held constant.
- When compared to 1-propanol, the three-carbon polyols propylene glycol and glycerol showed a decrease in regeneration efficiency in part due to increased viscosity and reduction in mass-transfer exchange occurrence.
- Similar regeneration of resin across cosolvent parameters for dodecylbenzene sulfonate and diclofenac compared to PFBA suggest that these two anions can serve as surrogates for future PFBA regeneration experiments.
- As alkyl chain length increases on monohydroxy alcohols and volume fraction increases, the solubility of NaCl decreases. This illustrates the trade-off between polarity of cosolvent solution and the miscibility and phase separation of dissolved salt. Other chloride salts and alternative counterion salts should be investigated for regeneration and solubility trends.

- Dissolved organic carbon (DOC) in natural groundwater can decrease both the adsorption capacity and regenerability of the AER flow-through columns. Such finding confirms the necessity of considering DOC pretreatment for extending the longevity of AER treatment systems
- The regeneration of PFCAs from some resins is faster in terms of releasing rate compared to PFSAs with the same chain length and longer-chain PFAS with the same head group generally desorb first compared to their short-chain analogs. The different regeneration profile relating to chain-length and head groups are likely caused by their difference in polarity and hydrophobicity.

PFAS Destruction in Regenerants

- Tests demonstrate that electrochemical oxidation processes employing BDD anodes can be effective for degradation and defluorination of PFASs present in AFFF-impacted synthetic brines being considered for AER regeneration processes. Fluoride mass balance analysis indicated that roughly half of the organic fluoride in a 500-fold diluted AFFF mixture is released as inorganic fluoride within 8 h of electrochemical treatment, and defluorination reaches >80% with extended treatment.
- Rates of electrochemical oxidation-based AFFF defluorination were found to be superior in sulfate- and bicarbonate-based brines compared to chloride-based brines, and tests showed similar results for sodium- and ammonium-based salt brines (the latter has been found to be more effective for resin regeneration in published reports). These results suggest that the sulfate and bicarbonate salts which have potential to scavenge hydroxyl radicals or produce secondary radicals, do not influence the net rate of PFAS defluorination inhibit reactions by competing for reactive sites on the BDD anode.
- Tests of a waste ion exchange still bottoms sample obtained from the former Naval Air Station at Willow Grove demonstrated effective destruction of the full suite of detected PFASs using hydrothermal alkaline treatment (HALT), a technology being developed under SERDP funding through Project ER18-1501.
- The electrochemical treatment of still bottom generated from waste regenerant showed significant PFAS degradation ratio even in the presence of high DOC (e.g., 200 mg/L).
- Consistent with previous studies, transient increases in the shorter-chained perfluorinated carboxylates were observed during the ECO treatment. The transient increases are likely due to the sequential head group oxidation reactions of the longer-chained perfluorinated carboxylates, but may also be due to the oxidation of PFAA precursor compounds to perfluorinated carboxylates.
- Trends for HALT treatment of individual PFASs are consistent with earlier tests for treatment of AFFF and AFFF-impacted groundwater, that is very rapid destruction of PFCAs and slower alkali-dependent destruction of PFSAs. Observed rate constants for destruction of individual PFASs in the still bottoms were similar to rate constants measured in other liquid matrices, highlighting the matrix-independent nature of HALT reactions.
- Dissolved organic carbon (DOD) was reduced by a marginal amount, highlighting that some components of natural organic matter are recalcitrant to the HALT process.

Life Cycle Analysis

- A life cycle assessment (LCA) framework was established and applied to compare the life cycle environmental impacts of anion exchange treatment systems for PFAS-contaminated water sources. The methodologies are initially being applied to address two questions: (1) Compare the sustainability of non-regenerable vs regenerable IX vs. GAC adsorption; and (2) Assess the influence of process design decisions on the sustainability of waste brine management options.
- LCA compared AER-based PFAS remediation system with different regeneration scenarios including disposing of waste regeneration solution via incineration, reusing the organic cosolvent and brine fractions of the waste regeneration solution, and altering the composition of the regeneration solution to avoid organic cosolvent or NaCl. The results show that disposing of waste regeneration solution via incineration, without recycling organic cosolvent or brine, had the greatest environmental impact, and that incineration accounted for the greatest impact among contributing processes.
- Recycling of the cosolvent (or cosolvent and brine) fraction of the waste regeneration solution resulted in lower environmental impacts due to reduced mass of waste disposed of via incineration. Replacing NaCl in the brine with an alternative salt resulted in higher environmental impacts, with salts derived from chemical production, such as ammonium chloride and potassium carbonate, showing the largest increases in impacts.
- Environmental impacts were sensitive to the amount of waste incinerated and the nature of the incineration process. Hence, further research is needed to refine the amount and characteristics of the waste generated for incineration, and emissions from the incineration process.
- The environmental impacts of AER regeneration options had greater impacts to human toxicity, ecotoxicity, and eutrophication than climate change. As the hypothetical scenarios from this study are supported with new experimental and field data on regeneration performance, the life cycle environmental impacts should be compared with life cycle costs to identify the regeneration options that minimize both harmful environmental impacts and cost.
- For a baseline treatment scenario, single-use AER was found to have the lowest treatment costs and environmental impacts for nearly all impact categories. Single-use GAC was found to be most costly and least sustainable, while regenerable AER treatment was found to have more environmental impact than thermally reactivated GAC, but at a lower cost.
- The large impacts from single-use GAC result from much higher media usage rates (MURs) than either AER system due to rapid PFAS breakthrough observed in field pilot studies. Differences in MURs shrink when more stringent PFAS breakthrough criteria are used since shorter chain perfluorocarboxylic acids (e.g., PFBA) breakthrough rapidly for all adsorbent media.
- On a person-normalized basis, carcinogens and ecotoxicity are supported as the categories of greatest concern during PFAS treatment. Single-use AER is shown to outperform single-use GAC in reducing these emissions across all criteria that may determine vessel changeout/regeneration.

- Environmental impacts and costs are most sensitive to media usage rates (MURs) or AER regeneration frequency, which are highly dependent upon the PFAS breakthrough criteria used to determine when media replacement or regeneration was required. Use of very stringent breakthrough criteria (e.g., detection of any PFASs in effluent waters) leads to much higher MURs or regeneration frequencies than less stringent criteria like 50% breakthrough of PFOS.

- Costs of using single-use AER prove to be much lower than GAC under the baseline scenario. However, GAC may prove cheaper when using very stringent PFAS breakthrough criteria.

- Incineration of wastes is a primary source of environmental impact; minimization of waste quantities sent for hazardous waste incineration can be accomplished by thermal reactivation and reuse of GAC, reduction in brine/cosolvent volumes used to regenerate AERs, and improvement of cosolvent recovery during distillation of waste regenerant solutions.

- Findings highlight the need for future research to address how adsorbents can be tailored to provide greater capacity and uptake of early eluting PFASs, how regenerant solution composition can be further optimized, how influent PFAS concentration influences MURs, and how adsorbent technologies can be coupled with destructive technologies for complete on-site PFAS treatment.

5. Literature Cited

Abbasian, M., Ghaderi, A., Namazi, H., & Entezami, A.A. (2011). Preparation of Anion-Exchange Resin Based on Styrene-Divinylbenzene Copolymer Obtained by Suspension Polymerization Method. Polymer-Plastics Technology & Engineering, 50(15), 1606–1612.

Abunada, Z., Alazaiza, M.Y.D. and Bashir, M.J.K. 2020. An Overview of Per- and Polyfluoroalkyl Substances (PFAS) in the Environment: Source, Fate, Risk and Regulations. Water 12(12), 3590.

Adam, C., Yang, L., & Cockroft, S. L. (2015). Partitioning Solvophobic and Dispersion Forces in Alkyl and Perfluoroalkyl Cohesion. Angewandte Chemie International Edition, 54(4), 1164-1167. https://doi.org/10.1002/anie.201408982

Ahmed, M.B., Alam, M.M., Zhou, J.L., Xu, B., Johir, M.A.H., Karmakar, A.K., Rahman, M.S., Hossen, J., Hasan, A.T.M.K. and Moni, M.A. 2020. Advanced treatment technologies efficacies and mechanism of per- and poly-fluoroalkyl substances removal from water. Process Safety and Environmental Protection 136, 1-14.

Akhadov, Y. Y. (1980). CHAPTER III - DIELECTRIC DATA FOR BINARY SYSTEMS — AQUEOUS SOLUTIONS. In Y. Y. Akhadov (Ed.), Dielectric Properties of Binary Solutions (pp. 266-338). Pergamon. https://doi.org/https://doi.org/10.1016/B978-0-08-023600-1.50009-X

Albert, M., Hahnenstein, I., Hasse, H., & Maurer, G. (2001). Vapor-liquid and liquid-liquid equilibria in binary and ternary mixtures of water, methanol, and methylal. Journal of Chemical and Engineering Data, 46(4), 897–903.

Alemdar, A., Güngör, N., & Erim, F. (2003). Effect of sodium dodecyl sulfate and sodium dodecyl benzene sulfonate on the flow behavior of purified bentonite dispersion. Journal of Materials Science Letters, 22(2), 89-90.

Allen, S.J., Gan, Q., Matthews, R. and Johnson, P.A. 2003. Comparison of optimised isotherm models for basic dye adsorption by kudzu. Bioresource Technology 88(2), 143-152.

Amini, A., Kim, Y., Zhang, J., Boyer, T. and Zhang, Q. 2015. Environmental and economic sustainability of ion exchange drinking water treatment for organics removal. Journal of Cleaner Production 104, 413-421.

Anderson, R.E. 1964. A contour map of anion exchange resin properties. Industrial & Engineering Chemistry Product Research and Development 3(2), 85-89.

Appleman, T.D., Higgins, C.P., Quiñones, O., Vanderford, B.J., Kolstad, C., Zeigler-Holady, J.C. and Dickenson, E.R.V. 2014. Treatment of poly- and perfluoroalkyl substances in U.S. full-scale water treatment systems. Water Res. 51, 246-255.

Astbury, G. R., Bugand-Bugandet, J., Grollet, E., & Stell, K. M. (2005). Flash points of aqueous solutions of flammable solvents. Institution of Chemical Engineers Symposium Series, 505-522.

Atamna, I.Z., Muschik, G.M., & Issaq, H.J. (1990). Effect of alcohol chain length, concentration and polarity on separations in high-performance liquid chromatography using bonded cyclodextrin columns. Journal of Chromatography A, 499(C), 477–488.

Ateia, M., Alsbaiee, A., Karanfil, T. and Dichtel, W. 2019a. Efficient PFAS Removal by Amine-Functionalized Sorbents: Critical Review of the Current Literature. Environmental Science & Technology Letters 6(12), 688-695.

Ateia, M., Arifuzzaman, M., Pellizzeri, S., Attia, M.F., Tharayil, N., Anker, J.N. and Karanfil, T. 2019b. Cationic polymer for selective removal of GenX and short-chain PFAS from surface waters and wastewaters at ng/L levels. Water Research 163, 114874.

Awual, M.R., Urata, S., Jyo, A., Tamada, M. and Katakai, A. 2008. Arsenate removal from water by a weak-base anion exchange fibrous adsorbent. Water Research 42(3), 689-696.

Azizi, O., Hubler, D., Schrader, G., Farrell, J. and Chaplin, B.P. 2011. Mechanism of Perchlorate Formation on Boron-Doped Diamond Film Anodes. Environmental Science & Technology 45(24), 10582-10590.

Backe, W.J., Day, T.C. and Field, J.A. 2013. Zwitterionic, Cationic, and Anionic Fluorinated Chemicals in Aqueous Film Forming Foam Formulations and Groundwater from U.S. Military Bases by Nonaqueous Large-Volume Injection HPLC-MS/MS. Environmental Science & Technology 47(10), 5226-5234.

Bagastyo, A.Y.; D.J. Batstone, I. Kristiana, W. Gernjak, C. Joll, and J. Radjenovic, J. Electrochemical oxidation of reverse osmosis concentrate on boron-doped diamond anodes at circumneutral and acidic pH. Water Res. 2012, 46, 6104−6112.

Bajpai, S., Gupta, S.K., Dey, A., Jha, M.K., Bajpai, V., Joshi, S. and Gupta, A. 2012. Application of Central Composite Design approach for removal of chromium (VI) from aqueous solution using weakly anionic resin: Modeling, optimization, and study of interactive variables. Journal of Hazardous Materials 227-228, 436-444.

Banks, D., Jun, B.-M., Heo, J., Her, N., Park, C.M. and Yoon, Y. 2020. Selected advanced water treatment technologies for perfluoroalkyl and polyfluoroalkyl substances: A review. Separation and Purification Technology 231, 115929.

Banzhaf, S., Filipovic, M., Lewis, J., Sparrenbom, C.J. and Barthel, R. 2017. A review of contamination of surface-, ground-, and drinking water in Sweden by perfluoroalkyl and polyfluoroalkyl substances (PFASs). Ambio 46(3), 335-346.

Bare, J. 2011. TRACI 2.0: the tool for the reduction and assessment of chemical and other environmental impacts 2.0. Clean Technologies and Environmental Policy 13(5), 687-696.

Bare, J. (2012) Tool for the Reduction and Assessment of Chemical and Other Environmental Impacts (TRACI) TRACI version 2.1 User's Guide EPA/600/R-12/554, U.S. Environmental Protection Agency, Cincinnati, OH.

Bare, J.C. 2010. Life cycle impact assessment research developments and needs. Clean Technologies and Environmental Policy 12(4), 341-351.

Barzen-Hanson, Krista A.; Roberts, Simon C.; Choyke, Sarah; Oetjen, Karl; McAlees, Alan; Riddell, Nicole; McCrindle, Robert; Ferguson, P. Lee; Higgins, Christopher P.; Field, Jennifer A., Discovery of 40 classes of per- and polyfluoroalkyl substances in historical aqueous film-forming foams (afffs) and afff-impacted groundwater. Environmental Science & Technology 2017, 51, (4), 2047-2057.

Bassler, J.; Ducatman, A.; Elliott, M.; Wen, S.; Wahlang, B.; Barnett, J.; Cave, M. C., Environmental perfluoroalkyl acid exposures are associated with liver disease characterized by apoptosis and altered serum adipocytokines. Environmental Pollution 2019, 1055-1063.

Becker, S., Bouzdine-Chameeva, T., & Jaegler, A. (2020). The carbon neutrality principle: A case study in the French spirits sector. Journal of Cleaner Production, 274, 122739. https://doi.org/https://doi.org/10.1016/j.jclepro.2020.122739

Bolster, C.H. and Hornberger, G.M. 2007. On the Use of Linearized Langmuir Equations. Soil Science Society of America Journal 71(6), 1796-1806.

Bolto, B., Dixon, D., Eldridge, R., King, S. and Linge, K. 2002. Removal of natural organic matter by ion exchange. Water Research 36(20), 5057-5065.

Boodoo, F., Begg, T., Funk, T., Kessler, T., Shaw, E., & Pickel, M. (2019). Polishing PFAS to non-detect levels using PFAS-selective resin. WaterOnline. https://www.wateronline.com/doc/polishing-pfas-to-non-detect-levels-using-pfas-selective-resin-0001

Boodoo, Francis. “Polishing PFAS to Non-Detect Levels Using PFAS-Selective Resin.” WaterOnline, 2019.

Boronow, K.E., Brody, J. G., Schaider, L.A., Peaslee, G.F., Havas, L., & Cohn, B.A. (2019). Serum concentrations of PFASs and exposure-related behaviors in African American and non-Hispanic white women. Journal of Exposure Science & Environmental Epidemiology, 29(2), 206–217. https://doi.org/10.1038/s41370-018-0109-y

Botelho, G., Anjos, O., Estevinho, L. M., & Caldeira, I. (2020). Methanol in Grape Derived, Fruit and Honey Spirits: A Critical Review on Source, Quality Control, and Legal Limits. Processes, 8(12), 1609. https://doi.org/10.3390/pr8121609

Boyer, T. H., Ellis, A., Fang, Y., Schaefer, C. E., Higgins, C. P., & Strathmann, T. J. (2021). Life cycle environmental impacts of regeneration options for anion exchange resin remediation of PFAS impacted water. Water research, 207, 117798. https://doi.org/https://doi.org/10.1016/j.watres.2021.117798

Boyer, T. H., Fang, Y., Ellis, A., Dietz, R., Choi, Y. J., Schaefer, C. E., Higgins, C. P., & Strathmann, T. J. (2021). Anion exchange resin removal of per- and polyfluoroalkyl substances (PFAS) from impacted water: A critical review. Water research, 200, 117244. https://doi.org/https://doi.org/10.1016/j.watres.2021.117244

Boyer, T.H. 2015. Removal of Dissolved Organic Matter by Magnetic Ion Exchange Resin. Current Pollution Reports 1(3), 142-154.

Boyer, T.H. and Singer, P.C. 2008. Stoichiometry of removal of natural organic matter by ion exchange. Environmental Science & Technology 42, 608-613.

Boyer, T.H., Singer, P.C. and Aiken, G.R. 2008. Removal of Dissolved Organic Matter by Anion Exchange: Effect of Dissolved Organic Matter Properties. Environmental Science & Technology 42(19), 7431-7437.

Brusseau, M.L.; and S. Van Glubt, The influence of surfactant and solution composition on PFAS adsorption at fluid-fluid interfaces. Water Res. 2019, 161, 17-26.

Buck, R.C., Franklin, J., Berger, U., Conder, J.M., Cousins, I.T., de Voogt, P., Jensen, A.A., Kannan, K., Mabury, S.A. and van Leeuwen, S.P. 2011. Perfluoroalkyl and polyfluoroalkyl substances in the environment: Terminology, classification, and origins. Integrated Environmental Assessment and Management 7(4), 513-541.

Burgess, J. (1978). Metal ions in solution. Ellis Horwood ; Distributed by Halsted Press.

Caldeira, I., Gomes, F., Mira, H., & Botelho, G. (2019). Distillates composition obtained of fermented Arbutus unedo L. fruits from different seedlings and clonal plants. Annals of Agricultural Sciences, 64(1), 21-28. https://doi.org/https://doi.org/10.1016/j.aoas.2019.05.009

Carter, K.E. and Farrell, J. 2010. Removal of Perfluorooctane and Perfluorobutane Sulfonate from Water via Carbon Adsorption and Ion Exchange. Sep. Sci. Technol. 45(6), 762-767.

Chaplin, B.P. Critical review of electrochemical advanced oxidation processes for water treatment applications. Environ. Sci.: Processes & Impacts, 2014, 16, 1182-1203.

Chaplin, B.P.; G. Schrader, and J. Farrell, Electrochemical destruction of N-nitrosodimethylamine in reverse osmosis concentrates using boron-doped diamond film electrodes. Environ. Sci. Technol. 2010, 44, 4264-4269.

Cheng, H., & Sabatini, D. A. (2002). Simultaneous uptake of anionic surfactants and micellar-solubilized contaminants using anion-exchange resins. Water research, 36(8), 2062-2076. https://doi.org/https://doi.org/10.1016/S0043-1354(01)00411-0

Chetverikov, S. P.; Sharipov, D. A.; Korshunova, T. Yu; Loginov, O. N., Degradation of perfluorooctanyl sulfonate by strain pseudomonas plecoglossicida 2.4-d. Applied Biochemistry and Microbiology 2017, 53, (5), 533-538.

Chin, Y.-P., Aiken, G. and O'Loughlin, E. 1994. Molecular Weight, Polydispersity, and Spectroscopic Properties of Aquatic Humic Substances. Environmental Science & Technology 28(11), 1853-1858.

Choe, J.K., Bergquist, A.M., Jeong, S., Guest, J.S., Werth, C.J. and Strathmann, T.J. 2015. Performance and life cycle environmental benefits of recycling spent ion exchange brines by catalytic treatment of nitrate. Water Research 80, 267-280.

Choe, J.K., Mehnert, M.H., Guest, J.S., Strathmann, T.J. and Werth, C.J. 2013. Comparative Assessment of the Environmental Sustainability of Existing and Emerging Perchlorate Treatment Technologies for Drinking Water. Environmental Science & Technology 47(9), 4644-4652.

Christoph, N., & Bauer-Christoph, C. (2007). Flavour of Spirit Drinks: Raw Materials, Fermentation, Distillation, and Ageing. In R. G. Berger (Ed.), Flavours and Fragrances: Chemistry, Bioprocessing and Sustainability (pp. 219-239). Springer Berlin Heidelberg. https://doi.org/10.1007/978-3-540-49339-6_10

Chularueangaksorn, P., Tanaka, S., Fujii, S. and Kunacheva, C. 2014. Batch and column adsorption of perfluorooctane sulfonate on anion exchange resins and granular activated carbon. Journal of Applied Polymer Science 131(3).

Chularueangaksorn, P., Tanaka, S., Fujii, S., & Kunacheva, C. (2013). Regeneration and reusability of anion exchange resin used in perfluorooctane sulfonate removal by batch experiments. Journal of Applied Polymer Science, 130(2), 884-890. https://doi.org/https://doi.org/10.1002/app.39169

Chularueangaksorn, Pattarawan; Tanaka, Shuhei; Fujii, Shigeo; Kunacheva, Chinagarn, Batch and column adsorption of perfluorooctane sulfonate on anion exchange resins and granular activated carbon. Journal of Applied Polymer Science 2014, 131, (3).

Clifford, D. and Weber, W.J. 1983. The determinants of divalent/monovalent selectivity in anion exchangers. Reactive Polymers, Ion Exchangers, Sorbents 1(2), 77-89.

Clifford, D., Sorg, T.J. and Ghurye, G.L. (2011) Water Quality & Treatment: A Handbook on Drinking Water. Edzwald, J.K. (ed), McGraw-Hill, Inc., New York.

Coffin, E.S., Reeves, D.M., & Cassidy, D.P. (2023). PFAS in municipal solid waste landfills: Sources, leachate composition, chemical transformations, and future challenges. Current Opinion in Environmental Science & Health, 31, 100418.

Comstock, S.E.H. and Boyer, T.H. 2014. Combined magnetic ion exchange and cation exchange for removal of DOC and hardness. Chemical Engineering Journal 241(0), 366-375.

Conte, L., Falletti, L., Zaggia, A. and Milan, M. 2015. Polyfluorinated organic micropollutants removal from water by ion exchange and adsorption. Chemical Engineering Transactions 43, 2257-2262.

Coperchini, Francesca, et al. “Thyroid Disrupting Effects of Old and New Generation PFAS.” Frontiers in Endocrinology, vol. 11, Frontiers Media S.A., Jan. 2021, p. 1077, doi:10.3389/FENDO.2020.612320/BIBTEX.

Cornelissen, E.R., Moreau, N., Siegers, W.G., Abrahamse, A.J., Rietveld, L.C., Grefte, A., Dignum, M., Amy, G. and Wessels, L.P. 2008. Selection of anionic exchange resins for removal of natural organic matter (NOM) fractions. Water Res. 42(1-2), 413-423.

Corominas, L., Byrne, D.M., Guest, J.S., Hospido, A., Roux, P., Shaw, A. and Short, M.D. 2020. The application of life cycle assessment (LCA) to wastewater treatment: A best practice guide and critical review. Water Research 184, 116058.

Crenna, Eleonora, et al. "Global Environmental Impacts: Data Sources and Methodological Choices for Calculating Normalization Factors for LCA." International Journal of Life Cycle Assessment, vol. 24, no. 10, Springer Verlag, Oct. 2019, pp. 1851–77, doi:10.1007/S11367-019-01604-Y/FIGURES/1.

Crone, B.C., Speth, T.F., Wahman, D.G., Smith, S.J., Abulikemu, G., Kleiner, E.J. and Pressman, J.G. 2019. Occurrence of per- and polyfluoroalkyl substances (PFAS) in source water and their treatment in drinking water. Critical Reviews in Environmental Science and Technology 49(24), 2359-2396.

Curzons, A. D., Constable, D. C., & Cunningham, V. L. (1999). Solvent selection guide: a guide to the integration of environmental, health and safety criteria into the selection of solvents. Clean Technologies and Environmental Policy, 1(2), 82-90. https://doi.org/10.1007/s100980050014

D'Agostino, Lisa A.; Mabury, Scott A., Identification of novel fluorinated surfactants in aqueous film forming foams and commercial surfactant concentrates. Environmental Science & Technology 2014, 48, (1), 121-129.

D'eon, Jessica C.; Mabury, Scott A., Exploring indirect sources of human exposure to perfluoroalkyl carboxylates (pfcas): Evaluating uptake, elimination, and biotransformation of polyfluoroalkyl phosphate esters (paps) in the rat. Environmental Health Perspectives 2011, 119, (3), 344-350.

da Silva, W. L., Lansarin, M. A., Livotto, P. R., & dos Santos, J. H. Z. (2015). Photocatalytic degradation of drugs by supported titania-based catalysts produced from petrochemical plant residue. Powder Technology, 279, 166-172. https://doi.org/https://doi.org/10.1016/j.powtec.2015.03.045

Davis, J.; J.C. Baygents, and J. Farrell, Understanding persulfate production at boron doped diamond film anodes. Electrochimica Acta, 2014, 150, 68-74.

del Moral, L., Choi, Y., & Boyer, T. (2020). Comparative removal of Suwannee River natural organic matter and perfluoroalkyl acids by anion exchange: Impact of polymer composition and mobile counterion. Water research, 178, 115846. https://doi.org/10.1016/j.watres.2020.115846

Deng, J.; Shao, Y.; Gao, N.; Xia, S.; Tan, C.; Zhou, S.; Hu, X., Degradation of the antiepileptic drug carbamazepine upon different uv-based advanced oxidation processes in water. Chemical Engineering Journal 2013, 222, 150-158.

Deng, S. B.; Yu, Q. A.; Huang, J.; Yu, G., Removal of perfluorooctane sulfonate from wastewater by anion exchange resins: Effects of resin properties and solution chemistry. Water Research 2010, 44, (18), 5188-5195.

De Santis, R., Marrelli, L., & Muscetta, P.N. (1976). Liquid—liquid equilibria in water—aliphatic alcohol systems in the presence of sodium chloride. The Chemical Engineering Journal, 11(3), 207–214.

D'Eon, Jessica C.; Mabury, Scott A., Production of perfluorinated carboxylic acids (pfcas) from the biotransformation of polyfluoroalkyl phosphate surfactants (paps): Exploring routes of human contamination. Environmental Science & Technology 2007, 41, (13), 4799-4805.

Dietz, R., Kassar, C., & Boyer, T. H. (2021). Regeneration efficiency of strong-base anion exchange resin for perfluoroalkyl and polyfluoroalkyl substances. AWWA Water Science, 3(6), e1259. https://doi.org/https://doi.org/10.1002/aws2.1259

Ding, G.; Peijnenburg, W. J. G. M., Physicochemical properties and aquatic toxicity of poly- and perfluorinated compounds. Critical Reviews in Environmental Science and Technology 2013, 43, (6), 598-678.

Dixit, F., Dutta, R., Barbeau, B., Berube, P., & Mohseni, M. (2021a). PFAS removal by ion exchange resins: A review. Chemosphere, 272, 129777.

Dixit, F., Barbeau, B., Mostafavi, S.G., & Mohseni, M. (2021b). PFAS and DOM removal using an organic scavenger and PFAS-specific resin: Trade-off between regeneration and faster kinetics. Science of The Total Environment, 754, 142107.

Dixit, F., Barbeau, B. and Mohseni, M. 2018. Characteristics of competitive uptake between Microcystin-LR and natural organic matter (NOM) fractions using strongly basic anion exchange resins. Water Res. 139, 74-82.

Dixit, F., Barbeau, B., Mostafavi, S. G., & Mohseni, M. (2020). Removal of legacy PFAS and other fluorotelomers: Optimized regeneration strategies in DOM-rich waters. Water research, 183, 116098. https://doi.org/https://doi.org/10.1016/j.watres.2020.116098

Dixit, F., Barbeau, B., Mostafavi, S.G. and Mohseni, M. 2019. PFOA and PFOS removal by ion exchange for water reuse and drinking applications: role of organic matter characteristics. Environmental Science: Water Research & Technology 5(10), 1782-1795.

Dixit, F., Barbeau, B., Mostafavi, S.G. and Mohseni, M. 2020. Efficient removal of GenX (HFPO-DA) and other perfluorinated ether acids from drinking and recycled waters using anion exchange resins. Journal of Hazardous Materials 384, 121261.

Dixit, F., Barbeau, B., Mostafavi, S.G. and Mohseni, M. 2021. PFAS and DOM removal using an organic scavenger and PFAS-specific resin: Trade-off between regeneration and faster kinetics. Science of The Total Environment 754, 142107.

Dixit, F., Barbeau, B., Mostafavi, S.G., & Mohseni, M. (2020). Efficient removal of GenX (HFPO-DA) and other perfluorinated ether acids from drinking and recycled waters using anion exchange resins. Journal of Hazardous Materials, 384,121261. https://doi.org/10.1016/j.jhazmat.2019.121261

Dixit, F., Barbeau, B., Mostafavi, S.G., & Mohseni, M. (2021a). PFAS and DOM removal using an organic scavenger and PFAS-specific resin: Trade-off between regeneration and faster kinetics. Science of The Total Environment, 754, 142107. https://doi.org/10.1016/j.scitotenv.2020.142107

Dixit, F., Dutta, R., Barbeau, B., Berube, P., & Mohseni, M. (2021b). PFAS removal by Ion Exchange Resins: A Review. Chemosphere, 272, 129777. https://doi.org/10.1016/j.chemosphere.2021.129777

Domingo, J.L. and Nadal, M. 2019. Human exposure to per- and polyfluoroalkyl substances (PFAS) through drinking water: A review of the recent scientific literature. Environmental Research 177, 108648.

Drennan, D.M.; R.E. Koshy, D.B. Gent, and C.E. Schaefer, Electrochemical treatment for greywater reuse: effects of cell configuration on COD reduction and disinfection byproduct formation and removal. Water Supply, 2019, 19, 891-898.

Dron, J. and Dodi, A. 2011a. Comparison of adsorption equilibrium models for the study of CL−, NO3− and SO42− removal from aqueous solutions by an anion exchange resin. Journal of Hazardous Materials 190(1), 300-307.

Dron, J. and Dodi, A. 2011b. Thermodynamic Modeling of Cl−, NO3− and SO42− Removal by an Anion Exchange Resin and Comparison with Dubinin−Astakhov Isotherms. Langmuir 27(6), 2625-2633.

Du, Z., Deng, S., Bei, Y., Huang, Q., Wang, B., Huang, J., & Yu, G. (2014). Adsorption behavior and mechanism of perfluorinated compounds on various adsorbents—a review. Journal of Hazardous Materials, 274, 443–454. https://doi.org/10.1016/j.jhazmat.2014.04.038

Du, Z., Deng, S., Chen, Y., Wang, B., Huang, J., Wang, Y. and Yu, G. 2015. Removal of perfluorinated carboxylates from washing wastewater of perfluorooctanesulfonyl fluoride using activated carbons and resins. Journal of Hazardous Materials 286, 136-143.

Du, Ziwen; Deng, Shubo; Bei, Yue; Huang, Qian; Wang, Bin; Huang, Jun; Yu, Gang, Adsorption behavior and mechanism of perfluorinated compounds on various adsorbents—a review. Journal of Hazardous Materials 2014, 274, 443-454.

Du, Ziwen; Deng, Shubo; Chen, Youguang; Wang, Bin; Huang, Jun; Wang, Yujue; Yu, Gang, Removal of perfluorinated carboxylates from washing wastewater of perfluorooctanesulfonyl fluoride using activated carbons and resins. Journal of Hazardous Materials 2015, 286, 136-143.

Dubois, M. A., Dozol, J. F., Nicotra, C., Serose, J., & Massiani, C. (1995). Pyrolysis and incineration of cationic and anionic ion-exchange resins — Identification of volatile degradation compounds. Journal of Analytical and Applied Pyrolysis, 31, 129-140. https://doi.org/https://doi.org/10.1016/0165-2370(94)00817-K

Dudley, L.-A. 2012. Removal of Perfluorinated Compounds by Powdered Activated Carbon, Superfine Powder Activated Carbon, and Anion Exchange Resin.

Edebali, S. and Pehlivan, E. 2010. Evaluation of Amberlite IRA96 and Dowex 1×8 ion-exchange resins for the removal of Cr(VI) from aqueous solution. Chemical Engineering Journal 161(1), 161-166.

Edgar, M. and Boyer, T.H. 2021. Removal of natural organic matter by ion exchange: Comparing regenerated and non-regenerated columns. Water Research 189, 116661.

Edwards, M. and Triantafyllidou, S. 2007. Chloride-to-sulfate mass ratio and lead leaching to water. J. Am. Water Work Assoc. 99(7), 96-109.

Ellis, Anderson C., et al. "Pilot Study Comparison of Regenerable and Emerging Single-Use Anion Exchange Resins for Treatment of Groundwater Contaminated by per- and Polyfluoroalkyl Substances (PFASs)." Water Research, vol. 223, Pergamon, Sept. 2022, p. 119019, doi:10.1016/J.WATRES.2022.119019.

A.C. Ellis, T.H. Boyer, Y. Fang, C.J. Liu, and T.J. Strathmann. (2023). Life cycle assessment and life cycle cost analysis of anion exchange and granular activated carbon systems for remediation of groundwater contaminated by per- and polyfluoroalkyl substances (PFAS). Manuscript in review.

Emery, Isaac, et al. "Evaluation of Treatment Options for Well Water Contaminated with Perfluorinated Alkyl Substances Using Life Cycle Assessment." International Journal of Life Cycle Assessment, vol. 24, no. 1, Springer Verlag, Jan. 2019, pp. 117–28, doi:10.1007/S11367-018-1499-8/FIGURES/5.

Environmental Protection Agency. (2023). Proposed PFAS National Drinking Water Regulation. https://www.epa.gov/sdwa/and-polyfluoroalkyl-substances-pfas

Environmental Protection Agency. (2022). Drinking Water Treatment Technology Unit Cost Models and Work Breakdown Structure (WBS). Https://Www.Epa.Gov/Sdwa/Drinking-Water-Treatment-Technology-Unit-Cost-Models.

Fang, Y., Ellis, A.C., Choi, Y.J., Boyer, T.H., Higgins, C.P., Schaefer, C.E., & Strathmann, T.J. (2021). Removal of per- and polyfluoroalkyl substances (PFASs) in aqueous film-forming foam (AFFF) using ion-exchange and nonionic resins. Environmental Science & Technology, 55(8), 5001–5011. https://doi.org/10.1021/acs.est.1c00769.

Fang, Y., Meng, P., Schaefer, C., & Knappe, D.R.U. (2023). Removal and destruction of perfluoroalkyl ether carboxylic acids (PFECAs) in an anion exchange resin and electrochemical oxidation treatment train. Water Research, 230, 119522.

Y. Fang, P. Meng, C. Schaefer, D. Knappe. (2023). Removal and destruction of perfluoroalkyl ether carboxylic acids (PFECAs) in an anion exchange resin and electrochemical oxidation treatment train. *Water Research*, 230, 119522. https://doi.org/10.1016/j.watres.2022.119522

Farhat, A., Keller, J., Tait, S. and Radjenovic, J. 2015. Removal of Persistent Organic Contaminants by Electrochemically Activated Sulfate. Environmental Science & Technology 49(24), 14326-14333.

Feng, Danyi, et al. "Environmental, Human Health, and Economic Implications of Landfill Leachate Treatment for per- and Polyfluoroalkyl Substance Removal." Journal of Environmental Management, vol. 289, Academic Press, July 2021, p. 112558, doi:10.1016/J.JENVMAN.2021.112558.

Fenton, Suzanne E., et al. "Per- and Polyfluoroalkyl Substance Toxicity and Human Health Review: Current State of Knowledge and Strategies for Informing Future Research." Environmental Toxicology and Chemistry, vol. 40, no. 3, John Wiley & Sons, Ltd, Mar. 2021, pp. 606–30, doi:10.1002/ETC.4890.

Ferrari, A.C.G., Corazza, M.L., & Voll, F.A.P. (2023). Modeling and experimental measurement of NaBr solubility in water, methanol, ethanol, 1-propanol, and its mixtures at different temperatures. Digital Chemical Engineering, 6, 100067.

Finkbeiner, P., Moore, G., Pereira, R., Jefferson, B. and Jarvis, P. 2020. The combined influence of hydrophobicity, charge and molecular weight on natural organic matter removal by ion exchange and coagulation. Chemosphere 238, 124633.

Foo, K.Y. and Hameed, B.H. 2010. Insights into the modeling of adsorption isotherm systems. Chemical Engineering Journal 156(1), 2-10.

Franke, V., McCleaf, P., Lindegren, K. and Ahrens, L. 2019. Efficient removal of per- and polyfluoroalkyl substances (PFASs) in drinking water treatment: nanofiltration combined with active carbon or anion exchange. Environmental Science: Water Research & Technology 5(11), 1836-1843.

Franke, Vera, et al. "The Price of Really Clean Water: Combining Nanofiltration with Granular Activated Carbon and Anion Exchange Resins for the Removal of Per- And Polyfluoralkyl Substances (PFASs) in Drinking Water Production." ACS ES&T Water, vol. 1, no. 4, American Chemical Society, Apr. 2021, pp. 782–95, doi:10.1021/ACSESTWATER.0C00141.

Gabarrón, S., Gernjak, W., Valero, F., Barceló, A., Petrovic, M., & Rodríguez-Roda, I. (2016). Evaluation of emerging contaminants in a drinking water treatment plant using electrodialysis reversal technology. Journal of Hazardous Materials, 309, 192-201. https://doi.org/https://doi.org/10.1016/j.jhazmat.2016.02.015

Gagliano, E., Sgroi, M., Falciglia, P. P., Vagliasindi, F. G. A., & Roccaro, P. (2020). Removal of poly- and perfluoroalkyl substances (PFAS) from water by adsorption: Role of PFAS chain length, effect of organic matter and challenges in adsorbent regeneration. Water research, 171, 115381. https://doi.org/https://doi.org/10.1016/j.watres.2019.115381

Gao, Y., Deng, S., Du, Z., Liu, K. and Yu, G. 2017. Adsorptive removal of emerging polyfluoroalky substances F-53B and PFOS by anion-exchange resin: A comparative study. Journal of Hazardous Materials 323, 550-557.

Gar Alalm, Mohamed, and Daria Camilla Boffito. "Mechanisms and Pathways of PFAS Degradation by Advanced Oxidation and Reduction Processes: A Critical Review." Chemical Engineering Journal, vol. 450, Elsevier, Dec. 2022, p. 138352, doi:10.1016/J.CEJ.2022.138352.

Giles, Spencer L.; Snow, Arthur W.; Hinnant, Katherine M.; Ananth, Ramagopal, Modulation of fluorocarbon surfactant diffusion with diethylene glycol butyl ether for improved foam characteristics and fire suppression. Colloids and Surfaces A: Physicochemical and Engineering Aspects 2019, 579, 123660.

Gobelius, L., Lewis, J., & Ahrens, L. (2017). Plant uptake of per- and polyfluoroalkyl substances at a contaminated fire training facility to evaluate the phytoremediation potential of various plant species. Environmental Science & Technology, 51(21), 12602–12610. https://doi.org/10.1021/acs.est.7b02926

Gomez-Ruiz, B.; S. G´omez-Lavín, N. Diban, V. Boiteux, A. Colin, X., Dauchy, and A. Urtiaga, Efficient electrochemical degradation of poly- and perfluoroalkyl substances (PFASs) from the effluents of an industrial wastewater treatment plant. Chem. Eng. J. 2017, 322, 196–204.

Goode, D.J., & Senior, L.A. (2020). Groundwater withdrawals and regional flow paths at and near Willow Grove and Warminster, Pennsylvania—data compilation and preliminary simulations for conditions in 1999, 2010, 2013, 2016, and 2017. Open-File Report. https://doi.org/10.3133/ofr20191137

Graf, K.C., Cornwell, D.A. and Boyer, T.H. 2014. Removal of dissolved organic carbon from surface water by anion exchange and adsorption: Bench-scale testing to simulate a two-stage countercurrent process. Sep. Purif. Technol. 122, 523-532.

Greluk, M. and Hubicki, Z. 2010. Kinetics, isotherm and thermodynamic studies of Reactive Black 5 removal by acid acrylic resins. Chemical Engineering Journal 162(3), 919-926.

Greluk, M. and Hubicki, Z. 2011. Comparison of the gel anion exchangers for removal of Acid Orange 7 from aqueous solution. Chemical Engineering Journal 170(1), 184-193.

Grieco, S.A., Chang, J., Maio, E.Y., & Hwang, M. (2021). Comparing conventional and emerging adsorbents for per- and polyfluoroalkyl substances: Kinetic, equilibrium, and column experiments. AWWA Water Science, 3(6). https://doi.org/10.1002/aws2.1256

Gu, B., Brown, G. M., Maya, L., Lance, M. J., & Moyer, B. A. (2001). Regeneration of Perchlorate (ClO4-)-Loaded Anion Exchange Resins by a Novel Tetrachloroferrate (FeCl4-) Displacement Technique. Environmental Science & Technology, 35(16), 3363-3368. https://doi.org/10.1021/es010604i

Gu, B., Brown, G.M., Bonnesen, P.V., Liang, L., Moyer, B.A., Ober, R. and Alexandratos, S.D. 2000. Development of Novel Bifunctional Anion-Exchange Resins with Improved Selectivity for Pertechnetate Sorption from Contaminated Groundwater. Environmental Science & Technology 34(6), 1075-1080.

Gu, B., Ku, Y.K., & Jardine, P.M. (2004). Sorption and binary exchange of nitrate, sulfate, and uranium on an anion-exchange resin. Environmental Science and Technology, 38(11), 3184–3188.

Gu, B., Ku, Y.-K. and Brown, G.M. 2005. Sorption and Desorption of Perchlorate and U(VI) by Strong-Base Anion-Exchange Resins. Environmental Science & Technology 39(3), 901-907.

Guelfo, Jennifer L.; Higgins, Christopher P., Subsurface transport potential of perfluoroalkyl acids at aqueous film-forming foam (afff)-impacted sites. Environmental Science & Technology 2013, 47, (9), 4164-4171.

Gustafson, R., Fillius, H. and Kunin, R. 1970. Basicities of weak base ion exchange resins. Industrial & Engineering Chemistry Fundamentals 9(2), 221-229.

Gustafson, R.L. and Lirio, J.A. 1968. Adsorption of organic ions by anion exchange resins. Industrial & Engineering Chemistry Product Research and Development 7(2), 116-120.

Harding-Marjanovic, Katie C.; Houtz, Erika F.; Yi, Shan; Field, Jennifer A.; Sedlak, David L.; Alvarez-Cohen, Lisa, Aerobic biotransformation of fluorotelomer thioether amido sulfonate (lodyne) in afff-amended microcosms. Environmental Science & Technology 2015, 49, (13), 7666-7674.

S. Hao, Y.J. Choi, B. Wu, C. Higgins, R. Deeb, and T.J. Strathmann. (2021). Hydrothermal alkaline treatment for destruction of per- and polyfluoroalkyl substances (PFASs) in aqueous film-forming foam (AFFF). Environmental Science & Technology. 55, 3283-3295.

Harland, C.E. (1994) Ion exchange: theory and practice, Royal society of Chemistry.

Hatton, J., Holton, C., & DiGuiseppi, B. (2018). Occurrence and behavior of per- and polyfluoroalkyl substances from aqueous film-forming foam in groundwater systems. Remediation Journal, 28(2), 89–99.

Haupert, L. M., Pressman, J. G., Speth, T. F., & Wahman, D. G. (2021). Avoiding pitfalls when modeling removal of per- and polyfluoroalkyl substances by anion exchange. AWWA Water Science, 3(2). https://doi.org/10.1002/aws2.1222

Hekmatzadeh, A.A., Karimi-Jashani, A., Talebbeydokhti, N. and Kløve, B. 2012. Modeling of nitrate removal for ion exchange resin in batch and fixed bed experiments. Desalination 284, 22-31.

Helfferich, F.G. (1995) Ion exchange, Courier Corporation.

Higgins, Christopher P.; Luthy, Richard G., Sorption of perfluorinated surfactants on sediments. Environmental Science & Technology 2006, 40, (23), 7251-7256.

Hinrichs, R.L. and Snoeyink, V.L. 1976. Sorption of benzenesulfonates by weak base anion exchange resins. Water Research 10(1), 79-87.

Hodgkins, L. M.; Mulligan, R. P.; McCallum, J. M.; Weber, K. P., Modelling the transport of shipborne per- and polyfluoroalkyl substances (pfas) in the coastal environment. Science of The Total Environment 2019, 658, 602-613.

Höll, W. and Kirch, R. 1978. Regeneration of weak base ion exchange resins. Desalination 26(2), 153-162.

Holmquist, H., Fantke, P., Cousins, I.T., Owsianiak, M., Liagkouridis, I. and Peters, G.M. 2020. An (Eco)Toxicity Life Cycle Impact Assessment Framework for Per- And Polyfluoroalkyl Substances. Environmental Science & Technology 54(10), 6224-6234.

Holmquist, Hanna, Sandra Roos, et al. "What Difference Can Drop-in Substitution Actually Make? A Life Cycle Assessment of Alternative Water Repellent Chemicals." Journal of Cleaner Production, vol. 329, Elsevier, Dec. 2021, p. 129661, doi:10.1016/J.JCLEPRO.2021.129661.

Hori, Hisao; Nagaoka, Yumiko; Sano, Taizo; Kutsuna, Shuzo, Iron-induced decomposition of perfluorohexanesulfonate in sub- and supercritical water. Chemosphere 2008, 70, (5), 800-806.

Hori, Hisao; Nagaoka, Yumiko; Yamamoto, Ari; Sano, Taizo; Yamashita, Nobuyoshi; Taniyasu, Sachi; Kutsuna, Shuzo; Osaka, Issey; Arakawa, Ryuichi, Efficient decomposition of environmentally persistent perfluorooctanesulfonate and related fluorochemicals using zerovalent iron in subcritical water. Environmental Science & Technology 2006, 40, (3), 1049-1054.

Houde, Magali; Martin, Jonathan W.; Letcher, Robert J.; Solomon, Keith R.; Muir, Derek C. G., Biological monitoring of polyfluoroalkyl substances: A review. Environmental Science & Technology 2006, 40, (11), 3463-3473.

Houtz, Erika F.; Higgins, Christopher P.; Field, Jennifer A.; Sedlak, David L., Persistence of perfluoroalkyl acid precursors in afff-impacted groundwater and soil. Environmental Science & Technology 2013, 47, (15), 8187-8195.

Howe, K.J., Hand, D.W., Crittenden, J.C., Trussell, R.R. and Tchobanoglous, G. (2012) Principles of water treatment, John Wiley & Sons.

Hu, X.C., Andrews, D.Q., Lindstrom, A.B., Bruton, T.A., Schaider, L.A., Grandjean, P., Lohmann, R., Carignan, C.C., Blum, A., Balan, S.A., Higgins, C.P., & Sunderland, E.M. (2016). Detection of poly- and perfluoroalkyl substances (PFASs) in U.S. drinking water linked to industrial sites, military fire training areas, and wastewater treatment plants. Environmental Science & Technology Letters, 3(10), 344–350. https://doi.org/10.1021/acs.estlett.6b00260

Hu, Y., Foster, J., & Boyer, T. H. (2016). Selectivity of bicarbonate-form anion exchange for drinking water contaminants: Influence of resin properties. Separation and Purification Technology, 163, 128-139. https://doi.org/https://doi.org/10.1016/j.seppur.2016.02.030

Huang, Shan; Jaffé, Peter R., Defluorination of perfluorooctanoic acid (pfoa) and perfluorooctane sulfonate (pfos) by acidimicrobium sp. Strain a6. Environmental Science & Technology 2019, 53, (19), 11410-11419.

Humbert, H., Gallard, H., Suty, H. and Croue, J.P. 2005. Performance of selected anion exchange resins for the treatment of a high DOC content surface water. Water Research 39(9), 1699-1708.

Humbert, H., Gallard, H., Suty, H. and Croue, J.P. 2008. Natural organic matter (NOM) and pesticides removal using a combination of ion exchange resin and powdered activated carbon (PAC). Water Res. 42(6-7), 1635-1643.

Interstate Technology & Regulatory Council (ITRC), (2021) PFAS - Per- and Polyfluoroalkyl Substances: 2.2 Chemistry, Terminology, and Acronyms [website], https://pfas-1.itrcweb.org/2-2-chemistry-terminology-and-acronyms/, accessed 05/21/2021.

Interstate Technology & Regulatory Council (ITRC), PFAS technical and regulatory guidance document and fact sheets PFAS-1. Washington, D.C.: Interstate Technology and Regulatory Council, PFAS team. Hiips://pfas-1.itrcweb.org/.

Jackson, M.B. and Bolto, B.A. 1990. Effect of ion-exchange resin structure on nitrate selectivity. Reactive Polymers 12(3), 277-290.

Jamil, S., Loganathan, P., Kandasamy, J., Listowski, A., Khourshed, C., Naidu, R., & Vigneswaran, S. (2019). Removal of dissolved organic matter fractions from reverse osmosis concentrate: Comparing granular activated carbon and ion exchange resin adsorbents. Journal of Environmental Chemical Engineering, 7(3), 103126. https://doi.org/https://doi.org/10.1016/j.jece.2019.103126

Janousek, Raphael M., et al. “Is the Phase-out of Long-Chain PFASs Measurable as Fingerprint in a Defined Area? Comparison of Global PFAS Concentrations and a Monitoring Study Performed in Hesse, Germany from 2014 to 2018.” TrAC Trends in Analytical Chemistry, vol. 120, Elsevier, Nov. 2019, p. 115393, doi:10.1016/J.TRAC.2019.01.017.

Jawando, W., Gayen, P. and Chaplin, B.P. 2015. The effects of surface oxidation and fluorination of boron-doped diamond anodes on perchlorate formation and organic compound oxidation. Electrochimica Acta 174, 1067-1078.

Jensen, V.B. and Darby, J.L. 2016. Brine Disposal Options for Small Systems in California's Central Valley. Journal AWWA 108(5), E276-E289.

Kanazawa, N., Urano, K., Kokado, N. and Urushigawa, Y. 2004. Exchange characteristics of monocarboxylic acids and monosulfonic acids onto anion-exchange resins. Journal of Colloid and Interface Science 271(1), 20-27.

Kärrman, A., Elgh-Dalgren, K., Lafossas, C. and Møskeland, T. 2011. Environmental levels and distribution of structural isomers of perfluoroalkyl acids after aqueous fire-fighting foam (AFFF) contamination. Environmental Chemistry 8(4), 372-380.

C. Kassar, C. Graham, and T.H. Boyer. (2022). Removal of perfluoroalkyl acids and common drinking water contaminants by weak-base anion exchange resins: Impacts of solution pH and resin properties. *Water Research X*, 17, 100159. https://doi.org/10.1016/j.wroa.2022.100159

C. Kassar and T.H. Boyer. (2023). Removal of PFAS from groundwater using weak-base anion exchange resins. AWWA Water Science, e1325. https://doi.org/10.1002/aws2.1325.

Kassar, C. (2022). Removal of Perfluoroalkyl Acids and Common Drinking Water Contaminants by Weak-Base Anion Exchange Resins (Publication Number 29164080) [M.S., Arizona State University].

Khan, M.Y., So, S. and da Silva, G. 2020. Decomposition kinetics of perfluorinated sulfonic acids. Chemosphere 238, 124615.

Kołodyńska, D. 2009. Polyacrylate anion exchangers in sorption of heavy metal ions with the biodegradable complexing agent. Chemical Engineering Journal 150(2), 280-288.

Kołodyńska, D. 2010. Cu(II), Zn(II), Ni(II), and Cd(II) Complexes with HEDP Removal from Industrial Effluents on Different Ion Exchangers. Industrial & Engineering Chemistry Research 49(5), 2388-2400.

Kotthoff, M., Müller, J., Jürling, H., Schlummer, M., & Fiedler, D. (2015). Perfluoroalkyl and polyfluoroalkyl substances in consumer products. Environmental Science and Pollution Research, 22(19), 14546–14559.

Kong, Zong Yang, et al. "Energy-Efficient Hybrid Reactive-Extractive Distillation with a Preconcentration Column for Recovering Isopropyl Alcohol and Diisopropyl Ether from Wastewater: Process Design, Optimization, and Intensification." Industrial and Engineering Chemistry Research, vol. 61, no. 30, American Chemical Society, Aug. 2022, pp. 11156–67, doi:10.1021/ACS.IECR.2C01768/ASSET/IMAGES/LARGE/IE2C01768_0008.JPEG.

Kortüm, G., Vogel, W. and Andrussow, K. 1960. Disssociation constants of organic acids in aqueous solution. Pure and Applied Chemistry 1(2-3), 187-536.

Kothawala, D.N., Köhler, S.J., Östlund, A., Wiberg, K. and Ahrens, L. 2017. Influence of dissolved organic matter concentration and composition on the removal efficiency of perfluoroalkyl substances (PFASs) during drinking water treatment. Water Res. 121, 320-328.

Krause, M.J., Thoma, E., Sahle-Damesessie, E., Crone, B., Whitehill, A., Shields, E., & Gullett, B. (2021). Supercritical Water Oxidation as an Innovative Technology for PFAS Destruction. Journal of Environmental Engineering, 148(2), 05021006.

Kucharzyk, K.H., Darlington, R., Benotti, M., Deeb, R. and Hawley, E. 2017. Novel treatment technologies for PFAS compounds: A critical review. Journal of Environmental Management 204, 757-764.

Kucharzyk, K.H., Darlington, R., Benotti, M., Deeb, R., & Hawley, E. (2017). Novel treatment technologies for PFAS compounds: A critical review. Journal of Environmental Management, 204, 757–764. https://doi.org/10.1016/j.jenvman.2017.08.016

Kumar, K.V. and Sivanesan, S. 2005. Comparison of linear and non-linear method in estimating the sorption isotherm parameters for safranin onto activated carbon. Journal of Hazardous Materials 123(1), 288-292.

Kuo, Yu Mei, et al. "Filtration and Loading Characteristics of Granular Bed Filters." Journal of Aerosol Science, vol. 41, no. 2, Pergamon, Feb. 2010, pp. 223–29, doi:10.1016/J.JAEROSCI.2009.09.011.

Kwon, Bum Gun; Lim, Hye-Jung; Na, Suk-Hyun; Choi, Bong-In; Shin, Dong-Soo; Chung, Seon-Yong, Biodegradation of perfluorooctanesulfonate (pfos) as an emerging contaminant. Chemosphere 2014, 109, 221-225.

Lampert, D.J., Frisch, M.A. and Speitel, G.E. 2007. Removal of Perfluorooctanoic Acid and Perfluorooctane Sulfonate from Wastewater by Ion Exchange. Practice Periodical of Hazardous, Toxic, and Radioactive Waste Management 11(1), 60-68.

Landry, K. A., & Boyer, T. H. (2013). Diclofenac removal in urine using strong-base anion exchange polymer resins. Water Res, 47(17), 6432-6444. https://doi.org/10.1016/j.watres.2013.08.015

Landry, K. A., Sun, P., Huang, C. H., & Boyer, T. H. (2015). Ion-exchange selectivity of diclofenac, ibuprofen, ketoprofen, and naproxen in ureolyzed human urine. Water Res, 68, 510-521. https://doi.org/10.1016/j.watres.2014.09.056

Lath, S., Knight, E.R., Navarro, D.A., Kookana, R.S. and McLaughlin, M.J. 2019. Sorption of PFOA onto different laboratory materials: Filter membranes and centrifuge tubes. Chemosphere 222, 671-678.

Lau, C., Anitole, K., Hodes, C., Lai, D., Pfahles-Hutchens, A., & Seed, J. (2007). Perfluoroalkyl Acids: A Review of Monitoring and Toxicological Findings. Toxicological Sciences, 99(2), 366-394. https://doi.org/10.1093/toxsci/kfm128

Laura del Moral, L., Choi, Y.J., & Boyer, T.H. (2020). Comparative removal of Suwannee River natural organic matter and perfluoroalkyl acids by anion exchange: Impact of polymer composition and mobile counterion. Water Research, 178, 115846. https://doi.org/10.1016/j.watres.2020.115846

Le, T.X.H.; H. Haflich, A.D. Shah, and B.P. Chaplin, Energy-Efficient Electrochemical Oxidation of Perfluoroalkyl Substances Using a Ti4O7 Reactive Electrochemical Membrane Anode. Environ. Sci. Technol. Letters, 2019, 6, 504-510.

Leeson, A., Thompson, T., Stroo, H.F., Anderson, R.H., Speicher, J., Mills, M.A., Willey, J., Coyle, C., Ghosh, R., Lebrón, C., & Patton, C. (2020). Identifying and managing aqueous film-forming foam-derived per- and polyfluoroalkyl substances in the environment. Environmental Toxicology and Chemistry, 40(1), 24–36. https://doi.org/https://doi.org/10.1002/etc.4894

Levchuk, I., Rueda Márquez, J.J. and Sillanpää, M. 2018. Removal of natural organic matter (NOM) from water by ion exchange – A review. Chemosphere 192, 90-104.

Lewis, R. C., Johns, L. E., & Meeker, J. D. (2015). Serum Biomarkers of Exposure to Perfluoroalkyl Substances in Relation to Serum Testosterone and Measures of Thyroid Function among Adults and Adolescents from NHANES 2011-2012. International Journal of

Environmental Research and Public Health, 12(6), 6098-6114. https://doi.org/10.3390/ijerph120606098

Li, F., Duan, J., Tian, S., Ji, H., Zhu, Y., Wei, Z. and Zhao, D. 2020. Short-chain per- and polyfluoroalkyl substances in aquatic systems: Occurrence, impacts and treatment. Chemical Engineering Journal 380, 122506.

Li, Gengyang, et al. "Environmental Life Cycle Assessment (LCA) of Treating PFASs with Ion Exchange and Electrochemical Oxidation Technology." ACS ES and T Water, vol. 2, no. 9, American Chemical Society, Sept. 2022, pp. 1555–64, doi:10.1021/ACSESTWATER.2C00196/ASSET/IMAGES/LARGE/EW2C00196_0010.JPEG.

Li, P. and Sengupta, A.K. 1998. Genesis of selectivity and reversibility for sorption of synthetic aromatic anions onto polymeric sorbents. Environmental Science & Technology 32(23), 3756-3766.

Li, P. and SenGupta, A.K. 2000. Intraparticle diffusion during selective ion exchange with a macroporous exchanger. Reactive and Functional Polymers 44(3), 273-287.

Li, P., & SenGupta, A. K. (2001). Entropy-driven selective ion exchange for aromatic ions and the role of cosolvents. Colloids and Surfaces A: Physicochemical and Engineering Aspects, 191(1), 123-132. https://doi.org/https://doi.org/10.1016/S0927-7757(01)00769-5

Li, P., & SenGupta, A. K. (2004). Sorption of hydrophobic ionizable organic compounds (HIOCs) onto polymeric ion exchangers. Reactive and Functional Polymers, 60, 27-39. https://doi.org/https://doi.org/10.1016/j.reactfunctpolym.2004.02.008

Liang, S.; R.D. Pierce Jr, H. Lin, S.Y. Chiang, and Q.J. Huang, Electrochemical oxidation of PFOA and PFOS in concentrated waste streams. Remediation J., 2018, 28, 127-134.

Liang, S., Mora, R., Huang, Q., Casson, R., Wang, Y., Woodard, S., & Anderson, H. (2022). Field demonstration of coupling ion-exchange resin with electrochemical oxidation for enhanced treatment of per- and polyfluoroalkyl substances (PFAS) in groundwater. Chemical Engineering Journal Advances, 9, 100216.

Lin, A.Y.-C., Panchangam, S.C. and Lo, C.-C. 2009. The impact of semiconductor, electronics and optoelectronic industries on downstream perfluorinated chemical contamination in Taiwanese rivers. Environmental Pollution 157(4), 1365-1372.

Lin, H.; J. Niu, S. Liang, C. Wang, Y. Wang, F. Jin, Q. Luo, and Q. Huang, Development of macroporous Magneli phase Ti4O7 ceramic materials: As an efficient anode for mineralization of poly-and perfluoroalkyl substances. Chemical Engin. J. 2018, 354, 1058-1067.

Liu, C.J., Murray, C.C., Marshall, E., Strathmann, T.J., Bellona, C. Removal of per- and polyfluoroalkyl substances from contaminated groundwater by granular activated carbon and anion exchange resins: A pilot-scale comparative assessment. Manuscript in review, Environmental Science: Water Research & Technology.

Liu, C.J., Werner, D., & Bellona, C. (2019). Removal of per- and polyfluoroalkyl substances (PFASs) from contaminated groundwater using granular activated carbon: A pilot-scale study with Breakthrough Modeling. Environmental Science: Water Research & Technology, 5(11), 1844–1853. https://doi.org/10.1039/c9ew00349e

Liu, Charlie J., et al. "Removal of Per- and Polyfluoroalkyl Substances (PFASs) from Contaminated Groundwater Using Granular Activated Carbon: A Pilot-Scale Study with Breakthrough Modeling." Environmental Science: Water Research & Technology, vol. 5, no. 11, The Royal Society of Chemistry, Oct. 2019, pp. 1844–53, doi:10.1039/C9EW00349E.

Liu, G., et al. "A Comparison of Additional Treatment Processes to Limit Particle Accumulation and Microbial Growth during Drinking Water Distribution." Water Research, vol. 47, no. 8, Pergamon, May 2013, pp. 2719–28, doi:10.1016/J.WATRES.2013.02.035.

Liu, Y.-L. and Sun, M. 2021. Ion exchange removal and resin regeneration to treat per- and polyfluoroalkyl ether acids and other emerging PFAS in drinking water. Water Research 207, 117781.

Liu, Y.-L., & Sun, M. (2021). Ion exchange removal and resin regeneration to treat per- and polyfluoroalkyl ether acids and other emerging PFAS in drinking water. Water research, 207, 117781. https://doi.org/https://doi.org/10.1016/j.watres.2021.117781

Long, Yuyang, et al. "Effect of Fe2O3 on the Leaching Behavior of Cr in Hazardous Waste Incineration Fly Ash after Thermal Treatment." Environmental Technology & Innovation, vol. 24, Elsevier, Nov. 2021, p. 102072, doi:10.1016/J.ETI.2021.102072.

Loos, R.; Locoro, G.; Comero, S.; Contini, S.; Schwesig, D.; Werres, F.; Balsaa, P.; Gans, O.; Weiss, S.; Blaha, L.; Bolchi, M.; Gawlik, B. M., Pan-european survey on the occurrence of selected polar organic persistent pollutants in ground water. Water Research 2010, 44, (14), 4115-4126.

Lu, D., Sha, S., Luo, J., Huang, Z. and Zhang Jackie, X. 2020. Treatment train approaches for the remediation of per- and polyfluoroalkyl substances (PFAS): A critical review. Journal of Hazardous Materials 386, 121963.

Lucca, F. D., Munizaga-Miranda, R., Jopia-Castillo, D., Gelmi, C. A., & Pérez-Correa, J. R. (2013). Operation Strategies to Minimize Methanol Recovery in Batch Distillation of Hydroalcoholic Mixtures. International Journal of Food Engineering, 9(3), 259-265. https://doi.org/doi:10.1515/ijfe-2013-0031

MacAdam, J. and Jarvis, P. (2015) Mineral Scales and Deposits. Amjad, Z. and Demadis, K.D. (eds), pp. 3-23, Elsevier, Amsterdam.

Macpherson, G.L. 2009. CO2 distribution in groundwater and the impact of groundwater extraction on the global C cycle. Chemical Geology 264(1), 328-336.

Maimati, A., Deng, S., Meng, P., Wang, W., Wang, B., Huang, J., Wang, Y., Yu, G. (2018). Competitive adsorption of perfluoroalkyl substances on anion exchange resins in simulated AFFF-

impacted groundwater. Chemical Engineering Journal, 348, 494-502. https://doi.org/10.1016/j.cej.2018.05.006

Marcus, Y. 1991. Thermodynamics of solvation of ions. Part 5.—Gibbs free energy of hydration at 298.15 K. Journal of the Chemical Society, Faraday Transactions 87(18), 2995-2999.

Martínez, P. J. G., Rus, E., & Compaña, J. M. (2005). FLASH POINT DETERMINATION OF BINARY MIXTURES OF ALCOHOLS , KETONES AND WATER.

Matthews, H. Scott, and Mitchell J. Small. "Extending the Boundaries of Life-Cycle Assessment through Environmental Economic Input-Output Models." Journal of Industrial Ecology, vol. 4, no. 3, 2001, www.eiolca.net.

Matzek, L.W., Tipton, M.J., Farmer, A.T., Steen, A.D. and Carter, K.E. 2018. Understanding Electrochemically Activated Persulfate and Its Application to Ciprofloxacin Abatement. Environmental Science & Technology 52(10), 5875-5883.

Maul, G. A., Kim, Y., Amini, A., Zhang, Q., & Boyer, T. H. (2014). Efficiency and life cycle environmental impacts of ion-exchange regeneration using sodium, potassium, chloride, and bicarbonate salts. Chemical Engineering Journal, 254, 198-209. https://doi.org/https://doi.org/10.1016/j.cej.2014.05.086

Maul, G.A., Kim, Y., Amini, A., Zhang, Q. and Boyer, T.H. 2014. Efficiency and life cycle environmental impacts of ion-exchange regeneration using sodium, potassium, chloride, and bicarbonate salts. Chemical Engineering Journal 254(0), 198-209.

Mazzoni, M.; Buffo, A.; Cappelli, F.; Pascariello, S.; Polesello, S.; Valsecchi, S.; Volta, P.; Bettinetti, R., Perfluoroalkyl acids in fish of italian deep lakes: Environmental and human risk assessment. Science of The Total Environment 2019, 653, 351-358.

McCleaf, P., Englund, S., Östlund, A., Lindegren, K., Wiberg, K., & Ahrens, L. (2017). Removal efficiency of multiple poly- and perfluoroalkyl substances (PFASs) in drinking water using granular activated carbon (GAC) and anion exchange (AE) column tests. Water Research, 120, 77–87. https://doi.org/10.1016/j.watres.2017.04.057

McCleaf, P.; Englund, S.; Ostlund, A.; Lindegren, K.; Wiberg, K.; Ahrens, L., Removal efficiency of multiple poly- and perfluoroalkyl substances (pfass) in drinking water using granular activated carbon (gac) and anion exchange (ae) column tests. Water Research 2017, 120, 77-87.

McDonough, C.A., Choyke, S., Ferguson, P.L., DeWitt, J.C., & Higgins, C.P. (2020a). Bioaccumulation of Novel Per- and Polyfluoroalkyl Substances in mice dosed with an aqueous film-forming foam. Environmental Science and Technology, 54(9), 5700-5709. https://doi.org/10.1021/acs.est.0c00234

McDonough, L.K., Santos, I.R., Andersen, M.S., O'Carroll, D.M., Rutlidge, H., Meredith, K., Oudone, P., Bridgeman, J., Gooddy, D.C., Sorensen, J.P., Lapworth, D.J., MacDonald, A. M., Ward, J., & Baker, A. (2020b). Changes in global groundwater organic carbon driven by climate

change and urbanization. Nature Communications, 11(1). https://doi.org/10.1038/s41467-020-14946-1

McGuire, M.E., Schaefer, C., Richards, T., Backe, W.J., Field, J.A., Houtz, E., Sedlak, D.L., Guelfo, J.L., Wunsch, A. and Higgins, C.P. 2014. Evidence of Remediation-Induced Alteration of Subsurface Poly- and Perfluoroalkyl Substance Distribution at a Former Firefighter Training Area. Environmental Science & Technology 48(12), 6644-6652.

Meegoda, J. N., Kewalramani, J. A., Li, B., & Marsh, R. W. (2020). A Review of the Applications, Environmental Release, and Remediation Technologies of Per- and Polyfluoroalkyl Substances. International Journal of Environmental Research and Public Health, 17(21), 8117. https://doi.org/10.3390/ijerph17218117

Mejia-Avendaño, S.; Munoz, G.; Vo Duy, S.; Desrosiers, M.; Benolt, P.; Sauvé, S.; Liu, J., Novel fluoroalkylated surfactants in soils following firefighting foam deployment during the lac-mégantic railway accident. Environmental Science and Technology 2017, 51, (15), 8313-8323.

Meot-Ner, M. (2005). The Ionic Hydrogen Bond. Chemical Reviews, 105(1), 213-284. https://doi.org/10.1021/cr9411785

Mifkovic, M., Van Hoomissen, D.J., & Vyas, S. (2022). Conformational distributions of helical perfluoroalkyl substances and impacts on stability. Journal of Computational Chemistry, 43(24),

Millar, G.J., Couperthwaite, S.J. and Leung, C.W. 2015. An examination of isotherm generation: Impact of bottle-point method upon potassium ion exchange with strong acid cation resin. Separation and Purification Technology 141, 366-377.

Miyazaki, Y. and Nakai, M. 2011. Protonation and ion exchange equilibria of weak base anion-exchange resins. Talanta 85(4), 1798-1804.

Moeini, Mohammadreza, et al. “Sustainability Assessment of PFAS Adsorbents for Groundwater Remediation.” Materials Today: Proceedings, vol. 60, Elsevier, Jan. 2022, pp. 2209–16, doi:10.1016/J.MATPR.2022.03.014.

Moldes, A.B., Alonso, J.L. and Parajó, J.C. 2003. Recovery of lactic acid from simultaneous saccharification and fermentation media using anion exchange resins. Bioprocess and Biosystems Engineering 25(6), 357-363.

Moody, C.A. and Field, J.A. 2000. Perfluorinated Surfactants and the Environmental Implications of Their Use in Fire-Fighting Foams. Environmental Science & Technology 34(18), 3864-3870.

Moore, Brian C., et al. “GAC Pore Structure in Cincinnati during Full-Scale Treatment/Reactivation.” Journal - American Water Works Association, vol. 95, no. 2, John Wiley & Sons, Ltd, Feb. 2003, pp. 103–12, doi:10.1002/J.1551-8833.2003.TB10296.X.

Murray, C.C., Marshall, R.E., Liu, C.J., Vatankhah, H., & Bellona, C.L. (2021). PFAS treatment with granular activated carbon and ion exchange resin: Comparing chain length, empty bed contact time, and cost. Journal of Water Process Engineering, 44, 102342. https://doi.org/10.1016/j.jwpe.2021.102342

Murray, C.C., Vatankhah, H., McDonough, C.A., Nickerson, A., Hedtke, T.T., Cath, T.Y., Higgins, C.P., & Bellona, C.L. (2019). Removal of per- and polyfluoroalkyl substances using super-fine powder activated carbon and ceramic membrane filtration. Journal of Hazardous Materials, 366. 160-168. https://doi.org/10.1016/j.jhazmat.2018.11.050

Mussabek, D., Ahrens, L., Persson, K.M., & Berndtsson, R. (2019). Temporal trends and sediment–water partitioning of per- and polyfluoroalkyl substances (PFAS) in lake sediment. Chemosphere, 227, 624–629. https://doi.org/10.1016/j.chemosphere.2019.04.074

Nancy, Merino; Yan, Qu; A., Deeb Rula; L., Hawley Elisabeth; R., Hoffmann Michael; Shaily, Mahendra, Degradation and removal methods for perfluoroalkyl and polyfluoroalkyl substances in water. Environmental Engineering Science 2016, 33, (9), 615-649.

National Center for Biotechnology Information (2022). PubChem Compound Summary for CID 887, Methanol. Retrieved June 19, 2022 from https://pubchem.ncbi.nlm.nih.gov/compound/Methanol.

National Center for Biotechnology Information (2022). PubChem Compound Summary for CID 702, Ethanol. Retrieved June 25, 2022 from https://pubchem.ncbi.nlm.nih.gov/compound/Ethanol.

National Center for Biotechnology Information (2022). PubChem Compound Summary for CID 1031, Propanol. Retrieved June 19, 2022 from https://pubchem.ncbi.nlm.nih.gov/compound/Propanol.

National Center for Biotechnology Information (2022). PubChem Compound Summary for CID 263, 1-Butanol. Retrieved June 19, 2022 from https://pubchem.ncbi.nlm.nih.gov/compound/1-Butanol.

National Center for Biotechnology Information (2022). PubChem Compound Summary for CID 1030, Propylene glycol. Retrieved June 25, 2022 from https://pubchem.ncbi.nlm.nih.gov/compound/Propylene-glycol.

National Center for Biotechnology Information (2022). PubChem Compound Summary for CID 753, Glycerol. Retrieved June 25, 2022 from https://pubchem.ncbi.nlm.nih.gov/compound/Glycerol.

National Center for Biotechnology Information (2022). PubChem Compound Summary for CID 57371080, Sodium dodecyl benzenesulfonate. Retrieved June 19, 2022 from https://pubchem.ncbi.nlm.nih.gov/compound/Sodium-dodecyl-benzenesulfonate.

National Center for Biotechnology Information (2022). PubChem Compound Summary for CID 5018304, Diclofenac sodium. Retrieved June 19, 2022 from https://pubchem.ncbi.nlm.nih.gov/compound/Diclofenac-sodium.

Ness, A.; and T.H. Boyer, Pilot-Scale Evaluation of Bicarbonate-Form Anion Exchange for DOC Removal in Small Systems. J.-American Water Works Assoc. 2017, 109, 13-26.

Nguyen, C.K., Stone, K.R., Dudi, A. and Edwards, M.A. 2010. Corrosive Microenvironments at Lead Solder Surfaces Arising from Galvanic Corrosion with Copper Pipe. Environ. Sci. Technol. 44(18), 7076-7081.

Nguyen, T.M.H., Braunig, J., Thompson, T., Thompson, J., Kabiri, S., Navarro, D.A., Kookana, R.S., Grimison, C., Barnes, C.M., Higgins, C.P., McLaughlin, M.J., & Mueller, J.F. (2020). Influences of chemical properties, soil properties, and solution pH on soil-water partitioning coefficients of per- and polyfluoroalkyl substances (PFASs). Environmental Science & Technology, 54(24), 15883-15892. https://doi.org/10.1021/acs.est.0c05705

Ni, X., Li, Z., & Wang, Y. (2018). Adsorption Characteristics of Anionic Surfactant Sodium Dodecylbenzene Sulfonate on the Surface of Montmorillonite Minerals. Frontiers in chemistry, 6, 390-390. https://doi.org/10.3389/fchem.2018.00390

Nickerson, Anastasia; Maizel, Andrew C.; Kulkarni, Poonam R.; Adamson, David T.; Kornuc, John J.; Higgins, Christopher P., Enhanced extraction of afff-associated pfass from source zone soils. Environmental Science & Technology 2020.

Nickerson, A., Rodowa, A.E., Adamson, D.T., Field, J.A., Kulkarni, P.R., Kornuc, J.J., & Higgins, C.P. (2021). Spatial Trends of Anionic, Zwitterionic, and Cationic PFASs at an AFFF-Impacted Site. Cite This: Environ. Sci. Technol, 55, 313–323.

Obolensky, A., Singer, P.C. and Shukairy, H.M. 2007. Information collection rule data evaluation and analysis to support impacts on disinfection by-product formation. Journal of Environmental Engineering-ASCE 133(1), 53-63.

OECD 2013. OECD/UNEP Global PFC Group, Synthesis paper on per- and polyfluorinated chemicals (PFCs). Environment, Health and Safety, Environment Directorate, OECD http://www.oecd.org/chemicalsafety/(https://www.oecd.org/env/ehs/risk-management/PFC_FINAL-Web.pdf), 59 pp.

Padungthon, S., German, M., Wiriyathamcharoen, S., & SenGupta, A. K. (2015). Polymeric anion exchanger supported hydrated Zr(IV) oxide nanoparticles: A reusable hybrid sorbent for selective trace arsenic removal. Reactive and Functional Polymers, 93, 84-94. https://doi.org/https://doi.org/10.1016/j.reactfunctpolym.2015.06.002

Park, M., Daniels, K. D., Wu, S., Ziska, A. D., & Snyder, S. A. (2020). Magnetic ion-exchange (MIEX) resin for perfluorinated alkylsubstance (PFAS) removal in groundwater: Roles of atomic charges for adsorption. Water research, 181, 115897.

Park, M., Wu, S., Lopez, I.J., Chang, J.Y., Karanfil, T. and Snyder, S.A. 2020. Adsorption of perfluoroalkyl substances (PFAS) in groundwater by granular activated carbons: Roles of hydrophobicity of PFAS and carbon characteristics. Water Res. 170, 115364.

Pelch, K.E., Reade, A., Wolffe, T.A.M. and Kwiatkowski, C.F. 2019. PFAS health effects database: Protocol for a systematic evidence map. Environment International 130, 104851.

Pennings, Jeroen L. A., et al. "Cord Blood Gene Expression Supports That Prenatal Exposure to Perfluoroalkyl Substances Causes Depressed Immune Functionality in Early Childhood." Journal of Immunotoxicology, vol. 13, no. 2, 2016, pp. 173–80, doi:10.3109/1547691X.2015.1029147.

Pica, N.; J. Funkhouser, Y. Yin, Z. Zhang, D.M. Ceres, T. Tong, and J. Blotevogel, Electrochemical Oxidation of Hexafluoropropylene Oxide Dimer Acid (GenX): Mechanistic insights and efficient treatment train with nanofiltration. Environ. Sci. Technol. 2019, 53, 12602-12609.

Place, Benjamin J.; Field, Jennifer A., Identification of novel fluorochemicals in aqueous film-forming foams used by the us military. Environmental Science & Technology 2012, 46, (13), 7120-7127.

Plummer, S., Gorman, C., Henrie, T., Shimabuku, K., Thompson, R. and Seidel, C. 2018. Optimization of strong-base anion exchange O&M costs for hexavalent chromium treatment. Water Research 139, 420-433.

Polcaro, A.M.; A.Vacca, M. Mascia, S. Palmas, and J.R. Ruiz, Electrochemical treatment of waters with BDD anodes: Kinetics of the reactions involving chlorides. J. Appl. Electrochem. 2009, 39, 2083–2092.

Pontius, F. 2019. Regulation of Perfluorooctanoic Acid (PFOA) and Perfluorooctane Sulfonic Acid (PFOS) in Drinking Water: A Comprehensive Review. Water 11(10).

Prevedouros, Konstantinos; Cousins, Ian T.; Buck, Robert C.; Korzeniowski, Stephen H., Sources, fate and transport of perfluorocarboxylates. Environmental Science & Technology 2006, 40, (1), 32-44.

Prézélus, F., Tiruta-Barna, L., Remigy, J.-C. and Guigui, C. 2021. Process-based LCA of ultrafiltration for drinking water production. Water Research 199, 117156.

Purolite. (2023). Best PFAS Treatment Options. https://www.purolite.com/index/core-technologies/industry/potable---groundwater/PFAS-In-Our-Environment/best-pfas-treatment-option

Radjenovic, J. and Petrovic, M. 2016. Sulfate-mediated electrooxidation of X-ray contrast media on boron-doped diamond anode. Water Research 94, 128-135.

Rahman, M.F., Peldszus, S., & Anderson, W.B. (2014). Behaviour and fate of perfluoroalkyl and polyfluoroalkyl substances (PFASs) in drinking water treatment: A review. Water Research, 50, 318–340. https://doi.org/10.1016/j.watres.2013.10.045

Rahmani, S. and Mohseni, M. 2017. The role of hydrophobic properties in ion exchange removal of organic compounds from water. The Canadian Journal of Chemical Engineering 95(8), 1449-1455.

Rao, P. S. C., Lee, L. S., & Pinal, R. (1990). Cosolvency and sorption of hydrophobic organic chemicals. Environmental Science & Technology, 24(5), 647-654.

Ras, C. and von Blottnitz, H. 2012. A comparative life cycle assessment of process water treatment technologies at the Secunda industrial complex, South Africa. Water Sa 38(4), 549-554.

Reichardt, C., & Welton, T. (2010). Solvents and Solvent Effects in Organic Chemistry: Fourth Edition. Solvents and Solvent Effects in Organic Chemistry: Fourth Edition. https://doi.org/10.1002/9783527632220

Remde, Armin; Debus, Reinhard, Biodegradability of fluorinated surfactants under aerobic and anaerobic conditions. Chemosphere 1996, 32, (8), 1563-1574.

Rhoads, Kurt R.; Janssen, Elisabeth M. L.; Luthy, Richard G.; Criddle, Craig S., Aerobic biotransformation and fate of n-ethyl perfluorooctane sulfonamidoethanol (n-etfose) in activated sludge. Environmental Science & Technology 2008, 42, (8), 2873-2878.

Riegel, M., Haist-Gulde, B., & Sacher, F. (2023). Sorptive removal of short-chain perfluoroalkyl substances (PFAS) during drinking water treatment using activated carbon and anion exchanger. Environmental Sciences Europe, 35(1), 1–12.

Rodowa, Alix E., et al. "Environmental Science Water Research & Technology Pilot Scale Removal of Per-and Polyfluoroalkyl Substances and Precursors from AFFF-Impacted Groundwater by Granular Activated Carbon †." Cite This: Environ. Sci.: Water Res. Technol, vol. 6, 2020, p. 1083, doi:10.1039/c9ew00936a.

Rokicki, C.A. and Boyer, T.H. 2011. Bicarbonate-form anion exchange: Affinity, regeneration, and stoichiometry. Water Res. 45(3), 1329-1337.

Rotander, Anna; Kärrman, Anna; Toms, Leisa-Maree L.; Kay, Margaret; Mueller, Jochen F.; Gómez Ramos, María José, Novel fluorinated surfactants tentatively identified in firefighters using liquid chromatography quadrupole time-of-flight tandem mass spectrometry and a case-control approach. Environmental Science & Technology 2015, 49, (4), 2434-2442.

Roth, Katherine, et al. "Exposure to a Mixture of Legacy, Alternative, and Replacement per- and Polyfluoroalkyl Substances (PFAS) Results in Sex-Dependent Modulation of Cholesterol Metabolism and Liver Injury." Environment International, vol. 157, Pergamon, Dec. 2021, p. 106843, doi:10.1016/J.ENVINT.2021.106843.

Routti, H.; Atwood, T. C.; Bechshoft, T.; Boltunov, A.; Ciesielski, T. M.; Desforges, J. P.; Dietz, R.; Gabrielsen, G. W.; Jenssen, B. M.; Letcher, R. J.; McKinney, M. A.; Morris, A. D.; Rigét, F. F.; Sonne, C.; Styrishave, B.; Tartu, S., State of knowledge on current exposure, fate and potential health effects of contaminants in polar bears from the circumpolar arctic. Science of The Total Environment 2019, 664, 1063-1083.

Ryberg, Morten, et al. "Updated US and Canadian Normalization Factors for TRACI 2.1." Clean Technologies and Environmental Policy, vol. 16, no. 2, Springer Verlag, May 2014, pp. 329–39, doi:10.1007/S10098-013-0629-Z/TABLES/4.

Saetta, D., Ishii, S.K.L., Pine, W.E. and Boyer, T.H. 2015. Case Study and Life Cycle Assessment of a Coastal Utility Facing Saltwater Intrusion. Journal - American Water Works Association 107(10), E543-E558.

Sági, G.; T. Csay, T., L. Szabó, G. Pátzay, E. Csonka, E.Takács, and L. Wojnárovits, Analytical approaches to the OH radical induced degradation of sulfonamide antibiotics in dilute aqueous solutions. J. Pharm. Biomed. Anal., 2015, 106, 52-60.

Samatya, S., Kabay, N., Yüksel, Ü., Arda, M. and Yüksel, M. 2006. Removal of nitrate from aqueous solution by nitrate selective ion exchange resins. Reactive and Functional Polymers 66(11), 1206-1214.

Schaefer, C.E., Nguyen, D., Culina, V.M., Guelfo, J., & Kumar, N. (2020). Application of Rapid Small-Scale Column Tests for Treatment of Perfluoroalkyl Acids Using Anion-Exchange Resins and Granular Activated Carbon in Groundwater with Elevated Organic Carbon. Industrial & Engineering Chemistry Research, 59(38), 16832-16837. https://doi.org/10.1021/acs.iecr.0c02290

Schaefer, C.E., Tran, D., Fang, Y., Choi, Y.J., Higgins, C.P. and Strathmann, T.J. 2020. Electrochemical treatment of poly- and perfluoroalkyl substances in brines. Environmental Science: Water Research & Technology In press, 10.1039/D1030EW00377H.

Schaefer, C.E.; C. Andaya, A. Burant, C.W. Condee, A. Urtiaga, T.J. Strathmann, and C.P. Higgins, Electrochemical treatment of perfluorooctanoic acid and perfluorooctane sulfonate: insights into mechanisms and application to groundwater treatment. Chem. Eng. J. 2017, 317, 424−432.

Schaefer, C.E.; S. Choyke, P.L. Ferguson, C. Andaya, A. Burant, A. Maizel, T.J. Strathmann, and C.P. Higgins, Electrochemical transformations of perfluoroalkyl acid (PFAA) precursors and PFAAs in groundwater impacted with aqueous film forming foams. Environ. Sci. Technol., 2018, 52, 10689-10697.

Schaefer, C.E.; V. Culina, D. Nguyen, and J. Field, Uptake of Poly-and Perfluoroalkyl Substances at the Air–Water Interface. Environ. Sci. Technol., 2019, 53, 12442-12448.

Schmalz, V.; T. Dittmar, D. Haaken, and E. Worch, Electrochemical disinfection of biologically treated wastewater from small treatment systems by using boron doped diamond (BDD) electrodes. Water Res. 2009, 43, 5260–5266.

Schultz, M.M., Barofsky, D.F., & Field, J.A. (2004). Quantitative determination of fluorotelomer sulfonates in groundwater by LC MS/MS. Environmental Science & Technology, 38(6), 1828–1835. https://doi.org/10.1021/es035031j

Schuricht, F., Borovinskaya, E.S. and Reschetilowski, W. 2017. Removal of perfluorinated surfactants from wastewater by adsorption and ion exchange — Influence of material properties, sorption mechanism and modeling. Journal of Environmental Sciences 54, 160-170.

Scott, M. J., & Jones, M. N. (2000). The biodegradation of surfactants in the environment. Biochimica et Biophysica Acta (BBA) - Biomembranes, 1508(1), 235-251. https://doi.org/https://doi.org/10.1016/S0304-4157(00)00013-7

Senevirathna, S.T.M.L.D., Tanaka, S., Fujii, S., Kunacheva, C., Harada, H., Ariyadasa, B.H.A.K.T. and Shivakoti, B.R. 2010a. Adsorption of perfluorooctane sulfonate (n-PFOS) onto non ion-exchange polymers and granular activated carbon: Batch and column test. Desalination 260(1), 29-33.

Senevirathna, S.T.M.L.D., Tanaka, S., Fujii, S., Kunacheva, C., Harada, H., Shivakoti, B.R. and Okamoto, R. 2010b. A comparative study of adsorption of perfluorooctane sulfonate (PFOS) onto granular activated carbon, ion-exchange polymers and non-ion-exchange polymers. Chemosphere 80(6), 647-651.

Sengupta, A.K. and Clifford, D. 1986. Some unique characteristics of chromate ion exchange. Reactive Polymers, Ion Exchangers, Sorbents 4(2), 113-130.

SenGupta, A.K., Ion exchange in environmental processes: Fundamentals, applications and sustainable technology. Wiley: 2017.

Seo, Sung-Hee; Son, Min-Hui; Choi, Sung-Deuk; Lee, Duk-Hee; Chang, Yoon-Seok, Influence of exposure to perfluoroalkyl substances (pfass) on the korean general population: 10-year trend and health effects. Environment International 2018, 113, 149-161.

Shoaff, Jessica, et al. “Prenatal Exposure to Perfluoroalkyl Substances: Infant Birth Weight and Early Life Growth.” Environmental Epidemiology (Philadelphia, Pa.), vol. 2, no. 2, Wolters Kluwer Health, June 2018, p. e010, doi:10.1097/EE9.0000000000000010.

Shuang, C., Pan, F., Zhou, Q., Li, A., Li, P. and Yang, W. 2012. Magnetic Polyacrylic Anion Exchange Resin: Preparation, Characterization and Adsorption Behavior of Humic Acid. Industrial & Engineering Chemistry Research 51(11), 4380-4387.

Shuang, C., Wang, J., Li, H., Li, A. and Zhou, Q. 2015. Effect of the chemical structure of anion exchange resin on the adsorption of humic acid: Behavior and mechanism. Journal of Colloid and Interface Science 437, 163-169.

Smith, J., Beuthe, B., Dunk, M., Demeure, S., Carmona, J. M. M., Medve, A., Spence, M. J., Pancras, T., Schrauwen, G., Held, T., Baker, K., Ross, I., & Slenders, H. (2016). Environmental fate and effects of polyand perfluoroalkyl substances (PFAS). 1-107.

Solo-Gabriele, H.M., Jones, A.S., Lindstrom, A.B. and Lang, J.R. 2020. Waste type, incineration, and aeration are associated with per- and polyfluoroalkyl levels in landfill leachates. Waste Management 107, 191-200.

Song, H., Zhou, Y., Li, A. and Mueller, S. 2012. Selective removal of nitrate from water by a macroporous strong basic anion exchange resin. Desalination 296, 53-60.

Song, H; L. Yan, J. Jiang, J. Ma, Z. Zhang, J. Zhang, P. Liu, and T. Yang, Electrochemical activation of persulfates at BDD anode: radical or nonradical oxidation?. Water Res. 2018, 128, 393-401.

Sörengård, M., Franke, V., Tröger, R. and Ahrens, L. 2020. Losses of poly- and perfluoroalkyl substances to syringe filter materials. Journal of Chromatography A 1609, 460430.

Steenland, Kyle, and Andrea Winquist. "PFAS and Cancer, a Scoping Review of the Epidemiologic Evidence." Environmental Research, vol. 194, Academic Press, Mar. 2021, p. 110690, doi:10.1016/J.ENVRES.2020.110690.

Subramonian, S. and Clifford, D. 1988. Monovalent/divalent selectivity and the charge separation concept. Reactive Polymers, Ion Exchangers, Sorbents 9(2), 195-209.

Sun, P.; Y. Li, T. Meng, R. Zhang, M. Song, and J. Ren, Removal of sulfonamide antibiotics and human metabolite by biochar and biochar/H2O2 in synthetic urine. Water Res. 2018, 147, 91-100.

Sunderland, E.M., Hu, X.C., Dassuncao, C., Tokranov, A.K., Wagner, C.C., & Allen, J.G. (2018). A review of the pathways of human exposure to poly- and perfluoroalkyl substances (PFASs) and present understanding of health effects. Journal of Exposure Science & Environmental Epidemiology, 29(2), 131–147. https://doi.org/10.1038/s41370-018-0094-1

Tenorio, R.; J. Liu, X. Xiao, A. Maizel, J.S. Guest, C.P. Higgins, C.E. Schaefer, and T.J. Strathmann, T.J., Destruction of per- and polyfluoroalkyl substances (PFAS) in aqueous film-forming foam (AFFF) with UV-sulfite photo-reductive treatment. Environ. Sci. Technol., 2020, 54, 6957-6967.

Tian, F.Y., Huang, L.F., Fan, L.W., Qian, H.L., & Yu, Z.T. (2016). Wall effects on the pressure drop in packed beds of irregularly shaped sintered ore particles. Powder Technology, 301, 1284–1293. https://doi.org/10.1016/j.powtec.2016.07.073

Todd, P., & Sorkin, E. (1998). Diclofenac sodium: a reappraisal of its pharmacodynamic and pharmaco-kinetic properties and therapeutic efficacy. Drugs 35, 244 regulations for continuing clinical trials. Pharmacol Res(37), 321.

Toms, L.M.L., Bräunig, J., Vijayasarathy, S., Phillips, S., Hobson, P., Aylward, L.L., Kirk, M.D. and Mueller, J.F. 2019. Per- and polyfluoroalkyl substances (PFAS) in Australia: Current levels and estimated population reference values for selected compounds. International Journal of Hygiene and Environmental Health 222(3), 387-394.

Tow, E.W., Ersan, M.S., Kum, S., Lee, T., Speth, T.F., Owen, C., Bellona, C., Nadagouda, M.N., Mikelonis, A.M., Westerhoff, P., Mysore, C., Frenkel, V.S., deSilva, V., Walker, W.S., Safulko, A.K. and Ladner, D.A. 2021. Managing and treating per- and polyfluoroalkyl substances (PFAS) in membrane concentrates. AWWA Water Science 3(5), e1233.

Tran, H.N., You, S.-J. and Chao, H.-P. 2017a. Fast and efficient adsorption of methylene green 5 on activated carbon prepared from new chemical activation method. Journal of Environmental Management 188, 322-336.

Tran, H.N., You, S.-J., Hosseini-Bandegharaei, A. and Chao, H.-P. 2017b. Mistakes and inconsistencies regarding adsorption of contaminants from aqueous solutions: A critical review. Water Research 120, 88-116.

Tsitonaki, Aikaterini; Petri, Benjamin; Crimi, Michelle; MosbÆK, Hans; Siegrist, Robert L.; Bjerg, Poul L., In situ chemical oxidation of contaminated soil and groundwater using persulfate: A review. Critical Reviews in Environmental Science and Technology 2010, 40, (1), 55-91.

U.S. Environmental Protection Agency. "Drinking Water Treatment Technology Unit Cost Models and Work Breakdown Structure (WBS)." Https://Www.Epa.Gov/Sdwa/Drinking-Water-Treatment-Technology-Unit-Cost-Models, 2022.

Urtiaga, A.; C. Fernandez-Gonzalez, S. Gomez-Lavin, and I. Ortiz, Kinetics of the electrochemical mineralization of perfluorooctanoic acid on ultrananocrystalline boron doped conductive diamond electrodes. Chemosphere 2015, 129, 20−26.

USEPA 2020. Interim Guidance on the Destruction and Disposal of Perfluoroalkyl and Polyfluoroalkyl Substances and Materials Containing Perfluoroalkyl and Polyfluoroalkyl Substances. U.S. Environmental Protection Agency Washington, DC, USA.

Vecitis, C.D., Park, H., Cheng, J., Mader, B.T., & Hoffmann, M.R. (2009). Treatment technologies for aqueous perfluorooctanesulfonate (PFOS) and perfluorooctanoate (PFOA). Frontiers of Environmental Science & Engineering in China, 3(2), 129–151. https://doi.org/10.1007/s11783-009-0022-7

Velazquez-Pena, S.; C. Sáez, P. Canizares, P., I. Linares-Hernández, V. Martínez-Miranda, C. Barrera-Díaz, and M.A. Rodrigo, Production of oxidants via electrolysis of carbonate solutions with conductive-diamond anodes. Chem. Engin. J. 2013, 230, 272-278.

Víctor-Ortega, M.D., Ochando-Pulido, J.M. and Martínez-Ferez, A. 2017. Impacts of main parameters on the regeneration process efficiency of several ion exchange resins after final purification of olive mill effluent. Separation and Purification Technology 173, 1-8.

Walker, K.M. and Boyer, T.H. 2011. Long-term performance of bicarbonate-form anion exchange: Removal of dissolved organic matter and bromide from the St. Johns River, FL, USA. Water Research 45(9), 2875-2886.

Wang, L., Nickelsen, M., Chiang, S.-Y., Woodard, S., Wang, Y., Liang, S., Mora, R., Fontanez, R., Anderson, H. and Huang, Q. 2021. Treatment of perfluoroalkyl acids in concentrated wastes from regeneration of spent ion exchange resin by electrochemical oxidation using Magnéli phase Ti4O7 anode. Chemical Engineering Journal Advances 5, 100078.

Wang, W., Li, M. and Zeng, Q. 2015. Adsorption of chromium (VI) by strong alkaline anion exchange fiber in a fixed-bed column: Experiments and models fitting and evaluating. Separation and Purification Technology 149, 16-23.

Wang, W., Maimaiti, A., Shi, H., Wu, R., Wang, R., Li, Z., Qi, D., Yu, G. and Deng, S. 2019. Adsorption behavior and mechanism of emerging perfluoro-2-propoxypropanoic acid (GenX) on activated carbons and resins. Chemical Engineering Journal 364, 132-138.

Wang, W., Mi, X., Zhou, Z., Zhou, S., Li, C., Hu, X., Qi, D., Deng, S. (2019). Novel insights into the competitive adsorption behavior and mechanism of per- and polyfluoroalkyl substances on the anion-exchange resin. Journal of Colloid and Interface Science, 557, 655-663. https://doi.org/10.1016/j.jcis.2019.09.066

Wang, Z., DeWitt, J.C., Higgins, C.P. and Cousins, I.T. 2017. A Never-Ending Story of Per- and Polyfluoroalkyl Substances (PFASs)? Environmental Science & Technology 51(5), 2508-2518.

Wawrzkiewicz, M. 2011. Comparison of gel anion exchangers of various basicity in direct dye removal from aqueous solutions and wastewaters. Chemical Engineering Journal 173(3), 773-781.

Wawrzkiewicz, M. and Hubicki, Z. 2009. Removal of tartrazine from aqueous solutions by strongly basic polystyrene anion exchange resins. Journal of Hazardous Materials 164(2), 502-509.

Wawrzkiewicz, M. and Hubicki, Z. 2011. Remazol Black B removal from aqueous solutions and wastewater using weakly basic anion exchange resins. Central European Journal of Chemistry 9(5), 867-876.

Wei, Z., Xu, T. and Zhao, D. 2019. Treatment of per- and polyfluoroalkyl substances in landfill leachate: status, chemistry and prospects. Environmental Science: Water Research & Technology 5(11), 1814-1835.

Weishaar, J.L., Aiken, G.R., Bergamaschi, B.A., Fram, M.S., Fujii, R. and Mopper, K. 2003. Evaluation of specific ultraviolet absorbance as an indicator of the chemical composition and reactivity of dissolved organic carbon. Environ. Sci. Technol. 37(20), 4702-4708.

Woodard, S., Berry, J., & Newman, B. (2017). Ion exchange resin for PFAS removal and pilot test comparison to GAC. Remediation, 27, 19-27. https://doi.org/10.1002/rem.21515

Woodard, Steve, et al. “Ion Exchange Resin for PFAS Removal and Pilot Test Comparison to GAC.” Remediation, vol. 27, no. 3, John Wiley and Sons Inc., June 2017, pp. 19–27, doi:10.1002/rem.21515.

Workman, C. E.; Becker, A. B.; Azad, M. B.; Moraes, T. J.; Mandhane, P. J.; Turvey, S. E.; Subbarao, P.; Brook, J. R.; Sears, M. R.; Wong, C. S., Associations between concentrations of perfluoroalkyl substances in human plasma and maternal, infant, and home characteristics in winnipeg, canada. Environmental Pollution 2019, 758-766.

Wu, B., Hao, S., Choi, Y., Higgins, C.P., Deeb, R., & Strathmann, T.J. (2019). Rapid Destruction and Defluorination of Perfluorooctanesulfonate by Alkaline Hydrothermal Reaction. Environmental Science and Technology Letters, 6(10), 630–636.

Xiao, F., Jin, B., Golovko, S.A., Golovko, M.Y., & Xing, B. (2019). Sorption and desorption mechanisms of cationic and zwitterionic per- and polyfluoroalkyl substances in natural soils:

Thermodynamics and hysteresis. Environmental Science & Technology, 53(20), 11818–11827. https://doi.org/10.1021/acs.est.9b05379

Xiao, F; R.A. Hanson, S.A., Golovko, M.Y. Golovko, and W.A. Arnold, PFOA and PFOS are generated from zwitterionic and cationic precursor compounds during water disinfection with chlorine or ozone. Environ. Sci. Technol. Letters, 2018, 5, 382-388.

Xiao, Xin; Ulrich, Bridget A.; Chen, Baoliang; Higgins, Christopher P., Sorption of poly- and perfluoroalkyl substances (pfass) relevant to aqueous film-forming foam (afff)-impacted groundwater by biochars and activated carbon. Environmental Science & Technology 2017, 51, (11), 6342-6351.

Xu, B., Liu, S., Zhou, J.L., Zheng, C., Weifeng, J., Chen, B., Zhang, T. and Qiu, W. 2021. PFAS and their substitutes in groundwater: Occurrence, transformation and remediation. Journal of Hazardous Materials 412, 125159.

Yang, S., Fernando, S., Holsen, T.M. and Yang, Y. 2019. Inhibition of Perchlorate Formation during the Electrochemical Oxidation of Perfluoroalkyl Acid in Groundwater. Environmental Science & Technology Letters 6(12), 775-780.

Yang, Shewei; Cheng, Jianhua; Sun, Jian; Hu, Yongyou; Liang, Xiaoyan, Defluorination of aqueous perfluorooctanesulfonate by activated persulfate oxidation. PLOS ONE 2013, 8, (10), e74877.

Yang, Y., Ding, Q., Yang, M., Wang, Y., Liu, N. and Zhang, X. 2018. Magnetic ion exchange resin for effective removal of perfluorooctanoate from water: study of a response surface methodology and adsorption performances. Environmental Science and Pollution Research 25(29), 29267-29278.

Yao, Y., Volchek, K., Brown, C.E., Robinson, A. and Obal, T. 2014. Comparative study on adsorption of perfluorooctane sulfonate (PFOS) and perfluorooctanoate (PFOA) by different adsorbents in water. Water Science and Technology 70(12), 1983-1991.

Yu, Q., Zhang, R., Deng, S., Huang, J. and Yu, G. 2009. Sorption of perfluorooctane sulfonate and perfluorooctanoate on activated carbons and resin: Kinetic and isotherm study. Water Res. 43(4), 1150-1158.

Yuchi LEE, Shanglien LO, Jeff KUO, Chinghong HSIEH, Decomposition of perfluorooctanoic acid by microwave-activated persulfate: Effects of temperature, ph, and chloride ions. Front. Environ. Sci. Eng. 2012, 6, (1), 17-25.

Zaggia, A., Conte, L., Falletti, L., Fant, M., & Chiorboli, A. (2016). Use of strong anion exchange resins for the removal of perfluoroalkylated substances from contaminated drinking water in batch and continuous pilot plants. Water Research, 91, 137–146. https://doi.org/10.1016/j.watres.2015.12.039

Zeng, C., Atkinson, A., Sharma, N., Ashani, H., Hjelmstad, A., Venkatesh, K. and Westerhoff, P. 2020. Removing per- and polyfluoroalkyl substances from groundwaters using activated carbon and ion exchange resin packed columns. AWWA Water Science 2(1), e1172.

Zeng, Chao; Atkinson, Ariel; Sharma, Naushita; Ashani, Harsh; Hjelmstad, Annika; Venkatesh, Krishishvar; Westerhoff, Paul, Removing per- and polyfluoroalkyl substances from groundwaters using activated carbon and ion exchange resin packed columns. AWWA Water Science 2020, 2, (1), e1172.

Zeng, Jicai, et al. "Model Validation and Analyses of Parameter Sensitivity and Uncertainty for Modeling Long-Term Retention and Leaching of PFAS in the Vadose Zone." Journal of Hydrology, vol. 603, Elsevier, Dec. 2021, p. 127172, doi:10.1016/J.JHYDROL.2021.127172.

Zhang, D.Q., Zhang, W.L. and Liang, Y.N. 2019. Adsorption of perfluoroalkyl and polyfluoroalkyl substances (PFASs) from aqueous solution - A review. Science of The Total Environment 694, 133606.

Zhang, H., Shields, A.J., Jadbabaei, N., Nelson, M., Pan, B. and Suri, R.P.S. 2014. Understanding and Modeling Removal of Anionic Organic Contaminants (AOCs) by Anion Exchange Resins. Environmental Science & Technology 48(13), 7494-7502.

Zhang, J., Amini, A., O'Neal, J. A., Boyer, T. H., & Zhang, Q. (2015). Development and validation of a novel modeling framework integrating ion exchange and resin regeneration for water treatment. Water research, 84, 255-265. https://doi.org/https://doi.org/10.1016/j.watres.2015.07.027

Zhang, Y., Geißen, S.-U., & Gal, C. (2008). Carbamazepine and diclofenac: Removal in wastewater treatment plants and occurrence in water bodies. Chemosphere, 73(8), 1151-1161. https://doi.org/https://doi.org/10.1016/j.chemosphere.2008.07.086

Zuber, A., Cardozo-Filho, L., Cabral, V. F., Checoni, R. F., & Castier, M. (2014). An empirical equation for the dielectric constant in aqueous and nonaqueous electrolyte mixtures. Fluid Phase Equilibria, 376, 116-123. https://doi.org/https://doi.org/10.1016/j.fluid.2014.05.037

APPENDIX A: Supporting Data

Table A3.1.1 *Suspect PFASs detected in an 1:93,000 diluted AFFF solution*

Class #	Compound class and structure	n	Compound Acronym	Formula	m/z	Ionic charge [h]	C_0 (µg/L) [i]
1[a]	N-dimethyl ammonio propyl perfluoroalkane sulfonamide (AmPr-FASA) 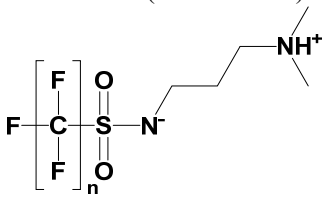	2	AmPr-FEtSA[f]	$C_7H_{13}O_2N_2SF_5$	285.069	Zwi	0.38±0.05
		3	AmPr-FPrSA	$C_8H_{13}O_2SN_2F_7$	333.051	Zwi	0.20±0.03
		4	AmPr-FBSA	$C_9H_{13}O_2SN_2F_9$	383.048	Zwi	2.23±0.06
		5	AmPr-FPeSA	$C_{10}H_{13}O_2SN_2F_{11}$	433.045	Zwi	1.90±0.06
		6	AmPr-FHxSA	$C_{11}H_{13}O_2SN_2F_{13}$	483.042	Zwi	13.4±1.46
2[b]	N-dimethyl ammonio propyl perfluoralkane sulfonamido propanoic acid (AmPr-FASA-PrA)[j] 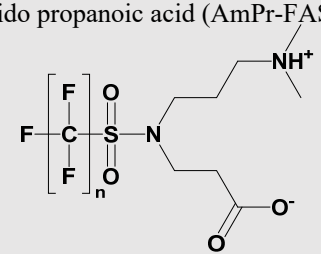	2	AmPr-FEtSA-PrA	$C_{10}H_{17}O_4N_2SF_5$	357.090	Zwi	1.65±0.17
		3	AmPr-FPrSA-PrA	$C_{11}H_{17}O_4SN_2F_7$	405.072	Zwi	1.12±0.04
		4	AmPr-FBSA-PrA	$C_{12}H_{17}O_4SN_2F_9$	455.069	Zwi	6.91±0.42
		5	AmPr-FPeSA-PrA	$C_{13}H_{17}O_4SN_2F_{11}$	505.066	Zwi	5.88±0.30
		6	AmPr-FHxSA-PrA	$C_{14}H_{17}O_4SN_2F_{13}$	555.063	Zwi	12.0±1.46
3[a]	N-carboxy ethyl dimethyl ammonio propyl-perfluoroalkane sulfonamido propanoic acid (CEtAmPr-FASA-PrA) 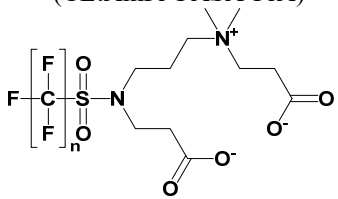	2	CEtAmPr-FEtSA-PrA	$C_{13}H_{21}O_6N_2SF_5$	429.111	Neg	0.70±0.08
		3	CEtAmPr-FPrSA-PrA	$C_{14}H_{21}O_6SN_2F_7$	477.094	Neg	0.07±0.00
		4	CEtAmPr-FBSA-PrA	$C_{15}H_{21}O_6SN_2F_9$	527.090	Neg	0.12±0.00
		5	CEtAmPr-FPeSA-PrA	$C_{16}H_{21}O_6SN_2F_{11}$	577.087	Neg	0.07±0.00
		6	CEtAmPr-FHxSA-PrA	$C_{17}H_{21}O_6SN_2F_{13}$	627.084	Neg	0.25±0.01
4[c]	Chloro-perfluorosulfonate (Cl-PFSA) 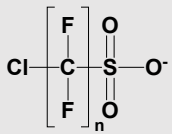	4	Cl-PFBS[g]	$C_4HO_3SClF_8$	314.913	Neg	0.05±0.00
		5	Cl-PFPeS	$C_5HO_3SClF_{10}$	364.910	Neg	0.03±0.00
		6	Cl-PFHxS	$C_6HO_3SClF_{12}$	414.907	Neg	0.32±0.01

Class #	Compound class and structure	n	Compound Acronym	Formula	m/z	Ionic charge [h]	C_0 (µg/L) [i]
5[c]	N-carboxy methyl dimethyl ammonio propyl-perfluoroalkane sulfonamide (CMeAmPr-FASA) 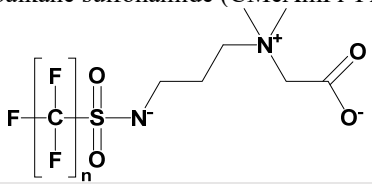	4	CMeAmPr-FBSA	$C_{11}H_{15}O_4SN_2F_9$	441.054	Neg	0.09±0.00
		5	CMeAmPr-FPeSA	$C_{12}H_{15}O_4SN_2F_{11}$	491.050	Neg	0.01±0
		6	CMeAmPr-FHxSA	$C_{13}H_{15}O_4SN_2F_{13}$	541.047	Neg	0.42±0.02
6[c]	N-carboxy methyl dimethyl ammonio propyl-perfluoroalkane sulfonamido propanoic acid (CMeAmPr-FAS-PrA) 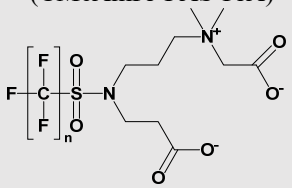	3	CMeAmPr-FPrSAPrA	$C_{13}H_{19}O_6SN_2F_7$	463.078	Neg	0.06±0.00
		4	CMeAmPr-FBSAPrA	$C_{14}H_{19}O_6SN_2F_9$	513.075	Neg	0.13±0.00
		5	CMeAmPr-FPeSAPrA	$C_{15}H_{19}O_6SN_2F_{11}$	563.072	Neg	0.06±0.00
		6	CMeAmPr-FHxSAPrA	$C_{16}H_{19}O_6SN_2F_{13}$	613.068	Neg	0.44±0.00
7[c]	Pentafluorosulfide-perfluoroalkane sulfonate (F5S-PFAS) 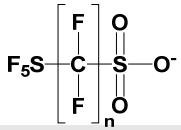	6	F_5S-PFHxS	$C_6HO_3S_2F_{17}$	506.902	Neg	0.05±0.00
8[c]	Perfluoroalkane sulfonamide (FASA) 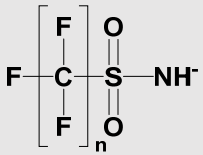	4	FBSA	$C_4H_2O_2SNF_9$	297.959	Neg	0.05±0.00
		6	FHxSA	$C_6H_2O_2SNF_{13}$	397.953	Neg	0.25±0.00
9[c]	Hydrido-perfluoroalkanoic acid (H-PFCA) 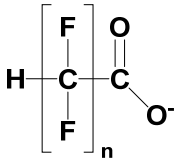	5	H-PFHxA	$C_6H_2O_2F_{10}$	294.982	Neg	0.16±0.00

Class #	Compound class and structure	n	Compound Acronym	Formula	m/z	Ionic charge [h]	C_0 (µg/L) [i]
10[c]	Hydrido-perfluoroalkane sulfonate (H-PFSA) 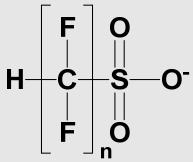	3	H-PFPrS	$C_3H_2O_3SF_6$	230.956	Neg	0.01±0.00
		4	H-PFBS	$C_4H_2O_3SF_8$	280.952	Neg	0.05±0.00
		6	H-PFHxS	$C_6H_2O_3SF_{12}$	380.946	Neg	0.04±0.00
		7	H-PFHpS	$C_7H_2O_3SF_{14}$	430.943	Neg	0.05±0.01
		8	H-PFOS	$C_8H_2O_3SF_{16}$	480.940	Neg	0.87±0.11
		10	H-PFDS	$C_{10}H_2O_3SF_{20}$	580.933	Neg	0.97±0.14
11[c]	Hydrido-Unsaturated perfluoroalkane sulfonate (H-UPFAS) 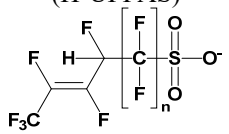	7	H-UPFHpS	$C_7H_2O_3SF_{12}$	392.946	Neg	0.02±0.00
		8	H-UPFOS	$C_8H_2O_3SF_{14}$	442.943	Neg	0.15±0.01
12[d]	Keto-perfluoroalkanesulfonate (K-PFAS) 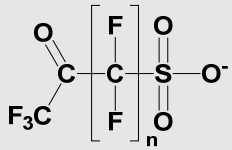	5	K-PFPeS	$C_5HO_4SF_9$	326.938	Neg	0.03±4.53
		6	K-PFHxS	$C_6HO_4SF_{11}$	376.935	Neg	0.03±0.00
		7	K-PFHpS	$C_7HO_4SF_{13}$	426.932	Neg	0.06±0.00
		8	K-PFOS	$C_8HO_4SF_{15}$	476.928	Neg	0.39±0.04
13[b]	N-methylethyl-carboxymethyl dimethyl ammonio propyl perfluoroalkane amide (MeEtCMeAmPr-FAAd) 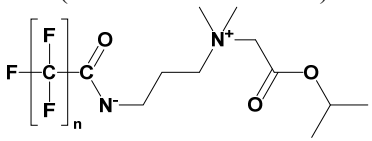	4	MeEtCMeAmPr-FPeAd	$C_{15}H_{21}O_3N_2F_9$	447.134	Zwi	10.9±0.46
14[c]	N-methylperfluoroalkanesulfonamidoacetic acid (MeFASAA) 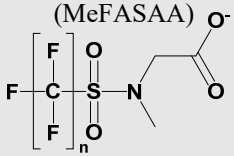	5	MeFPeSAA	$C_8H_6O_4SNF_{11}$	419.977	Neg	0.77±0.02
		6	MeFHxSAA	$C_9H_6O_4SNF_{13}$	469.974	Neg	4.78±0.43

Class #	Compound class and structure	n	Compound Acronym	Formula	m/z	Ionic charge [h]	C_0 (µg/L) [i]
15[b]	N-oxidedimethylammoniopropyl-perfluoroalkanesulfonamide (OAmPr-FASA) 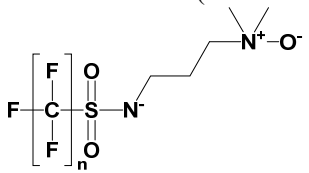	5	OAmPr-FPeSA	$C_{10}H_{13}O_3SN_2F_{11}$	451.054	Neg	1.23±0.06
		6	OAmPr-FHxSA	$C_{11}H_{13}O_3SN_2F_{13}$	499.037	Neg	3.46±0.16
16[c]	Oxa-perfluoroalkanesulfonate (O-PFAS) 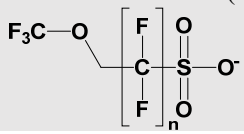	6	O-PFHxS	$C_5HO_4SF_{11}$	364.935	Neg	0.00±0.00
		7	O-PFHpS	$C_6HO_4SF_{13}$	414.932	Neg	0.07±0.00
17[c]	Perfluoroalkanesulfinate (PFASi) 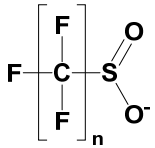	4	PFBSi	$C_4HO_2SF_9$	282.948	Neg	0.03±0.00
		5	PFPeSi	$C_5HO_2SF_{11}$	332.945	Neg	0.01±0.00
		6	PFHxSi	$C_6HO_2SF_{13}$	382.942	Neg	0.33±0.02
18[e]	Perfluoro cyclohexane carboxylic acid (PFCPeCA) 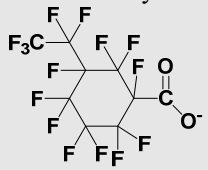	6	PFMeCHxCA	$C_8HO_2F_{13}$	374.970	Neg	0.20±0.03
19[c]	N-trimethylammoniopropyl perfluoroalkanesulfonamide (TAmPr-FASA) 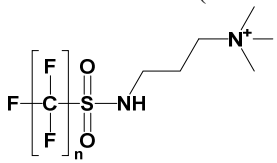	3	TAmPr-FPrSA	$C_9H_{15}O_2SN_2F_7$	349.082	Pos	1.04±0.46
		4	TAmPr-FBSA	$C_{10}H_{15}O_2SN_2F_9$	399.078	Pos	1.38±0.15
		5	TAmPr-FPeSA	$C_{11}H_{15}O_2SN_2F_{11}$	449.075	Pos	1.51±0.56
		6	TAmPr-FHxSA	$C_{12}H_{15}O_2SN_2F_{13}$	499.072	Pos	2.04±0.03

Class #	Compound class and structure	n	Compound Acronym	Formula	m/z	Ionic charge [h]	C_0 (µg/L) [i]
20[c]	N-trimethylammoniopropyl perfluoroalkanesulfonamido propanoic acid (TAmPr-FASAPrA) 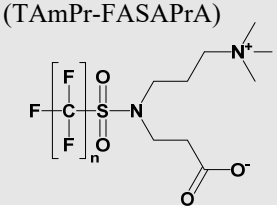	3	TAmPr-FPrSAPrA	$C_{12}H_{19}O_4SN_2F_7$	421.103	Zwi	1.12±0.07
		4	TAmPr-FBSAPrA	$C_{13}H_{19}O_4SN_2F_9$	471.099	Zwi	2.08±0.11
		5	TAmPr-FPeSAPrA	$C_{14}H_{19}O_4SN_2F_{11}$	521.096	Zwi	2.34±0.21
		6	TAmPr-FHxSAPrA	$C_{15}H_{19}O_4SN_2F_{13}$	571.093	Zwi	2.34±0.04
21[c]	Unsaturated perfluoroalkane sulfonate (UPFSA)[j] 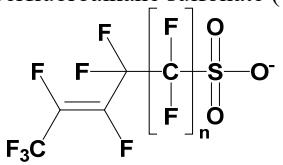	6	UPFHxS	$C_6HO_3SF_{11}$	360.940	Neg	0.15±0.01
		7	UPFHpS	$C_7HO_3SF_{13}$	410.937	Neg	0.08±0.00
		8	UPFOS	$C_8HO_3SF_{15}$	460.933	Neg	3.09±0.37

a. Class structure adopted from Place et al. based on m/z value and q-TOF-MS data.
b. Class structure adopted from D'Agostino et al. based on m/z value and q-TOF-MS data.[89]
c. Class structure adopted from Barzen-Hanson et al. based on m/z value and q-TOF-MS data.[90]
d. Class structure adopted from Rotander et al. based on m/z value and q-TOF-MS data.[91]
e. Predicted class structure using q-TOF-MS data.
f. Orange highlighted compounds are only detected under ESI+ mode during LC-qTOF-MS analysis
g. Blue highlighted compounds are only detected under ESI- mode during LC-qTOF-MS analysis
h. Predicted base on the pK_a values calculated using Sparc (Archem LLC)
i. Initial concentration of suspect PFAS is estimated using a semi-quantification method. Details on this method is provided in main text's method section
j. For class 2, the structures shown are one possible structural isomer class. An alternative isomer class is N-carboxy ethyl dimethyl ammonio propyl-perfluoroalkane sulfonamide (CEtAmPr-FASA). For class 21, the structures shown are one possible isomer class. An alternative isomer class is perfluoroethylcyclosulfonates (PFEtCSA).

Table A3.1.2. Targeted analysis of adsorption of PFAAs in AFFF by 50 mg/L GAC, AER, PAER, CER, and NIR

Compound Acronym	% Adsorbed													
	GAC	**AER**					***PAER***			**CER**		***NIR***		
	Cal F400	A300	A520E	A532E	A600E	A860	*PFA694E*	*CalRes23 01*	*CalRes23 04*	C100	C150	*XAD-2*	*XAD-4*	*XAD-7HP*
PFBA	5.86±0.50	18.9±1.23	25.3±3.81	67.1±0.71	22.7±3.29	5.30±5.25	82.6±0.35	82.1±0.11	76.9±0.69	2.35±0.09	5.74±0.06	3.84±0.08	12.5±0.34	15.0±0.53
PFPeA	8.80±2.28	41.9±0.69	43.4±2.26	83.5±1.15	36.8±3.45	6.41±0.70	85.1±0.73	89.7±0.97	82.7±1.16	1.74±0.01	0.18±0.01	3.57±0.08	4.19±0.01	4.00±0.06
PFHxA	24.7±2.09	56.2±0.39	63.8±2.95	94.8±0.18	56.0±4.10	7.39±2.08	95.1±0.41	96.0±0.15	94.3±0.47	1.85±0.00	0.00±0.00	3.19±0.11	3.40±0.07	0.56±0.01
PFHpA	68.6±0.33	72.2±0.91	85.8±1.35	96.9±0.00	78.2±2.06	9.90±2.22	97.1±0.00	97.7±0.00	96.8±0.00	10.9±0.01	0.00±0.00	0.33±0.00	18.7±0.04	0.73±0.01
PFOA	88.4±0.99	80.6±0.13	94.6±0.61	99.4±0.00	93.8±0.61	18.0±2.74	99.5±0.00	99.5±0.00	99.2±0.00	10.8±0.22	8.11±0.40	12.7±0.26	15.3±0.00	13.5±0.40
PFPrS	17.9±1.91	90.4±1.33	79.9±0.64	98.6±0.04	75.9±1.02	7.83±3.14	98.8±0.05	98.9±0.09	98.4±0.09	0.00±0.00	0.00±0.00	0.00±0.00	0.00±0.00	0.33±0.01
PFBS	31.3±2.72	92.9±1.08	89.7±0.89	99.3±0.03	86.1±1.96	10.0±2.12	99.4±0.18	99.6±0.06	99.2±0.00	0.38±0.00	0.00±0.00	1.26±0.03	2.25±0.01	0.16±0.00
PFPeS	85.0±0.25	95.3±0.52	96.1±0.44	99.6±0.00	94.2±1.62	15.7±2.34	99.7±0.03	99.7±0.05	99.6±0.02	12.8±0.07	1.52±0.01	7.52±0.56	2.57±0.01	10.5±0.01
PFHxS	93.4±0.56	96.7±0.57	98.1±0.68	99.9±0.00	98.4±0.14	23.3±1.08	99.9±0.03	99.9±0.06	99.9±0.00	2.91±0.00	0.00±0.00	0.60±0.01	2.33±0.05	0.00±0.00
PFHpS	98.0±0.30	98.6±0.18	99.1±0.53	99.8±0.01	98.8±5.64	62.3±7.61	99.8±0.00	99.8±0.00	99.9±0.00	10.9±0.15	2.56±0.18	6.72±0.33	14.3±0.22	0.00±0.00
PFOS	89.0±1.04	98.4±0.14	99.9±0.01	99.9±0.00	99.8±0.07	89.9±0.67	99.9±0.00	99.9±0.06	99.9±0.00	2.48±0.04	12.2±0.73	6.1±0.15	15.4±0.58	6.52±0.47
Cl-PFOS	90.9±1.92	99.0±0.48	99.6±0.35	99.9±0.00	99.0±0.98	93.8±0.80	99.8±0.00	99.9±0.00	99.9±0.00	5.30±0.14	9.83±0.58	7.19±0.10	5.79±0.09	5.50±2.04

Table A3.1.3. Suspect screening analysis of adsorption of PFASs in AFFF by 50 mg/L GAC, AER, PAER, CER, and NIR

Class #	Compound Acronym	Ionic charge [a]	% Adsorbed													
			GAC	**AER**					***PAER***			**CER**		***NIR***		
			Cal F400	A300	A520E	A532E	A600E	A860	*PFA694E*	*CalRes23 01*	*CalRes23 04*	C100	C150	*XAD-2*	*XAD-4*	*XAD-7HP*
1	AmPr-FEtSA [b]	Zwi	N/A [c]	N/A	20±1	3±0	N/A	N/A	5±0	12±2	N/A	1±0	1±0	1±0	10±1	1±0
	AmPr-FPrSA	Zwi	13±3	11±0	29±5	32±4	19±1	9±0	25±3	19±4	1±0	1±0	1±0	1±0	48±5	13±1
	AmPr-FBSA	Zwi	14±3	10±0	29±4	39±6	15±1	6±0	30±4	44±4	8±0	1±0	1±0	24±2	66±7	13±1
	AmPr-FPeSA	Zwi	15±3	12±0	30±4	44±7	15±1	6±0	38±6	50±8	21±1	1±0	1±0	64±4	76±3	42±4
	AmPr-FHxSA	Zwi	47±6	5±0	15±3	39±5	7±0	4±0	41±8	59±10	32±2	1±0	1±0	91±10	81±2	75±12
2	AmPr-FEtSA-PrA	Zwi	N/A	N/A	16±0	18±1	N/A	N/A	9±0	26±2	N/A	1±0	2±0	1±0	9±0	1±0
	AmPr-FPrSA-PrA	Zwi	52±3	41±4	84±7	85±8	66±1	8±0	70±10	69±9	41±8	1±0	1±0	1±0	1±0	1±0
	AmPr-FBSA-PrA	Zwi	77±5	44±2	85±2	88±2	68±0	12±0	75±11	82±4	56±6	1±0	1±0	1±0	1±0	1±0
	AmPr-FPeSA-PrA	Zwi	77±12	35±3	69±9	82±15	65±0	10±1	76±13	77±15	53±5	1±0	1±0	1±0	1±0	1±0
	AmPr-FHxSA-PrA	Zwi	83±3	39±1	85±9	88±2	68±5	14±0	86±13	89±3	76±7	1±0	1±0	1±0	1±0	1±0
3	CEtAmPr-FEtSA-PrA	Neg	N/A	N/A	11±1	5±0	N/A	N/A	0±0	1±0	N/A	3±0	3±0	6±0	8±0	11±1
	CEtAmPr-FPrSA-PrA	Neg	37±6	1±0	41±2	80±4	62±3	17±0	47±2	57±9	46±2	1±0	1±0	1±0	1±0	1±0
	CEtAmPr-FBSA-PrA	Neg	50±3	40±2	47±2	77±16	64±3	10±0	71±4	72±4	33±6	1±0	1±0	1±0	1±0	1±0
	CEtAmPr-FPeSA-PrA	Neg	38±3	41±7	83±4	73±4	68±2	4±0	74±4	68±12	37±7	1±0	1±0	1±0	1±0	1±0
	CEtAmPr-FHxSA-PrA	Neg	50±2	50±9	85±7	83±13	71±6	11±0	78±10	82±3	52±8	1±0	1±0	1±0	1±0	1±0
4	Cl-PFBS [d]	Neg	38±2	*>96* [e]	*>96*	*>96*	*>96*	16±1	*>96*	*>96*	*>96*	4±0	32±2	17±1	24±1	30±2
	Cl-PFPeS	Neg	*>95*	*>95*	*>95*	*>95*	*>95*	40±2	*>95*	*>95*	*>95*	2±0	36±2	7±1	16±1	6±0
	Cl-PFHxS	Neg	*>99*	*>99*	*>99*	*>99*	*>99*	22±0	*>99*	*>99*	*>99*	1±0	6±0	1±0	20±1	17±1

Class #	Compound Acronym	Ionic charge [a]	*Cal F400*	A300	A520E	A532E	A600E	A860	*PFA694E*	*CalRes23 01*	*CalRes23 04*	C100	C150	*XAD-2*	*XAD-4*	*XAD-7HP*
5	CMeAmPr-FBSA	Neg	54±3	30±1	66±3	47±2	29±1	9±0	65±3	77±4	54±3	1±0	1±0	1±0	25±5	9±2
	CMeAmPr-FPeSA	Neg	66±17	51±4	68±3	48±3	54±3	13±1	68±3	81±4	36±2	1±0	1±0	9±1	62±3	7±1
	CMeAmPr-FHxSA	Neg	77±20	55±4	75±6	59±8	56±4	13±0	68±7	85±4	64±3	1±0	1±0	15±2	25±2	10±1
6	CMeAmPr-FPrSAPrA	Neg	*>97*	*>97*	*>97*	*>97*	*>97*	9±1	*>97*	*>97*	*>97*	1±0	1±0	1±0	1±0	1±0
	CMeAmPr-FBSAPrA	Neg	*>99*	*>99*	*>99*	*>99*	*>99*	10±0	*>99*	*>99*	*>99*	1±0	1±0	1±0	1±0	1±0
	CMeAmPr-FPeSAPrA	Neg	*>97*	*>97*	*>97*	*>97*	*>97*	20±2	*>97*	*>97*	*>97*	1±0	1±0	1±0	1±0	1±0
	CMeAmPr-FHxSAPrA	Neg	*>98*	*>98*	*>98*	*>98*	*>98*	34±1	*>98*	*>98*	*>98*	1±0	1±0	1±0	1±0	1±0
7	F_5S-PFHxS	Neg	*>96*	*>96*	*>96*	*>96*	*>96*	*>96*	*>96*	*>96*	*>96*	1±0	1±0	1±0	1±0	1±0
8	FBSA	Neg	1±0	1±0	45±4	61±7	40±1	12±0	79±6	87±4	67±2	1±0	1±0	1±0	1±0	1±0
	FHxSA	Neg	18±3	48±3	64±6	85±4	65±8	12±0	84±1	90±14	80±4	1±0	1±0	1±0	1±0	1±0
9	H-PFHxA	Neg	26±2	*>97*	*>97*	*>97*	*>97*	10±0	*>97*	*>97*	*>97*	6±0	3±0	23±1	16±1	1±0
10	H-PFPrS	Neg	26±1	*>90*	*>90*	*>90*	*>90*	17±1	*>90*	*>90*	*>90*	1±0	4±0	1±0	5±0	1±0
	H-PFBS	Neg	24±1	*>96*	*>96*	*>96*	*>96*	14±0	*>96*	*>96*	*>96*	1±0	1±0	1±0	1±0	3±0
	H-PFHxS	Neg	*>96*	*>96*	*>96*	*>96*	*>96*	25±1	*>96*	*>96*	*>96*	11±0	16±1	32±2	43±2	37±3
	H-PFHpS	Neg	*>96*	*>96*	*>96*	*>96*	*>96*	25±1	*>96*	*>96*	*>96*	22±2	17±0	9±0	19±1	27±1
	H-PFOS	Neg	97±15	98±5	*>99*	*>99*	*>99*	75±6	*>99*	*>99*	*>99*	31±2	34±0	24±3	48±9	73±5
	H-PFDS	Neg	95±15	*>96*	*>96*	*>96*	*>96*	88±4	*>96*	*>96*	*>96*	8±0	6±0	10±0	65±3	60±3
11	H-UPFHpS	Neg	67±1	66±3	*>90*	*>90*	82±4	1±0	*>90*	*>90*	*>90*	2±0	1±0	7±0	4±0	5±0
	H-UPFOS	Neg	69±3	94±14	*>99*	*>99*	98±11	23±3	*>99*	*>99*	*>99*	13±1	23±0	20±2	34±3	36±7
12	K-PFPeS	Neg	49±5	*>94*	*>94*	*>94*	*>94*	13±0	*>94*	*>94*	*>94*	1±0	1±0	1±0	1±0	1±0
	K-PFHxS	Neg	81±10	*>93*	*>93*	*>93*	*>93*	25±4	*>93*	*>93*	*>93*	3±0	22±1	22±1	38±2	10±1
	K-PFHpS	Neg	*>34*	*>34*	*>34*	*>34*	34±0	29±1	*>34*	*>34*	*>34*	*>34*	*1±0*	*>34*	*>34*	*23±1*
	K-PFOS	Neg	*>99*	*>99*	*>99*	*>99*	*>99*	67±11	*>99*	*>99*	*>99*	34±2	38±2	37±7	52±4	42±2
13	MeEtCMeAmPr-FPeAd	Zwi	5±0	33±1	29±2	23±3	11±0	1±0	15±1	1±0	1±0	1±0	1±0	36±2	60±8	28±4

Class #	Compound Acronym	Ionic charge [a]	*Cal F400*	A300	A520E	A532E	A600E	A860	*PFA694E*	*CalRes2301*	*CalRes2304*	C100	C150	*XAD-2*	*XAD-4*	*XAD-7HP*
14	MeFPeSAA	Neg	1±0	88±4	84±4	91±5	47±2	39±4	90±4	*>97*	*>97*	1±0	1±0	1±0	1±0	1±0
	MeFHxSAA	Neg	54±5	90±1	94±10	93±18	44±2	60±3	93±5	99±5	99±5	1±0	1±0	1±0	1±0	1±0
15	OAmPr-FPeSA	Neg	N/A	N/A	1±0	1±0	N/A	N/A	1±0	1±0	N/A	1±0	1±0	25±4	54±2	13±3
	OAmPr-FHxSA	Neg	N/A	N/A	1±0	1±0	N/A	N/A	1±0	1±0	N/A	1±0	1±0	53±5	46±1	39±7
16	O-PFHxS	Neg	*>48*	*>48*	*>48*	*>48*	*>48*	*>48*	*>48*	*>48*	*>48*	*>48*	*>48*	*>48*	*>48*	*>48*
	O-PFHpS	Neg	*>50*	*>50*	*>50*	*>50*	*>50*	36±1	*>50*	*>50*	*>50*	21±1	20±1	1±0	36±2	*>50*
17	PFBSi	Neg	1±0	63±3	55±3	61±3	51±3	17±1	*>94*	*>94*	*>94*	1±0	1±0	11±1	7±0	1±0
	PFPeSi	Neg	1±0	*>84*	*>84*	*>84*	*>84*	1±0	*>84*	*>84*	*>84*	32±2	43±2	22±1	42±7	16±1
	PFHxSi	Neg	83±8	82±7	*>88*	*>88*	*>88*	14±1	*>88*	*>88*	*>88*	1±0	7±0	7±0	19±0	10±0
18	PFMeCHxCA	Neg	59±3	87±4	*>99*	*>99*	*>99*	28±2	*>99*	*>99*	*>99*	29±1	27±4	9±0	36±2	23±0
19	TAmPr-FPrSA	Pos	N/A	N/A	15±1	2±0	N/A	N/A	12±1	22±1	N/A	2±0	9±0	10±1	17±1	8±1
	TAmPr-FBSA	Pos	N/A	N/A	1±0	00±0	N/A	N/A	2±0	2±0	N/A	1±0	1±0	1±0	38±2	4±0
	TAmPr-FPeSA	Pos	N/A	N/A	1±0	9±0	N/A	N/A	3±0	1±0	N/A	1±0	2±0	23±1	47±2	22±2
	TAmPr-FHxSA	Pos	N/A	N/A	1±0	1±0	N/A	N/A	1±0	1±0	N/A	1±0	1±0	39±8	54±5	8±0
20	TAmPr-FPrSAPrA	Zwi	N/A	N/A	7±0	1±0	N/A	N/A	3±0	1±0	N/A	8±0	1±0	3±0	24±0	1±0
	TAmPr-FBSAPrA	Zwi	N/A	N/A	1±0	5±0	N/A	N/A	3±0	1±0	N/A	0±0	1±0	1±0	40±0	12±0
	TAmPr-FPeSAPrA	Zwi	N/A	N/A	1±0	1±0	N/A	N/A	1±0	1±0	N/A	1±0	1±0	1±0	35±1	9±2
	TAmPr-FHxSAPrA	Zwi	N/A	N/A	1±0	1±0	N/A	N/A	1±0	1±0	N/A	1±0	3±0	33±2	56±3	42±1
21	UPFHxS	Neg	85±10	*99*	96±5	*99*	97±14	10±0	99±8	99±8	99±6	7±0	3±0	6±0	9±0	10±1
	UPFHpS	Neg	61±3	*98*	*98*	*98*	*98*	24±0	98±12	98±12	98±12	60±3	62±8	65±4	52±3	71±10
	UPFOS	Neg	66±3	*99*	*99*	*99*	92±5	36±2	99±3	99±6	99±9	83±4	49±3	43±5	55±2	89±14

a. Predicted base on the pK_a values calculated using Sparc (Archem LLC)
b. Orange highlighted compounds are only detected under ESI+ screening mode
c. Data not available from ESI+ screening
d. Blue highlighted compounds are only detected under ESI- mode during LC-qTOF-MS analysis
e. Data with italic formatting are calculated based on the limit of quantification (i.e., %Ads > $100\times(C_{init} - LOQ)/C_{init}$)

Table A3.1.4. Log (K_{ex}) values for AERs and PAERs

Class #	Compound Acronym	Ionic charge [a]	*AER*					PAER		
			A300	*A520E*	*A532E*	*A600E*	*A860*	PFA694E	CalRes2301	CalRes2304
1	AmPr-FEtSA[b]	Zwi	N/A[c]	1.46±0.04	0.72±0.04	N/A	N/A	0.75±0.00	1.07±0.19	N/A
	AmPr-FPrSA	Zwi	1.00±0.00	1.68±0.13	1.91±0.07	1.24±0.05	1.12±0.01	1.52±0.09	1.28±0.21	0.04±0.00
	AmPr-FBSA	Zwi	0.96±0.02	1.70±0.09	2.04±0.08	1.10±0.03	0.90±0.02	1.64±0.12	1.82±0.08	0.95±0.02
	AmPr-FPeSA	Zwi	1.01±0.02	1.70±0.10	2.13±0.08	1.12±0.03	0.91±0.01	1.80±0.13	1.92±0.15	1.45±0.02
	AmPr-FHxSA	Zwi	0.65±0.01	1.34±0.14	2.05±0.07	0.71±0.05	0.70±0.04	1.85±0.15	2.07±0.16	1.69±0.05
2	AmPr-FEtSA-PrA	Zwi	N/A	1.35±0.00	1.58±0.02	N/A	N/A	0.99±0.00	1.46±0.06	N/A
	AmPr-FPrSA-PrA	Zwi	1.73±0.07	2.78±0.06	2.98±0.04	2.15±0.02	1.08±0.00	2.38±0.11	2.27±0.13	1.87±0.15
	AmPr-FBSA-PrA	Zwi	1.79±0.03	2.81±0.01	3.09±0.01	2.19±0.00	1.27±0.02	2.49±0.12	2.57±0.05	2.14±0.09
	AmPr-FPeSA-PrA	Zwi	1.62±0.05	2.42±0.09	2.90±0.09	2.13±0.00	1.18±0.04	2.50±0.13	2.45±0.19	2.09±0.07
	AmPr-FHxSA-PrA	Zwi	1.70±0.03	2.82±0.07	3.12±0.01	2.19±0.05	1.34±0.02	2.78±0.13	2.82±0.03	2.54±0.06
3	CEtAmPr-FEtSA-PrA	Neg	N/A	1.17±0.04	0.97±0.02	N/A	N/A	-0.95±0.04	-0.30±0.05	N/A
	CEtAmPr-FPrSA-PrA	Neg	-0.10±0.00	1.91±0.03	2.84±0.02	2.06±0.04	1.45±0.01	1.96±0.04	2.05±0.15	1.96±0.04
	CEtAmPr-FBSA-PrA	Neg	1.71±0.03	2.02±0.03	2.76±0.10	2.10±0.03	1.19±0.01	2.39±0.04	2.33±0.05	1.73±0.15
	CEtAmPr-FPeSA-PrA	Neg	1.73±0.11	2.77±0.03	2.68±0.02	2.18±0.02	0.74±0.01	2.46±0.04	2.24±0.17	1.81±0.14
	CEtAmPr-FHxSA-PrA	Neg	1.90±0.13	2.84±0.06	2.93±0.08	2.24±0.06	1.23±0.00	2.56±0.10	2.58±0.03	2.06±0.11
4	Cl-PFBS[d]	Neg	*3.30* [e]	*3.49*	*3.65*	*3.26*	1.42±0.03	*3.41*	*3.33*	*3.44*
	Cl-PFPeS	Neg	*3.16*	*3.34*	*3.51*	*3.12*	1.95±0.03	*3.27*	*3.19*	*3.30*
	Cl-PFHxS	Neg	*3.74*	*3.93*	*4.09*	*3.70*	1.57±0.01	*3.85*	*3.77*	*3.88*
5	CMeAmPr-FBSA	Neg	1.51±0.04	2.36±0.03	2.19±0.02	1.47±0.04	1.14±0.03	2.27±0.04	2.45±0.05	2.10±0.04
	CMeAmPr-FPeSA	Neg	1.91±0.05	2.41±0.03	2.21±0.03	1.92±0.04	1.30±0.03	2.34±0.04	2.54±0.05	1.78±0.04
	CMeAmPr-FHxSA	Neg	1.99±0.05	2.55±0.05	2.40±0.06	1.95±0.05	1.31±0.01	2.33±0.08	2.66±0.05	2.28±0.04
6	CMeAmPr-FPrSAPrA	Neg	*3.37*	*3.56*	*3.72*	*3.34*	1.14±0.06	*3.49*	*3.40*	*3.52*
	CMeAmPr-FBSAPrA	Neg	*3.72*	*3.90*	*4.07*	*3.68*	1.16±0.03	*3.83*	*3.75*	*3.86*
	CMeAmPr-FPeSAPrA	Neg	*3.36*	*3.54*	*3.70*	*3.32*	1.53±0.08	*3.47*	*3.38*	*3.50*
	CMeAmPr-FHxSAPrA	Neg	*3.53*	*3.71*	*3.88*	*3.49*	1.84±0.02	*3.64*	*3.56*	*3.67*
7	F_5S-PFHxS	Neg	*3.28*	*3.46*	*3.63*	*3.24*	*3.52*	*3.39*	*3.31*	*3.42*
8	FBSA	Neg	-0.11±0.00	1.99±0.06	2.42±0.05	1.68±0.02	1.25±0.02	2.58±0.06	2.74±0.05	2.34±0.02
	FHxSA	Neg	1.86±0.05	2.33±0.07	3.01±0.02	2.13±0.09	1.26±0.00	2.74±0.01	2.89±0.15	2.63±0.04

Class #	Compound Acronym	Ionic charge [a]	*A300*	*A520E*	*A532E*	*A600E*	*A860*	PFA694E	CalRes2301	CalRes2304
9	H-PFHxA	Neg	*3.45*	*3.64*	*3.80*	*3.41*	1.16±0.02	*3.57*	*3.48*	*3.59*
10	H-PFPrS	Neg	*2.85*	*3.03*	*3.203*	*2.81*	1.44±0.03	*2.96*	*2.88*	*2.99*
	H-PFBS	Neg	*3.32*	*3.51*	*3.67*	*3.28*	1.35±0.02	*3.43*	*3.35*	*3.46*
	H-PFHxS	Neg	*3.24*	*3.42*	*3.59*	*3.20*	1.64±0.04	*3.35*	*3.27*	*3.38*
	H-PFHpS	Neg	*3.32*	*3.51*	*3.67*	*3.29*	1.65±0.03	*3.44*	*3.35*	*3.46*
	H-PFOS	Neg	3.66±0.03	*4.35*	*4.51*	*4.13*	2.60±0.05	*4.28*	*4.20*	*4.31*
	H-PFDS	Neg	*3.26*	*3.45*	*3.61*	*3.22*	2.99±0.03	*3.38*	*3.29*	*3.40*
11	H-UPFHpS	Neg	2.18±0.04	*3.04*	*3.21*	2.53±0.04	0.13±0.08	*2.97*	*2.89*	*3.00*
	H-UPFOS	Neg	3.07±0.11	*3.97*	*4.13*	3.49±0.08	1.60±0.10	*3.90*	*3.81*	*3.93*
12	K-PFPeS	Neg	*3.09*	*3.28*	*3.44*	*3.06*	1.31±0.00	*3.21*	*3.12*	*3.23*
	K-PFHxS	Neg	*3.04*	*3.22*	*3.39*	2.88±0.04	1.66±0.10	*3.15*	*3.07*	*3.18*
	K-PFHpS	Neg	*1.60*	*1.79*	*1.95*	*1.56*	1.73±0.03	*1.72*	*1.63*	*1.74*
	K-PFOS	Neg	*4.18*	*4.37*	*4.53*	*4.15*	2.45±0.11	*4.30*	*4.21*	*4.33*
13	MeEtCMeAmPr-FPeAd	Zwi	1.59±0.03	1.69±0.05	1.71±0.07	0.94±0.03	0.13±0.02	1.27±0.07	-0.08±0.00	0.04±0.00
14	MeFPeSAA	Neg	2.74±0.03	2.80±0.04	3.23±0.02	1.81±0.04	1.93±0.07	2.96±0.04	*3.50*	*3.61*
	MeFHxSAA	Neg	2.83±0.01	3.24±0.07	3.33±0.09	1.76±0.04	2.30±0.04	3.16±0.04	3.92±0.05	4.03±0.04
15	OAmPr-FPeSA	Neg	N/A	-0.05±0.00	0.11±0.00	N/A	N/A	-0.12±0.00	-0.21±0.00	N/A
	OAmPr-FHxSA	Neg	N/A	0.03±0.00	0.20±0.00	N/A	N/A	-0.04±0.00	-0.12±0.00	N/A
16	O-PFHxS	Neg	*1.86*	*2.04*	*2.20*	*1.82*	*2.10*	*1.97*	*1.88*	*2.00*
	O-PFHpS	Neg	*1.89*	*2.07*	*2.24*	*1.85*	1.88±0.01	*2.00*	*1.92*	*2.03*
17	PFBSi	Neg	2.12±0.04	2.17±0.03	2.43±0.02	1.88±0.04	1.46±0.02	*3.22*	*3.13*	*3.25*
	PFPeSi	Neg	*2.60*	*2.78*	*2.94*	*2.56*	0.13±0.04	*2.71*	*2.63*	*2.74*
	PFHxSi	Neg	2.55±0.06	*2.94*	*3.10*	*2.72*	1.35±0.03	*2.87*	*2.78*	*2.90*
18	PFMeCHxCA	Neg	2.70±0.04	*4.08*	*4.25*	*3.86*	1.71±0.06	*4.01*	*3.93*	*4.04*
19	TAmPr-FPrSA	Pos	N/A	1.33±0.03	0.64±0.02	N/A	N/A	1.15±0.04	1.37±0.05	N/A
	TAmPr-FBSA	Pos	N/A	0.08±0.00	-0.09±0.04	N/A	N/A	0.20±0.03	0.22±0.11	N/A
	TAmPr-FPeSA	Pos	N/A	0.08±0.00	1.23±0.02	N/A	N/A	0.42±0.04	-0.08±0.00	N/A
	TAmPr-FHxSA	Pos	N/A	0.08±0.00	0.24±0.00	N/A	N/A	0.01±0.00	-0.08±0.00	N/A

Class #	Compound Acronym	Ionic charge [a]	*A300*	*A520E*	*A532E*	*A600E*	*A860*	PFA694E	CalRes2301	CalRes2304
20	TAmPr-FPrSAPrA	Zwi	N/A	0.96±0.03	0.25±0.02	N/A	N/A	0.45±0.01	-0.08±0.00	N/A
	TAmPr-FBSAPrA	Zwi	N/A	0.08±0.00	0.95±0.01	N/A	N/A	0.45±0.00	-0.08±0.00	N/A
	TAmPr-FPeSAPrA	Zwi	N/A	0.08±0.00	0.24±0.00	N/A	N/A	0.01±0.00	-0.08±0.00	N/A
	TAmPr-FHxSAPrA	Zwi	N/A	0.08±0.00	0.24±0.00	N/A	N/A	0.01±0.00	-0.08±0.00	N/A
21	UPFHxS	Neg	*3.76*	3.45±0.04	*4.11*	3.40±0.11	1.16±0.02	*3.87*	*3.79*	*3.90*
	UPFHpS	Neg	*3.53*	*3.72*	*3.88*	*3.49*	1.62±0.01	*3.65*	*3.56*	*3.67*
	UPFOS	Neg	*4.07*	*4.26*	*4.42*	2.91±0.04	1.89±0.03	*4.19*	*4.10*	*4.21*

a. Predicted base on the pK_a values calculated using Sparc (Archem LLC)
b. Orange highlighted compounds are only detected under ESI+ screening mode
c. Data not available from ESI+ screening
d. Blue highlighted compounds are only detected under ESI- mode during LC-qTOF-MS analysis
e. Data with italic formatting are calculated based on the limit of quantification

Table A3.2.1. Measured density of anion exchange resin; gram dry resin per milliliter wet settled resin.

Resin	Chloride-form	Sulfate-form
A520E	0.4403	0.4912
A860	0.6218	0.8280

Table A3.2.2. Composition of Tempe groundwater used as background matrix for all test waters, and other test waters. Values are averages.

Constituent	Unit	GW	GW + SRNOM	GW + PFAAs	GW + SRNOM + PFAAs
pH		8.1	8.0		
Conductivity	µS/cm	1800	1700		
Chloride	mg/L	290	280		
Sulfate	mg/L	98	94		
Sodium	mg/L	270	250		
Magnesium	mg/L	27	26		
Calcium	mg/L	64	61		
DOC	mg/L as C	1.4	8.1	1.5	8.4
DOC[a]	meq/L		0.081		0.084
UVA254	1/cm	0.016	0.314	0.022	0.325
SUVA254[b]	L/mg·m	1.1	3.9	1.4	3.9
PFBA	µg/L			319	399
PFHxA	µg/L			586	565
PFOA	µg/L			252	274
PFBS	µg/L			410	428
PFHxS	µg/L			363	342
PFOS	µg/L			271	286
sumPFAA	mg/L as C			0.45	0.47
sumPFAA/DOC	mg C/mg C			0.29	0.056
sumPFAA	meq/L			0.0068	0.0072
sumPFAA/DOC	meq/meq				0.086

[a] Assuming SRNOM charge density of 10 meq/g C. [b] SUVA254 = (UVA254 (1/cm)/DOC (mg/L)) × 100.

Table A3.2.3. Tandem mass spectrometry parameters for PFAAs analysis.

Name	Parent Mass (Da)	Product Mass (Da)	Retention time (min)	DP (V)	EP (V)	CE (V)	CXP (V)	LOQ (µg/L)	Internal standard	R^2
PFBA[a]	212.8	168.9	3.6	-10	-4.5	-12	0	5	[$^{13}C_4$]PFBA	0.992
PFBS (1)[b]	298.9	80	4.2	-45	-8	-50	-2	1	[$^{13}C_3$]PFBS	0.993
PFBS (2)[b]	298.9	98.9	4.2	-45	-8	-42	0	0.5	[$^{13}C_3$]PFBS	0.992
PFHxA (1)	312.9	118.8	4.53	-10	-6	-30	-4	5	[$^{13}C_2$]PFHxA	0.996
PFHxA (2)	312.9	269	4.53	-10	-6	-12	0	5	[$^{13}C_2$]PFHxA	0.986
PFHxS (1)	398.8	79.9	4.8	-65	-8	-56	-6	0.5	[$^{13}C_4$]PFHxS	0.997
PFHxS (2)	398.8	98.9	4.8	-65	-8	-50	0	1	[$^{13}C_4$]PFHxS	0.995
PFOA (1)	412.9	168.9	5.2	-10	-4.5	-24	-4	1	[$^{13}C_4$]PFOA	0.993
PFOA (2)	412.9	369	5.2	-10	-4.5	-14	-2	0.5	[$^{13}C_4$]PFOA	0.985
PFOS (1)	498.9	98.9	5.45	-70	-7.5	-54	0	5	[$^{13}C_4$]PFOS	0.998
PFOS (2)	498.9	79.9	5.45	-70	-7.5	-86	-6	0.5	[$^{13}C_4$]PFOS	0.987
[$^{13}C_4$]PFBA	216.9	171.8	3.6	-10	-4.5	-16	0			
[$^{13}C_3$]PFBS	301.9	79.9	4.2	-40	-11	-50	-2			
[$^{13}C_2$]PFHxA	315	270	4.53	-10	-6	-12	-2			
[$^{13}C_4$]PFHxS	402.9	83.9	4.8	-60	-10	-64	-6			
[$^{13}C_4$]PFOA	416.9	372.1	5.2	-10	-4	-14	0			
[$^{13}C_4$]PFOS	503	79.9	5.45	-70	-7	-74	-6			

Composition for injection was 1:1 MeOH:water.

a: PFBA has only one valid transition. b: (1) Transition for quantification, (2) transition for confirmation.

DP: declustering potential. EP: entrance potential. CE: collision energy. CXP: collision exit potential. Internal standard: selected isotope-labeled compound for internal standardization. R^2: Coefficient of determination

Table A3.2.4. Two factor ANOVA with replication results for Figure 1 using significance level α = 0.05. ANOVA conducted using C/C_0 values after AER treatment.

Anova: Two-Factor With Replication						
SUMMARY	R-Cl	R-SO4	Total			
A520E						
Count	13	13	26			
Sum	7.860	4.253	12.113			
Average	0.605	0.327	0.466			
Variance	0.030	0.018	0.043			
A860						
Count	13	13	26			
Sum	3.761	2.967	6.729			
Average	0.289	0.228	0.259			
Variance	0.004	0.009	0.007			
Total						
Count	26	26				
Sum	11.621	7.220				
Average	0.447	0.278				
Variance	0.042	0.016				
ANOVA						
Source of Variation	*SS*	*df*	*MS*	*F*	*P-value*	*F crit*
Sample	0.557	1	0.557	36.45	2.2E-07	4.04
Columns	0.372	1	0.372	24.35	1.0E-05	4.04
Interaction	0.152	1	0.152	9.95	2.8E-03	4.04
Within	0.734	48	0.015			
Total	1.816	51				

Because "Interaction" term was significant, post-hoc analysis using one-sided, paired t-tests with Bonferroni correction was conducted (corrected α = 0.0125) with the following results:

$(C/C_0)a - (C/C_0)b$	**mean**	**p-value**
A520E/Cl – A860/Cl	0.32	5.1E-7
A520E/SO4 – A860/SO4	0.10	4.0E-4
A520E/Cl – A520E/SO4	0.26	8.0E-8
A860/Cl – A860/SO4	0.06	0.007

Table A3.2.5. Two factor ANOVA with replication results for Figure 2 using significance level α = 0.05. ANOVA conducted using C/C_0 values after AER treatment.

Anova: Two-Factor With Replication						
SUMMARY	R-Cl	R-SO4	Total			
A520E						
Count	14	14	28			
Sum	7.365	3.764	11.130			
Average	0.526	0.269	0.397			
Variance	0.057	0.027	0.057			
A860						
Count	14	14	28			
Sum	4.896	3.521	8.417			
Average	0.350	0.251	0.301			
Variance	0.008	0.003	0.008			
Total						
Count	28	28				
Sum	12.262	7.285				
Average	0.438	0.260				
Variance	0.039	0.014				
ANOVA						
Source of Variation	*SS*	*df*	*MS*	*F*	*P-value*	*F crit*
Sample	0.131	1	0.131	5.538	0.022	4.027
Columns	0.442	1	0.442	18.644	7.10E-05	4.027
Interaction	0.088	1	0.088	3.729	0.059	4.027
Within	1.233	52	0.024			
Total	1.896	55				

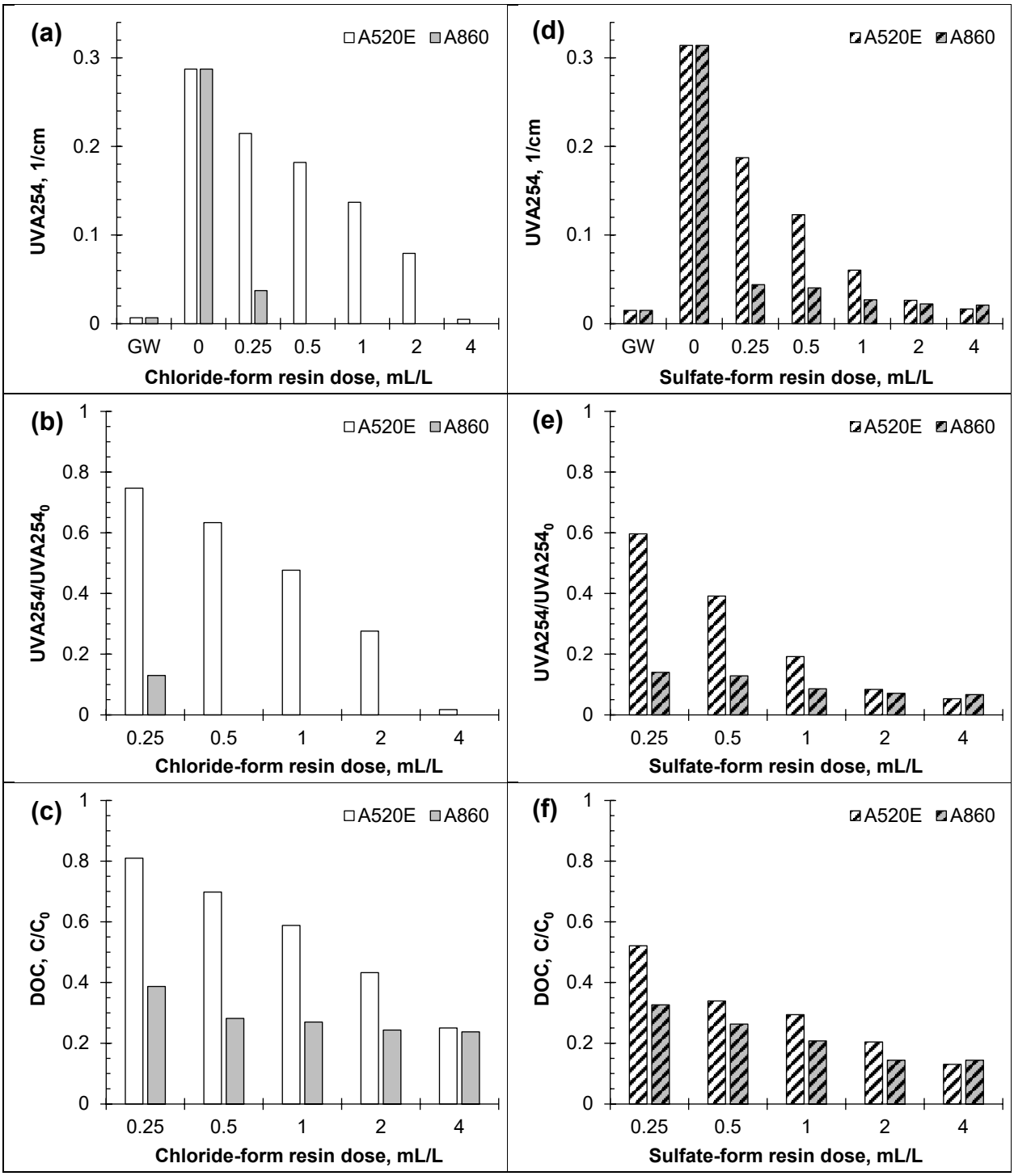

Figure A3.2.1. Impact of resin polymer composition (polystyrene A520E resin vs. polyacrylic A860 resin) and mobile counterion (chloride vs. sulfate) on removal of UVA254 and DOC by AER in the presence of SRNOM. GW is groundwater. Test water (resin dose 0–4 mL/L) is combination of groundwater NOM and SRNOM. (a), (b): measured UV absorbance (per cm); (c), (d): relative UV absorbance in comparison to initial sample (0, without resin); (e), (f): relative concentration of DOC remaining in water.

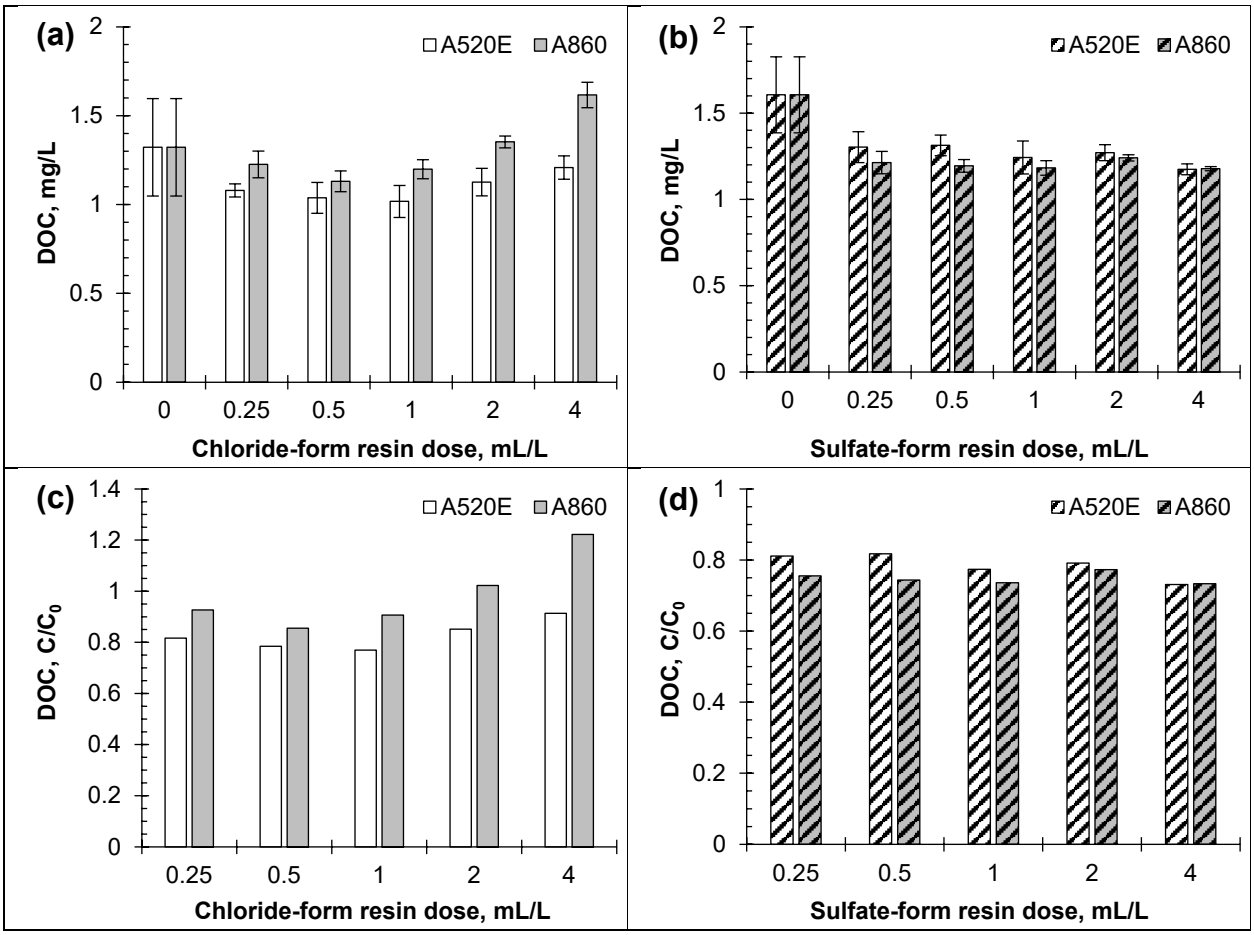

Figure A3.2.2. Impact of resin polymer composition (polystyrene A520E resin vs. polyacrylic A860 resin) and mobile counterion (chloride vs. sulfate) on DOC removal by AER. Test water is natural groundwater. (a), (b): concentration of DOC remaining in water (mg/L); (c), (d): relative concentration of DOC remaining in water.

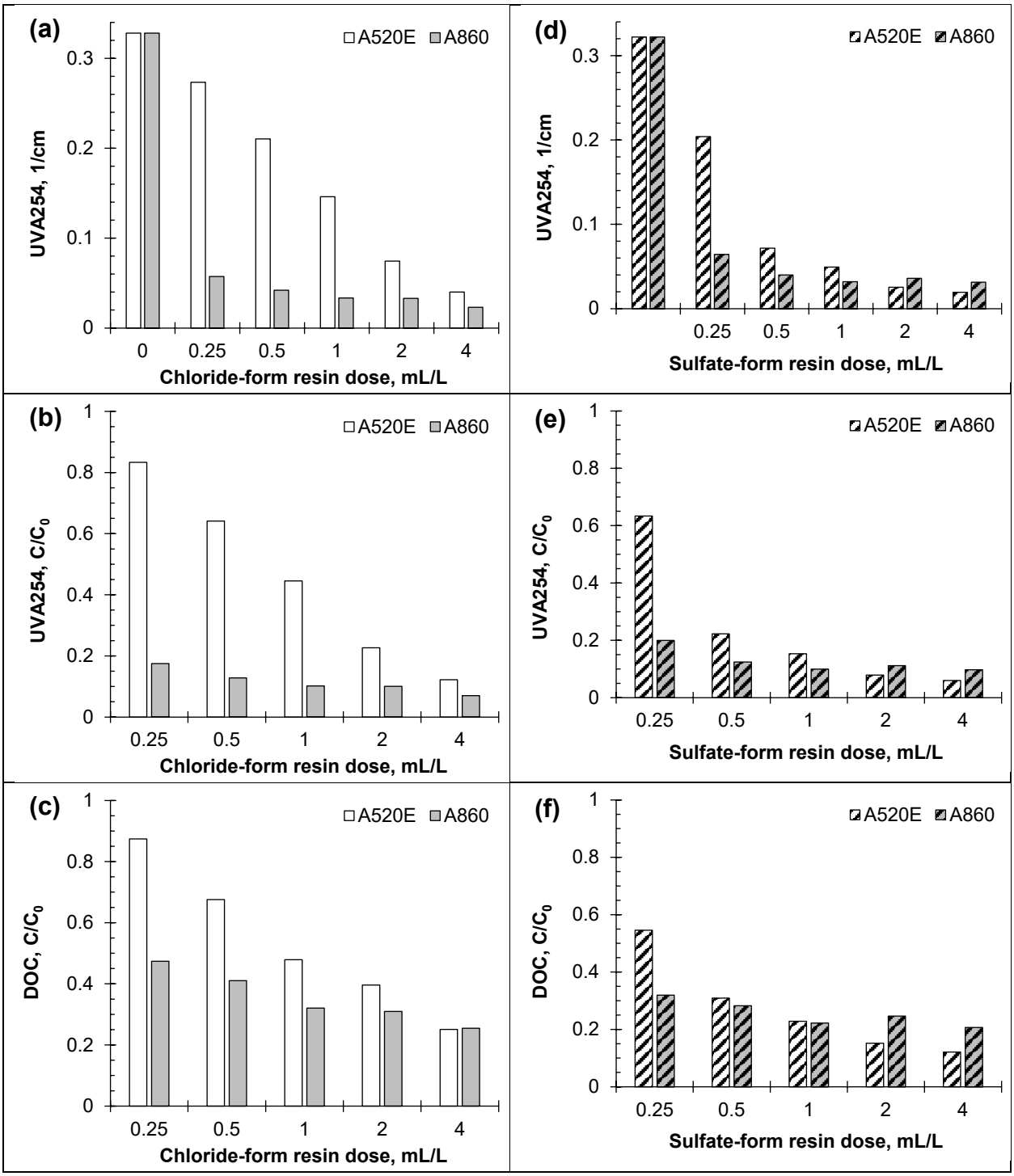

Figure A3.2.3. Impact of resin polymer composition (polystyrene A520E resin vs. polyacrylic A860 resin) and mobile counterion (chloride vs. sulfate) on removal of UVA254 and DOC by AER in presence of perfluoroalkyl acids (PFAAs). Test water (resin dose 0–4 mL/L) is combination of groundwater DOC, SRNOM, and six PFAAs. (a), (b): measured UV absorbance (per cm); (c), (d): UV absorbance normalized by initial sample (0, without resin); (e), (f): relative concentration of DOC remaining in water.

Table A3.3.1. Groundwater characteristics used to prepare test water for ion-exchange treatment.

Constituent	Unit	Groundwater
pH	–	8.1
Conductivity	µS/cm	2179
UVA 254	1/cm	0.064
DOC	mg/L as C	4.2
Chloride	mg/L	410
Sulfate	mg/L	103
Sodium	mg/L	230
Magnesium	mg/L	49
Calcium	mg/L	84
Potassium	mg/L	8.9

Table A3.3.2. Mass spectrometry parameters for PFAA analysis.

Name	Precursor Ion (m/z)	Product Ion (m/z)	Retention Time (min)	Internal Standard
PFBA[a]	213.0	169.0	2.106	$[^{13}C_2]$PFHxA
PFBS (1)[b]	289.9	80.0	2.438	$[^{13}C_3]$PFBS
PFBS (2)[b]	289.9	98.9	2.444	$[^{13}C_3]$PFBS
PFHxA (1)	313.0	269.1	2.756	$[^{13}C_2]$PFHxA
PFHxA (2)	313.0	119.0	2.756	$[^{13}C_2]$PFHxA
PFHxS (1)	398.9	79.9	3.074	$[^{18}O_2]$PFHxS
PFHxS (2)	398.9	99.0	3.081	$[^{18}O_2]$PFHxS
PFOA (1)	413.0	369.0	3.074	$[^{13}C_4]$PFOA
PFOA (2)	413.0	169.0	3.406	$[^{13}C_4]$PFOA
PFOS (1)	498.9	79.9	3.672	$[^{13}C_4]$PFOS
PFOS (2)	498.9	98.9	3.679	$[^{13}C_4]$PFOS
$[^{13}C_3]$PFBS	217.0	172.0	2.106	
$[^{13}C_2]$PFHxA	315.0	270.0	2.756	
$[^{18}O_2]$PFHxS	403.0	103.0	3.087	
$[^{13}C_4]$PFOA	417.0	372.0	3.399	
$[^{13}C_4]$PFOS	503.0	89.9	3.685	

Composition for injection was 1:1 methanol:water.
[a] PFBA has only one valid transition. [b] (1) Transition for quantification, (2) transition for confirmation.

Table A3.3.3. Molar speciation of the six PFAS studied in the influent and the molar speciation of PFAS that adsorbed onto AER over multiple regeneration cycles. Molar speciation data are given as percentage.

		Experiment 1[a,c,f]	Experiment 2[a,d,f]	Experiment 3[a,c,g]	Experiment 4[a,c,g]	Experiment 5[b,e,h]
Influent	PFBA	15	15	9	15	14
	PFHxA	23	23	22	25	21
	PFOA	30	30	32	27	29
	PFBS	12	12	7	9	10
	PFHxS	12	12	16	14	13
	PFOS	8	8	14	10	13
Regeneration cycle 1	PFBA	13	13	12	12	3
	PFHxA	23	23	24	24	4
	PFOA	30	30	28	28	33
	PFBS	13	13	9	9	8
	PFHxS	13	13	16	16	19
	PFOS	8	8	11	11	33
Regeneration cycle 2	PFBA	13	13	7	11	5
	PFHxA	22	23	23	24	8
	PFOA	30	30	26	28	33
	PFBS	13	13	11	9	5
	PFHxS	14	13	19	16	15
	PFOS	8	8	14	12	34
Regeneration cycle 3	PFBA	14	13	6	10	3
	PFHxA	22	22	20	25	6
	PFOA	30	31	30	28	30
	PFBS	13	13	12	9	4
	PFHxS	14	13	19	16	15
	PFOS	7	8	13	12	42
Regeneration cycle 4	PFBA	-	-	8	10	5
	PFHxA	-	-	20	24	6
	PFOA	-	-	25	28	33
	PFBS	-	-	9	9	5
	PFHxS	-	-	16	16	15
	PFOS	-	-	22	13	36
Regeneration cycle 5	PFBA	-	-	0	12	7
	PFHxA	-	-	22	7	9
	PFOA	-	-	29	35	30
	PFBS	-	-	12	11	4
	PFHxS	-	-	21	20	13
	PFOS	-	-	16	15	37

Dash (-) used to indicate that no sample was collected; experiments 1 and 2 show no values for regeneration cycles 4 and 5 because only three regeneration cycles were tested.[a] Polystyrene A520E resin used. [b] Polyacrylic A860 resin used. [c] Regeneration solution used 0.5% $(NH_4)_2SO_4$ + 0.5% NH_4OH. [d] Regeneration solution used 0.5% $(NH_4)_2SO_4$ + 50% methanol. [e] Regeneration solution used 8% $NaHCO_3$. [f] Total initial PFAS concentration was 0.28 mg/L. [g] Total initial PFAS concentration was 11.2 mg/L. [h] Total initial PFAs concentration was 6.23 mg/L.

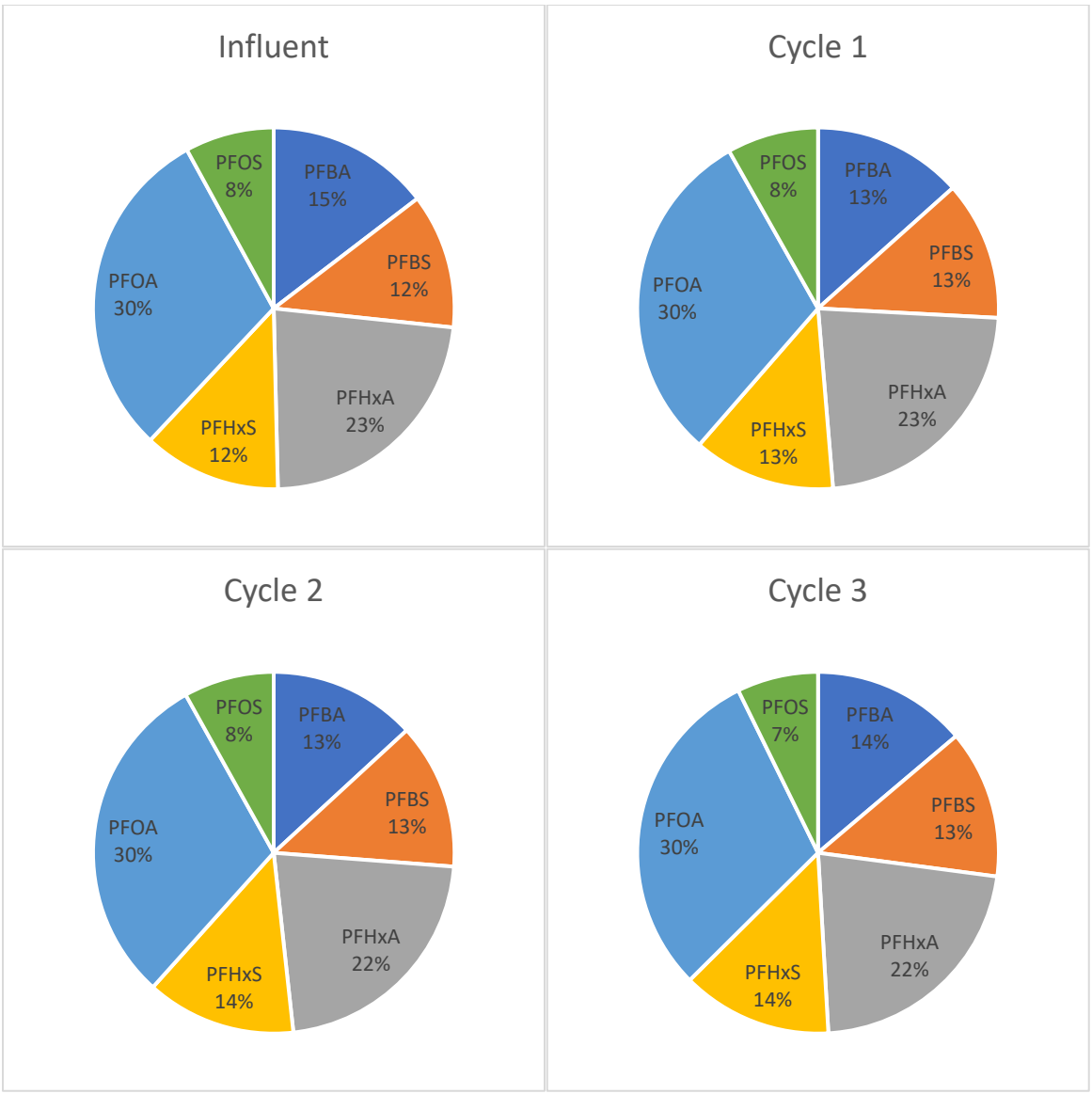

Figure A3.3.1: Experiment 1 molar speciation of the six PFAS studied in the influent (top left), and the molar speciation of PFAS that adsorbed onto A520E resin during the first (top right), second (bottom left), and third regeneration cycle (bottom right). Total initial PFAS concentration equal to 280 µg/L; individual initial concentrations listed in Table 2.5.1.

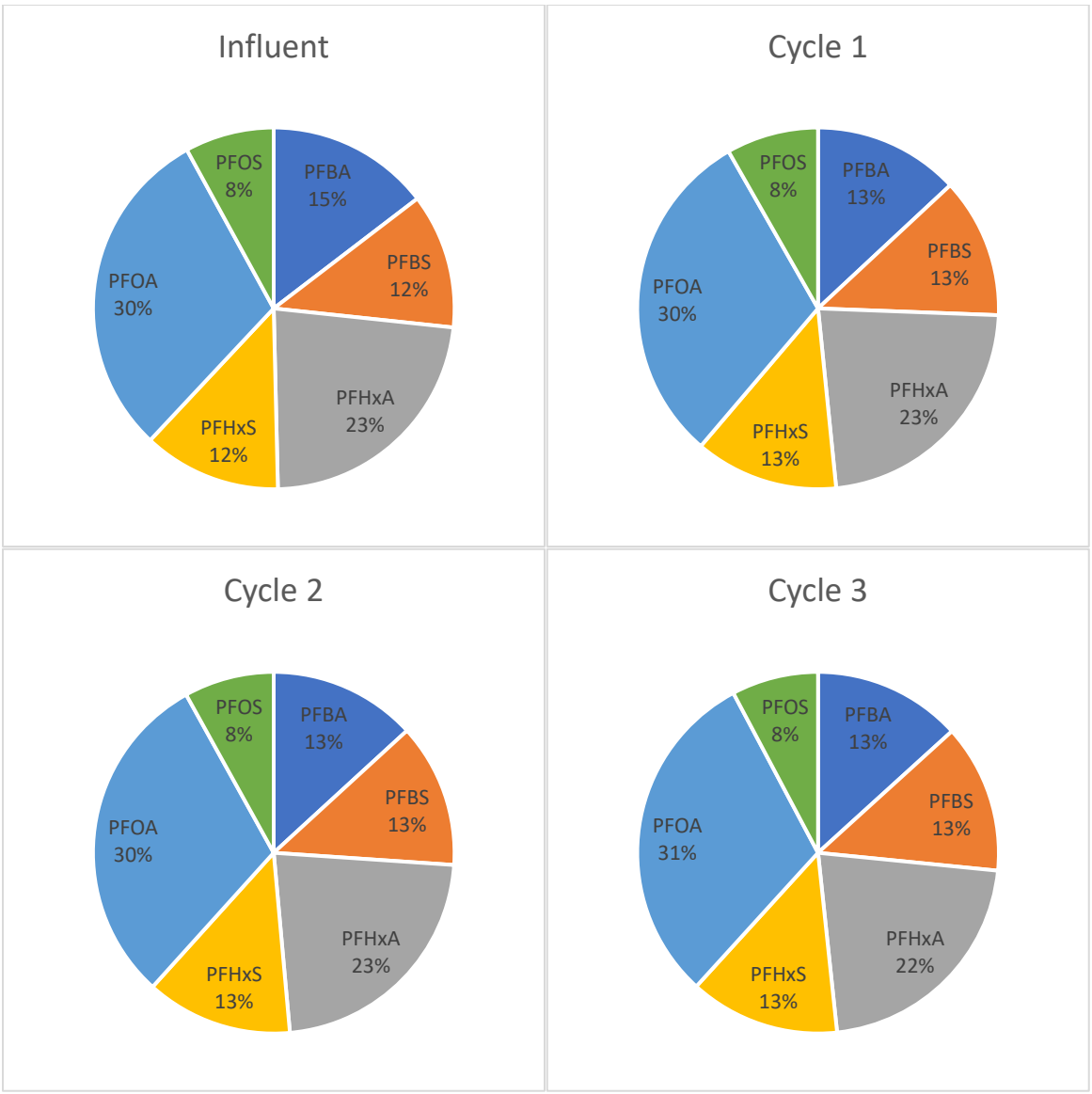

Figure A3.3.2: Experiment 2 molar speciation of the six PFAS studied in the influent (top left), and the molar speciation of PFAS chemicals that adsorbed onto A520E resin during the first (top right), second (bottom left), and third regeneration cycle (bottom right). Total initial PFAS concentration equal to 280 µg/L; individual initial concentrations listed in Table 2.5.1.

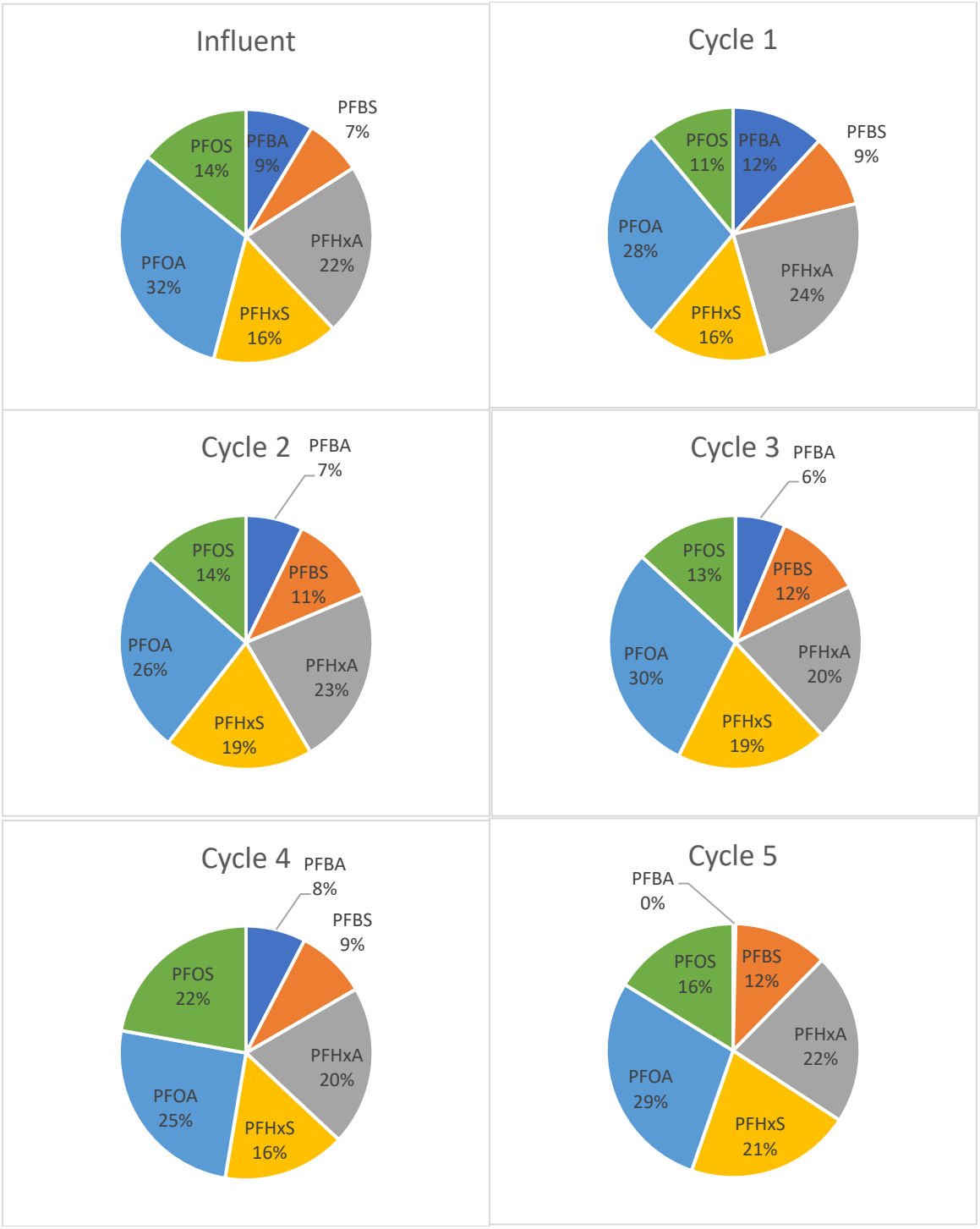

Figure A3.3.3: Experiment 3 molar speciation of the six PFAS chemicals in the influent (top left), and the molar speciation of PFAS chemicals that adsorbed onto A520E resin during the first (top right), second (middle left), third (middle right), fourth (bottom left), and fifth regeneration cycle (bottom right). Total initial PFAS concentration equal to 11,200 µg/L; individual initial concentrations listed in Table 2.5.1.

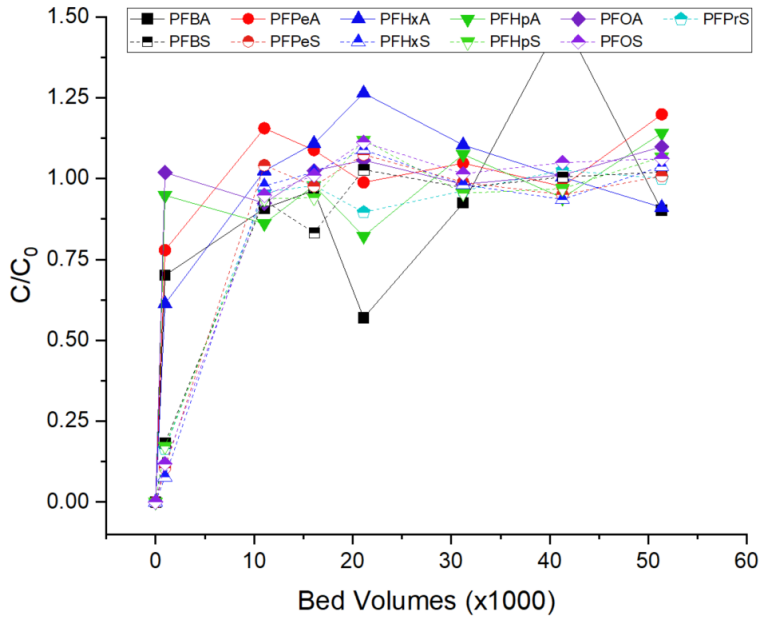

Figure A3.4.1. Breakthrough data after sourcewater treatment using A860 (2-min EBCT).

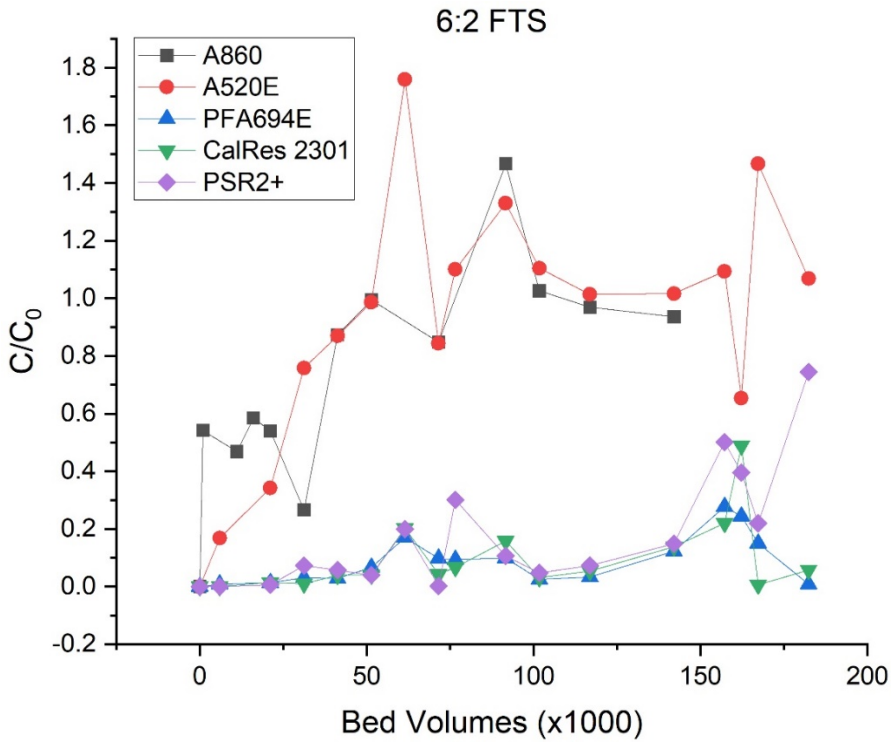

Figure A3.4.2. Breakthrough of 6:2 FTS through the five AER beds (2-min EBCT).

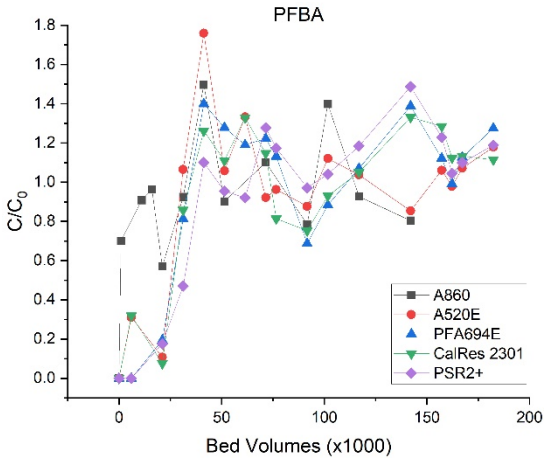

Figure A3.4.3. Breakthrough of PFBA through different AER beds (2-min EBCT).

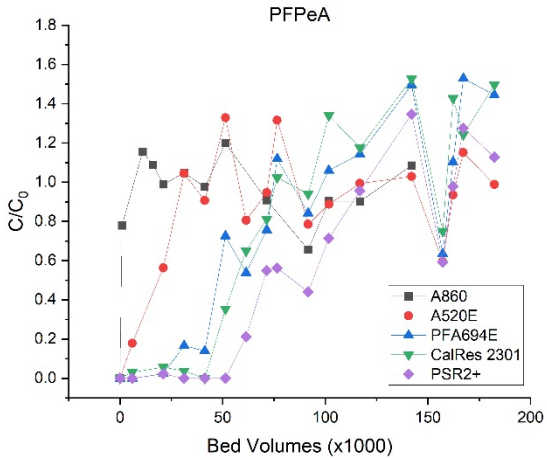

Figure A3.4.4. Breakthrough of PFPeA through different AER beds (2-min EBCT).

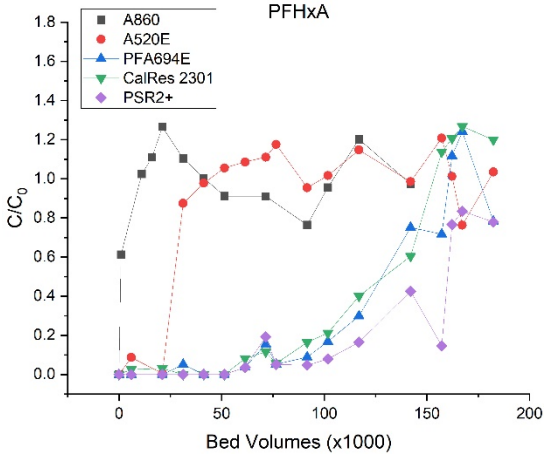

Figure A3.4.5. Breakthrough of PFHxA through different AER beds (2-min EBCT).

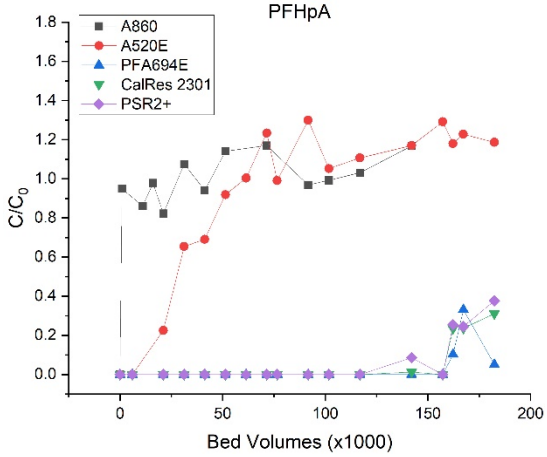

Figure A3.4.6. Breakthrough of PFHpA through different AER beds (2-min EBCT).

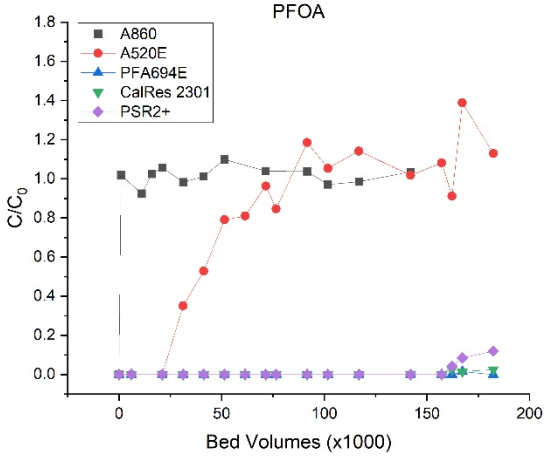

Figure A3.4.7. Breakthrough of PFOA through different AER beds (2-min EBCT).

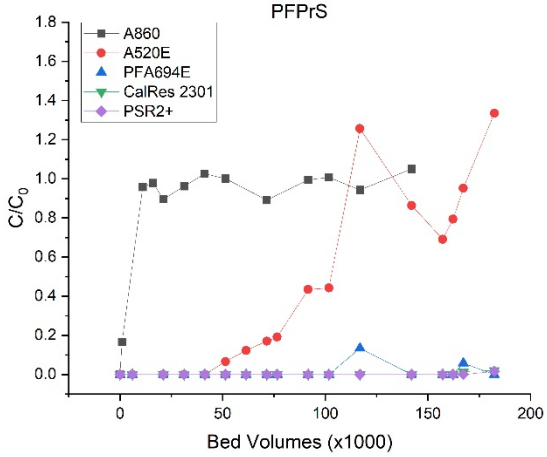

Figure A3.4.8. Breakthrough of PFPrS through different AER beds (2-min EBCT).

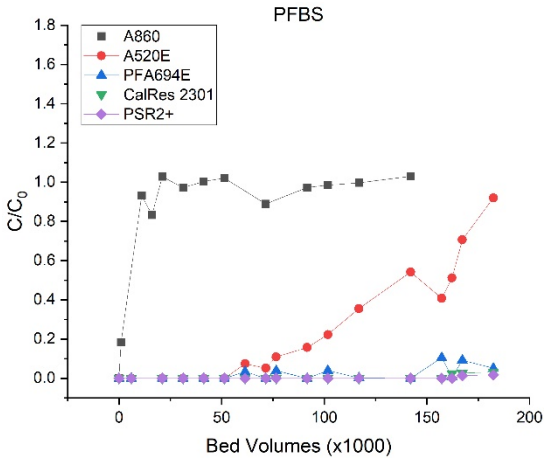

Figure A3.4.9. Breakthrough of PFBS through different AER beds (2-min EBCT).

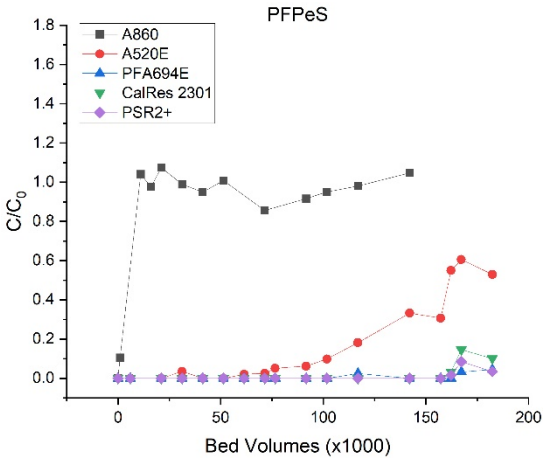

Figure A3.4.10. Breakthrough of PFPeS through different AER beds (2-min EBCT).

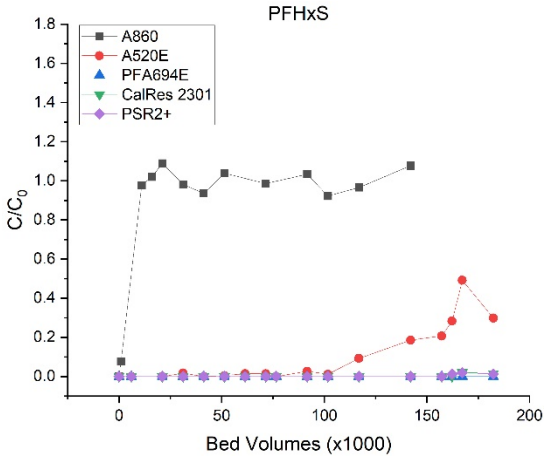

Figure A3.4.11. Breakthrough of PFHxS through the four AER beds at a 2-min EBCT

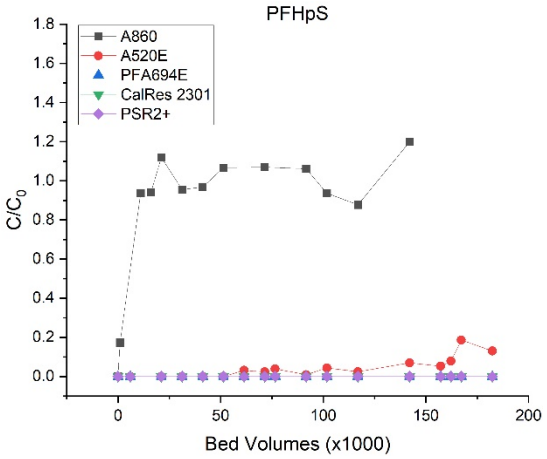

Figure A3.4.12. Breakthrough of PFHpS through different AER beds (2-min EBCT).

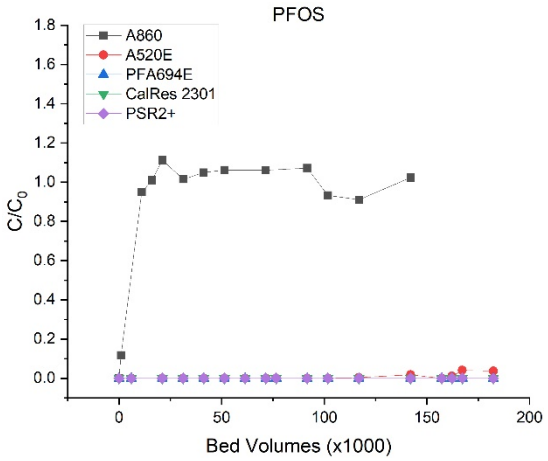

Figure A3.4.13. Breakthrough of PFOS through different AER beds (2-min EBCT).

Figures A3.4.14-A3.4.25 shows the effects of varying EBCT on PFAS breakthrough data with one of the single-use resins, PSR2+. Breakthrough data is presented for individual PFASs on a bed volume-equivalent basis when monitoring effluent after 30-sec and 2-min EBCT. Data is only shown for the first 205,000 BVs because effluent from 2-min EBCT only reached 180,000 BVs at the time the pilot study ended. **Figures A3.4.26-A3.4.37** compares breakthrough data observed for individual PFASs in effluent from the regenerable A50E resin following 2-min and 3-min EBCT. Again, data is presented on a bed volume equivalent basis.

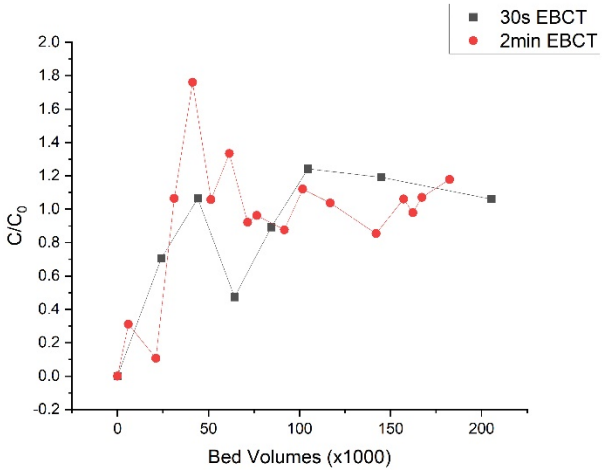

Figure A3.4.14. PFBA breakthrough on A520E after 30-sec and 2-min EBCTs.

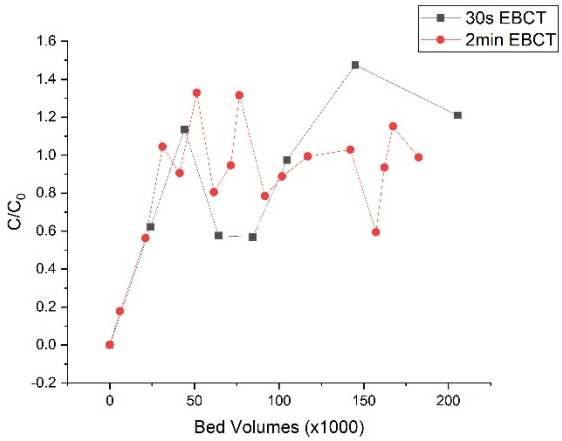

Figure A3.4.15. PFPeA breakthrough on A520E after 30-sec and 2-min EBCTs.

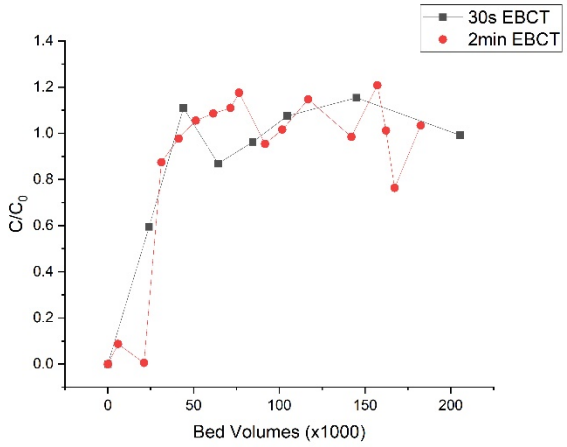

Figure A3.4.16. PFHxA breakthrough on A520E after 30-sec and 2-min EBCTs.

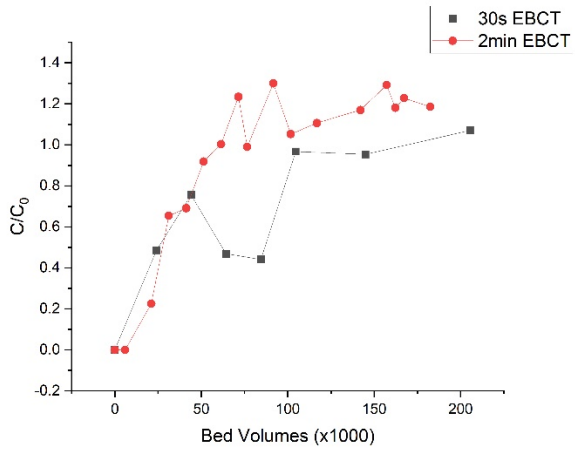

Figure A3.4.17. PFHpA breakthrough on A520E after 30-sec and 2-min EBCTs.

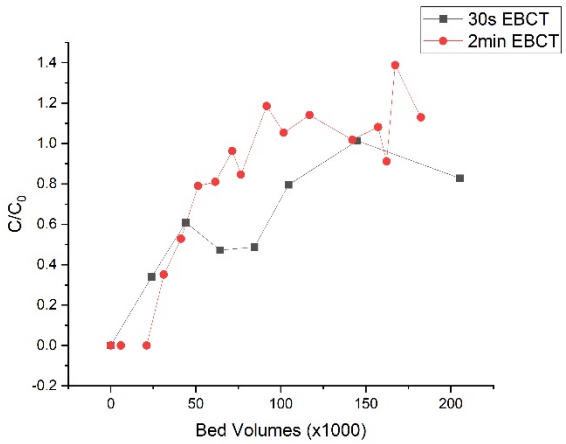

Figure A3.4.18. PFOA breakthrough on A520E after 30-sec and 2-min EBCTs.

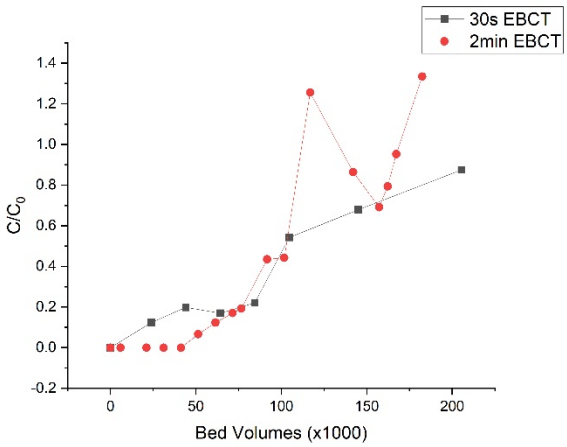

Figure A3.4.19. PFPrS breakthrough on A520E after 30-sec and 2-min EBCTs

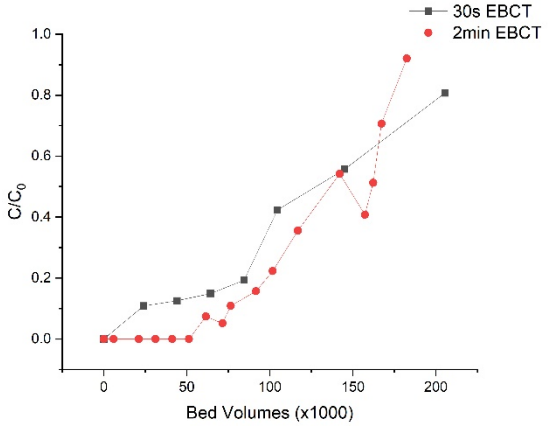

Figure A3.4.20. PFBS breakthrough on A520E after 30-sec and 2-min EBCTs.

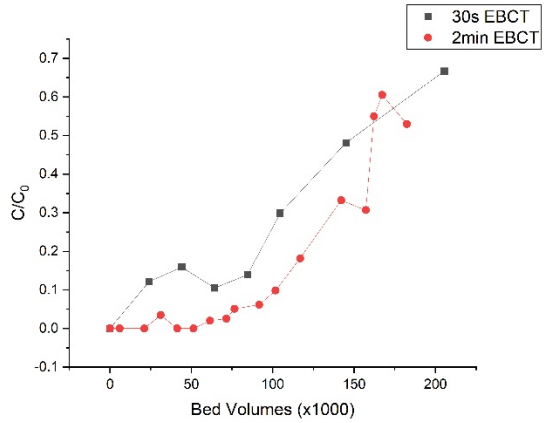

Figure A3.4.21. PFPeS breakthrough on A520E after 30-sec and 2-min EBCTs

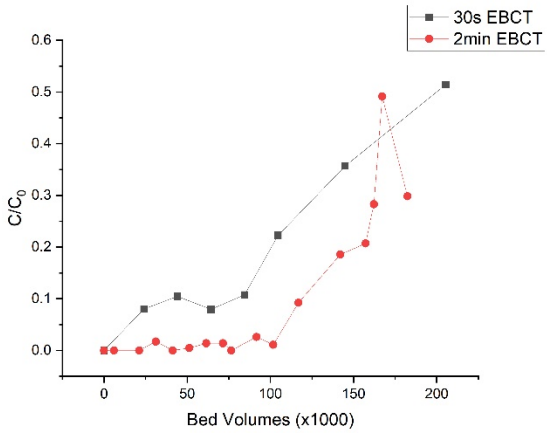

Figure A3.4.22. PFHxS breakthrough on A520E after 30-sec and 2-min EBCTs.

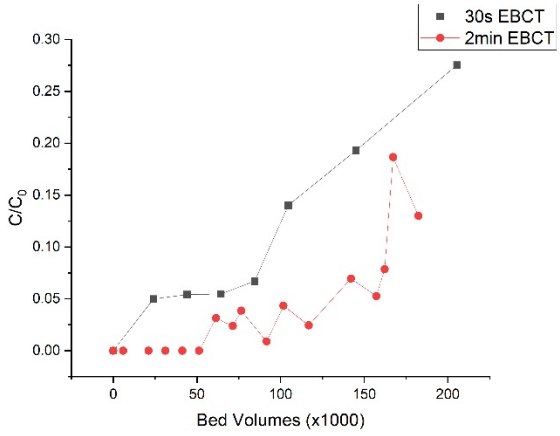

Figure A3.4.23. PFHpS breakthrough on A520E after 30-sec and 2-min EBCTs.

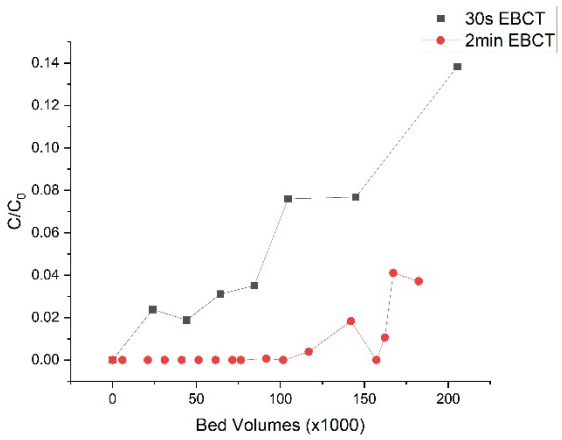

Figure A3.4.24. PFOS breakthrough on A520E after 30-sec and 2-min EBCTs.

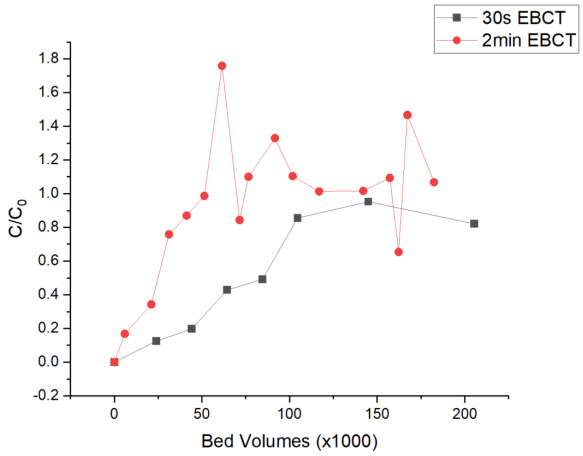

Figure A3.4.25. 6:2 FTS breakthrough on A520E after 30-sec and 2-min EBCTs.

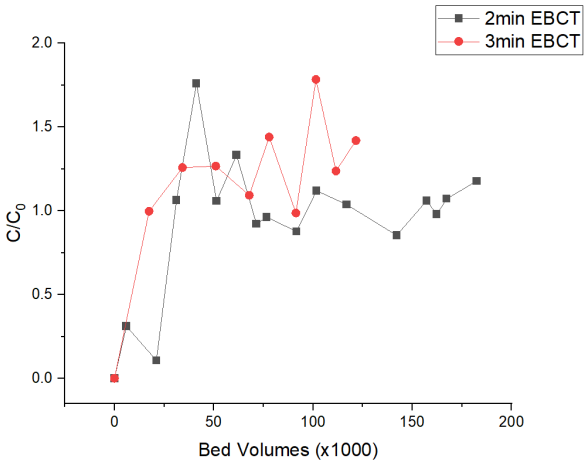

Figure A3.4.26. PFBA breakthrough on A520E after 2-min and 3-min EBCTs.

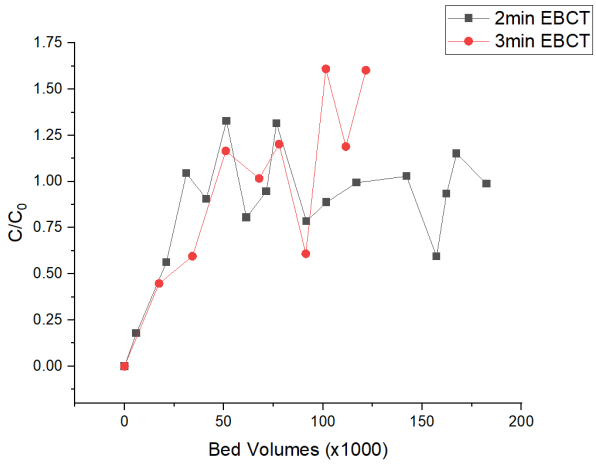

Figure A3.4.27. PFPeA breakthrough on A520E after 2-min and 3-min EBCTs.

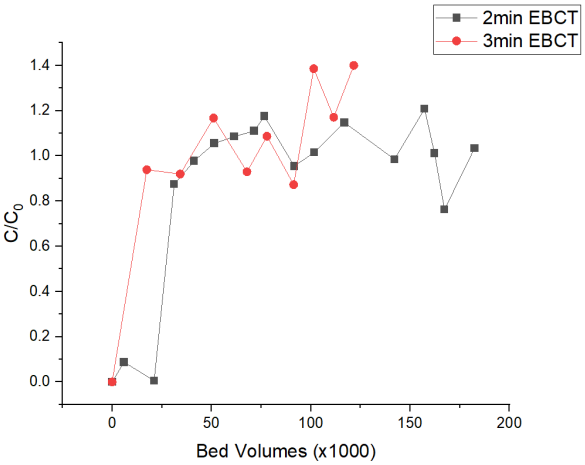

Figure A3.4.28. PFHxA breakthrough on A520E after 2-min and 3-min EBCTs.

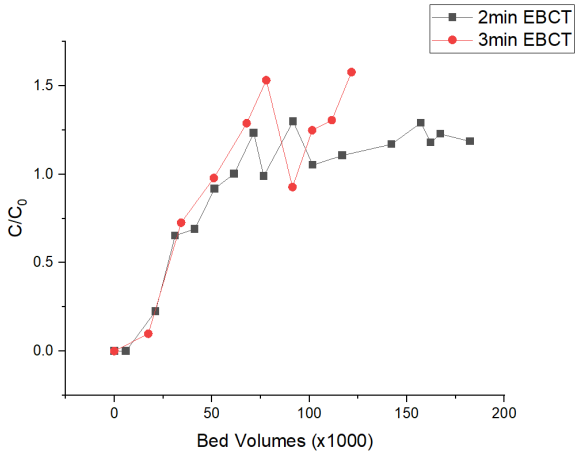

Figure A3.4.29. PFHpA breakthrough on A520E after 2-min and 3-min EBCTs.

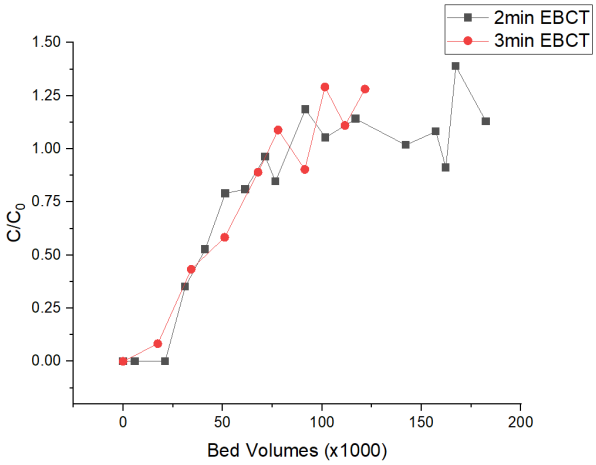

Figure A3.4.30. PFOA breakthrough on A520E after 2-min and 3-min EBCTs.

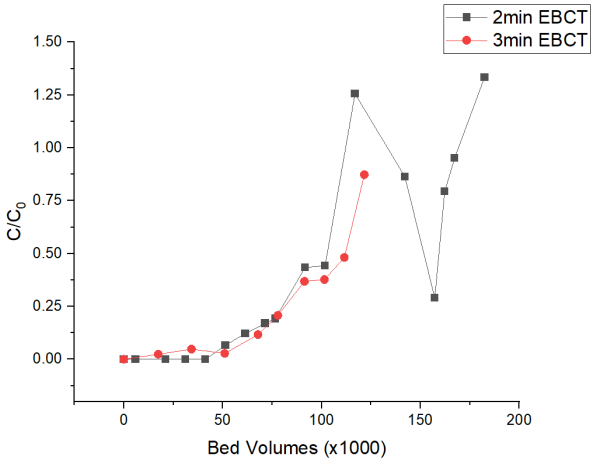

Figure A3.4.31. PFPrS breakthrough on A520E after 2-min and 3-min EBCTs.

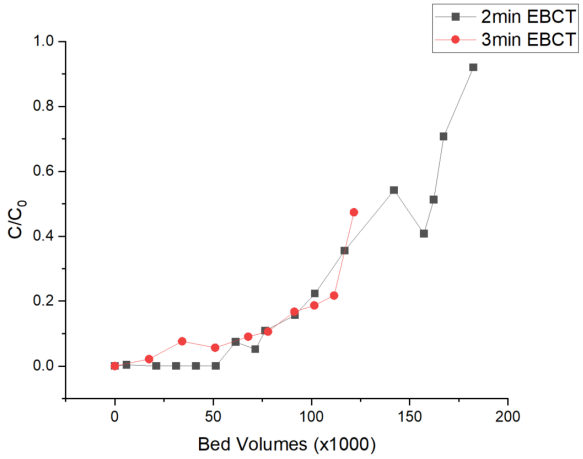

Figure A3.4.32. PFBS breakthrough on A520E after 2-min and 3-min EBCTs.

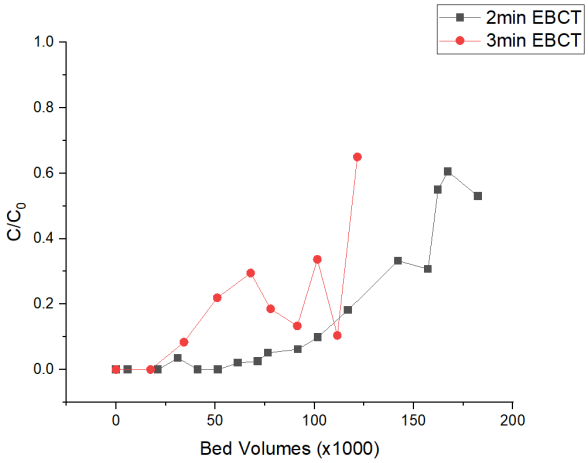

Figure A3.4.33. PFPeS breakthrough on A520E after 2-min and 3-min EBCTs.

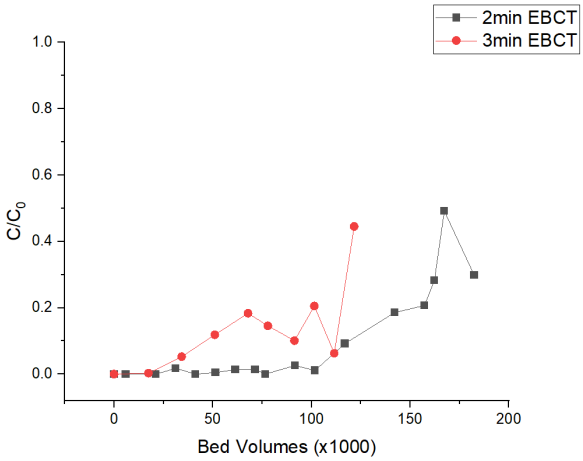

Figure A3.4.34. PFHxS breakthrough on A520E after 2-min and 3-min EBCTs.

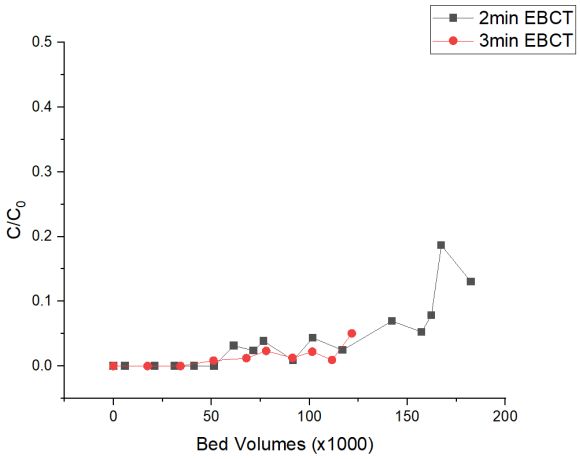

Figure A3.4.35. PFHpS breakthrough on A520E after 2-min and 3-min EBCTs.

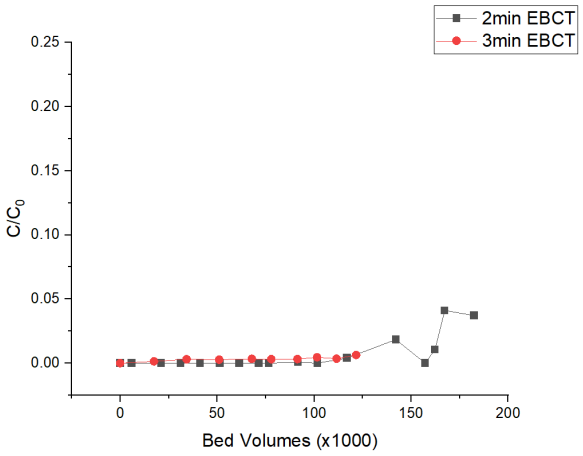

Figure A3.4.36. PFOS breakthrough on A520E after 2-min and 3-min EBCTs.

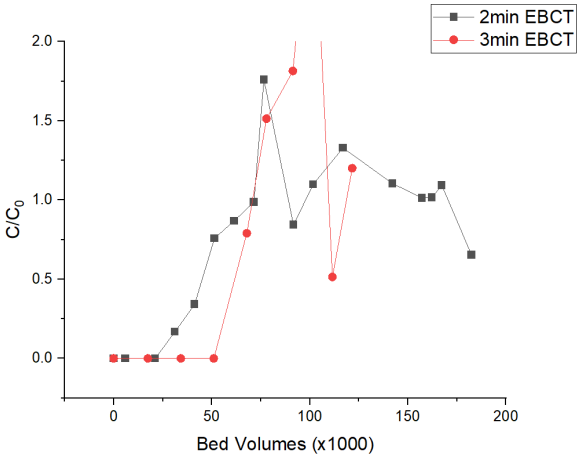

Figure A3.4.37. 6:2 FTS breakthrough on A520E after 2-min and 3-min EBCTs.

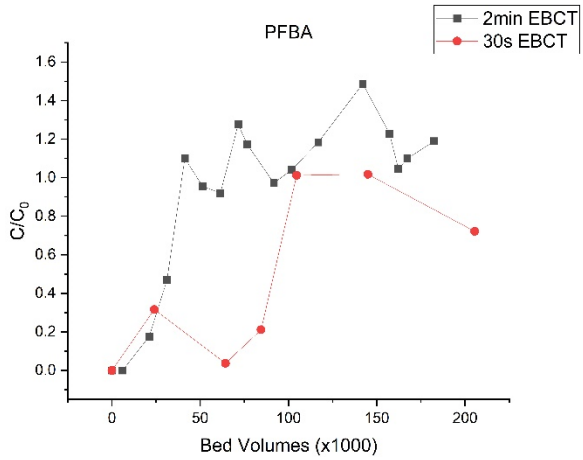

Figure A3.4.38. PFBA breakthrough on PSR2+ after 30-sec and 2-min EBCTs.

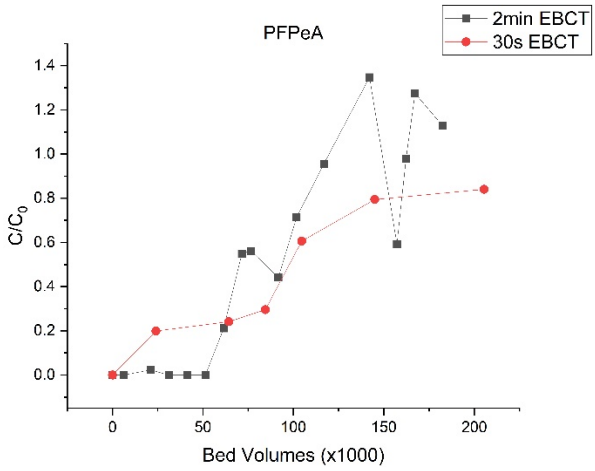

Figure A3.4.39. PFPeA breakthrough on PSR2+ after 30-sec and 2-min EBCTs.

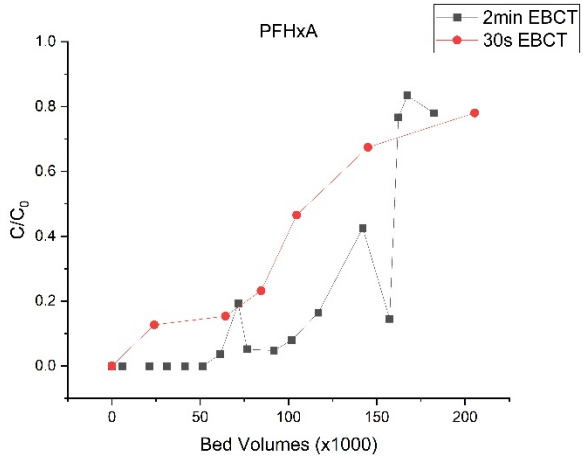

Figure A3.4.40. PFHxA breakthrough on PSR2+ after 30-sec and 2-min EBCTs.

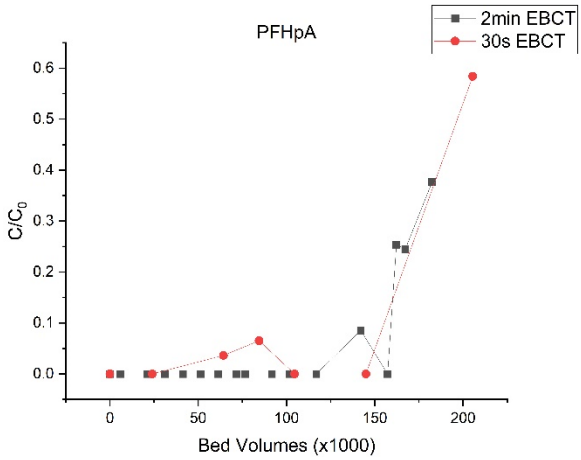

Figure A3.4.41. PFHpA breakthrough on PSR2+ after 30-sec and 2-min EBCTs.

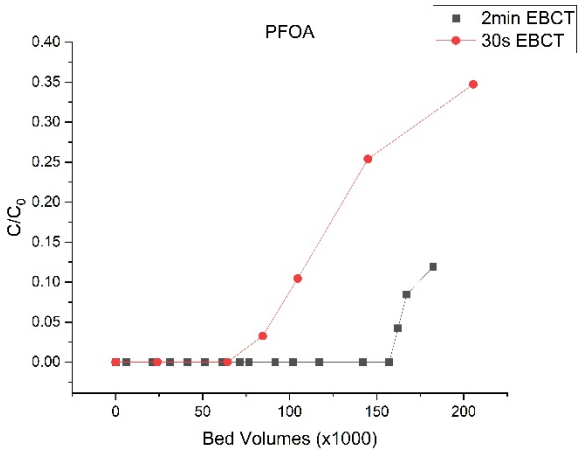

Figure A3.4.42. PFOA breakthrough on PSR2+ after 30-sec and 2-min EBCTs.

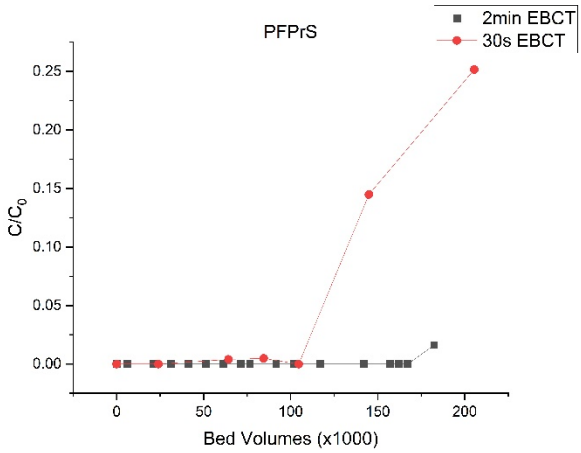

Figure A3.4.43. PFPrS breakthrough on PSR2+ after 30-sec and 2-min EBCTs

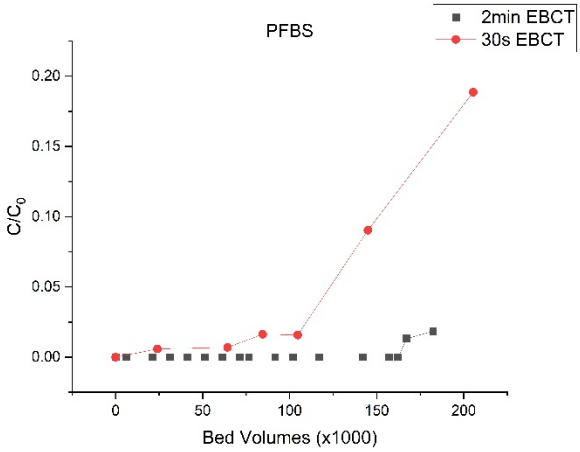

Figure A3.4.44. PFBS breakthrough on PSR2+ after 30-sec and 2-min EBCTs.

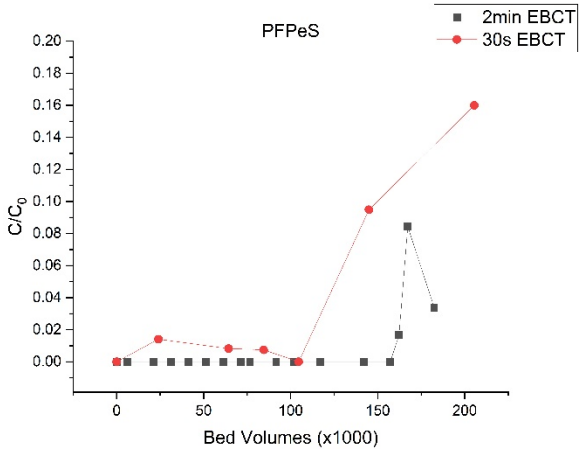

Figure A3.4.45. PFPeS breakthrough on PSR2+ after 30-sec and 2-min EBCTs

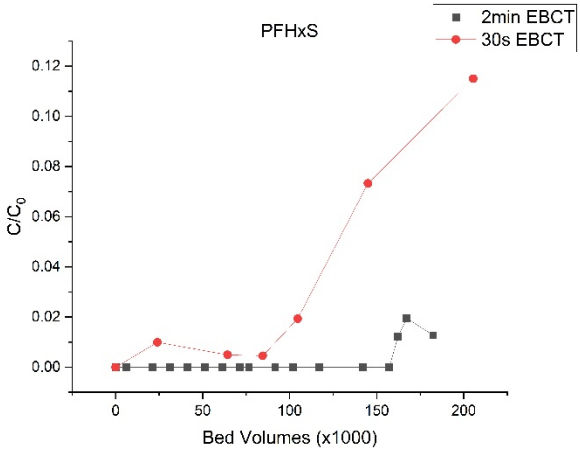

Figure A3.4.46. PFHxS breakthrough on PSR2+ after 30-sec and 2-min EBCTs.

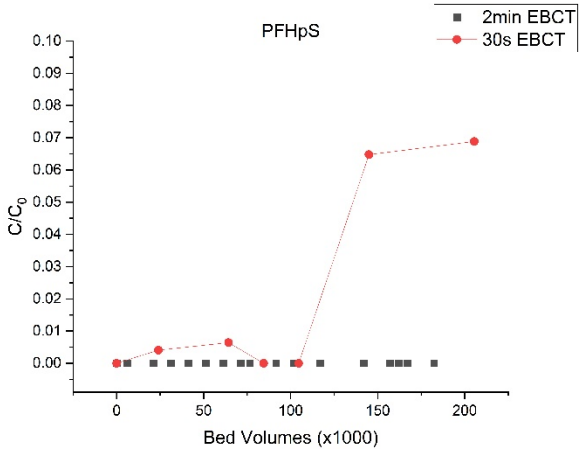

Figure A3.4.47. PFHpS breakthrough on PSR2+ after 30-sec and 2-min EBCTs.

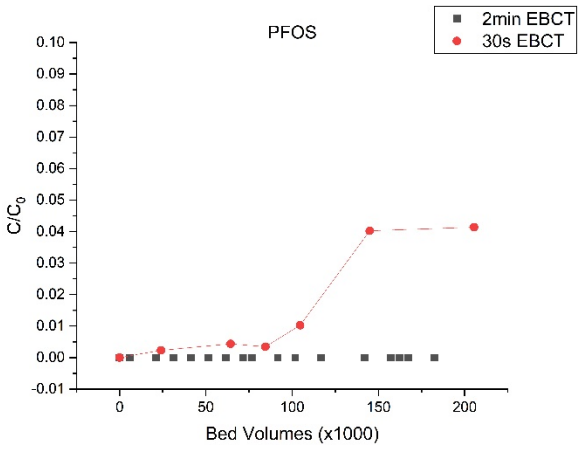

Figure A3.4.48. PFOS breakthrough on PSR2+ after 30-sec and 2-min EBCTs.

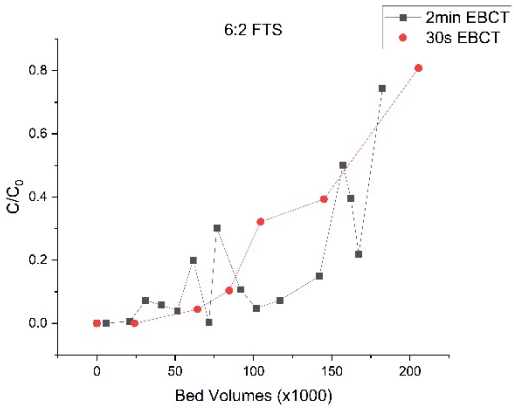

Figure A3.4.49. 6:2 FTS breakthrough on PSR2+ after 30-sec and 2-min EBCTs

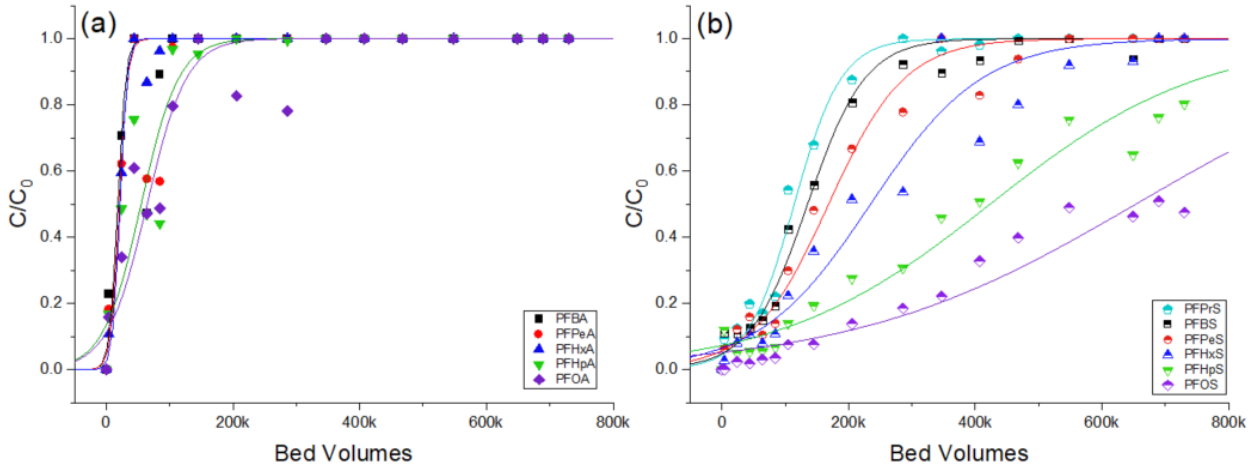

Figure A3.4.50. Thomas Model fits of breakthrough data for (a) PFCAs and (b) PFSAs after 30-sec EBCT treatment with A520E. Fit-derived parameters listed in Table A3.4.1.

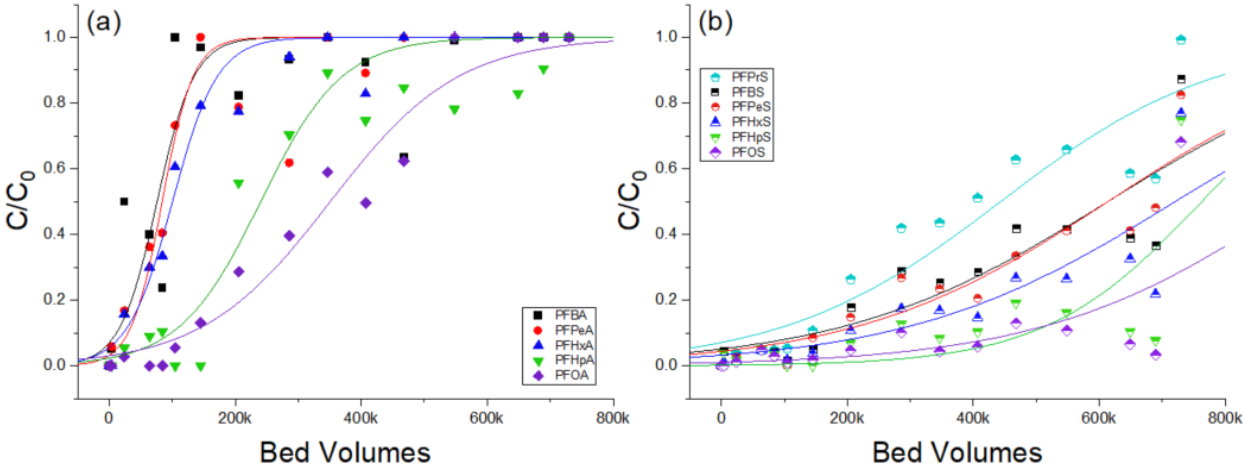

Figure A3.4.51. Thomas Model fits of breakthrough data for (a) PFCAs and (b) PFSAs after 30-sec EBCT treatment with PFA694E. Fit-derived parameters listed in Table A3.4.1.

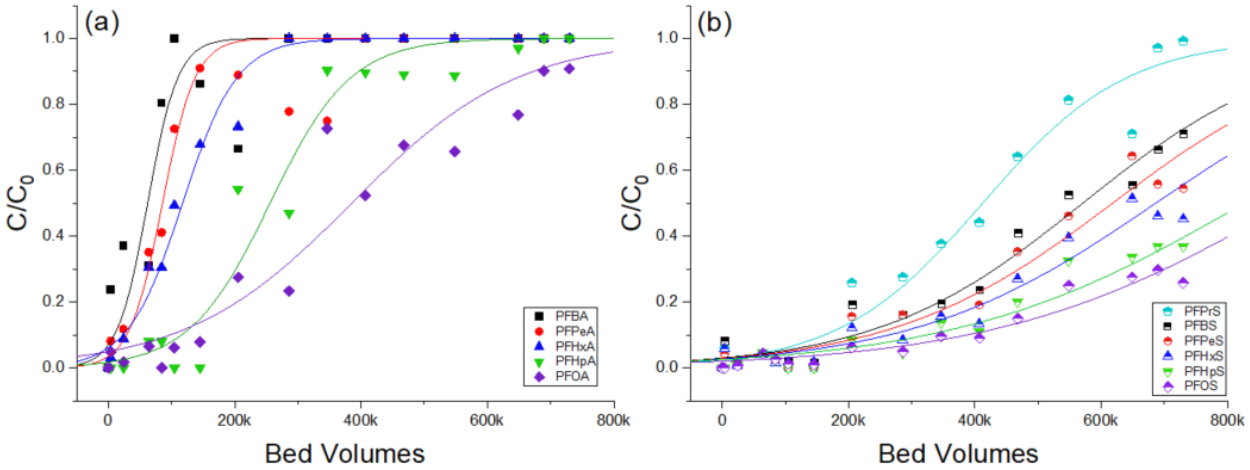

Figure A3.4.52. Thomas Model fits of breakthrough data for (a) PFCAs and (b) PFSAs after 30-sec EBCT treatment with CalRes 2301. Fit-derived parameters listed in Table A3.4.1.

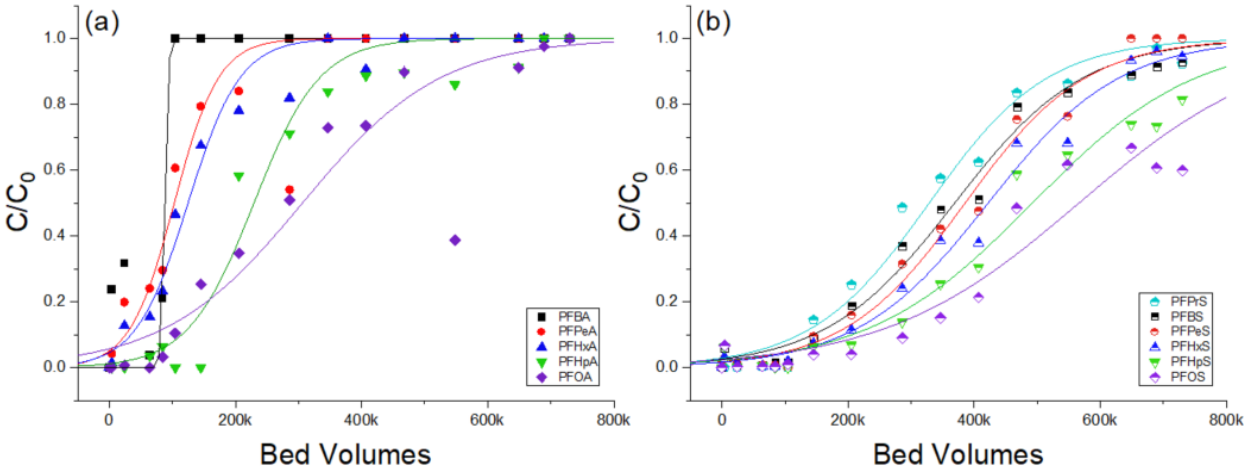

Figure A3.4.53. Thomas Model fits of breakthrough data for (a) PFCAs and (b) PFSAs after 30-sec EBCT treatment with PSR2+. Fit-derived parameters listed in Table S5.1.

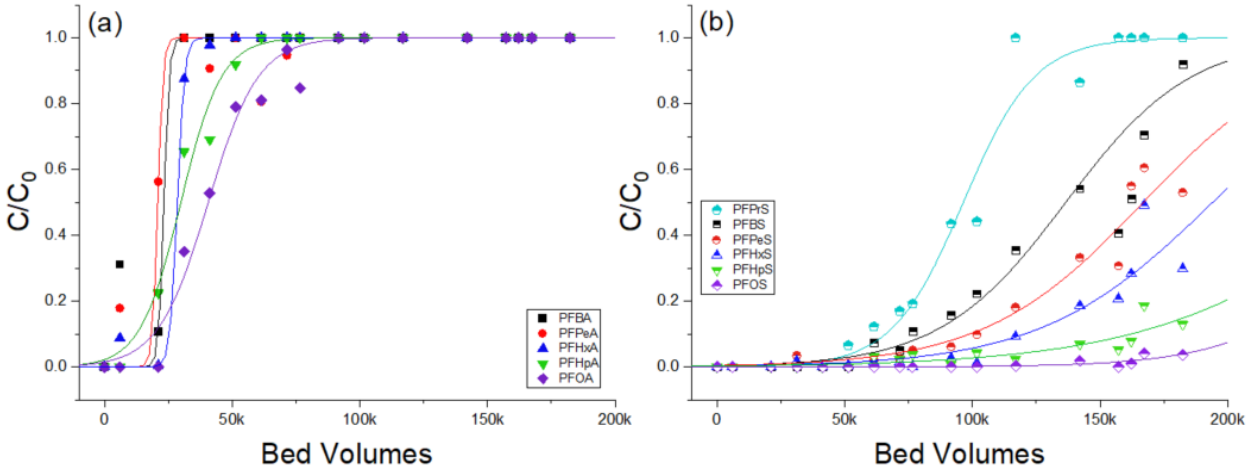

Figure A3.4.54. Thomas Model fits of breakthrough data for (a) PFCAs and (b) PFSAs after 2-min EBCT treatment with A520E. Fit-derived parameters listed in Table A3.4.1.

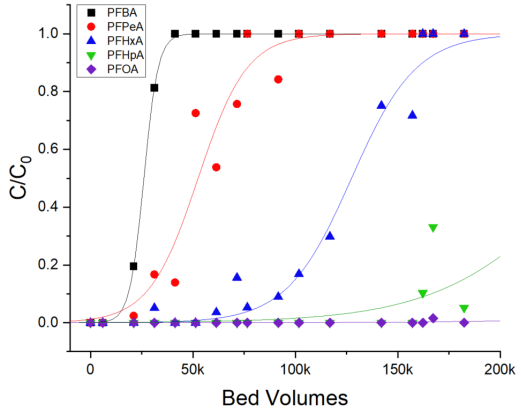

Figure A3.4.55. Thomas Model fits of breakthrough data for PFCAs after 2-min EBCT treatment with PFA694E. Fit-derived parameters listed in Table A3.4.1.

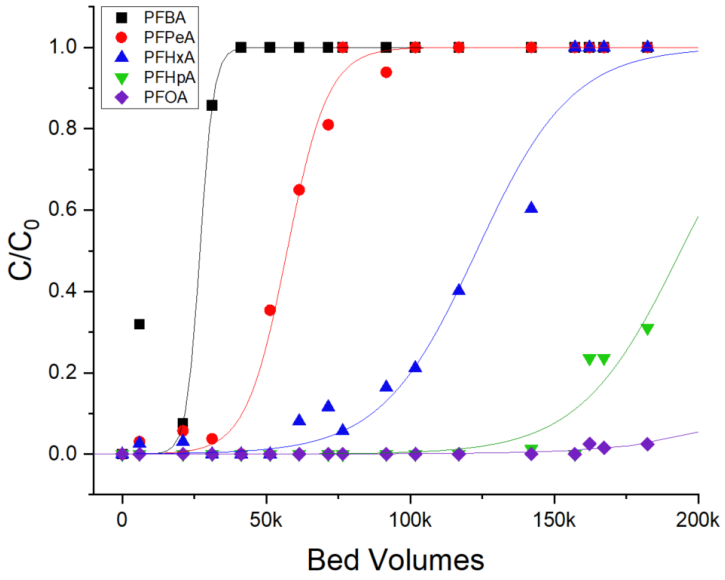

Figure A3.4.56. Thomas Model fits of breakthrough data for PFCAs after 2-min EBCT treatment with CalRes 2301. Fit-derived parameters listed in Table A3.4.1.

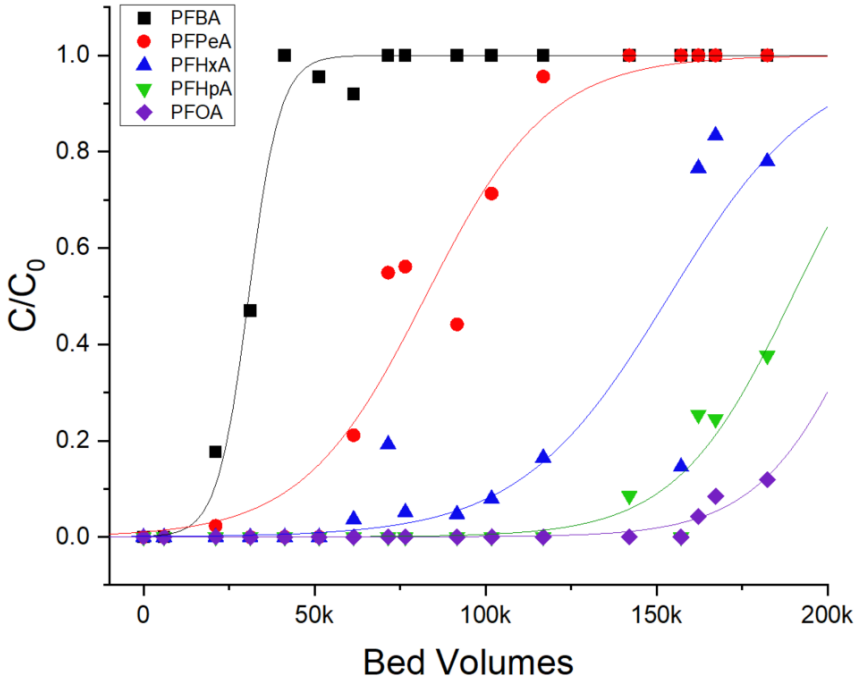

Figure A3.4.57. Thomas Model fits of breakthrough data for PFCAs after 2-min EBCT treatment with PSR2+. Fit-derived parameters listed in Table A3.4.1.

Table A3.4.2. Thomas model breakthrough curve fit parameters derived from field pilot data[a,b]

Resin	A520E			PFA694E			CalRes 2301			PSR2+		
Parameter	k_{Th}	q_e	R^2	k_{Th}	q_e	R^2	k_{Th}	q_e	R^2	k_{Th}	q_e	R^2
30-second EBCT Breakthrough Curve Fit Parameters												
PFBA	0.184±0.072	0.017±0.004	0.8	0.042±0.016	0.072±0.014	0.76	0.048±0.013	0.057±0.009	0.85	0.562±2.936	0.086±0.021	0.94
PFPeA	0.046±0.016	0.035±0.010	0.76	0.045±0.014	0.097±0.010	0.89	0.043±0.010	0.100±0.008	0.93	0.028±0.008	0.123±0.014	0.89
PFHxA	0.086±0.013	0.052±0.003	0.99	0.015±0.003	0.249±0.016	0.96	0.012±0.001	0.290±0.013	0.98	0.013±0.002	0.311±0.017	0.97
PFHpA	0.074±0.020	0.026±0.005	0.85	0.043±0.010	0.123±0.010	0.91	0.043±0.008	0.132±0.008	0.95	0.053±0.010	0.118±0.007	0.96
PFOA	0.010±0.002	0.220±0.029	0.89	0.004±0.000	1.263±0.057	0.96	0.003±0.000	1.386±0.086	0.92	0.003±0.001	1.110±0.115	0.86
PFPrS	0.061±0.006	0.067±0.003	0.99	0.014±0.002	0.258±0.018	0.87	0.021±0.002	0.241±0.009	0.96	0.026±0.002	0.192±0.007	0.98
PFBS	0.023±0.002	0.174±0.007	0.99	0.005±0.001	0.793±0.054	0.80	0.007±0.000	0.729±0.017	0.97	0.011±0.001	0.471±0.012	0.99
PFPeS	0.018±0.002	0.204±0.010	0.98	0.006±0.001	0.747±0.034	0.89	0.007±0.001	0.743±0.023	0.94	0.012±0.001	0.463±0.011	0.99
PFHxS	0.002±0.000	1.804±0.137	0.94	9.1E-4±2.1E-4	5.606±0.393	0.74	9.2E-4±9.4E-5	5.389±0.165	0.94	1.7E-3±1.3E-4	3.249±0.073	0.99
PFHpS	0.008±0.001	0.430±0.017	0.95	0.009±0.004	0.804±0.080	0.49	0.006±0.001	0.818±0.028	0.94	0.011±0.001	0.504±0.013	0.97
PFOS	1.9E-4±2.0E-5	20.975±0.843	0.92	0.004±0.002	23.081±0.129	0.86	1.8E-4±2.0E-5	29.176±1.233	0.92	2.8E-4±3.7E-5	18.148±0.685	0.92
2-minute EBCT Breakthrough Curve Fit Parameters												
PFBA	2.072±2E4	0.022±1.753	0.95	0.421±0.004	0.026±0.000	0.99	0.618±0.195	0.026±0.001	0.95	0.319±0.044	0.030±0.000	0.99
PFPeA	0.205±0.040	0.021±0.002	0.96	0.101±0.019	0.062±0.003	0.95	0.172±0.018	0.067±0.001	0.99	0.072±0.012	0.096±0.004	0.96
PFHxA	0.408±0.243	0.070±0.004	0.99	0.037±0.004	0.314±0.007	0.98	0.035±0.004	0.303±0.007	0.98	0.027±0.007	0.379±0.013	0.83
PFHpA	0.330±0.037	0.015±0.001	0.99	0.081±0.057	0.125±0.028	0.34	0.157±0.033	0.101±0.003	0.84	0.161±0.030	0.098±0.002	0.88
PFOA	0.040±0.005	0.147±0.005	0.98	0.010±0.011	1.474±1.043	0.15	0.017±0.005	0.962±0.100	0.74	0.025±0.004	0.770±0.022	0.90
PFPrS	0.176±0.026	0.056±0.001	0.98	---	---	---	---	---	---	---	---	---
PFBS	0.036±0.005	0.187±0.005	0.93	---	---	---	---	---	---	---	---	---
PFPeS	0.038±0.005	0.201±0.004	0.94	---	---	---	---	---	---	---	---	---
PFHxS	0.006±0.001	1.495±0.061	0.85	---	---	---	---	---	---	---	---	---
PFHpS	0.030±0.007	0.269±0.025	0.77	---	---	---	---	---	---	---	---	---
PFOS	0.002±0.001	8.516±0.920	0.73	---	---	---	---	---	---	---	---	---

a. Units for kTh values as provided are in *L / bed volume-mg PFAS*

b. Units for qe values as provided are in *mg PFAS / g of resin*

The fit-derived Thomas Model parameters were used to predict 50% breakthrough BV estimates for all analytes after treatment using resins at both a 30-sec and 2-min EBCT. To better understand the effects of EBCT on AER treatment of PFAS, estimated BVs at which 50% breakthrough is reached were compared between the two contact times in cases where >10% elution was observed at both contact times. As shown in **Figure A3.4.58**, the fit-derived estimates are generally in agreement at both contact times, with the majority of data points falling very near the 1:1 line. While the 30-sec EBCT data may be assumed to routinely underpredict breakthrough BVs due to the lack of time needed to ensure sufficient kinetic loading of PFASs, 16 of the 25 analytes were found to have slightly earlier fitted 50% breakthrough estimates from the Thomas model fits compared to 2-min. This can be attributed to the significantly larger uptake of PFAS mass in the 30-second vessel compared to the subsequent 90-second vessel as determined by the postmortem resin extractions (**Figure 3.4.3**). Additionally, the lack of PFSA breakthrough after single-use resin treatment at a 2-min EBCT means the majority of analytes cannot be compared at the two contact times, thus precluding a more detailed analysis of how contact times influence Thomas Model predictions. While many analytes may experience larger estimated BVs treated before 50% breakthrough at a 30-second EBCT compared to 2-min, these analytes are detected in effluent samples far sooner using a 30-sec EBCT as shown in **Figures A3.4.26-A3.4.37**. Therefore, it may be expected that shorter EBCTs lead to more rapid initial elution, but that the breakthrough profiles at a short EBCT may be more gradual (lower k_{Th} values), thus leading to extended periods of incomplete removal of PFAS from groundwater.

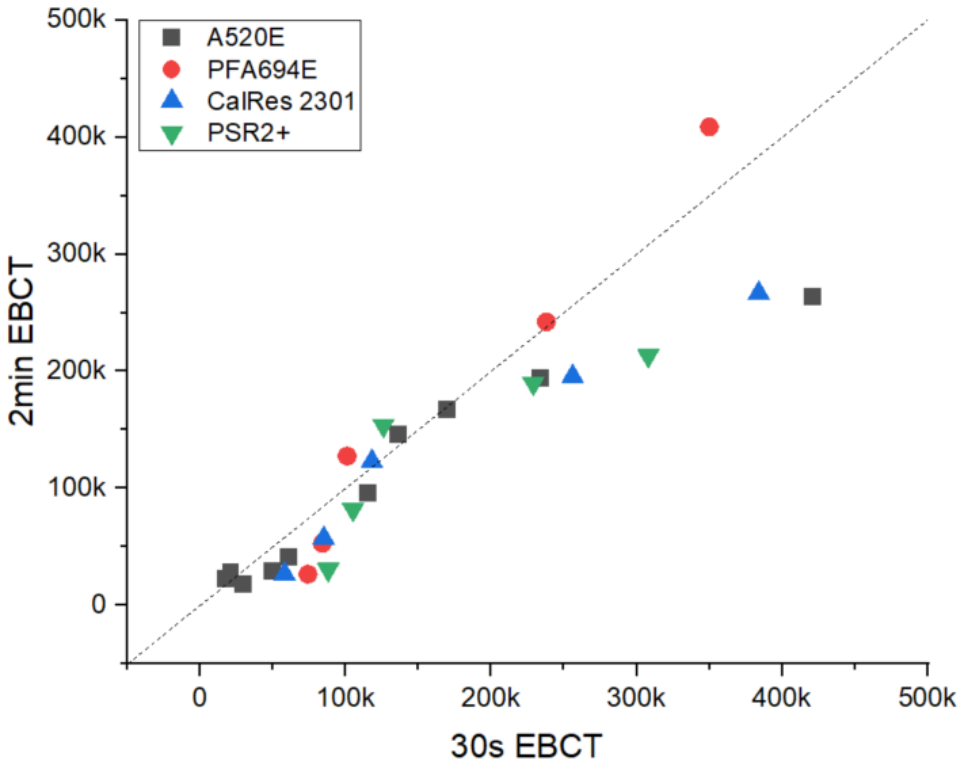

Figure A3.4.58. Cross-comparison of 50% breakthrough values obtained using the Thomas Model at both a 2-min and 30-sec EBCT for all analytes with observed breakthrough at both EBCTs

Figures A3.4.59-A3.4.62 show the relationships between PFAS-chloride ion exchange coefficients measure in batch experiments (logK_{ex}) and the Thomas Model fit-derived bed volume values at which 50% breakthrough is observed for the same PFAS-resin combination. Batch-derived exchange coefficient values can be found in Fang et al. (2021). Linear regression fits and the resulting empirical equations are also shown.

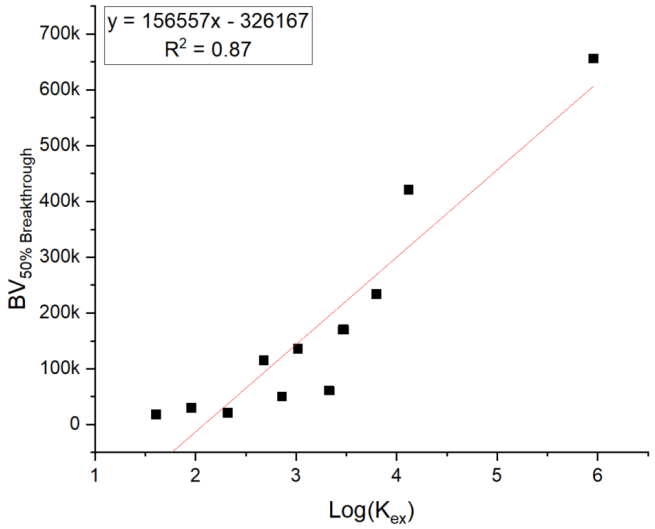

Figure A3.4.59. Relationship between pilot system breakthrough data and batch-derived PFAS-chloride ion exchange coefficients for A520E.

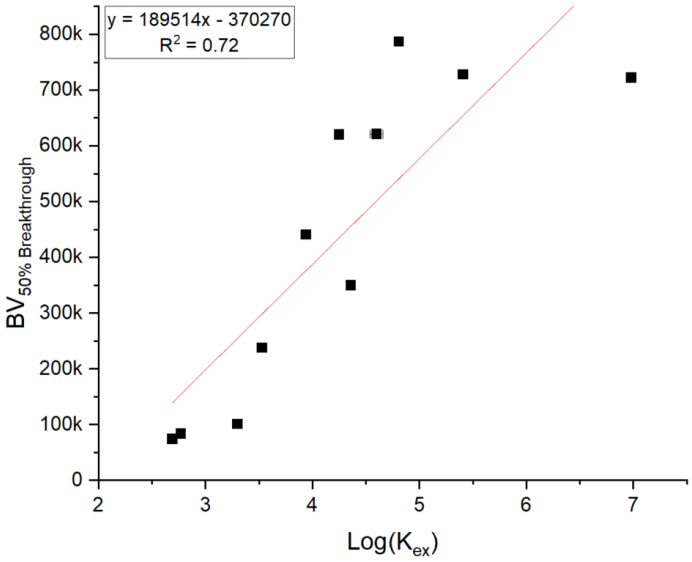

Figure A3.4.60. Relationship between pilot system breakthrough data and batch-derived PFAS-chloride ion exchange coefficients for PFA694E.

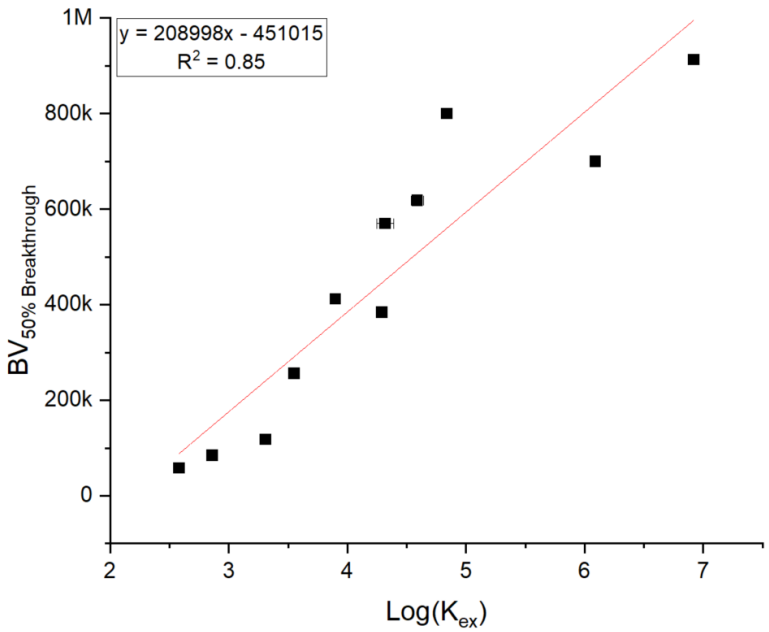

Figure A3.4.61. Relationship between pilot system breakthrough data and batch-derived PFAS-chloride ion exchange coefficients for CalRes 2301.

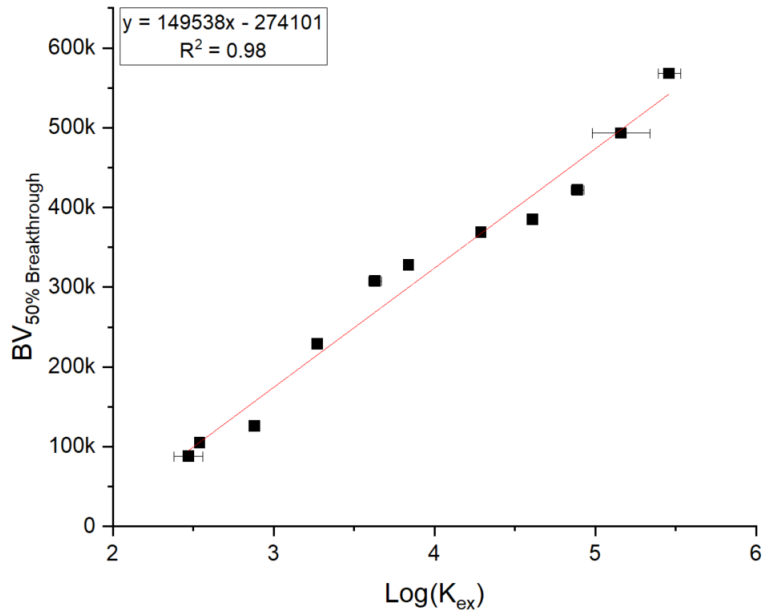

Figure A3.4.62. Relationship between pilot system breakthrough data and batch-derived PFAS-chloride ion exchange coefficients for PSR2+.

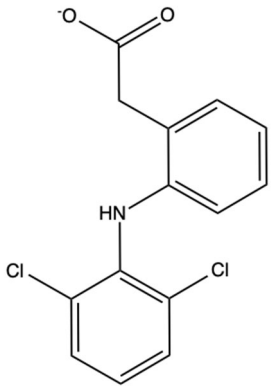

Figure A3.5.1. Diclofenac anion molecular structure.

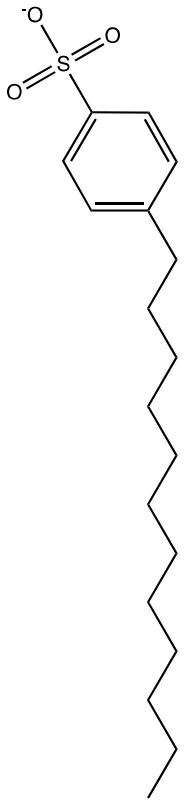

Figure A3.5.2. Dodecylbenzene sulfonate anion molecular structure.

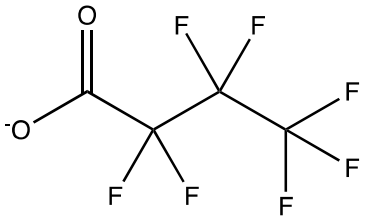

Perfluorooctanoic Acid (PFOA)

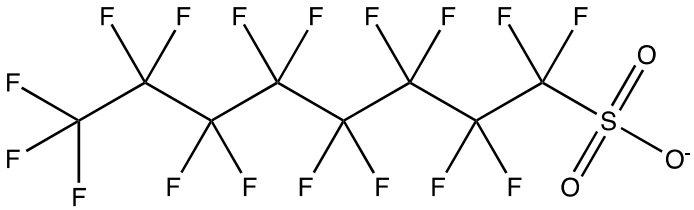

Perfluorooctanesulfonic Acid (PFOS)

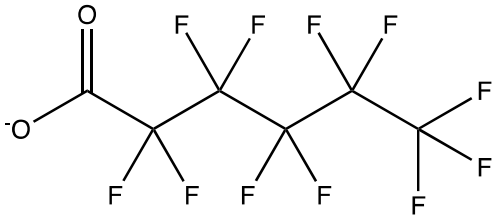

Perfluorohexanoic (PFHxA)

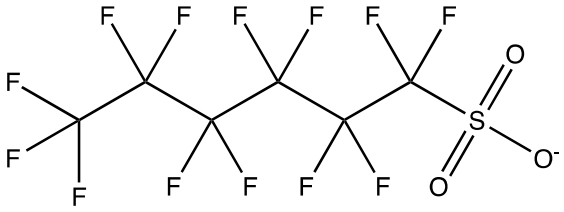

Perfluorohexanesulfonic Acid (PFHxS)

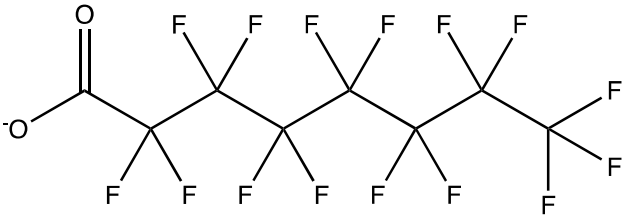

Perfluorobutanoate (PFBA)

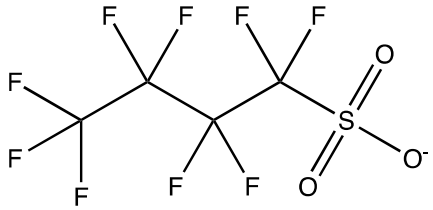

Perfluorobutanesulfonic Acid (PFBS)

Figure A3.5.3. Six deprotonated perfluoroalkyl acid anions.

Table A3.5.1. Solubility of NaCl in pure alcohol solvent conditions at 25 °C.

Solvent	**Solubility of NaCl [a] (g NaCl / kg solvent)**
Water	360
Methanol	14
Ethanol	0.65
1-Propanol	0.12
1-Butanol	0.050
Propylene glycol	71
Glycerol	83

[a] Sourced from (Burgess, 1978)

Table A3.5.2. Empirically determined miscibility of monoalcohol cosolvent and brine solutions.

		Cosolvent Volume Fraction			
Alcohol	**Salt Content (m/m)**	**0.05**	**0.25**	**0.5**	**0.75**
Methanol	0.05	Miscible	Miscible	Miscible	Miscible
	0.5	Miscible	Miscible	Miscible	Miscible
	5	Miscible	Miscible	Miscible	Miscible
Ethanol	0.05	Miscible	Miscible	Miscible	Miscible
	0.5	Miscible	Miscible	Miscible	Miscible
	5	Miscible	Miscible	Immiscible	Immiscible
1-Propanol	0.05	Miscible	Miscible	Miscible	Miscible
	0.5	Miscible	Miscible	Miscible	Miscible
	5	Miscible	Miscible	Immiscible	Immiscible
1-Butanol	0.05	Miscible	Immiscible	Immiscible	Immiscible
	0.5	Miscible	Immiscible	Immiscible	Immiscible
	5	Miscible	Immiscible	Immiscible	Immiscible

Table A3.6.1. PFAS in the diluted (1:500) AFFF used in this study. Transient oxidation products during electrochemical treatment are noted.

PFAAs	**Formal Name**	**Concentration (µg/L)**
PFBA	perfluorobutanoic acid	64
PFPeA	perfluoropentanoic acid	110
PFHxA	perfluorohexanoic acid	290
PFHpA	perfluoroheptanoic acid	74
PFOA	perfluorooctanoic acid	290
PFPrS	perfluoropropane sulfonic acid	170
PFBS	perfluorobutane sulfonic acid	350
PFPeS	perfluoropentane sulfonic acid	390
PFHxS	perfluorohexane sulfonic acid	1,900
PFHpS	perfluoroheptane sulfonic acid	230
PFOS	perfluorooctane sulfonic acid	15,200
Suspect Analytes (>10^5 area) Representing 84% of the Organic Fluorine Present in the Total Identified Suspect Analytes		
AmPr-FASA-PrA (perfluorinated chain lengths of 3 to 6)		
AmPr-FASA (perfluorinated chain lengths of 3 to 6)		
OAmPr-FASA (perfluorinated chain lengths of 3 to 5) [oxidation product]		
MeFASAA (perfluorinated chain lengths of 3 to 5) [oxidation product]		
FASA (perfluorinated chain lengths of 3 to 5) [oxidation product]		

AmPr-FASA-PrA = *N-dimethyl ammonio propyl perfluoroalkane sulfonamido propanoic acid*
Ampr-FASA = *N-oxidedimethylammoniopropyl-perfluoroalkane sulfonamide*
OAmPr-FASA = *N-oxidedimethylammoniopropyl-perfluoro sulfonamides*
MeFASAA = *N-methylperfluoroalkane sulfonamido acetic acids*
FASA = *perfluorosulfonamides*

Table A3.6.2. Brine solutions evaluated in this study.

Salt (wt. %)	Base (0.2 wt. %)
NaCl (0.2, 1, 5)	NaOH
Na_2SO_4 (0.2, 1, 5)	NaOH
Na_2HCO_3 (0.2, 1, 2.5)[a]	NaOH
$NaClO_4$ (0.2)	NaOH
$(NH_4)_2SO_4$ (0.2)	NH_4OH

[a]Na_2HCO_3 had an upper limit of 2.5 weight percent due to solubility limits.

Table A3.6.3. First order rate constants for fluoride generation in the various brine solutions shown in Figure 1. First order rate constants are based on a maximum fluorine content of 27 mg/L based on ^{19}F-NMR. The ± values indicate the 95% confidence intervals. TBA = tert-butyl alcohol at 100 mM (except where noted).

Brine & wt%	First-order Rate Constant (h^{-1})	R^2
NaCl		
0.2	0.065 ± 0.0074	0.98
1	0.032 ± 0.0060	0.93
5	0.0079 ± 0.0029	0.65
Na_2SO_4		
0.2	0.098 ± 0.024	0.90
1	0.11 ± 0.022	0.95
5	0.088 ± 0.022	0.90
Na_2HCO_3		
0.2	0.098 ± 0.030	0.84
1	0.96 ± 0.018	0.94
2.5	0.10 ± 0.021	0.93
$NaClO_4$		
0.2	0.10 ± 0.028	0.88
$(NH_4)_2SO_4$		
0.2	0.070 ± 0.0066	0.98
$NaClO_4$ + TBA		
0.2	0.019 ± 0.0065	0.68
Na_2SO_4 + TBA		
0.2	0.015 ± 0.0040	0.75
Na_2SO_4 + 10 mM TBA		
0.2	0.047 ± 0.0056	0.97

Table A3.6.4. First order rate constants for the removal of polyfluorinated compounds (Figure S11) in 0.2% Na_2SO_4 or $NaClO_4$ brines, with and without TBA. The ± values indicate the 95% confidence intervals.

System	First-order Rate Constant (h^{-1})	R^2
Na_2SO_4	0.71 ± 0.034	0.99
Na_2SO_4 + TBA	0.32 ± 0.085	0.96
$NaClO_4$	0.40 ± 0.043	0.99
$NaClO_4$ + TBA	0.20 ± 0.052	0.96

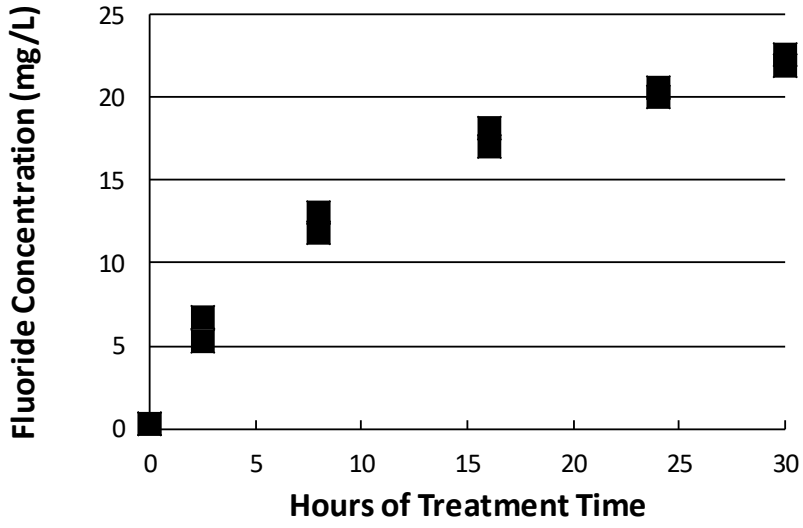

Figure A3.6.1. Electrochemical fluoride generation over 30 hours in the 0.2% sodium sulfate solution. The current density was 40 mA/cm^2. Results of duplicate experiments are shown. No foam layer was present by 24 hours of treatment time.

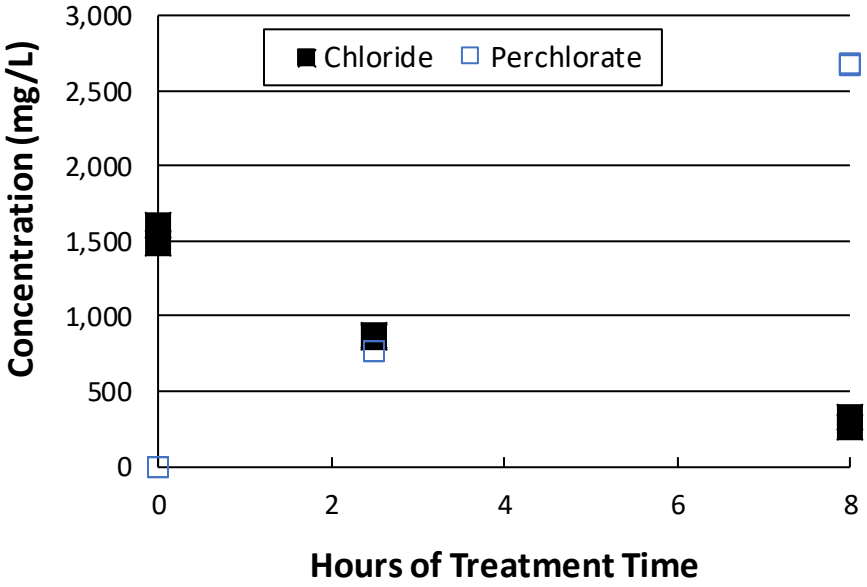

Figure A3.6.2. Removal of chloride and generation of perchlorate in the 0.2% NaCl brine during electrochemical treatment using 40 mA/cm^2. Results from duplicate experiments are shown, but often overlap. Perchlorate was observed as the primary transformation product. Decreases in chloride also were observed in the 1% and 5% chloride solutions.

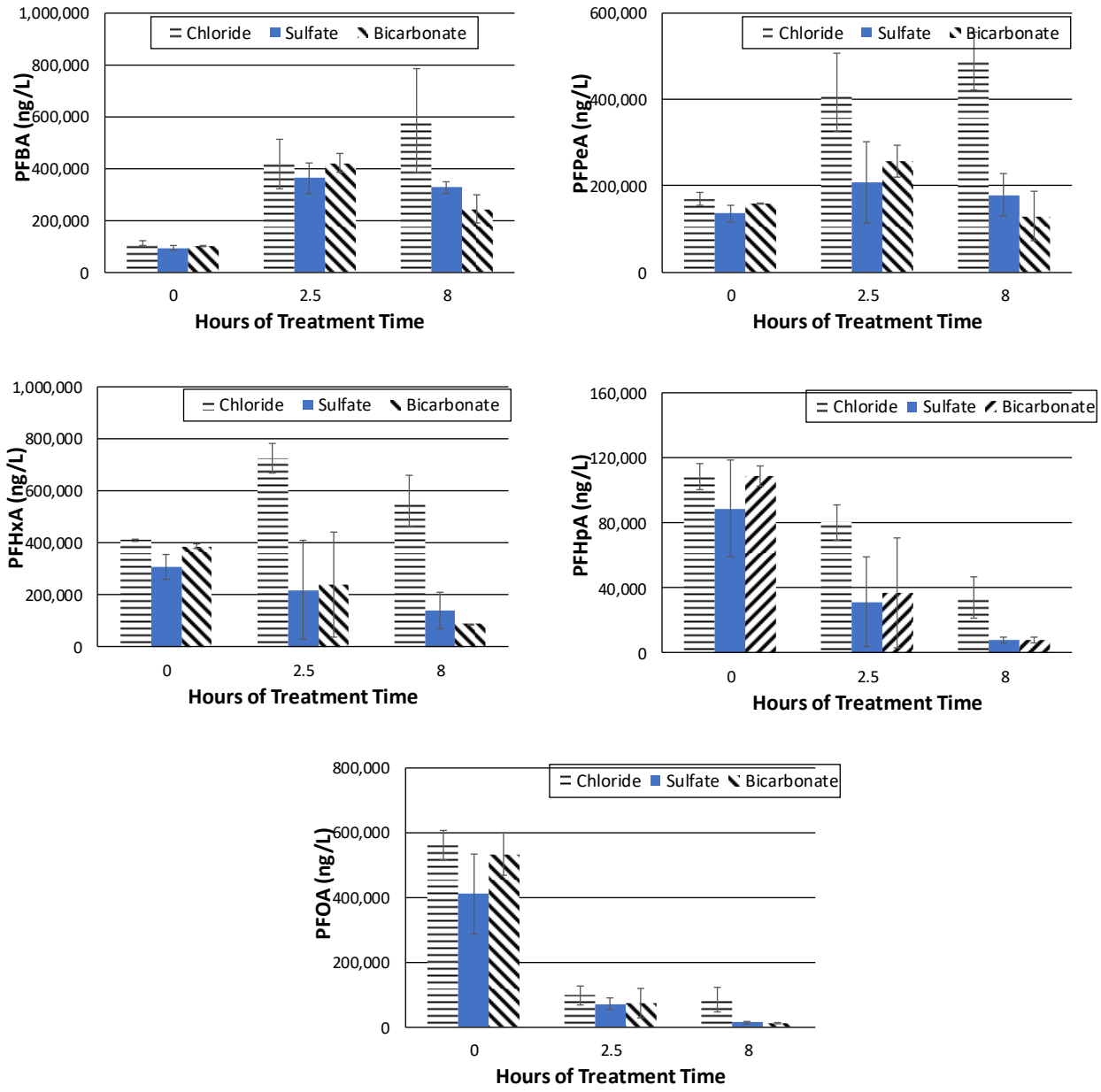

Figure A3.6.3. Removal of perfluorinated carboxylates during electrochemical treatment (5% NaCl, 5% Na_2SO_4, and 2.5% $NaHCO_3$ brines) using 40 mA/cm^2. Averages of duplicate experiments are shown. Error bars represent 95% confidence intervals. *PFBA=perfluorobutanoic acid, PFPeA=perfluoropentanoic acid, PFHxA=perfluorohexanoic acid, PFHpA = perfluoroheptanoic acid, PFOA=perfluorooctanoic acid.*

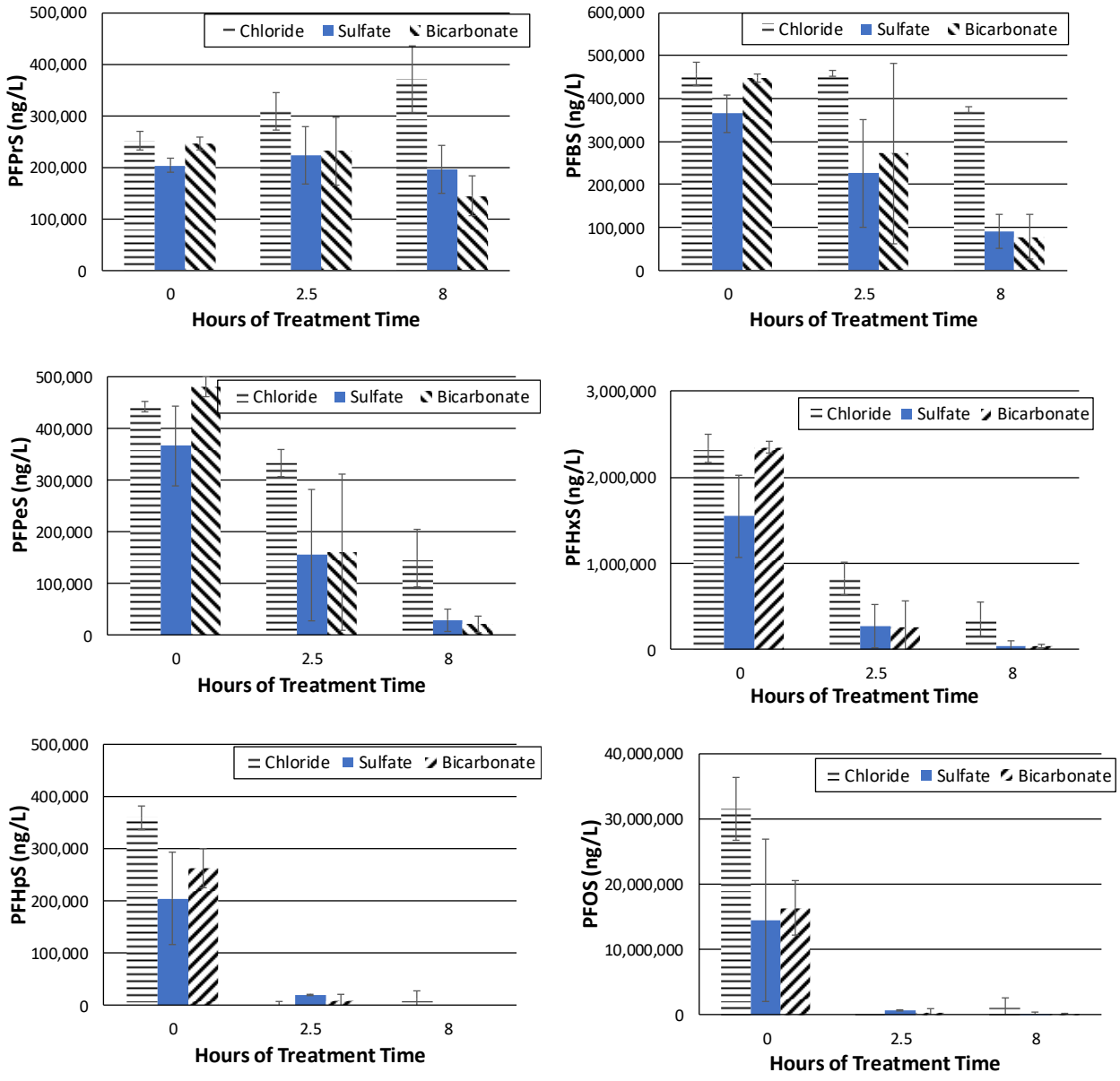

Figure A3.6.4. Removal of perfluorinated sulfonates during electrochemical treatment (5% NaCl, 5% Na_2SO_4, and 2.5% $NaHCO_3$ brines) using 40 mA/cm^2. Averages of duplicate experiments are shown. Error bars represent 95% confidence intervals. *PFPrS = perfluoropropane sulfonate, PFBS = perfluorobutane sulfonate, PFPeS=perfluoropentane sulfonate, PFHxS = perfluorohexane sulfonate, PFHpS = perfluoroheptane sulfonate, PFOS = perfluorooctane sulfonate*

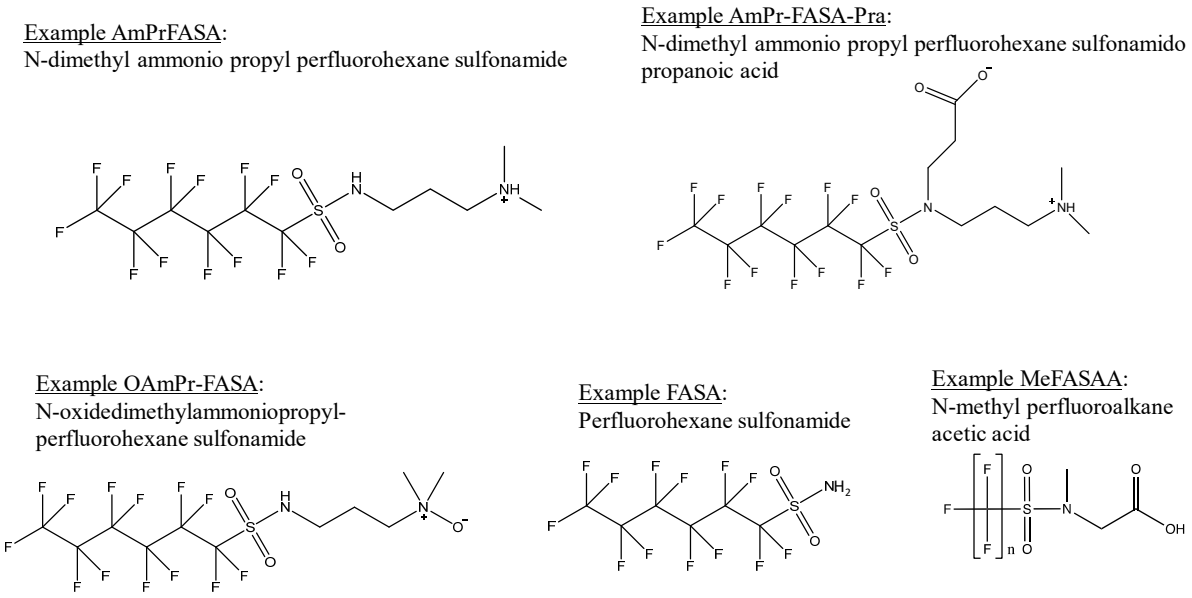

Figure A3.6.5. Representative structures for the most abundant suspect analytes, and potential PFAA precursors, identified in the diluted AFFF solution are shown in the top row. The bottom row shows representative structures for identified transient intermediates.

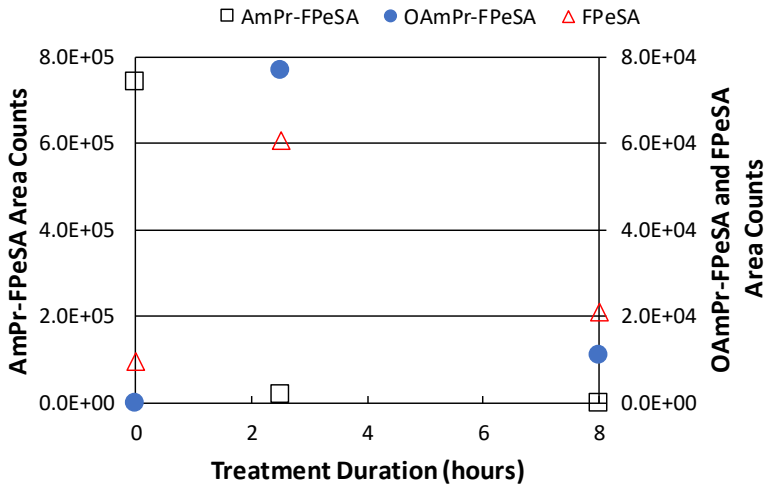

Figure A3.6.6. Removal of N-dimethyl ammonio propyl perfluoropentane sulfonamide (AmPr-FPeSA) during electrochemical treatment in the 5% Na_2SO_4 brine using 40 mA/cm^2, with oxidative formation of N-oxidedimethylammoniopropyl-perfluorohexane sulfonamide (OAmPr-FPeSA) and perfluoropentane sulfonamide (FPeSA). Average of duplicate results are shown.

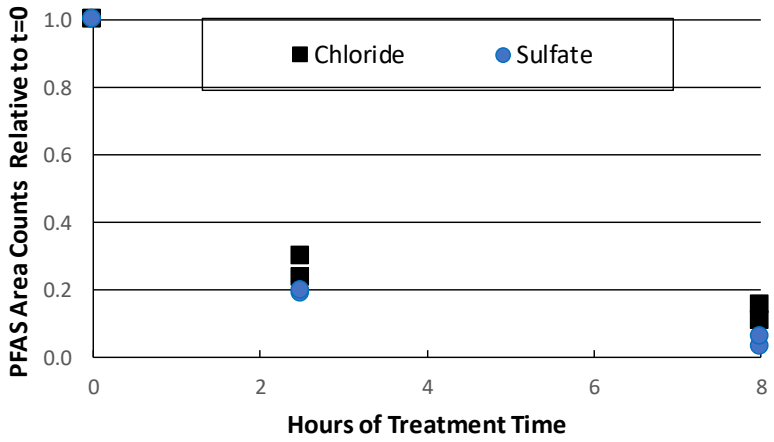

Figure A3.6.7. Relative (to t=0 hours) removal of polyfluorinated compounds during electrochemical treatment in 5% Na_2SO_4 and 5% NaCl using 40 mA/cm^2. Duplicate results are shown.

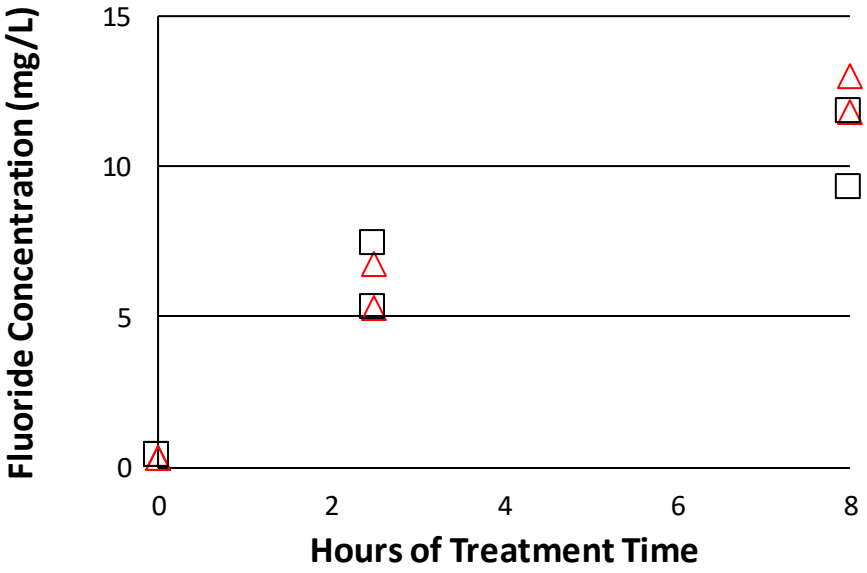

Figure A3.6.8. Electrochemical fluoride generation over 8 hours in the 0.2% sodium sulfate solution The current density was 40 mA/cm^2. Results of duplicate experiments are shown. The triangle symbols are from experiments where the foam layer was present, and the squares are from experiments where the foam layer was continuously skimmed from the surface. Foam formation ceased at approximately 6 hours. Skimming of the foam had no measurable impact on fluoride generation over 8 hours, indicating that no measurable re-dissolution and defluorination of PFAS from the foam occurred over the 8 hour experiment.

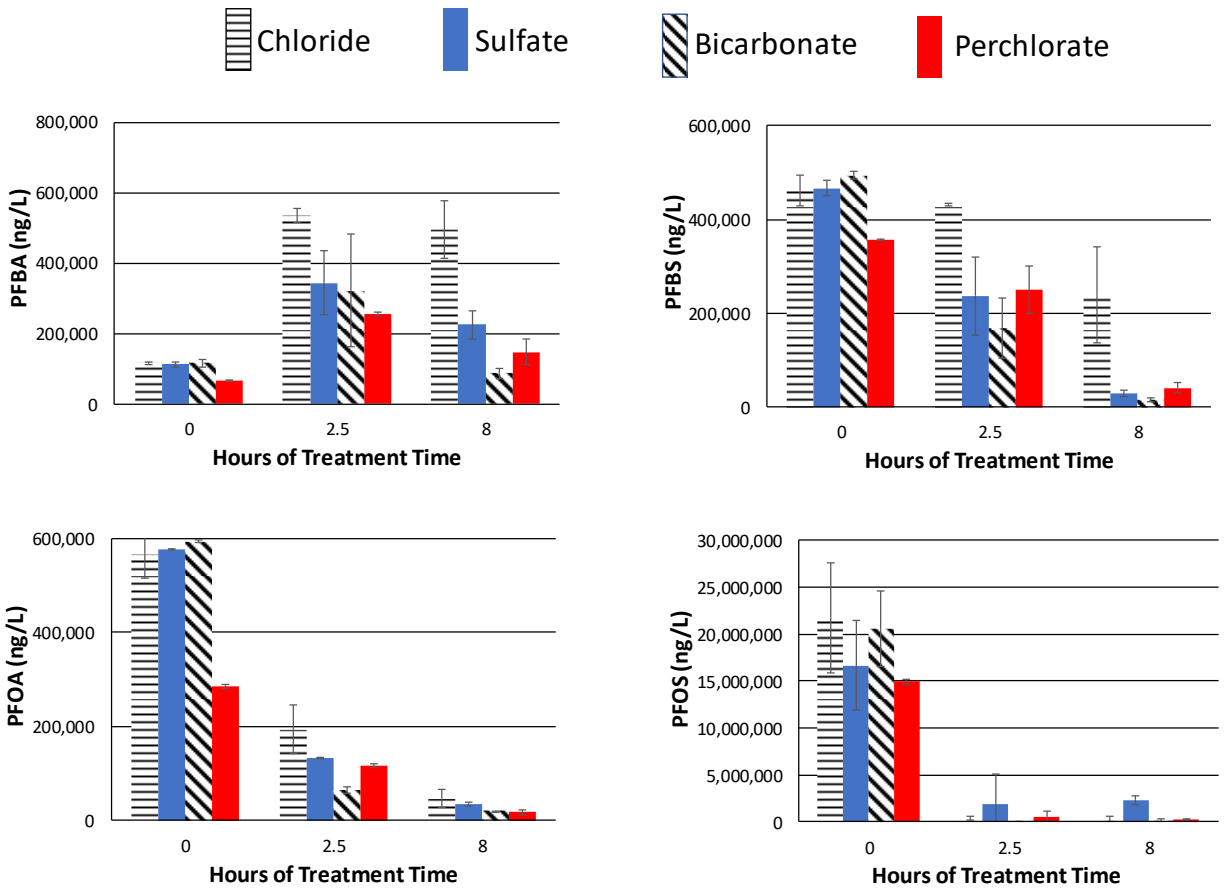

Figure A3.6.9. Removal of representative PFAAs during electrochemical treatment in 0.2% sodium brine solutions. The applied current density was 40 mA/cm^2. Average of duplicate experiments are shown. Error bars represent 95% confidence intervals.

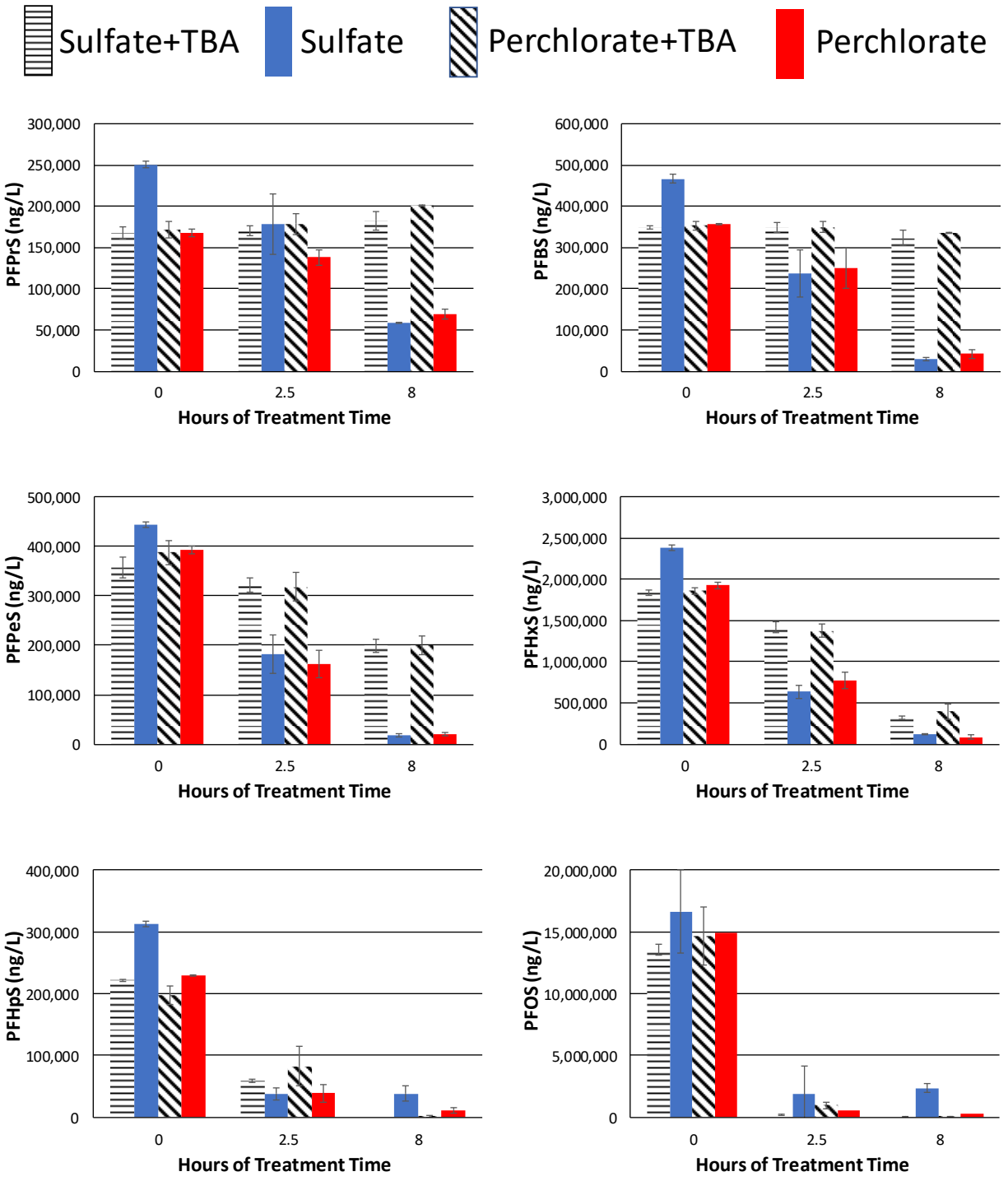

Figure A3.6.10. Removal of perfluorinated sulfonates during electrochemical treatment in 0.2% Na_2SO_4 and $NaClO_4$ brines using 40 mA/cm^2, with and without TBA. Averages of duplicate experiments are shown. Error bars indicate the 95% confidence intervals.

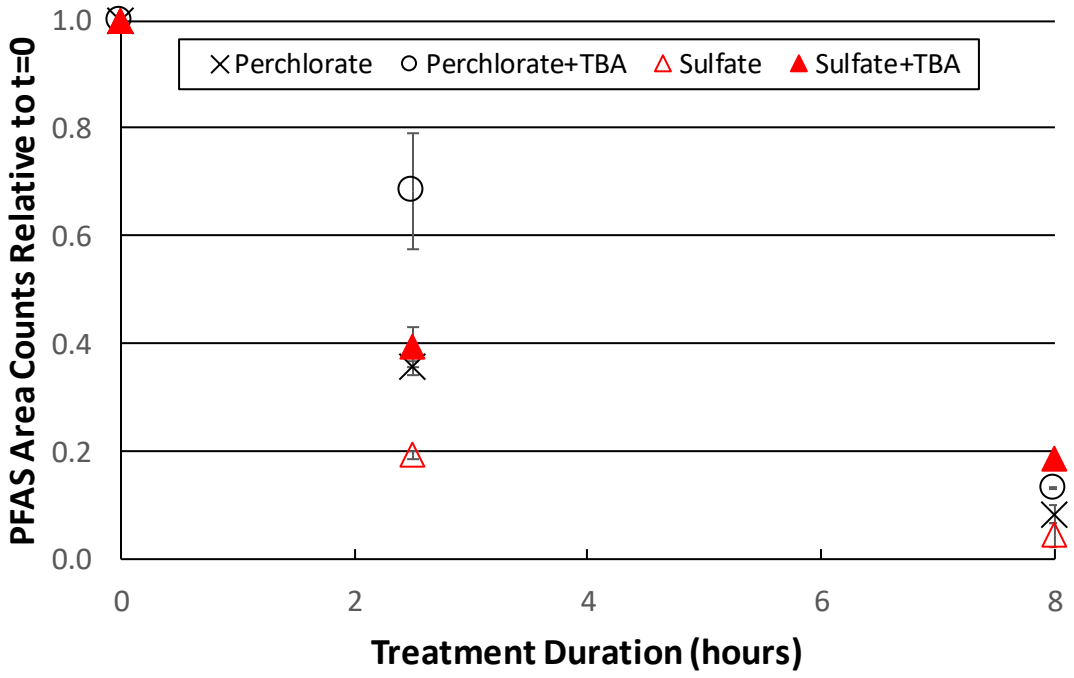

Figure A3.6.11. Relative (to t=0 hours) removal of polyfluorinated compounds during electrochemical treatment in 0.2% Na_2SO_4 and $NaClO_4$ using 40 mA/cm^2, with and without TBA. Average of duplicate results are shown. Error bars represent 95% confidence intervals

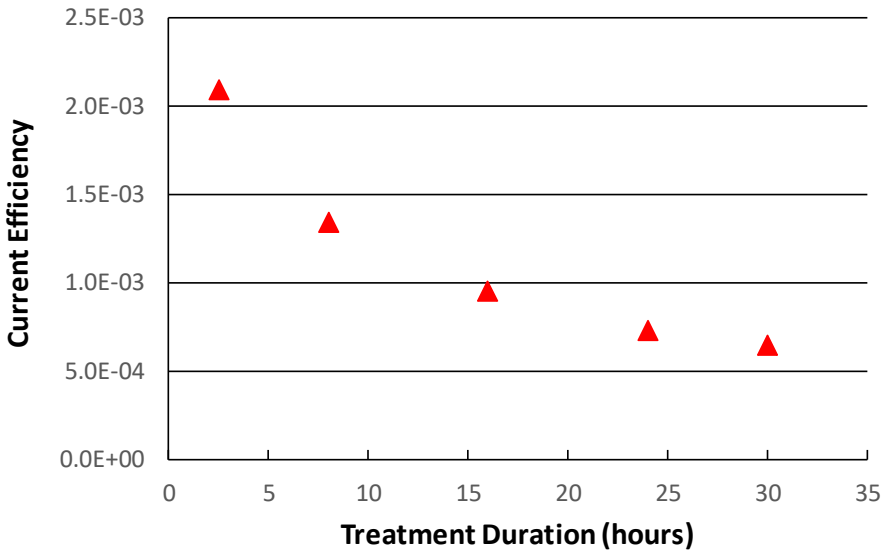

Figure A3.6.12. Current efficiency (CE) for fluoride generation in the 0.2% sodium sulfate brine solution in the long-term experiment. The current density was 40 mA/cm^2.

Additional Methods for Section 2.10.1

The general procedure followed in SimaPro was:

1. Specify the known outputs to the technosphere (amount and unit). This is the functional unit that the LCA is based on. In the case of this LCA study, for all scenarios, amount = 1, unit = m^3, i.e., 1 m^3 AER-treated groundwater to remove PFAS.
2. Specify the inventory items in steps 3 and 4 based on the system and boundary.
    a. Inventory items were selected from databases to best reflect operational inputs used in PFAS treatment. Emphasis was given to items linked to AER treatment (e.g., spent solvent incineration) and items with data obtained from the United States or North America (e.g., US or RNA, respectively).
3. Determine the known inputs from the technosphere (amount and unit) such as materials/fuels and electricity/heat. These are the material and electricity input items listed in Table 2.10.1 and shown in Figure 2.10.1. For scenario 1a the items were:
    a. Sodium chloride, at plant/RNA
    b. Methanol, at plant/RNA
    c. Tap water (RoW)|market for
    d. Transport, combination truck, diesel powered/US
    e. Electricity, at grid, US/US
4. Determine known outputs to technosphere. Waste and emissions to treatment (amount and unit). This is for incineration or other disposal methods. For scenario 1a the item was:
    a. Spent solvent mixture (RoW)|treatment of, hazardous waste incineration
5. The inventory items in steps 3 and 4 include the following information: item name (e.g., sodium chloride), location (e.g., US = United States, RNA = North America), and additional information about the nature of the item (e.g., “at plant” means the item includes all inputs associated with the production of the item).
6. The inventory items can be viewed to see additional details such as technology used and inputs required from the technosphere.
7. Following the specification of all inputs and outputs, the LCA is analyzed following a specified method. For this LCA study, the method was TRACI 2.1, version 1.02 with normalization following US 2008, which is the impact associated with one person in the US in 2008.
    a. TRACI (the Tool for Reduction and Assessment of Chemicals and Other Environmental Impacts) was chosen as the method for impact assessment in this study due to its reliance on EPA impact data, synthesis of numerous existing methodologies, and applicability to US operations.
8. The output of the LCA model show the results of the impact assessment that includes characterization values (ozone depletion, global warming, smog, etc.), which are midpoint environmental impacts as defined in TRACI, and normalization values, which normalize the characterization values to the impact of a US citizen in 2008.

a. One can use the interconnected model built-in to SimaPro to run sensitivity analyses, as changes to input quantities will be propagated through the entire model and adjust quantities of constituent inputs accordingly.

9. Many resources are available for LCA including SimaPro tutorial (Goedkoop et al., 2016), TRACI user guide (Bare, 2012; Ryberg et al., 2014), and critical review articles on LCA for water and wastewater research (Corominas et al., 2020).

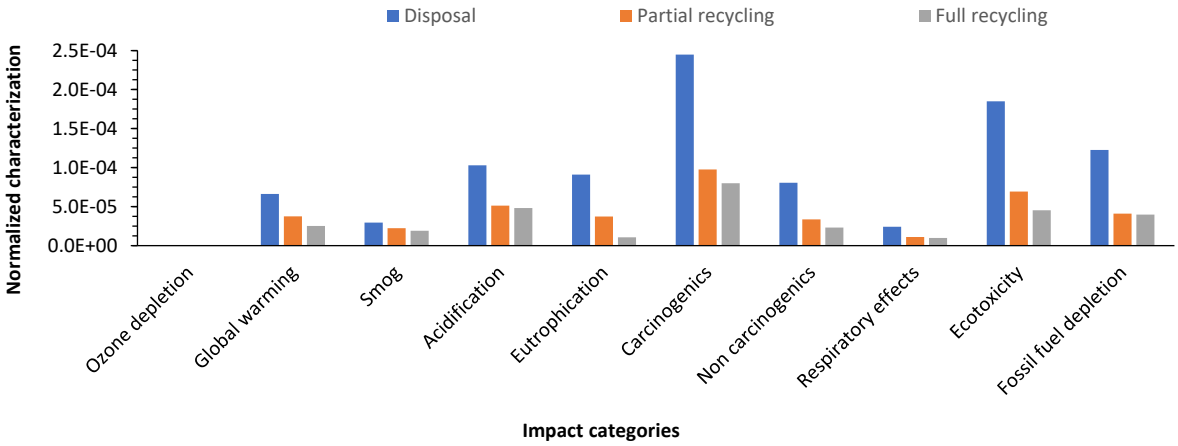

Figure A3.7.1. Overall environmental impact for each AER regeneration option calculated by TRACI 2.1 normalized to the average annual impact of a U.S. citizen in 2008.

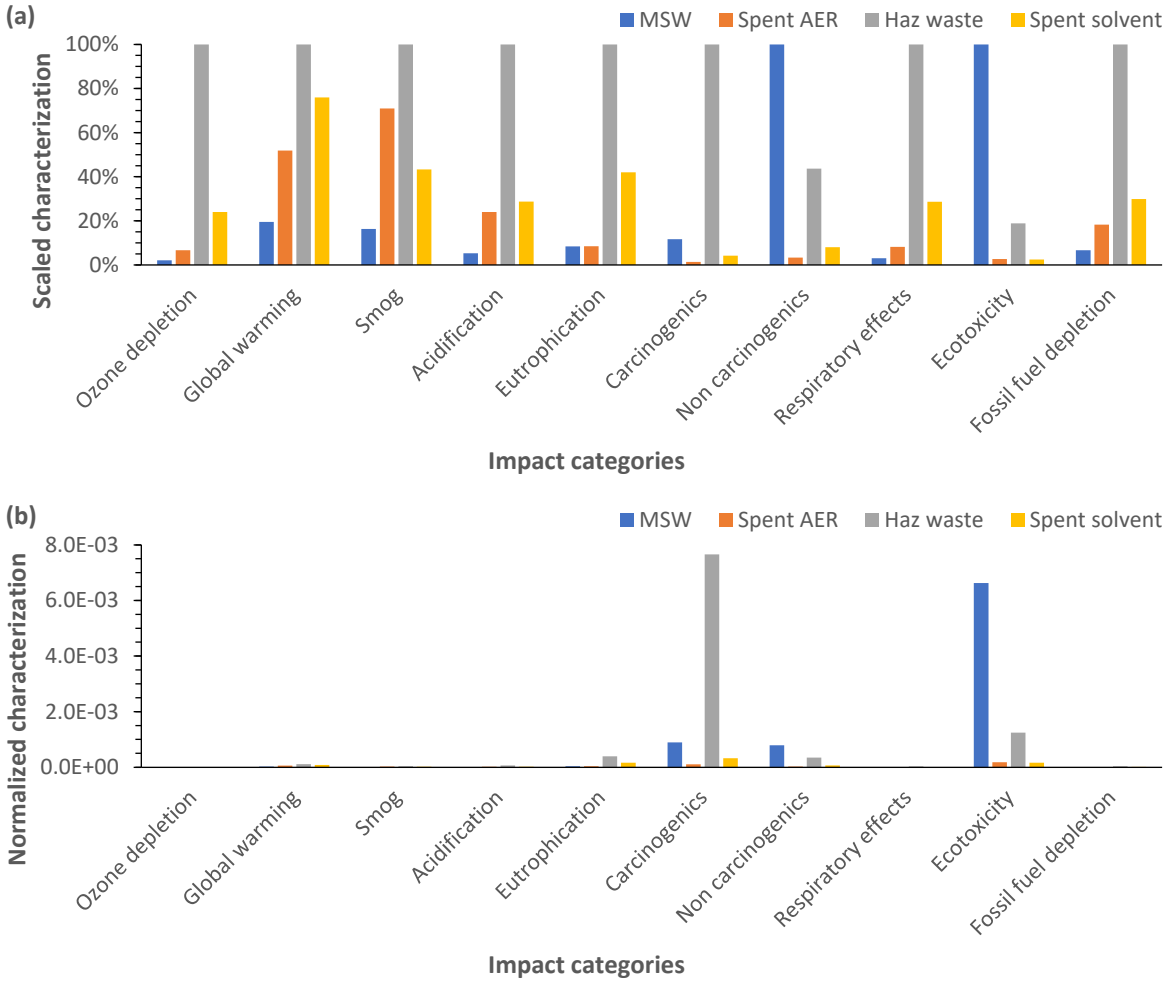

Figure A3.7.2. Overall environmental impact for different incineration inventory items calculated by TRACI 2.1 **(a)** results expressed such that the item with the greatest impact for a given impact category is 100% and the other items are a percentage of that item, and **(b)** normalized to the average annual impact of a U.S. citizen in 2008. **Incineration process**, SimaPro inventory item (database): **MSW**, Municipal solid waste {RoW}| treatment of, incineration | Alloc Def, U (Ecoinvent 3); **Spent AER**, Spent anion exchange resin from potable water production {RoW}| treatment of, municipal incineration | Alloc Def, U (Ecoinvent 3); **Haz waste**, Hazardous waste, for incineration {RoW}| treatment of hazardous waste, hazardous waste incineration | Alloc Def, U (Ecoinvent 3); **Spent solvent**, Spent solvent mixture {RoW}| treatment of, hazardous waste incineration | Alloc Def, U (Ecoinvent 3).

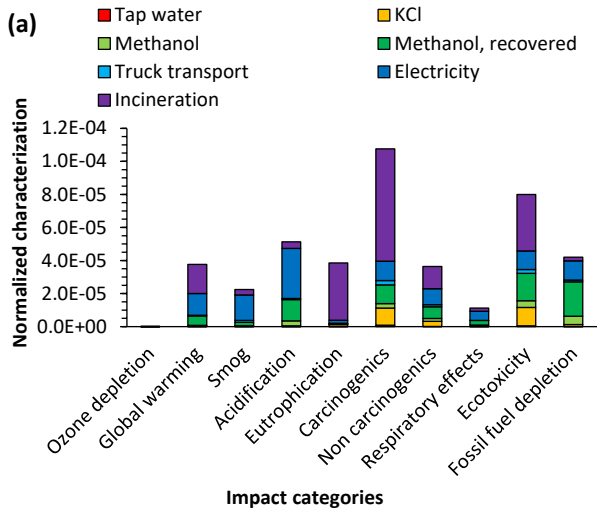
(a)
Tap water
KCl
Methanol
Methanol, recovered
Truck transport
Electricity
Incineration
Normalized characterization
1.2E-04
1.0E-04
8.0E-05
6.0E-05
4.0E-05
2.0E-05
0.0E+00
Ozone depletion
Global warming
Smog
Acidification
Eutrophication
Carcinogenics
Non carcinogenics
Respiratory effects
Ecotoxicity
Fossil fuel depletion
Impact categories

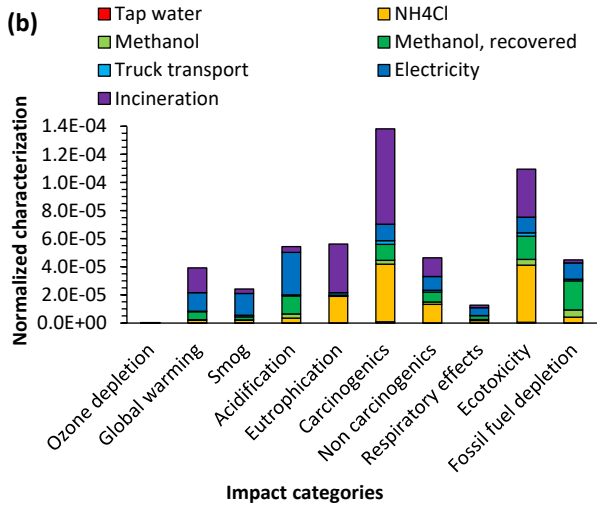
(b)
Tap water
NH4Cl
Methanol
Methanol, recovered
Truck transport
Electricity
Incineration
Normalized characterization
1.4E-04
1.2E-04
1.0E-04
8.0E-05
6.0E-05
4.0E-05
2.0E-05
0.0E+00
Ozone depletion
Global warming
Smog
Acidification
Eutrophication
Carcinogenics
Non carcinogenics
Respiratory effects
Ecotoxicity
Fossil fuel depletion
Impact categories

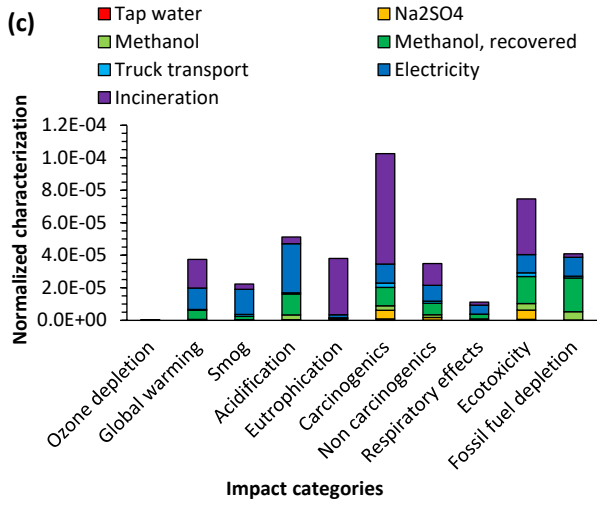
(c)
Tap water
Na2SO4
Methanol
Methanol, recovered
Truck transport
Electricity
Incineration
Normalized characterization
1.2E-04
1.0E-04
8.0E-05
6.0E-05
4.0E-05
2.0E-05
0.0E+00
Ozone depletion
Global warming
Smog
Acidification
Eutrophication
Carcinogenics
Non carcinogenics
Respiratory effects
Ecotoxicity
Fossil fuel depletion
Impact categories

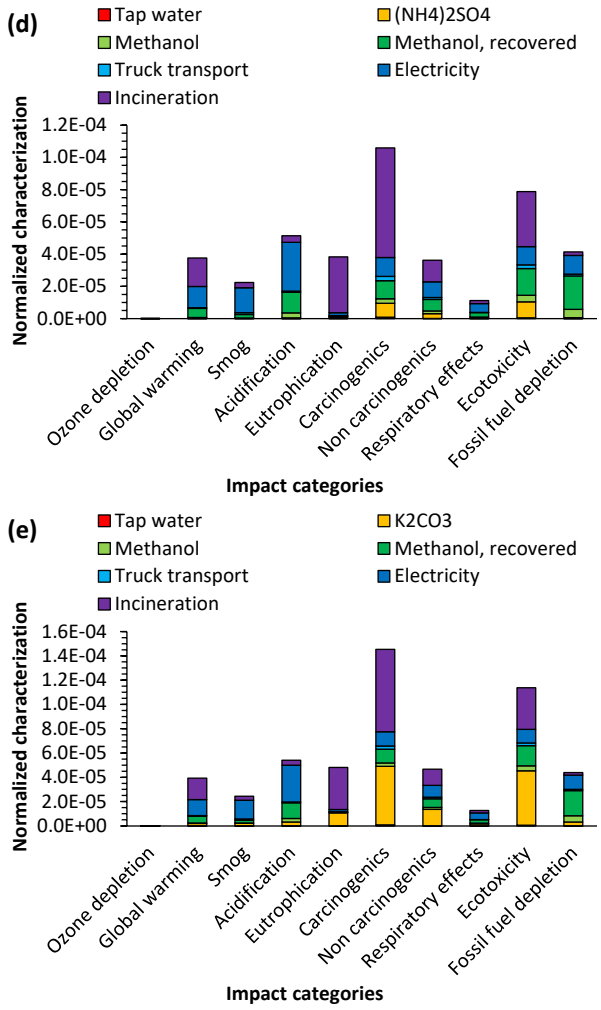

Figure A3.7.3. Impact assessment results for AER regeneration option of partial recycling for the salts **(a)** KCl, **(b)** NH_4Cl, **(c)** Na_2SO_4, **(d)** $(NH_4)_2SO_4$, and **(e)** K_2CO_3 calculated by TRACI 2.1 normalized to the average annual impact of a U.S. citizen in 2008. Color coding for each inventory item is consistent across subplots.

Table A3.7.1. Overall environmental impact for different salt inventory items calculated by TRACI 2.1 **(a)** results expressed such that the item with the greatest impact for a given impact category is 1.000 and the other items are a fraction of that item with blue-white-red heatmap included for emphasis, and **(b)** normalized to the average annual impact of a U.S. citizen in 2008 with white-red heatmap added for emphasis.

(a)

Impact category	Max[a]	NaCl[b]	NaCl[c]	NaCl[d]	KCl[e]	KCl[f]	NH_4Cl[g]	NH_4Cl[h]	Na_2SO_4	K_2SO_4	$(NH_4)_2SO_4$	Na_2CO_3[i]	Na_2CO_3[j]	K_2CO_3	$(NH_4)_2CO_3$
Ozone depletion	7.39E-7	0.002	0.017	0.028	0.109	0.001	1.000	0.212	0.020	0.165	0.039	0.014	0.140	0.336	0.256
Global warming	2.56E0	0.059	0.054	0.094	0.210	0.085	0.949	0.512	0.074	0.320	0.148	0.201	0.338	1.000	0.612
Smog	1.66E-1	0.038	0.052	0.089	0.143	0.032	0.903	0.509	0.071	0.369	0.103	0.152	0.336	1.000	0.630
Acidification	1.60E-2	0.067	0.064	0.106	0.132	0.021	1.000	0.498	0.084	0.546	0.139	0.250	0.329	0.914	0.598
Eutrophication	2.11E-2	0.001	0.044	0.068	0.067	0.001	1.000	0.409	0.040	0.171	0.054	0.002	0.270	0.573	0.638
Carcinogenics	1.26E-7	0.007	0.157	0.200	0.216	0.001	0.851	0.539	0.111	0.489	0.180	0.011	0.356	1.000	0.436
Non carcinogenics	7.33E-7	0.022	0.199	0.236	0.234	0.000	0.979	0.617	0.125	0.691	0.224	0.098	0.407	1.000	0.505
Respiratory effects	2.16E-3	0.028	0.073	0.121	0.135	0.006	1.000	0.469	0.097	0.392	0.132	0.118	0.310	0.950	0.527
Ecotoxicity	2.56E1	0.007	0.210	0.234	0.248	0.000	0.907	0.629	0.129	0.630	0.221	0.009	0.415	1.000	0.518
Fossil fuel depletion	3.71E0	0.066	0.032	0.052	0.294	0.145	1.000	0.572	0.040	0.363	0.143	0.112	0.377	0.764	0.791

[a] Maximum value for salt with scaled value of 1.000; units: kg CFC-11 eq, kg CO2 eq, kg)3 eq, kg SO2 eq, kg N eq, CTUh, CTUh, kg PM2.5 eq, CTUe, MJ surplus, respectively. [b] Default from scenario 1. [c] Brine solution. [d] Powder. [e] Default. [f] Alternative. [g] Default [h] Alternative. [i] Default. [j] Alternative. **Salt**, SimaPro inventory item (database): **NaCl[b]**, Sodium chloride, at plant/RNA (USLCI); **NaCl[c]**, Sodium chloride, brine solution {RoW}| production | Alloc Def, U (Ecoinvent 3); **NaCl[d]**, Sodium chloride, powder {RoW}| production | Alloc Def, U (Ecoinvent 3); **KCl[e]**, Potassium chloride, as K2O {RoW}| potassium chloride production | Alloc Def, U (Ecoinvent 3); **KCl[f]**, Potassium chloride (NPK 0-0-60), at plant/RER Mass (Agri-footprint); **NH_4Cl[g]**, Ammonium chloride {GLO}| production | Alloc Def, U (Ecoinvent 3); **NH_4Cl[h]**, Ammonium chloride {GLO}| modified Solvay process, Hou's process | Alloc Def, U (Ecoinvent 3); **Na_2SO_4**, Sodium sulfate, anhydrite {RoW}| sodium sulfate production, from natural sources | Alloc Def, U (Ecoinvent 3); **K_2SO_4**, Potassium sulfate, as K2O {RoW}| potassium sulfate production | Alloc Def, U (Ecoinvent 3); **$(NH_4)_2SO_4$**, Ammonium sulfate, as N {RoW}| ammonium sulfate production | Alloc Def, U (Ecoinvent 3); **Na_2CO_3[i]**, Soda, powder, at plant/US (USLCI); **Na_2CO_3[j]**, Soda ash, dense {GLO}| modified Solvay process, Hou's process | Alloc Def, U (Ecoinvent 3); **K_2CO_3**, Potassium carbonate {GLO}| production, from potassium hydroxide | Alloc Def, U (Ecoinvent 3); **$(NH_4)_2CO_3$**, Ammonium carbonate {RoW}| production | Alloc Def, U (Ecoinvent 3).

(b)

Impact category	NaCl[b]	NaCl[c]	NaCl[d]	KCl[e]	KCl[f]	NH_4Cl[g]	NH_4Cl[h]	Na_2SO_4	K_2SO_4	$(NH_4)_2SO_4$	Na_2CO_3[i]	Na_2CO_3[j]	K_2CO_3	$(NH_4)_2CO_3$
Ozone depletion	6.91E-9	7.56E-8	1.27E-7	4.98E-7	3.28E-9	4.58E-6	9.73E-7	9.32E-8	7.57E-7	1.78E-7	6.34E-8	6.42E-7	1.54E-6	1.17E-6
Global warming	6.28E-6	5.66E-6	9.94E-6	2.21E-5	8.98E-6	1.00E-4	5.40E-5	7.80E-6	3.38E-5	1.57E-5	2.12E-5	3.57E-5	1.06E-4	6.46E-5
Smog	4.56E-6	6.15E-6	1.06E-5	1.71E-5	3.82E-6	1.08E-4	6.07E-5	8.41E-6	4.40E-5	1.23E-5	1.81E-5	4.01E-5	1.19E-4	7.51E-5
Acidification	1.18E-5	1.13E-5	1.87E-5	2.32E-5	3.67E-6	1.76E-4	8.79E-5	1.48E-5	9.63E-5	2.45E-5	4.41E-5	5.80E-5	1.61E-4	1.05E-4

Eutrophication	7.21E-7	4.32E-5	6.62E-5	6.58E-5	8.45E-7	9.79E-4	4.00E-4	3.96E-5	1.67E-4	5.32E-5	2.37E-6	2.64E-4	5.61E-4	6.25E-4
Carcinogenics	1.67E-5	3.91E-4	4.99E-4	5.38E-4	2.41E-6	2.12E-3	1.34E-3	2.76E-4	1.22E-3	4.49E-4	2.76E-5	8.87E-4	2.49E-3	1.09E-3
Non carcinogenics	1.51E-5	1.39E-4	1.65E-4	1.63E-4	2.26E-7	6.83E-4	4.30E-4	8.70E-5	4.82E-4	1.56E-4	6.86E-5	2.84E-4	6.98E-4	3.52E-4
Respiratory effects	2.50E-6	6.53E-6	1.08E-5	1.20E-5	5.46E-7	8.91E-5	4.18E-5	8.65E-6	3.50E-5	1.17E-5	1.05E-5	2.76E-5	8.46E-5	4.69E-5
Ecotoxicity	1.63E-5	4.88E-4	5.43E-4	5.76E-4	3.59E-7	2.10E-3	1.46E-3	2.99E-4	1.46E-3	5.14E-4	2.07E-5	9.63E-4	2.32E-3	1.20E-3
Fossil fuel depletion	1.41E-5	6.79E-6	1.11E-5	6.32E-5	3.12E-5	2.15E-4	1.23E-4	8.53E-6	7.80E-5	3.07E-5	2.41E-5	8.10E-5	1.64E-4	1.70E-4

See footnote a above for impact category units. See footnotes above for Salt, SimaPro inventory item (database).

Table A3.7.2. Contribution of processes within partial recycling scenario to overall environmental impact.

Scenario	Tap water	Salt	Methanol	Methanol, recovered	Truck transport	Electricity	Incineration
1b/NaCl	0.36%	0.43%	4.5%	20%	2.4%	28%	45%
2a/KCl	0.34%	6.7%	4.2%	19%	2.3%	26%	42%
2a/NH_4Cl	0.28%	24%	3.4%	15%	1.9%	21%	34%
2a/Na_2SO_4	0.35%	3.5%	4.3%	19%	2.4%	27%	43%
2a/$(NH_4)_2SO_4$	0.34%	5.8%	4.2%	19%	2.3%	26%	42%
2a/K_2CO_3	0.27%	25%	3.4%	15%	1.8%	21%	34%

Table A3.7.3. One-at-a-time sensitivity analysis on inputs to anion exchange resin regeneration options of partial recycling, scenario 1b/NaCl and scenario 2a/KCl, NH_4Cl, Na_2SO_4, $(NH_4)_2SO_4$, and K_2CO_3. Each input amount was varied by 0.5× and 2× from the baseline value in Table 3.7.1, and the percent decrease and percent increase, respectively, is listed.[a]

Impact category	NaCl		KCl		NH_4Cl		Na_2SO_4		$(NH_4)_2SO_4$		K_2CO_3	
Ozone depletion	0%	0%	-7%	13%	-29%	59%	-1%	3%	-3%	5%	-16%	33%
Global warming	0%	0%	-1%	1%	-2%	5%	0%	0%	0%	1%	-3%	5%
Smog	0%	0%	-1%	1%	-4%	9%	0%	1%	-1%	1%	-5%	9%
Acidification	0%	0%	0%	1%	-3%	6%	0%	1%	0%	1%	-3%	6%
Eutrophication	0%	0%	-2%	3%	-17%	34%	-1%	2%	-1%	3%	-11%	23%
Carcinogenics	0%	0%	-5%	10%	-15%	30%	-3%	5%	-4%	8%	-17%	33%
Non carcinogenics	0%	1%	-4%	9%	-14%	28%	-2%	5%	-4%	8%	-14%	29%
Respiratory effects	0%	0%	-1%	2%	-7%	14%	-1%	1%	-1%	2%	-6%	13%
Ecotoxicity	0%	0%	-7%	14%	-19%	37%	-4%	8%	-6%	13%	-20%	39%
Fossil fuel depletion	0%	1%	-1%	3%	-5%	9%	0%	0%	-1%	1%	-4%	7%

[a] For input varied by 0.5× from baseline, the results were considered: Not sensitive, <5% decrease; low sensitivity, 5 to <12.5% decrease; medium sensitivity, 12.5 to <25% decrease; high sensitivity, >25% decrease. For input varied by 2× from baseline, the results were considered: Not sensitive, <10% increase; low sensitivity, 10 to <25% increase; medium sensitivity, 25 to <50% increase; high sensitivity, >50% increase.

Table A3.8.1. List of assumptions made in LCA models for sorbent comparisons (Section 3.8)	
Category	***Assumption***
Treatment Site Assumptions	Remediation site is assumed to treat a flow rate of 6,000 LPH (0.038 MGD) to reflect remediation operations at a source zone rather than drinking water treatment at the point of use
	Site groundwater is assumed to contain an average of 50 ug/L of total PFAS to reflect site conditions at the Willow Grove, PA field pilot system (Ellis et al., 2022)
	PFSAs are assumed to dominate the total PFAS concentration (60-75% of total PFAS), consistent with sites contaminated by historical use of AFFF
	Flow rates at the site are assumed to be constant, and time needed for minimal stoppages necessary to change sorbent beds are assumed to be negligible
	Site infrastructure, including sorbent contactors and pipes, are assumed to experience minimal degradation that does not require additional capital costs for replacement
	Pressure drops from sorbent fouling or microbial growth are assumed to occur at a rate less than the sorbent changeout rate due to the high PFAS concentrations, consistent with observations at the Willow Grove field pilot
	Groundwater co-constituents including nitrate and sulfate are assumed to be well below levels that could be expected to compete with PFAS for exchange sites
	Concentrations of organic carbon (TOC) are assumed to be between 0 and 3 mg/L, consistent with field pilot observations and median concentrations found in groundwater
	Water quality parameters like pH and alkalinity are assumed to be within the expected bounds of natural waters (e.g., circumneutral pH of 6-8) and do not affect sorbents
	Presence of PFAA precursors and other fluorochemicals is assumed to be consistent with levels observed in field pilots, with no additional impact on sorbent performance
	Treatment site is assumed to be, on average, located approximately 500km from suppliers of sorbent media and hazardous waste incinerators for generalizability
	Treatment site is assumed to have an existing well from which contaminated groundwater is pumped, with a pump in place capable of handling 6,000 L/hr
	Treatment as modeled in this study is assumed to exhibit similar performance results on a bed volume-equivalent basis as field pilot-derived data for PFA694E and CalRes 2301 (single-use AER), A520E (regenerable AER), and F400 (both GAC models)
Operation of Remediation Systems	Remediation system is assumed to be immune to weather effects and located in an enclosure that provides constant temperature
	Remediation system operators are assumed to perform labor in hours and at a pay rate consistent with expected hours and pay rates provided by the EPA costing tool
	Operator hours are assumed to scale linearly with the number of changeouts per year
	Transportation of consumable materials is assumed to occur on full trucks such that the 500km transport distance is accurate and does not include any return trips or detours
	PFAS and co-constituent concentrations are assumed to stay constant throughout operation, with media usage rates assumed to stay constant as well
	Ten bed volumes of regenerant solution is assumed to be adequate for regeneration of the regenerable AER system
	Ten bed volumes of water used to flush the regenerable AER system after regeneration are assumed to be slowly blended back into the system influent stream. Residual solvent in the flushed solution is assumed to have no effect on sorbent performance.
	Regeneration efficiency is assumed to be 100% for each cycle over the course of the 5-year AER bed lifetime, with no impact on available AER capacity for PFAS

	Sampling of PFAS in vessel effluent is assumed to occur rapidly and provides adequate data to enable sorbent changeout without delays to treatment
	Treated effluent waters are assumed to be pumped back into the subsurface downstream of the PFAS plume, and are assumed to have no effect on influent PFAS concentrations
	Regenerant brine is assumed to maintain a fully-aqueous state without any salt precipitation that may affect flow rates or sorbent performance
Life Cycle Inventories and Impact Assessment (LCI+LCIA)	Inventory items selected using the decision tree in Appendix A are assumed to best reflect inputs that would be used in real-world PFAS treatment operations
	Inventories are designed to be generalizable across a range of treatment sites, and any other potential inputs are assumed to be negligible compared to sorbent usage rates
	As LCIs are compiled from field pilot-derived MURs, it is assumed that inputs of consumables and disposal of waste outputs scale linearly with sorbent usage
	Impacts as determined through SimaPro and associated databases from LCIs are assumed to optimally reflect impacts stemming from real-world PFAS treatment
	TRACI-derived impact categories and their associated units (e.g., comparative toxicity units, CTUs) are assumed to accurately reflect environmental impacts as of 2023
	Inventory items selected for use in these LCA models are assumed to best reflect the expected inputs/outputs required for the system in accordance with Appendix A
Waste Disposal	As all incineration and reactivation processes are modeled to reflect disposal of hazardous substances; it is assumed that items accurately capture the temperatures and breadth of waste operations required to destroy PFASs and reactivate GAC
	Hazardous waste incineration is assumed to occur at a temperature of approximately 1200°C while GAC reactivation is assumed to take place at approximately 815°C
	It is assumed that no additional environmental impact from disposal processes (incineration and reactivation) are incurred from potential PFAS volatilization
	Slightly higher costs of GAC reactivation compared to incineration are assumed to be a facet of increased hazardous material handling and pooling costs at a GAC-specific reactivation plant rather than bulk hazardous waste incineration
	GAC reactivation is assumed to yield complete separation of PFASs from the media and full recovery of carbon capacity for PFAS adsorption in the next treatment cycle
	While GAC reactivation is assumed to take place in pooled reactors with other GAC media, it is assumed that no other contaminants are loaded onto the GAC sent back to the treatment site for use in the next treatment cycle
	Offsite thermal reactivation of GAC is assumed to lose approximately 10% of its mass in the process, which is assumed to include any losses from heat and handling
	Waste material sent for incineration is assumed to contain a moisture content within the bounds of typical hazardous wastes, and requires no additional heat sources to evaporate
Life Cycle Costing (LCCA)	Treatment system infrastructure as modeled and priced by the LCCA analysis using the CoST tool are assumed to reflect equipment that would be used in remediation
	As suggested by the CoST tool, a 10% allowance for miscellaneous expenses was assumed to account for potential labor overages and repairs to site infrastructure
	Costs of labor are assumed to scale in a linear fashion with MUR and regeneration frequency. Labor costs for the baseline scenario were obtained from the WBS, and labor estimates for other changeout criteria scale with relative MURs.
	Where possible, equipment was selected to ensure its utility over a 30-year lifetime, thus it is assumed that no additional expenses are incurred beyond the assumed 10%
	Prices of consumable materials including adsorbents are assumed to stay constant over the duration of treatment, or purchased in quantities that render price fluxes irrelevant

	Prices for treatment of and resupply of reactivated GAC are assumed to follow pricing provided by Franke et al. (2021)
	Analysis of effluent samples for PFAS data is assumed to be equivalent for all systems, and thus has been excluded for LCCA data

APPENDIX B: LIST OF SCIENTIFIC/TECHNICAL PUBLICATIONS

Articles in peer-reviewed journals

1. del Moral, L., Choi, Y.-J., Boyer, T.H. (2020). Comparative removal of Suwanee River natural organic matter and perfluoroalkyl acids by anion exchange: Impact of polymer composition and mobile counterion. *Water Research*, 178, 115846. https://doi.org/10.1016/j.watres.2020.115846.
2. C.E. Schaefer, D. Tran, Y. Fang, Y. Choi, C.P. Higgins, and T.J. Strathmann. (2020). Electrochemical Treatment of Poly- and Perfluoroalkyl Substances in Brines. *Environmental Science: Water Research & Technology, 6, 2704.* https://doi.org/10.1039/d0ew00377h.
3. Y. Fang, A. Ellis, Y. Choi , T. Boyer, C.P. Higgins , C.E. Schaefer, T.J. Strathmann. (2021). Removal of poly- and perfluoroalkyl substance (PFAS) in aqueous film-forming foam (AFFF) impacted water using ion exchange and non-ionic resins. *Environ. Sci. Technol. 55, 5001.* https:/doi.org/10.1021/acs.est.1c00769.
4. T.H. Boyer, R. Dietz, Y. Fang, A. Ellis, Y.J. Choi, C. Schaefer, C.P. Higgins, and T.J. Strathmann (2021). Anion exchange resin removal of perfluoroalkyl acids (PFAAs) from impacted water: A critical review. *Water Research, 200, 117244.* https:/doi.org/10.1016/j.watres.2021.117244.
5. R. Dietz, C. Kassar and T.H. Boyer. (2021). Regeneration efficiency of strong-base anion exchange resin for PFAS. *AWWA Water Science,* 3, e1259. https://doi.org/10.1002/aws2.1259.
6. T.H. Boyer, A. Ellis, Y. Fang, C.E. Schaefer, C.P. Higgins, and T.J. Strathmann. (2021). Life cycle environmental impacts of regeneration options for anion exchange resin remediation of PFAS impacted groundwater. *Water Research*, 207, 117798. https://doi.org/10.1016/j.watres.2021.117798.
7. A. Ellis, C.J. Liu, Y. Fang, C. Bellona, T.H. Boyer, C.E. Schaefer, C.P. Higgins, and T.J. Strathmann. (2022). A pilot study comparison of regenerable and emerging single-use anion exchange resins for treatment of groundwater contaminated by per- and polyfluoroalkyl substances (PFASs). *Water Research*, 223, 119010. https://doi.org/10.1016/j.watres.2022.119019
8. C. Kassar, C. Graham, and T.H. Boyer. (2022). Removal of perfluoroalkyl acids and common drinking water contaminants by weak-base anion exchange resins: Impacts of solution pH and resin properties. *Water Research X*, 17, 100159. https://doi.org/10.1016/j.wroa.2022.100159
9. Y. Fang, P. Meng, C. Schaefer, D. Knappe. (2023). Removal and destruction of perfluoroalkyl ether carboxylic acids (PFECAs) in an anion exchange resin and electrochemical oxidation treatment train. *Water Research*, 230, 119522. https://doi.org/10.1016/j.watres.2022.119522

10. C. Kassar and T.H. Boyer. (2023). Removal of PFAS from groundwater using weak-base anion exchange resins. AWWA Water Science, e1325. https://doi.org/10.1002/aws2.1325.
11. A.C. Ellis, T.H. Boyer, Y. Fang, C.J. Liu, and T.J. Strathmann. Life cycle assessment and life cycle cost analysis of anion exchange and granular activated carbon systems for remediation of groundwater contaminated by per- and polyfluoroalkyl substances (PFAS). **Status:** Manuscript in review.
12. C. Graham, C. Kassar, and T.H. Boyer. (2022) Novel cosolvent regeneration for spent anion exchange resin saturated with hydrophobic ionizable organic compounds and perfluoroalkyl substances (PFASs). **Status:** Manuscript in preparation.
13. C. Graham and T.H. Boyer. (2022) Sustainability considerations for novel cosolvent regeneration of spent anion exchange resin saturated with perfluoroalkyl substances (PFASs). **Status:** Manuscript in preparation.
14. A.C. Ellis, T.H. Boyer, and T.J. Strathmann. (2023) Regeneration of regenerable and single-use anion exchange resins to treat PFAS-contaminated water. **Status**: Manuscript in preparation.

Conference Presentations and Lectures

T.J. Strathmann, C. Bellona, C.P. Higgins, T. Boyer, and C. Schaefer. *Developing and evaluating hybrid concentration-destruction treatment trains for water contaminated with per- and polyfluoroalkyl substances (PFASs).* Special invited Keynote presentation in Symposium on Innovative & Practical Approaches for Treatment of Per- and Polyfluoroalkyl Substances (PFASs) and Fluorinated Alternatives at the American Chemical Society National Meeting, San Diego, CA, March 22, 2022.

C. Kassar, C. Graham, and T.H. Boyer. *Removal of perfluoroalkyl acids (PFAAs) by weak-base anion exchange resins*. Presentation in Symposium on Ion Exchange, Sustainable Separations, & Humanitarian Engineering at the American Chemical Society National Meeting, San Diego, CA, March 20, 2022.

A. Ellis, T.H. Boyer, C.P. Higgins, C.E. Schaefer, T.J. Strathmann. *Pilot study comparison of regenerable and single-use ion exchange resins for remediation of PFASs.* Presentation in the Symposium on Ion Exchange, Sustainable Separations, & Humanitarian Engineering at the American Chemical Society National Meeting, San Diego, CA, March 20, 2022.

Boyer, T.H. *Insights on ion-exchange processes and operation through life cycle assessment: Example of PFAS remediation.* Presentation in Symposium on Ion Exchange, Sustainable Separations, & Humanitarian Engineering at the American Chemical Society National Meeting, San Diego, CA, March 20, 2022.

T.J. Strathmann. *Developing and evaluating hybrid concentration-destruction treatment trains for water contaminated with per- and polyfluoroalkyl substances (PFASs).* Invited webinar to Nanjing University, Nanjing, China, May 19, 2022.

A. Ellis, C. Liu, Y. Fang, T. Boyer, C.P. Higgins, C.E. Schaefer, T.J. Strathmann. *Assessment of various anion exchangers for the remediation of a diverse PFAS mixture at a highly concentrated source zone.* Presentation to be given at the RemTEC & Emerging Contaminants Summit, Westminster, CO, October 5, 2022.

A. Ellis, Y. Fang, T. Boyer, C.P. Higgins, C.E. Schaefer, T.J. Strathmann. *Use of anion exchange resins in removing per- and polyfluoroalkyl substances (PFASs) from real groundwater at an AFFF-impacted source zone.* Presentation to be given at the FLUOROS Australian Meeting, Brisbane, Australia, October 20, 2022.

Y.J. Choi, T.J. Strathmann, and C.P. Higgins. *Microbial transformation of polyfluoroalkyl substances in aqueous film forming foam: finding missing links using intermediate prediction database*. To be presented at the American Chemical Society National Meeting & Exposition. San Francisco, CA, August 2020.

A. Ellis, Y. Fang, T. Boyer, C.P. Higgins, C.E. Schaefer. and T.J. Strathmann. *Development and Application of a Forward-Predictive Model for Continuous Ion Exchange Treatment of PFAS.* Poster to be presented at the American Chemical Society National Meeting & Exposition. San Francisco, CA, August 2020.

Y. Fang, A. Ellis, Y.J. Choi, T. Boyer, C.P. Higgins, C.E. Schaefer, and T.J. Strathmann. *Removal of PFASs in aqueous film-forming foam (AFFF) using ion exchange and non-ionic resins*. Presented at the Emerging Contaminants Summit. Westminster, CO, March 2020.

A. Ellis, Y. Fang, T. Boyer, C.P. Higgins, C.E. Schaefer. and T.J. Strathmann. *Development of a Predictive Model for Continuous PFAS Treatment Using Ion Exchange Resins.* Poster presented at the Emerging Contaminants Summit. Westminster, CO, March 2020.

T.H. Boyer, L. del Moral, R. Dietz, Y.J. Choi, C.P. Higgins, C.E. Schaefer, and T.J. Strathmann. *PFAS Ion Exchange Treatment and Life Cycle Impacts*. Invited presentation at AZ Water Research Symposium: PFAS Occurrence, Research and Treatment Implementation in Arizona, Tempe, Arizona, 9 January 2020.

A. Ellis, Y. Fang, Y.J. Choi, R. Dietz, T. Boyer, C.P. Higgins, C.E. Schaefer, T.J. Strathmann. *Removal of PFAS from AFFF-Impacted Groundwater Using Ion Exchange Resins*. Poster Presented at the Herbert L. and Doris S. Young Environmental Issues Symposium. Golden, CO, January 2020.

T.J. Strathmann, T. Boyer, C.P. Higgins, C. Schaefer, Y. Fang, A. Ellis, Y.J. Choi, and R. Dietz. (2019). *Application and Life Cycle Assessment of Regenerable and Non-Regenerable Ion Exchange Treatment Technologies for Remediation of Aqueous Film-Forming Foam (AFFF)-Impacted Groundwater (ER18-1063)*. Poster presented at the 2019 SERDP-ESTCP Partners Meeting, Washington, DC, December 2019.

T. Strathmann, C. Bellona, C.P. Higgins, C. Schaefer, T. Boyer, H. Wright, G. McKay, C. Liu, R. Tenorio, Y. Fang, and A. Ellis. (2019) *Laboratory and Pilot-Scale Studies on Innovative Pathways for Removal and Destruction of Perfluoroalkyl Substances (PFAS).* Special invited keynote

presentation at the 2019 International Water Association (IWA) Micropol Conference, Seoul, South Korea, October 2019.

T. Strathmann (2019) *Accomplishing Removal and Destruction of Per- and Polyfluoroalkyl Substances (PFASs) in Contaminated Groundwater*. Invited lecture at the Seoul National University, October 2019.

T. Strathmann (2019) *Accomplishing Removal and Destruction of Per- and Polyfluoroalkyl Substances (PFASs) in Contaminated Groundwater*. Special invited lecture at the 6th International Workshop on Frontiers in Environmental Chemical Research, Pohang University of Science and Technology (POSTECH), Pohang, South Korea, October 2019.

T. Strathmann. Invited lecture, *Laboratory and Pilot-Scale Studies on Innovative Pathways for Removal and Destruction of Per- and Polyfluoroalkyl Substances (PFASs)*, University of Texas at Austin, Department of Civil, Architectural, and Environmental Engineering, Austin, TX, November 14, 2019.

T. Strathmann. Invited lecture, *Accomplishing Removal and Destruction of Per- and Polyfluoroalkyl Substances (PFASs) in Contaminated Groundwater*, University of New Mexico, Department of Civil & Environmental Engineering, Albuquerque, NM, September 18, 2019

T. Strathmann. Invited lecture, *Research to Advance Treatment of Per- and Polyfluoroalkyl Substances (PFAS).* Colorado Department of Public Health and Environment (CDPHE). Invited Panelist and Speaker, Water Quality Forum, Denver, CO, September 16, 2019.

Y. Fang, A. Ellis, Y.J. Choi, T. Boyer, C.P. Higgins, C.E. Schaefer, and T.J. Strathmann. *Removal of Poly- and Perfluoroalkyl Substances (PFAS) in Aqueous Film-Forming Foam (AFFF) Impacted Water using Ion Exchange and Non-Ionic Resins*. Presented at the American Chemical Society National Meeting, San Diego, CA, August 2019.

T.J. Strathmann, T. Boyer, C.P. Higgins, C. Schaefer, Y. Fang, A. Ellis, Y.J. Choi, and R. Dietz. (2019). *Resin Sorbent Technologies for Sustainable Treatment of PFAS (ER18-1063)*. Poster presented at the SERDP-ESTCP PFAS Workshop, San Diego, CA, July 2019.

T. Strathmann, C. Liu, G. McKay, L. Del Moral, Y. Fang, A. Ellis, J. Brown. Y.J. Choi, T. Boyer, C. Bellona, C. Higgins, H. Wright, R. Deeb, C. Schaefer. *Hybrid Treatment Strategies for Remediation of Groundwater Contaminated by PFAS*. Invited Presentation. Association of Environmental Engineering and Science Professors (AEESP) Biannual Conference, Tempe, AZ, May 2019.

A. Ellis, Y. Fang, T. Boyer, C.P. Higgins, C.E. Schaefer, T.J. Strathmann. *PFAS Remediation Using Combined & Noval Ion Exchange Systems: An Analysis of Viability and Sustainability*. Presentation given at the Rocky Mountain AWWA Student Conference. Boulder, CO, May 2019.

T. Strathmann, T. Boyer, C. Higgins, C. Schaefer, L. del Moral, Y. Fang, A. Ellis, and Y.J. Choi. *SERDP ER-1064: Regenerable Resin Sorbent Technologies with Regenerant Recycling for Sustainable Treatment of Per- and Polyfluoroalkyl Substances (PFASs)*. Poster presented at the 2018 SERDP-ESTCP Partners Meeting, Washington, DC, November 2018.

T. Strathmann, Invited Panelist, Emerging Contaminant Summit, Expert Panel on Perfluoro- and Polyfluoroalkyl Substances Treatment Technologies, Westminster, CO, March 2018.